AD619153

AD

USAAML TECHNICAL REPORT 65-28

EFFECT OF MACH NUMBER, REYNOLDS NUMBER, AND THICKNESS RATIO ON THE AERODYNAMIC CHARACTERISTICS OF NACA 63A-SERIES AIRFOIL SECTIONS

Lockheed Report LR 18596

By

O. E. Sipe, Jr
N. B. Gorenberg

COPY ___ OF ___
HARD COPY $. 7.75
MICROFICHE $. 2.25
47 1 p

June 1965

U. S. ARMY AVIATION MATERIEL LABORATORIES
FORT EUSTIS, VIRGINIA

CONTRACT DA 44-177-AMC-144(T)
LOCKHEED-CALIFORNIA COMPANY

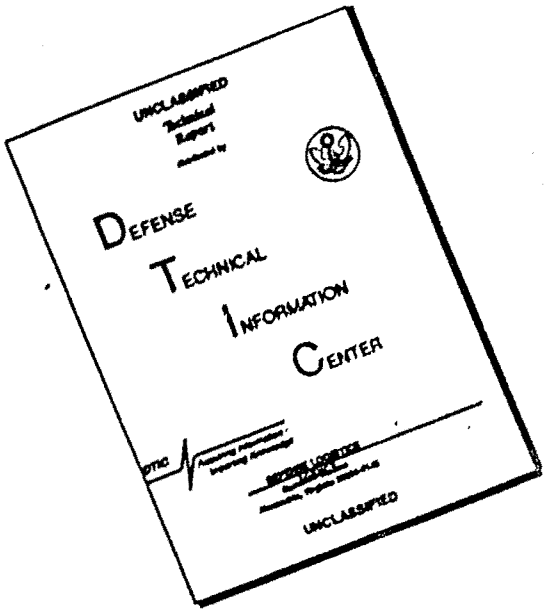
U S ARMY MATERIEL COMMAND

TISIA E

PROCESSING COPY

ARCHIVE COPY

DISCLAIMER NOTICE



THIS DOCUMENT IS BEST QUALITY AVAILABLE. THE COPY FURNISHED TO DTIC CONTAINED A SIGNIFICANT NUMBER OF PAGES WHICH DO NOT REPRODUCE LEGIBLY.

DDC Availability Notice

Qualified requesters may obtain copies of this report from DDC.

This report has been furnished to the Department of Commerce for sale to the public.

Disclaimer

The findings in this report are not to be construed as an official Department of the Army position, unless so designated by other authorized documents.

When Government drawings, specifications, or other data are used for any purpose other than in connection with a definitely related Government procurement operation, the United States Government thereby incurs no responsibility nor any obligation whatsoever; and the fact that the Government may have formulated, furnished, or in any way supplied the said drawings, specifications, or other data is not to be regarded by implication or otherwise as in any manner licensing the holder or any other person or corporation, or conveying any rights or permission, to manufacture, use or sell any patented invention that may in any way be related thereto.

Disposition Instructions

Destroy this report when it is no longer needed. Do not return it to the originator.

HEADQUARTERS
U S ARMY TRANSPORTATION RESEARCH COMMAND
FORT EUSTIS, VIRGINIA 23604

The report has been reviewed by the U. S. Army Transportation Research Command, and the data contained in it are considered to be valid. The report is published for the dissemination of information.

NOTE

On 1 March 1965, *after this report had been prepared,* the name of this command was changed from U.S. Army Transportation Research Command to:

U.S. ARMY AVIATION MATERIEL LABORATORIES

Task 1P125901A14203
Contract DA 44-177-AMC-144(T)
USAAVLABS Technical Report 65-28
June 1965

EFFECT OF MACH NUMBER, REYNOLDS NUMBER, AND THICKNESS RATIO ON THE AERODYNAMIC CHARACTERISTICS OF NACA 63A-SERIES AIRFOIL SECTIONS

Lockheed Report LR 18596

by

O. E. Sipe, Jr.
N. B. Gorenberg

Prepared by

Lockheed-California Company
Burbank, California

for

U. S. ARMY AVIATION MATERIEL LABORATORIES
FORT EUSTIS, VIRGINIA

ABSTRACT

Force and moment data are presented from wind tunnel tests of two-dimensional symmetrical NACA 63A-Series airfoils of thickness ratios from 9 to 18 percent. The tests were conducted at Mach numbers ranging from M = .30 to M = .94, with Reynolds numbers varying from R = 2.0 X 10^6 to R = 9.5 X 10^6 and at angles of attack as high as 29 degrees.

Comparisons are made, wherever possible, with NACA tests of the same or similar airfoils. The transonic similarity rule is used to evaluate the consistency of the data.

PREFACE

This program presents the results of a wind tunnel test program to obtain two-dimensional force and moment data for symmetrical NACA 63A-Series airfoils extending into the thicker range of the series. The thickness ratios tested were from 9 to 18 percent. Angle-of-attack, Mach number, and Reynolds number conditions encompass the principal portion of the helicopter rotor blade airfoil operating environment.

The program was conducted by the Fluid Dynamics Laboratory of the Lockheed-California Company under Contract DA 44-177-AMC-144(T) with the U.S. Army Transportation Research Command. Technical cognizance was maintained by the Aeromechanics Group of the U.S. Army Transportation Research Command. Mr. P. A. Cancro served as project officer for this group.

Messrs. J. C. Heitmeyer and G. Sim were project managers for Lockheed. Other principal Lockheed personnel associated with the program were Messrs. O. E. Sipe, Jr., B. H. Robinson, and N. B. Gorenberg.

CONTENTS

Section		Page
	ABSTRACT	iii
	PREFACE	v
	LIST OF ILLUSTRATIONS	viii
	LIST OF SYMBOLS	xi
	SUMMARY	1
	CONCLUSIONS	3
	RECOMMENDATIONS	5
1.0	INTRODUCTION	7
2.0	BACKGROUND INFORMATION	9
2.1	Scope of Bibliographies	9
2.2	Results of Test Data Search	9
2.3	Airfoil Section Data and Rotor Performance	13
3.0	DESCRIPTION OF TEST ITEMS	15
4.0	EXPERIMENTAL PROCEDURE	21
4.1	Wind Tunnel Facility	21
4.2	Tests	21
4.3	Data Reduction	22
5.0	DISCUSSION	31
5.1	Experimental Results	31
5.2	Experimental Problem Areas	31
5.3	Evaluation of Results	34
5.4	Aerodynamic Characteristics Variation With Reynolds Number	42
	PLOTTED AERODYNAMIC DATA	45
	BIBLIOGRAPHY - Section A - Airfoil Test Data and Data Correlation Methods	451
	BIBLIOGRAPHY - Section B - Rotor Test Data	456
	DISTRIBUTION	459
Appendix -	Equations to Determine Aerodynamic Coefficients	461

ILLUSTRATIONS

Figure		Page
1	Test Condition Envelope	10-11
2	Lockheed Two-Dimensional Balance System	16
3	Model Pitch Mechanism	17
4	Balance Installation	17
5	Airfoil Installation in Test Section	18
6	Wake Rake and Boundary Layer Rake Installation	18
7	Comparison of Aerodynamic Parameters	45-49
8	Comparison Data, 9-Percent Sections	50-52
9	Comparison Data, 12-Percent Sections	53-67
10	Comparison Data, 15-Percent Sections	68-70
11	Correlation of Experimental Data Using Transonic Similarity Rule	71-74
12	Variation of Maximum Section Lift Coefficient With Mach Number	75-78
13	Variation of Lift-Curve Slope at $C_l = 0$ With Mach Number	79-82
14	Variation of Section Drag Coefficient at $\alpha = 0$ With Mach Number	83-86
15	Variation of Angle of Attack at $C_l = 0$ With Mach Number	87-90
16	Variation of Section Pitching Moment Coefficient at $\alpha = 0$ With Mach Number	91-94
17	Variation of Aerodynamic Center With Mach Number	95-98
18	Variation of Maximum Section Lift Coefficient With Reynolds Number	99-102
19	Variation of Lift-Curve Slope at $C_l = 0$ With Reynolds Number	103-107
20	Variation of Section Drag Coefficient at $\alpha = 0$ With Reynolds Number	108-113
21	Variation of Zero-Lift Angle of Attack at $C_l = 0$ With Reynolds Number	114-119
22	Variation of Section Pitching Moment Coefficient at $\alpha = 0$ With Reynolds Number	120-125
23	Variation of Aerodynamic Center With Reynolds Number	126-131
24	Section Lift Coefficient Comparison for Various Thickness Ratios, $R = 3.5 \times 10^6$	132-145
25	Section Drag Coefficient Comparison for Various Thickness Ratios, $R = 3.5 \times 10^6$	146-159
26	Section Pitching Moment Coefficient Comparison for Various Thickness Ratios, $R = 3.5 \times 10^6$	160-173
27	Variation of Section Lift Coefficient With Angle of Attack at Constant Mach Number, NACA Section 63A009	174-179

Figure		Page
28	Variation of Section Lift Coefficient With Angle of Attack at Constant Mach Number, NACA Section 63A012	180-185
29	Variation of Section Lift Coefficient With Angle of Attack at Constant Mach Number, NACA Section 63A015	186-191
30	Variation of Section Lift Coefficient With Angle of Attack at Constant Mach Number, NACA Section 63A018	192-197
31	Variation of Section Drag Coefficient With Angle of Attack at Constant Mach Number, NACA Section 63A009	198-203
32	Variation of Section Drag Coefficient With Angle of Attack at Constant Mach Number, NACA Section 63A012	204-211
33	Variation of Section Drag Coefficient With Angle of Attack at Constant Mach Number, NACA Section 63A015	212-219
34	Variation of Section Drag Coefficient With Angle of Attack at Constant Mach Number, NACA Section 63A018	220-227
35	Variation of Section Pitching Moment Coefficient With Angle of Attack at Constant Mach Number, NACA Section 63A009	228-233
36	Variation of Section Pitching Moment Ccefficient With Angle of Attack at Constant Mach Number, NACA Section 63A012	234-239
37	Variation of Section Pitching Moment Coefficient With Angle of Attack at Constant Mach Number, NACA Section 63A015	240-245
38	Variation of Section Pitching Moment Coefficient With Angle of Attack at Constant Mach Number, NACA Section 63A018	246-251
39	Variation of Section Lift Coefficient With Mach Number at Constant Angle of Attack, R = 3.5 X 10^6 .	252-259
40	Variation of Section Drag Coefficient With Mach Number at Constant Angle of Attack, R = 3.5 X 10^6 .	260-271
41	Variation of Section Pitching Moment Coefficient With Mach Number at Constant Angle of Attack, R = 3.5 X 10^6	272-283
42	Variation of Section Lift Coefficient With Angle of Attack, NACA Section 63A009.	284-292
43	Variation of Section Lift Coefficient With Angle of Attack, NACA Section 63A012.	293-302
44	Variation of Section Lift Coefficient With Angle of Attack, NACA Section 63A015.	303-311
45	Variation of Section Lift Coefficient With Angle of Attack, NACA Section 63A018.	312-320
46	Variation of Section Drag Coefficient With Angle of Attack, NACA Section 63A009.	321-336
47	Variation of Section Drag Coefficient With Angle of Attack, NACA Section 63A012.	337-351

Figure		Page
48	Variation of Section Drag Coefficient With Angle of Attack, NACA Section 63A015	352-365
49	Variation of Section Drag Coefficient With Angle of Attack, NACA Section 63A018	366-379
50	Variation of Section Pitching Moment Coefficient With Angle of Attack, NACA Section 63A009	380-388
51	Variation of Section Pitching Moment Coefficient With Angle of Attack, NACA Section 63A012	389-398
52	Variation of Section Pitching Moment Coefficient With Angle of Attack, NACA Section 63A015	399-407
53	Variation of Section Pitching Moment Coefficient With Angle of Attack, NACA Section 63A018	408-416
54	Wind Tunnel Wall Boundary Layer	417-425
55	Wake Rake Survey, NACA Section 63A009	426-428
56	Wake Rake Survey, NACA Section 63A012	429-431
57	Wake Rake Survey, NACA Section 63A015	432-434
58	Wake Rake Survey, NACA Section 63A018	435-438
59	Repeatability Data, NACA Section 63A009	439-444
60	Pitch Rate Comparison Data, NACA Section 63A009 . . .	445-450

SYMBOLS

a.c. = Aerodynamic center

H_L = Local stream total pressure, p.s.i.a.

H_R = Stream total pressure from wake rake orifice, p.s.i.a.

K_d = Factor for reduced drag coefficient, $\dfrac{\left[(\gamma+1)\,M^2\right]^{1/3}}{(t/c)^{5/3}}$

K_{l_α} = Factor for reduced lift slope, $\left[(\gamma+1)\,M^2\right]^{1/3} \cdot (t/c)^{1/3}$

$K_{l,m}$ = Factor for reduced lift and moment coefficients, $\dfrac{\left[(\gamma+1)\,M^2\right]^{1/3}}{(t/c)^{2/3}}$

M = Free stream Mach number

M_R = Mach number at wake rake based on pressure ratio, H_{R/p_s}

R = Reynolds number based on airfoil chord

c = Airfoil chord, inches

c_d = Section drag coefficient

c'_d = $2\,\dfrac{M_R}{M}\left(\sqrt{\dfrac{1+0.2M_R^2}{1+0.2M^2}} - \dfrac{M_R}{M}\right)$

$\Delta c_{,c_{l=0}}$ = Drag coefficient increment at zero lift: drag coefficient at pertinent Mach number minus minimum drag coefficient (occurring between M = .5 and M = .7)

$\Delta c_{d,\alpha/(t/c)}$ = Drag coefficient increment obtained from drag coefficient at $\alpha/(t/c)$ and pertinent Mach number minus drag coefficient occurring at zero lift and the same Mach number

$\Delta c_{d,c_{l=0}}$ = Reduced form of $\Delta c_{d,c_{l=0}}$; $\left[\Delta c_{d,c_{l=0}}\right] \cdot \left[K_d\right]$

$\Delta c_{d,\alpha/(t/c)}$ = Reduced form of $\Delta c_{d,\alpha/(t/c)}$; $\left[\Delta c_{d,\alpha/(t/c)}\right] \cdot \left[K_d\right]$

c_l = Section lift coefficient

$\tilde{c}_l$ = Reduced form of c_l ; $\left[c_l\right] \cdot \left[K_{l,m}\right]$

$c_{l,\alpha/(t/c)\,=\,.4}$ = c_l at $\alpha/(t/c) = .4$

$c_{l_{\alpha,c_l\,=\,0}}$ = Lift slope at $c_l = 0$, per degree

$\tilde{c}_{l_{\alpha,c_l\,=\,0}}$ = Reduced form of $c_{l_{\alpha,c_l\,=\,0}}$; $\left[c_{l_{\alpha,c_l\,=\,0}}\right] \cdot \left[K_{l_\alpha}\right]$

$c_{m_{.25}}$ = Section pitching moment coefficient about .25 c

$\tilde{c}_{m_{.25}}$ = Reduced form of $c_{m_{.25}}$; $\left[c_{m_{.25}}\right] \cdot \left[K_{l,m}\right]$

$c_{m_{.25,\alpha/(t/c)\,=\,.4}}$ = $c_{m_{.25}}$ at $\alpha/(t/c) = .4$

p_s = Free stream static pressure, p.s.i.a.

q_L = Local compressible dynamic pressure, p.s.i.a.

q_c = Free stream compressible dynamic pressure, p.s.i.a.

(t/c) = Airfoil thickness ratio

(y/c) = Ratio of vertical distance in wake to airfoil chord

α = Angle of attack with respect to airfoil chord line, degrees

$\alpha/(t/c)$ = Angle of attack in radians divided by airfoil thickness ratio

γ = Ratio of specific heats

ξ = Reduced Mach number, $\dfrac{(M^2 - 1)}{\left[(\gamma + 1)M^2\right]^{2/3} (t/c)^{2/3}}$

SUMMARY

The two-dimensional aerodynamic characteristics of NACA 63A009, 63A012, 63A015, and 63A018 airfoil sections have been determined at angles of attack, Mach numbers, and Reynolds numbers which cover a principal portion of the helicopter rotor blade airfoil operating environment. Tests were made for angles of attack as high as 29 degrees and for Mach numbers ranging from M = .30 to M = .94 with corresponding Reynolds numbers varying from R = 2.0 X 10^6 to R = 9.5 X 10^6. Some data were obtained on NACA 63A012 over a full 180-degree angle-of-attack range at M = .30.

The absolute levels of the aerodynamic coefficients compared well, in general, with the aerodynamic coefficients obtained from force and pressure data on NACA tests of the same or similar airfoils in those regimes where comparison test data were available.

Application of the transonic similarity rule to the data showed very consistent trends within the family of airfoils. In general, the data showed greater consistency without modification of parameters than is normally experienced with two-dimensional airfoils of thickness ratios not greater than 10 percent.

CONCLUSIONS

1. The data obtained in this test fall, in general, between NACA data obtained by force measurements and NACA data obtained from pressure integrations.

2. There are portions of the data which are not well defined in absolute level or in trend. These include: drag coefficients near zero angle of attack at Mach numbers of .30 and .40 at low Reynolds numbers; the angle of attack for zero lift of the 18-percent airfoil; and the variation of maximum lift coefficient with Reynolds number for the 12- and 15-percent sections at a Mach number of .60. These data are discussed in Sections 5.3.3.1, 5.4.1, and 5.4.3.

3. From correlations with the transonic similarity rule and from comparisons between the airfoils tested, it is concluded that the results of the program are valid in both trend and absolute value except for the limitations noted above.

RECOMMENDATIONS

1. The problem areas encountered in correlating the two-dimensional test data have been resolved. However, additional testing is recommended to clarify those areas of questionable data from the present test program.

2. Data correlations for tests conducted on the same airfoil in different facilities are poor. Since the NACA 0012 airfoil has been a principal reference airfoil in the past, it is suggested that this airfoil section be tested in the present 4-foot tunnel system to provide a more complete base for section comparisons.

3. Whirl tower tests have recently been made on cambered NACA 63A-Series airfoils (References B-17, B-18, and B-19). Two-dimensional characteristics obtained from wind tunnel tests for these sections would provide valuable additional data for correlation purposes.

1.0 INTRODUCTION

The concept of powering rotary wing aircraft by tip propulsion systems encompasses a requirement for thick rotor blade airfoil sections. The requirement arises from either the need to duct gases, hot or cold, to tip mounted pressure-jet units or the need to provide depth for increased structural reliability in the case of tip mounted integral engines. At the inception of this program, very little two-dimensional performance data existed for suitably thick airfoils at the pertinent Mach number and angle-of-attack conditions. In addition, a need existed for section data on thinner airfoils at the combinations of angle of attack, Mach number, and Reynolds number which occur in the orthodox rotor blade airfoil environment.

On the basis of these needs, the United States Army Transportation Research Command (USA TRECOM) requested a wind tunnel test program to obtain two-dimensional data on several NACA 63A-Series airfoils ranging in thickness ratio from 9 to 18 percent. A test envelope was established to encompass a principal portion of helicopter blade environment. Also, a search was requested by USA TRECOM to determine whether or not test data obtained under comparable test conditions were available for the selected airfoils. The basic program was subject to review to assure no duplication of effort other than to obtain check points or a base line for comparisons.

The intent of this project was to provide two-dimensional test results to serve as a basis from which rotor analysis parameters could be evolved. Although it is beyond the scope of this project to specify the procedures for such application of these data, acknowledgement of the requirement for that phase of effort is noted in Section 2.3.

2.0 BACKGROUND INFORMATION

2.1 SCOPE OF BIBLIOGRAPHY

The Bibliography comprises the significant references examined in a search of test data. The search was conducted to determine whether or not section data were available for symmetrical 63A-Series airfoils ranging in thickness ratio from 9 to 18 percent at Reynolds number, Mach number, and angles of attack occurring in the test envelope described in Figures 1A and 1B. Sources of such data are listed only if the data are considered to be directly related to the subject matter of the current investigation and are also non-proprietary.

Section A of the Bibliography includes coverage of two-dimensional tests, selected fixed-wing three-dimensional tests, and pertinent transonic correlation techniques. Section B is grouped as an entity of the references which are further characterized by the inclusion of rotor test data. Reference B-2* provides previously unpublished compressible flow lift and drag data for the NACA 0012 airfoil which are used in the comparisons of Section 5.3.2 of this report.

2.2 RESULTS OF TEST DATA SEARCH

2.2.1 Nonduplication of Effort and Comparative Data

In general, previously existing section data for the symmetrical NACA 63A-Series airfoils of 9- to 18-percent thickness ratio were conspicuously limited in the range of one or more of the test parameters defining the test envelope of this program. Examples of these limitations are represented by the test data of References A-32 and A-10*. Data for a 16A010 appear in Reference A-32 for Reynolds numbers up to 9×10^6 and through angle-of-attack settings defining stall; however, the test series was conducted only at Mach numbers below M = .20. Reference A-10 includes data for the 63A009 airfoil for Mach numbers

*The letter refers either to Section A or to Section B of the Bibliography, and the numeral refers to the corresponding reference.

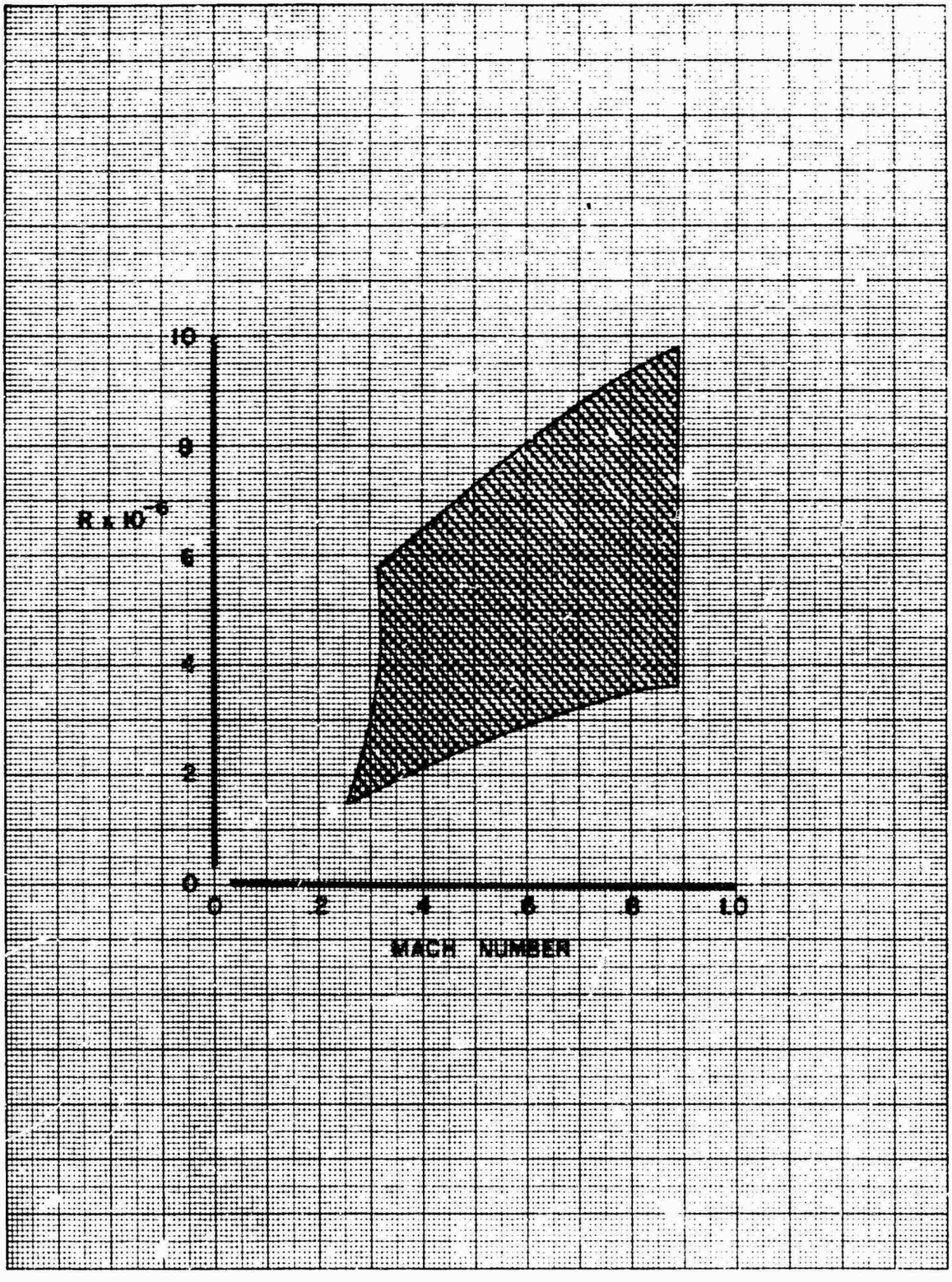


Figure 1A. Test Condition Envelope, Reynolds Number - Mach Number

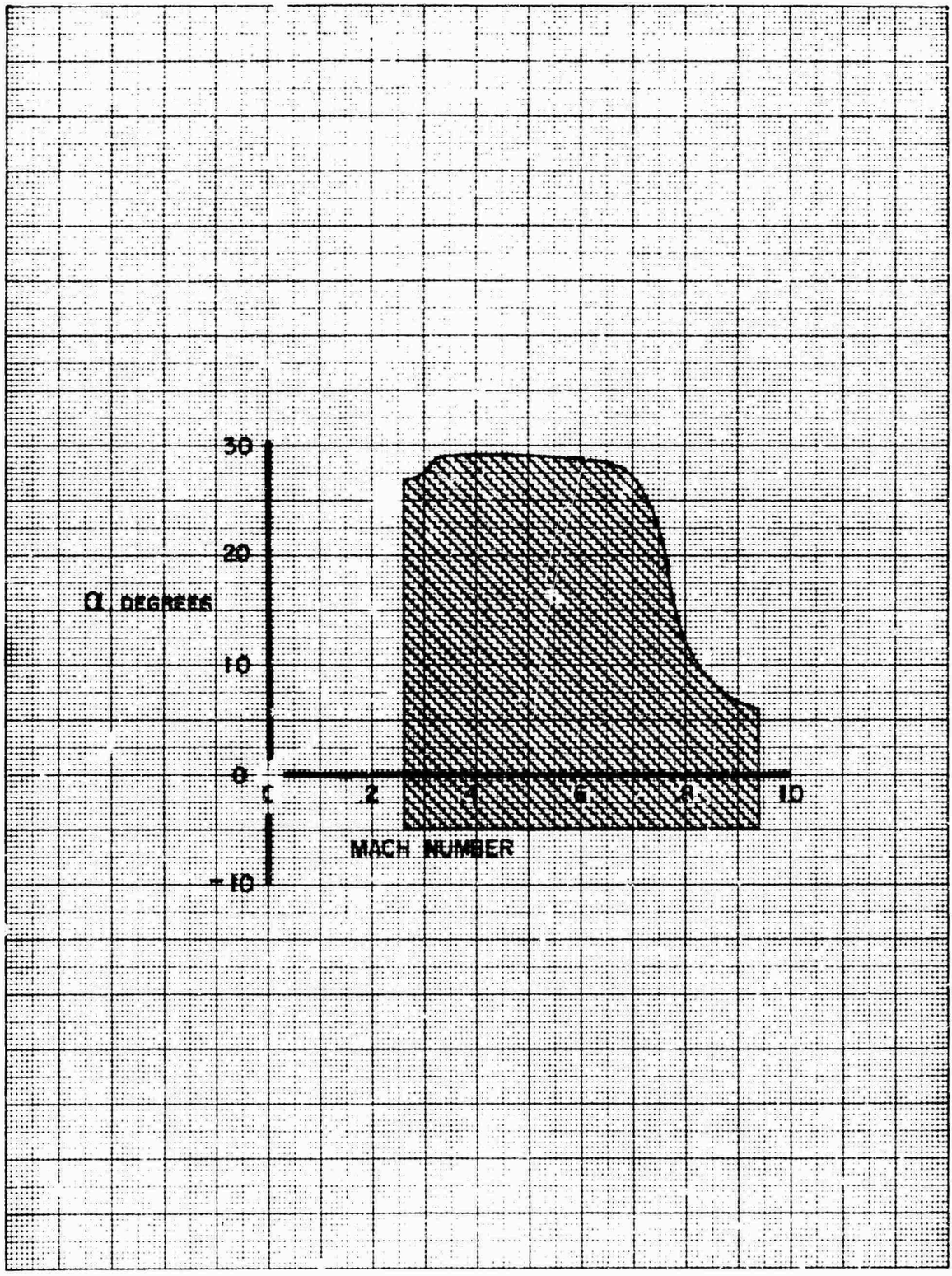


Figure 1B. Test Condition Envelope, Angle of Attack - Mach Number

from .30 to 1.0 but only at Reynolds numbers below R = 1.6 X 10^6. Also, angles of attack ranged from zero to 12 degrees, only, and drag data were limited to angles of attack not exceeding 8 degrees.

Similar limitations occur in the test parameters of section data for the basic 63-Series symmetrical airfoils. Reference A-30 includes test data for models which cover the required thickness ratio range. Test Reynolds numbers extend to 25 X 10^6, and the angle-of-attack settings through those defining stall are included. Again, the test series was conducted at Mach numbers below M = .20.

From the results of the section test data search, the conclusion reached was that this program for testing the specified airfoils does not represent a duplication of previous effort.

Section test data for related airfoils were somewhat less limited and are used for comparative purposes as feasible. Reference A-63 is an example in which test data for the basic 64-Series symmetrical airfoils are provided. Thickness ratios up to 12 percent are represented and test conditions ranged from low to high subsonic Mach numbers. Reynolds numbers up to 5.0 X 10^6 were achieved for angles of attack through stall and Reynolds numbers up to 2.4 X 10^6 were achieved at higher angles of attack. The data of Reference A-63 were subsequently to be complemented by the results of the tests reported in Reference A-7.1. The latter program included tests of the 64-Series airfoils for 15- and 18-percent thickness ratios as well as tests of the NACA 0012 airfoil. The report of the program was released on a preliminary basis for limited circulation. Later, several types of discrepancies were found in the data. Although these were partially explained, they could not be corrected and, as a result, the formal presentation of the report was cancelled. Accordingly, the unmodified data of Reference A-7.1 are not used for comparative purposes of this report.

NACA effort to assemble a better representation of the NACA 0012 section test data was continued. The data and information of References A-33, A-7, A-2, A-63, A-14 and A-46 were applied with the data of Reference A-7.1 to assemble the two-dimensional lift and drag data published in Reference B-2. These data are used in the comparisons of Section 5.3.2.

Comparative section test data for symmetrical airfoils of thickness ratios above 12 percent are, however, more limited. Reference A-14 provides test data on the NACA 0015 airfoil which are used in the comparison of Section 5.3.2. No section test data are directly applicable for comparison purposes at the appropriate Mach numbers for thickness ratio of 18 percent.

2.3 AIRFOIL SECTION DATA AND ROTOR PERFORMANCE

The effects of rotor performance and, therefore, vehicle performance, as a function of rotor airfoil section are reflected in the references of Section B of the Bibliography. These references include test data which pertain to both hover and forward flight conditions. A review of the rotor experimental results and the accompanying analyses presented in these reports makes evident the need for analytic processing or "synthesizing" of section data in proceeding from two-dimensional test results to integrated rotor results.

Some significant deficiencies found by comparing rotor test results and analytically integrated results are rotor test indicated delays in airfoil section stall and in airfoil force and moment divergence Mach numbers. These and similar differences have resulted in the consideration of elastic blade twist, centrifugal pumping of boundary layer, radial skin-friction, azimuthal as well as radial induced velocity distribution and flow separation as a function of rate-of-change of cyclic angle-of-attack variation. Presumably, a more rigorous treatment of these topics would minimize the need to synthesize the two-dimensional data.

The exploration of these subjects, however, continues to support the approach that differences in rotor performance are fundamentally a function of the two-dimensional characteristics of the airfoils being considered. It is in this light that the subject two-dimensional tests of 63A-Series airfoils were conducted.

3.0 DESCRIPTION OF TEST ITEMS

The four models tested consisted of NACA 63A009, 63A012, 63A015, and 63A018 airfoil sections, the coordinates for which were obtained and/or developed from Reference A-1 and A-2. The 63A015 and 63A018 models were fabricated of aluminum but model strength and deflection considerations dictated the use of heat-treated steel for the 63A009 and 63A012 models. Each had a chord of 8 inches and completely spanned the 4-foot tunnel. The maximum deviation of the section coordinates from the specified values listed in Table I was less than .005 inch.

Special model support structure and actuating mechanisms were required for this test. This equipment (See Figures 2, 3, and 4) included two six-component strain gauge balances, two ring and worm gear assemblies, and a single electric drive motor and associated shafts and couplings; the equipment was housed in the plenum chamber between the inner and outer walls of the transonic test section cart.

In order to minimize the deviation from two-dimensional flow at the airfoil-tunnel wall junctures, the normally perforated tunnel sidewalls were lined with dural sheets. The perforations in the floor and ceiling of the test section were, of course, left open. The models were tip-supported. They extended through cutouts in nonmetric discs which were flush with the inner walls of the tunnel. The 1/8-inch gaps between the model and the cutouts in the discs were sealed with soft rubber. The airfoil installation is shown in Figure 5.

The metric support system provided for varying the angle of attack of the models about the 25-percent chord point through a 360-degree angle range. The tunnel wall discs and force balances were rotated with the airfoil by the airfoil actuating mechanism but were nonmetric. Model angle of attack was sensed by a potentiometer directly coupled with the drive system.

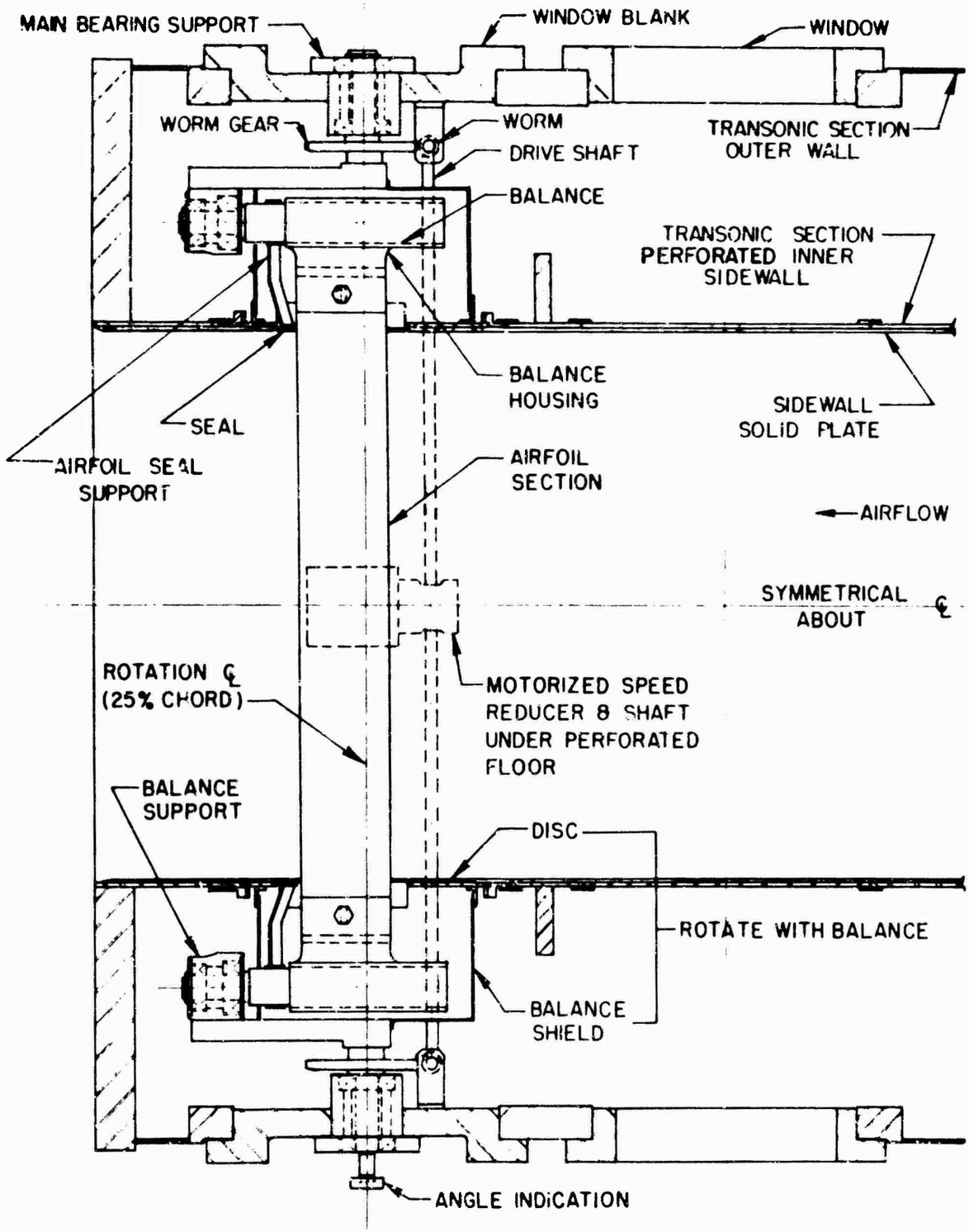


Figure 2. Lockheed Two-Dimensional Balance System

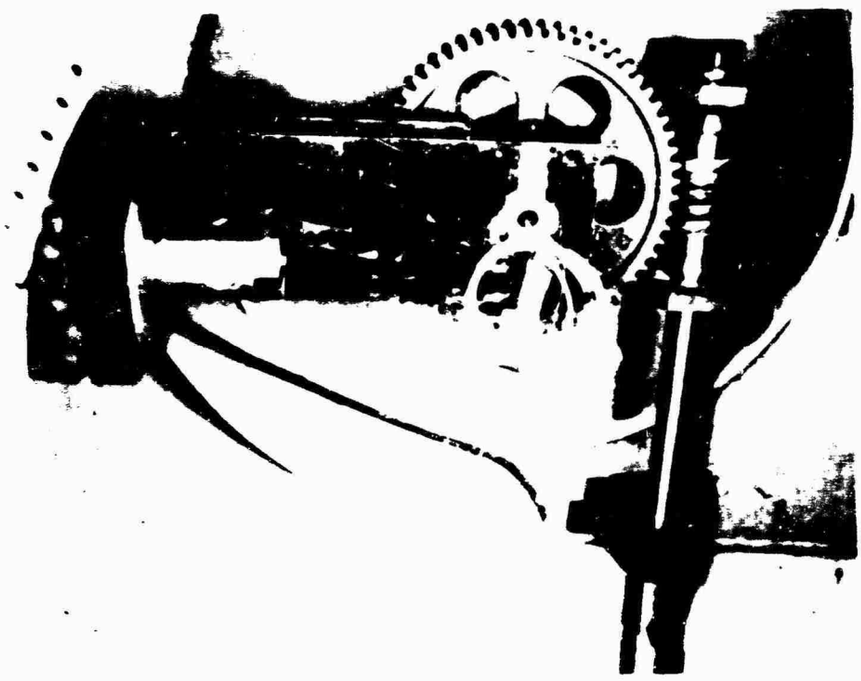


Figure 3. MODEL PITCH MECHANISM

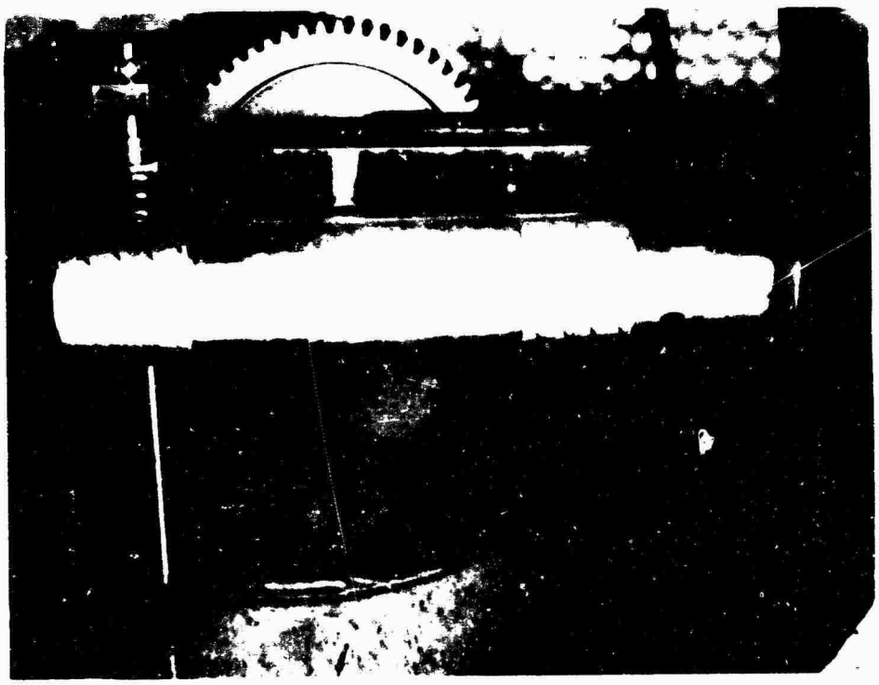


Figure 4. BALANCE INSTALLATION

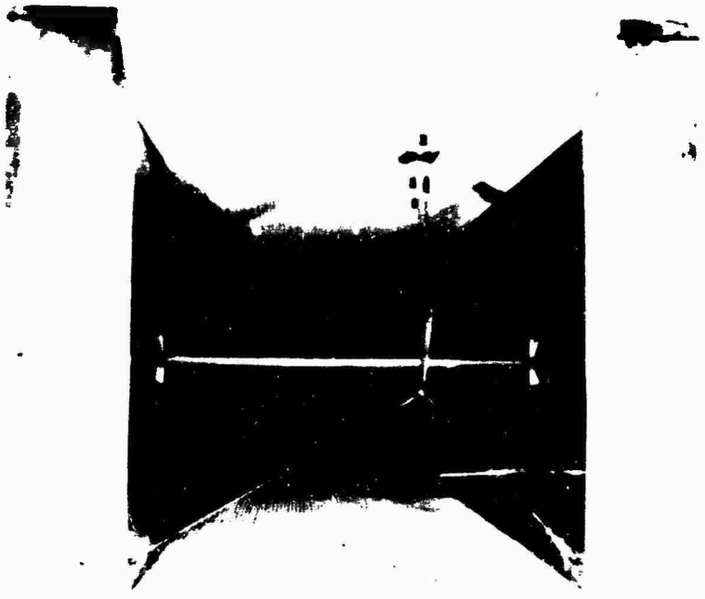


Figure 5. AIRFOIL INSTALLATION IN TEST SECTION

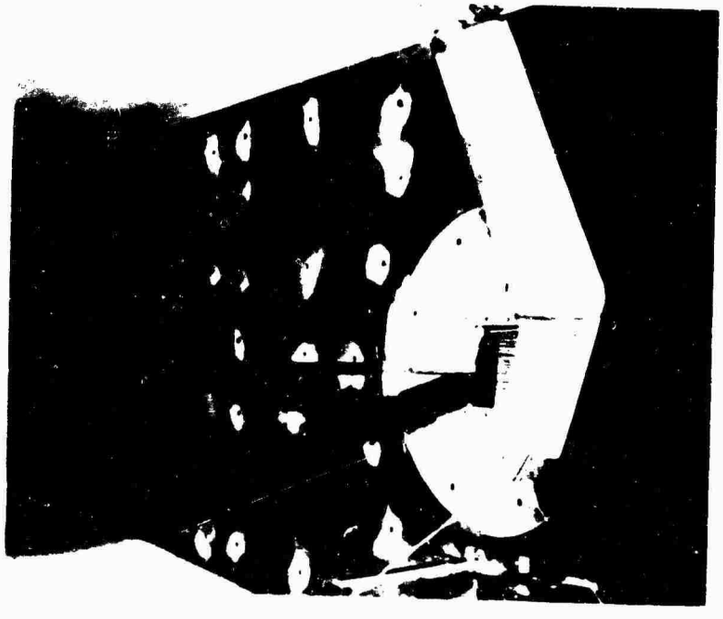


Figure 6. WAKE RAKE AND BOUNDARY LAYER RAKE INSTALLATION

TABLE 1

AIRFOIL SECTION DATA

X	± Y			
Horizontal Distance Along Chord, Inches	Vertical Distance Above and Below Chord, Inches			
	63A009	63A012	63A015	63A018
0	0	0	0	0
.040	0.0590	0.0778	0.0962	0.1138
.060	0.0710	0.0938	0.1158	0.1369
.100	0.0901	0.1194	0.1475	0.1739
.200	0.1251	0.1662	0.2063	0.2450
.400	0.1737	0.2316	0.2894	0.3473
.600	0.2100	0.2803	0.3506	0.4208
.800	0.2392	0.3195	0.3998	0.4800
1.200	0.2842	0.3798	0.4754	0.5711
1.600	0.3166	0.4230	0.5295	0.6370
2.000	0.3392	0.4531	0.5673	0.6818
2.400	0.3535	0.4721	0.5907	0.7093
2.800	0.3596	0.4796	0.5997	0.7198
3.200	0.3578	0.4766	0.5948	0.7127
3.600	0.3486	0.4634	0.5772	0.6904
4.000	0.3327	0.4414	0.5486	0.6545
4.400	0.3112	0.4118	0.5110	0.6101

TABLE 1 (contd.)

X	± Y			
Horizontal Distance Along Chord, Inches	Vertical Distance Above and Below Chord, Inches			
	63A009	63A012	63A015	63A018
4.800	0.2847	0.3760	0.4656	0.5563
5.200	0.2542	0.3349	0.4138	0.4910
5.600	0.2200	0.2897	0.3574	0.4237
6.000	0.1840	0.2421	0.2985	0.3538
6.400	0.1475	0.1541	0.2393	0.2837
6.800	0.1110	0.1461	0.1802	0.2136
7.200	0.0745	0.0980	0.1210	0.1434
7.600	0.0380	0.0500	0.0760	0.0734
8.000	0.0016	0.0020	0.0026	0.0032
Leading Edge Radius	0.0486	0.0860	0.1304	0.1624
Trailing Edge Radius	0.0018	0.0022	0.0030	0.0038

4.0 EXPERIMENTAL PROCEDURE

4.1 WIND TUNNEL FACILITY

The tests were conducted in the Lockheed-California Company Fluid Dynamics Laboratory 4-by-4-foot supersonic wind tunnel. The tunnel is of the blow-down type and uses air as the test medium. For testing in the transonic range, a portable test section cart having perforated walls enclosed within a vented plenum chamber is inserted into the circuit. For these tests, the perforations in the sidewalls only were covered in order to minimize span-wise flow.

4.2 TESTS

The nominal ranges of test Mach number, Reynolds number, and angle of attack through which the models were tested are tabulated below. A detailed outline of the test program is presented in Table 2. The minimum Reynolds number attainable at each Mach number was set by tunnel flow control limitations; and the maximum Reynolds number and angle of attack at each Mach number, by model strength and deflection limitations.

Mach No.	Reynolds No.	Angle of Attack
.3 to .94	2×10^6 to 9.5×10^6	-4° to 25° for $M < .80$
		-5° to 5° for $M > .80$

The pitch actuating mechanism provided the capability of varying the model angle of attack at a rate of 5.9 degrees per second. Data were continuously recorded as each model was pitched at this rate from a negative angle of attack through the angle-of-attack range. A data system with the high sampling rate of 7000 samples per second assures data compatability within .02 degree. To verify that the pitch rate did not affect the data, check runs were made with data recording occurring at fixed angles of attack (See Figure 60).

The duration of each run was dependent on the test conditions, Mach number, Reynolds number, and angle-of-attack range and varied from 15 seconds to 50 seconds.

A 40-tube total pressure rake (See Figure 6) was installed 20 inches behind the model pivot station to measure the wake drag of each model.

4.3 DATA REDUCTION

The data are presented in the form of the following dimensionless aerodynamic section coefficients:

c_l = section lift coefficient = L/qS

c_d = section drag coefficient = D/qS

$c_{m_{.25}}$ = section pitching moment coefficient = m/qSc

where

L	=	net lift, positive upwards; pounds
D	=	net drag, positive aft; pounds
m	=	net pitching moment about .25c, positive nose up; inch-pounds
c	=	airfoil chord; inches = 8
S	=	airfoil area; square inches = 384
q	=	incompressible free stream dynamic pressure; psia

4.3.1 Data Computation

The forces on the model were sensed as electrical outputs in millivolts from each strain gauge component of the balances, and recorded on magnetic tape in digital form. These data were then transformed to forces using a calibration matrix, and thence into the appropriate aerodynamic coefficients through the equations of the Appendix.

4.3.2 Corrections to Data

Since the test section had perforated top and bottom walls, no corrections for wind tunnel wall interference are applied. The data have been corrected for a flow inclination of -.2 degree at M = .30.

The wind tunnel wall boundary layer profiles measured along the side walls are presented in Figure 54. The force data in this report have not been corrected for the effects of the tunnel wall boundary layer.

4.3.3 Data Precision

Consideration of the processes involved in the measurement and computation of the data, repeatability of the data, and experimental data point scatter results in the following limitations on the accuracy of the data:

$$c_{\ell} = \pm .01$$

$$*c_{\ell_{max}} = \pm .05$$

$$c_d = \pm .0007$$

$$c_{m_{.25}} = \pm .004$$

$$M = .01$$

*See Section 5.2

TABLE 2

TEST PROGRAM

NACA Airfoil Section 63A009

Mach No.	Reynolds No. X 10^{-6}	Angle-of-Attack Range (degrees)
.32	5.8	-4 to +24
.37	2.1	-4 to +27
.38	3.9	-4 to +28
.47	2.5	-4 to +24
.49	4.7	-4 to +26
.49	7.0	-4 to +27
.58	2.8	-4 to +28
.60	5.2	-4 to +27
.59	7.9	-4 to +24
.67	3.2	-4 to +24
.69	5.9	-4 to +26
.68	8.7	-4 to +6
.73	8.2	-4 to +25
.74	6.0	-4 to +21
.74	8.8	-4 to +7
.78	3.4	-5 to +26
.79	6.0	-5 to +12
.79	9.3	-5 to +5

TABLE 2 (contd.)

Mach No.	Reynolds No. X 10^{-6}	Angle-of-Attack Range (degrees)
	NACA Airfoil Section 63A009	
.88	3.6	-5 to +5
.89	6.3	-5 to +5
.89	9.5	-5 to +5
.93	3.7	-5 to +5
.94	6.5	-5 to +4
.94	9.8	-5 to +4
	NACA Airfoil Section 63A012	
.26	1.6	-5 to +24
.30	3.0	-5 to +180
.32	5.9	-4 to +26
.35	2.1	-5 to +27
.39	3.8	-5 to +25
.47	2.4	-4 to +26
.49	4.6	-4 to +24
.49	7.1	-4 to +22
.57	2.9	-4 to +25
.58	5.2	-4 to +24
.59	7.8	-4 to +27

TABLE 2 (contd.)

NACA Airfoil Section 63A012		
Mach No.	Reynolds No. X 10^{-6}	Angle-of-Attack Range (degrees)
.68	3.2	-4 to +25
.69	5.7	-5 to +28
.69	8.5	-4 to +26
.73	3.3	-4 to +20
.74	5.7	-4 to +20
.74	8.8	-5 to +17
.78	3.4	-4 to +13
.78	6.1	-6 to +12
.79	9.0	-5 to +13
.89	3.6	-5 to +5
.89	6.3	-5 to +5
.89	9.5	-5 to +5
.93	3.6	-5 to +6
.94	6.5	-5 to +6
.94	9.5	-5 to +6

TABLE 2 (cont'd.)

NACA Airfoil Section 63A015

Mach No.	Reynolds No. X 10^{-6}	Angle-of-Attack Range (degrees)
.26	1.6	-5 to +27
.29	2.9	-5 to +27
.36	2.0	-5 to +29
.38	3.8	-5 to +29
.47	2.5	-5 to +28
.49	4.5	-5 to +27
.49	6.9	-5 to +27
.57	2.8	-4 to +27
.59	5.1	-4 to +26
.59	7.8	-4 to +8
.65	2.2	-5 to +28
.69	5.9	-4 to +6
.70	8.6	-5 to +6
.73	3.3	-4 to +22
.74	5.8	-5 to +6
.74	8.5	-4 to +6
.78	3.4	-5 to +17

TABLE 2 (contd.)

Mach No.	Reynolds No. X 10^{-6}	Angle-of-Attack Range (degrees)
	NACA Airfoil Section 63A015	
.79	5.9	-4 to +6
.79	9.0	-5 to +6
.88	3.6	-5 to +7
.89	6.1	-5 to +6
.90	9.6	-5 to +6
.93	3.7	-5 to +6
.94	6.4	-5 to +6
.94	9.8	-5 to +6
	NACA Airfoil Section 63A018	
.27	1.6	-5 to +27
.29	2.9	-5 to +27
.32	4.4	-5 to +27
.36	2.1	-5 to +28
.38	3.8	-5 to +23
.35	5.8	-5 to +19
.52	2.5	-5 to +29

TABLE 2 (contd.)

NACA Airfoil Section 63A018

Mach No.	Reynolds No. X 10^{-6}	Angle-of-Attack Range (degrees)
.49	4.6	-3 to +27
.57	2.9	-4 to +27
.59	5.2	-4 to +27
.59	7.8	-4 to +27
.67	3.2	-4 to +27
.69	6.0	-4 to +28
.69	8.5	-4 to +26
.73	3.3	-5 to +21
.74	5.9	-4 to +21
.74	8.8	-4 to +21
.78	3.5	-5 to +14
.79	6.0	-5 to +14
.79	9.1	-5 to +12
.88	3.6	-5 to +5
.89	6.3	-5 to +5
.89	9.6	-5 to +5
.93	3.7	-5 to +5
.94	6.4	-5 to +5
.94	9.7	-5 to +6

5.0 DISCUSSION

5.1 EXPERIMENTAL RESULTS

The basic test results are presented in graphic form in Figures 42 through 53. Because of slight variations in the actual Reynolds number and Mach number at which comparable runs were made, the data have been cross-plotted at constant values of Reynolds number between $R = 2.0 \times 10^6$ and $R = 9.5 \times 10^6$ in increments of $R = 1.5 \times 10^6$. The aerodynamic coefficients are shown varying with angle of attack at constant Mach number and with Mach number at constant angle of attack (Figures 27 through 41).

A Reynolds number of $R = 3.5 \times 10^6$ was selected as the basic condition for analysis and comparison. Test data over the largest range of Mach numbers were obtained at this Reynolds number. Also, most of the test data available from other sources were run at a comparable Reynolds number. Data from this test program are presented in Figures 7 through 11 in a form suitable for comparison with other test data, and in Figures 12 through 26 for direct evaluation of thickness ratio effects.

5.2 EXPERIMENTAL PROBLEM AREAS

Some of the basic plots show minor gaps in the data. During the course of these runs, the normal force recorded by one of the balances was, for unknown reasons, significantly lower than that recorded by the second balance. Where this discrepancy occurred, the data are omitted. Runs for which a large number of data points were affected by this condition were computed using twice the lift and drag measured by the unaffected balance. This is a valid procedure since each of the force balances measured one-half of the force on the model, as can be determined from an analysis of the model as a simple beam supported at either end.

A series of calibration runs using the test model in the transonic section revealed that the value of maximum lift for a two-dimensional airfoil was affected by the downstream diffuser throat setting and the associated amount of bleed required to produce the desired Mach number - Reynolds number combination. These calibration data provided throat settings at $R = 6 \times 10^6$ for each of the Mach numbers required for this test such that the true maximum lift was realized; tests were not run at values of R other than 6×10^6 due to lack of time. It is possible that the throat settings chosen were not optimum for

the other values of Reynolds number; in fact, during the analysis of the data after conclusion of the test, it was discovered that some of the values of maximum lift at $R = 6 \times 10^6$ were low. However, since by this time the experimental setup had been removed from the test section, it was impossible to rerun these points using a different throat setting.

In general, the shape of the drag polars is consistent with previously recorded data. However, several of the polars (Figures 46B-1 and -2, 47A-1, -2, 47C-1, -2, 47D-1, -2, 49A-1, -2, and 49B-1, -2) are not well defined. These include the 9-percent section at M = .40 at all Reynolds numbers, the 12-percent section at M = .30 and M = .40 at all Reynolds numbers, and at M = .50 at the lowest Reynolds numbers, the 18-percent section at M = .30 at all Reynolds numbers and at M = .40 at the lowest Reynolds numbers. The poor definition of the polar at these test conditions seems to be primarily a result of excessive data scatter; this, in turn, is a result of the low level of loads at these conditions.

The structural characteristics of the models limited on occasion the maximum angle of attack at which tests could be run without risking structural failure. The models affected include the 9-percent section at M = .70 and M = .75 for the highest Reynolds number, and the 15-percent section from M = .70 to M = .80 except at the lowest Reynolds number.

A wake survey rake was incorporated at the test installation to provide a check on the value of the drag coefficient for zero angle of attack. However, excessive data scatter in the Mach number range M = .30 to M = .50 prevented definition of the wake profile in this region. In addition, Mach numbers greater than M = .74 produced a wake that was too wide to be accurately defined by the rake.

The drag coefficient at zero angle of attack is based upon the value obtained from the wake survey at M = .60 to M = .74, where the wake profiles were well defined (Figures 55 through 58 represent typical examples). Force data were adjusted to agree with the wake survey value where appreciable differences existed. Longitudinal pressure gradients, which would affect the drag data, were believed to account for these differences when they occurred.

Normal manufacturing tolerances in the teeth of the actuating gears and associated mechanism resulted in very small angle-of-attack differences at the two ends of the model airfoils. This action produced pitching moment tares sinusoidal in nature and of opposite signs for the two balances. The average pitching moment tare that was used for data reduction could produce discrepancies in the pitching moment coefficient data, particularly in the area near zero angle of attack where the values of pitching moment are small.

The wind tunnel boundary layer was determined for the various test conditions by means of a survey rake installed in conjunction with the 9-percent airfoil section model. Integration of a few typical boundary layer profiles showed that a reduction in the measured forces of from 3.5 to 6.5 percent was possible, depending on Mach number.

5.3 EVALUATION OF TEST RESULTS

5.3.1 Comparative Data and Theory

The test results of this program are evaluated on the bases of comparisons with other test results and on the application of Spreiter's form of the Von Karman Transonic Similarity Rule.

Testing the same airfoil or near identical airfoils in different wind tunnels has produced different results at corresponding test parameters (see Reference A-24, for example). Test data on airfoils which are compared with the results of this program show large differences which cannot be fully explained. It is not reasonable, however, to exclude any of these sets of data from the comparisons.

The transonic similarity rule provides a useful tool for evaluating the relative characteristics of a family of airfoils. It is accepted that the application of the transonic similarity rule to the results for thicker airfoils is essentially empirical since the theoretical development is related to assumptions for thinner airfoils.

It is with these acknowledged limitations in theory and in other test data that the evaluation of the results of this program is made.

5.3.2 Comparisons With Other Test Results

Presented below are comparisons of the test data of this report and NACA test data on the same or similar airfoil sections.

5.3.2.1 9-Percent Thickness Ratio

Reference A-10 provides some test data on the NACA 63A009. Limitations of these data, other than for range of angle of attack and upper value of Reynolds number, are related to the fact that no suitable correction could be applied to the angle of attack for jet deflection. Results from Reference A-10, with the c_n data recalculated to provide c_ℓ data, are compared with the results of this program in Figures 8A, 8B and 8C as well as in Figure 7B.

The major effect of no correction for jet deflection in the data of Reference A-10 is a higher geometric angle of attack than that sensed by the airfoil. Page 10 of that reference states that because of this effect, all the corresponding normal force slope data are low.

This explanation accounts for the fact that lift data of Reference A-10 shown in Figure 7B are lower than the data determined in this program.

The angle-of-attack disparity also applies for the generally lower level of drag data shown for Reference A-10 in Figures 8B and 7B. Data for $c_{m_{.25}}$ versus Mach number are compared in Figure 8C. Both airfoils show similar trends with Mach number, but the data from Reference A-10 tend to be more positive with increasing angle of attack.

Comparative data for $c_{\ell\ max}$ have been obtained with representative data for an NACA 64-009 airfoil by cross-plotting for a 9-percent thickness ratio with the data from Reference A-63. The $c_{\ell\ max}$ data comparison for that airfoil and the airfoil of this program appears in Figure 7B. The data show similar trends up to M = .60 at which $c_{\ell\ max}$ values for the 64-009 airfoil exceed those of the 63A009 airfoil.

5.3.2.2 12-Percent Thickness Ratio

This portion of the comparisons for the airfoil of 12-percent thickness ratio excludes comparisons related to the rotation of the airfoil through 180 degrees in angle of attack. Comparisons associated with that range in angle of attack and the corresponding unstalled angles of attack in forward and reverse flow are presented in Section 5.3.2.5.

Data pertinent to the comparisons of this section are presented in Figures 7-C, 9A-1, 9A-2, 9E-1, 9E-2, 9I-1, and 9I-2. Coefficient data for angles of attack through 8 degrees are again included from Reference A-10 but, at this thickness ratio, the airfoil is of the NACA 64A-Series. Again, the c_n data have been recalculated to provide c_ℓ data; and again, the comment about no correction to the angle of attack due to jet deflection is applicable to data for this reference.

Coefficient data for all angles of attack shown in the comparison have been obtained for the NACA 64_1-012 airfoil from Reference A-63. Lift coefficient data through α = 10 degrees have been obtained for NACA 0012 airfoil from Reference B-2. Additional data for all coefficients have been obtained for the NACA 0012 airfoil at angles of attack up to 4 degrees from Reference A-11.

In the angle-of-attack range for zero to 8 degrees, test data are shown for the NACA 64A012 and NACA 64_1-012 airfoils in addition to that for the NACA 63A012 airfoil tested in this program (See Figures 9A-1, 9E-1, 9E-2, and 9I-1). It is pertinent to note that the c_ℓ, c_d and $c_{m_{.25}}$ data for the NACA 63A012 airfoil fall between the corresponding data of the other two NACA 6-series airfoils over the greatest portion of the Mach number range and through the 8-degree angle-of-attack range. An examination of the test techniques of Reference A-63 and A-10 makes it evident that the NACA 64_1-012 airfoil data were balanced-measured while

the NACA 64A012 airfoil data were pressure-contour and wake-measured. The balance-measured data for the NACA 63A012 airfoil of this program generally fall between the other data. It may be further noted that in a check of data differences, the c_ℓ data spread at $\alpha = 4$ degrees for data from two NACA 0012 airfoil data sources is found to be as great as the c_ℓ data spread for the NACA 64A012 and the NACA 64_1-012 airfoils at all of these angles of attack.

In Figures 9A-2, 9E-2, and 9I-2 for $\alpha > 8$ degrees, data for the 64_1-012 airfoil are further compared with the data for the NACA 63A012 airfoil. The c_ℓ and the c_d data continue the trend for the lower angles and are generally higher for the NACA 64_1-012 airfoil than for the NACA 63A012 airfoil. The c_m data reverse the trend of the lower angles and become more negative for the NACA 64_1-012 airfoil with increasing angle of attack.

The c_d data comparison of the summary graph of Figure 7C has already been discussed. The lift slope data for the NACA 63A012 airfoil is consistent with the other comparisons in that these data fall between the corresponding data for the NACA 64A012 and the NACA 64_1-012 airfoils. The $c_{\ell\ max}$ data for the NACA 63A012 is shown as less than that for either NACA 64_1-012 and the NACA 0012 airfoils.

5.3.2.3 15-Percent Thickness Ratio

Comparative data for the 15-percent thickness ratio are obtained for the NACA 0015 airfoil from Reference A-14. These data are presented in Figures 10A, 10B, and 10C as well as in Summary Figure 7D. The largest range of c_ℓ and c_d data from Reference A-14 was measured in the positive angle-of-attack range, but the c_d data, which were obtained separately by wake-rake, were measured through a negative angle-of-attack range. For the comparisons made here, these c_d data are applied as if for a positive angle-of-attack range.

In light of the large differences in test data results shown for airfoils within the NACA 6-Series family, the comparison of data for the NACA 63A015 airfoil of this program and the test data for the NACA 0015 airfoil of Reference A-14 cannot be considered as absolute.

In Figure 10A, it may be seen that the lift coefficient data are generally higher for the NACA 63A015 airfoil and that a higher Mach number can be attained at $\alpha > 2$ degrees before lift loss due to compressibility occurs. In Figure 7D, the lift slopes do not differ appreciably, but the $c_{\ell\ max}$ tends to remain higher with increasing Mach number for the NACA 63A015 airfoil.

Examination of the drag coefficient data in Figures 10B and 7D show acceptable experimental difference at the low Mach numbers and low angles of attack. With increasing angle of attack, the force data measurements for the 63A015 airfoil of the program are probably more applicable than the wake-rake measurements of Reference A-14. In any case, the comparison shows a delay in drag divergence Mach number for the 63A015 airfoil.

The pitching moment coefficient comparison is presented in Figure 10C. The negative $c_{m,25}$ values for the NACA 0015 airfoil at low angles of attack and low Mach number are questionable and, therefore, the data for that airfoil should be reviewed for incremental changes with increasing angle of attack and Mach number. Again, the comparison shows a delay in compressibility effects for the NACA 63A015 airfoil. Moment divergence occurs later for the 63A015 airfoil, and $c_{m,25}$ for this airfoil displays only a slight tendency toward the negative before increasing positively with an increase in Mach number beyond moment divergence.

5.3.2.4 18-Percent Thickness Ratio

Obvious difficulties have been demonstrated in the process of evaluating test results by comparisons with other test data. Other test data for airfoils of 18-percent thickness ratio are not directly applicable to such comparison, especially for the Mach number range of this program. The data of Reference A-32 that apply to this thickness ratio correspond to the data of Reference A-7.1 which are not used in this comparison because of the reason explained in Section 2.2.1. The evaluation of the data for the 63A018 airfoil is, therefore, based on comparisons made within the family of airfoils tested.

5.3.2.5 180-Degree Angle-of-Attack Sweep, 12-Percent Thickness Ratio

Comparisons of other test data with the test data of the 63A012 airfoil for an angle of attack variation from zero to 180 degrees at a Reynolds number of 3×10^6 and a Mach number of .30 are shown in various subfigures of Figure 9. Lift, drag, and moment data for the entire range are presented in Figures 9C, 9G, and 9K. Similar data for forward flow and for reverse flow through stall are shown in Figures 9B, 9F, and 9J and in Figures 9D, 9H, and 9L, using expanded scales, and include results from additional references for the shorter ranges in angle of attack.

Test data for the whole sweep in angle of attack are available for the NACA 0012 airfoil in Reference A-7 for low-speed incompressible conditions at a Reynolds number of 1.8×10^6. The data used in this comparison are those shown for the first of two wall corrections to which reference is made in that source. Additional data for the NACA

0012 airfoil which are used in the comparisons at small angles of forward and reversed flow are obtained from Reference A-11. These data are for a Mach number of .30 and for a Reynolds number of 1.0 to 2.0 X 10^6. The c_ℓ and c_d data of Reference A-11 for reverse flow are readily applied to the angle-of-attack region in the vicinity of 180 degrees. The moment coefficient data for reverse flow require a correction for the change in axis from 25 percent of the chord from the trailing edge to 25 percent from the nose.

Test data from both References A-7 and A-11 are presented in test point form, as are the basic data from this program. The larger number of test points taken through the angle-of-attack range more clearly reflect the test scatter which accompanies the angles of attack at which severe flow separation occurs at the airfoil.

Examination is first made of Figures 9C, 9G, and 9K for overall characteristics of the data in the range between forward flow and reverse flow stall. The maximum positive and negative values of lift coefficient which occur in the regions of 45 degrees and 135 degrees, respectively, agree closely for the NACA 63A012 and the NACA 0012 airfoils, but the lift slope through α = 90 degrees is more negative for the NACA 63A012 airfoil.

The drag coefficient at α = 90 degrees is higher for the NACA 63A012 airfoil than that for the NACA 0012 airfoil. The higher value of drag coefficient was actually measured in the tests for the NACA 0012 airfoil but was reduced with the application of the wall corrections.

The maximum negative moment coefficient in the region of α = 110 degrees is significantly more negative ($\Delta c_{m_{.25}} = -.1$) for the NACA 63A012 than for the NACA 0012 airfoil. It would appear that a more detailed examination than can be applied here would be required before attributing this difference to the difference in thickness distribution of the two airfoils. The data for the two airfoils display a similar variation of moment coefficient with angle of attack in this region.

The reverse flow regions from reverse-flow stall to α = 180 degrees may be examined on expanded scales in Figures 9D, 9H, and 9L. It may be noted that for the unstalled condition between α = 172 degrees and α = 180 degrees, the NACA 63A012 data show lower absolute values than the data for the NACA 0012 airfoil for all the coefficients and slopes. These include c_ℓ, c_{ℓ_α}, $c_{m_{.25\alpha}}$. At reverse-flow stall, maximum negative lift coefficient and maximum negative moment coefficient values are about the same for the two airfoils.

The forward flow data for angles of attack through conventional stall may be examined in standard format in Figures 9B, 9F, and 9J. Data

for the NACA 64A012 and the NACA 64_1-012 airfoils from Reference A-10 and A-63, corresponding to the data used in Section 5.3.2.2, are introduced to complement the comparisons. These data are shown in curve form.

The lift data for the NACA 0012 airfoil illustrate the typical low speed, low turbulence c_{ℓ} max. The lift curve for the NACA 63A012 airfoil falls between the data for the NACA 64A012 and the NACA 64_1-012 airfoils and displays a c_{ℓ} maximum consistent with that for the 6-Series airfoils at a Mach number of .30 (See References A-2, A-32, and A-46.)

The drag coefficient and moment coefficient data for the NACA 63A012 airfoil at angles of attack up to 8 degrees reflect some of the difficulties that were encountered at the lower Reynolds numbers and Mach numbers during a portion of this program. (See Section 5.2.) These data in the low angle-of-attack range are regarded as questionable. (The moment data do not vary appreciably from zero, however.) Beyond this low angle-of-attack range, the drag coefficient and the moment coefficient data for the NACA 63A012 follow the previous trend of falling between the data for the NACA 64A012 and the NACA 64_1-012 airfoils.

5.3.2.6 Evaluation of Comparisons With Other Test Results

The general procedure of comparing the test results of this program with the results of other tests has made evident the similarities and differences of these and other data. In addition, it has brought to light the problem areas associated with the majority of such programs.

The test data of this program are shown to include some limited regions of questionable data. Also, some explicit additional corrections are recommended, in other portions of the evaluation, for applying the data of this program. Generally, however, on the basis of the observations made in the systematic examination of the comparative data, it is concluded that the results of the program are valid. With the incorporation of the recommended corrections, these data are considered reasonable in absolute value.

5.3.3 Relative Characteristics of the Airfoils Tested

5.3.3.1 Examination of Test Results

An examination of some relative characteristics of the airfoils tested is permitted by the presentation of data for several principal airfoil parameters in Figures 7A-1 and 7A-2.

In Figures 7A-2, it is observed that the angle of attack of zero lift for the 63A018 airfoil is shown to be approximately .5 degrees. Flow characteristics of the wind tunnel are known not to display any flow inclination at a Mach number higher than .30. In addition, a

careful examination of the model reveals no disparities which could cause a flow asymmetry of this magnitude. It is suggested that a possible misalignment may have occurred in mounting the model, and that on this basis, application of the data for this model should include the correction to the angle of attack.

Other data shown in Figure 7A-2 are now considered. The c_m data for $\alpha = 0$ degrees over the Mach number range covered are acceptably close to zero and warrant no special attention. The aerodynamic center data demonstrate overall similar trends for all thicknesses with increasing Mach number and, generally, the data for all thickness ratios display a consistent trend with increasing Mach number in regard to each other. This effect is demonstrated by the fact that the rapid divergence in aerodynamic center with increasing Mach number occurs first for the thickest airfoil and then successively with each representation of a reduction in thickness ratio. The variation of the data for the 12-percent thickness ratio with Mach numbers below that of divergence appears somewhat severe. An examination of Figures 23-A through F shows that this characteristic for the 12-percent airfoil is generally limited to the lower range of test Reynolds numbers.

In Figures 7A-1, the lift slope data for $c_l = 0$ and the drag coefficient data for $\alpha = 0$ degrees show reasonable and consistent variation with Mach number and for thickness ratio. The data for $c_{l\ max}$ do not show trends which are as straightforward. The thicker sections show a falloff in $c_{l\ max}$ with increasing Mach number after an initial drop. These are the general characteristics that would be expected on the basis of a careful evaluation of the results in References A-46, A-59, and A-63.

5.3.3.2 Application of Transonic Similarity Rule

Spreiter's form of the Von Karman Transonic Similarity Rule (References A-26, A-52, A-53, A-15, and A-37) is useful for correlating aerodynamic characteristics of a family of airfoils. The literature is generally directed to applications for wings of finite span, but the required information for infinite aspect ratio are also included. Its usefulness is evident in the transonic region where it offers a form of data presentation. The linearized Glauert-Prandtl Rule and the Kaplan Rule which are applicable to Mach numbers between .6 and .8 are indeterminate at a Mach number of one. The transonic similarity rule is applicable at the lower Mach numbers but is somewhat more complicated to use than the linearized rules. Reference A-5 explains that the transonic expression is valid for only thin airfoil sections, but indicates that the rule may be applied with discretion to extrapolate to conditions for thicker sections. In this regard, the rule has usefulness in helicopter airfoil work because published data for thin airfoils passing through a Mach number of one could be applied to

somewhat thicker airfoils at high subsonic Mach numbers beyond the applicability of the linearized rules.

The transonic similarity rule is applied here as another tool for evaluating the consistency of the aerodynamic data for the airfoils tested. It is accepted that the application of this rule to the data for thicker airfoils under consideration is essentially an empirical process.

Examples of the applications of the transonic similarity rule to two-dimensional data are provided in References A-10 and A-24. It is to be noted that in Reference A-10, the constant term of $(\gamma + 1)^{2/3}$ is omitted in the denominator of the reduced Mach number, and that the constant term of $(\gamma + 1)^{1/3}$ is omitted in the numerator of the reduced coefficients. These terms are included in the reduced Mach number and in the reduced coefficients derived for this report as well as in the corresponding expressions of Reference A-24. The reduced Mach number and the reduced coefficient expressions are adequately defined in the symbol section of this report.

The reduced coefficient data are calculated for the condition of $c_l = 0$, Figures 11-A and 11-B, and for the condition of $\alpha/(t/c) = .4$, Figures 11-C and 11-D. Alpha is measured from the angle of attack for zero lift. The data presented in Figures 11-A to 11-D correspond to forms shown in Figure 23 of Reference A-10, except for the constants noted in the previous paragraph.

Each group of data presented in Figures 11-A through 11-D shows consistent trends with reduced Mach number for all thickness ratios. These data are considered to display good correlation whether considered independently or whether compared with the data of Figure 23 in Reference A-10 and of Figure 14 in Reference A-24. The correlation shown for reduced drag coefficient in Figure 11-B is exceptionally good.

5.3.3.3 Evaluation of Related Characteristics

On the basis of a simple visual examination of several principal characteristics of the airfoils tested, the correlation of test data with thickness ratio is generally good. Some problem areas exist and some corrections may be applied in making use of the data. The aerodynamic center travel for the 12-percent-thick airfoil below Mach divergence at the low Reynolds numbers is excessive. Use of the data for the 12-percent-thick airfoil should be accompanied by a correction in angle of attack from zero lift which may be as much as .5 of a degree.

A complementary evaluation of the relation of several aerodynamic characteristics on the basis of thickness ratio has been made with the transonic similarity rule. Although this scale may be considered empirical for the thickness ratios of the airfoils of this program, the correlation of characteristics is very good.

On the bases of general observations and on analytic correlation, it is concluded that the aerodynamic characteristics obtained in this program are generally consistent for thickness ratio.

5.4 AERODYNAMIC CHARACTERISTICS VARIATION WITH REYNOLDS NUMBER

The basic evaluation of the test results has been made for the condition of 3.5×10^6. In this section, an examination is made of the test results to establish the effects of Reynolds number on some of the principal aerodynamic characteristics.

5.4.1 $c_{\ell\ max}$

Data for $c_{\ell\ max}$ variation with Reynolds number at constant Mach numbers are shown in Figures 18A to 18D. Except for the data of $M = .6$, $c_{\ell\ max}$ versus Reynolds number varies less than .05 unit of c_ℓ, and this variation displays no consistent pattern. At $M = .6$, the 12- and 15-percent airfoils show peak values of $c_{\ell\ max}$ at $R = 5 \times 10^6$. From this condition, the data show a drop of $c_{\ell\ max}$ of more than .1 unit of c_ℓ at either the high or the low end of the Reynolds number range. This inconsistent trend in $c_{\ell\ max}$ is attributed to the fact that optimum wall positions were not established and applied at each test combination of Reynolds number and Mach number.

5.4.2 $c_{\ell\alpha}$ at $\alpha = 0$ degrees

Data for the variation of $c_{\ell\alpha}$ at $c_\ell = 0$ with Reynolds number are presented in Figures 19A through 19E. At $M = .4$, $c_{\ell\alpha}$ is essentially invariant with Reynolds number. With increasing Mach number, $c_{\ell\alpha}$ demonstrates an increase with Reynolds number at all thicknesses except for the 18-percent-thick airfoil. This airfoil shows a decrease in $c_{\ell\alpha}$ between $R = 3.5$ to 5.0×10^6 before reverting to the trend of the thinner airfoils. At a Mach number of .80, only the lower Reynolds number portion of the curve is available for the 18-percent-thick airfoil. The general pattern of $c_{\ell\alpha}$ with Reynolds number and thickness ratio for increasing constant values of Mach number is reasonable.

5.4.3 α for $c_\ell = 0$

Data for the angle of attack for zero lift are presented in Figures

21A through 21F. Information on this parameter for a symmetrical airfoil is more related to the symmetry of the test conditions than to an expected variation in Reynolds number. With the exception of the data for the 18-percent-thick airfoil, α for $c_\ell = 0$ does not vary more than $\pm$ .25 degrees. In the case of the 18-percent airfoil, a 1.5-degree difference from zero angle of attack is shown over almost the entire range of Reynolds numbers and Mach numbers. This result is the same as that noted in the general evaluation of the test data made at $R = 3.5 \times 10^6$. At that point, it was noted that correct use of the data for this airfoil would require the necessary adjustment for angle of attack at zero lift. The recommended correction for the previous case is equally applicable now.

5.4.4 c_d at $\alpha = 0$ degrees

Drag coefficient data for $\alpha = 0$ degrees are presented versus Reynolds number at constant Mach number in Figures 20A through 20F. For the Mach numbers from .40 through .70, c_d for $\alpha = 0$ degrees is essentially invariant with Reynolds number. Two areas of conspicuously poor variation are shown for the 18-percent-thick airfoil at a Mach number of .80 and for the 15-percent-thick airfoil at a Mach number of .90. In these two cases, c_d for zero lift increases from .02 to .03 units as the Reynolds number increases in value from the lowest to the highest values of Reynolds number.

5.4.5 $c_{m_{.25}}$ at $\alpha = 0$ degrees

Quarter-chord pitching moment coefficient data for $\alpha = 0$ degrees are shown versus Reynolds number at constant Mach number in Figures 22A through 22F. These data are essentially invariant with Reynolds number and are generally within .01 unit of zero.

5.4.6 Aerodynamic Center

Data for aerodynamic center versus Reynolds number at constant value of Mach number are shown in Figures 23A through 23F. For most conditions, there are no significant variations in aerodynamic center with Reynolds number. For the 12-percent-thick airfoil, however, M = .50 through .70 (i.e., below Mach divergence), the increase and decrease of 5 percent in chord for the aerodynamic center with increasing Reynolds number does not appear reasonable. At constant Reynolds numbers below drag divergence Mach number, a wide variation in aerodynamic center with Mach number occurs and is limited to the low Reynolds number condition. This was previously noted in the evaluation of the test results at $R = 3.5 \times 10^6$. Another disparity in aerodynamic center variation with Reynolds number occurs at M = .80 for the NACA 63A015 airfoil.

5.4.7 Results of Examination of Data With Variation in Reynolds Number

The examination of the variation of the aerodynamic characteristics with Reynolds number reveals some disparities similar to those noted in the evaluation of the data at $R = 3.5 \times 10^6$. However, the data generally show little variation with Reynolds number, and that variation which occurs is reasonable.

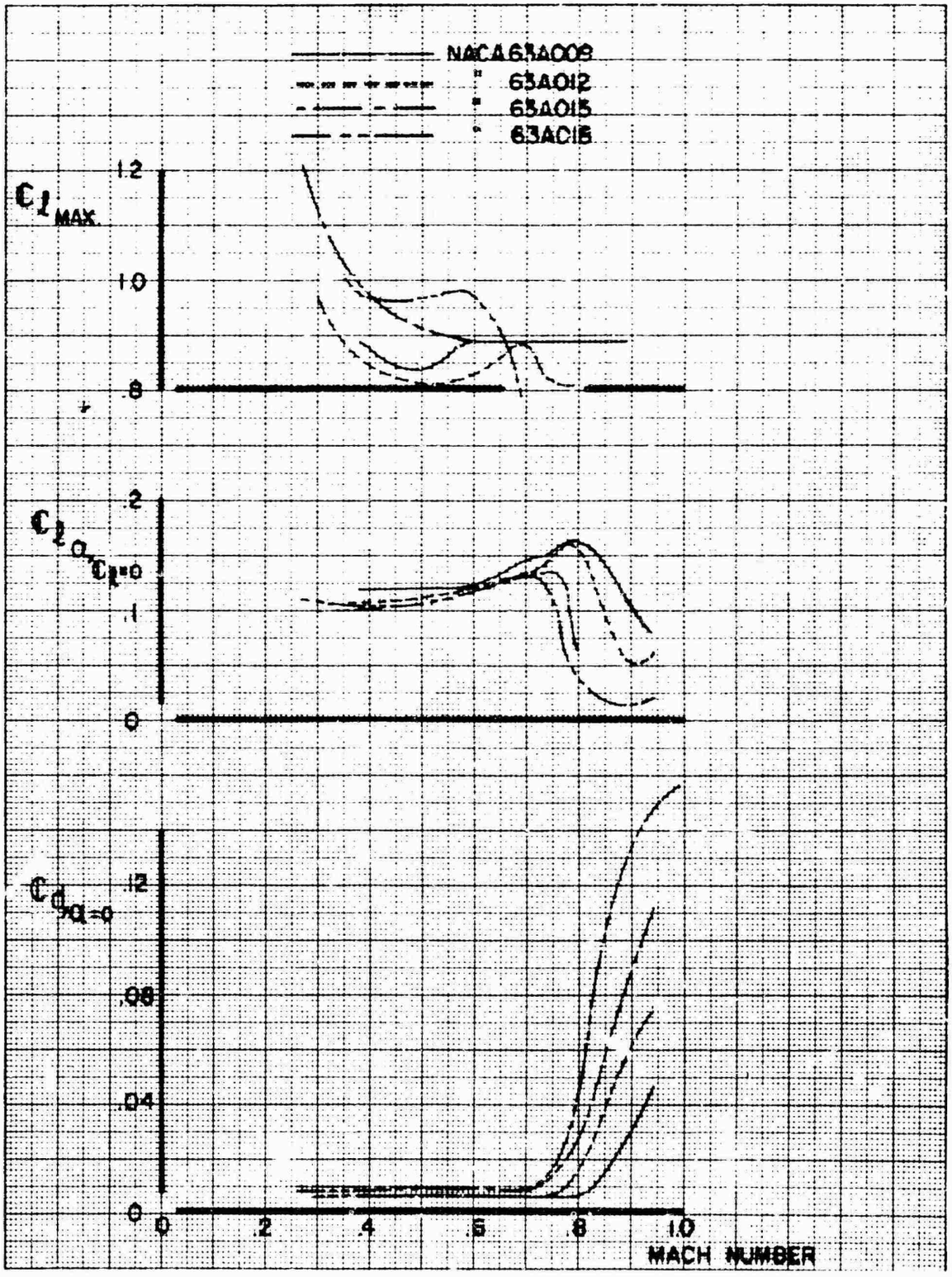


Figure 7A-1. Comparison of Aerodynamic Parameters for Varying Thickness Ratios, $R = 3.5 \times 10^6$

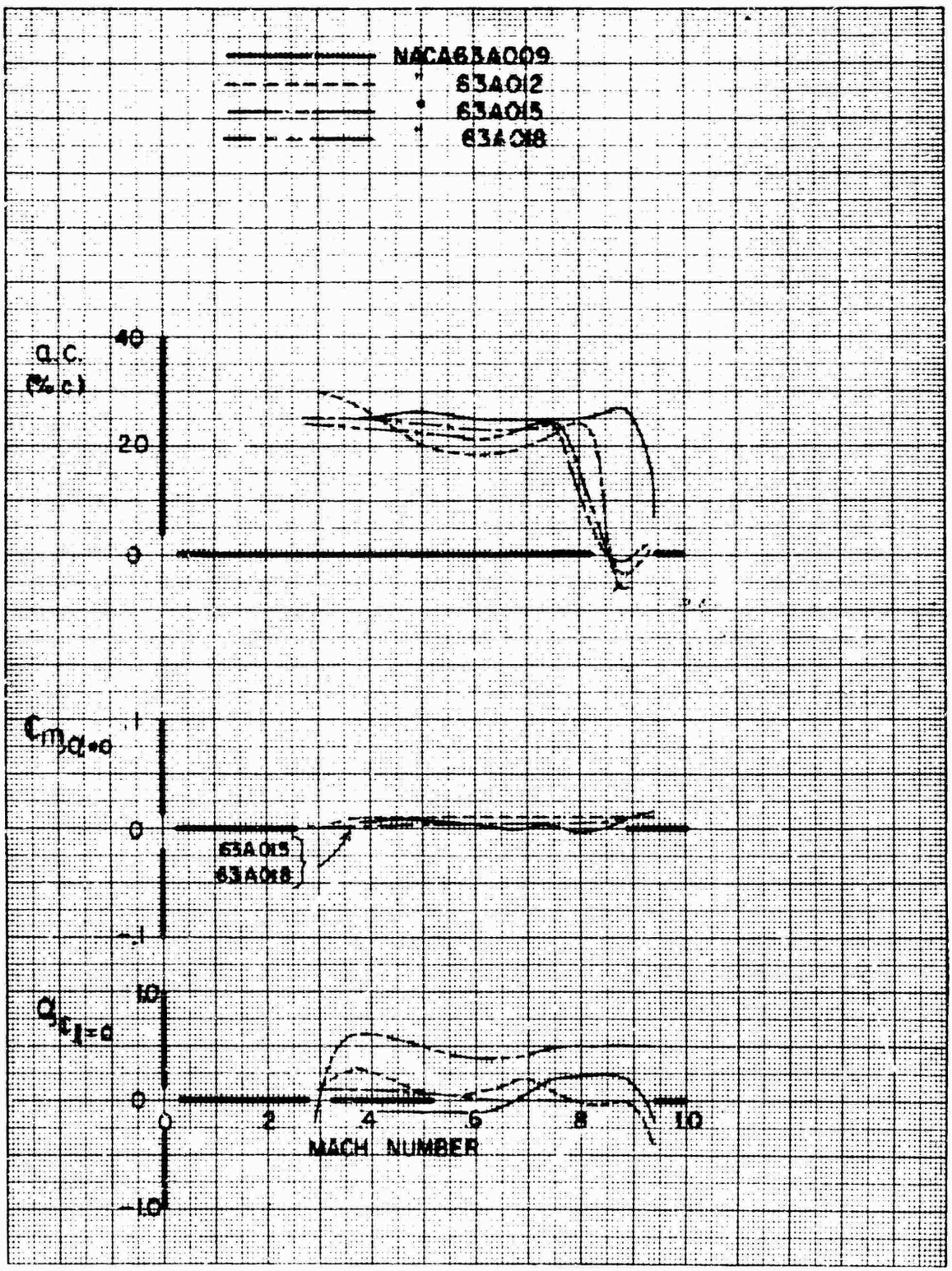


Figure 7A-2. Comparison of Aerodynamic Parameters for Varying Thickness Ratios, R= 3.5 x 10^6

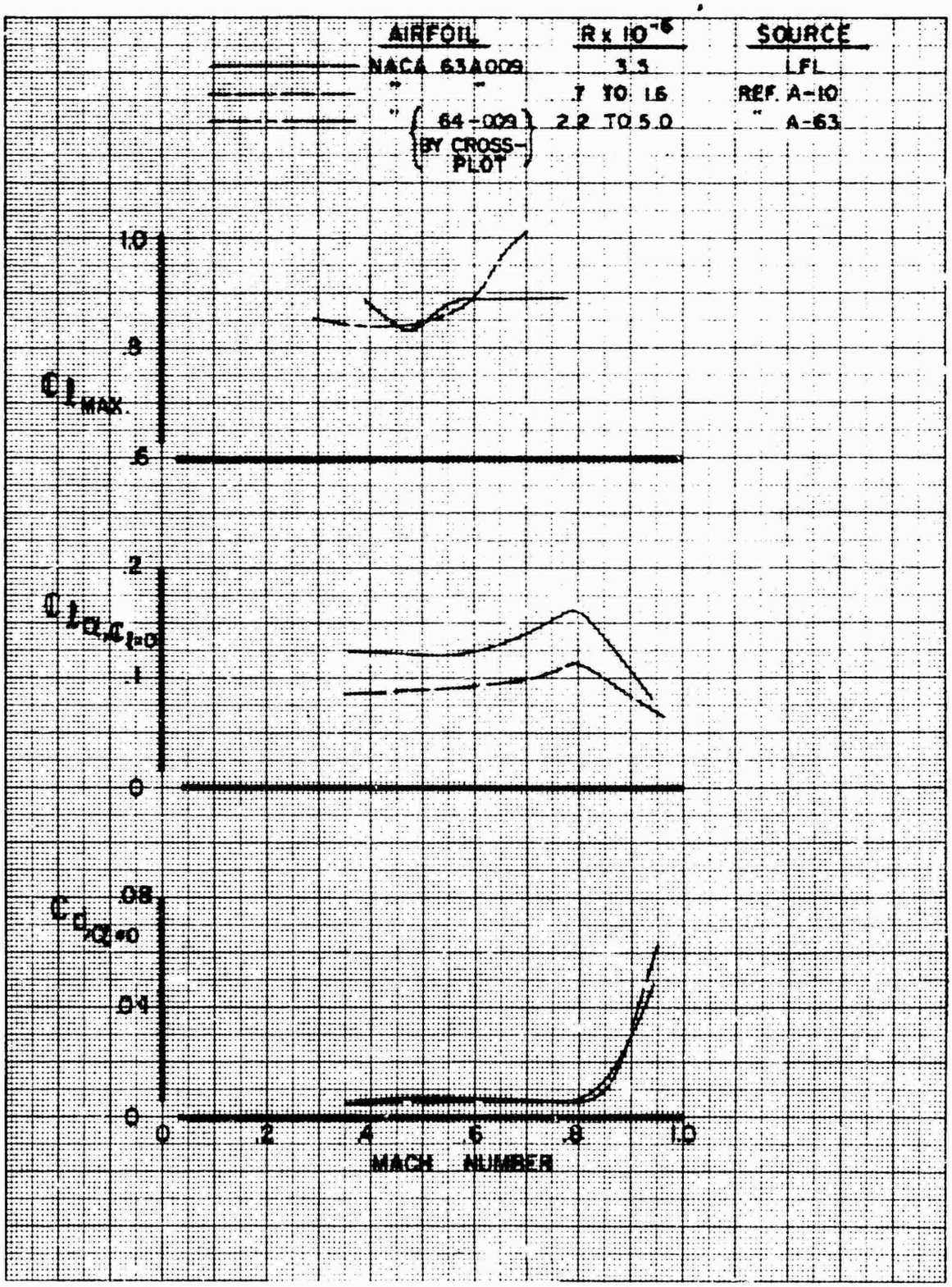


Figure 7B. Comparison of Aerodynamic Parameters - 9-Percent Sections

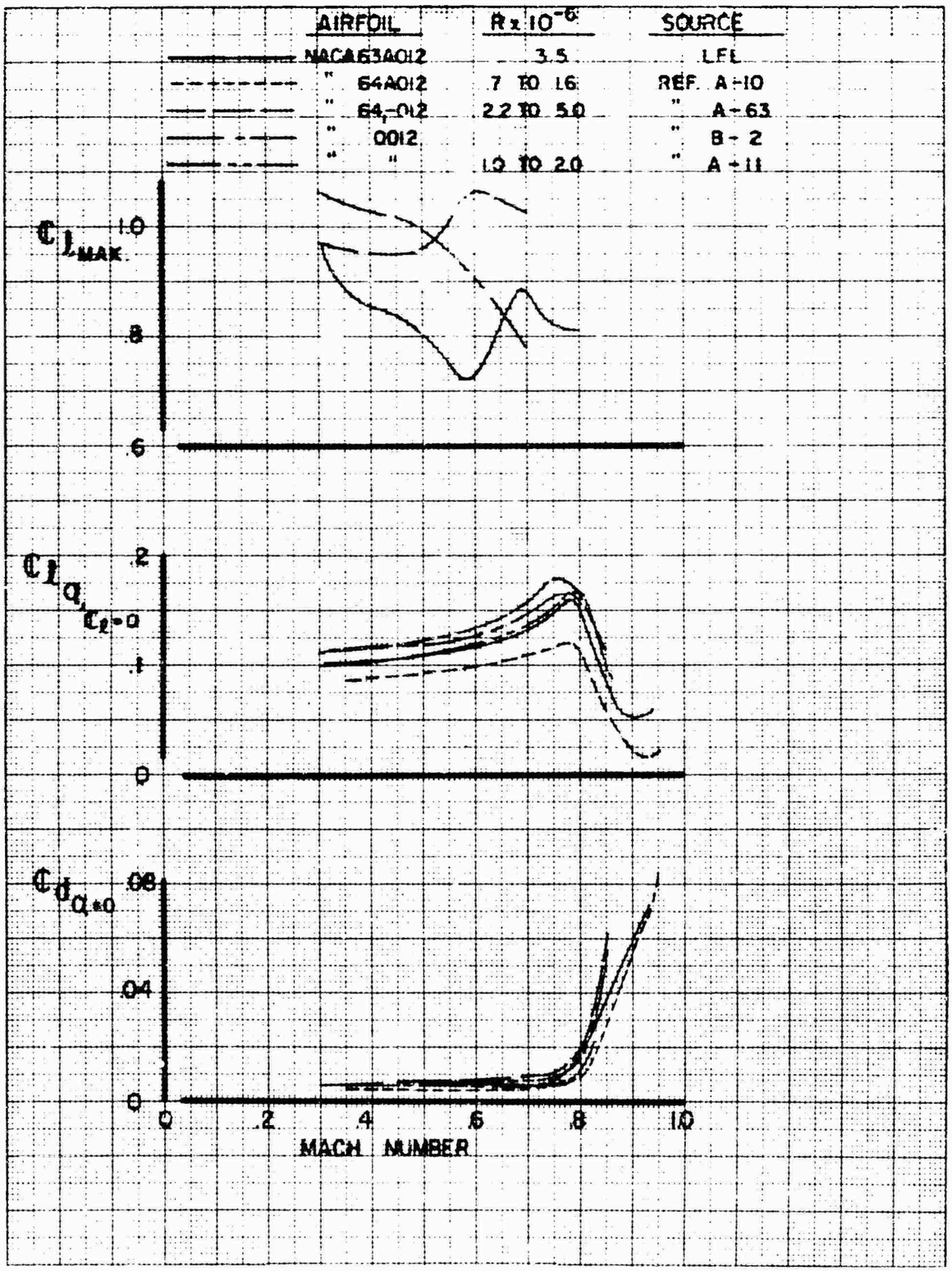


Figure 7C. Comparison of Aerodynamic Parameters - 12-Percent Sections

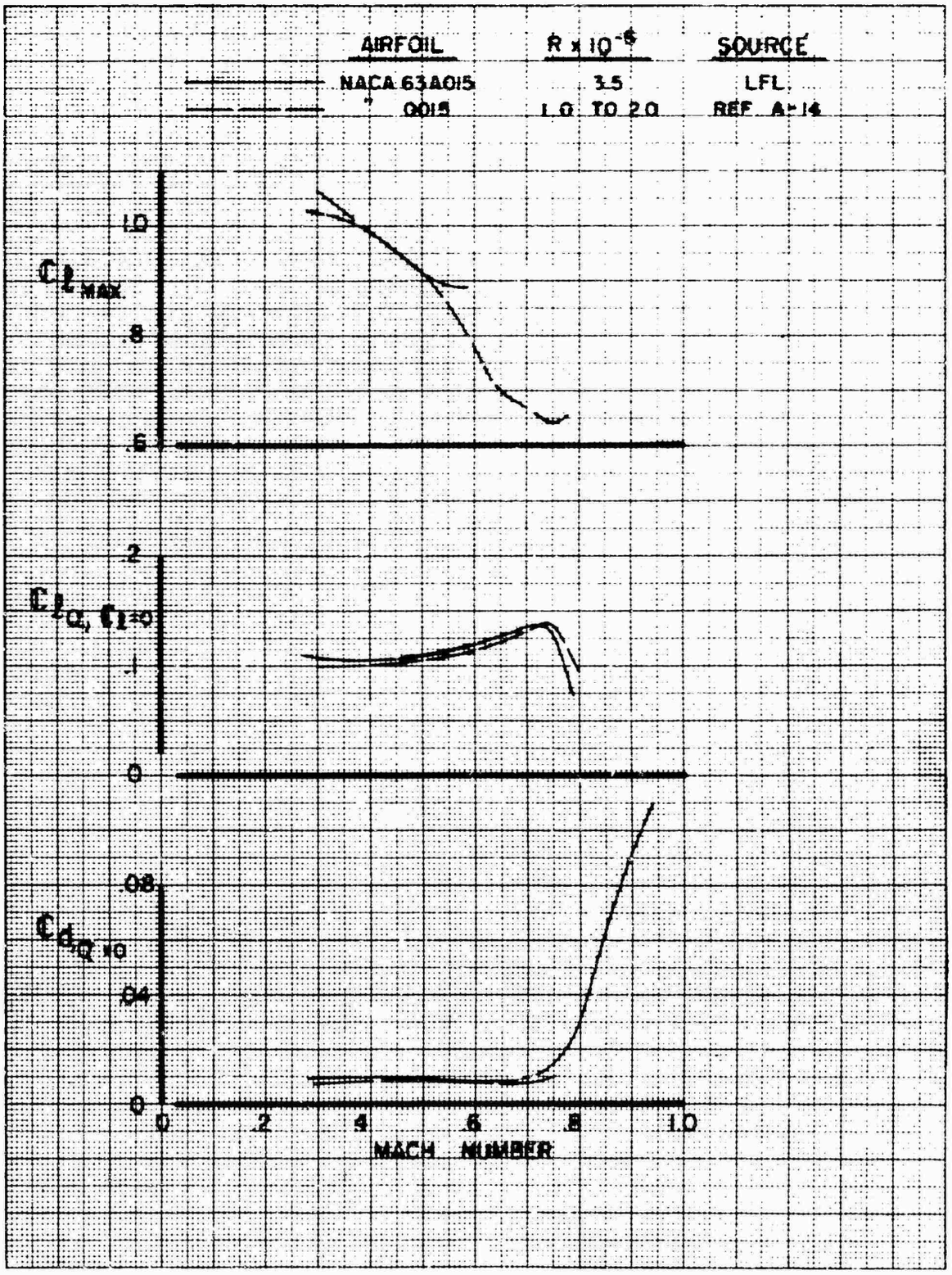


Figure 7D. Comparison of Aerodynamic Parameters - 15-Percent Sections

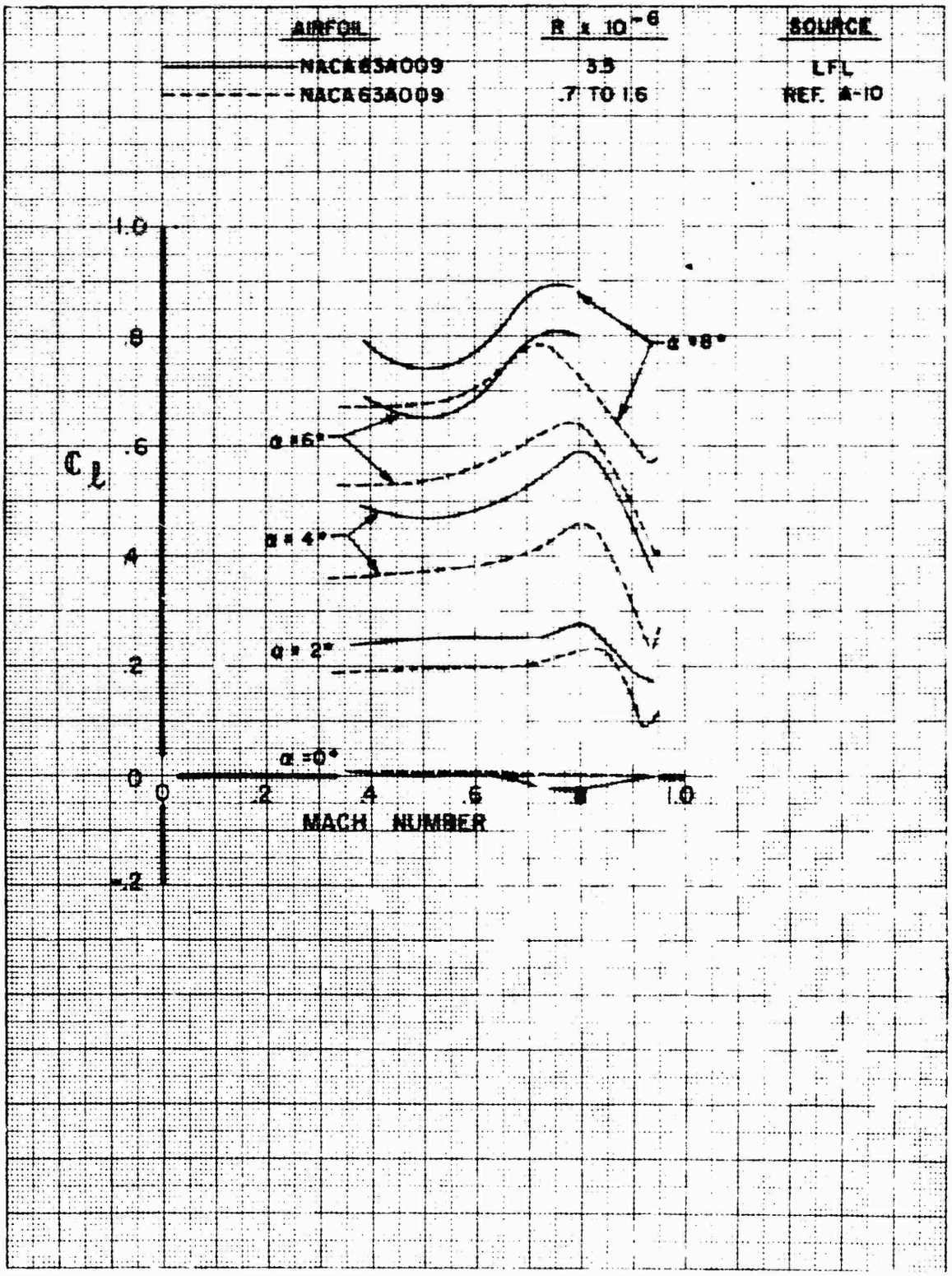


Figure 8A. Comparison Data, Section Lift Coefficient - 9-Percent Sections

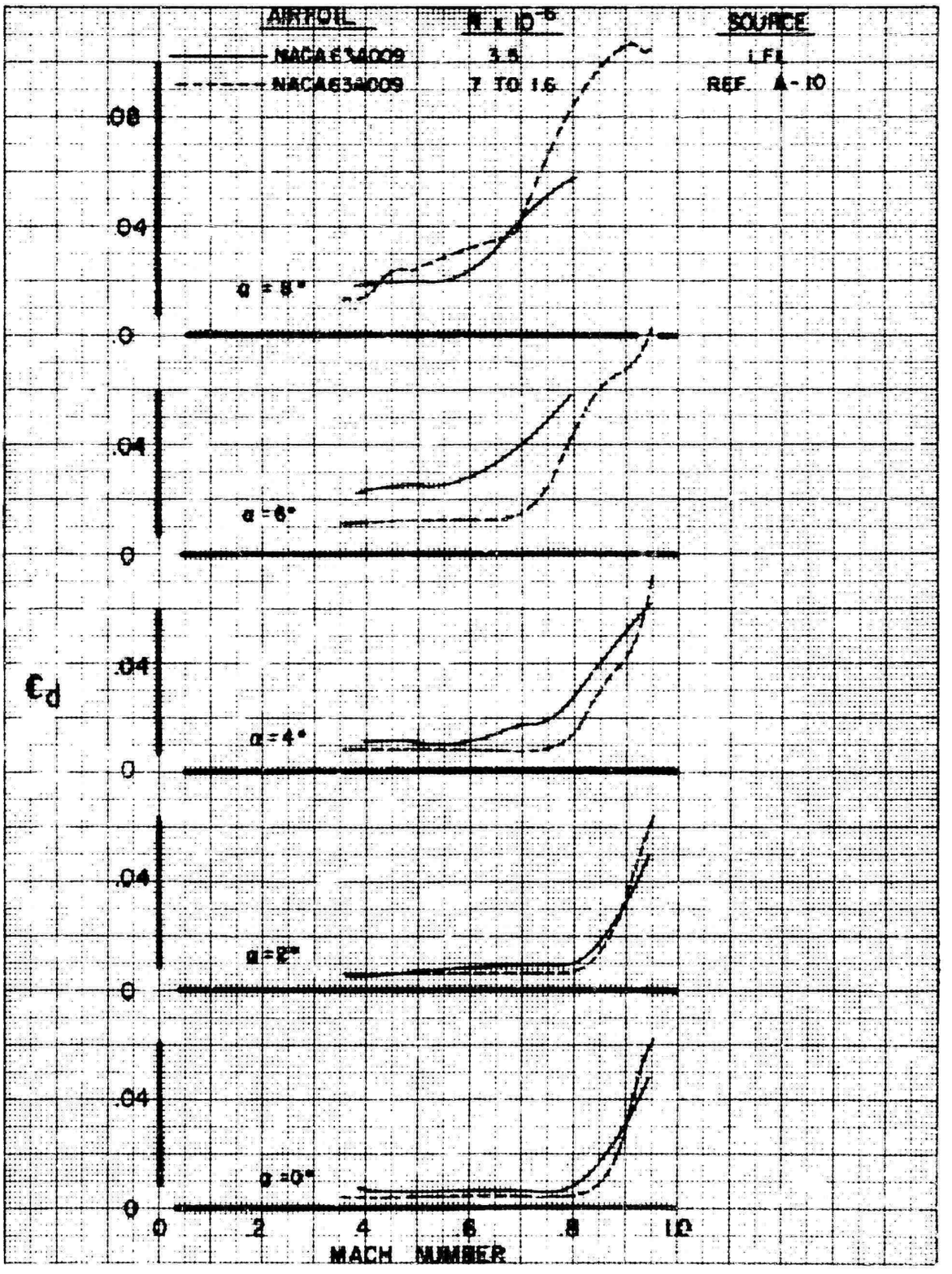


Figure 8B. Comparison Data, Section Drag Coefficient - 9-Percent Sections

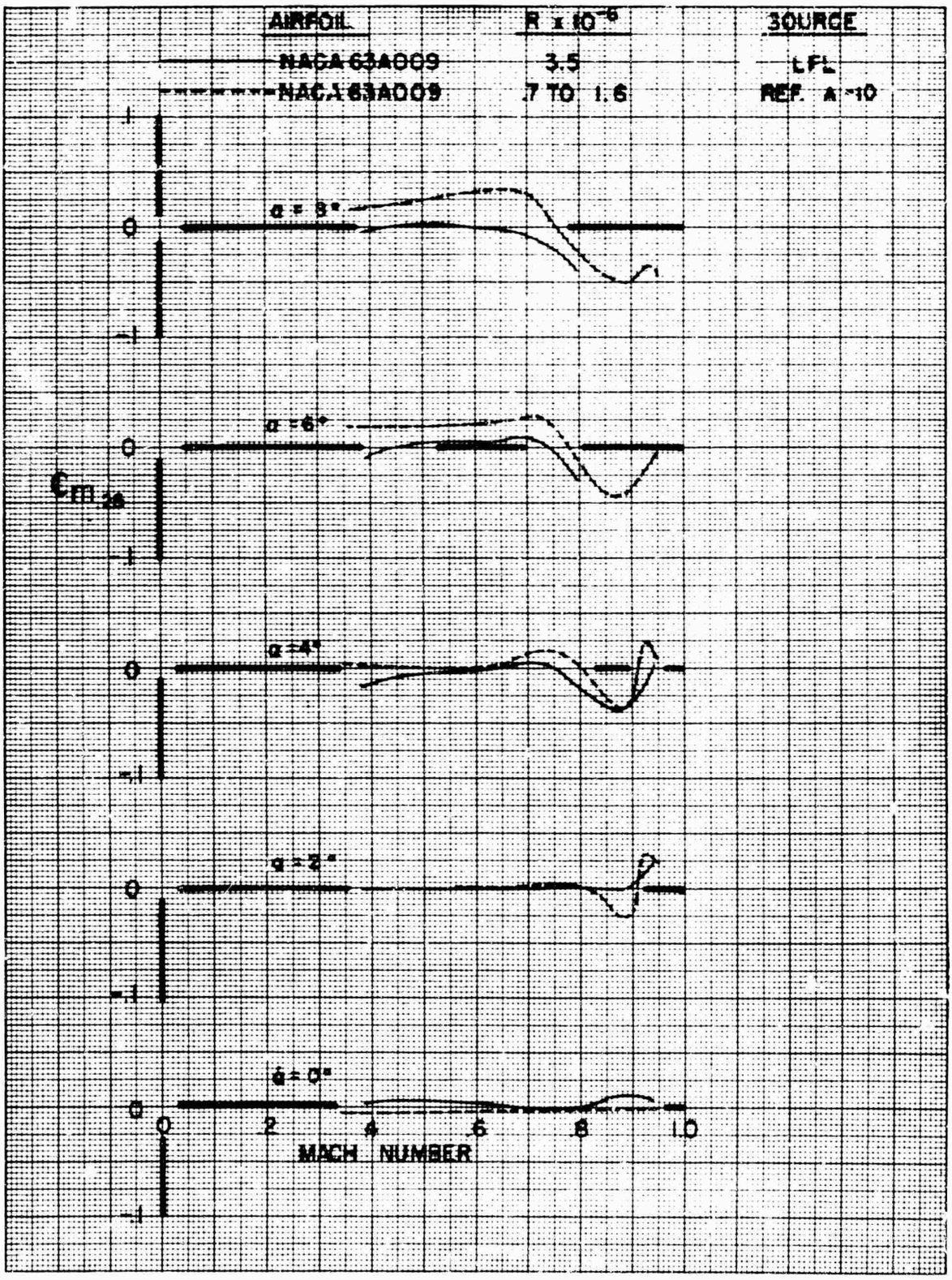


Figure 8C. Comparison Data, Section Pitching Moment Coefficient - 9-Percent Sections

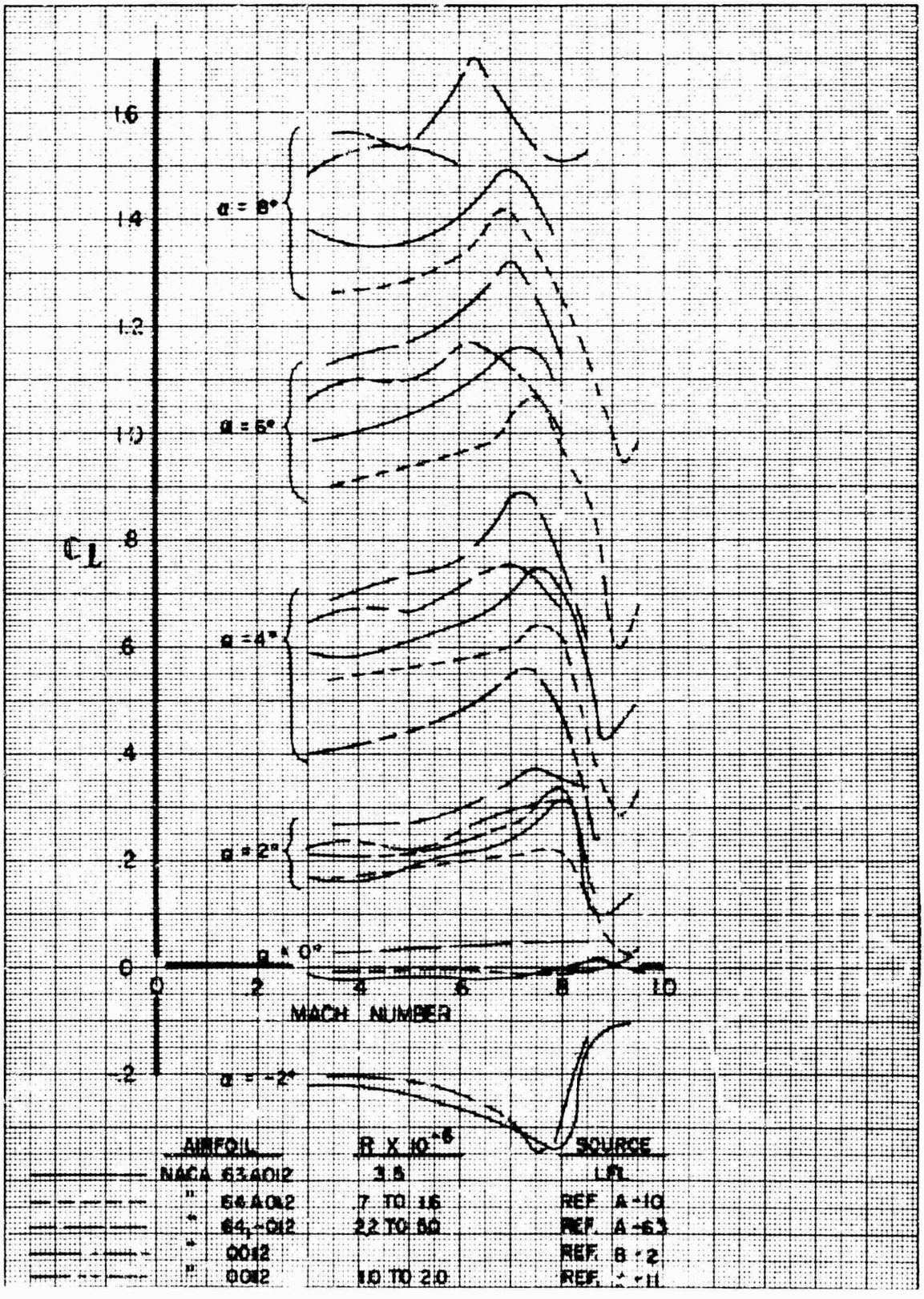


Figure 9A-1. Comparison Data, Section Lift Coefficient - 12-Percent Sections

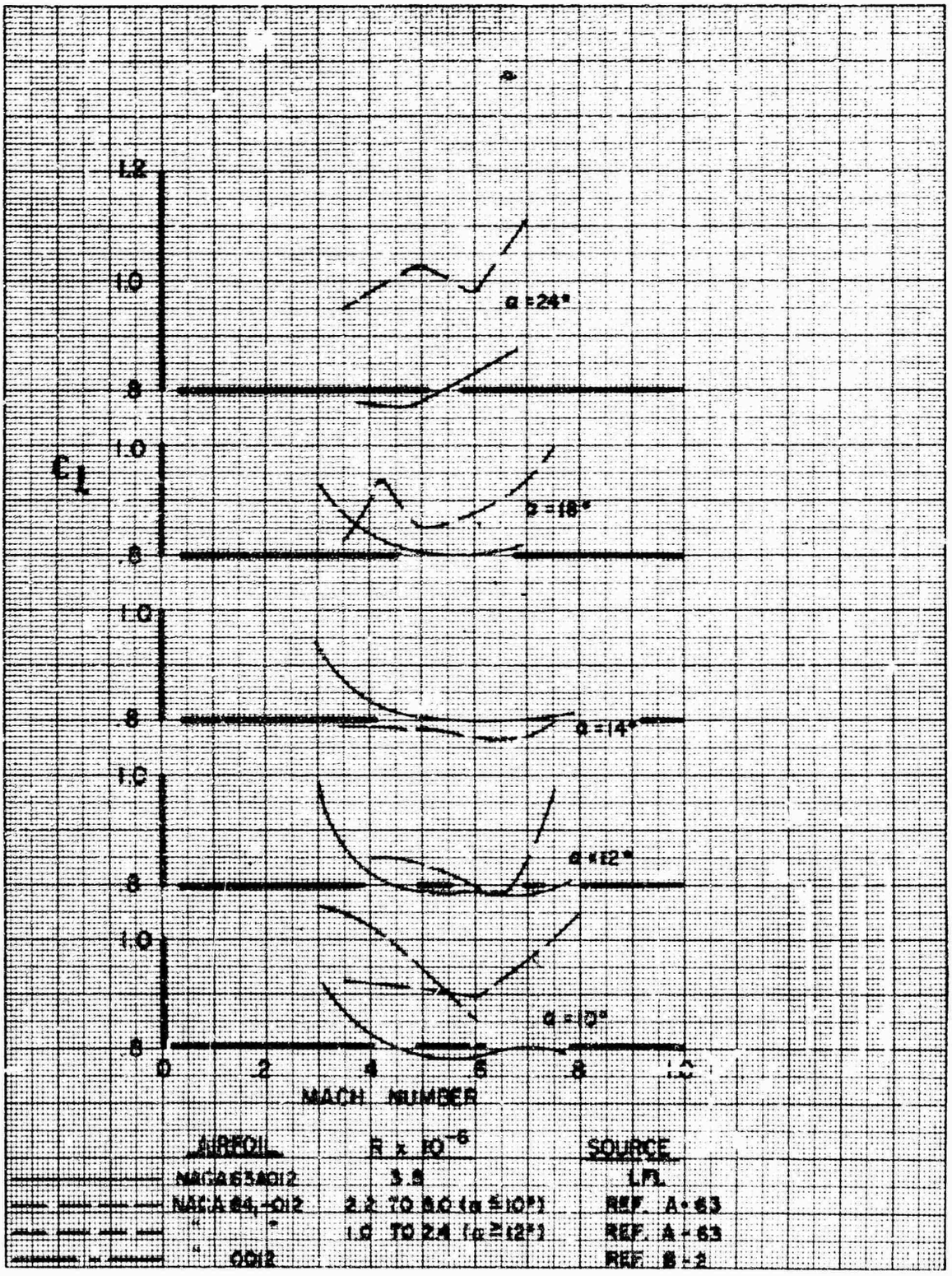


Figure 9A-2. Comparison Data, Section Lift Coefficient - 12-Percent Sections

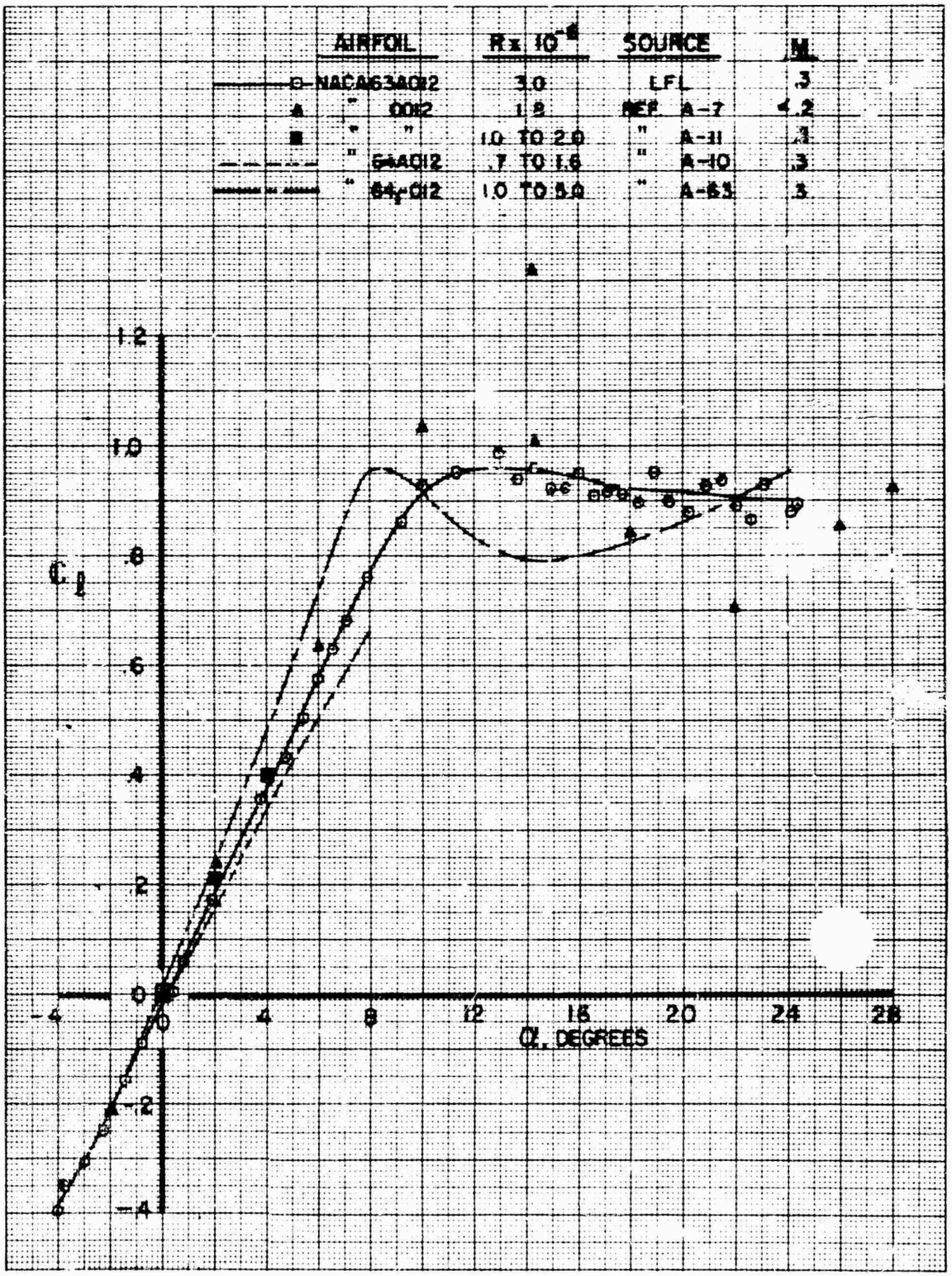


Figure 9B. Comparison Data, Section Lift Coefficient in Forward Flow Region - 12-Percent Sections

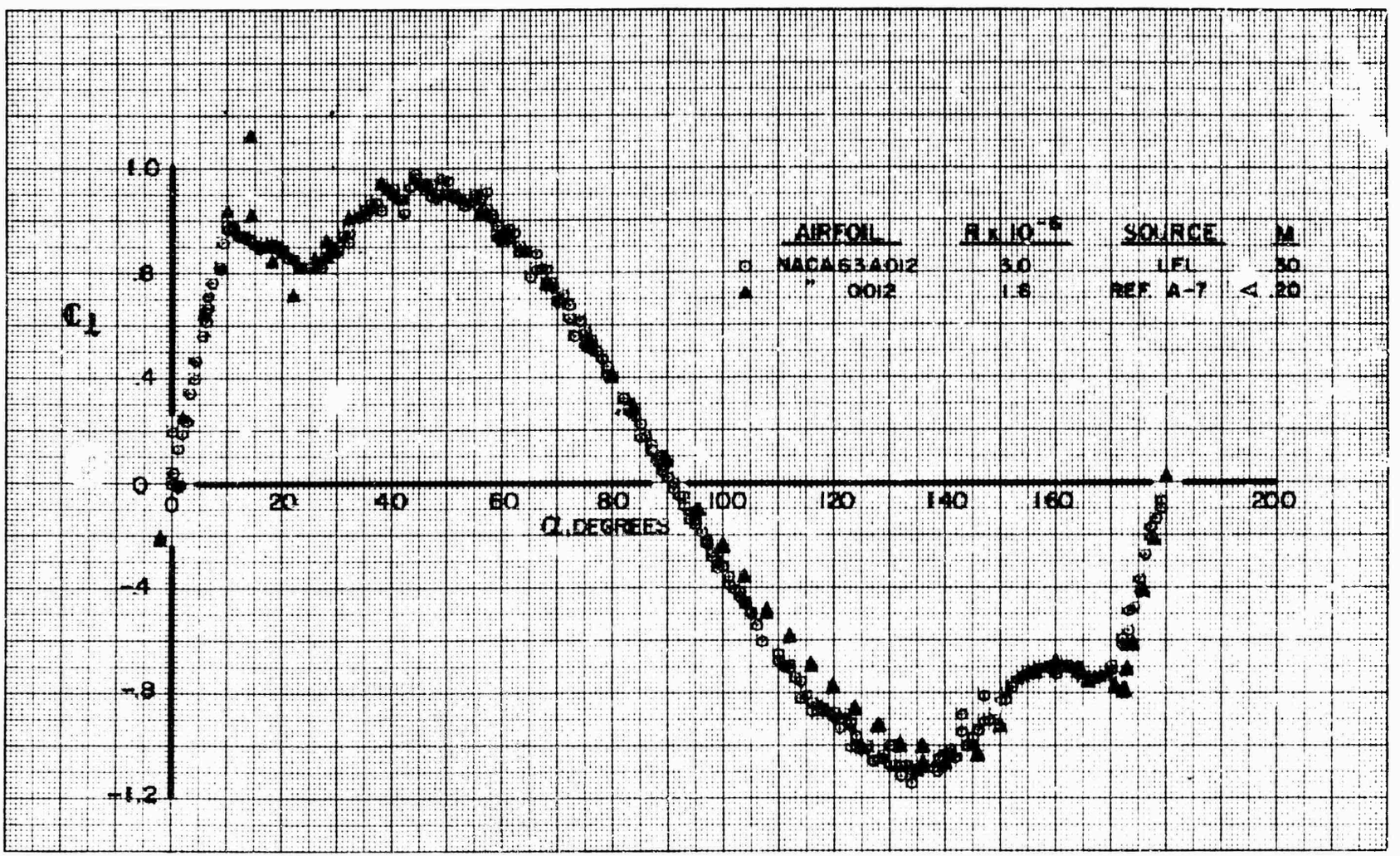


Figure 9C. Comparison Data, Section Lift Coefficient Over 180 Degree Range - 12-Percent Sections

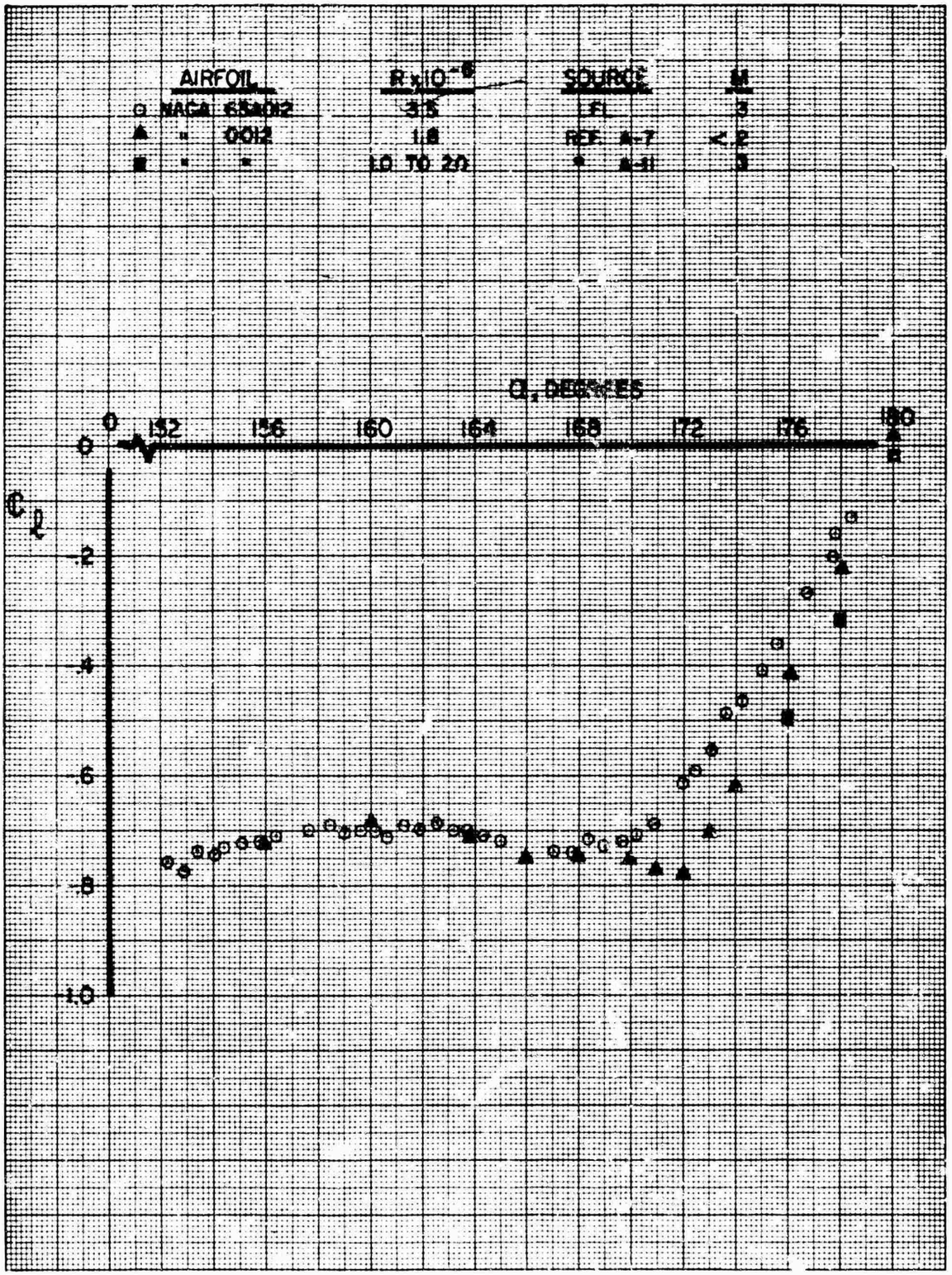


Figure 9D. Comparison Data, Section Lift Coefficient in Reverse Flow Region - 12-Percent Sections

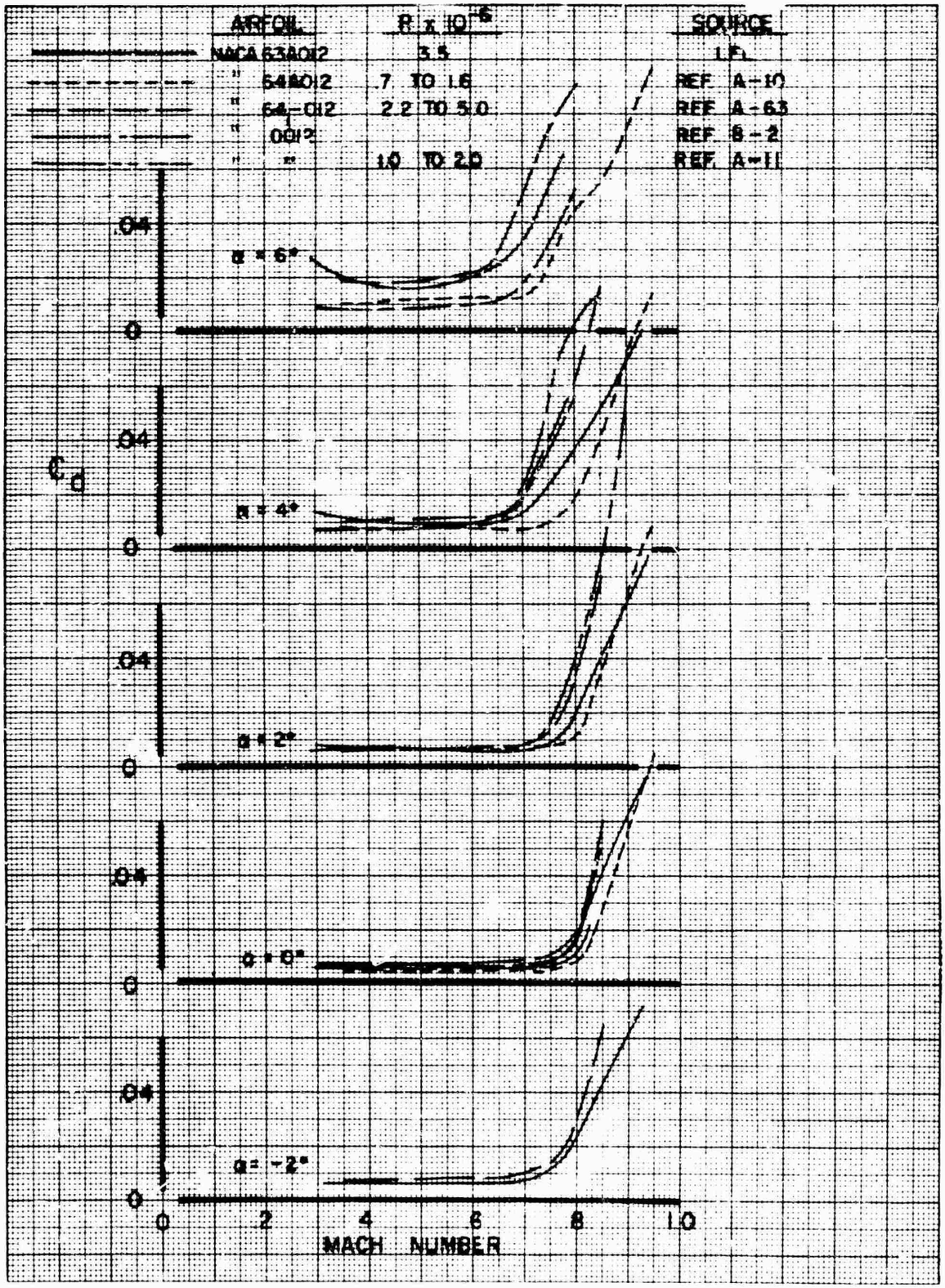


Figure 9E-1. Comparison Data, Section Drag Coefficient - 12-Percent Sections

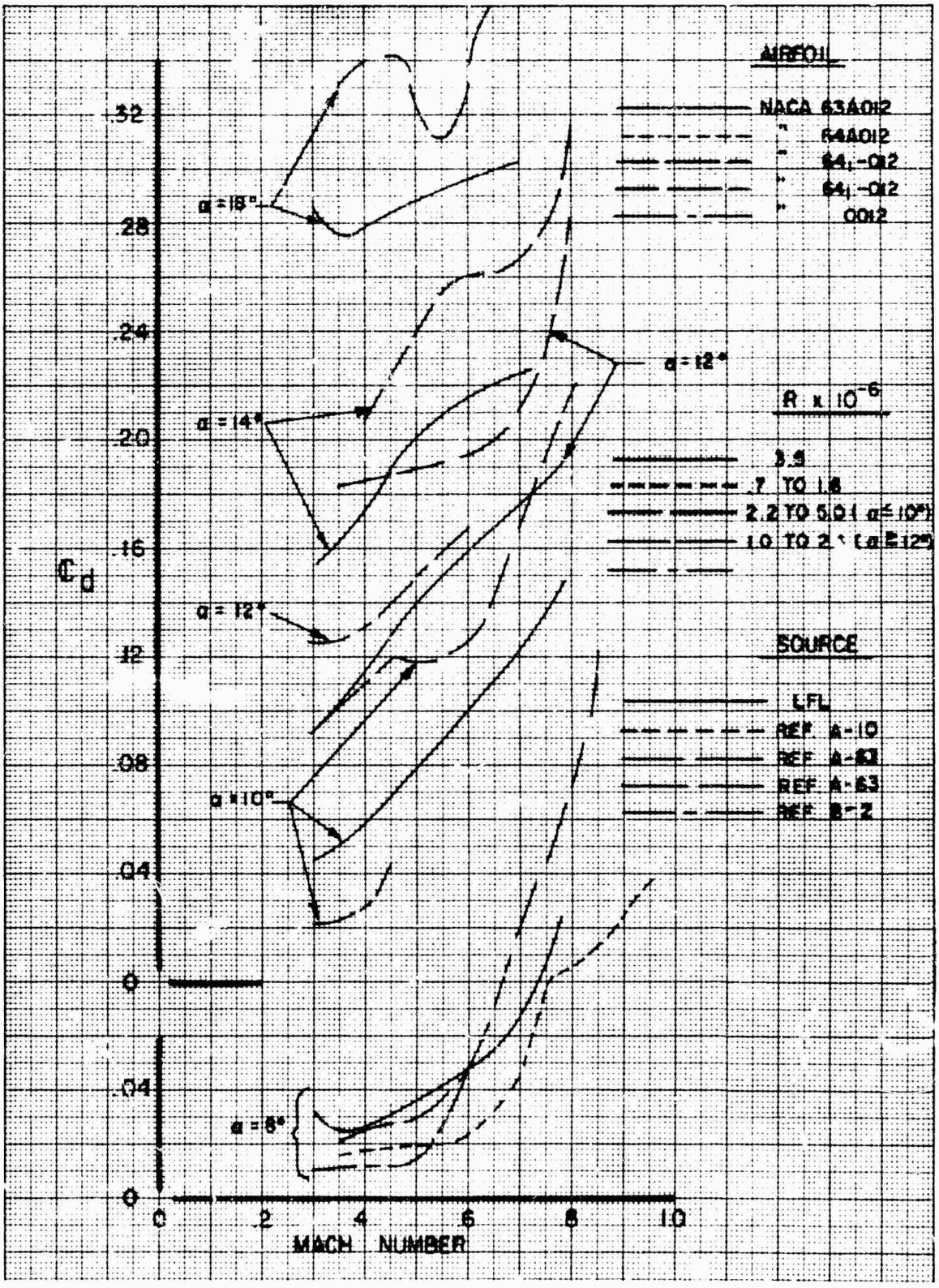


Figure 9E-2. Comparison Data, Section Drag Coefficient - 12-Percent Sections

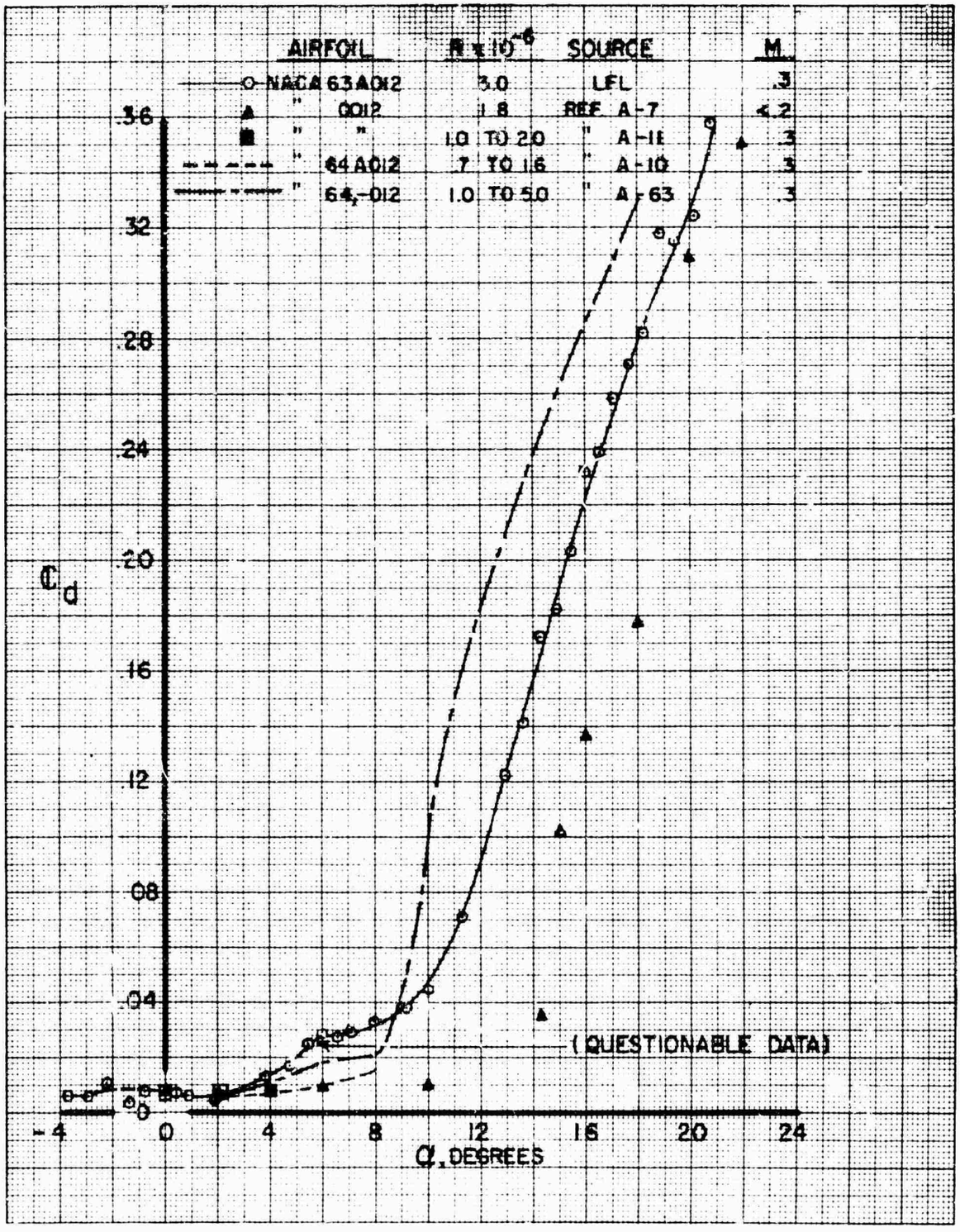


Figure 9F. Comparison Data, Section Drag Coefficient in Forward Flow Region - 12-Percent Sections

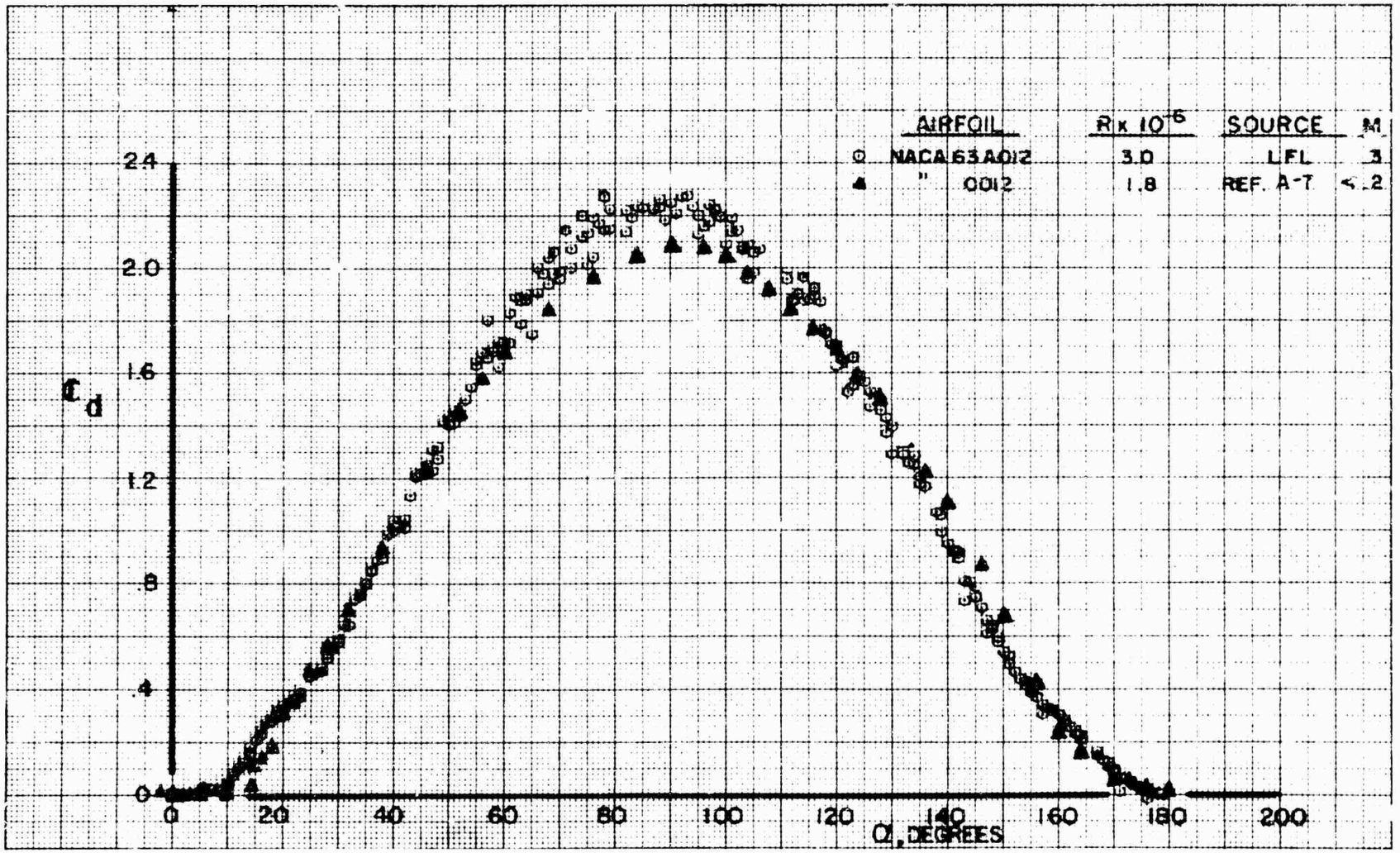


Figure 9G. Comparison Data, Section Drag Coefficient Over 180 Degree Range - 12-Percent Sections

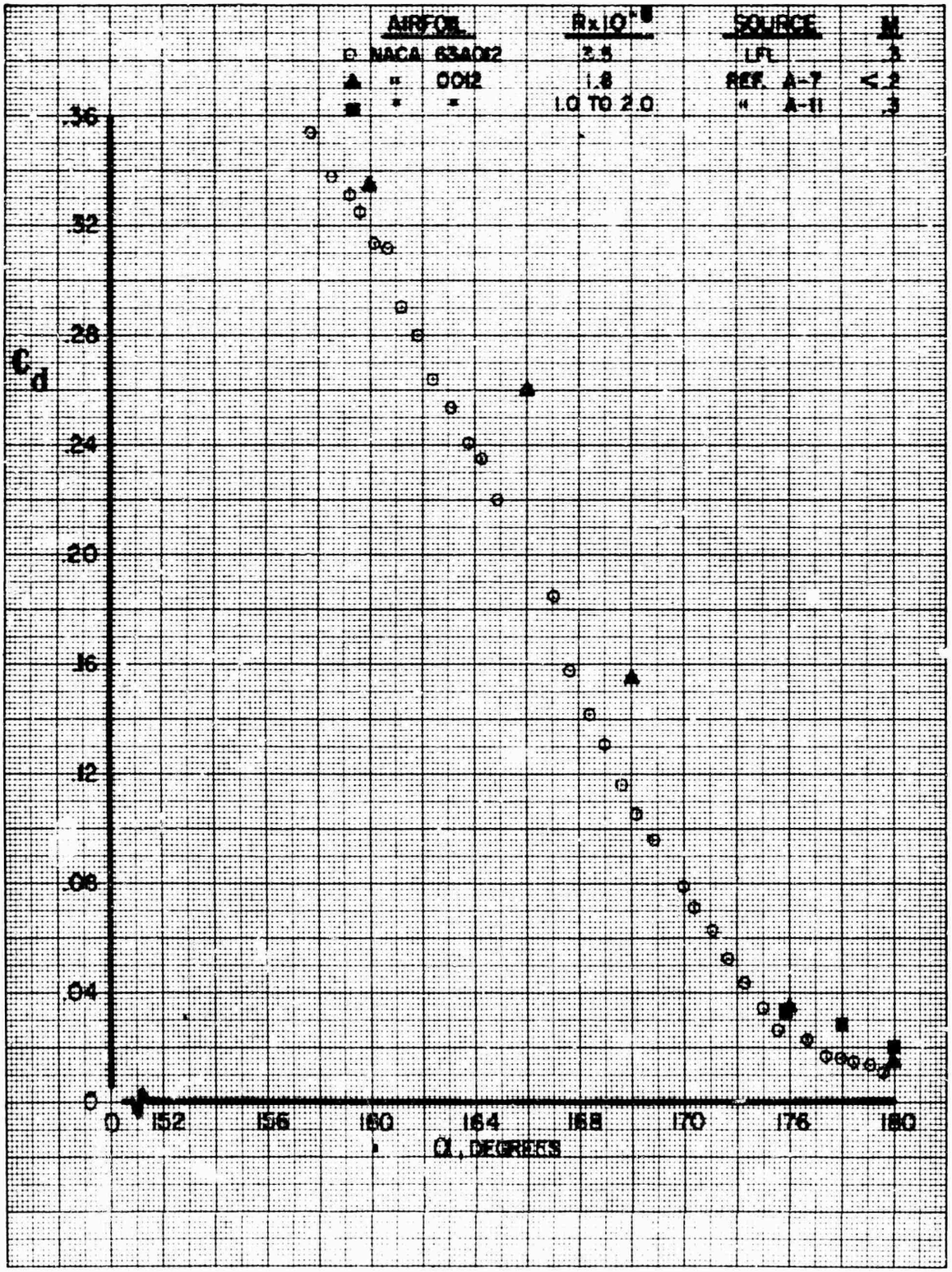


Figure 9H. Comparison Data, Section Drag Coefficient in Reverse Flow Region - 12-Percent Sections

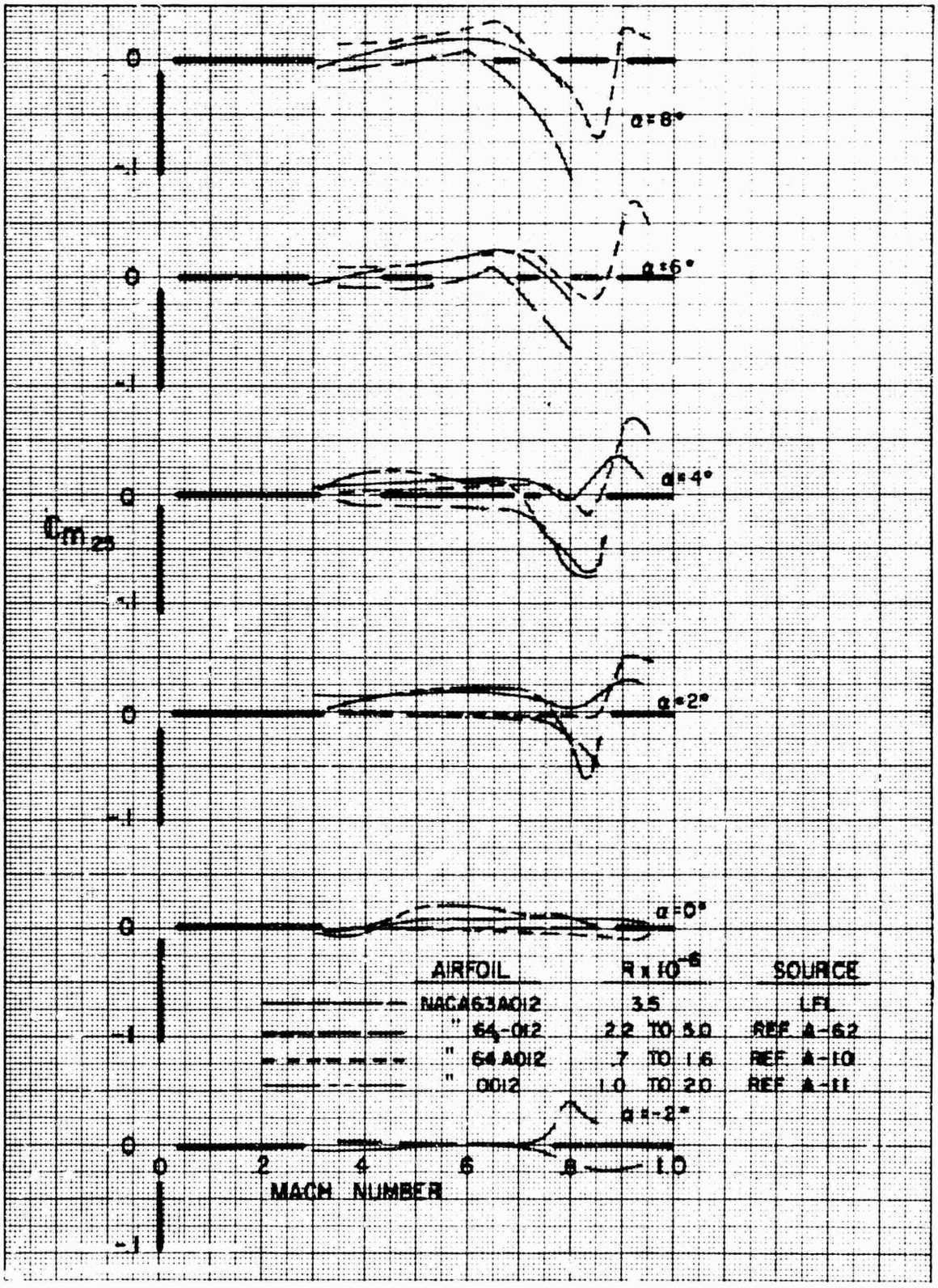


Figure 9I-1. Comparison Data, Section Pitching Moment Coefficient - 12-Percent Sections

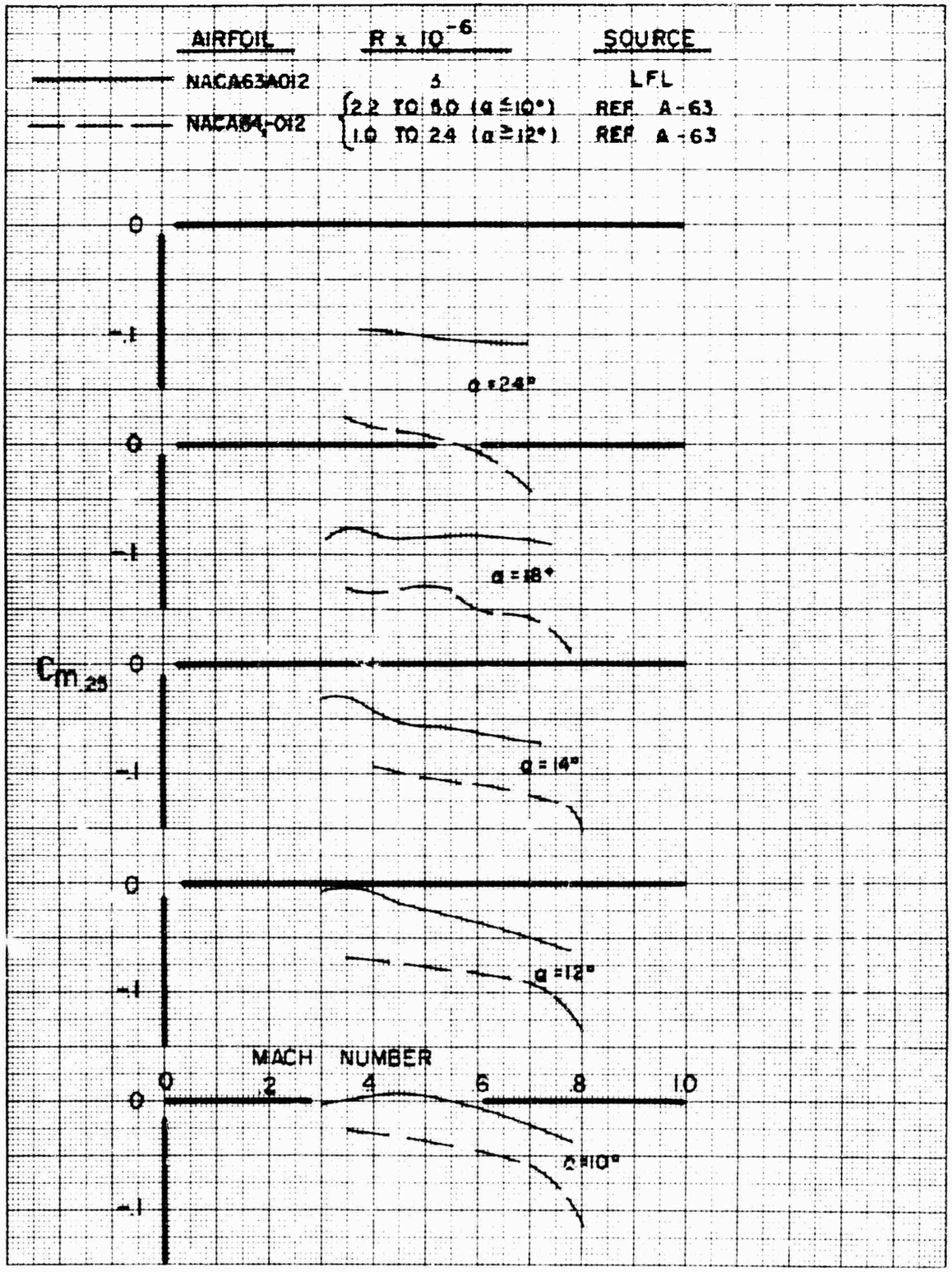


Figure 9I-2. Comparison Data, Section Pitching Moment Coefficient - 12-Percent Sections

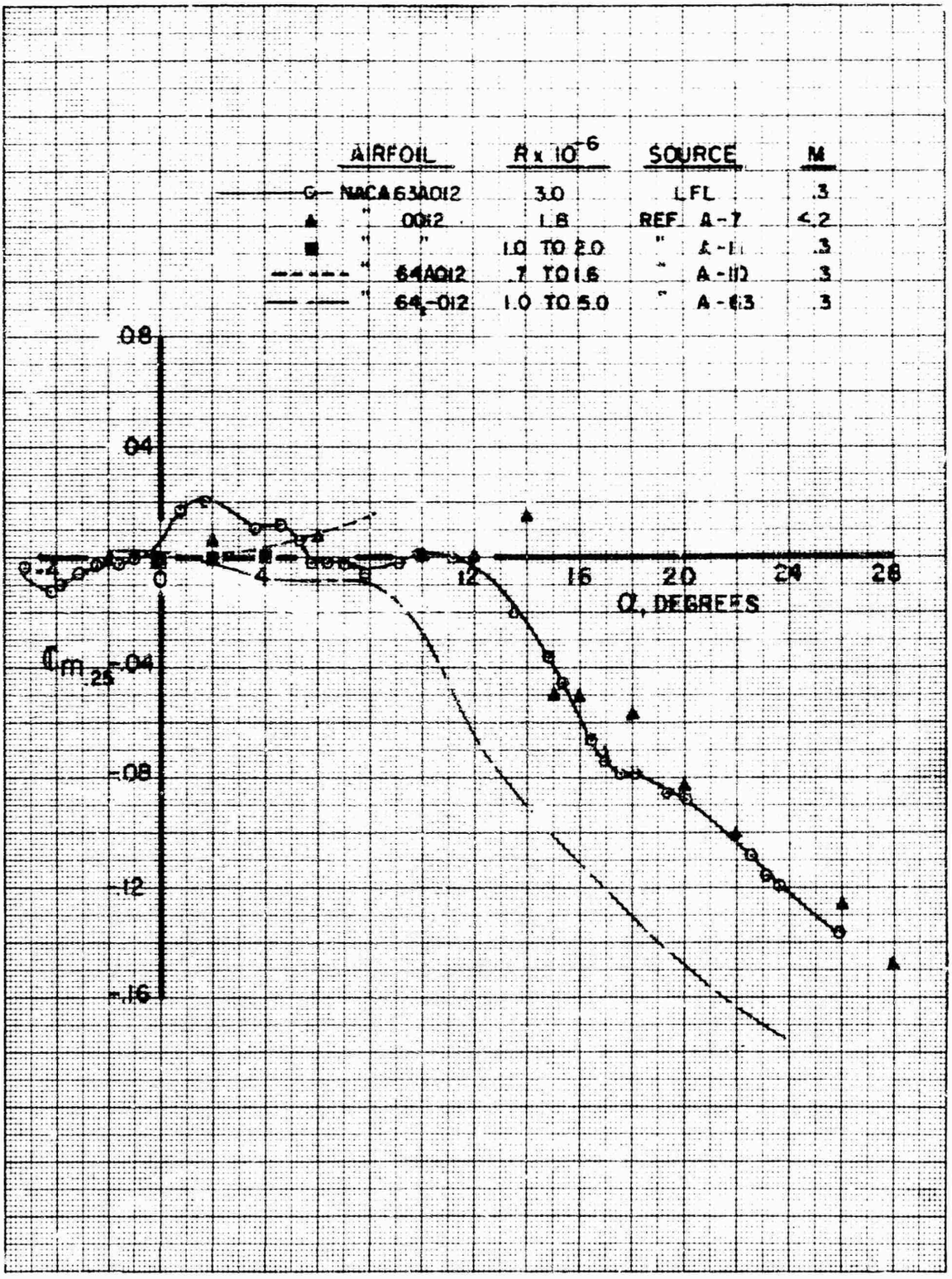


Figure 9J. Comparison Data, Section Pitching Moment Coefficient in Forward Flow Region - 12-Percent Sections

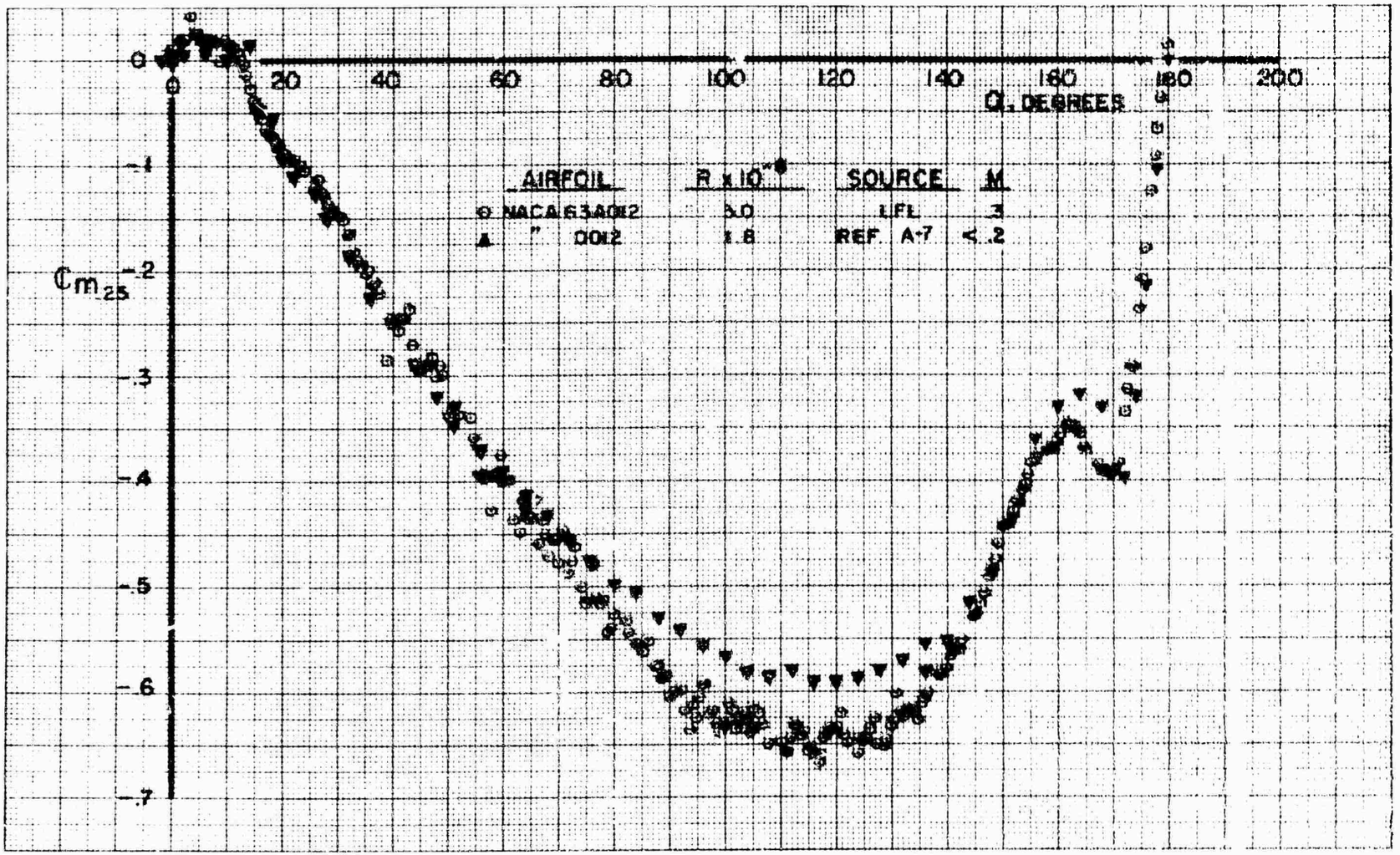


Figure 9K. Comparison Data, Section Pitching Moment Coefficient Over 180 Degree Range - 12-Percent Sections

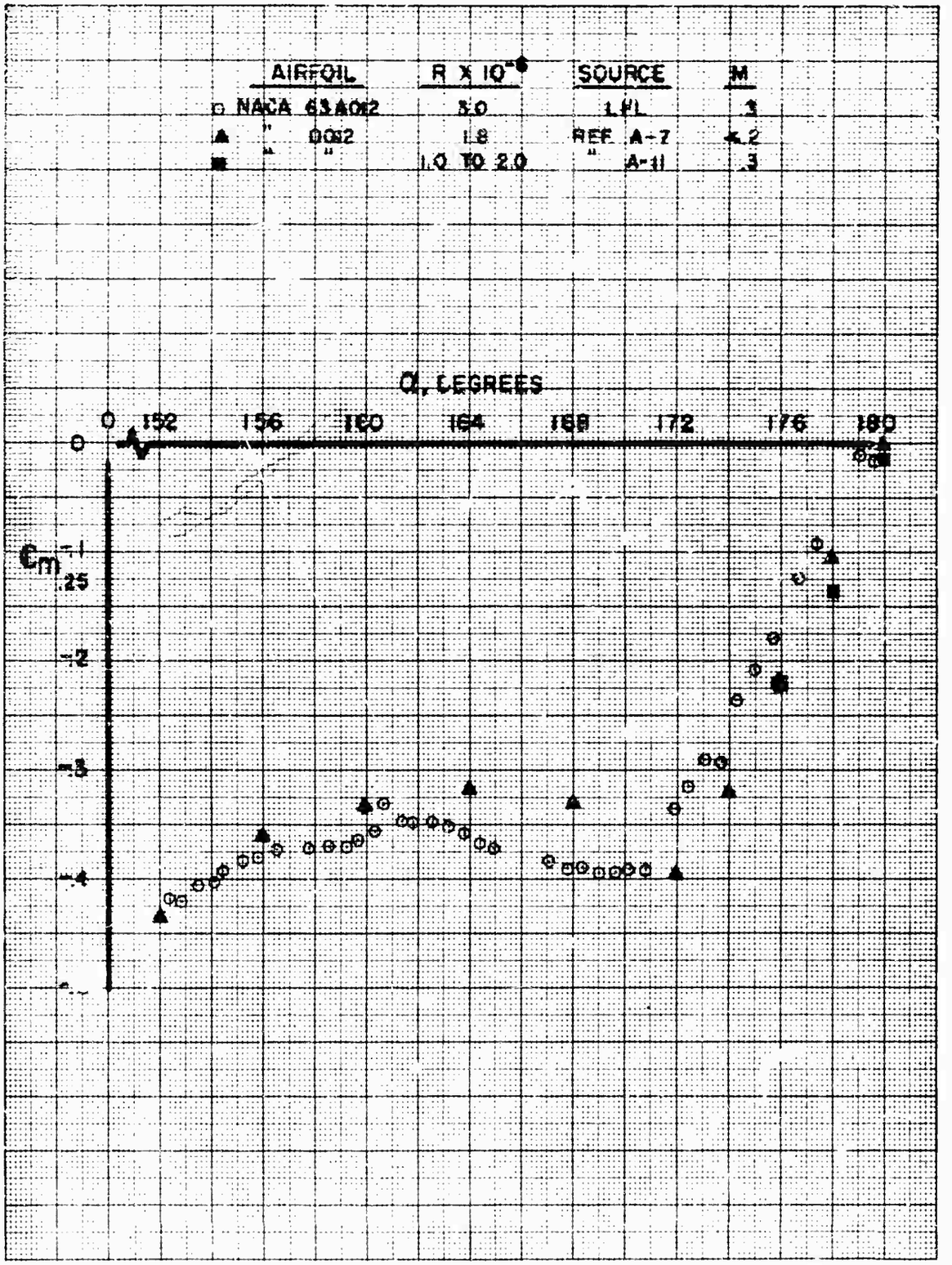


Figure 9L. Comparison Data, Section Pitching Moment Coefficient in Reverse Flow Region - 12-Percent Sections

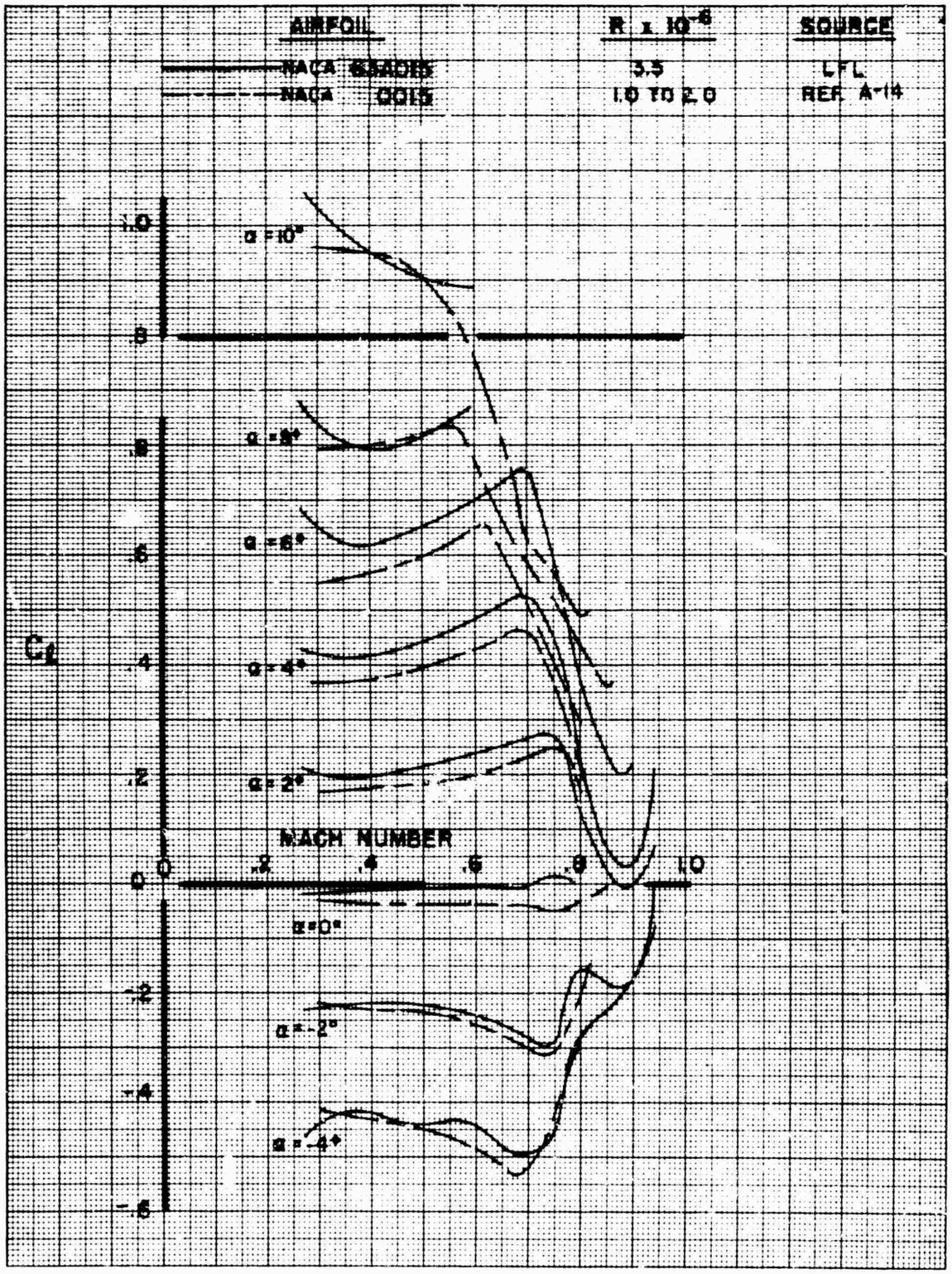


Figure 10A. Comparison Data, Section Lift Coefficient - 15-Percent Sections

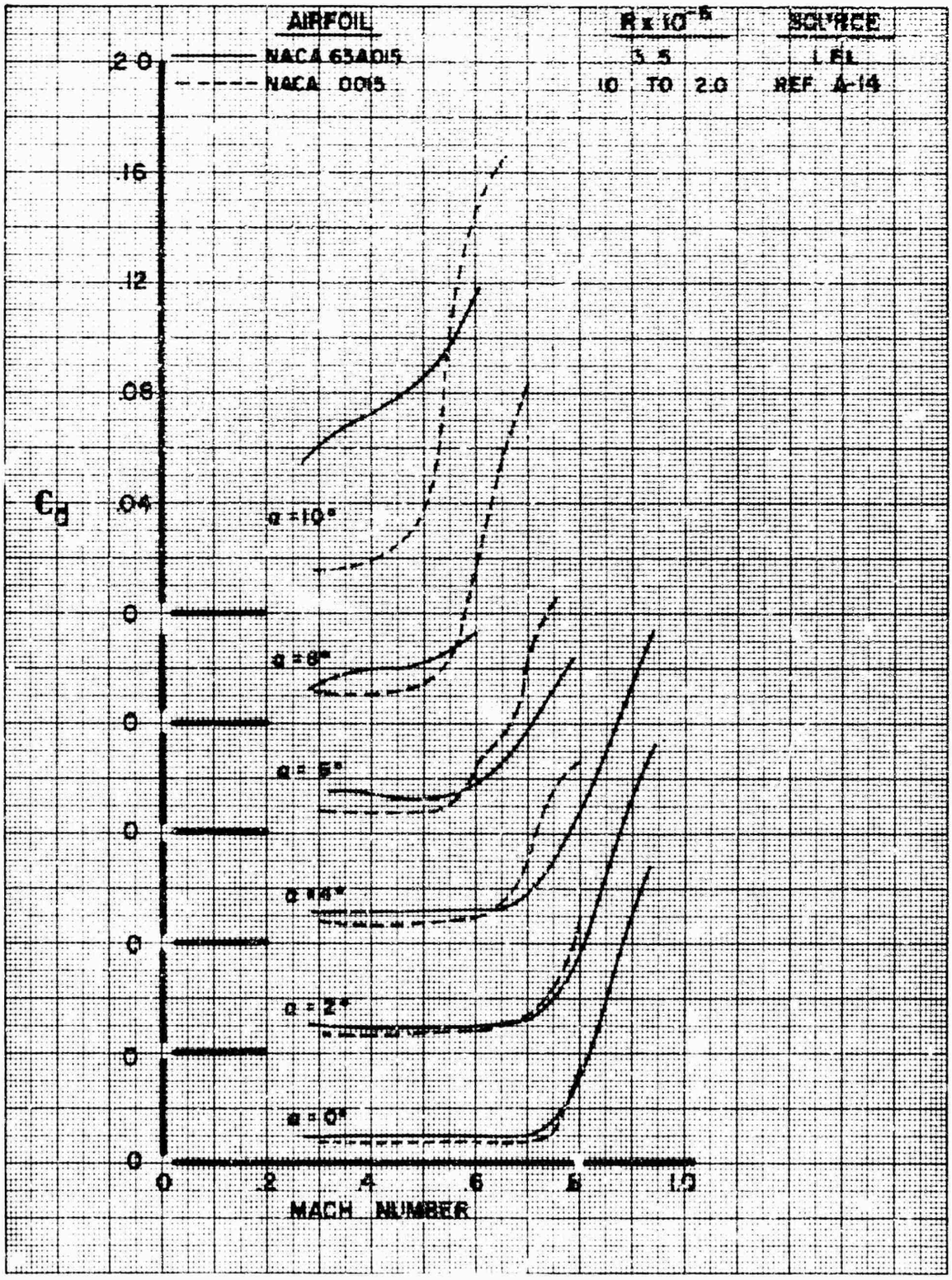


Figure 10B. Comparison Data, Section Drag Coefficient - 15-Percent Sections

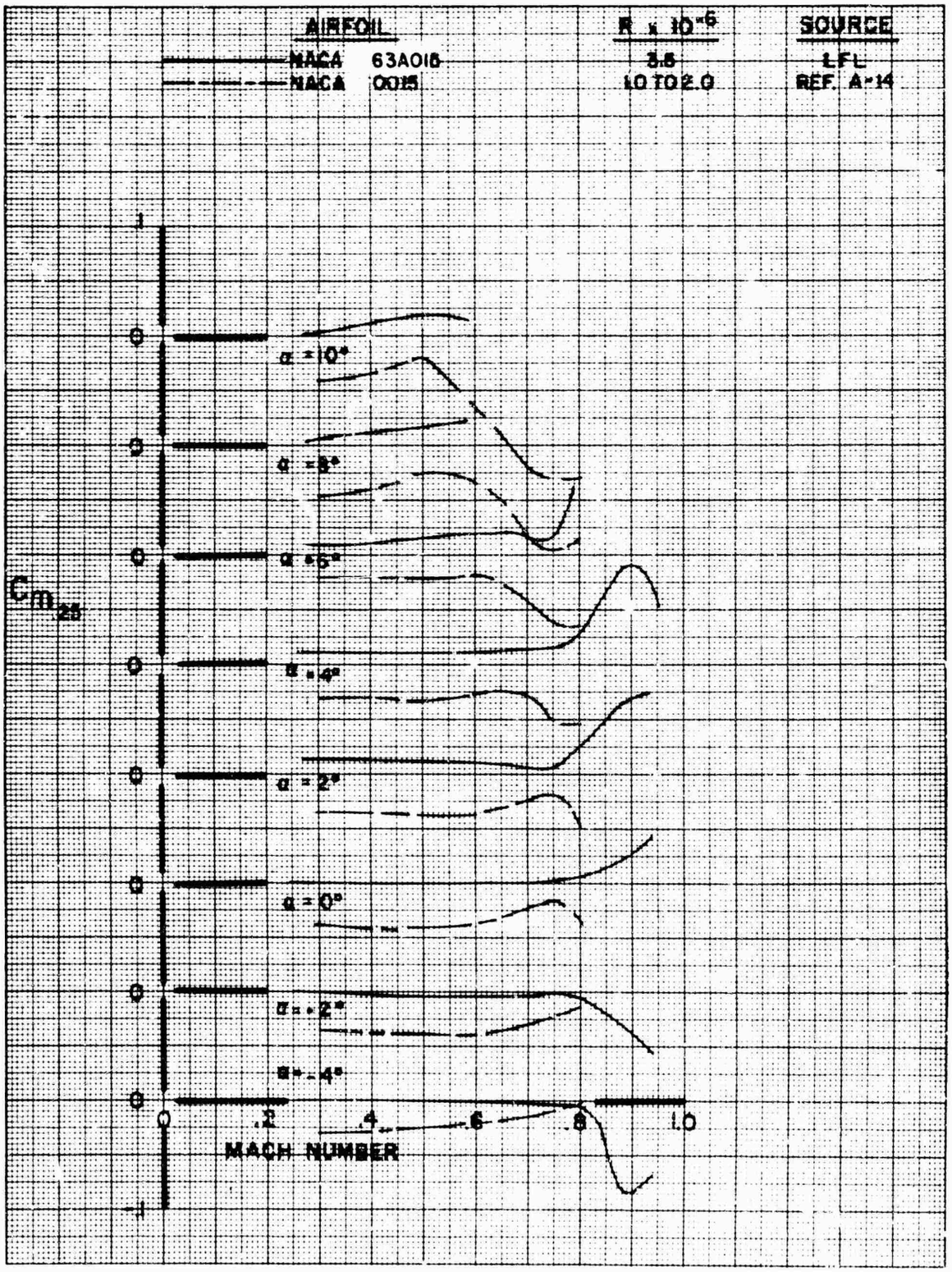


Figure 10C. Comparison Data, Section Pitching Moment Coefficient - 15-Percent Sections

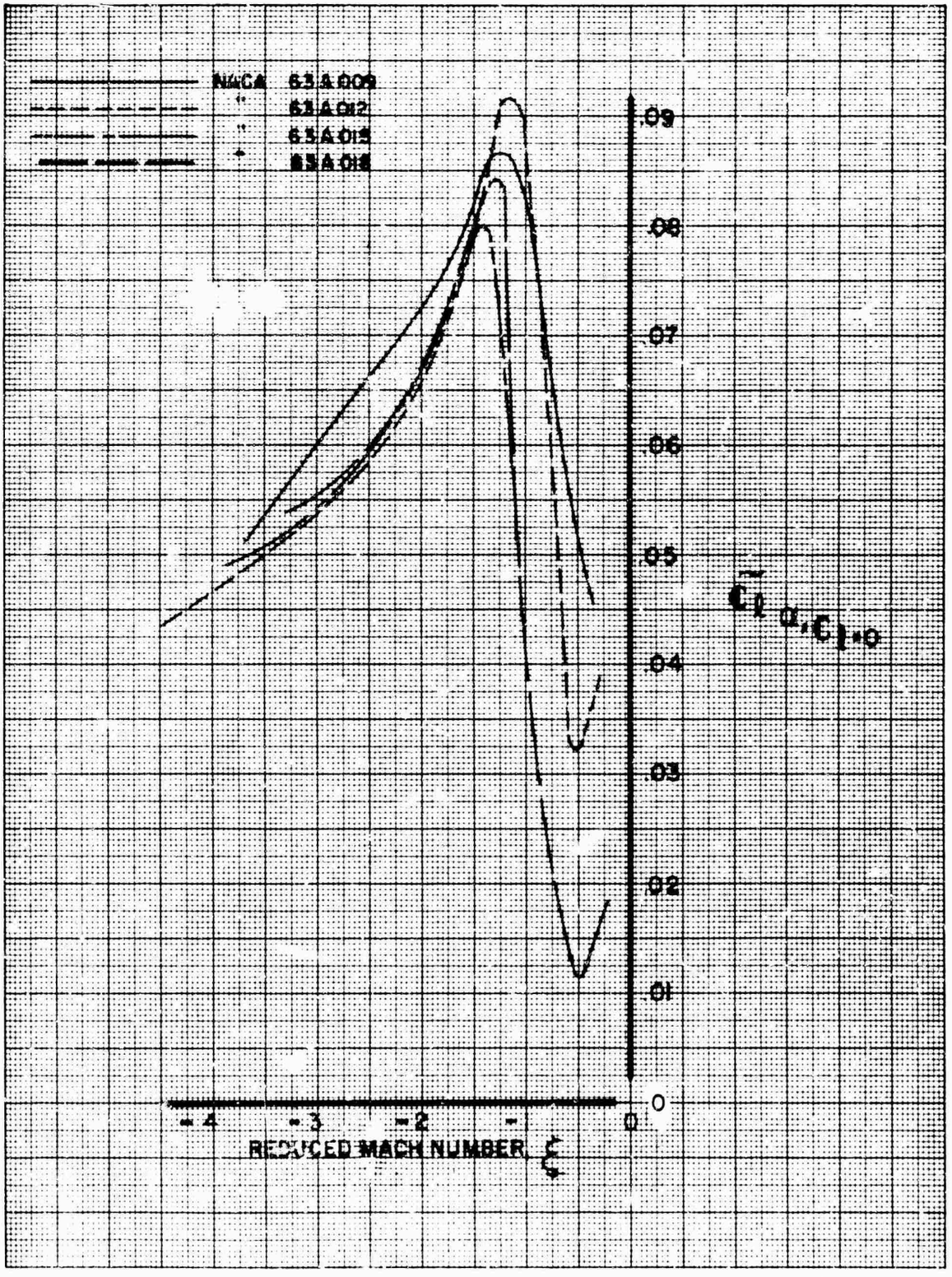


Figure 11A. Correlation of Experimental Data Using Transonic Similarity Rule - Reduced Lift Slope at $C_\ell = 0$

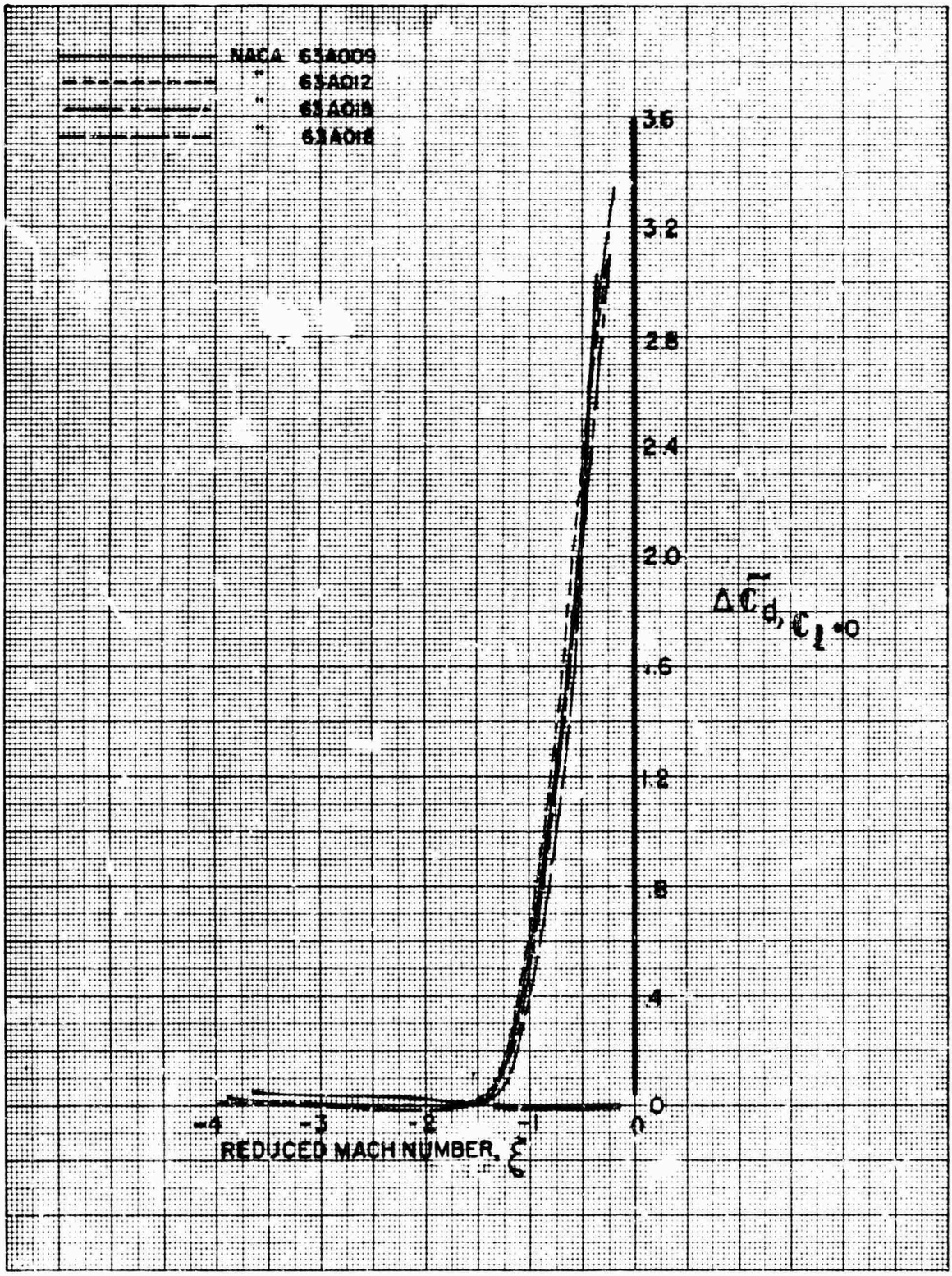


Figure 11B. Correlation of Experimental Data Using Transonic Similarity Rule - Reduced Drag Coefficient Increment at $C_l = 0$

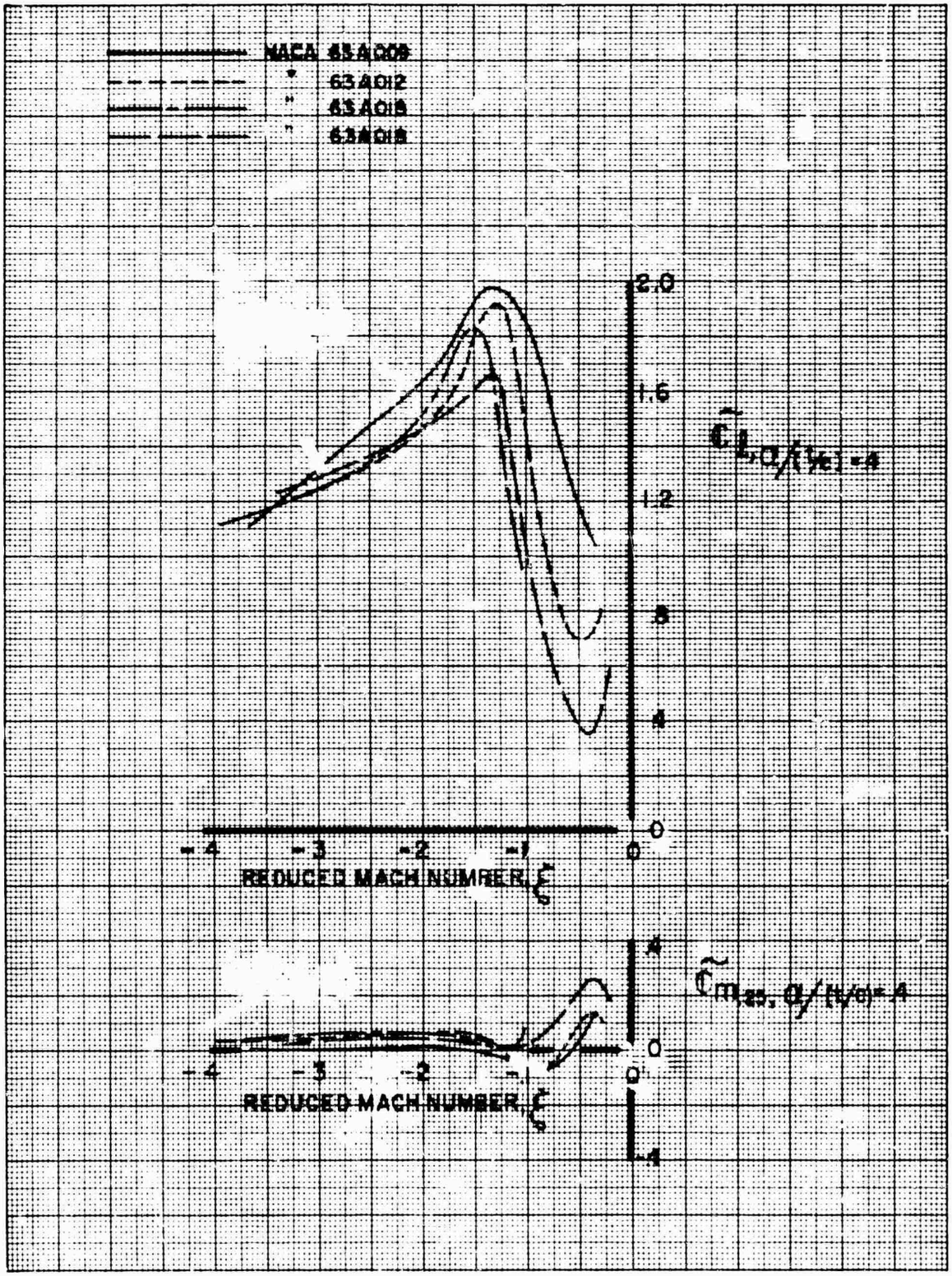


Figure 11C. Correlation of Experimental Data Using Transonic Similarity Rule - Reduced Lift Coefficient and Reduced Moment Coefficient at $\alpha/(t/c) = .4$

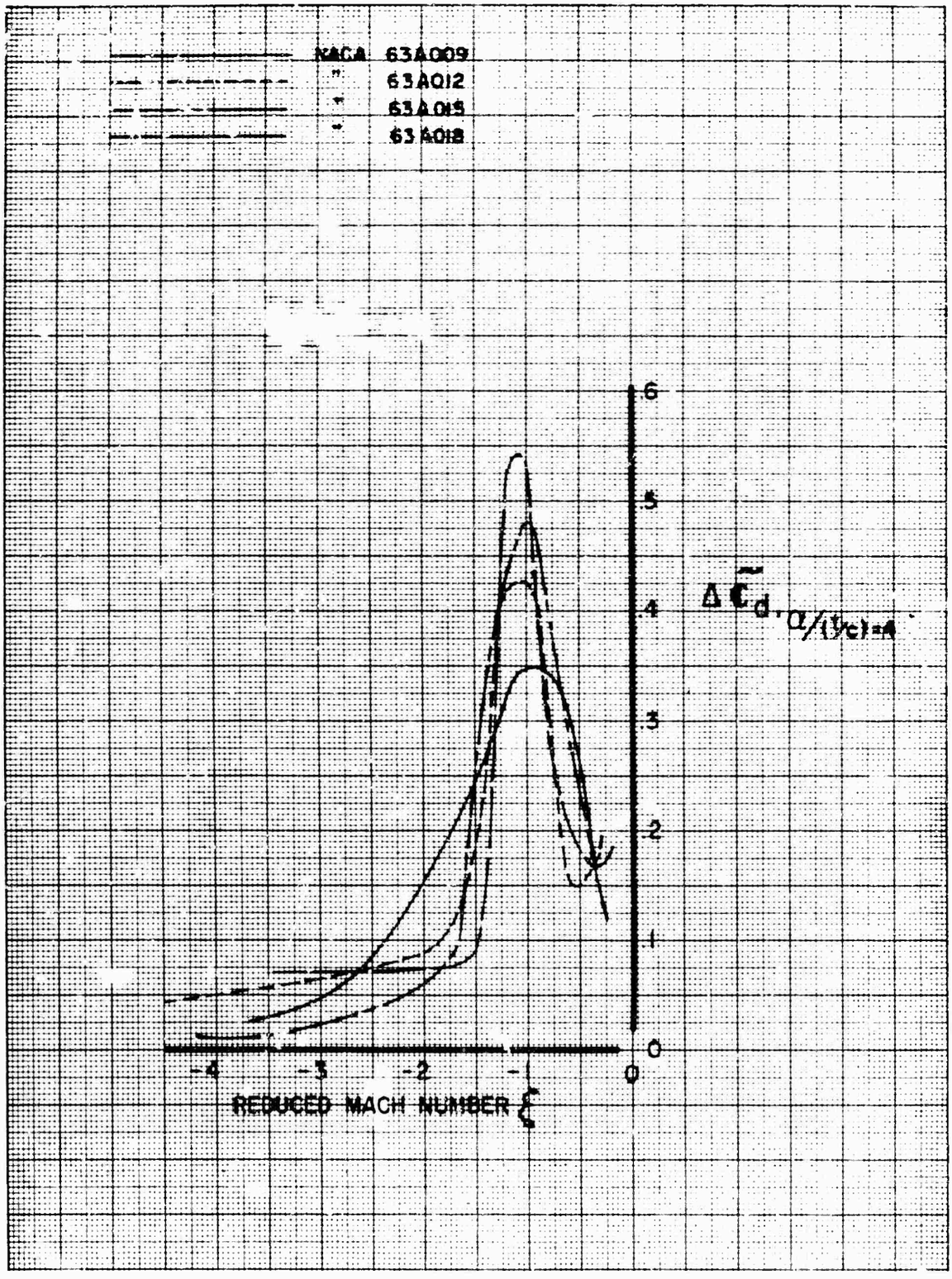


Figure 11D. Correlation of Experimental Data Using Transonic Similarity Rule - Reduced Drag Coefficient Increment at $\alpha/(t/c) = .4$

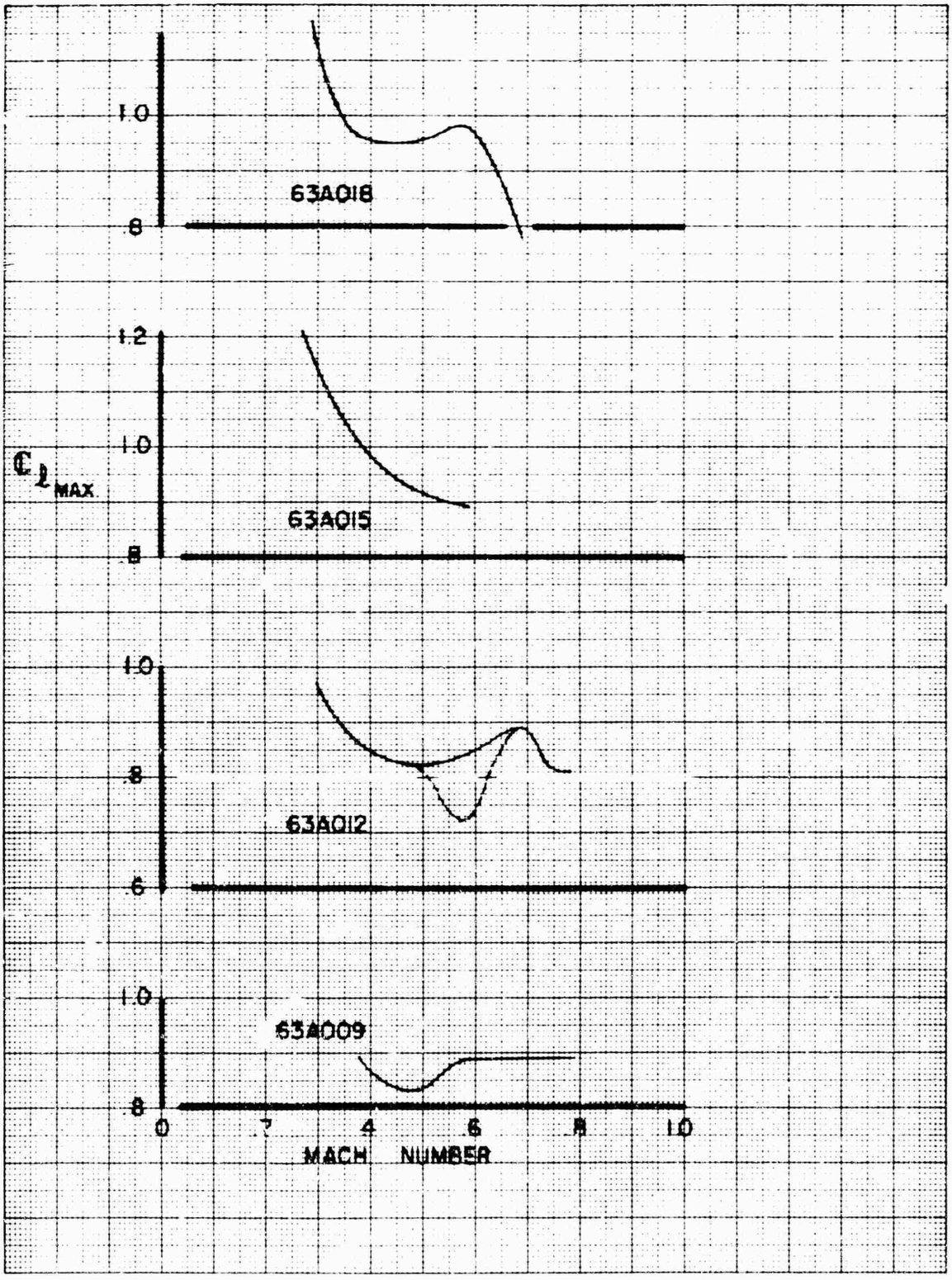


Figure 12A. Variation of Section Maximum Lift Coefficient With Mach Number - R = 3.5×10^6

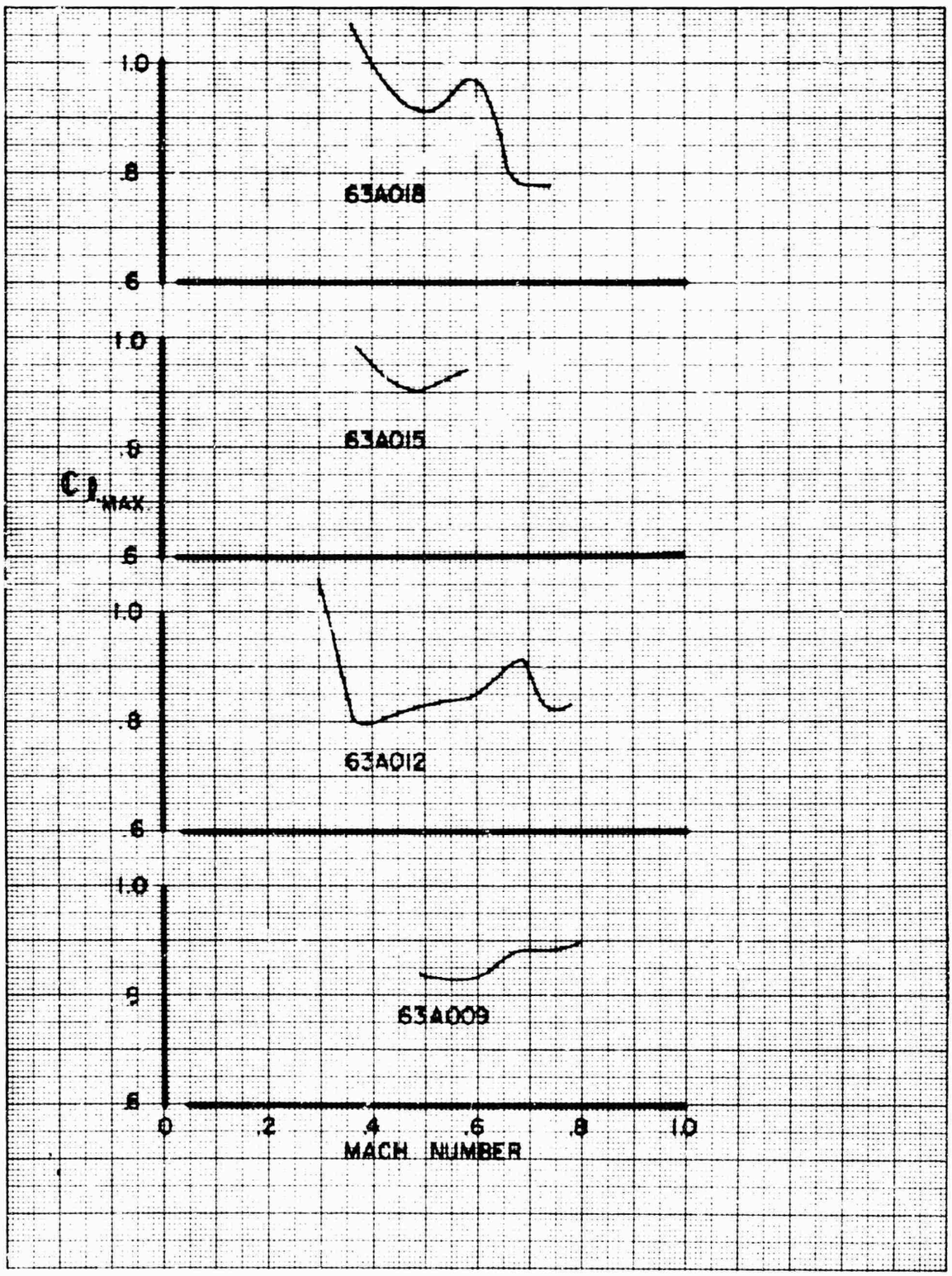


Figure 12B. Variation of Section Maximum Lift Coefficient With Mach Number - $R = 5.0 \times 10^6$

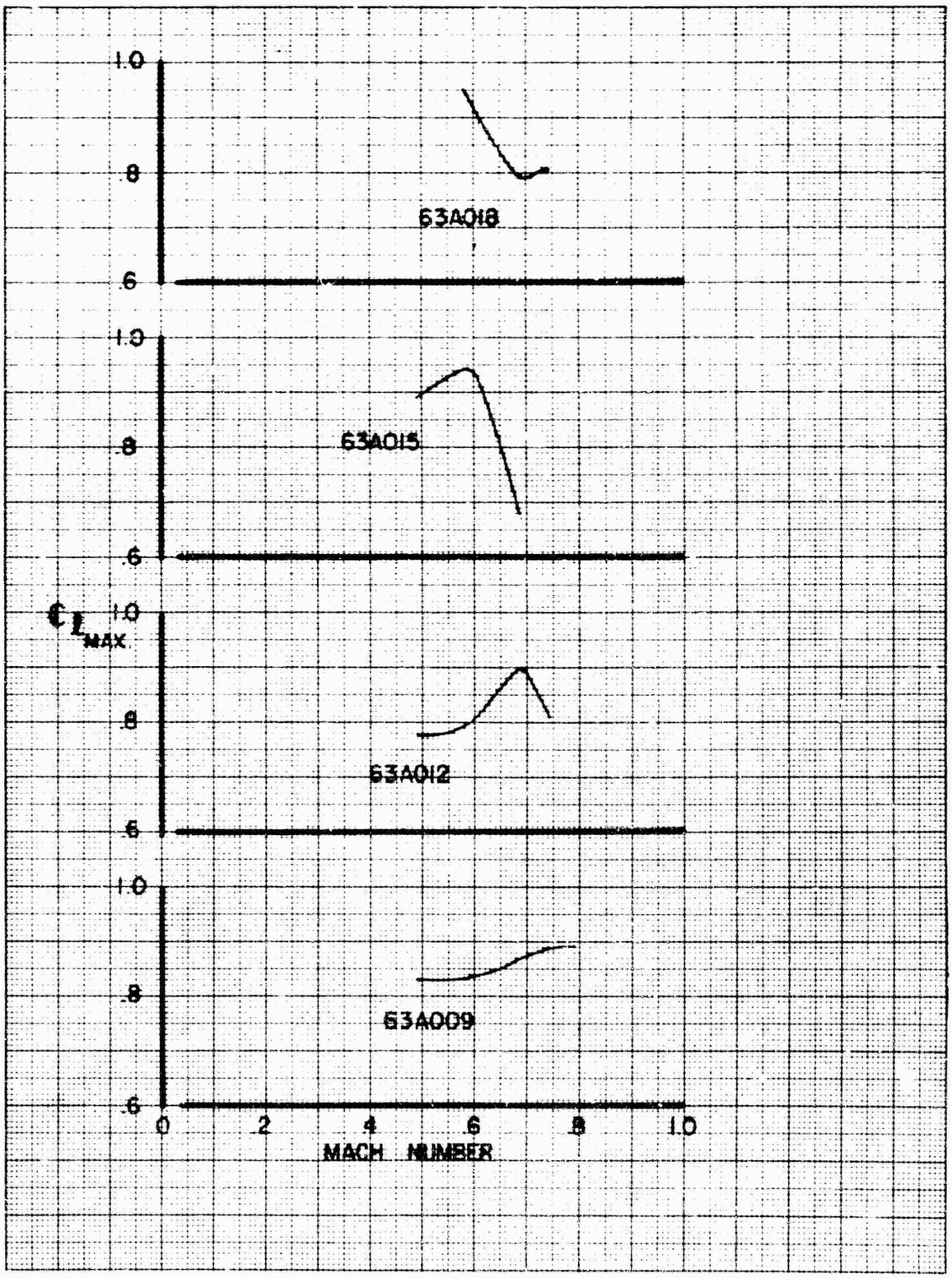


Figure 12C. Variation of Section Maximum Lift Coefficient With Mach Number - $R = 6.5 \times 10^6$

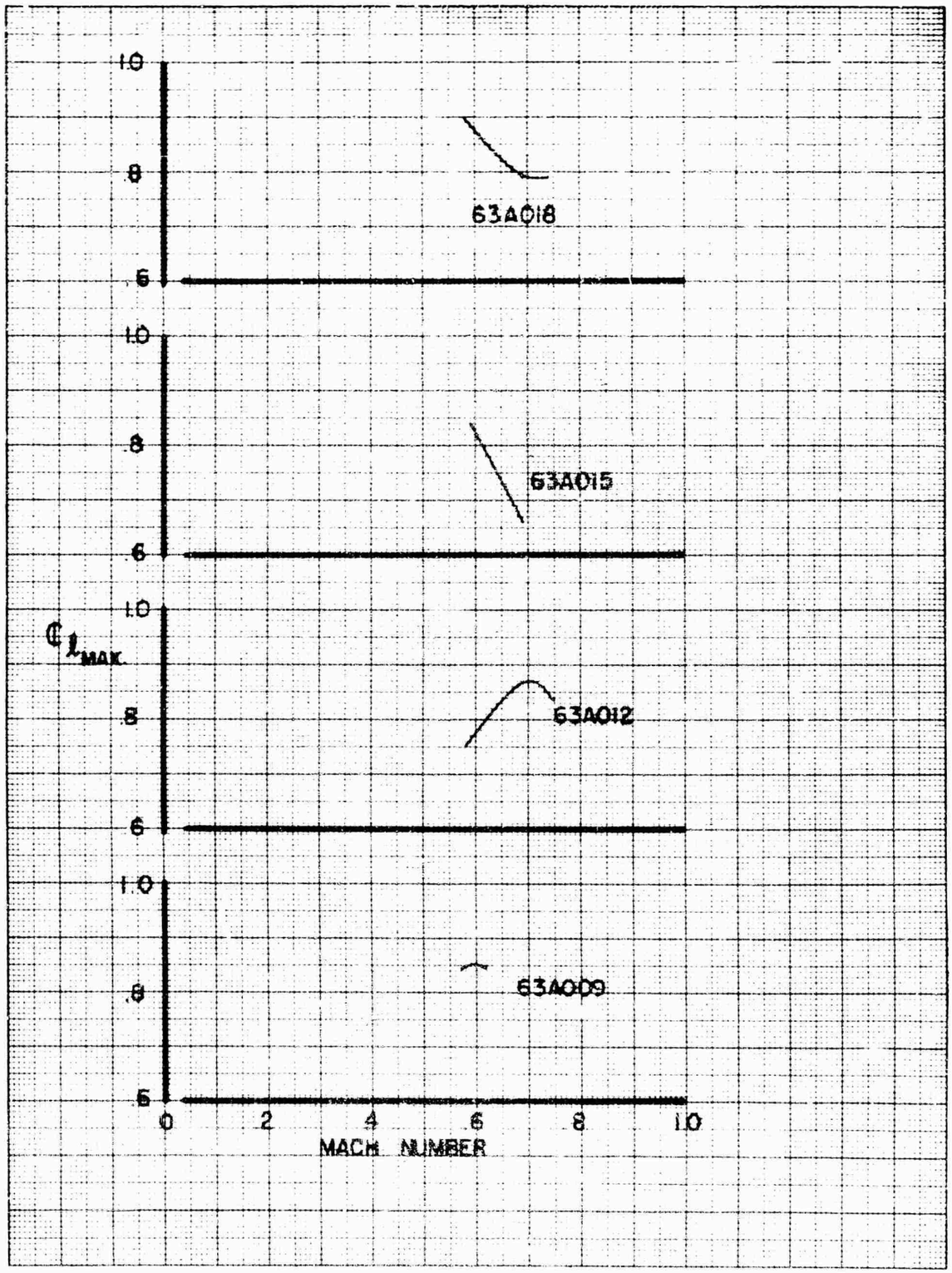


Figure 12D. Variation of Section Maximum Lift Coefficient With Mach Number - R = 8.0 x 10^6

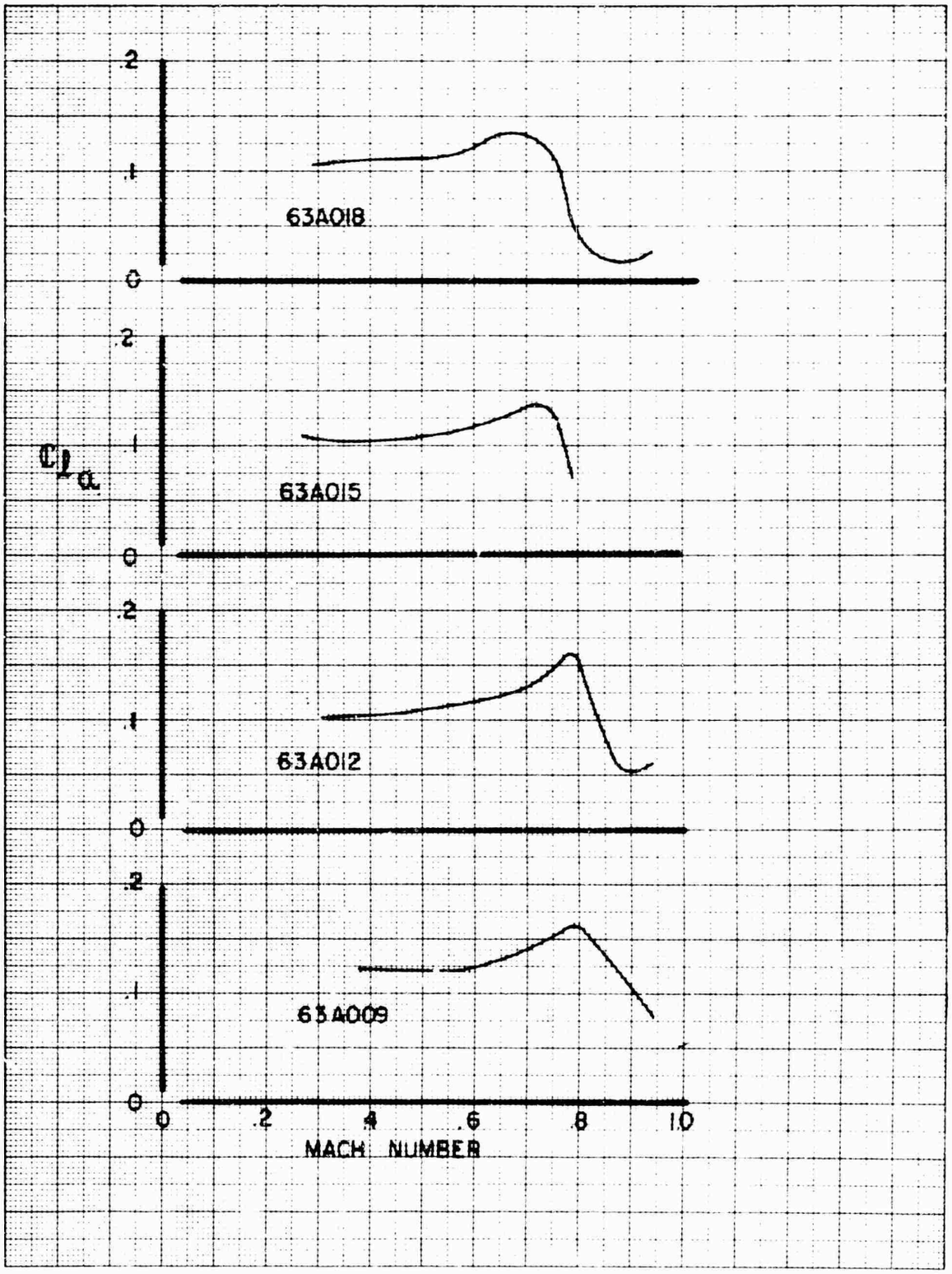


Figure 13A. Variation of Lift-Curve Slope at $C_l = 0$ With Mach Number - $R = 3.5 \times 10^6$

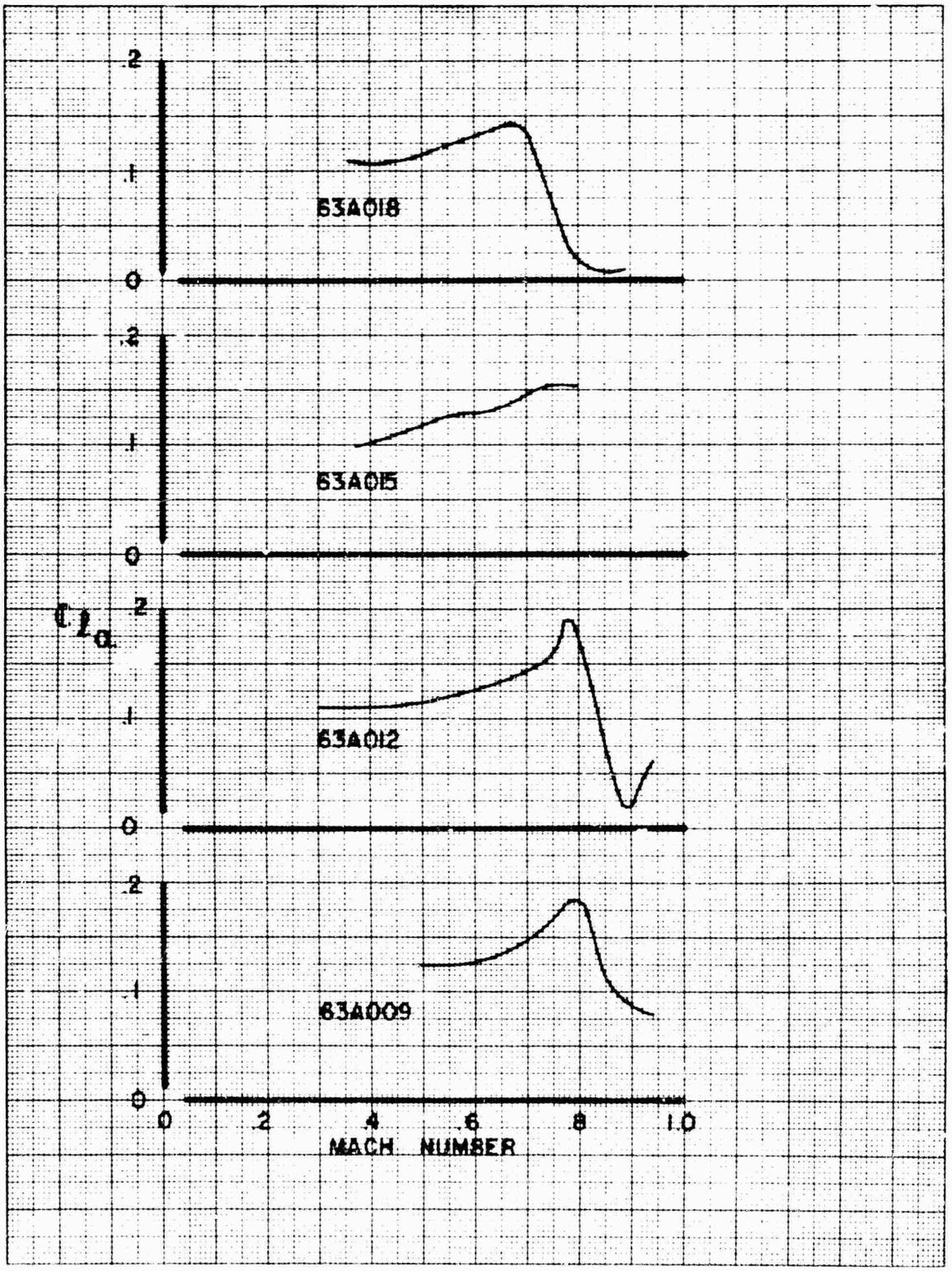


Figure 13B. Variation of Lift-Curve Slope at $C_l = 0$ With Mach Number - $R = 5.0 \times 10^6$

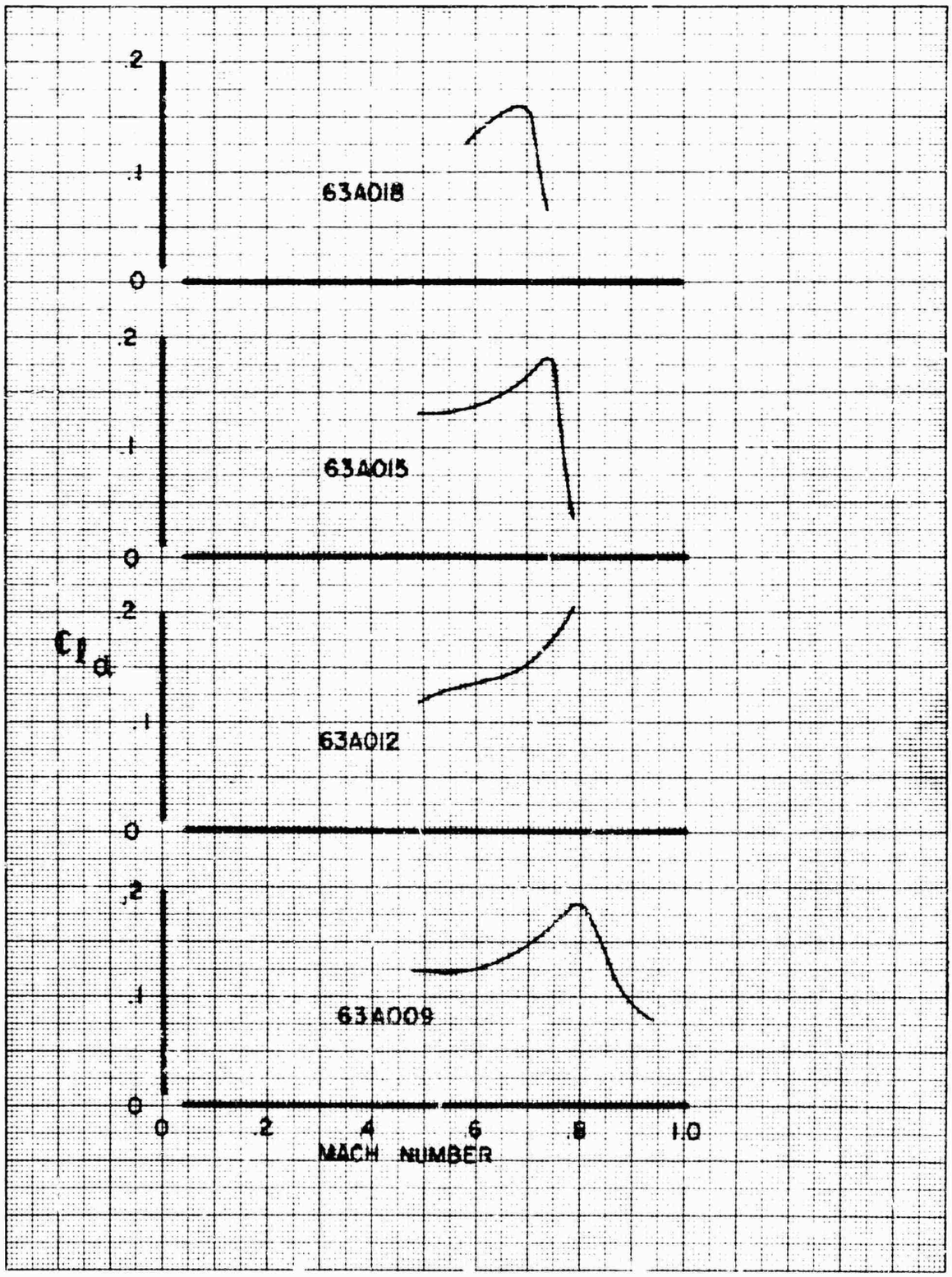


Figure 13C. Variation of Lift-Curve Slope at $C_l = 0$ With Mach Number - $R = 6.5 \times 10^6$

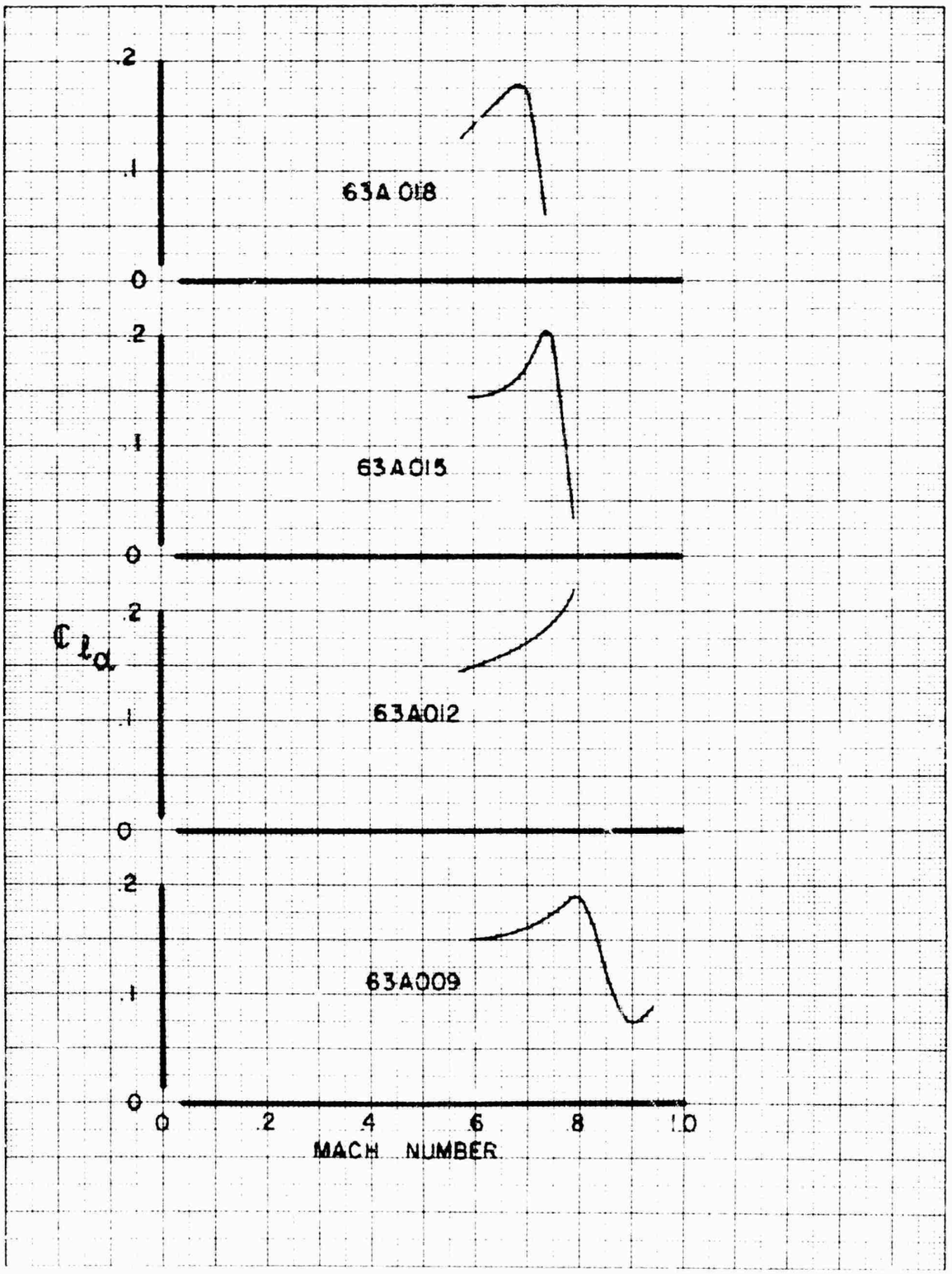


Figure 13D. Variation of Lift-Curve Slope at $C_l = 0$ With Mach Number - $R = 8.0 \times 10^6$

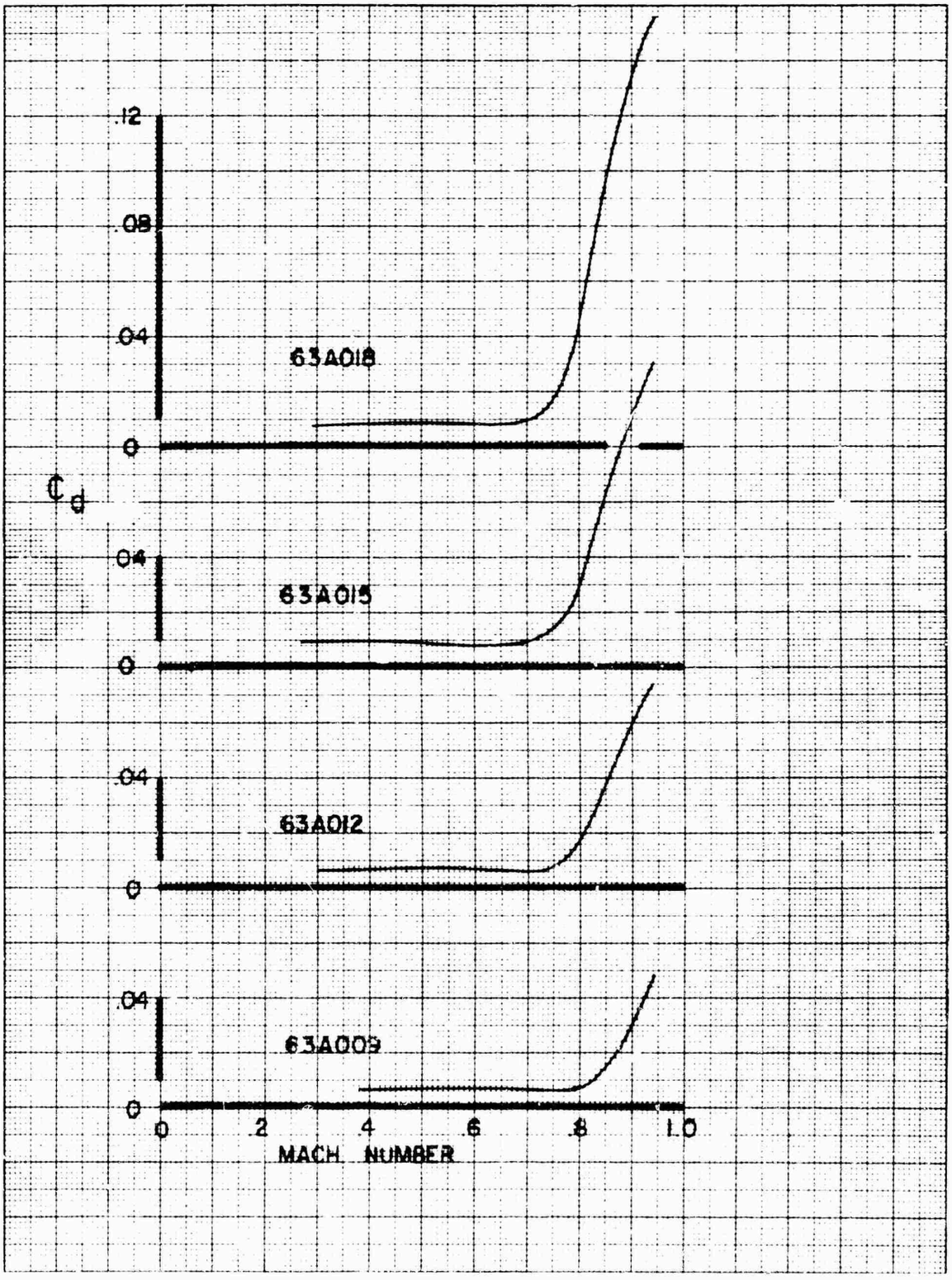


Figure 14A. Variation of Section Drag Coefficient at $\alpha = 0$ With Mach Number - $R = 3.5 \times 10^6$

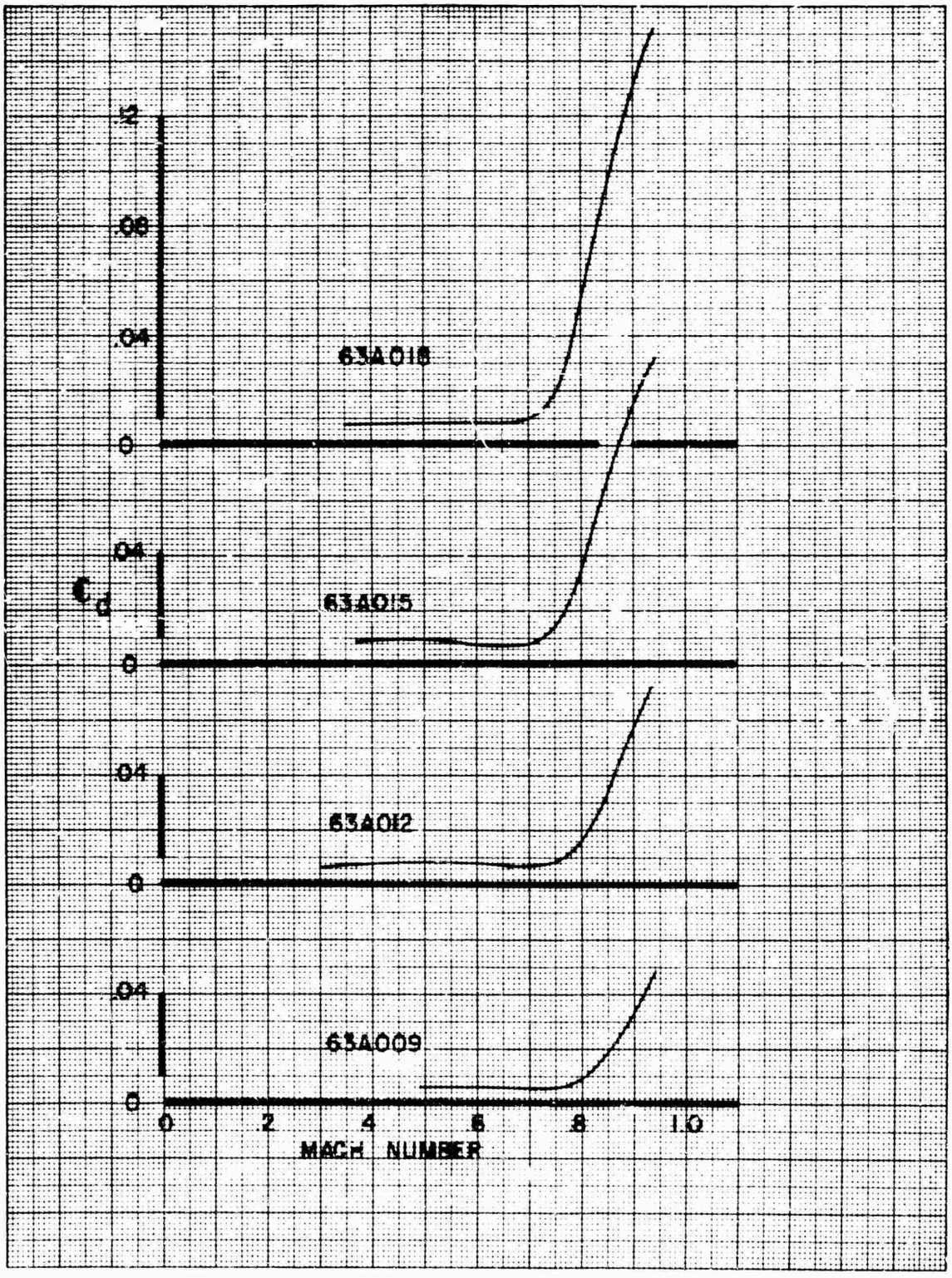


Figure 14B. Variation of Section Drag Coefficient at $\alpha = 0$ With Mach Number - $R = 5.0 \times 10^6$

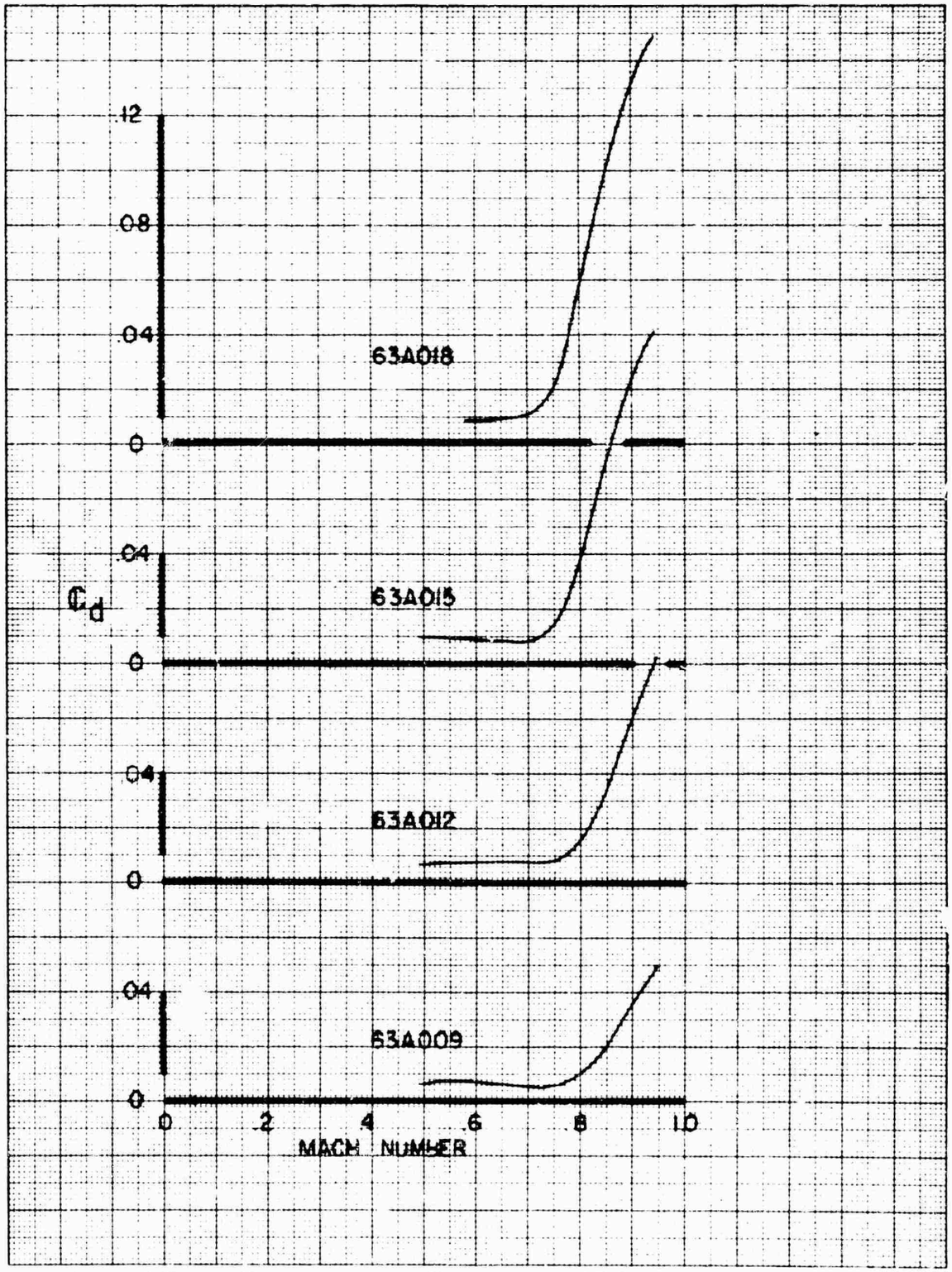


Figure 14C. Variation of Section Drag Coefficient at $\alpha = 0$ With Mach Number - $R = 6.5 \times 10^6$

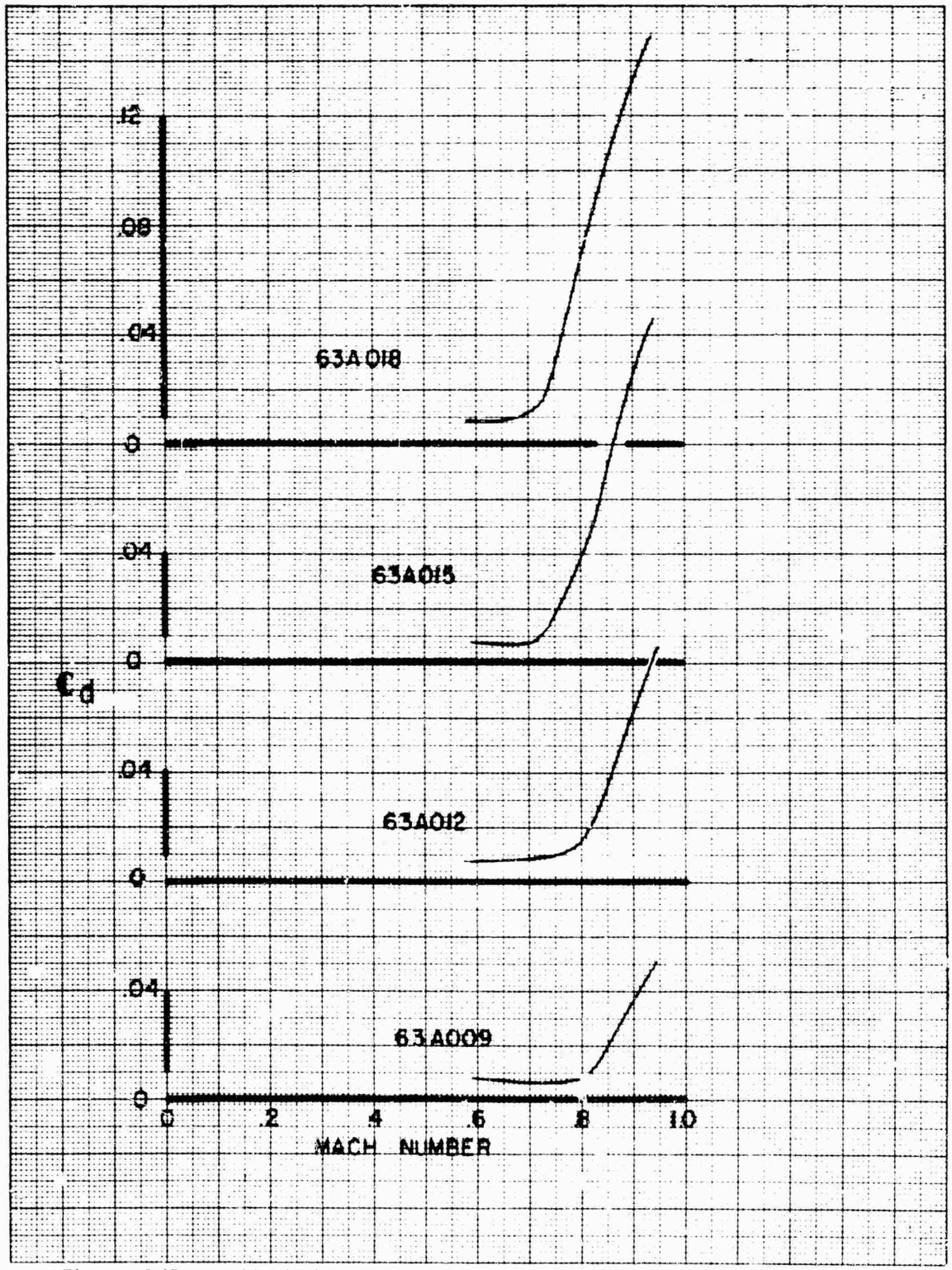


Figure 14D. Variation of Section Drag Coefficient at $\alpha = 0$ With Mach Number - $P = 8.0 \times 10^6$

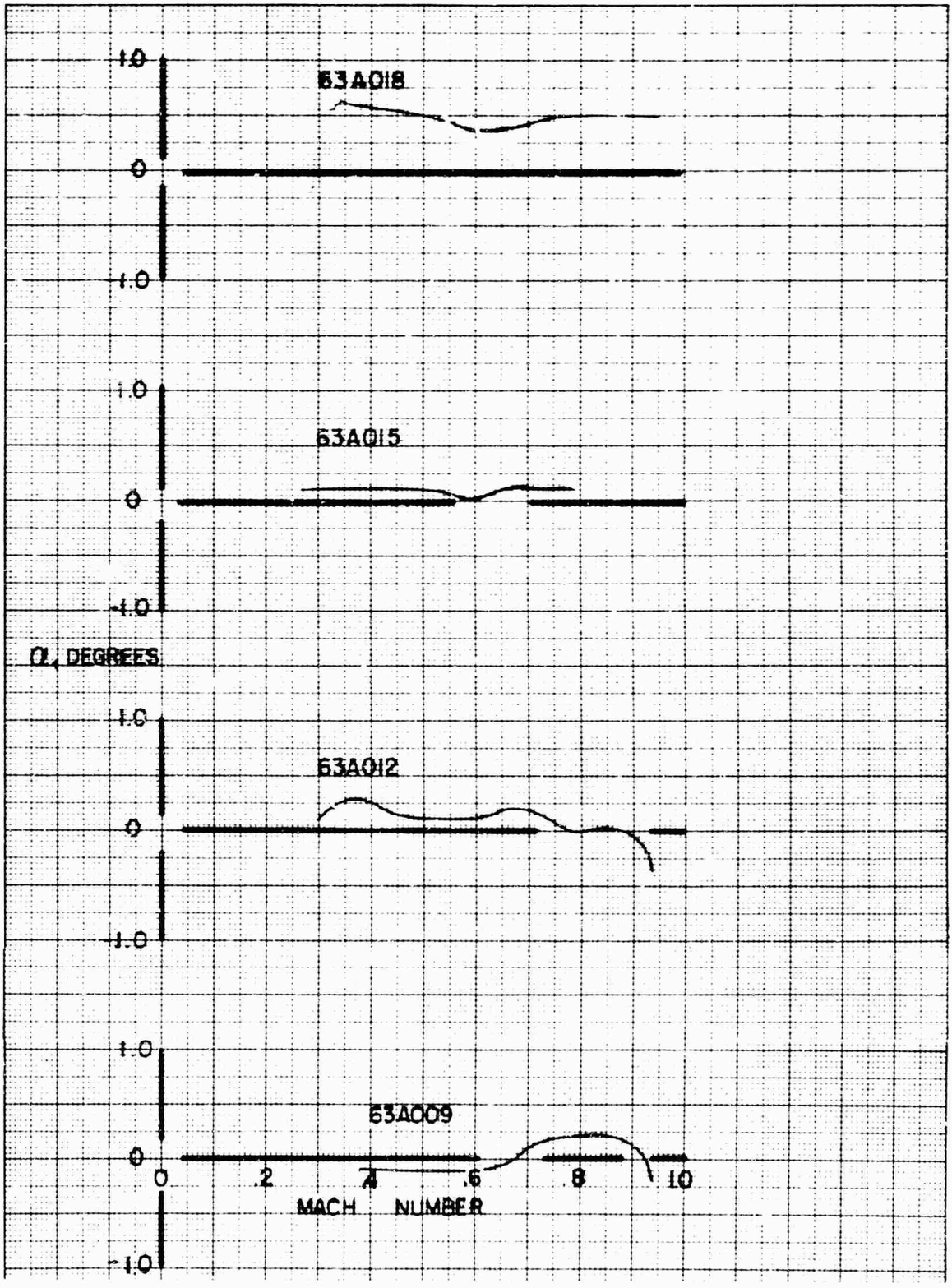


Figure 15A. Variation of Angle of Attack at $C_\ell = 0$ With Mach Number, $R = 3.5 \times 10^6$

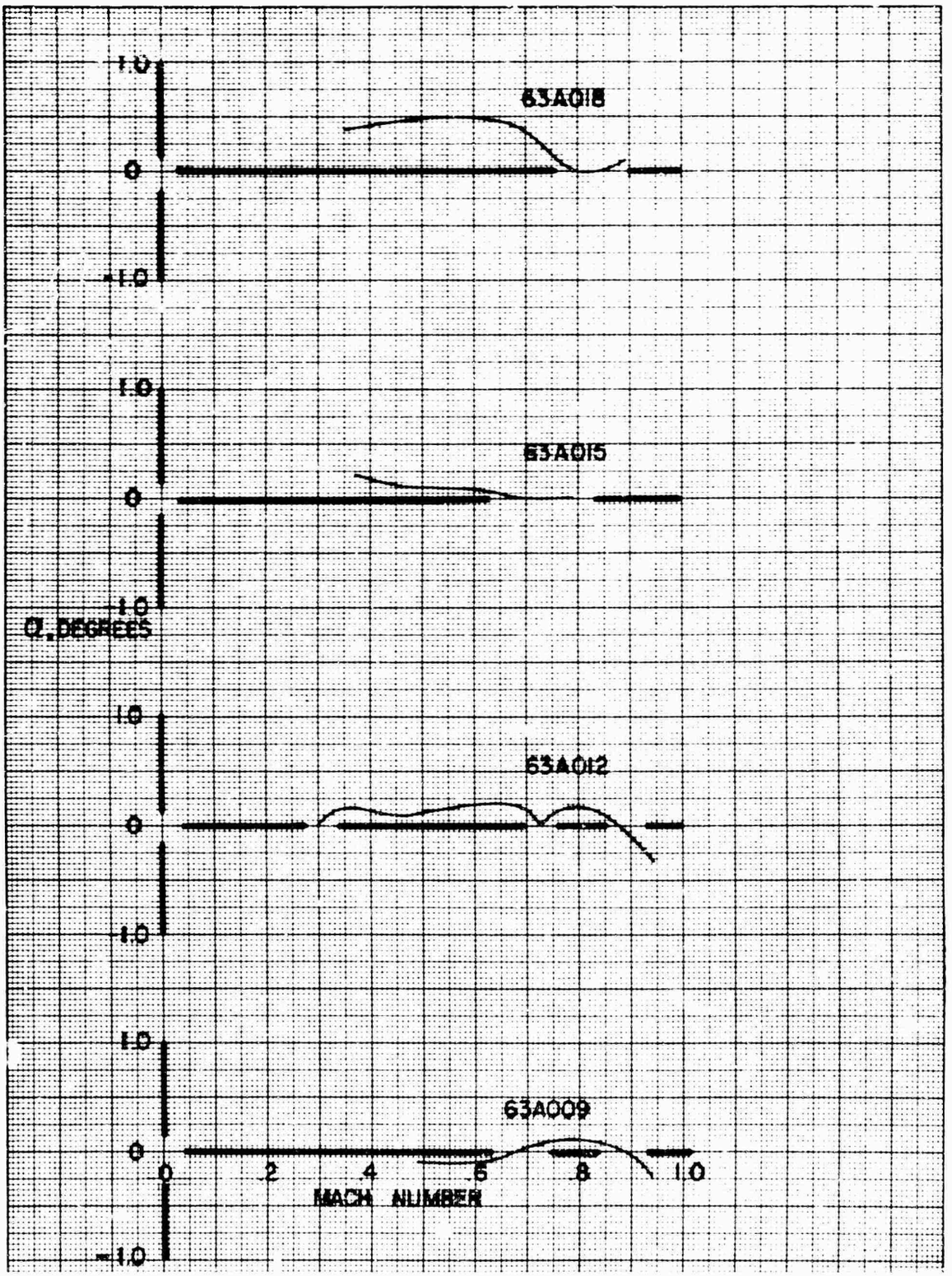


Figure 15B. Variation of Angle of Attack at $C_\ell = 0$ With Mach Number, $R = 5.0 \times 10^6$

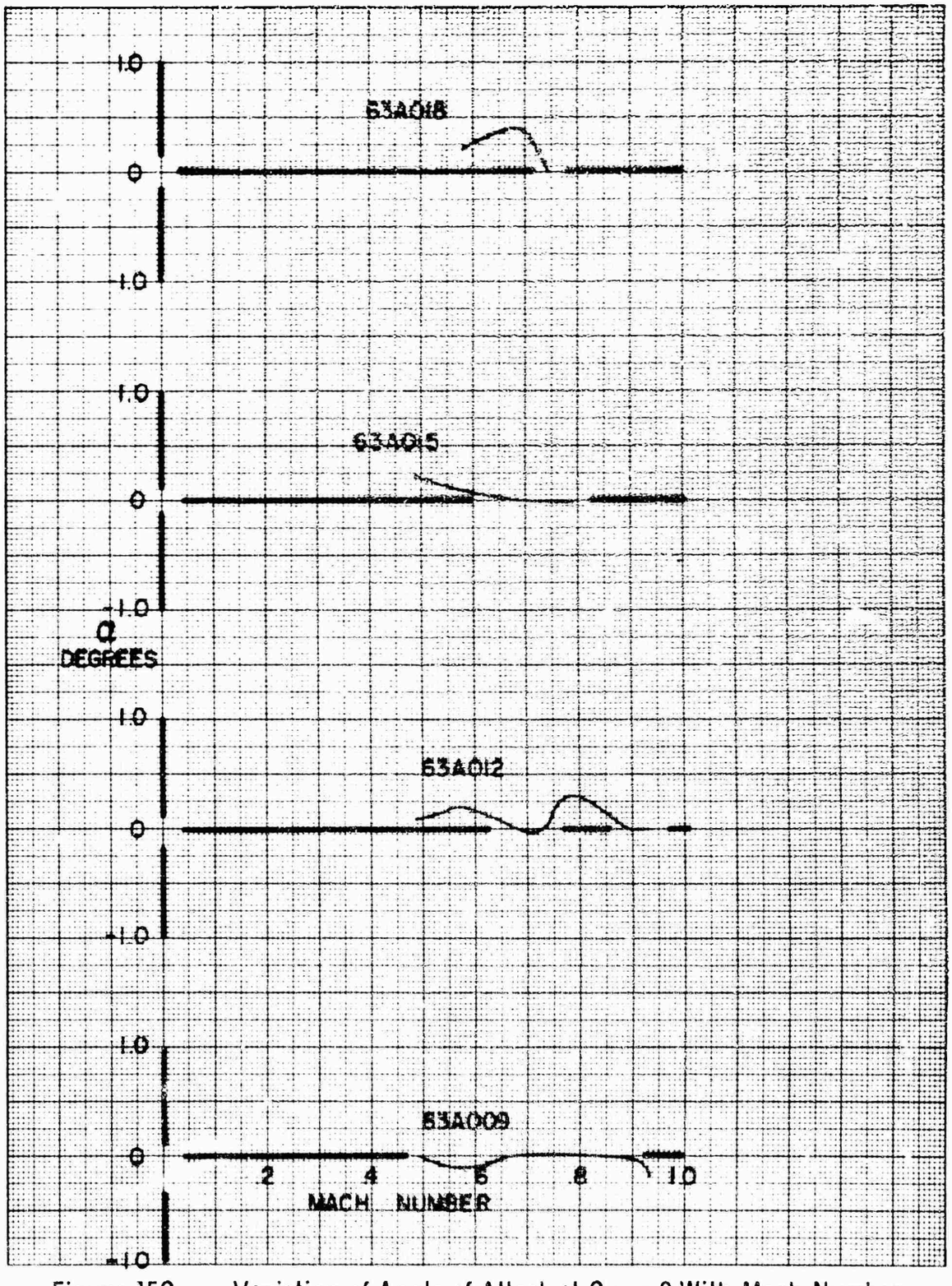


Figure 15C. Variation of Angle of Attack at C_l = 0 With Mach Number - R = 6.5 x 10^6

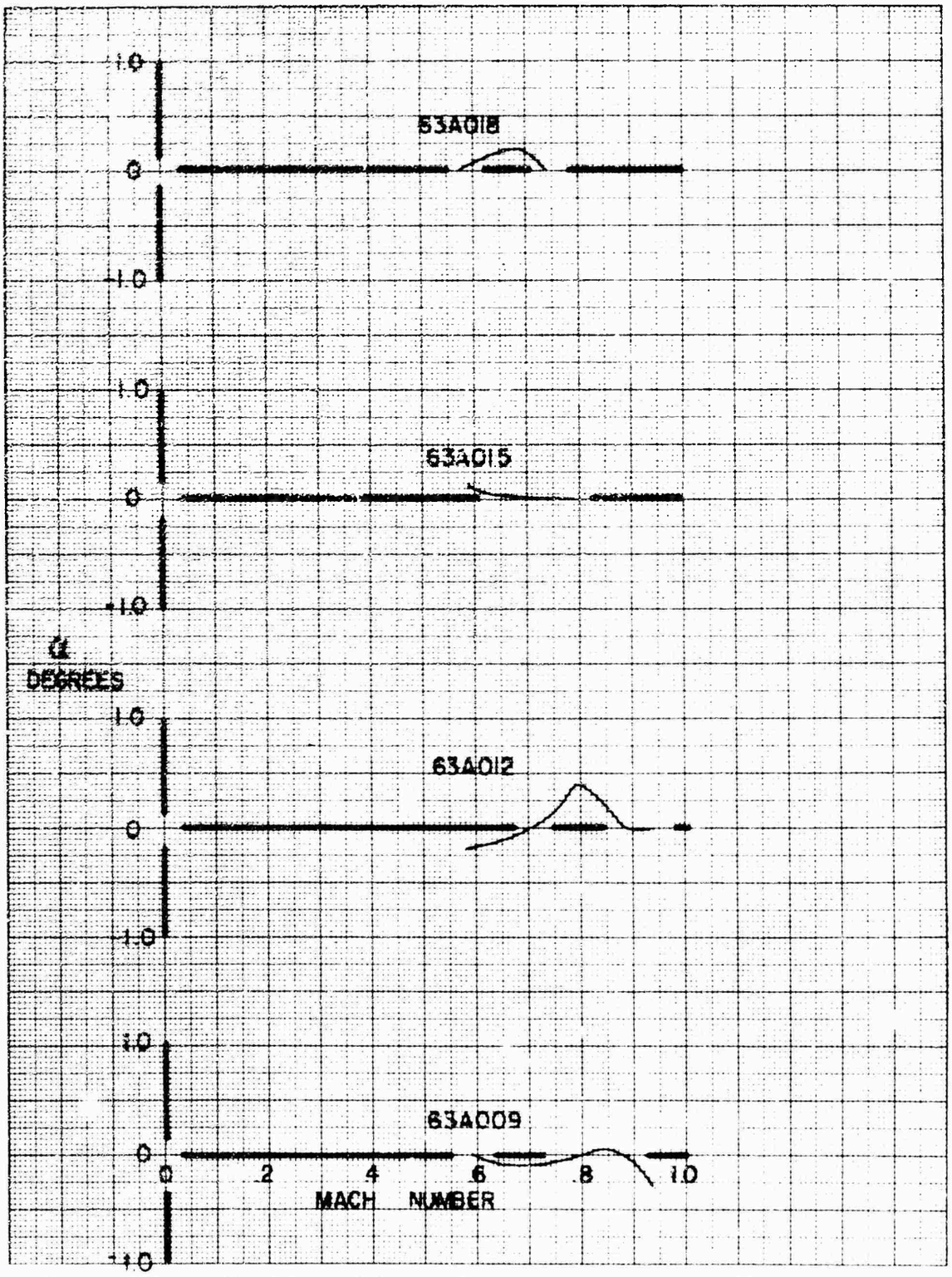


Figure 15D. Variation of Angle of Attack at $C_\ell = 0$ With Mach Number - R = 8.0 x 10^6

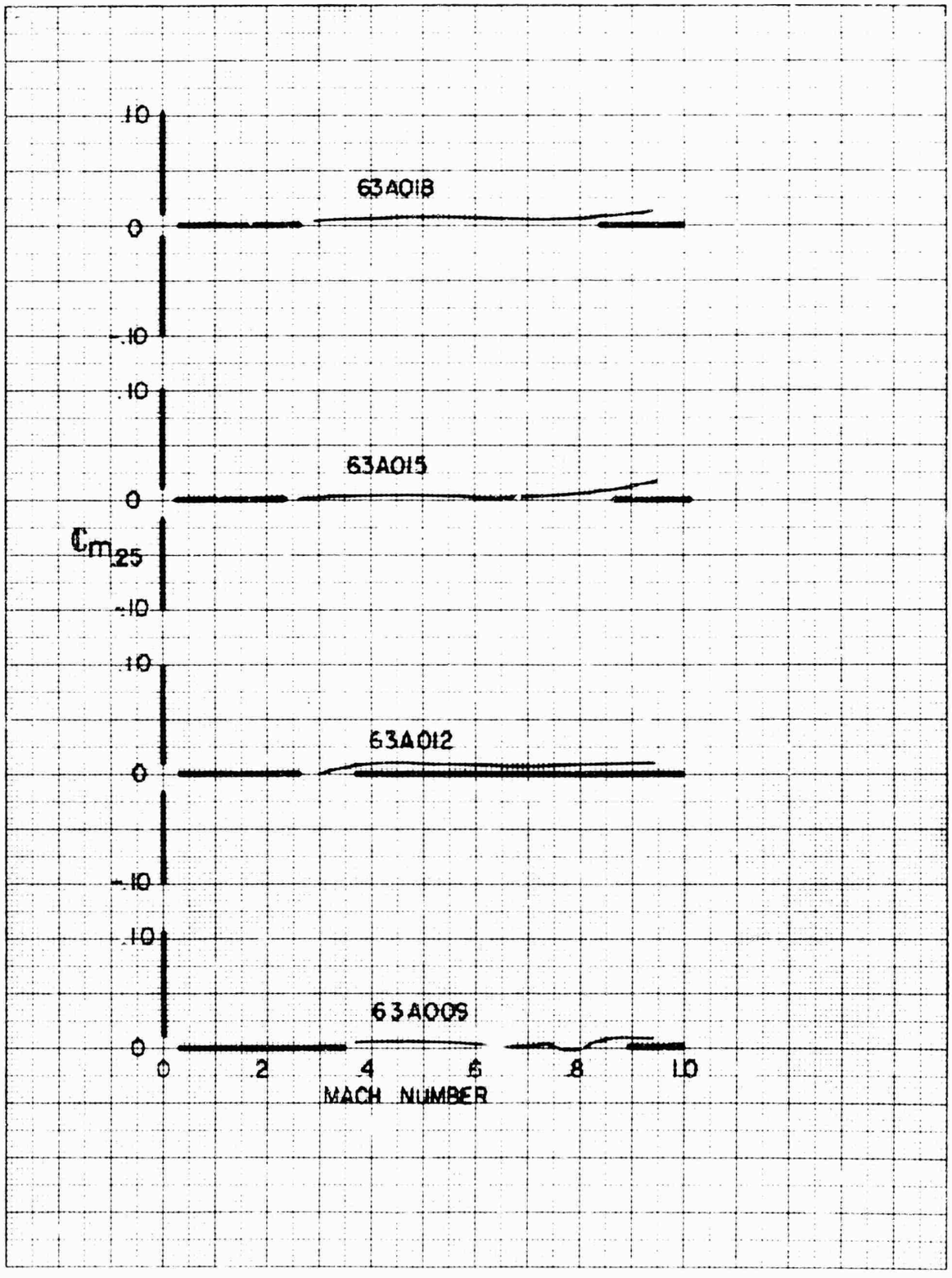


Figure 16A. Variation of Section Pitching Moment Coefficient at $\alpha = 0$ With Mach Number - R = 3.5×10^6

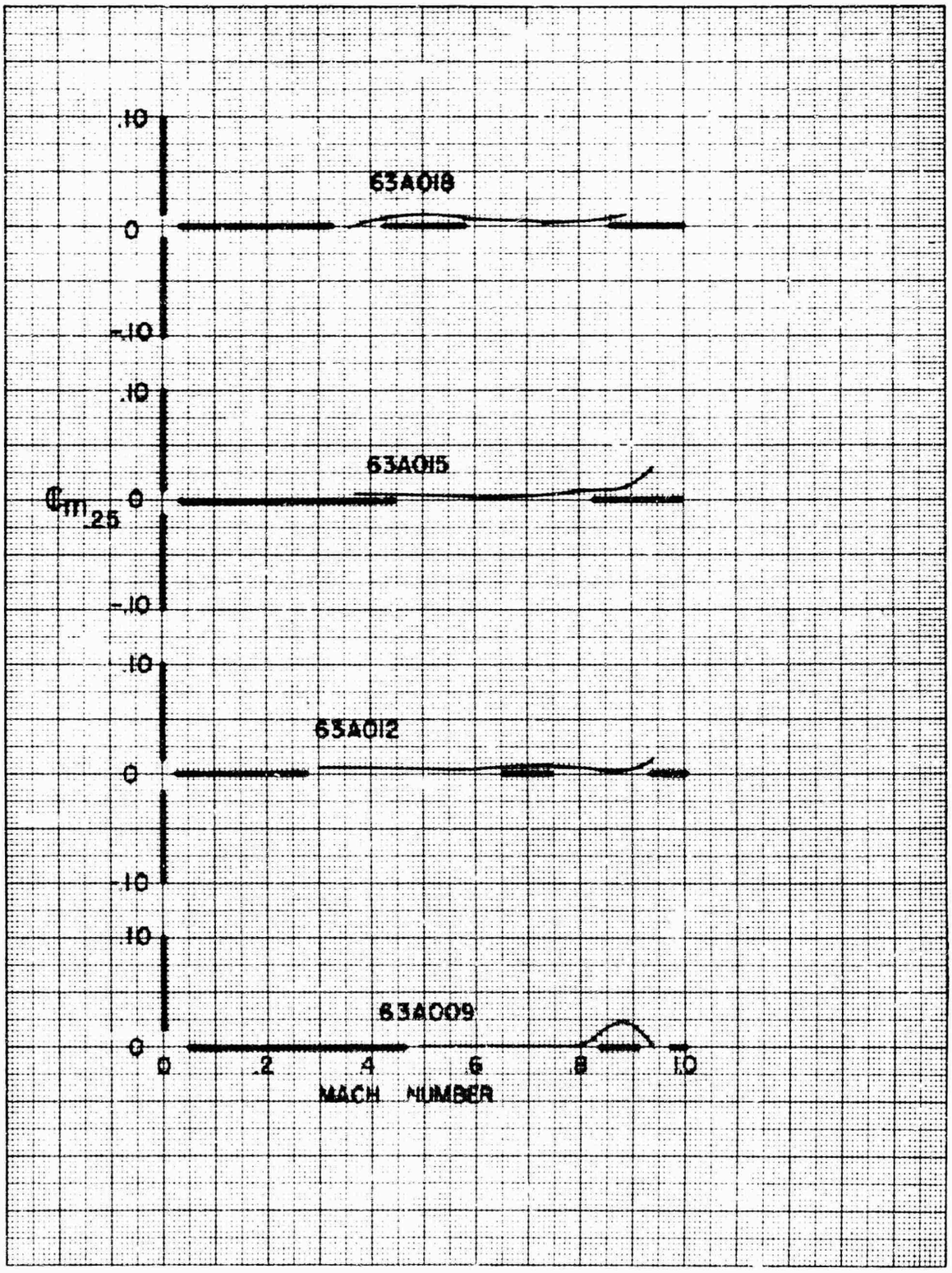


Figure 16B. Variation of Section Pitching Moment Coefficient at $\alpha = 0$ With Mach Number - $R = 5.0 \times 10^6$

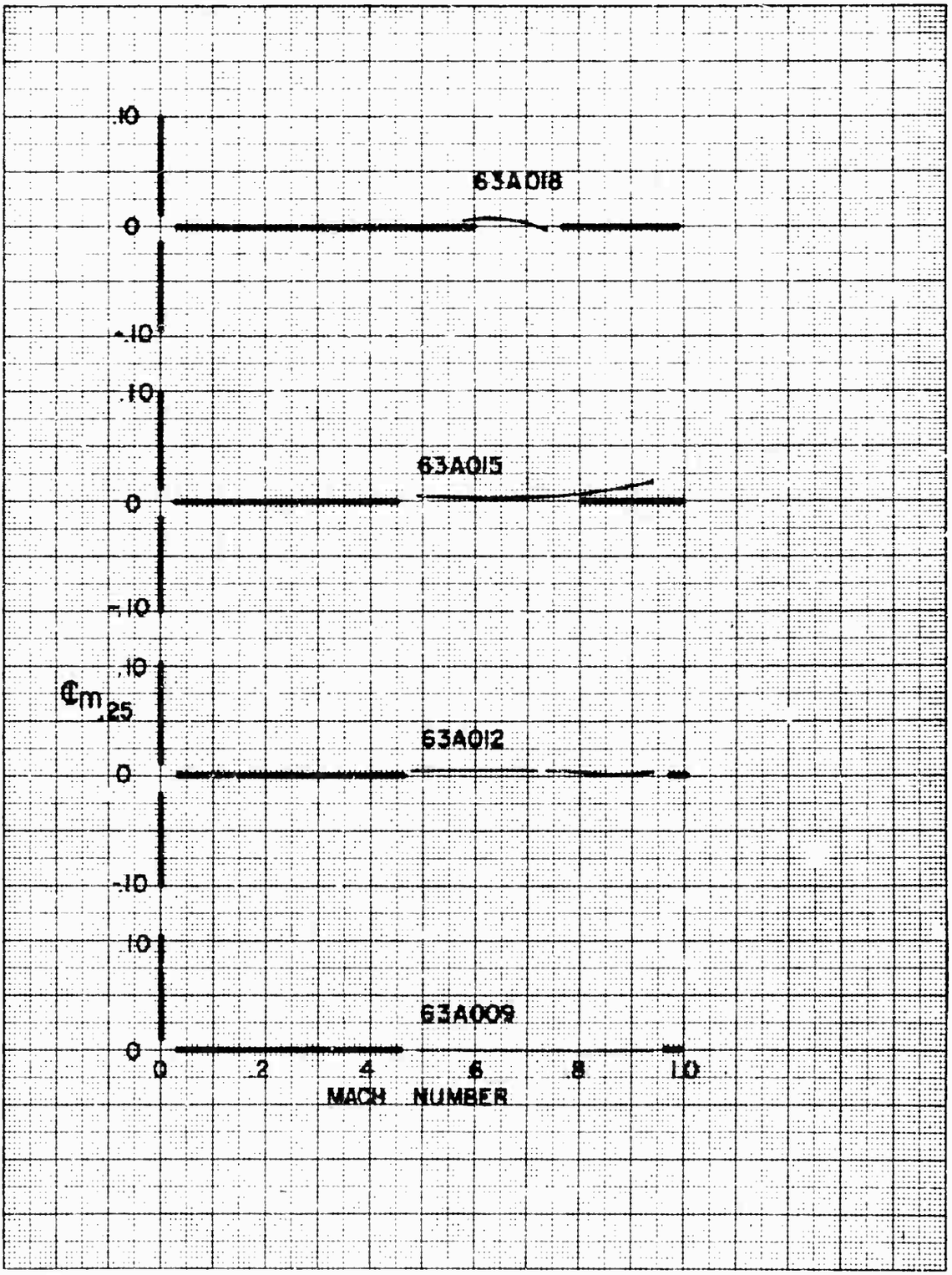


Figure 16C. Variation of Section Pitching Moment Coefficient at $\alpha = 0$ With Mach Number - $R = 6.5 \times 10^6$

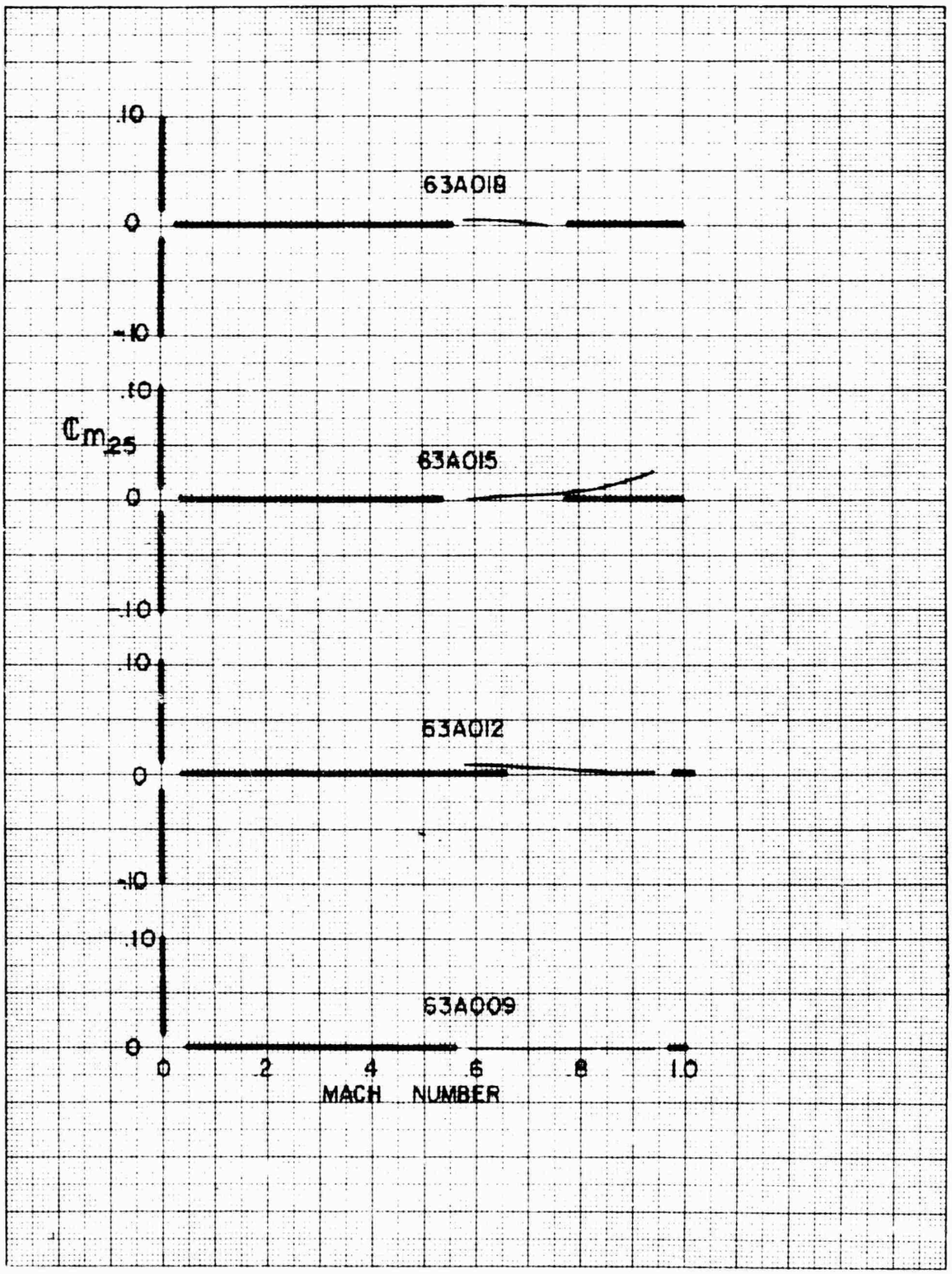


Figure 16D. Variation of Section Pitching Moment Coefficient at $\alpha = 0$ With Mach Number - $R = 8.0 \times 10^6$

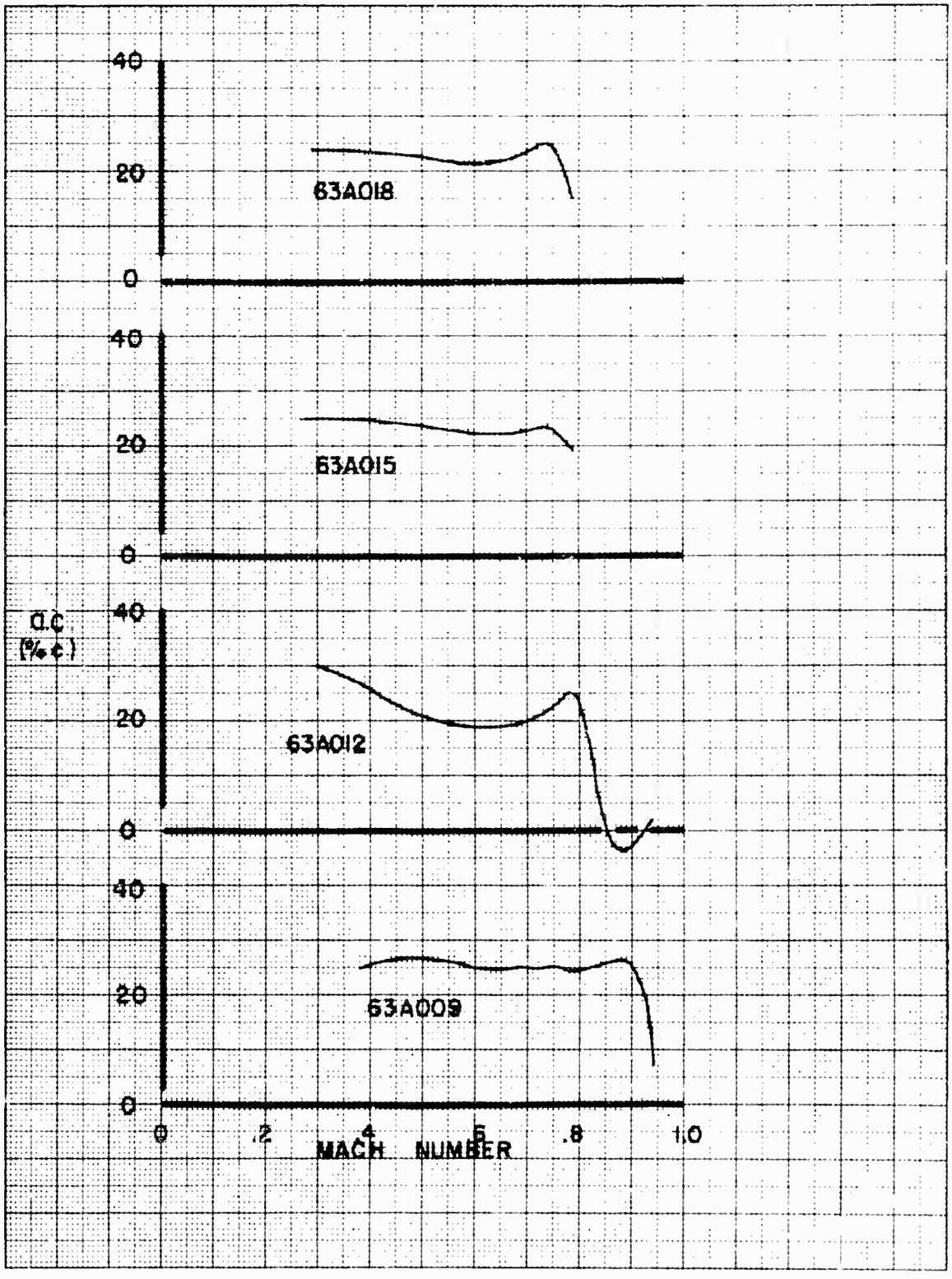


Figure 17A. Variation of Aerodynamic Center with Mach Number - $R = 3.5 \times 10^6$

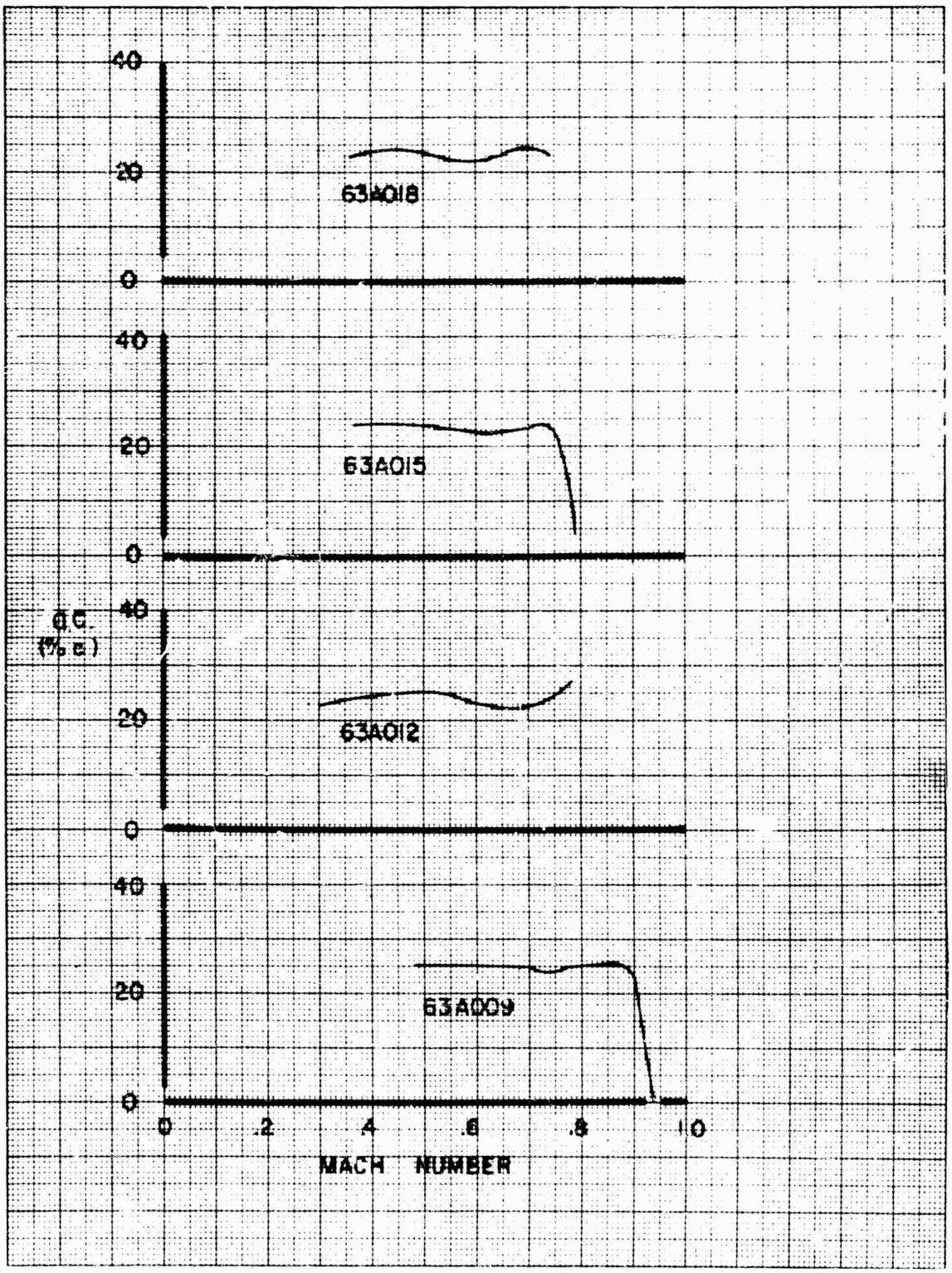


Figure 17B. Variation of Aerodynamic Center with Mach Number - $R = 5.0 \times 10^6$

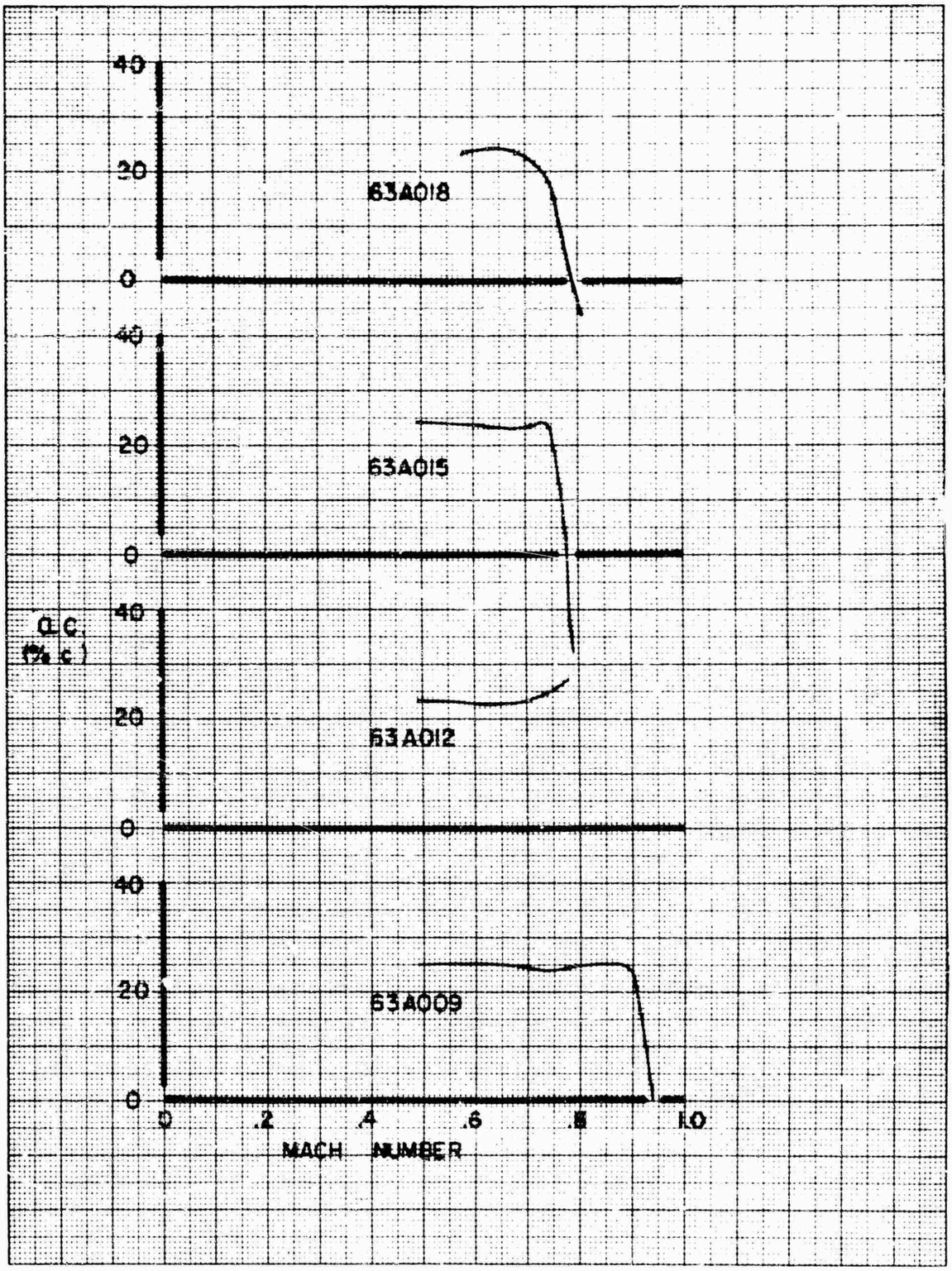


Figure 17C. Variation of Aerodynamic Center With Mach Number - $R = 6.5 \times 10^6$

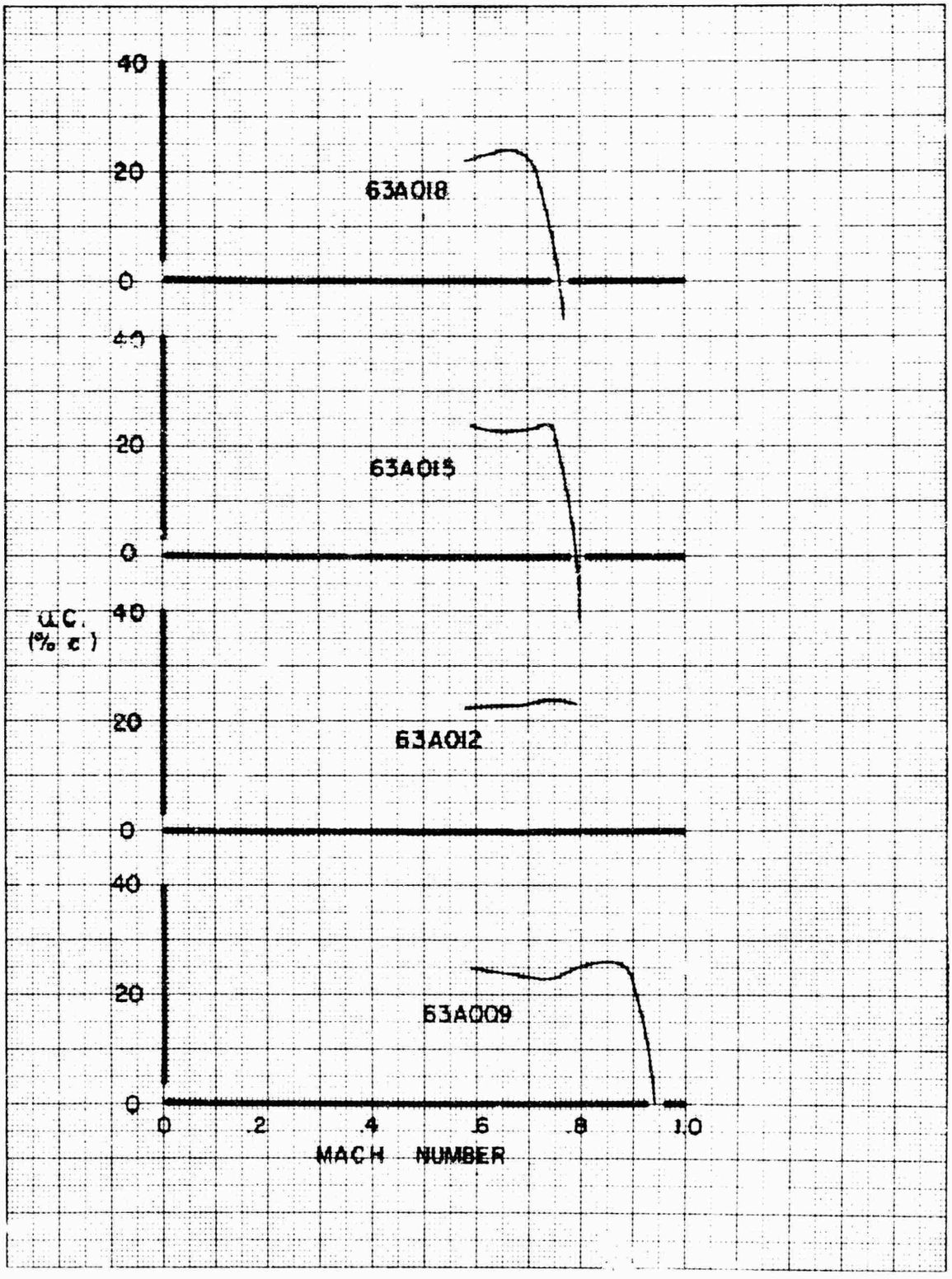


Figure 17D. Variation of Aerodynamic Center With Mach Number - $R = 8.0 \times 10^6$

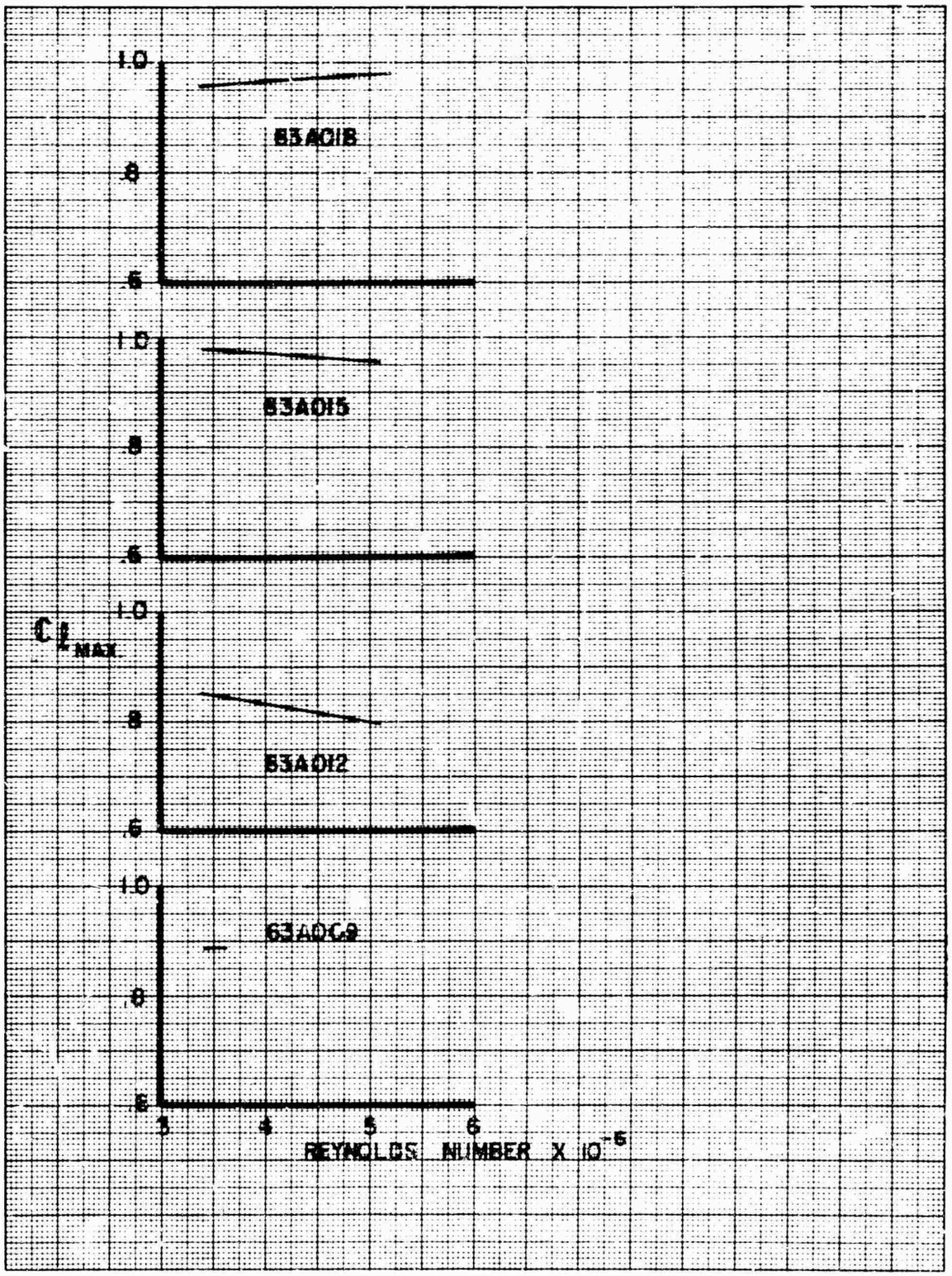


Figure 18A. Variation of Section Maximum Lift Coefficient With Reynolds Number - M = .40

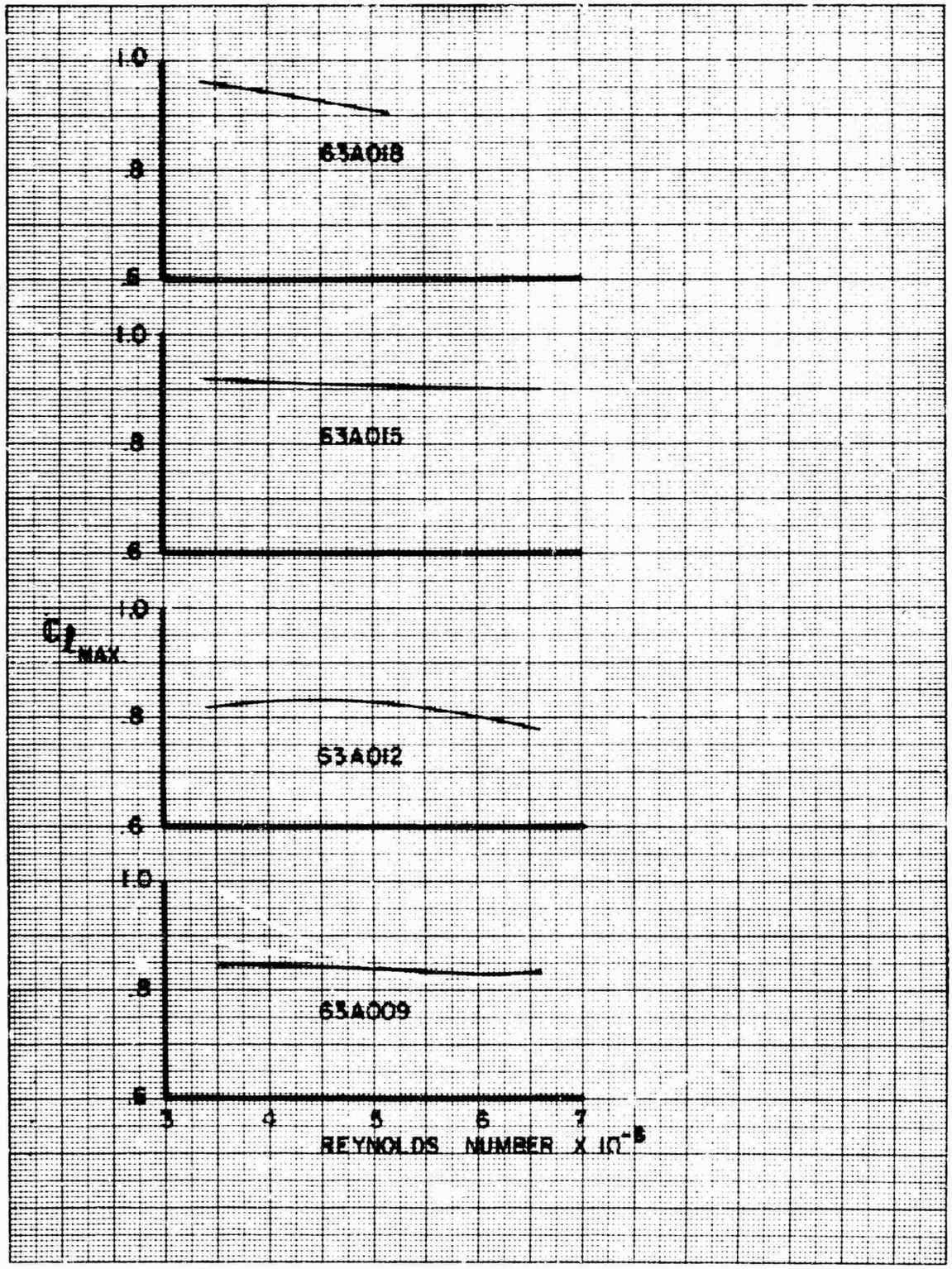


Figure 18B. Variation of Section Maximum Lift Coefficient With Reynolds Number - M = .50

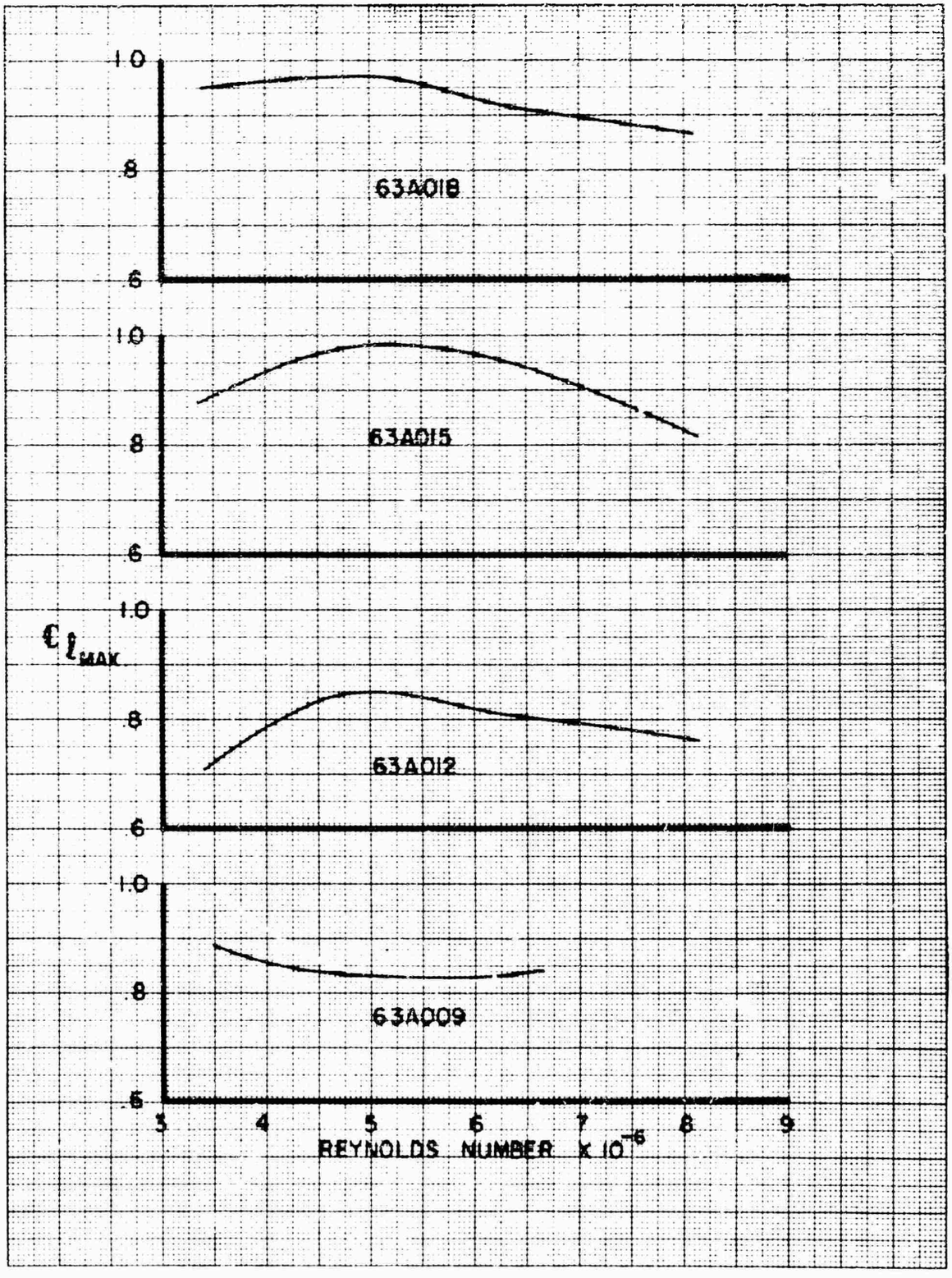


Fig re 18C. Variation of Section Maximum Lift Coefficient With Reynolds Number - M = .60

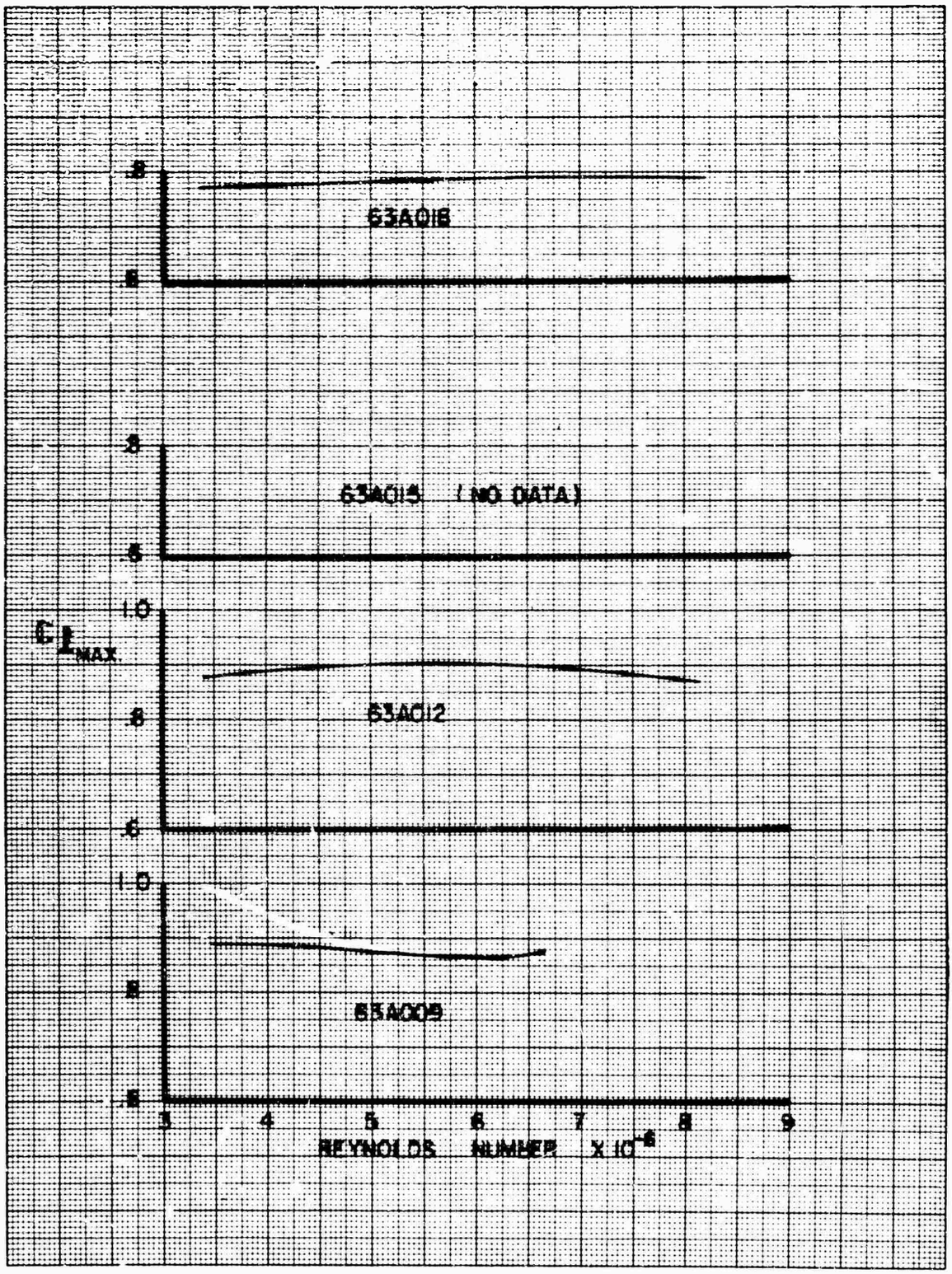


Figure 18D. Variation of Section Maximum Lift Coefficient With Reynolds Number - M = .70

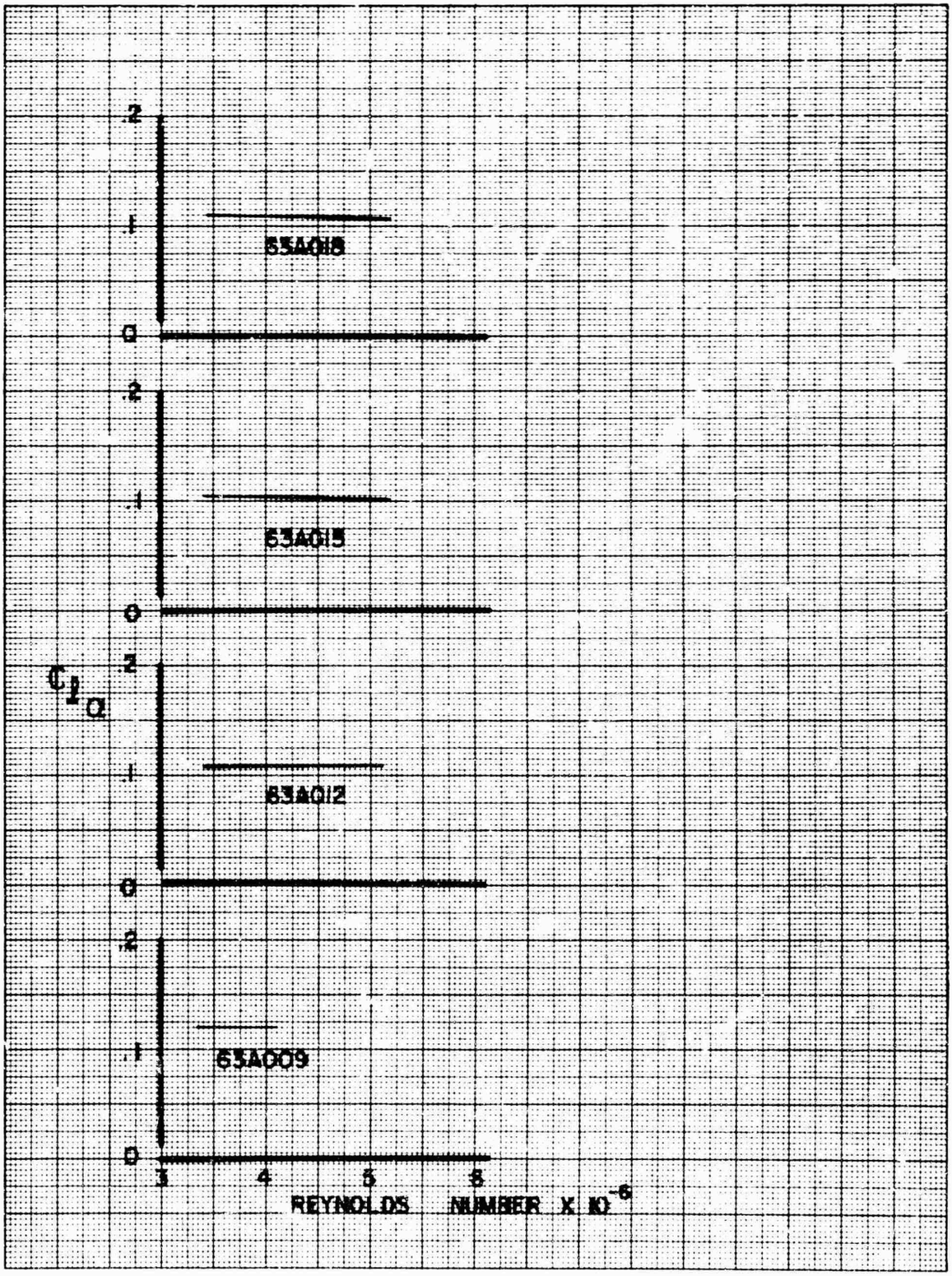


Figure 19A. Variation of Lift-Curve Slope at $C_l = 0$ With Reynolds Number - M = .40

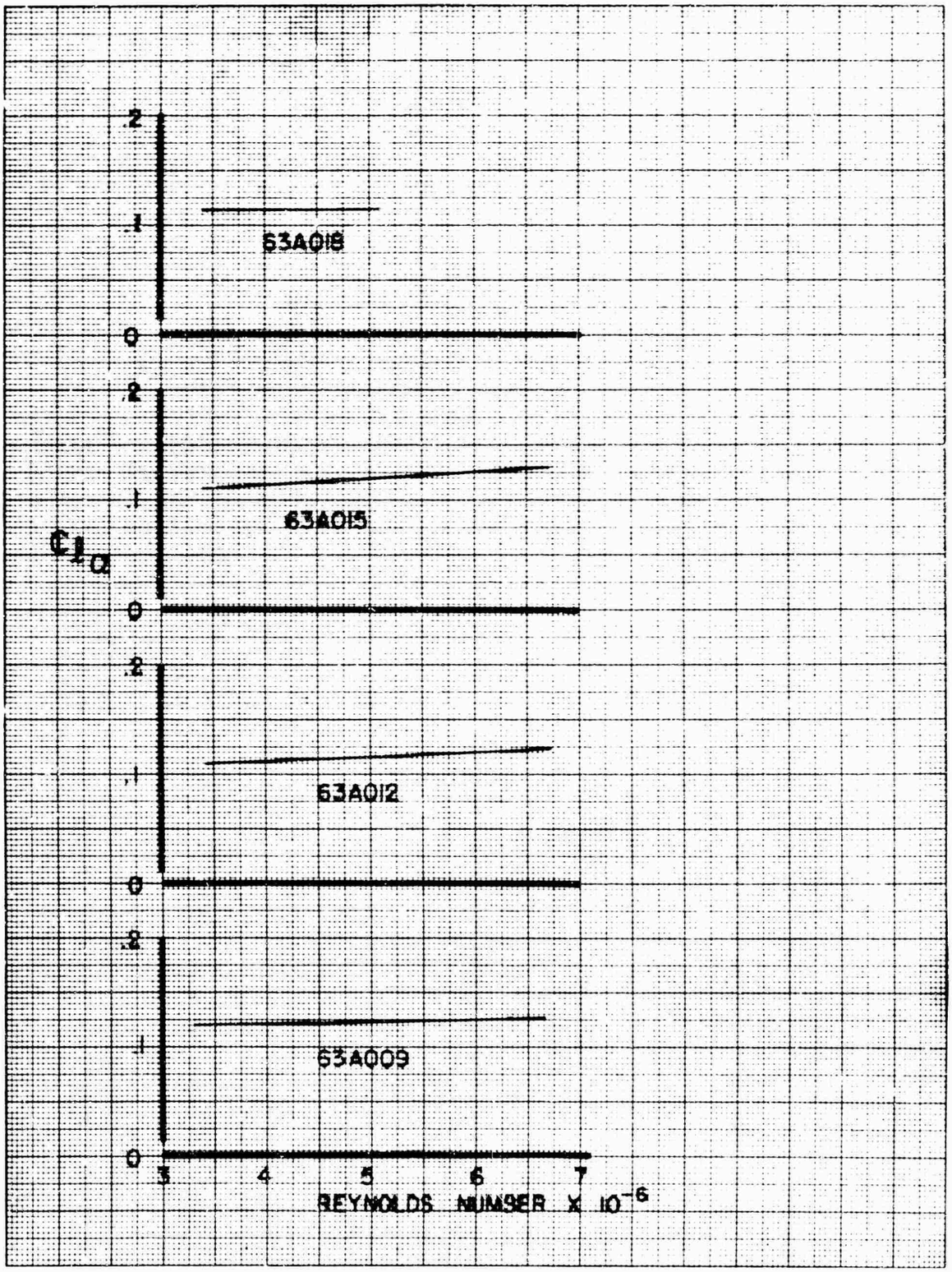


Figure 19B. Variation of Lift-Curve Slope at $C_\ell = 0$ With Reynolds Number - M = .50

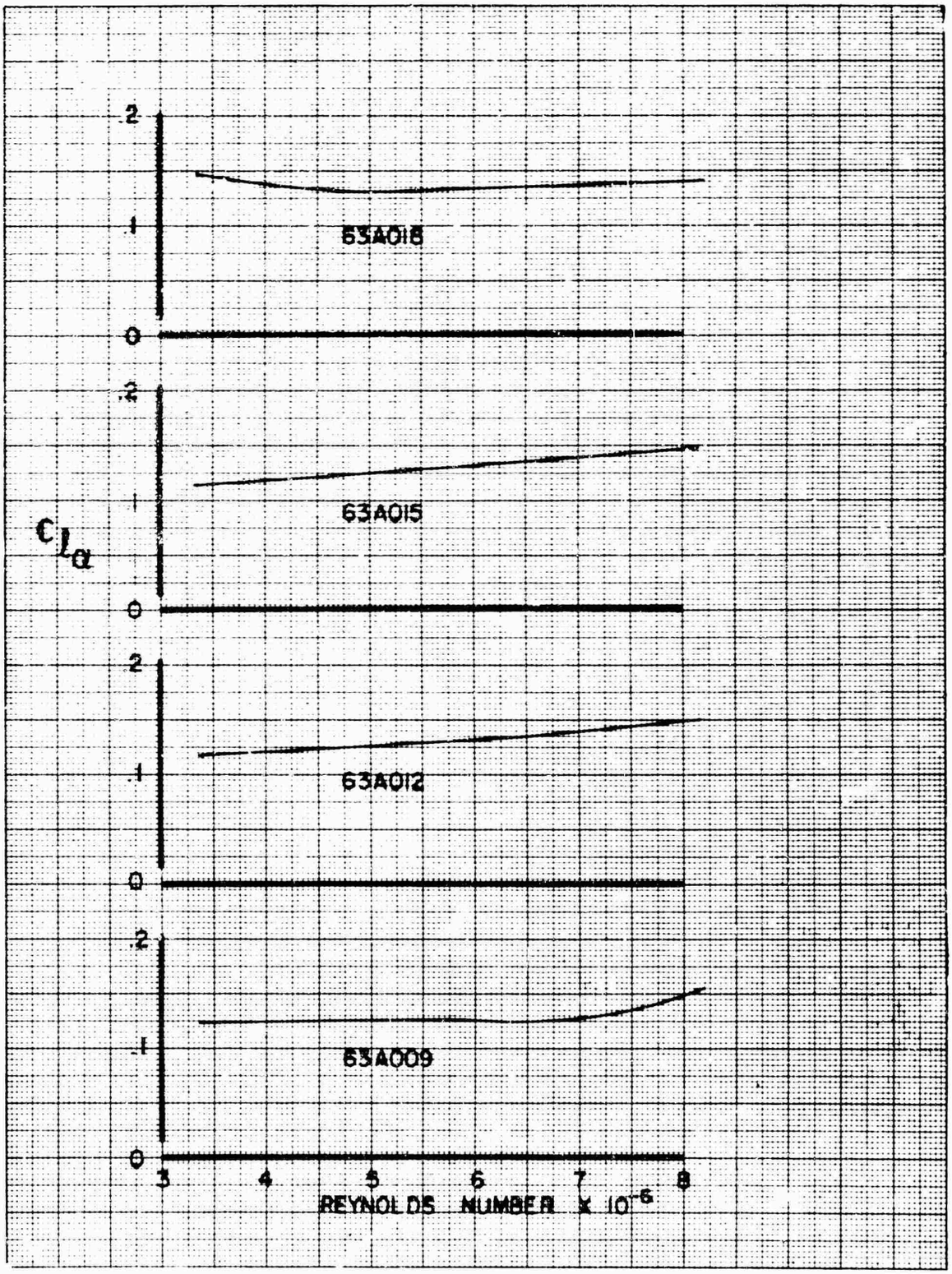


Figure 19C. Variation of Lift-Curve Slope at $C_l = 0$ With Reynolds Number - M = .60

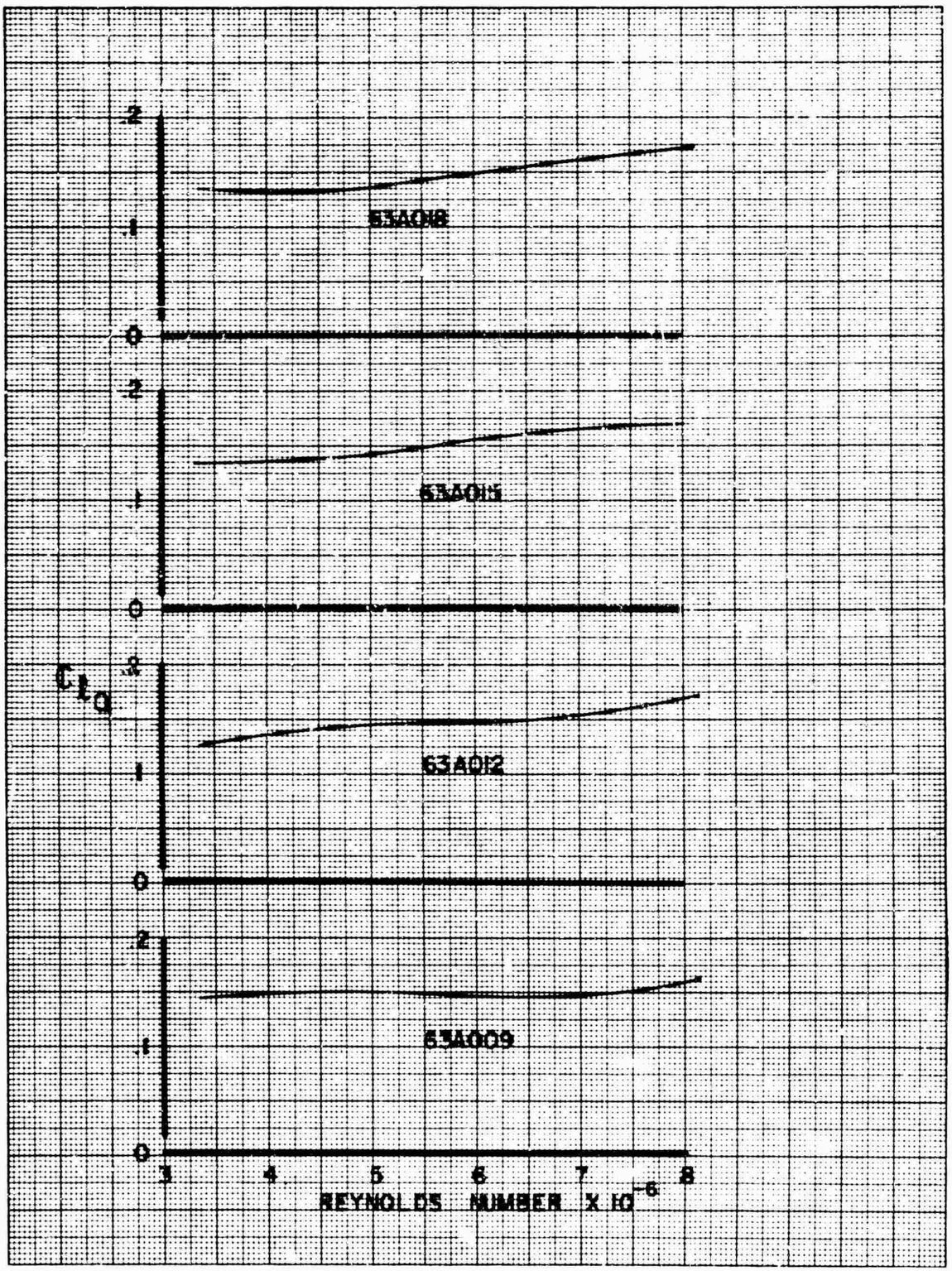


Figure 19D. Variation of Lift-Curve Slope at $C_l = 0$ With Reynolds Number - M = .70

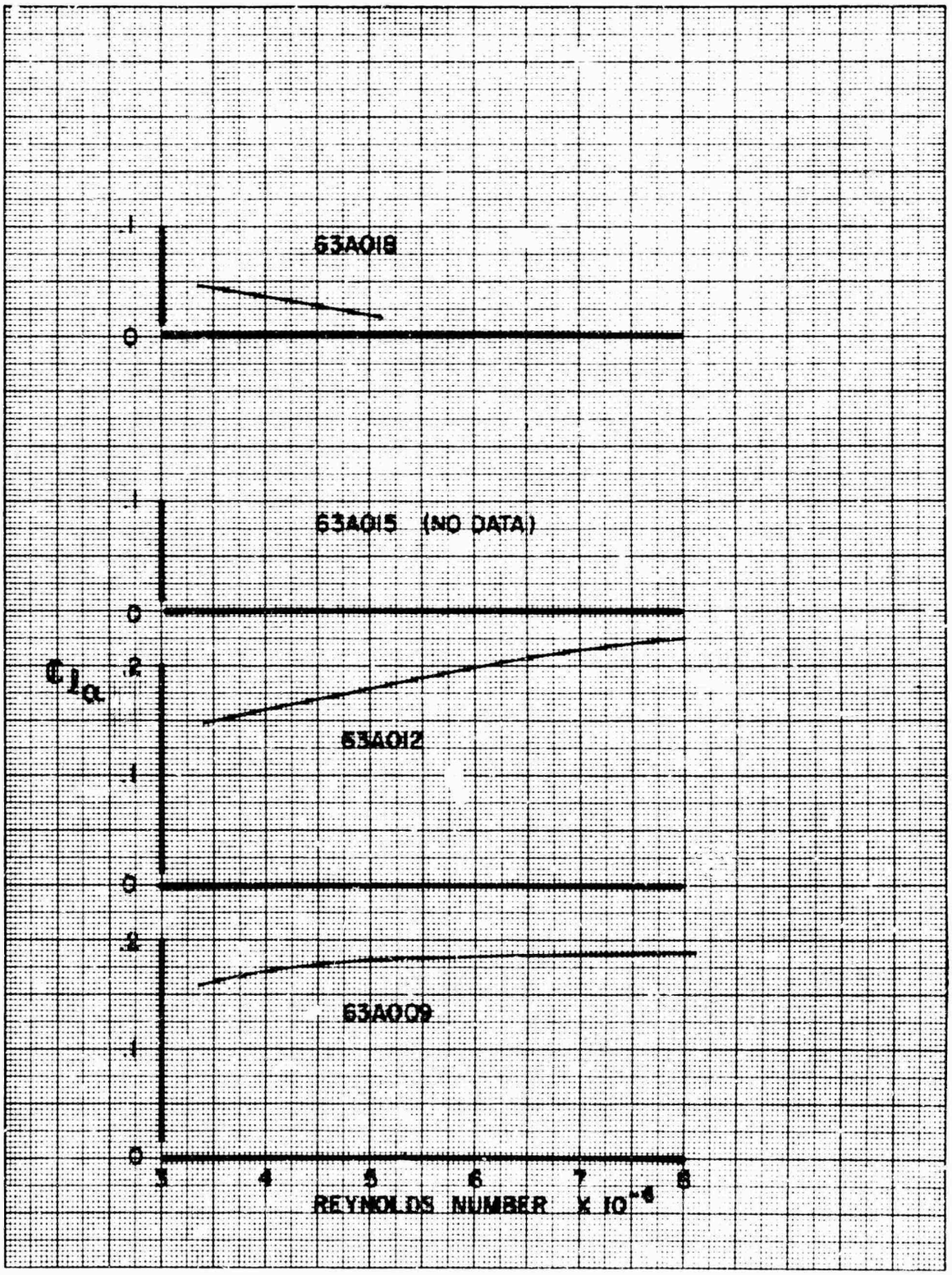


Figure 19E. Variation of Lift-Curve Slope at $C_\ell = 0$ With Reynolds Number - M = .80

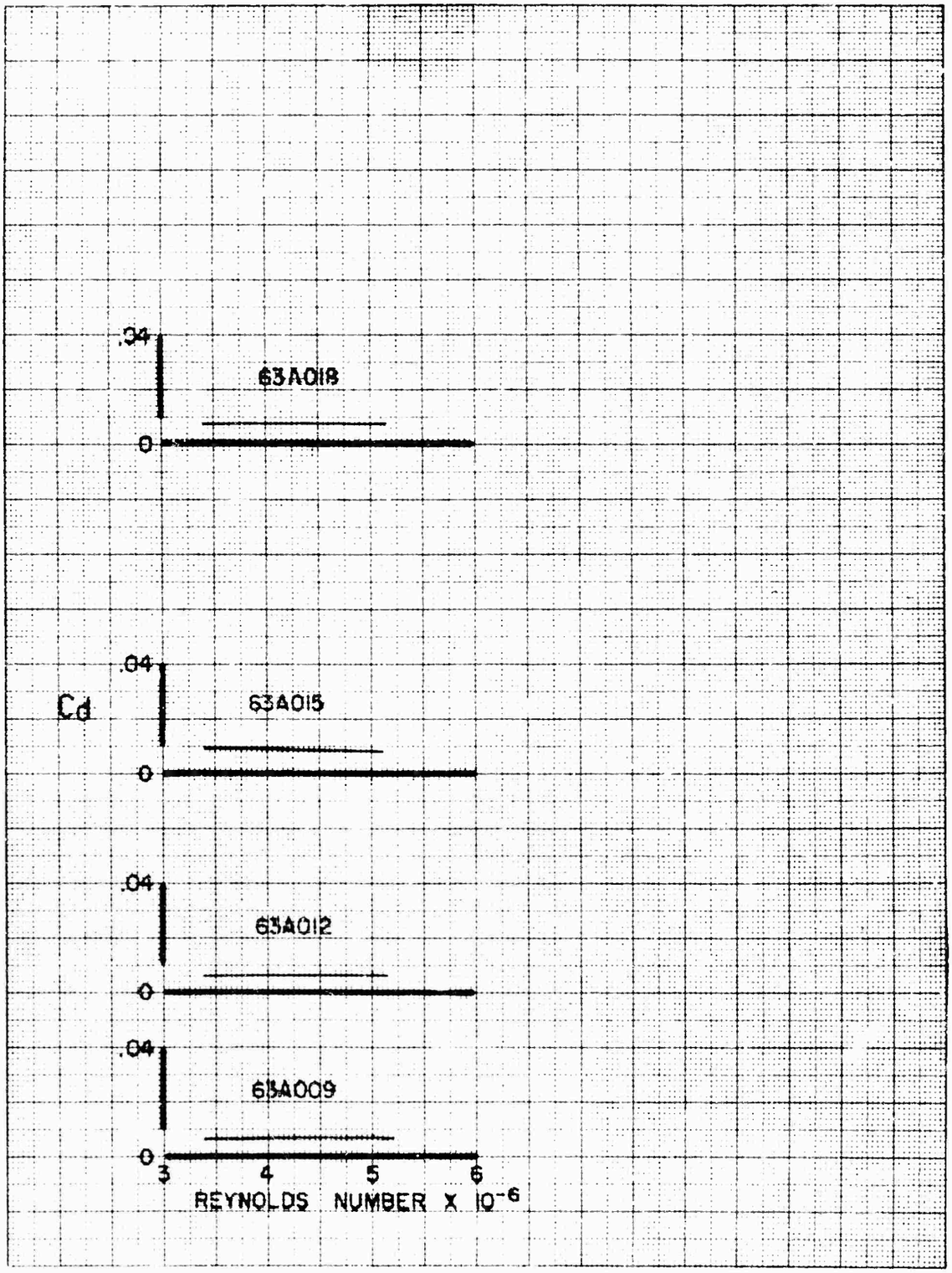


Figure 20A. Variation of Section Drag Coefficient at $\alpha = 0$ With Reynolds Number - M = .40

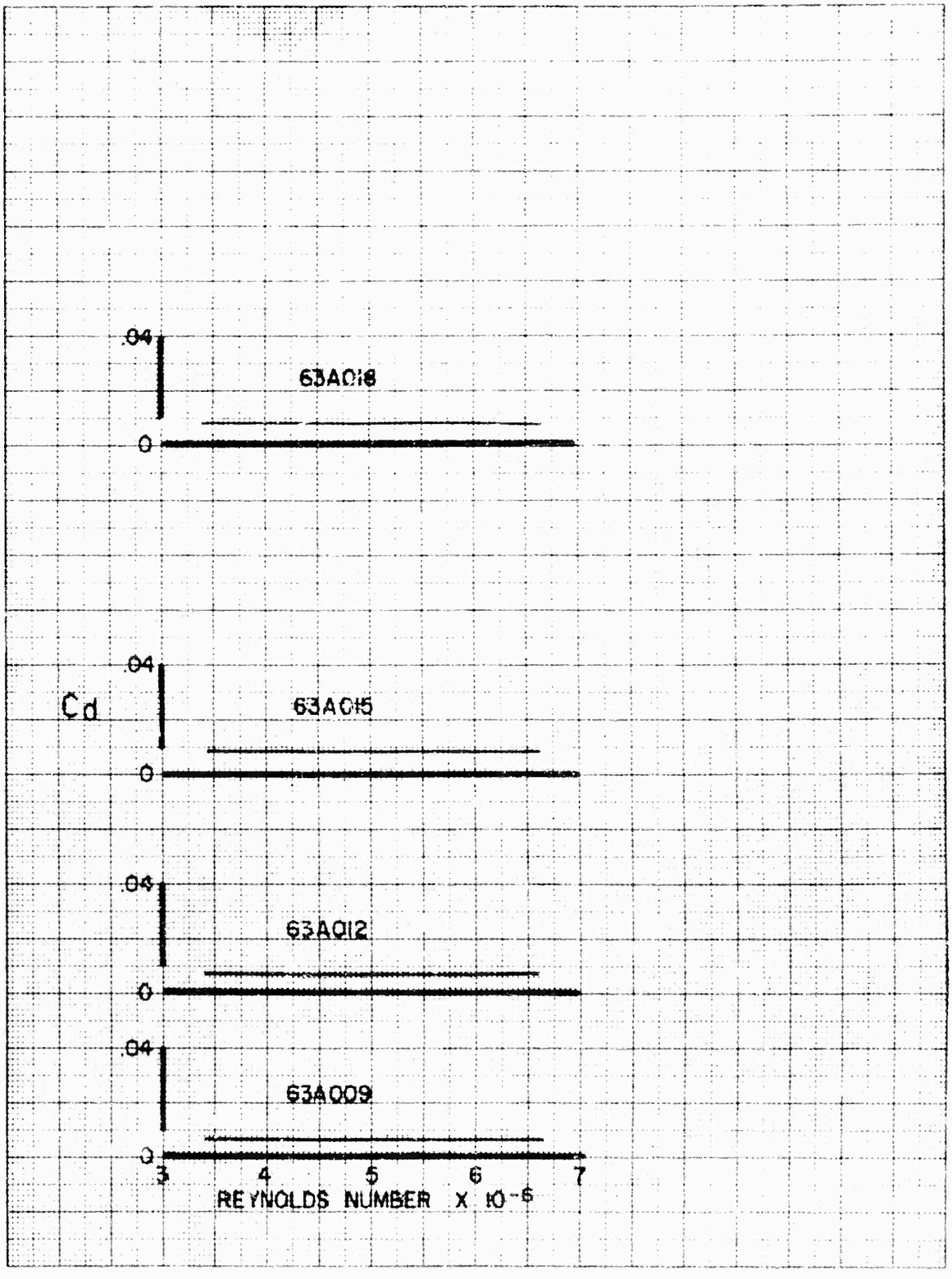


Figure 20B. Variation of Section Drag Coefficient at $\alpha = 0$ With Reynolds Number - M = .50

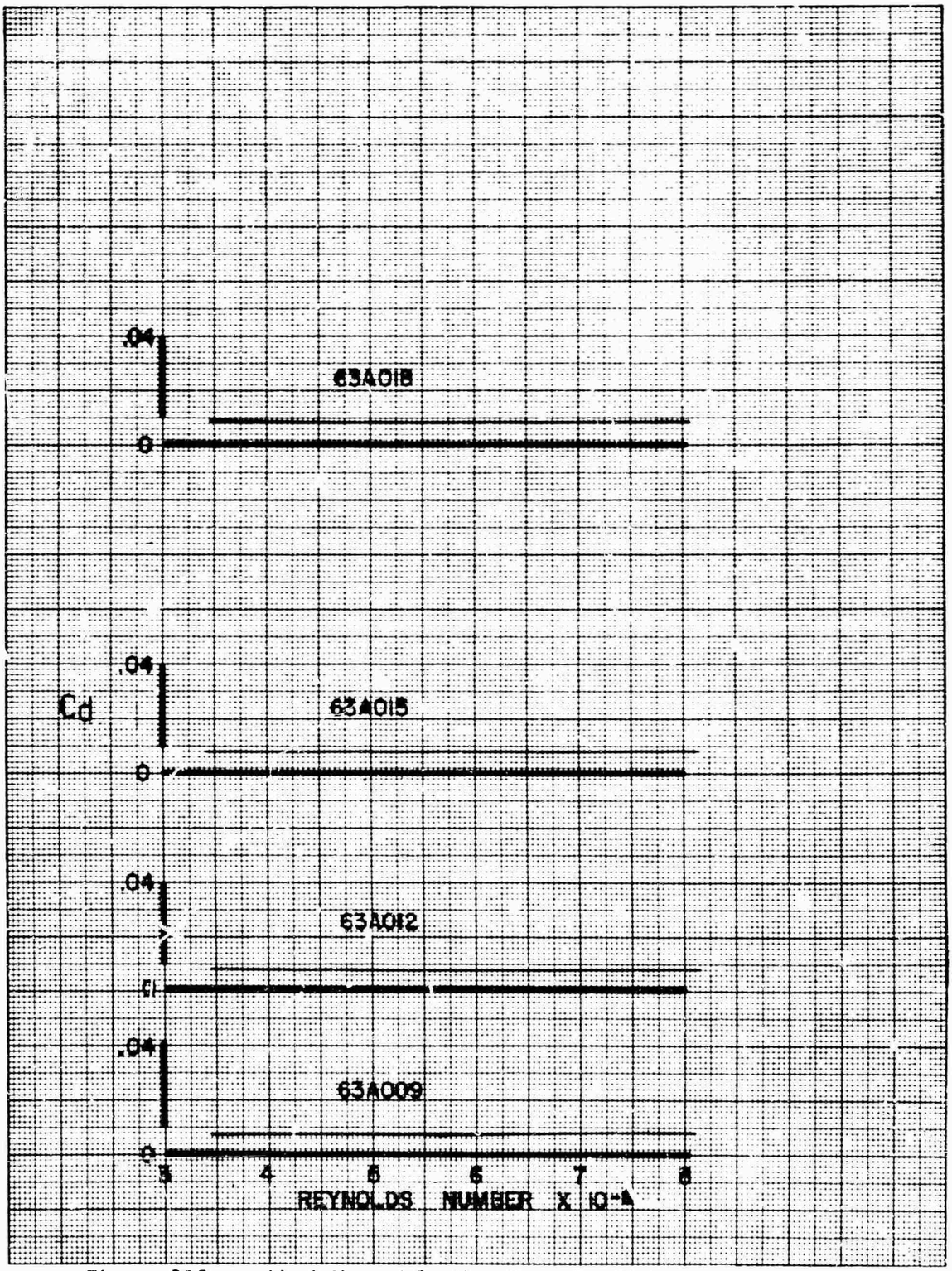


Figure 20C. Variation of Section Drag Coefficient at $\alpha = 0$ With Reynolds Number - M = .60

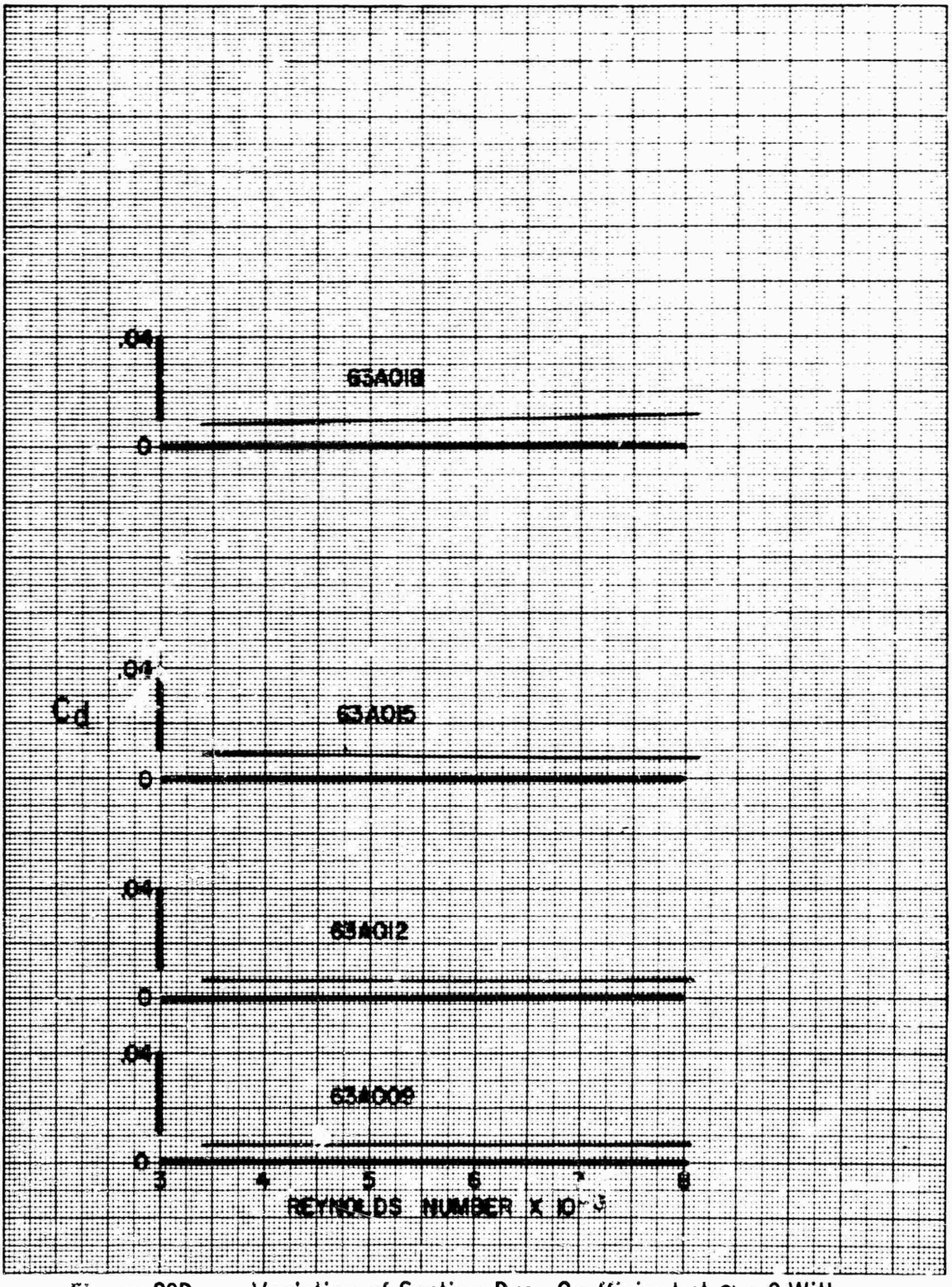


Figure 20D. Variation of Section Drag Coefficient at $\alpha = 0$ With Reynolds Number - M = .70

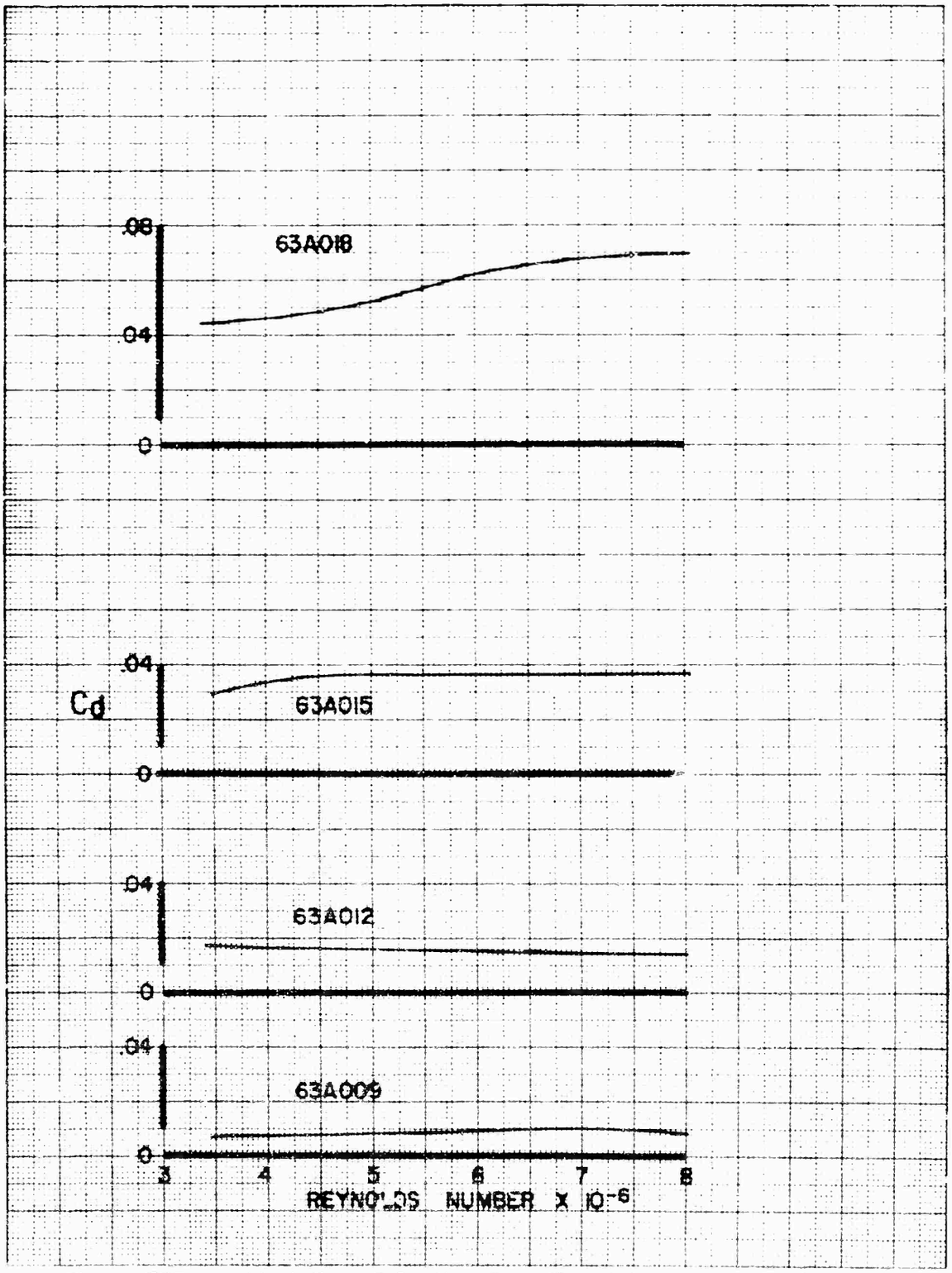


Figure 20E. Variation of Section Drag Coefficient at α = 0 With Reynolds Number - M = .80

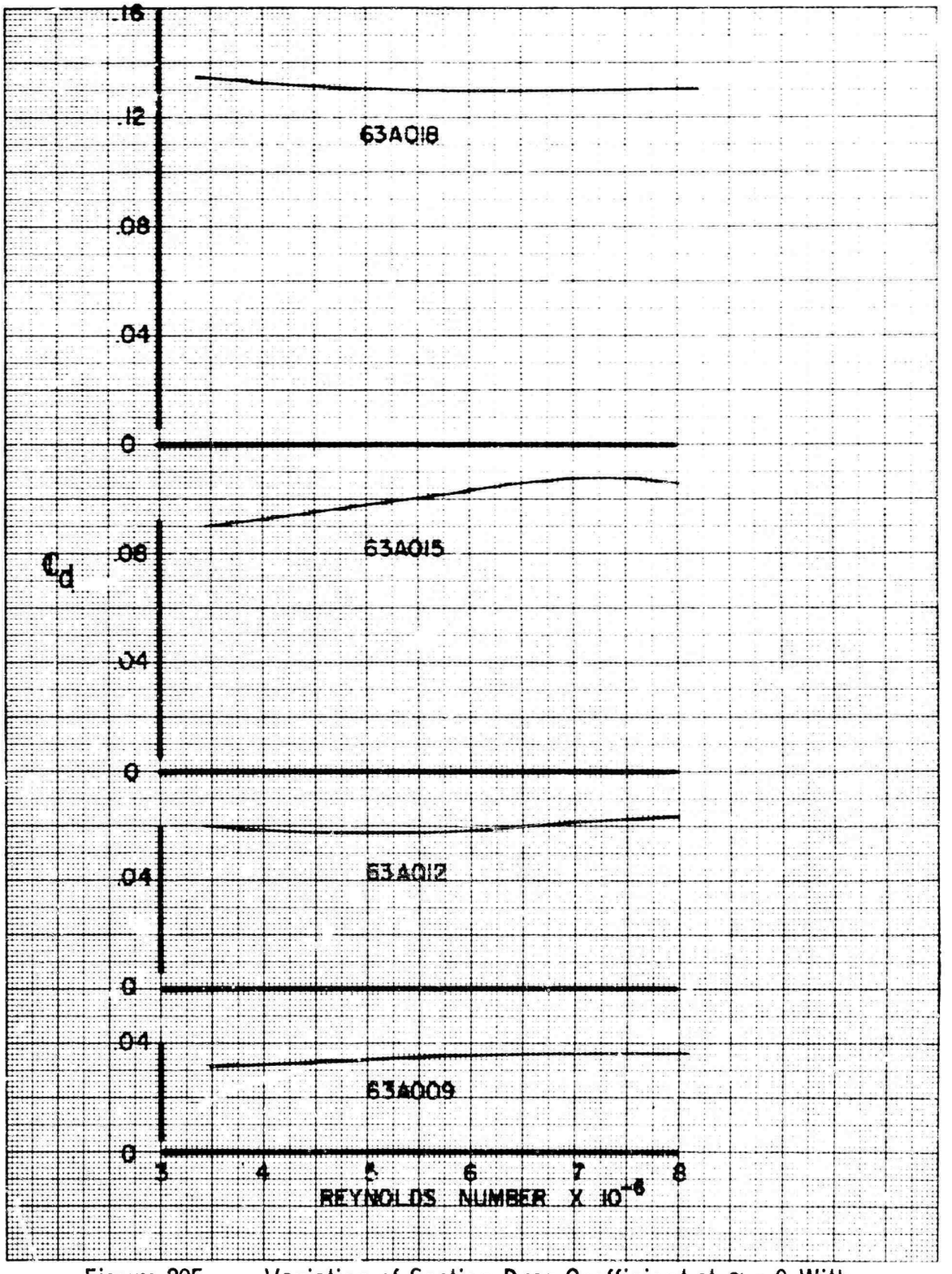


Figure 20F. Variation of Section Drag Coefficient at $\alpha = 0$ With Reynolds Number - M = .90

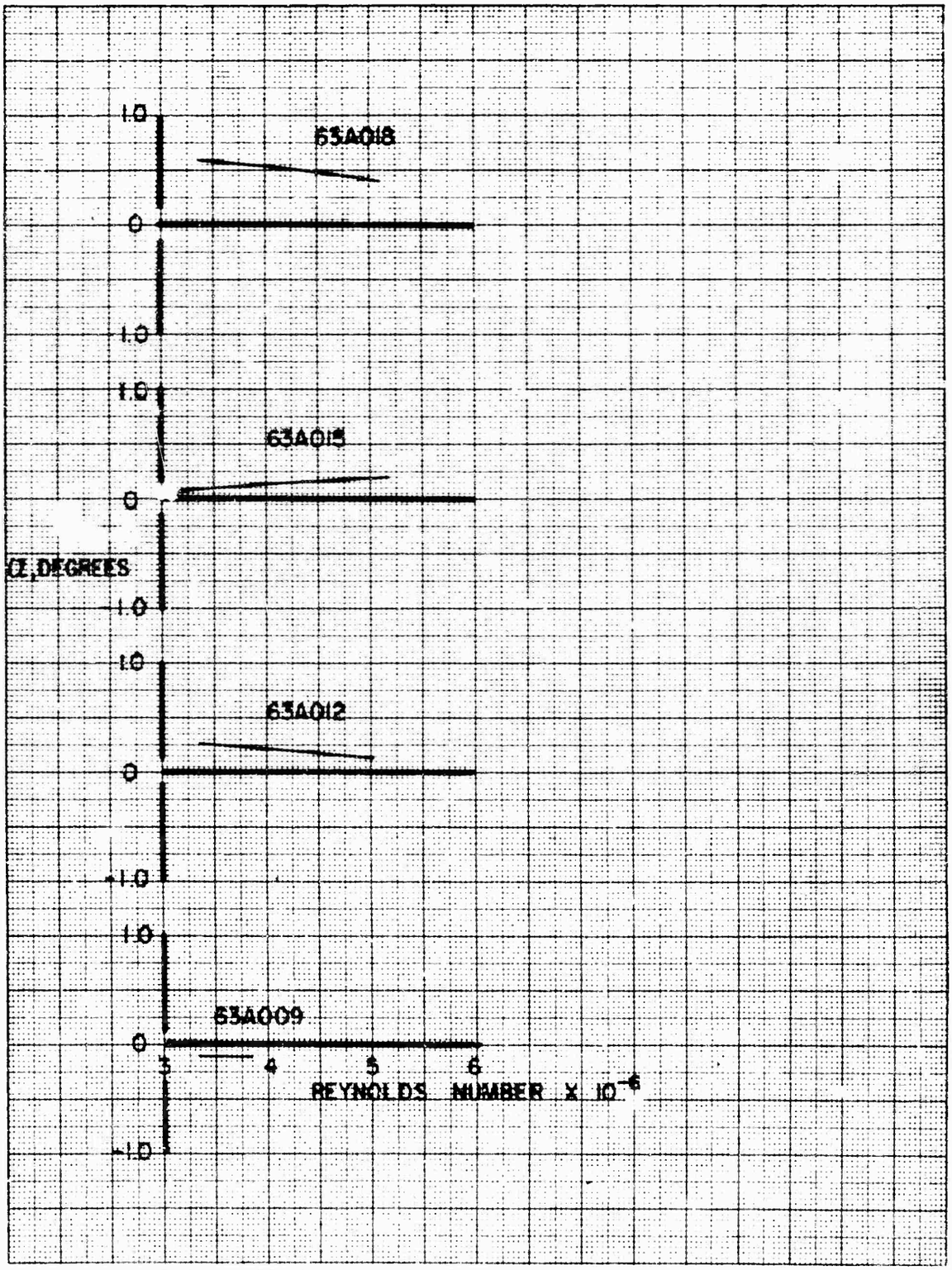


Figure 21A. Variation of Angle of Attack at $C_\ell = 0$ With Reynolds Number - M = .40

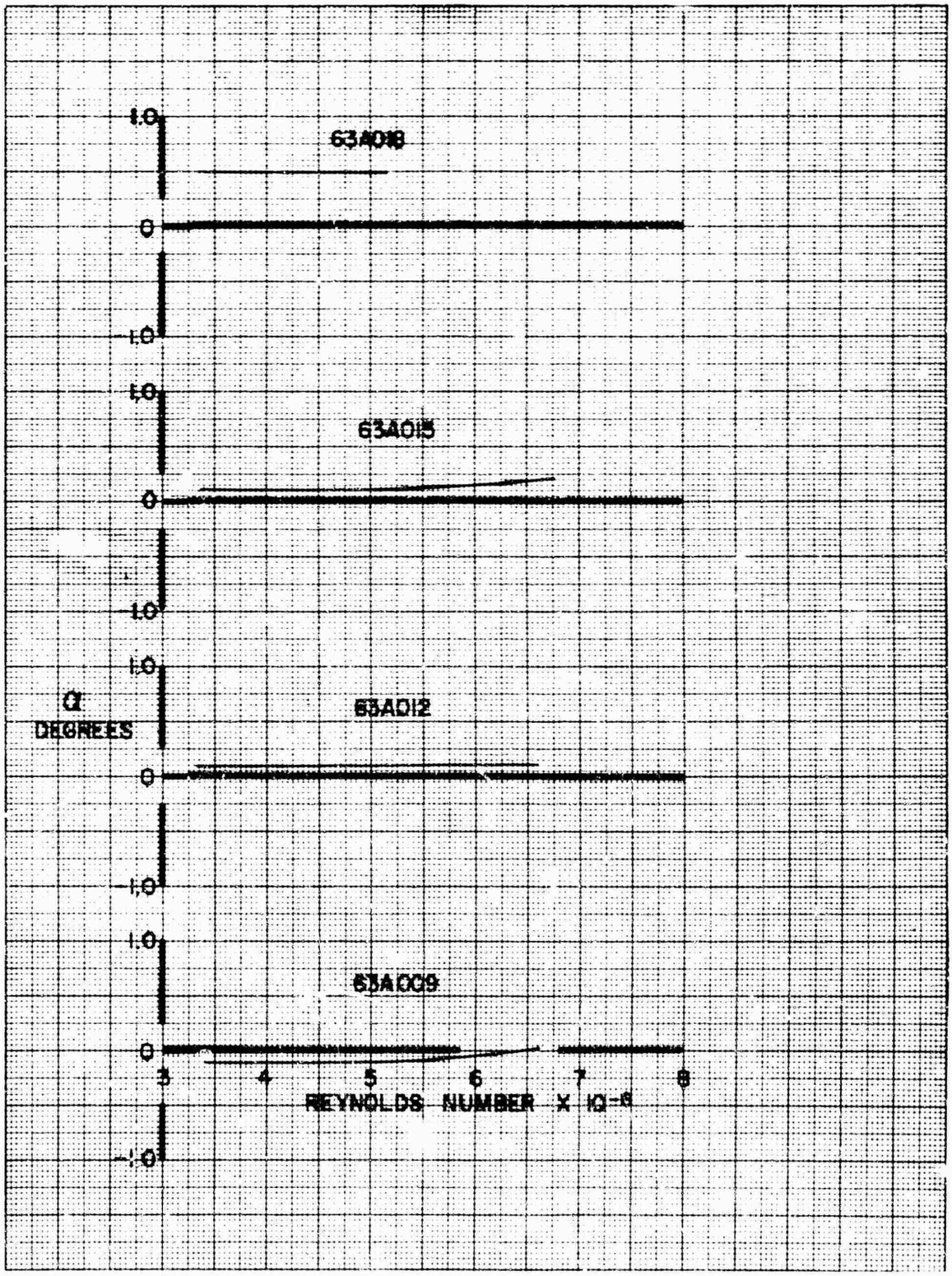


Figure 21B. Variation of Angle of Attack at $C_\ell = 0$ With Reynolds Number - M = .50

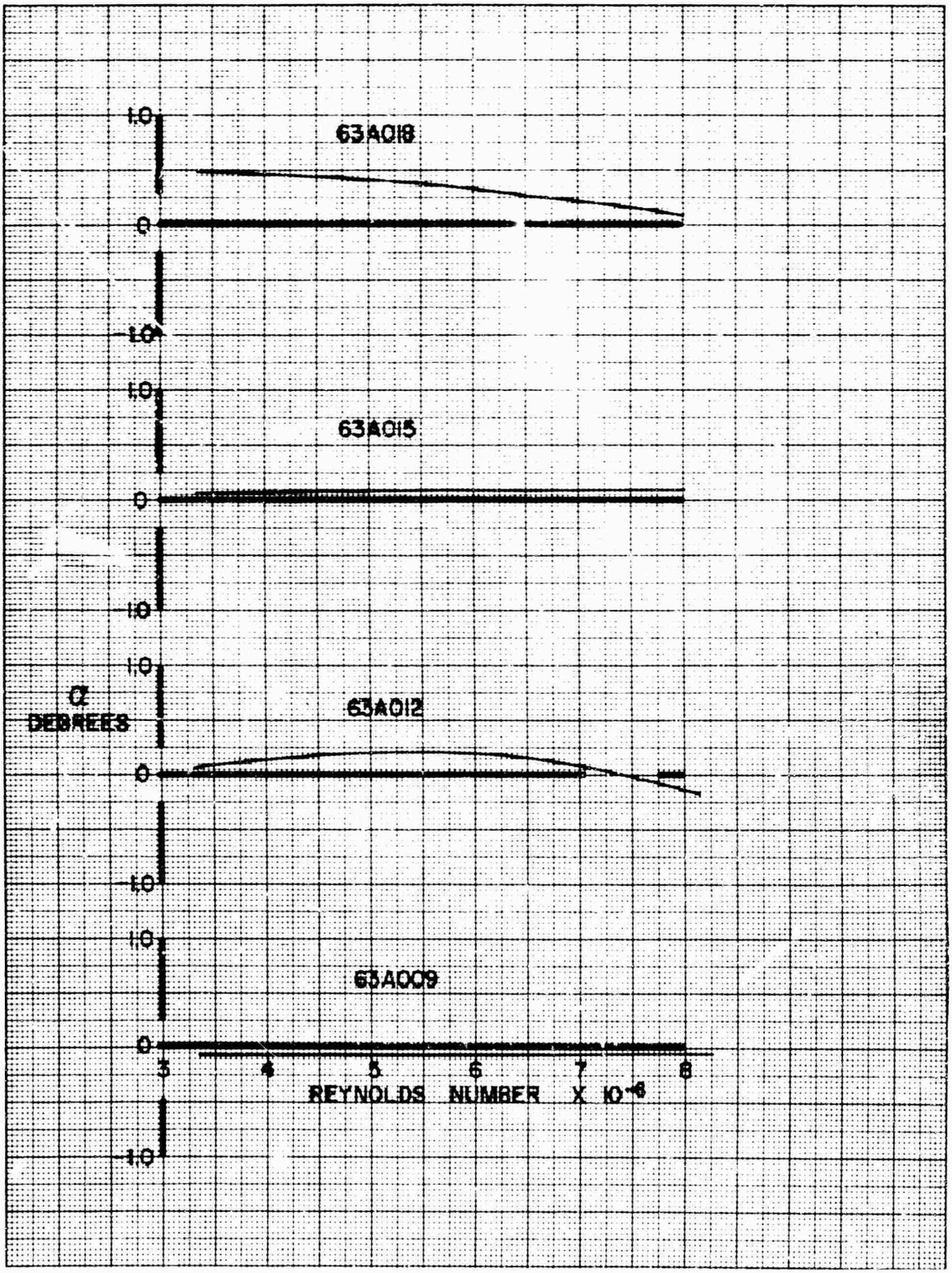


Figure 21C. Variation of Angle of Attack at $C_\ell = 0$ With Reynolds Number - M = .60

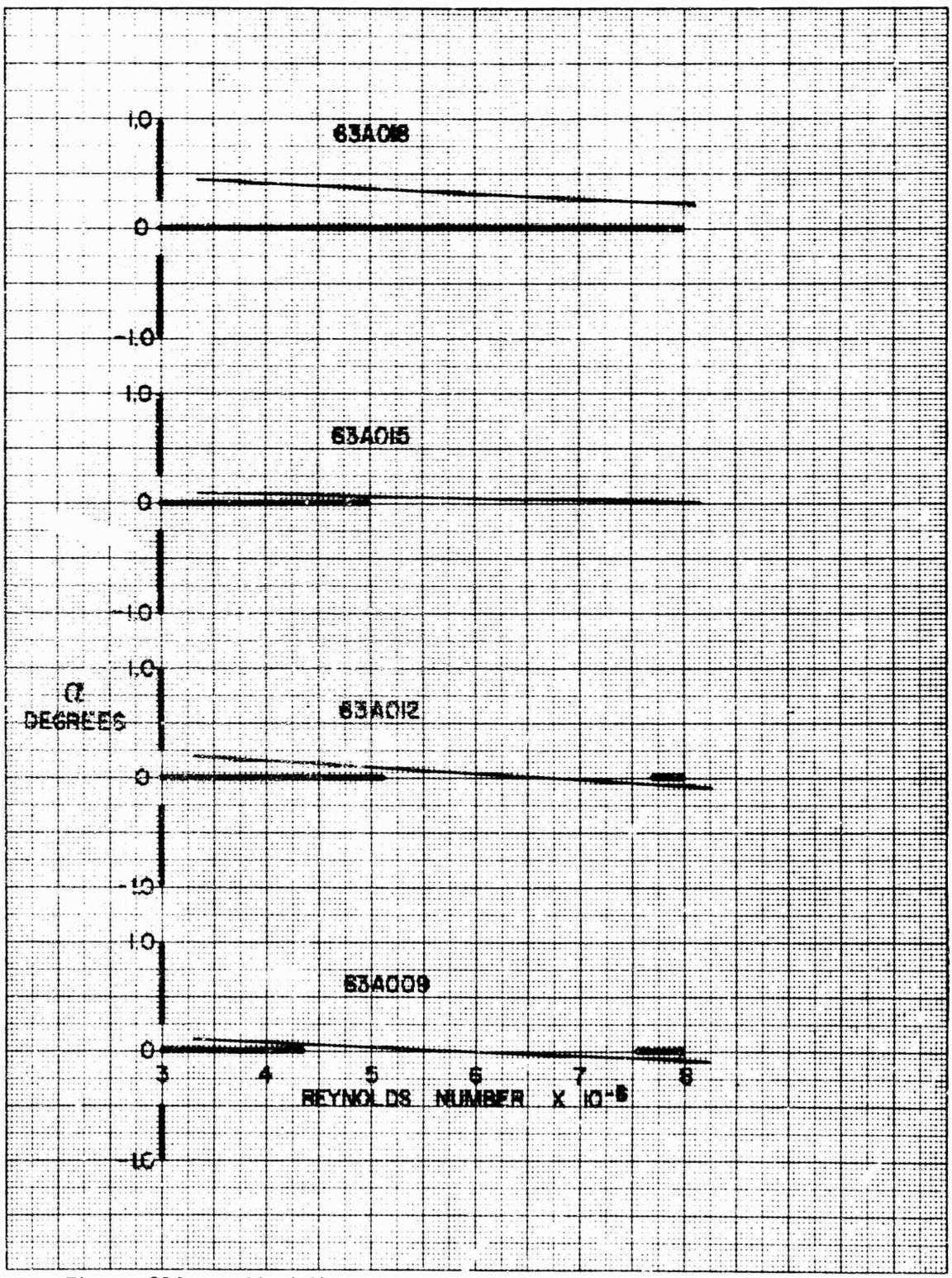


Figure 21D. Variation of Angle of Attack at $C_\ell = 0$ With Reynolds Number - M = .70

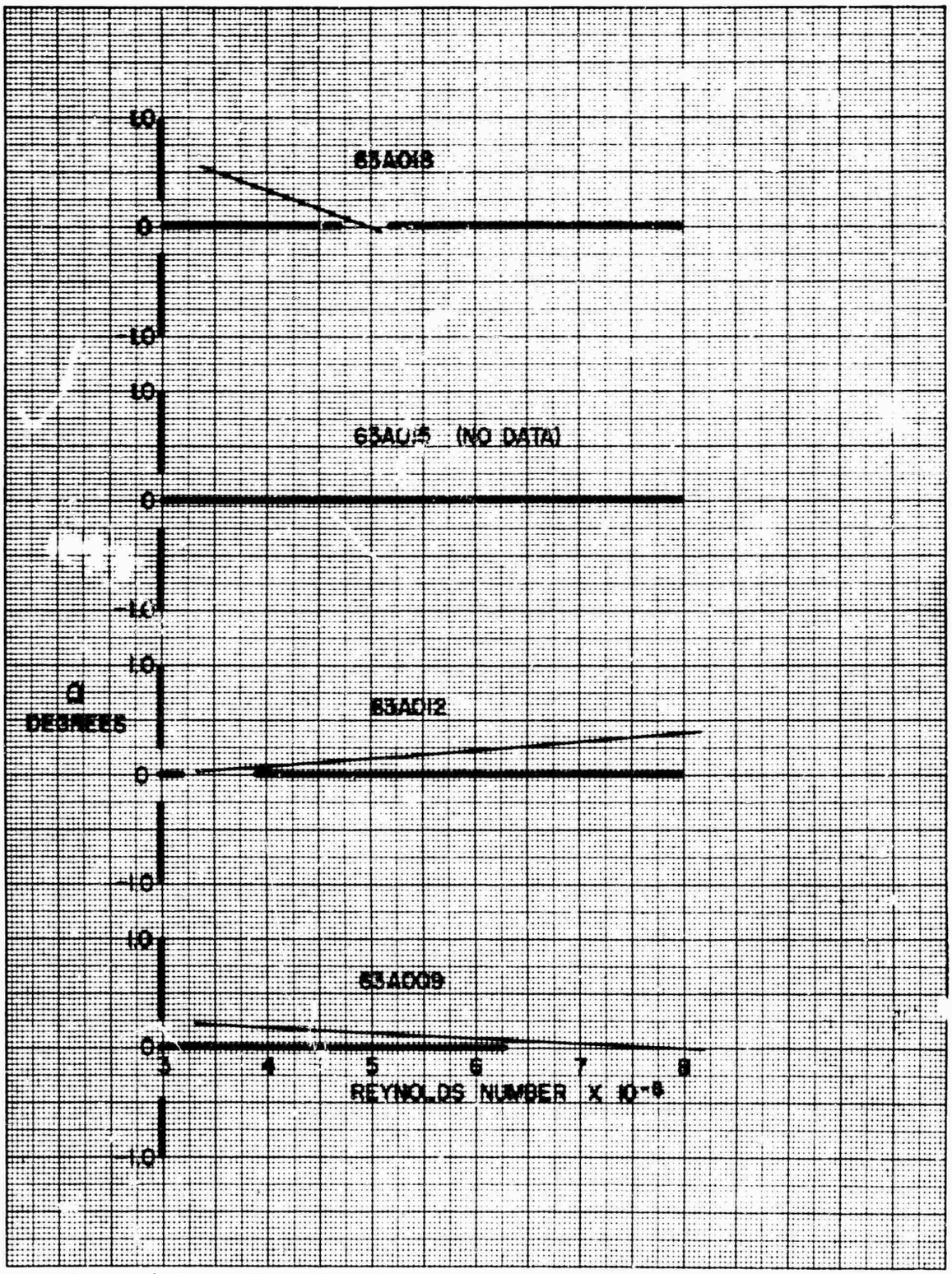


Figure 21E. Variation of Angle of Attack at $C_\ell = 0$ With Reynolds Number - M = .80

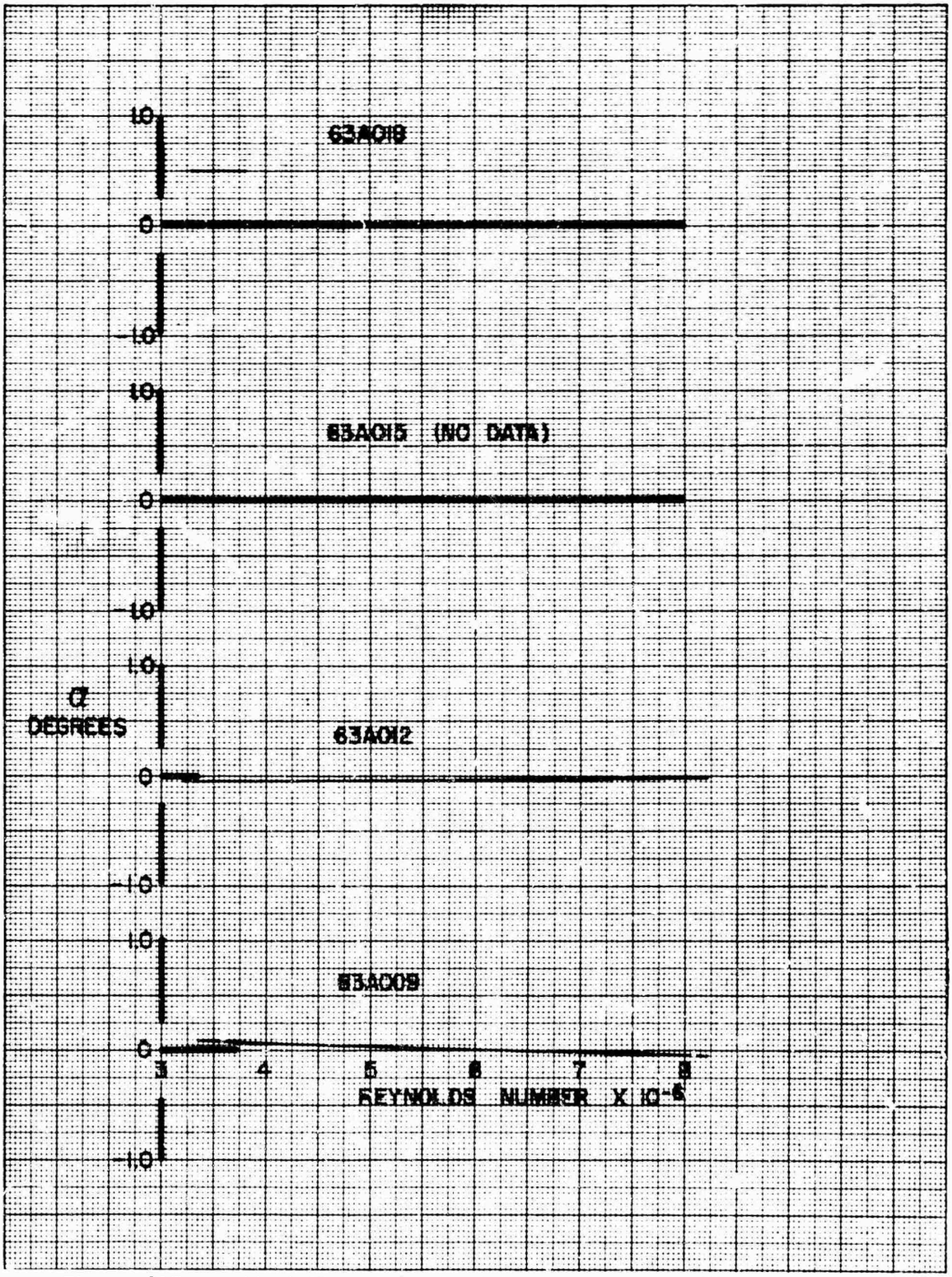


Figure 21F. Variation of Angle of Attack at $C_\ell = 0$ With Reynolds Number - M = .90

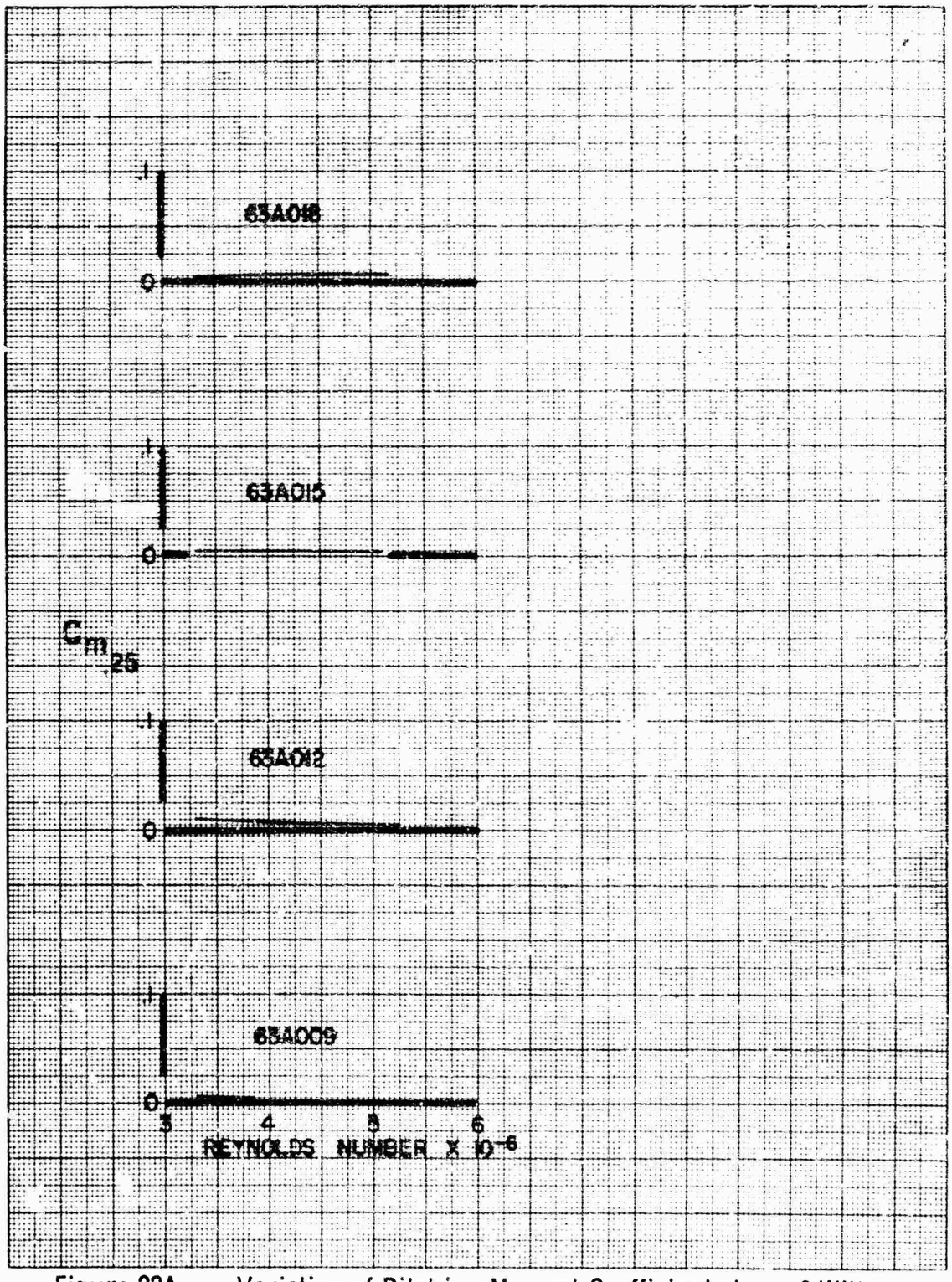


Figure 22A. Variation of Pitching Moment Coefficient at $\alpha = 0$ With Reynolds Number - M = .40

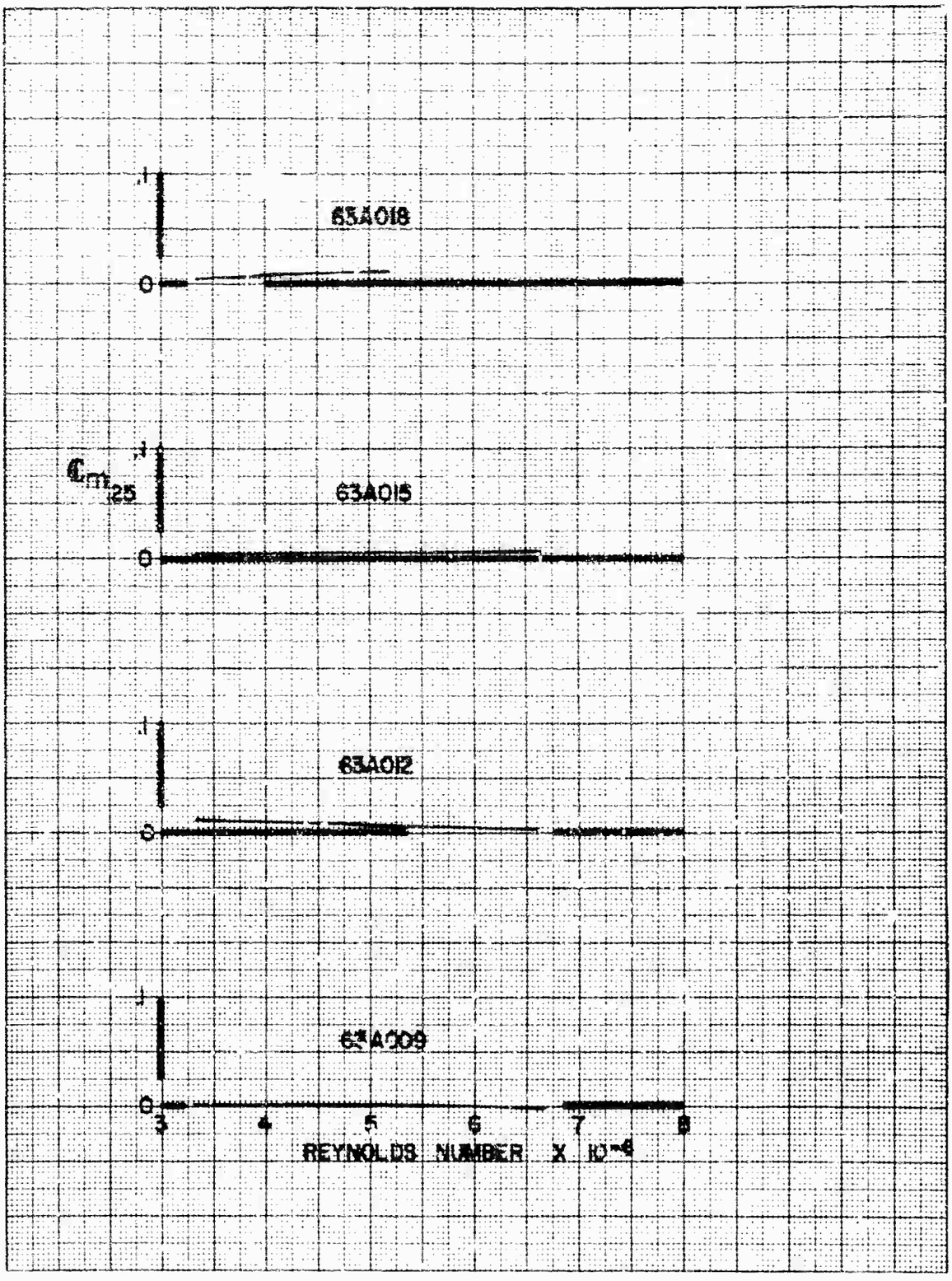


Figure 22B. Variation of Section Pitching Moment Coefficient at $\alpha = 0$ With Reynolds Number - M = .50

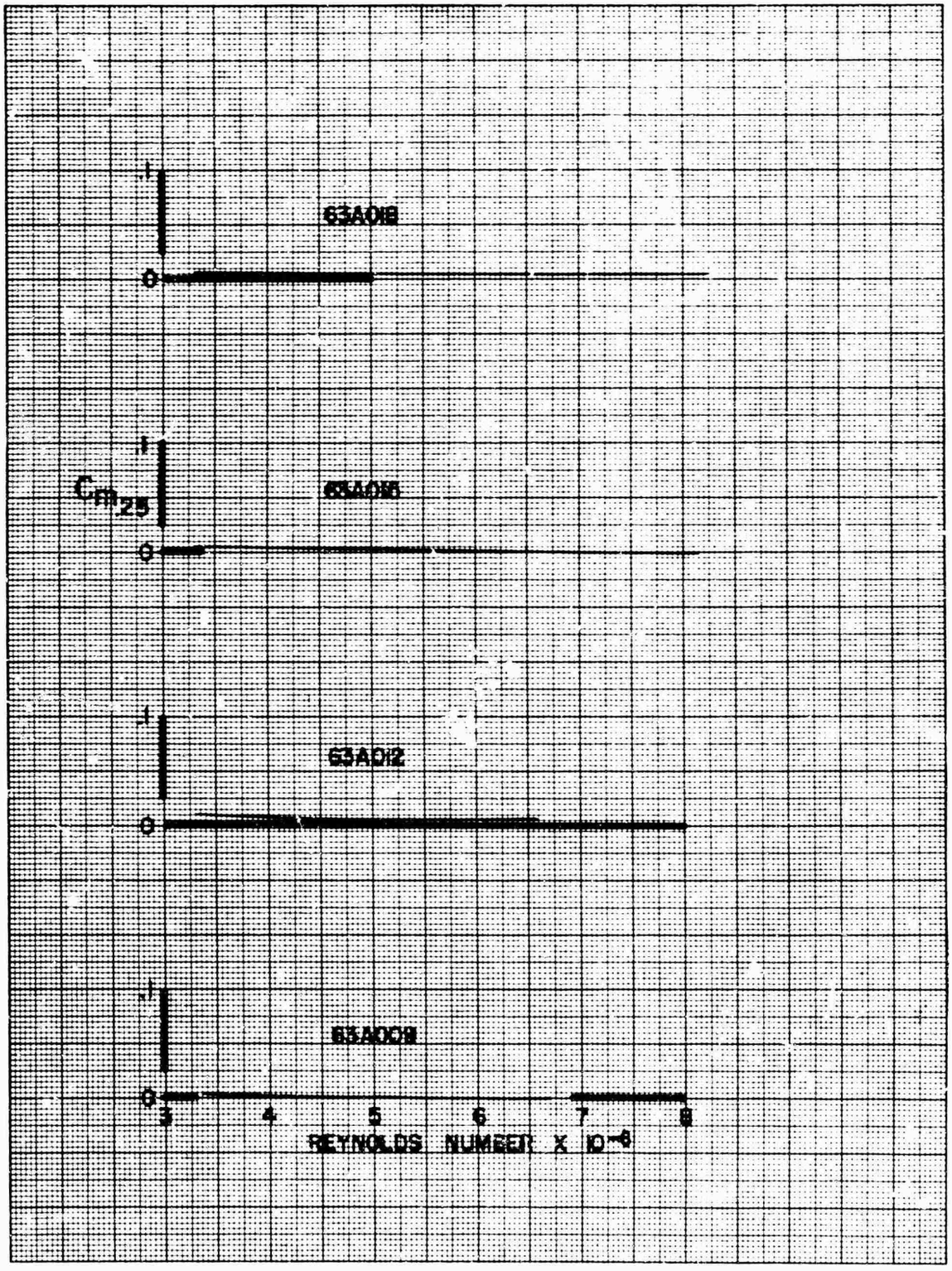


Figure 22C. Variation of Section Pitching Moment Coefficient at $\alpha = 0$ With Reynolds Number - M = .60

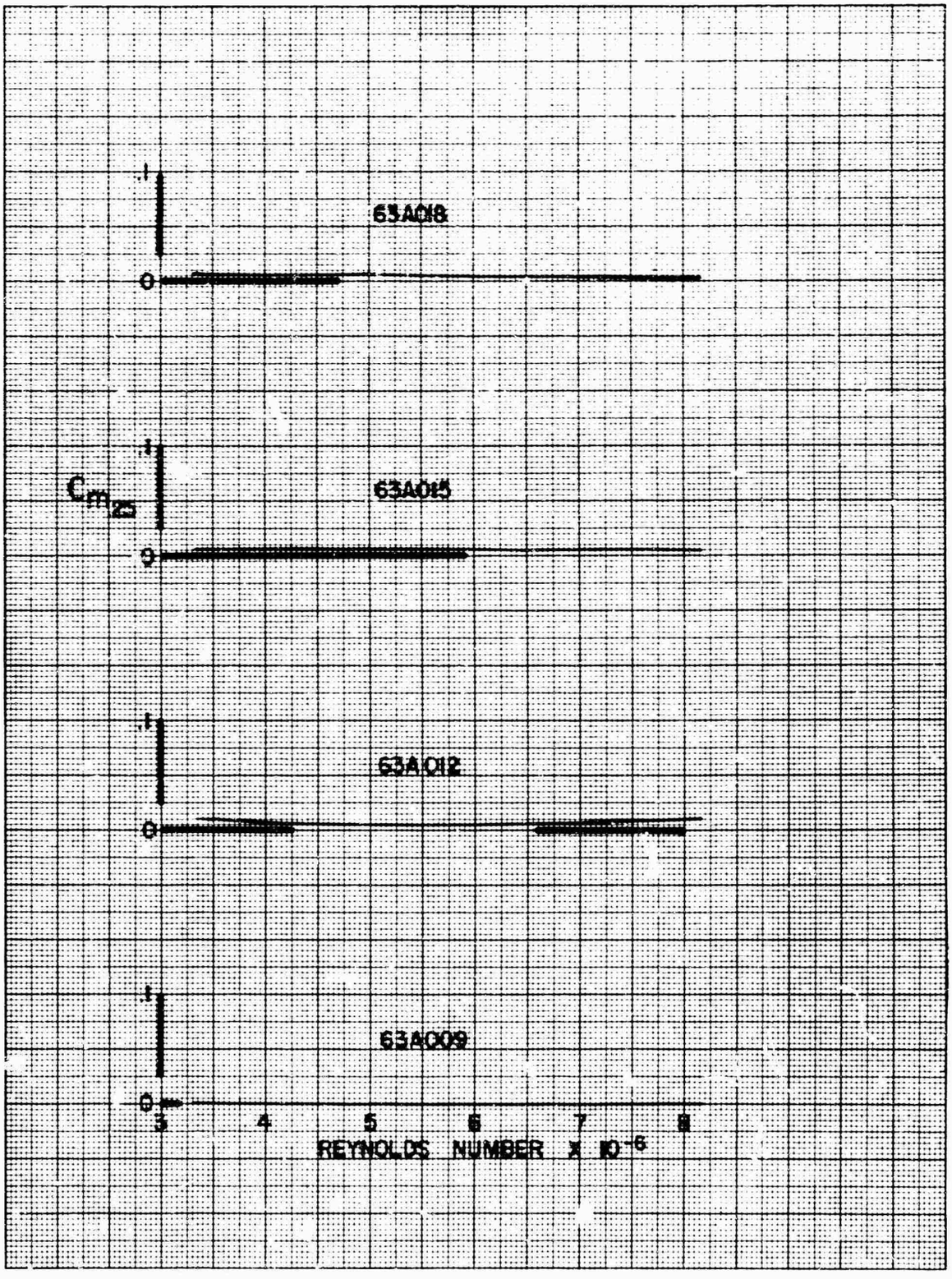


Figure 22D. Variation of Section Pitching Moment Coefficient at $\alpha = 0$ With Reynolds Number - M = .70

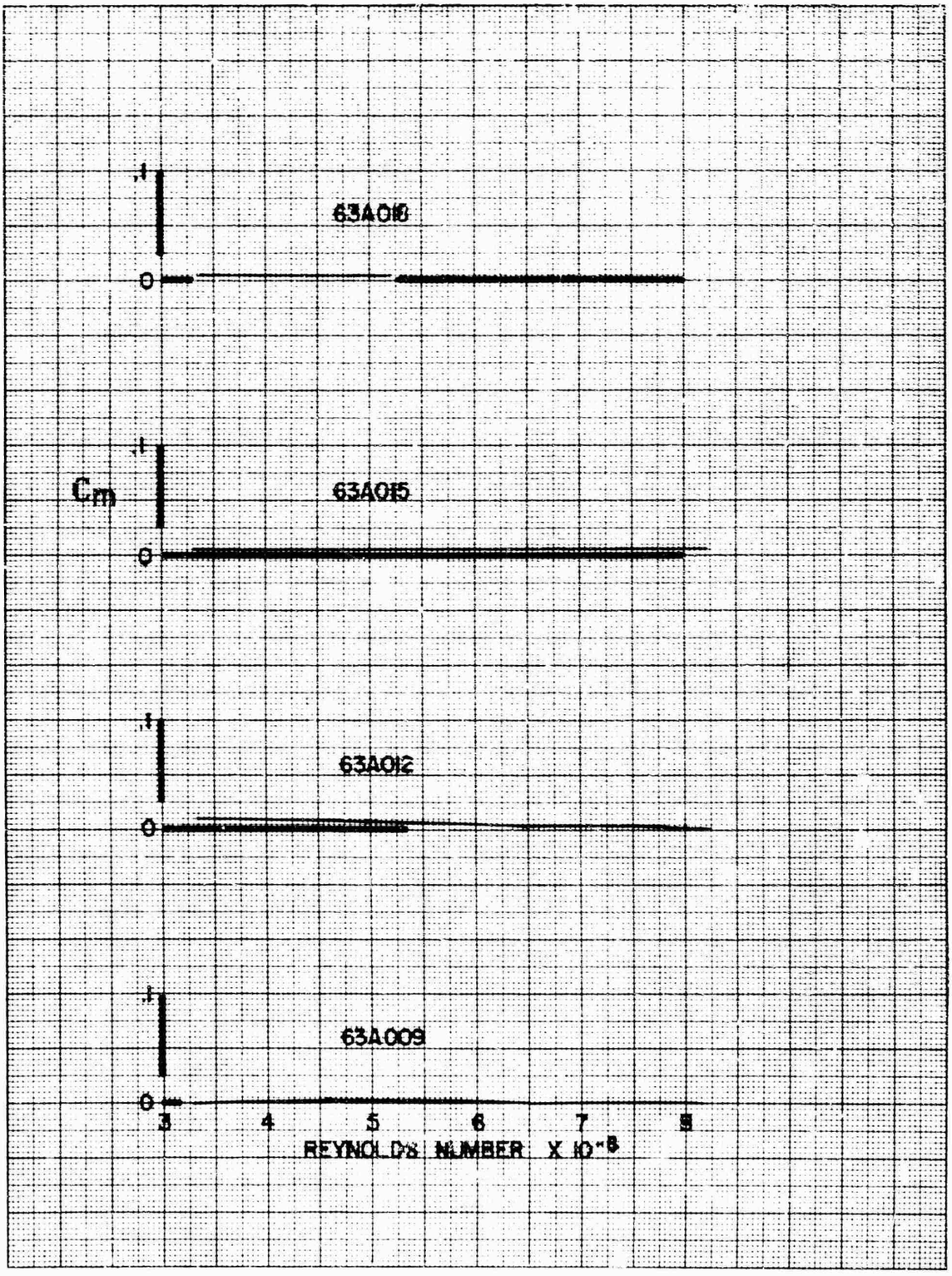


Figure 22E. Variation of Section Pitching Moment Coefficient at $\alpha = 0$ With Reynolds Number - M = .80

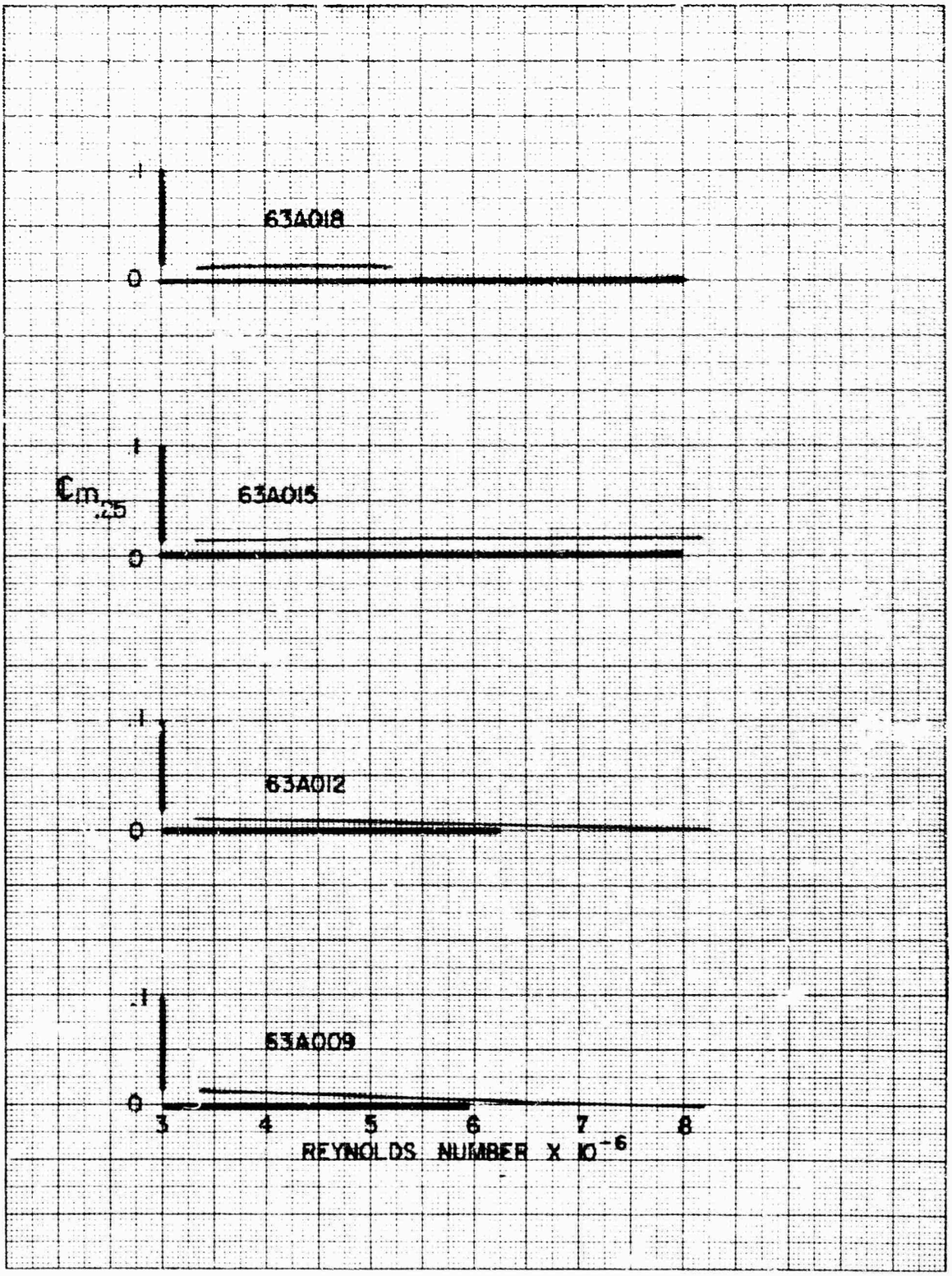


Figure 22F. Variation of Section Pitching Moment Coefficient at $\alpha = 0$ With Reynolds Number - M = .90

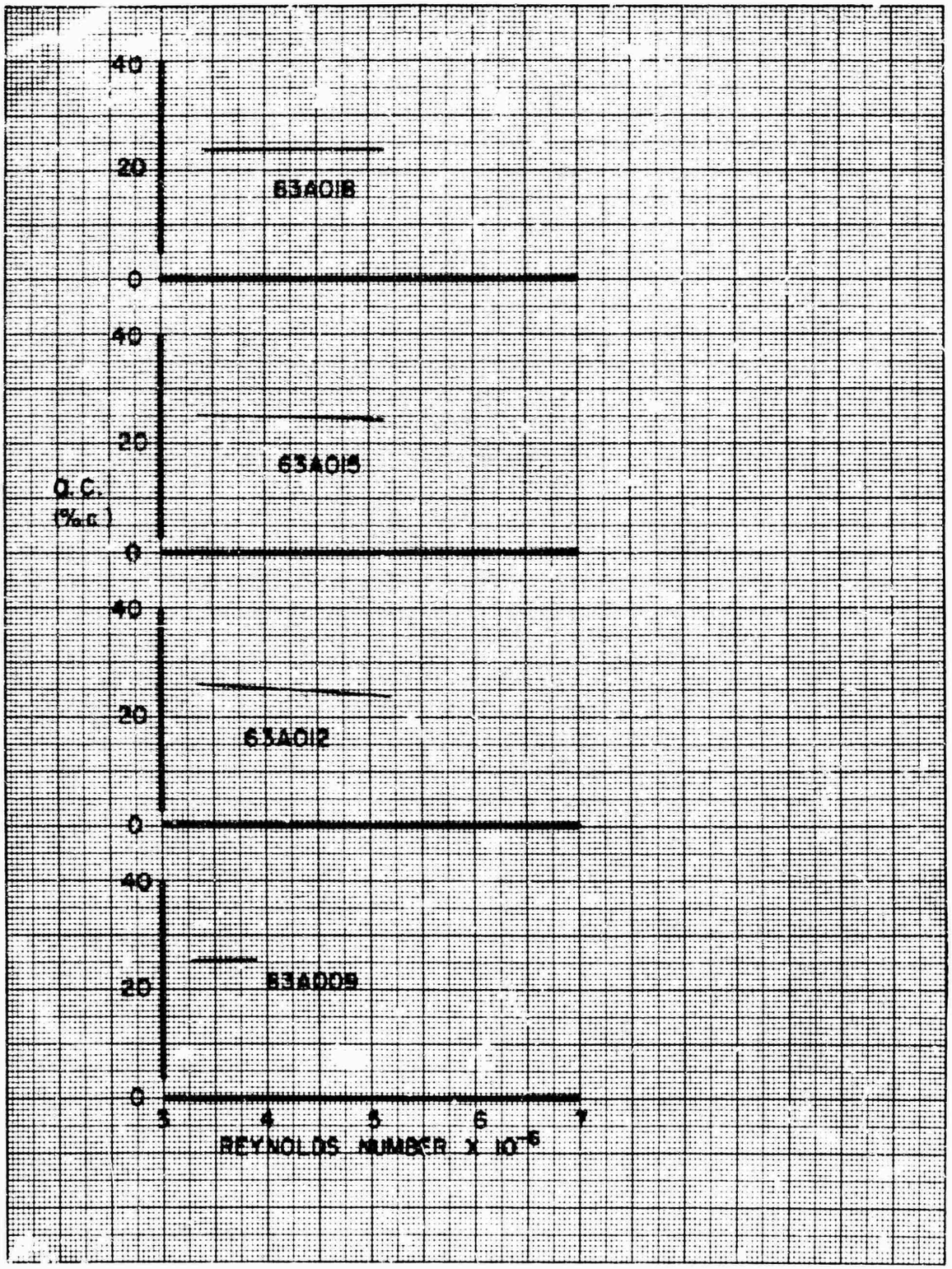


Figure 23A. Variation of Aerodynamic Center With Reynolds Number - M = .40

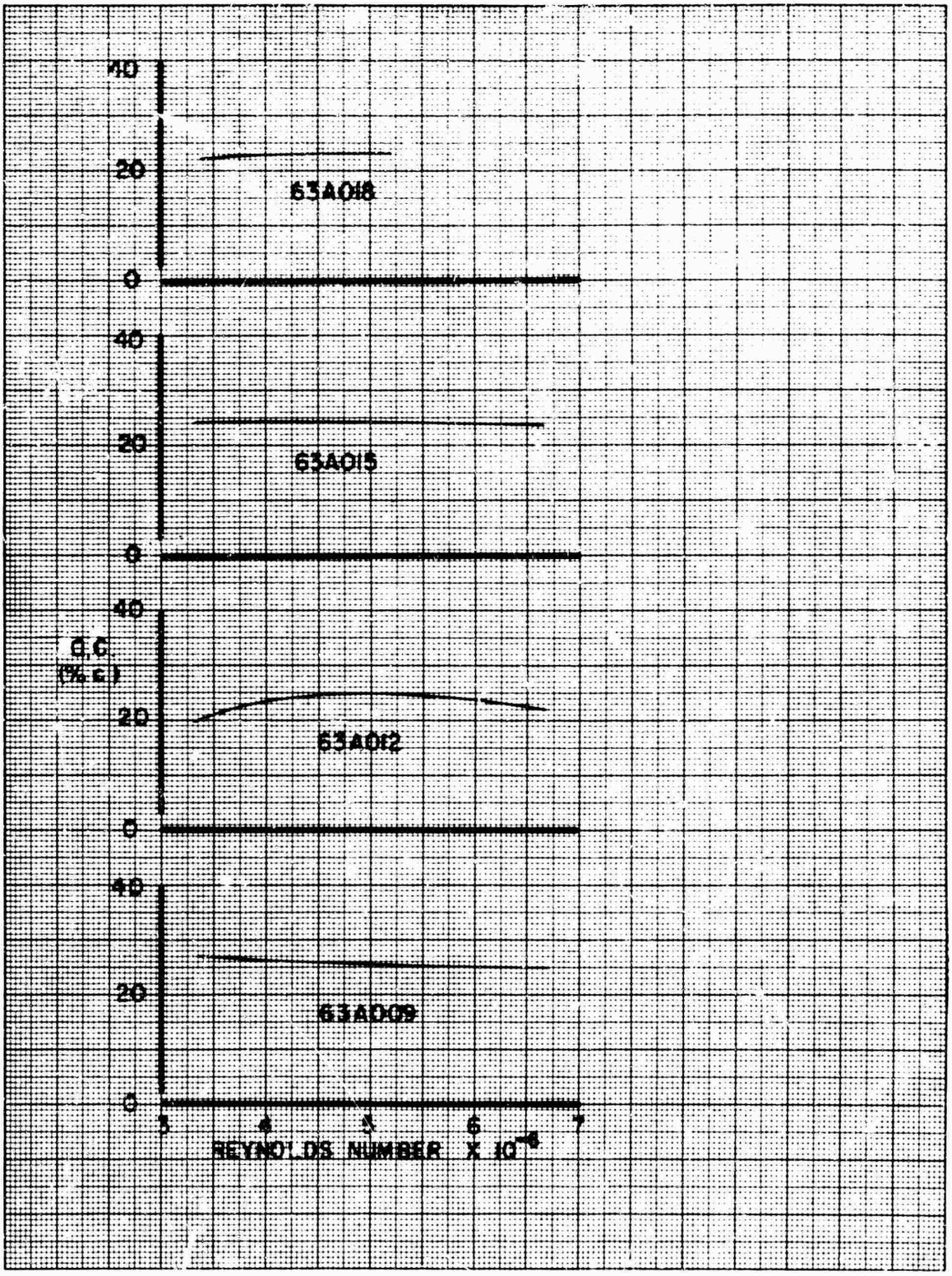


Figure 23B. Variation of Aerodynamic Center With Reynolds Number - M = .50

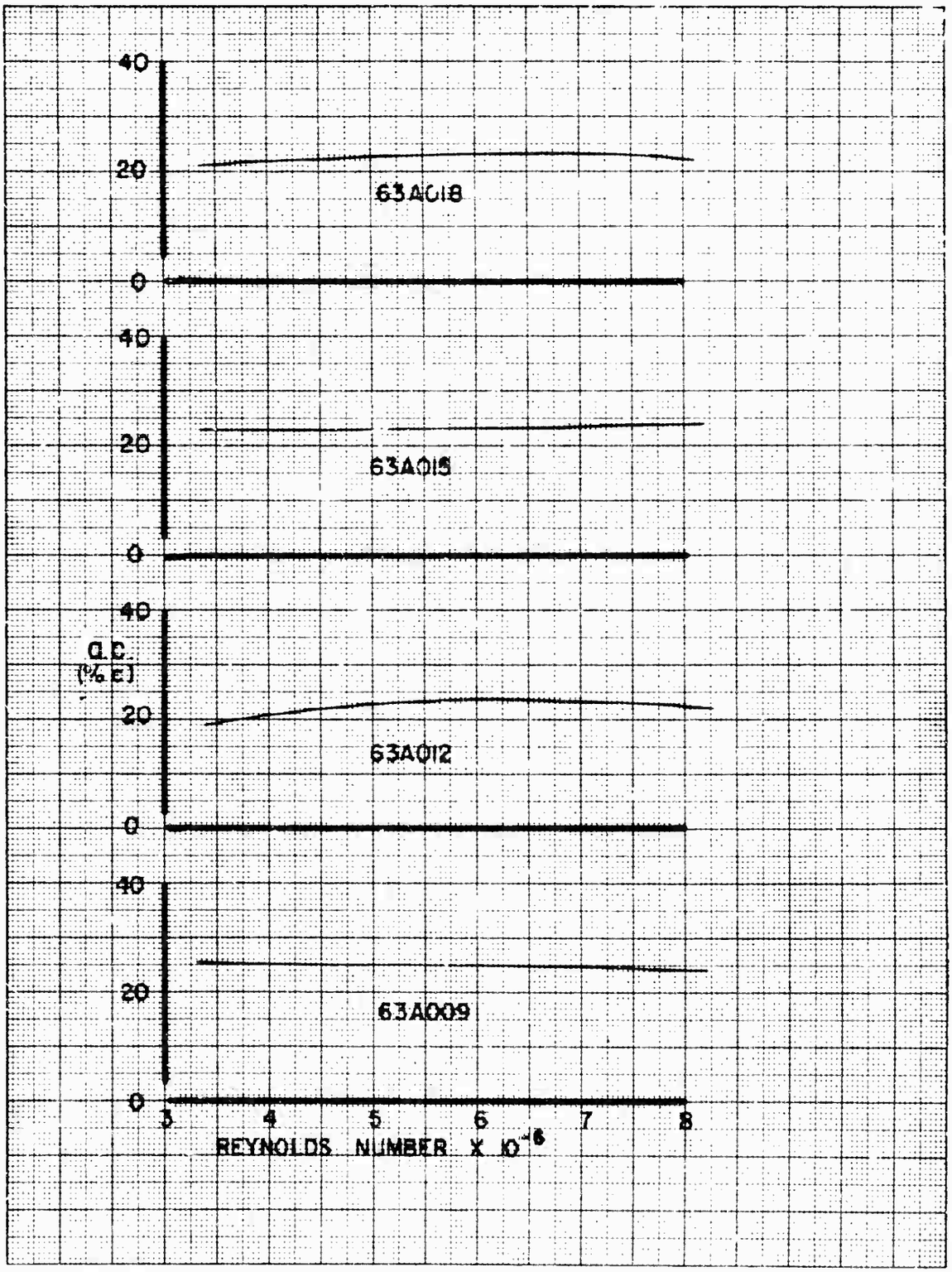


Figure 23C. Variation of Aerodynamic Center With Reynolds Number - M = .60

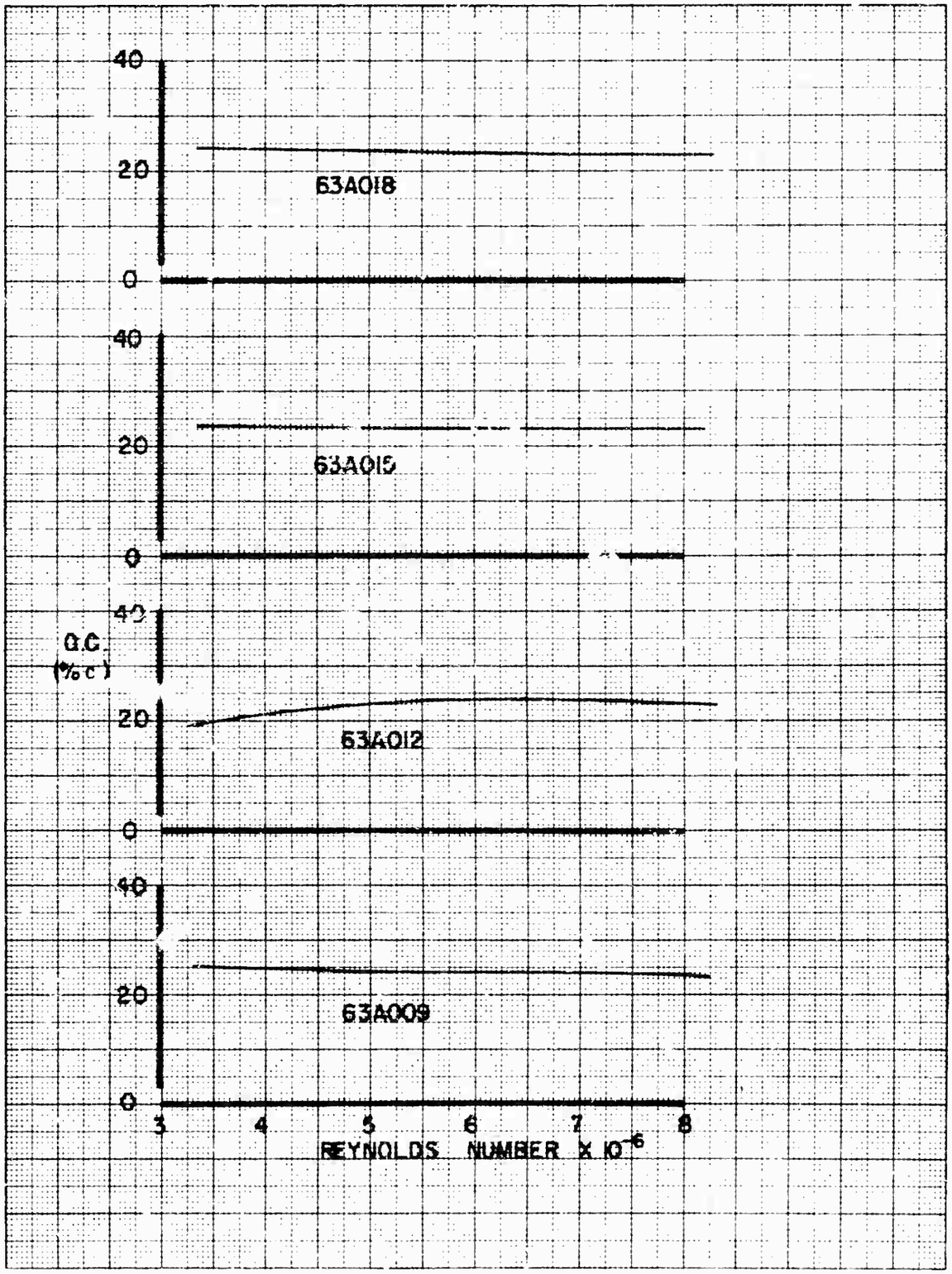


Figure 23D. Variation of Aerodynamic Center With Reynolds Number - M = .70

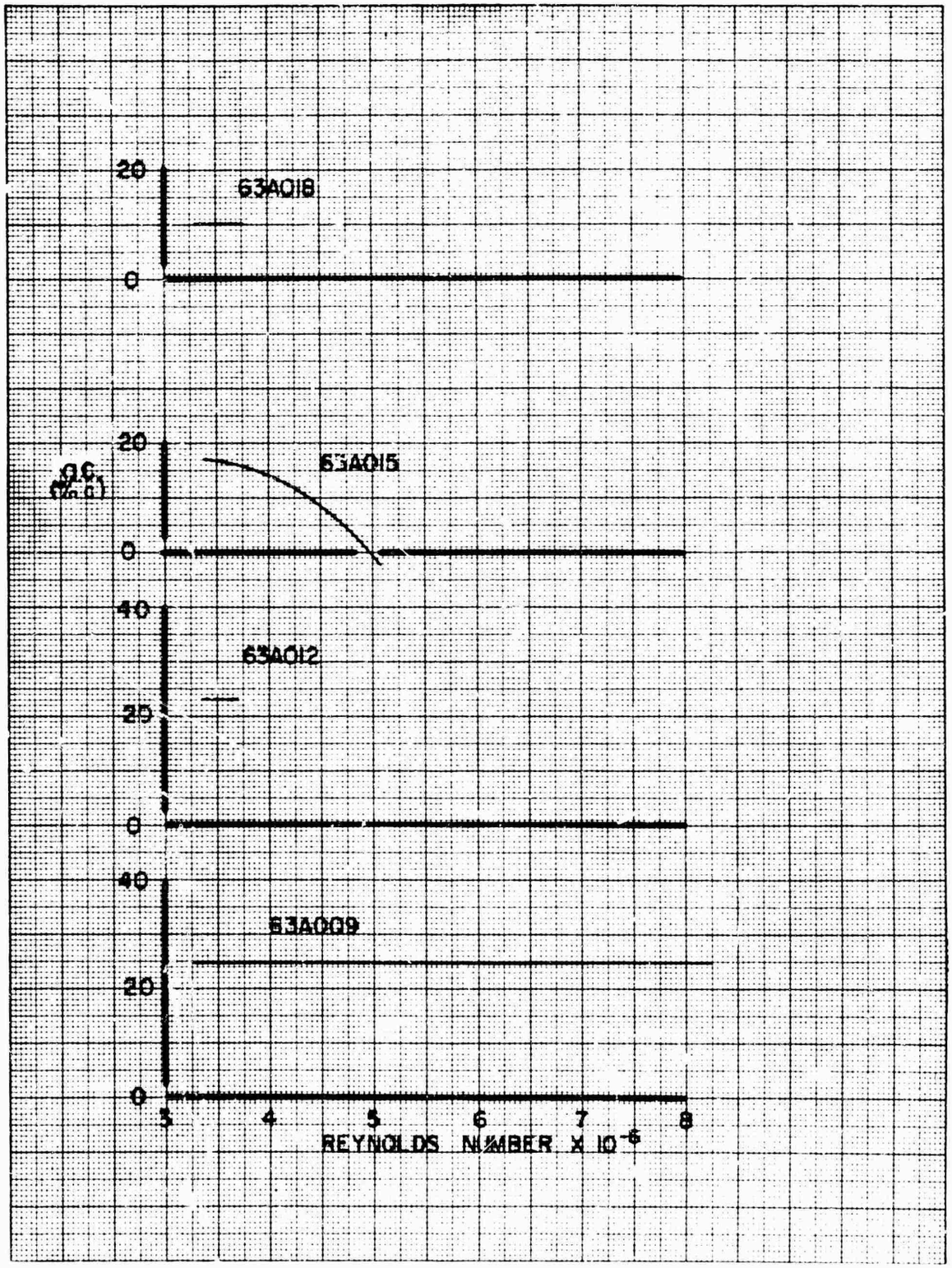


Figure 23E. Variation of Aerodynamic Center With Reynolds Number - M = .80

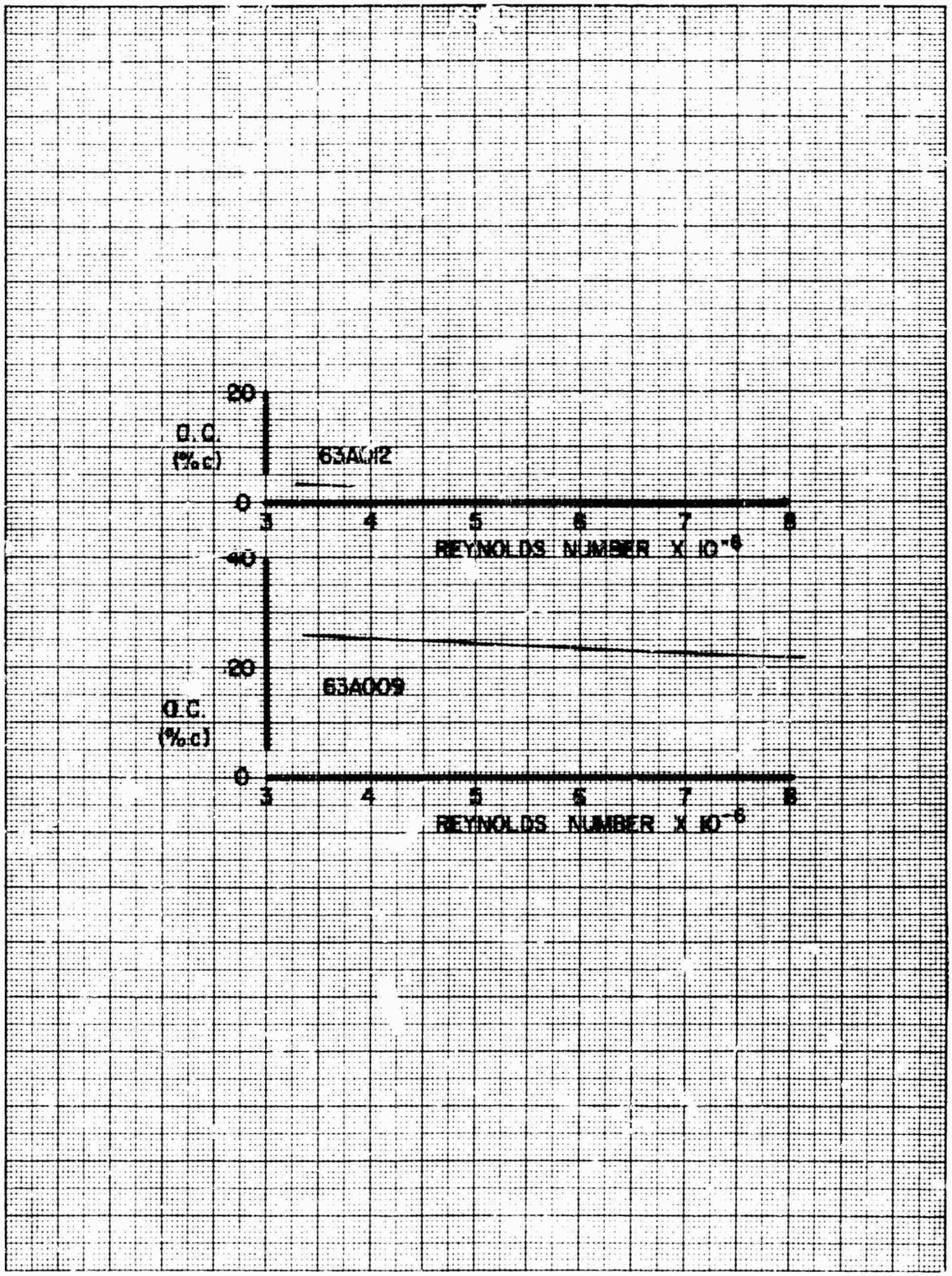


Figure 23F. Variation of Aerodynamic Center With Reynolds Number - M = .90

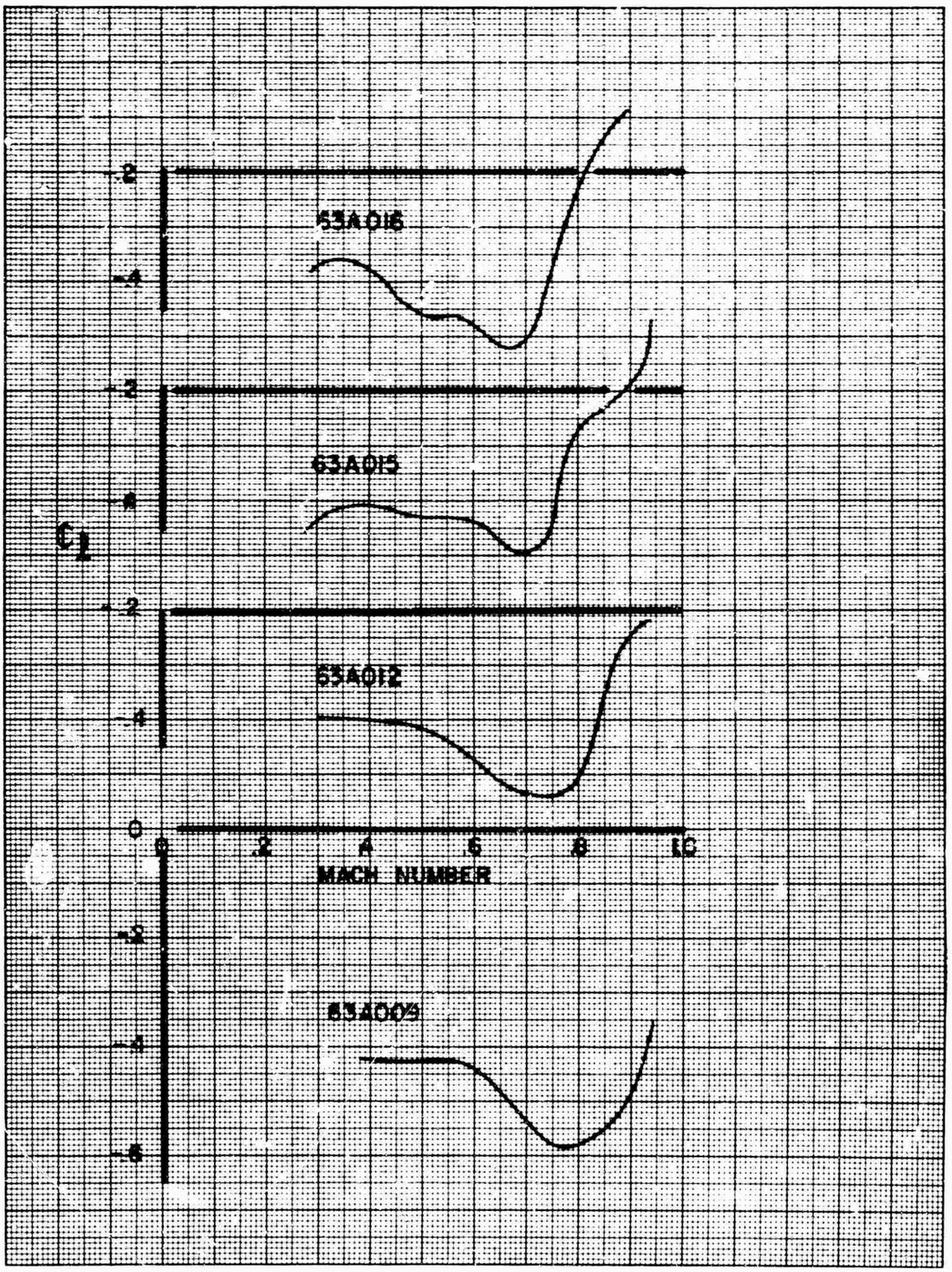


Figure 24A. Section Lift Coefficient Comparison for Various Thickness Ratios, $R = 3.5 \times 10^6$, $\alpha = -4$ Degrees

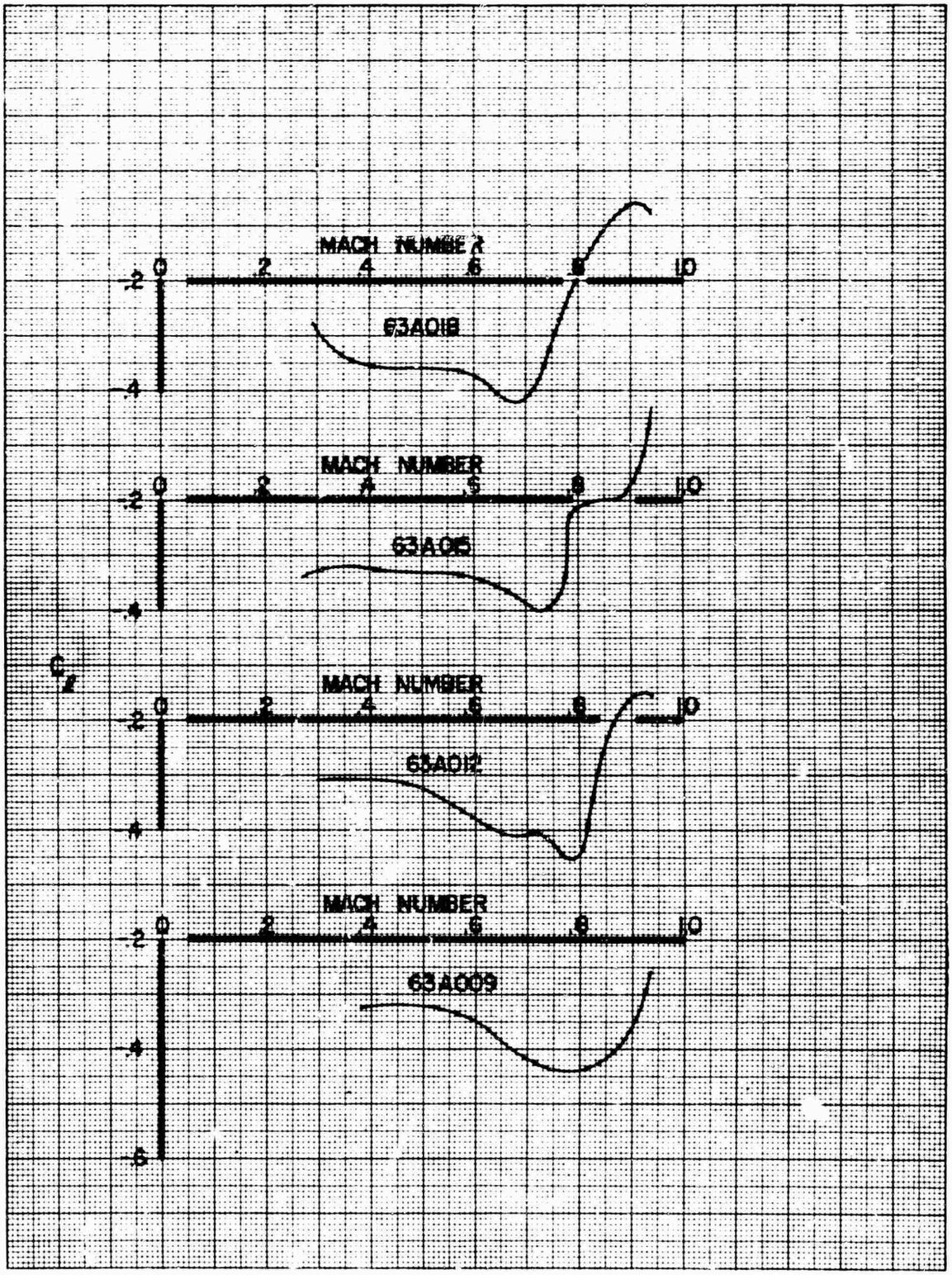


Figure 24B. Section Lift Coefficient Comparison for Various Thickness Ratios, $R = 3.5 \times 10^6$, $\alpha = -3$ Degrees

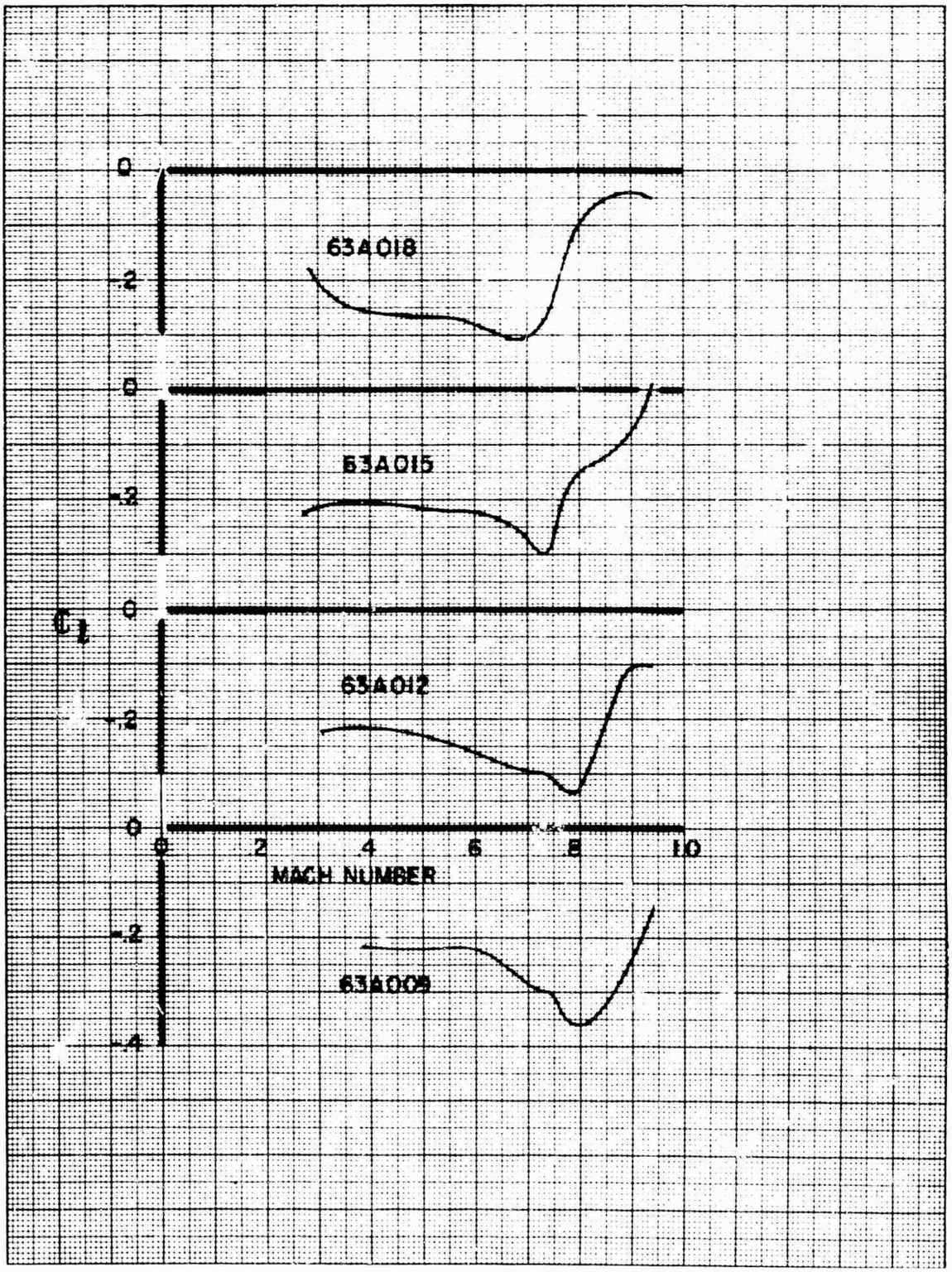


Figure 24C. Section Lift Coefficient Comparison for Various Thickness Ratios, $R = 3.5 \times 10^6$, $\alpha = -2$ Degrees

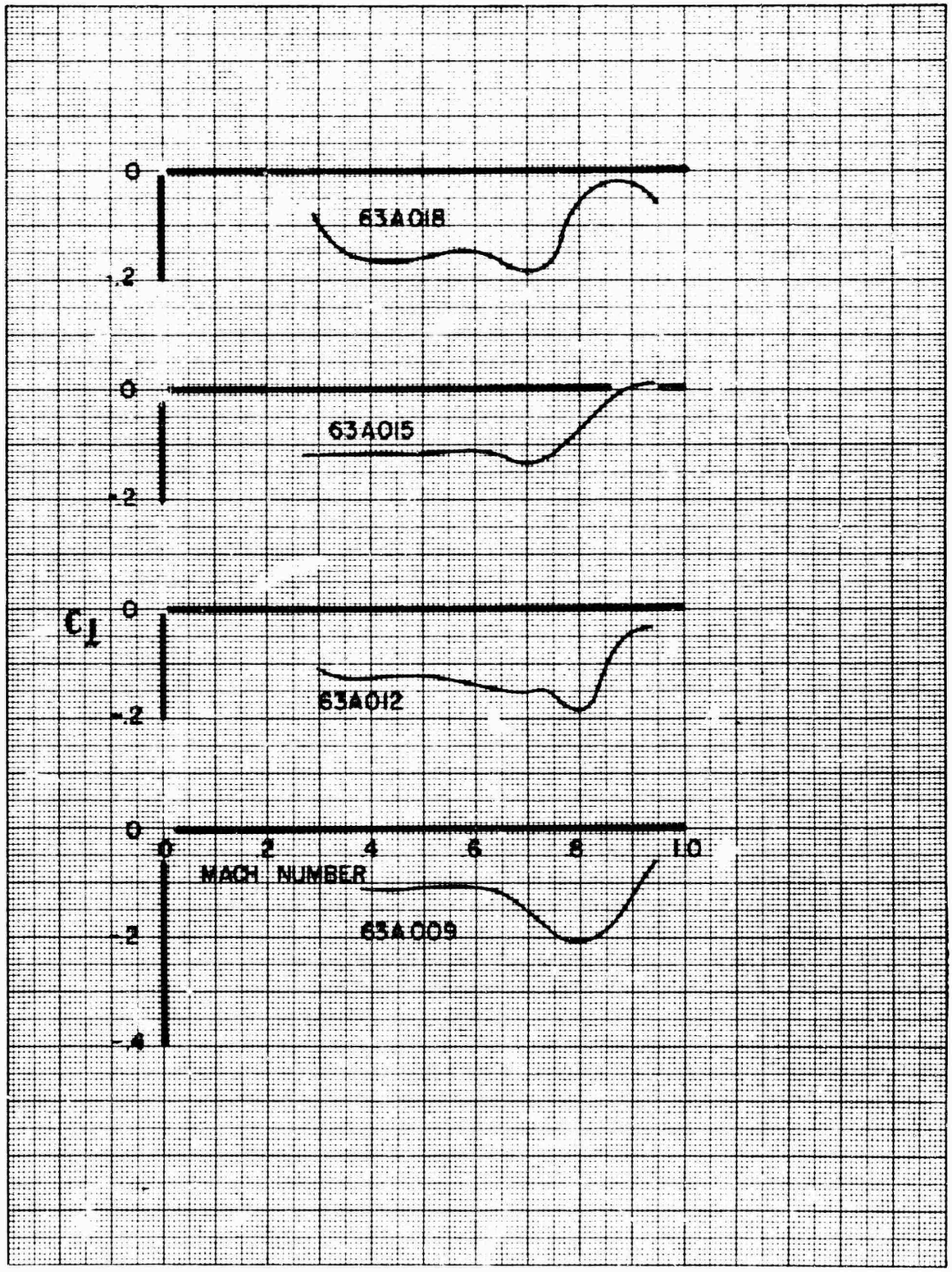


Figure 24D. Section Lift Coefficient Comparison for Various Thickness Ratios, $R = 3.5 \times 10^6$, $\alpha = -1$ Degree

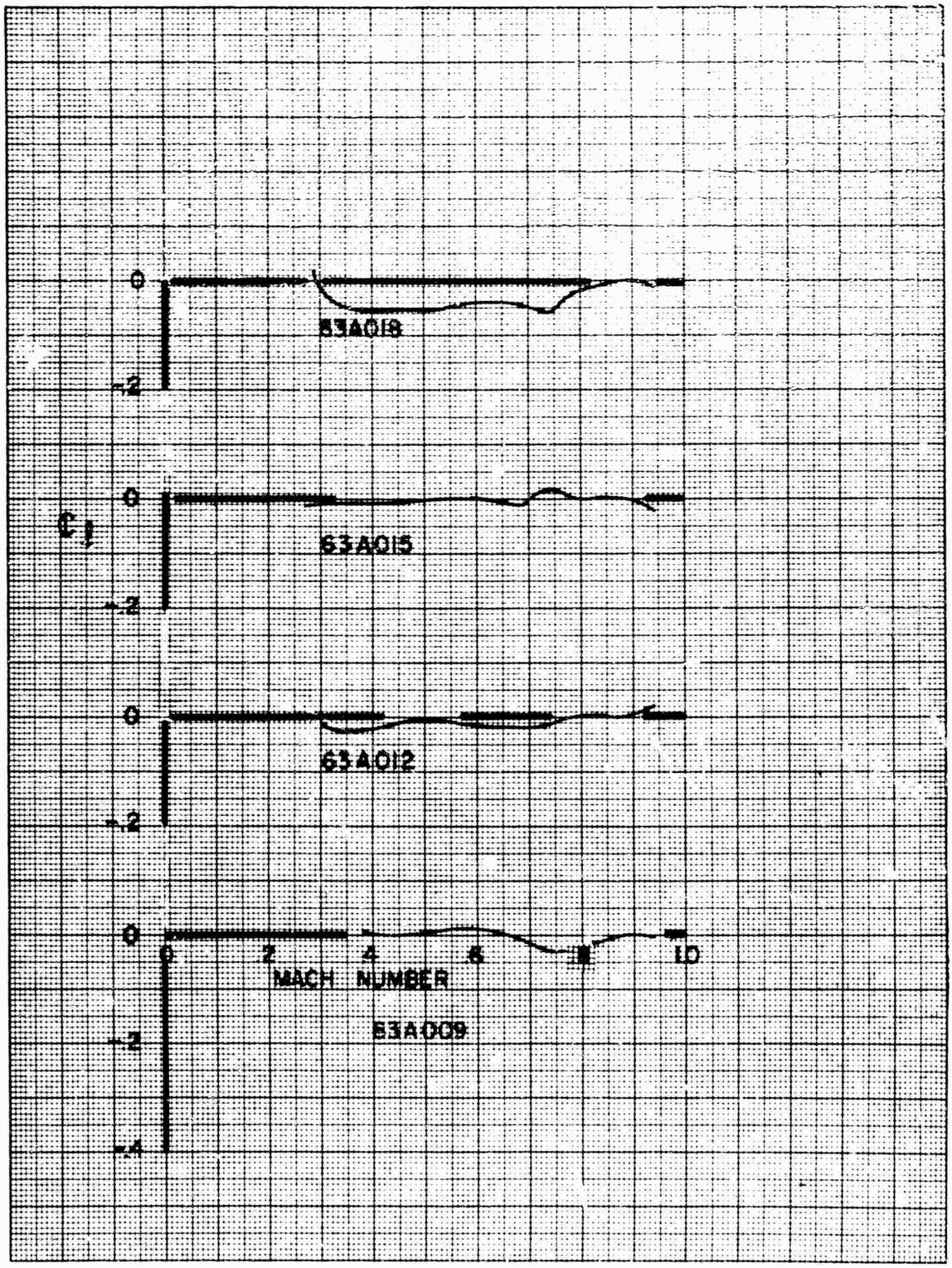


Figure 2.1E. Section Lift Coefficient Comparison for Various Thickness Ratios, $R = 3.5 \times 10^6$, $\alpha = 0$ Degrees

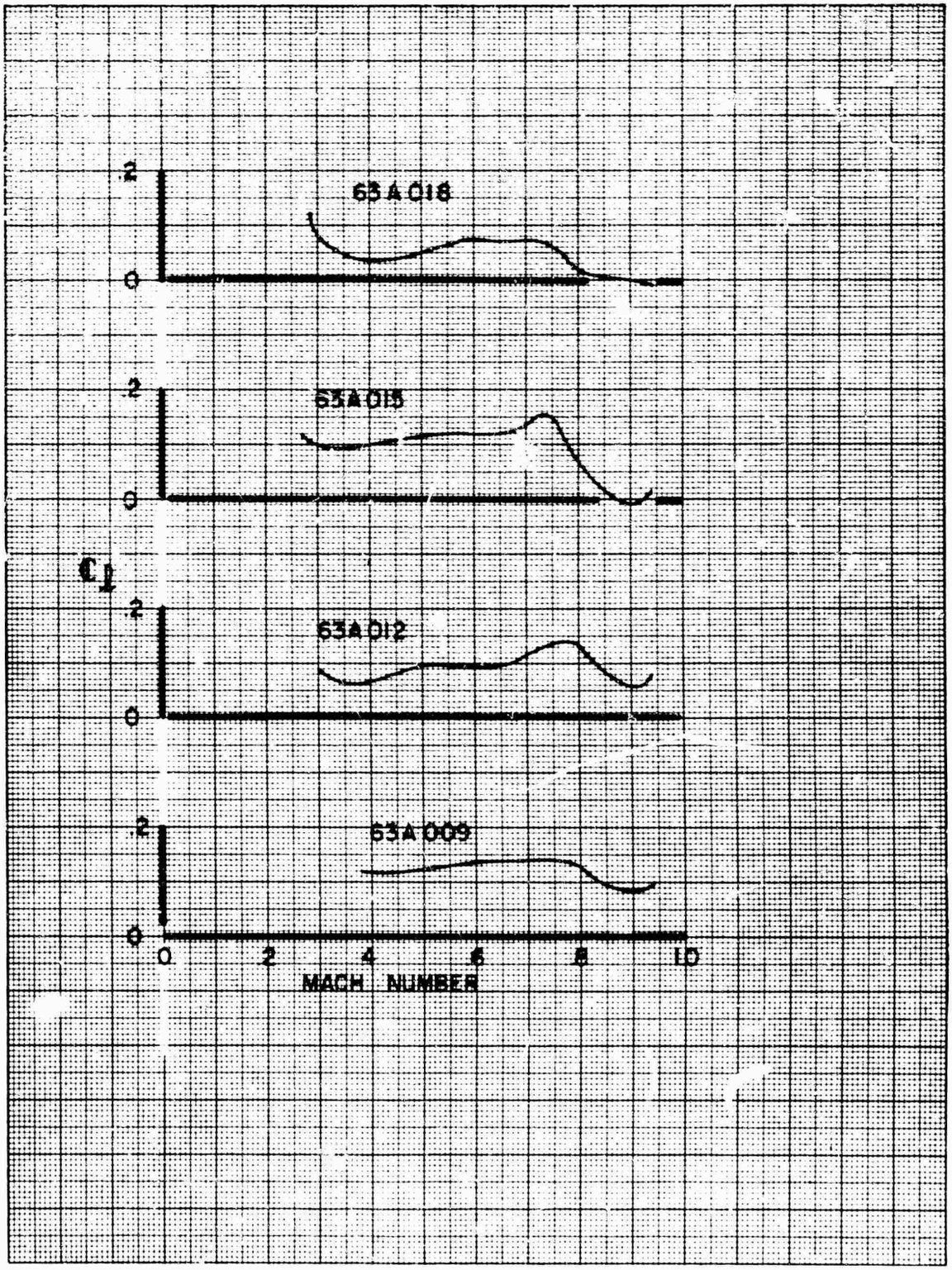


Figure 24F. Section Lift Coefficient Comparison for Various Thickness Ratios, $R = 3.5 \times 10^6$, $\alpha = 1$ Degree

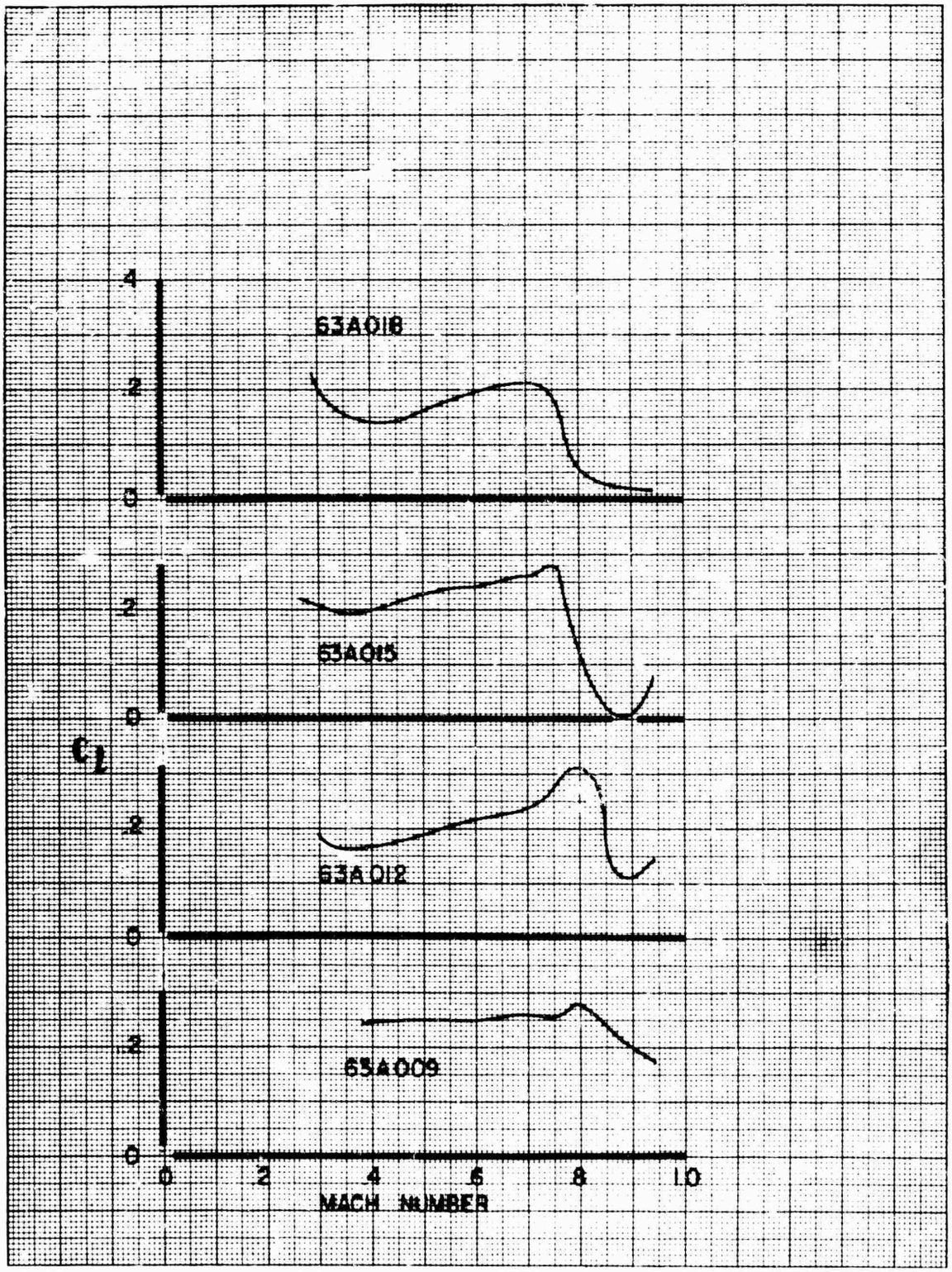


Figure 24G. Section Lift Coefficient Comparison for Various Thickness Ratios, $R = 3.5 \times 10^6$, $\alpha = 2$ Degrees

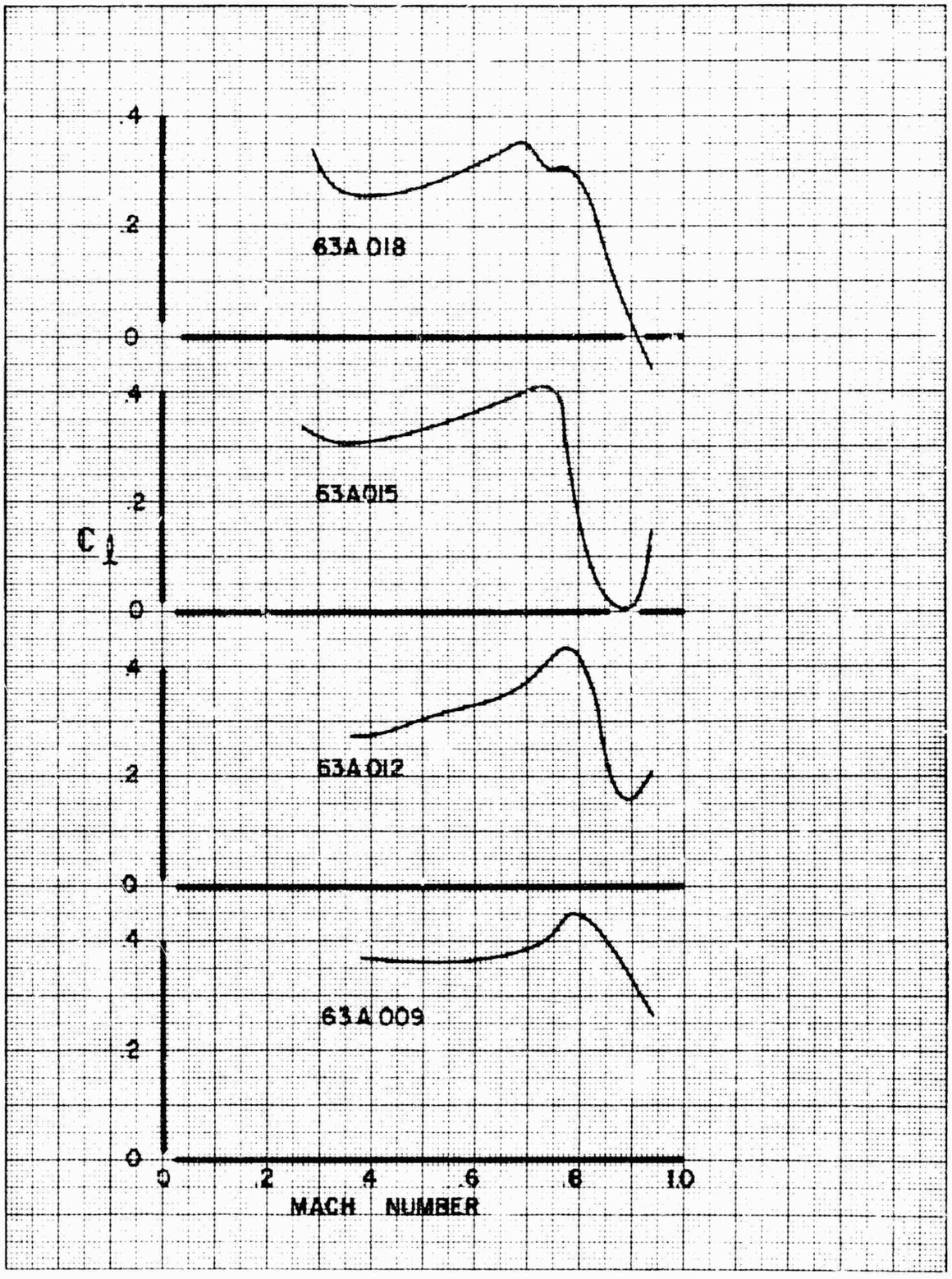


Figure 24H. Section Lift Coefficient Comparison for Various Thickness Ratios, $R = 3.5 \times 10^6$, $\alpha = 3$ Degrees

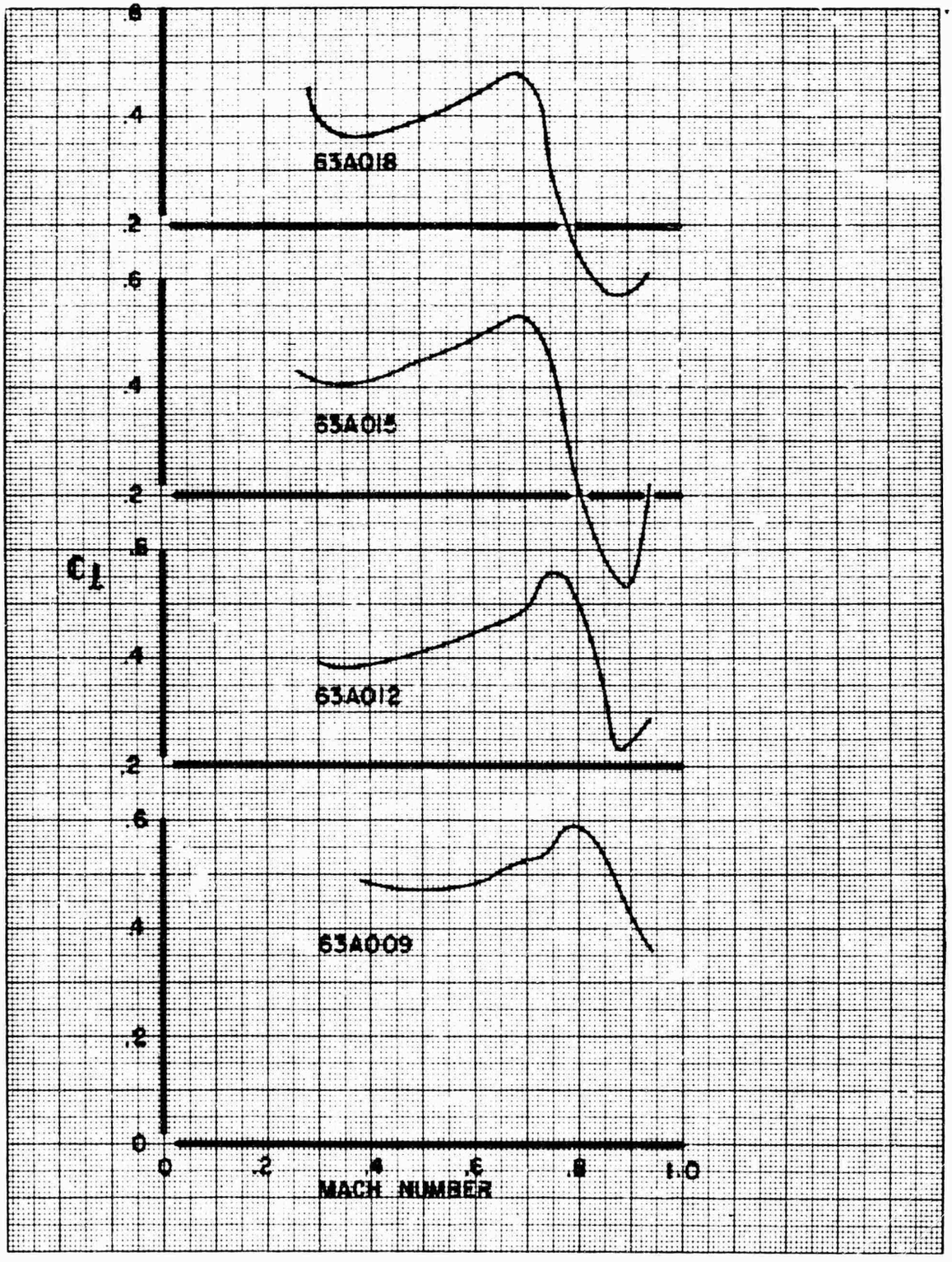


Figure 241. Section Lift Coefficient Comparison for Various Thickness Ratios, $R = 3.5 \times 10^6$, $\alpha = 4$ Degrees

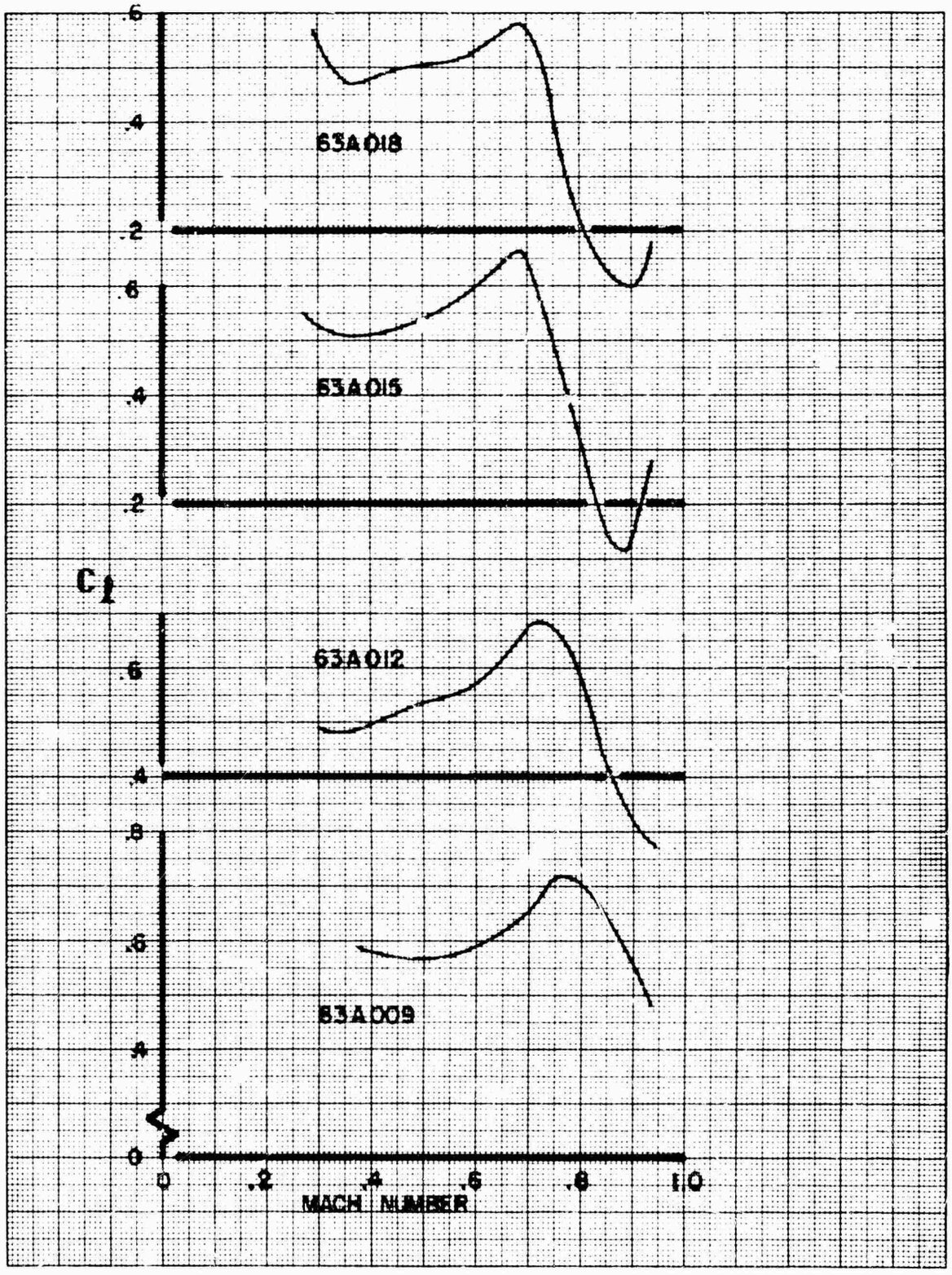


Figure 24J. Section Lift Coefficient Comparison for Various Thickness Ratios, $R = 3.5 \times 10^6$, $\alpha = 5$ Degrees

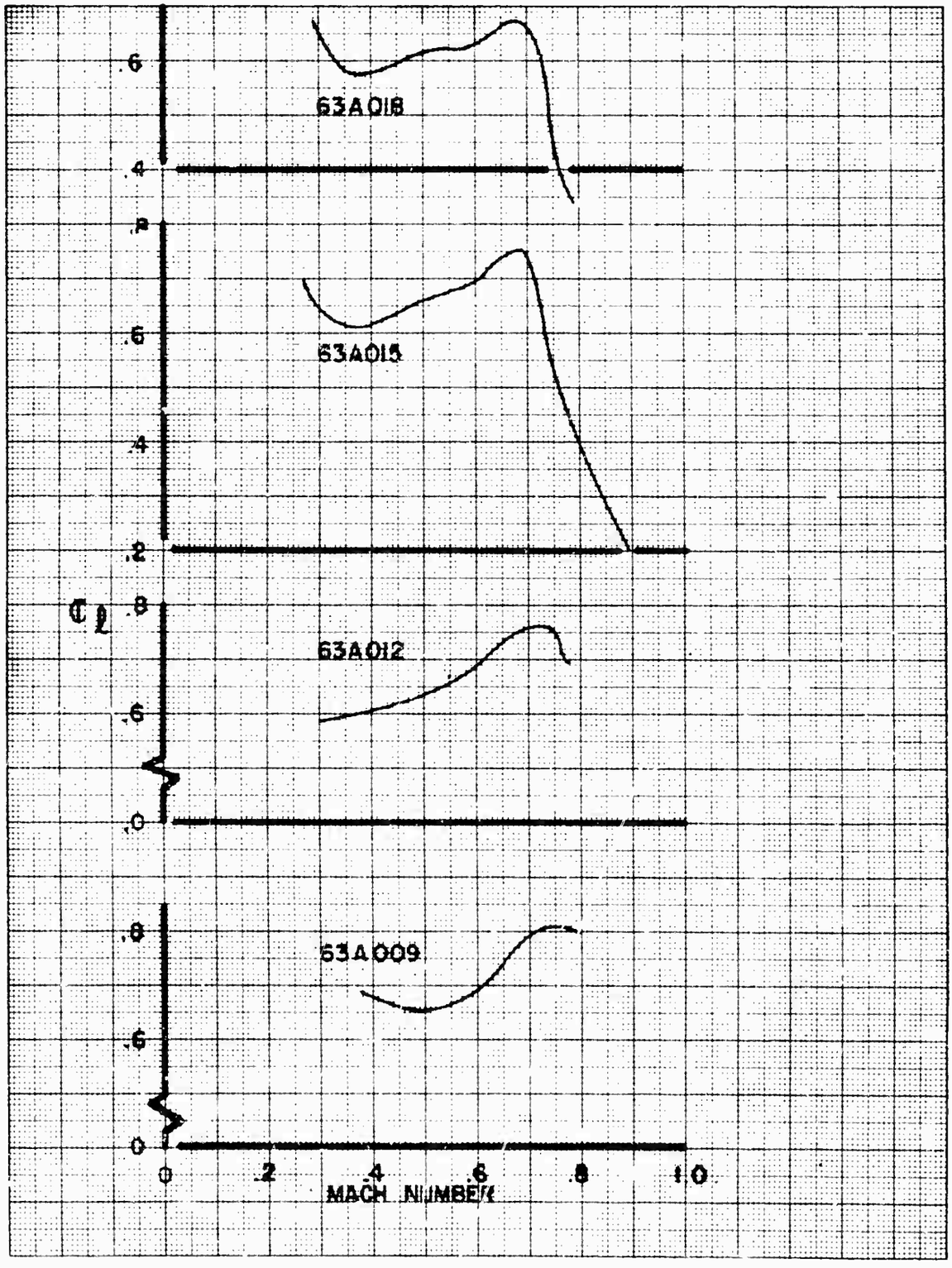


Figure 24K. Section Lift Coefficient Comparison for Various Thickness Ratios, $R = 3.5 \times 10^6$, $\alpha = 6$ Degrees

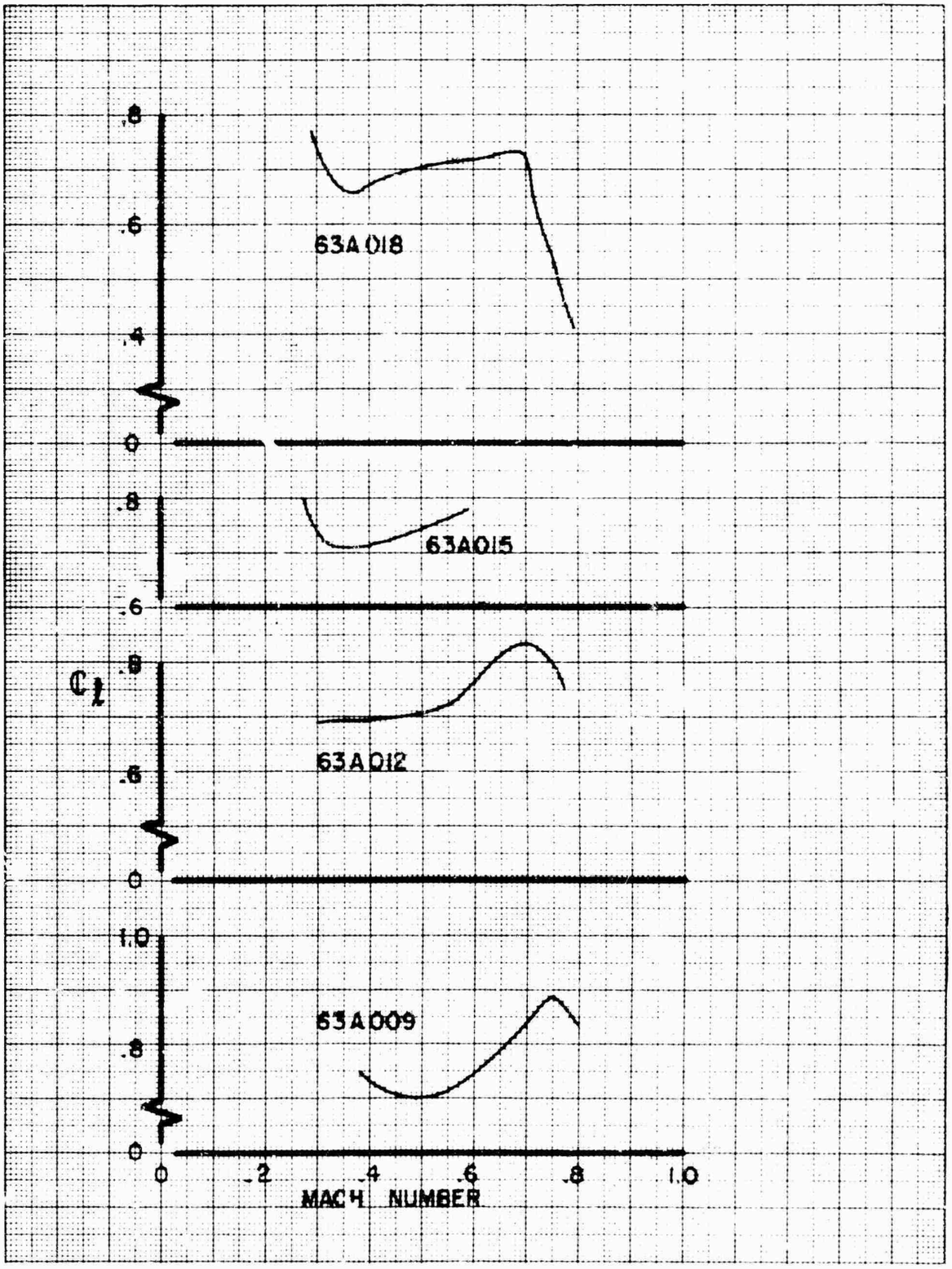


Figure 24L Section Lift Coefficient Comparison for Various Thickness Ratios, R = 3.5 x 10^6, α = 7 Degrees

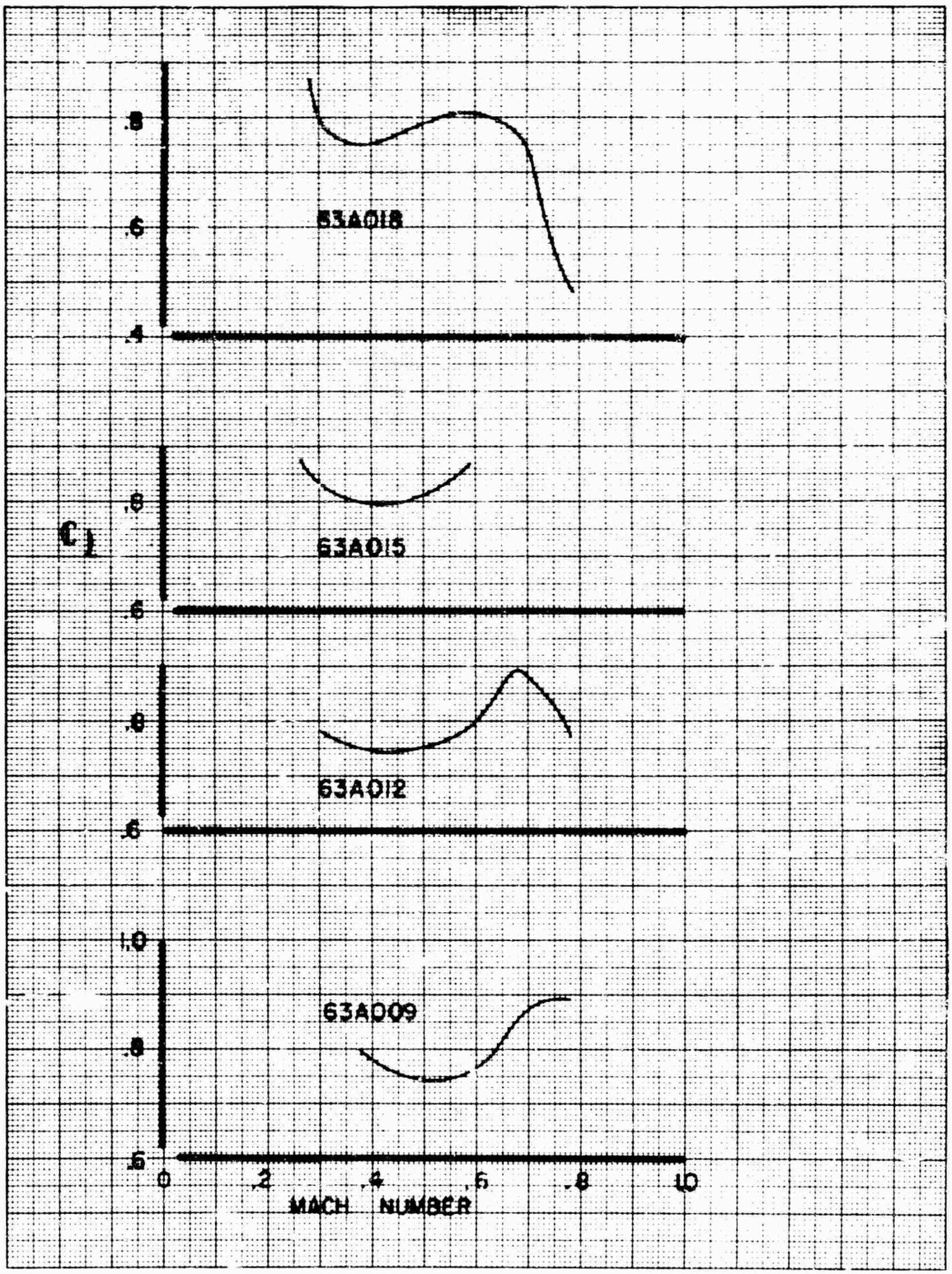


Figure 24M. Section Lift Coefficient Comparison for Various Thickness Ratios, $R = 3.5 \times 10^6$, $\alpha = 8$ Degrees

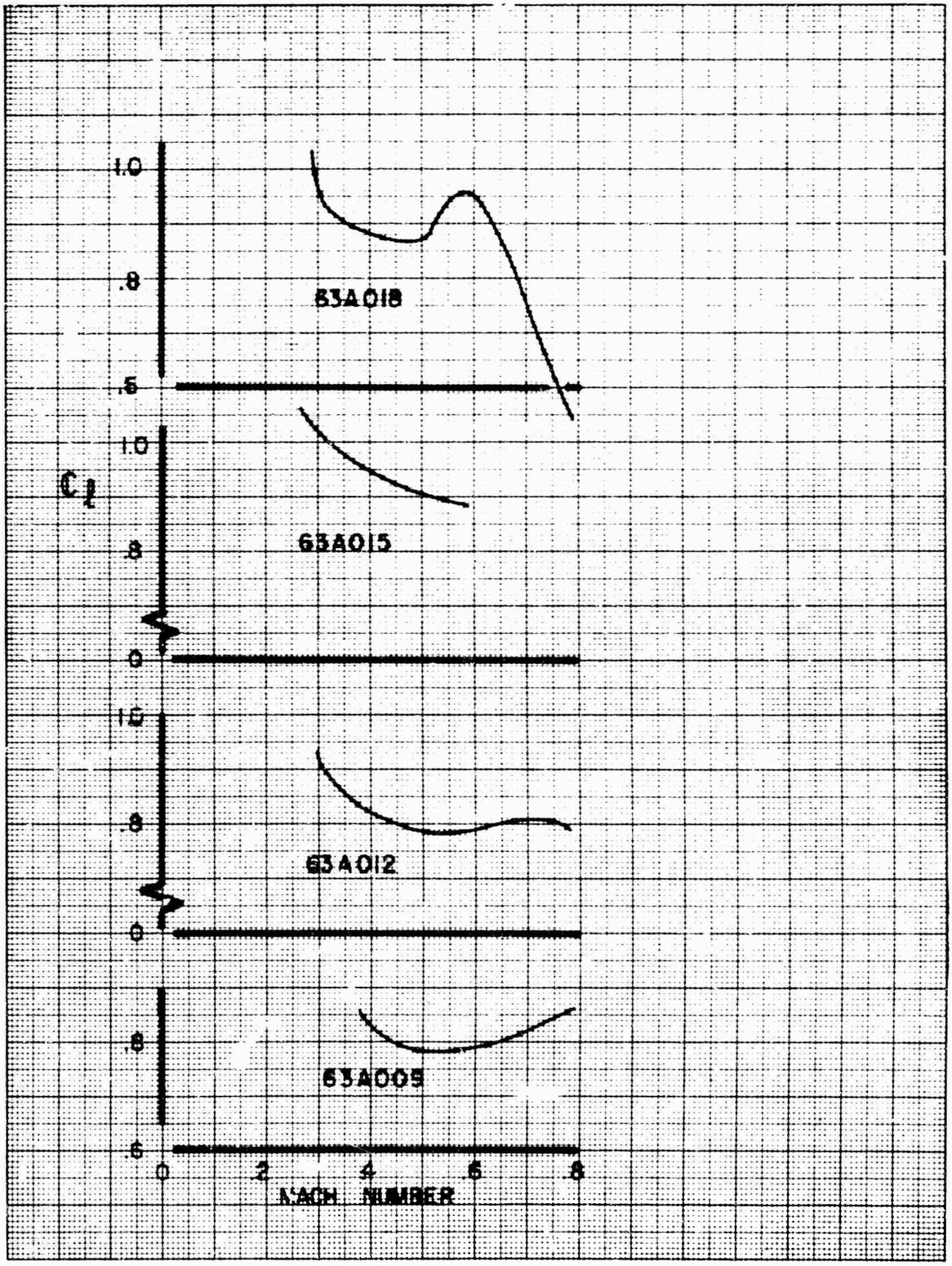


Figure 24N. Section Lift Coefficient Comparison for Various Thickness Ratios, $R = 3.5 \times 10^6$, $\alpha = 10$ Degrees

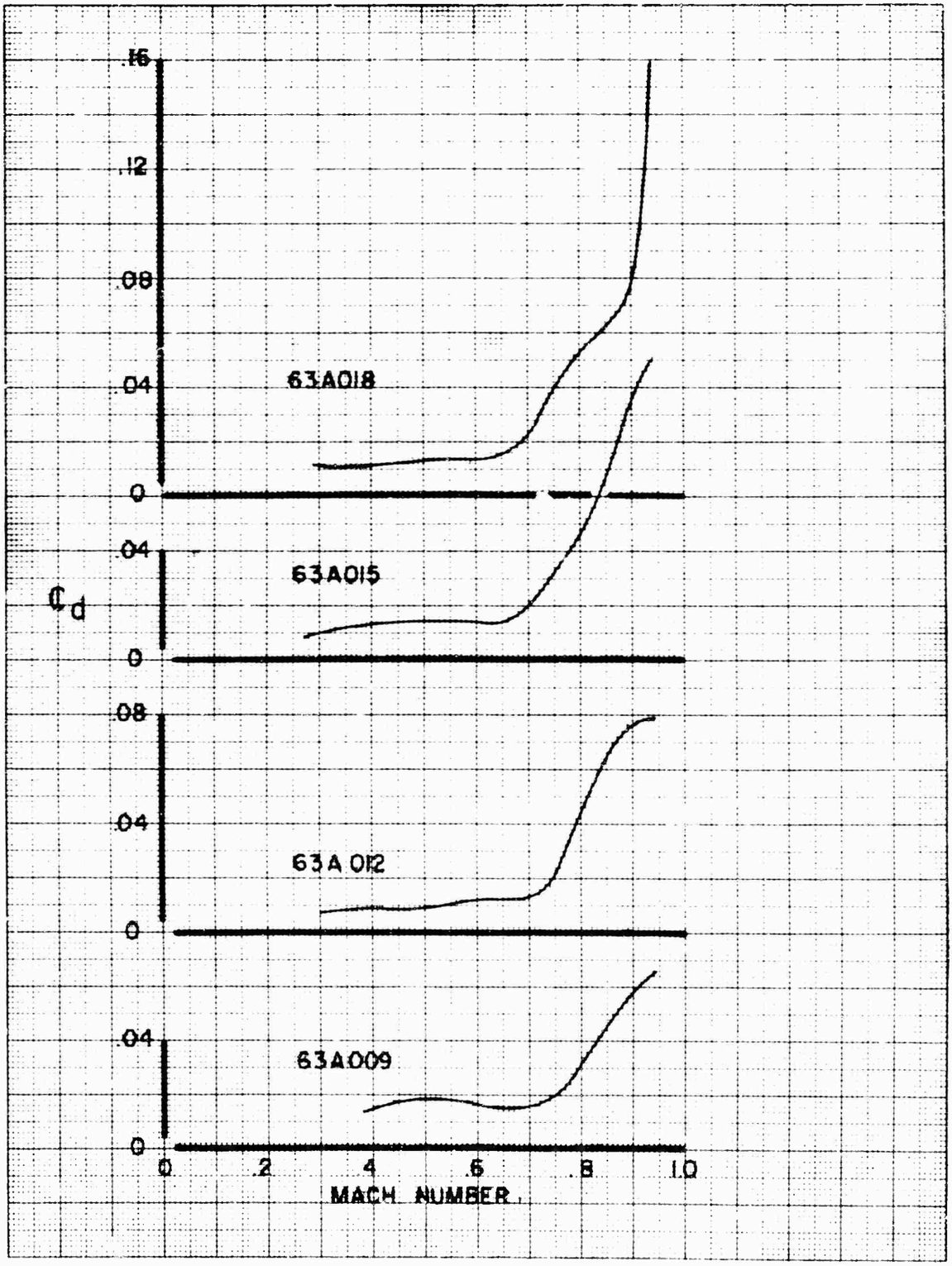


Figure 25A. Section Drag Coefficient Comparison for Various Thickness Ratios, $R = 3.5 \times 10^6$, $\alpha = -4$ Degrees

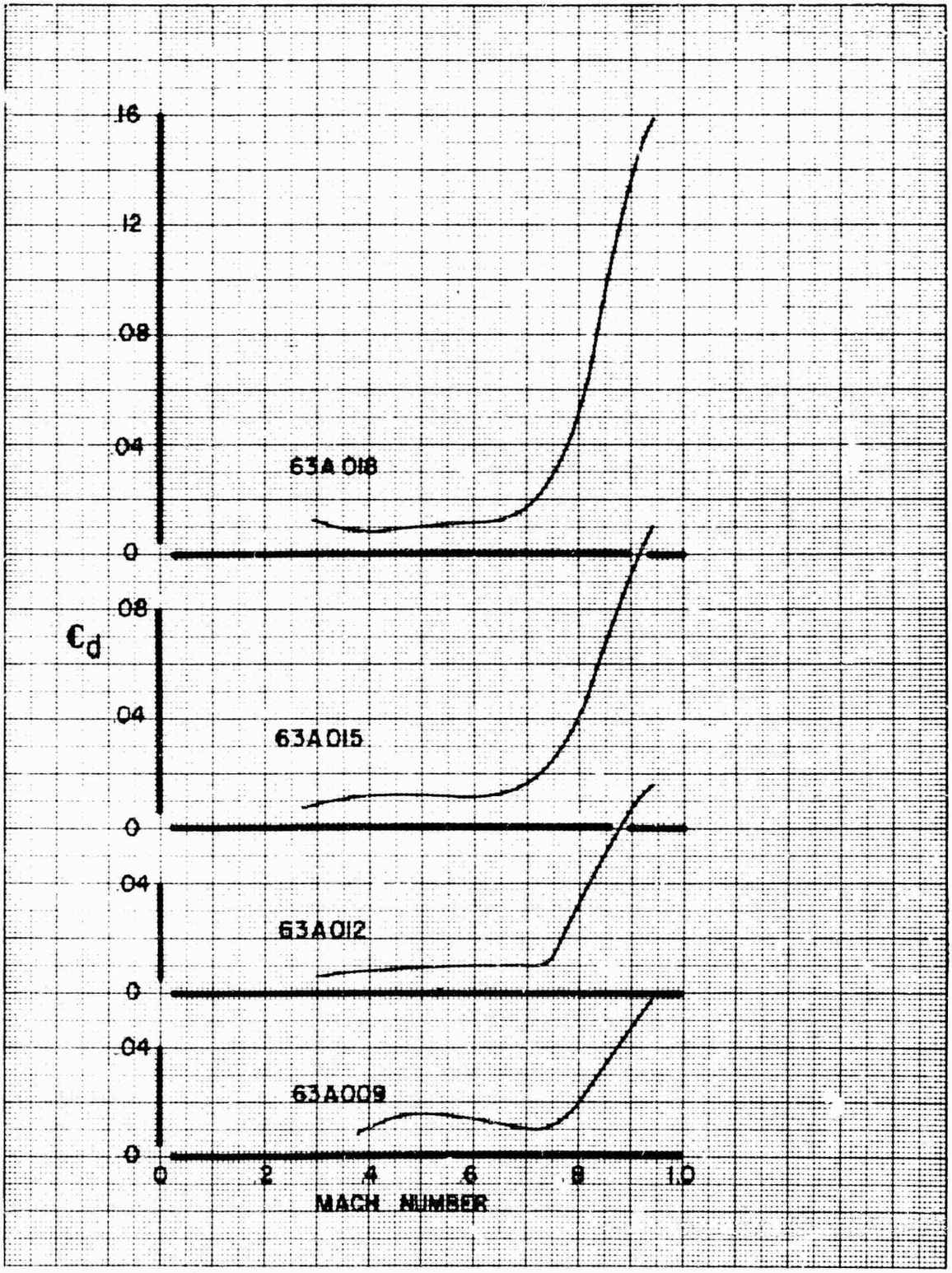


Figure 25B. Section Drag Coefficient Comparison for Various Thickness Ratios, $R = 3.5 \times 10^6$, $\alpha = -3$ Degrees

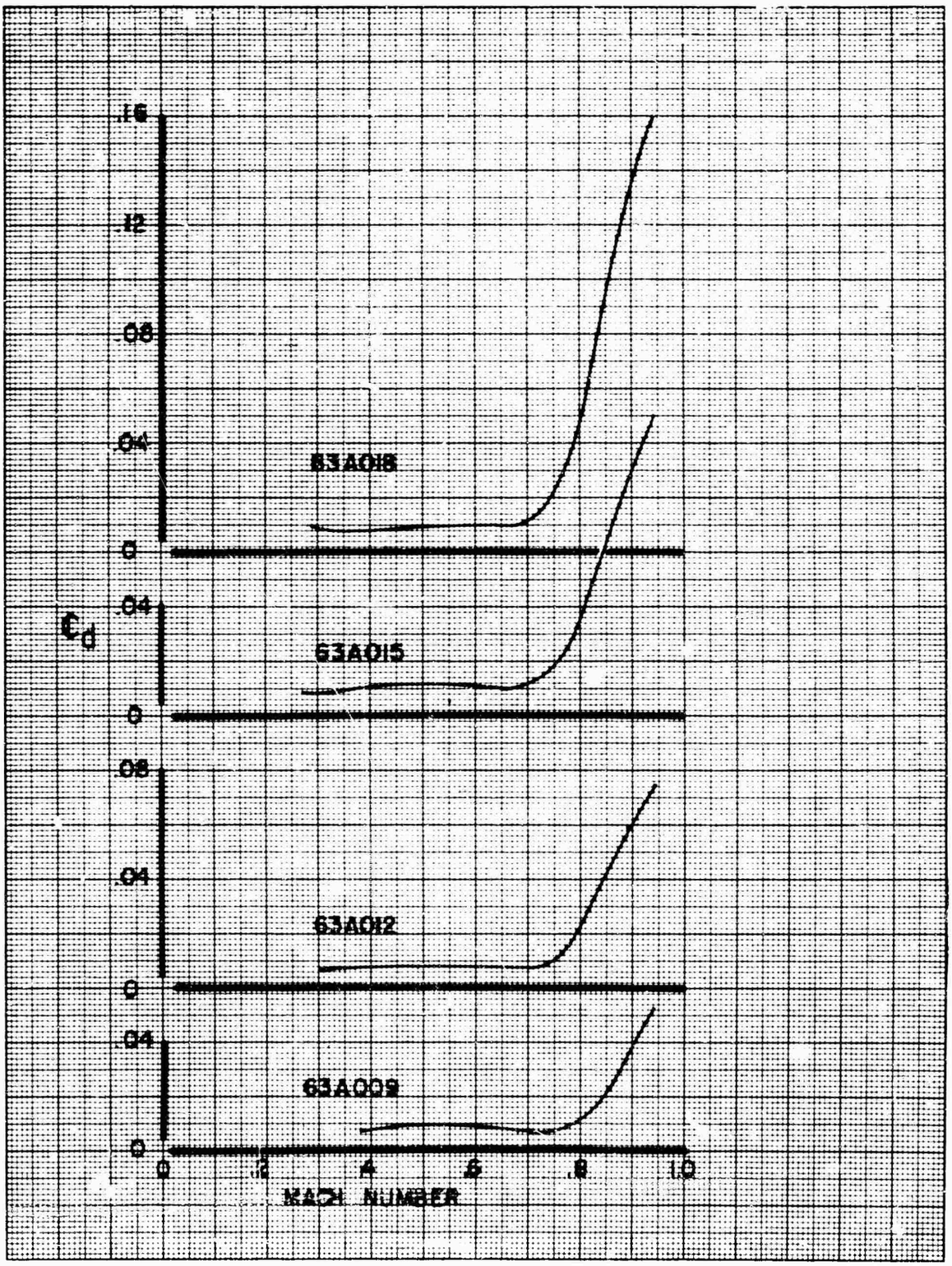


Figure 25C. Section Drag Coefficient Comparison for Various Thickness Ratios, R = 3.5 x 10^6, α = -2 Degrees

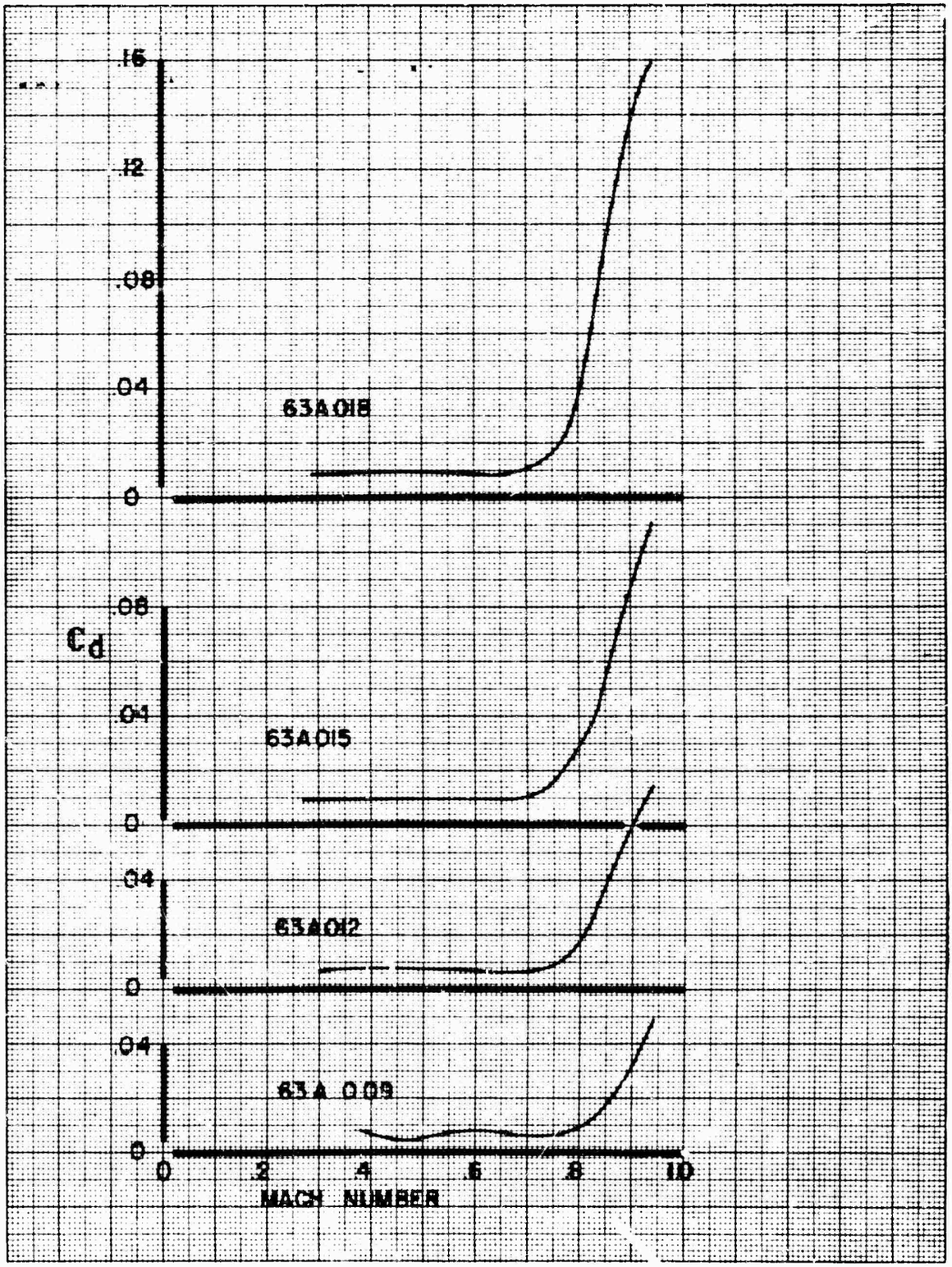


Figure 25D. Section Drag Coefficient Comparison for Various Thickness Ratios, $R = 3.5 \times 10^6$, $\alpha = -1$ Degree

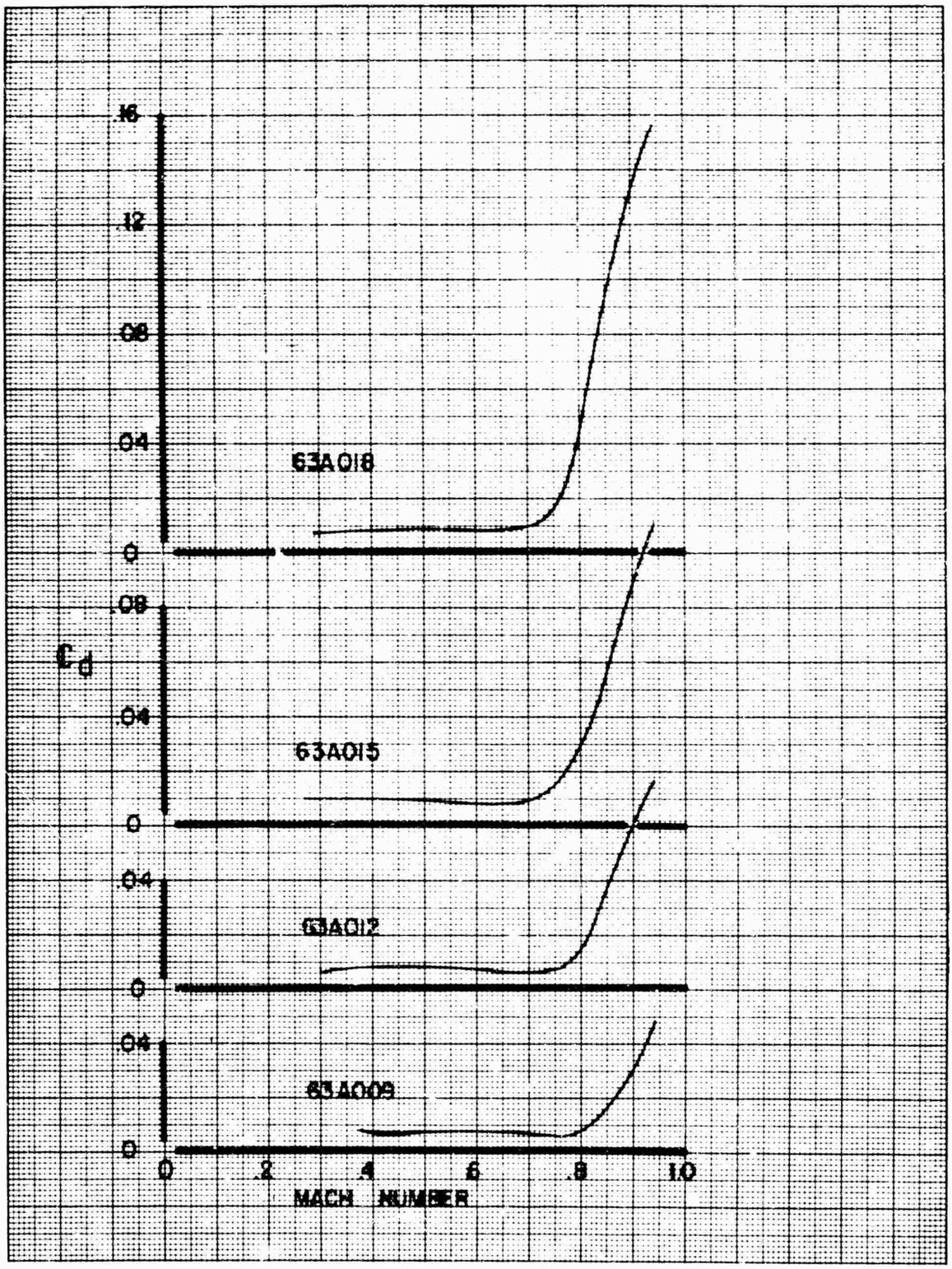


Figure 25E. Section Drag Coefficient Comparison for Various Thickness Ratios, $R = 3.5 \times 10^6$, $\alpha = 0$ Degrees

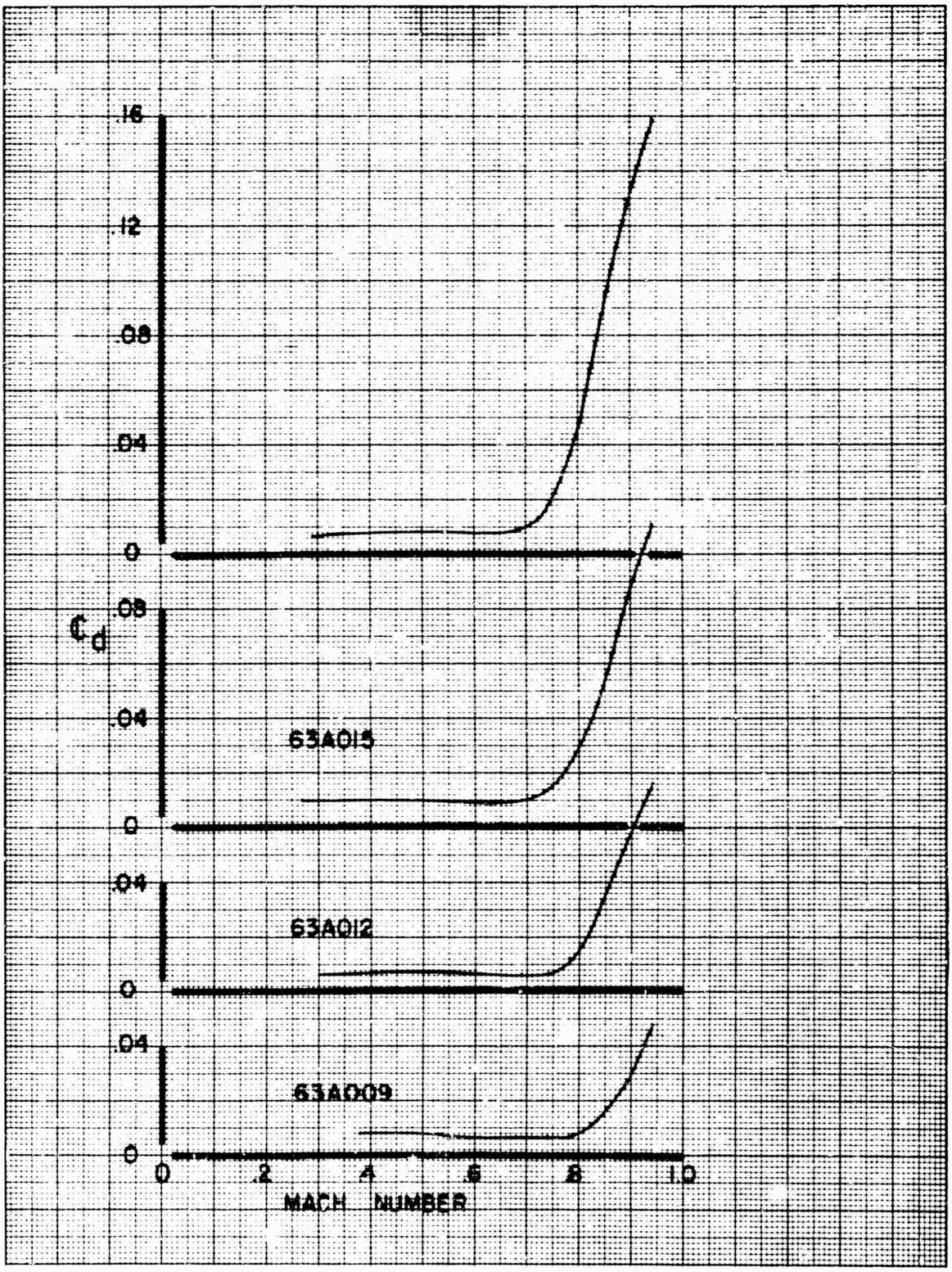


Figure 25F. Section Drag Coefficient Comparison for Various Thickness Ratios, $R = 3.5 \times 10^6$, $\alpha = 1$ Degree

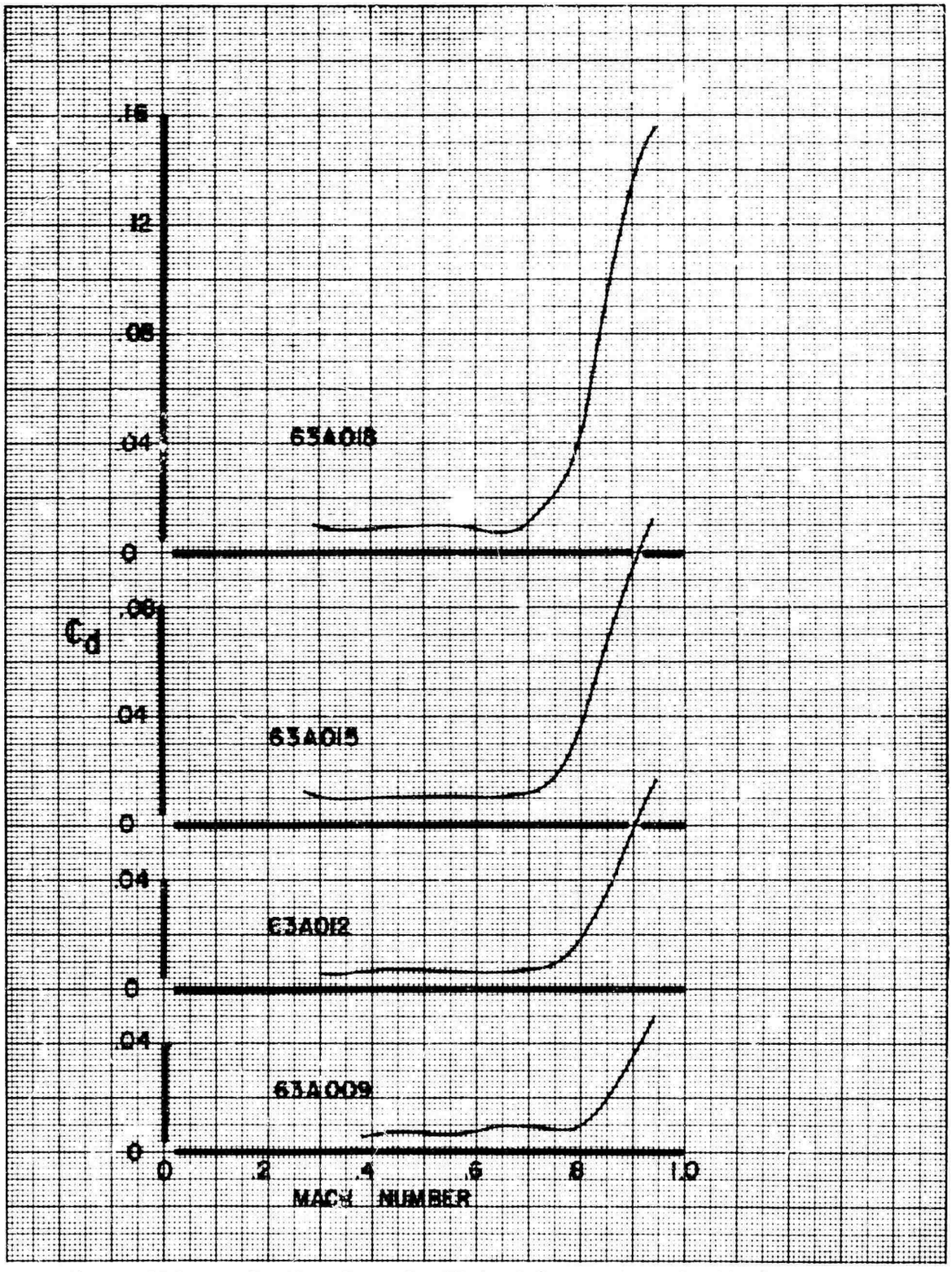


Figure 25G. Section Drag Coefficient Comparison for Various Thickness Ratios, $R = 3.5 \times 10^6$, $\alpha = 2$ Degrees

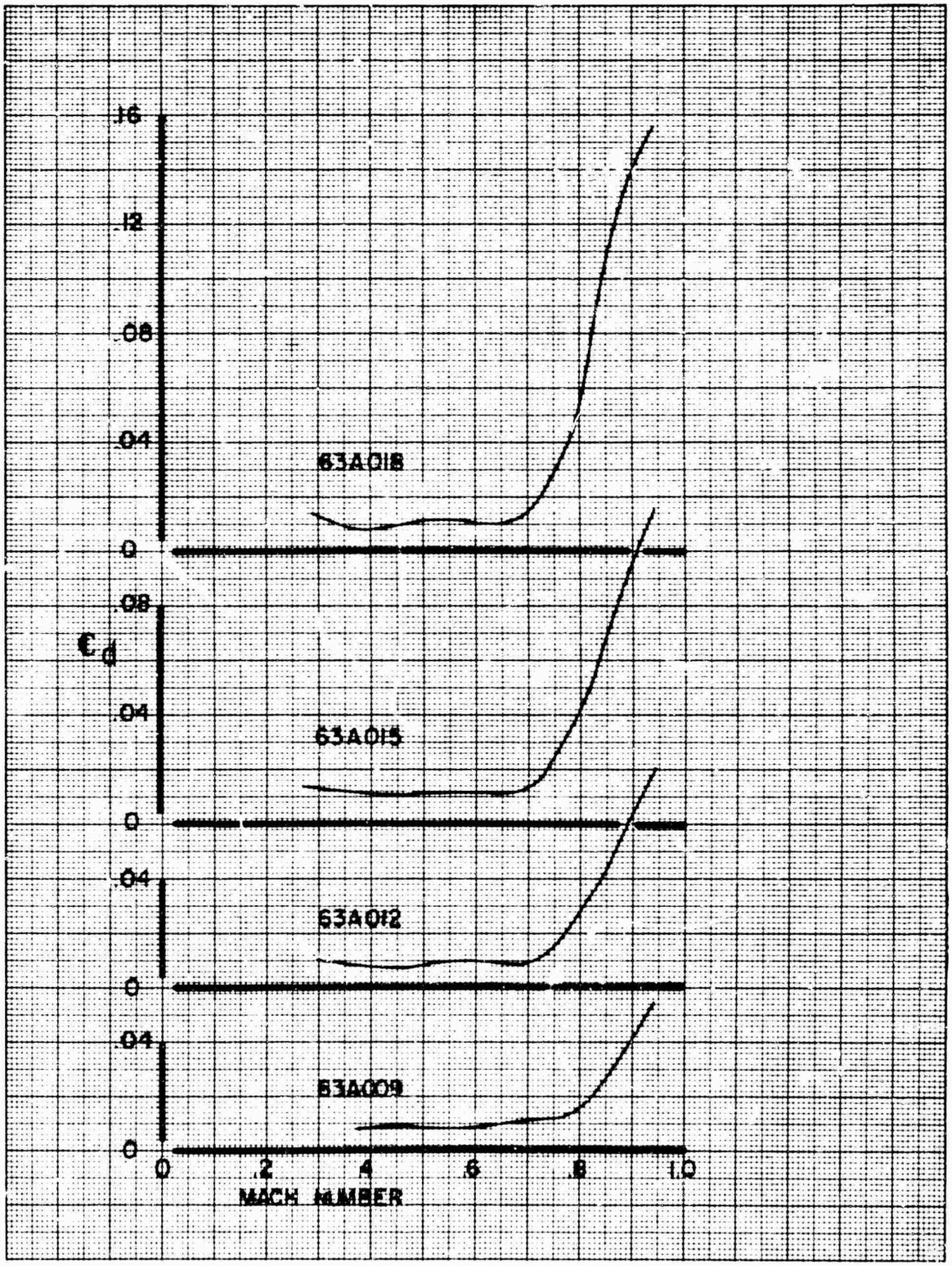


Figure 25H. Section Drag Coefficient Comparison for Various Thickness Ratios, $R = 3.5 \times 10^6$, $\alpha = 3$ Degrees

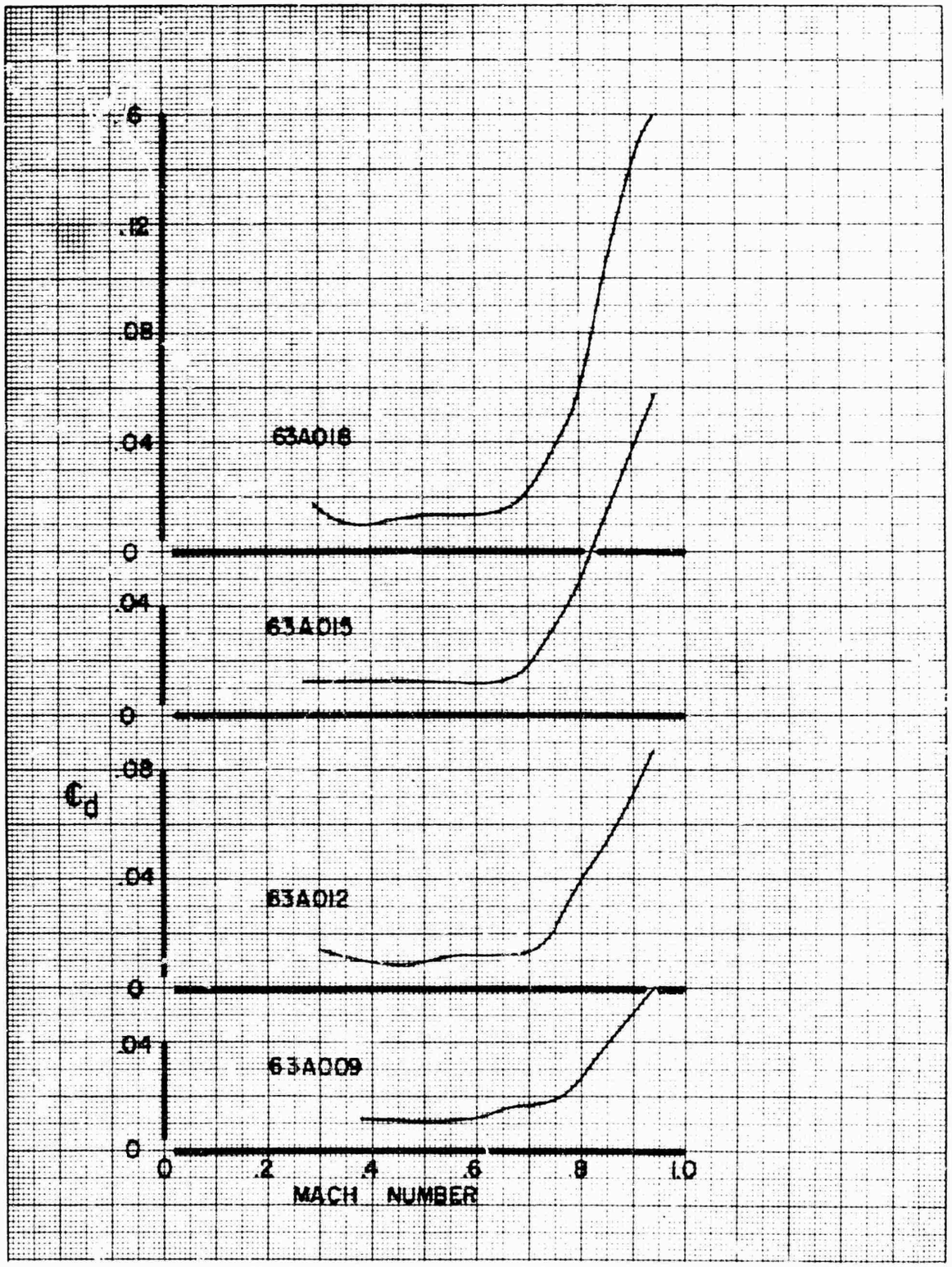


Figure 251. Section Drag Coefficient Comparison for Various Thickness Ratios, $R = 3.5 \times 10^6$, $\alpha = 4$ Degrees

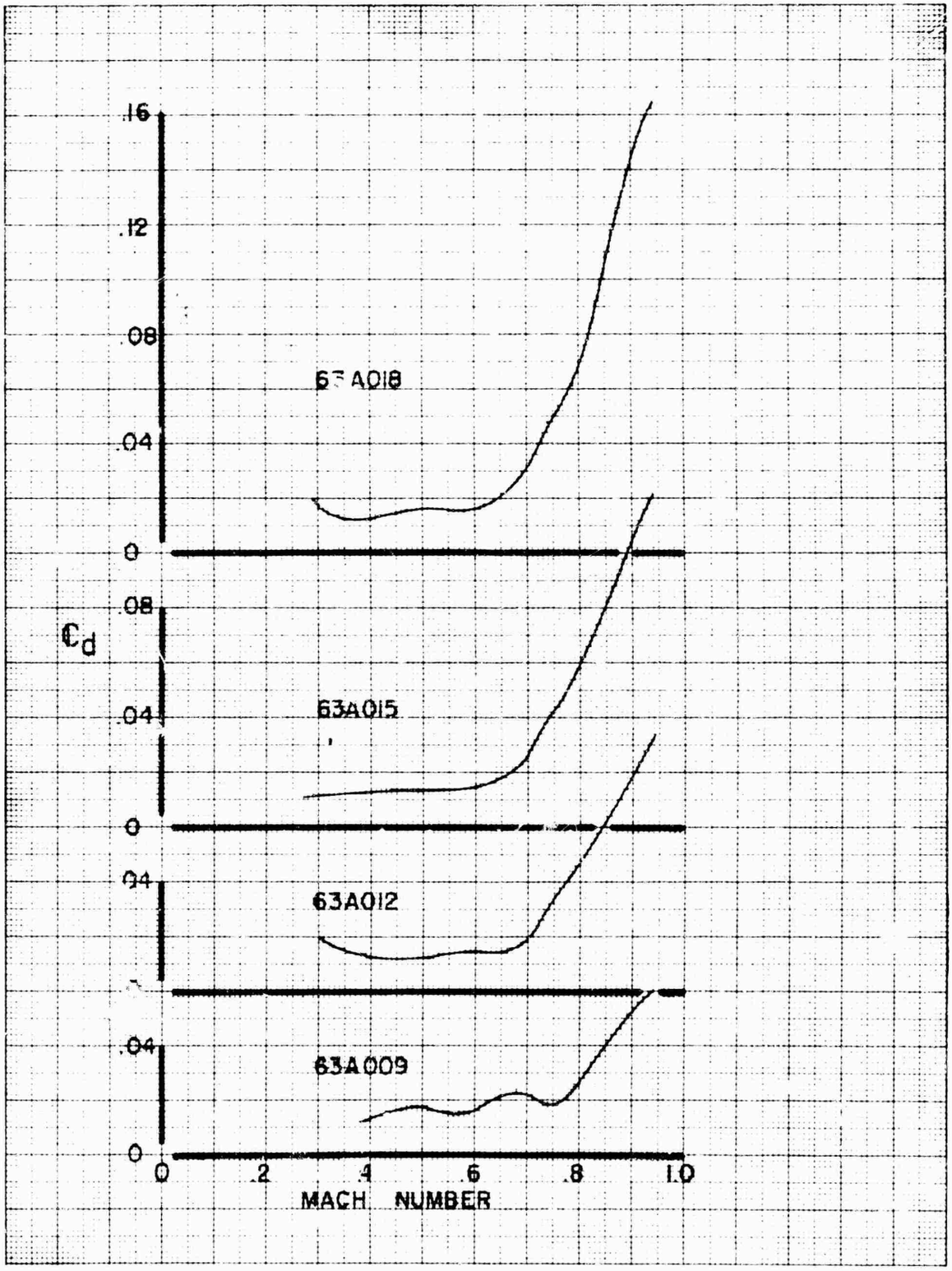


Figure 25J. Section Drag Coefficient Comparison for Various Thickness Ratios, $R = 3.5 \times 10^6$, $\alpha = 5$ Degrees

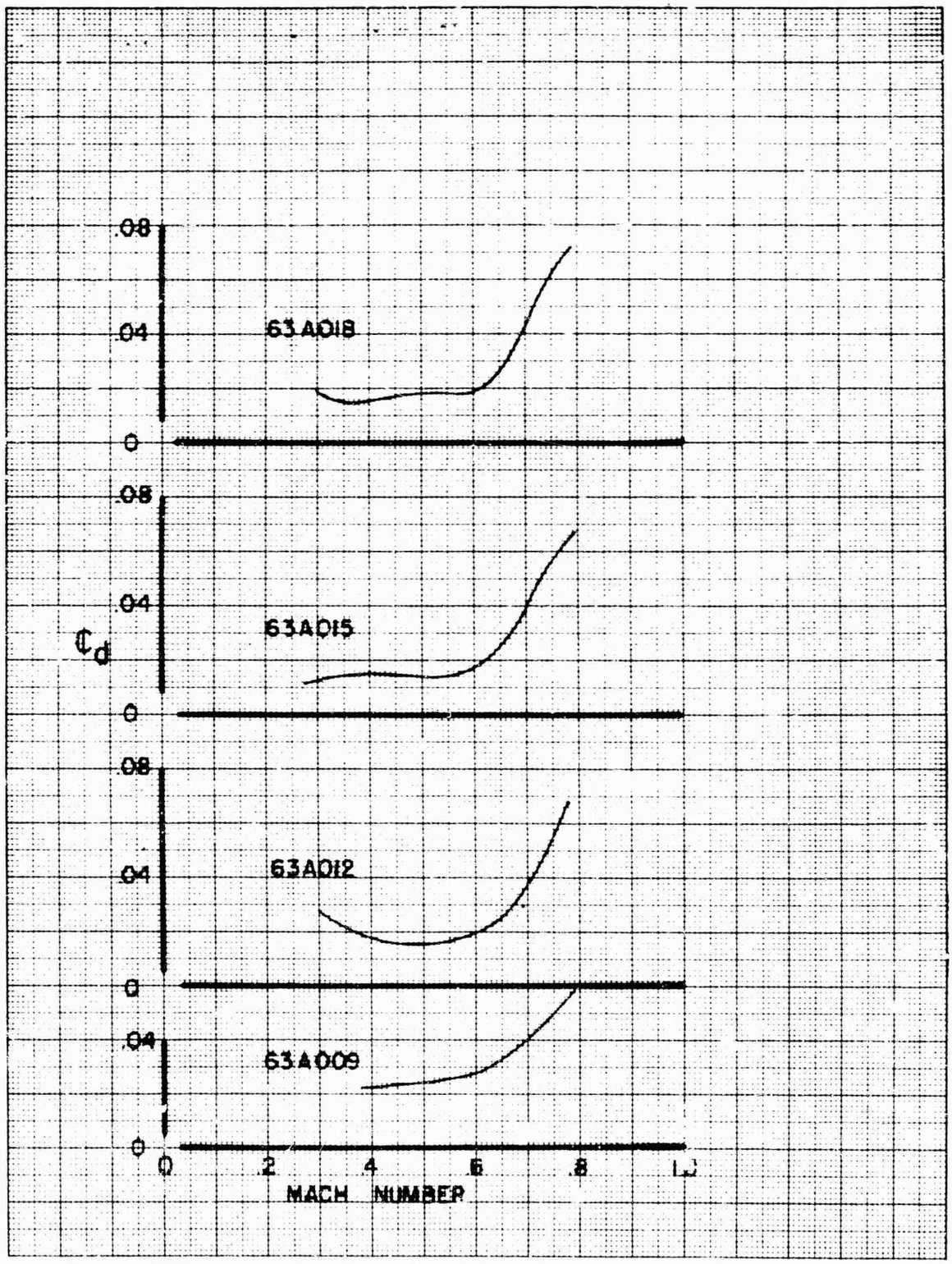


Figure 25K. Section Drag Coefficient Comparison for Various Thickness Ratios, $R = 3.5 \times 10^6$, $\alpha = 6$ Degrees

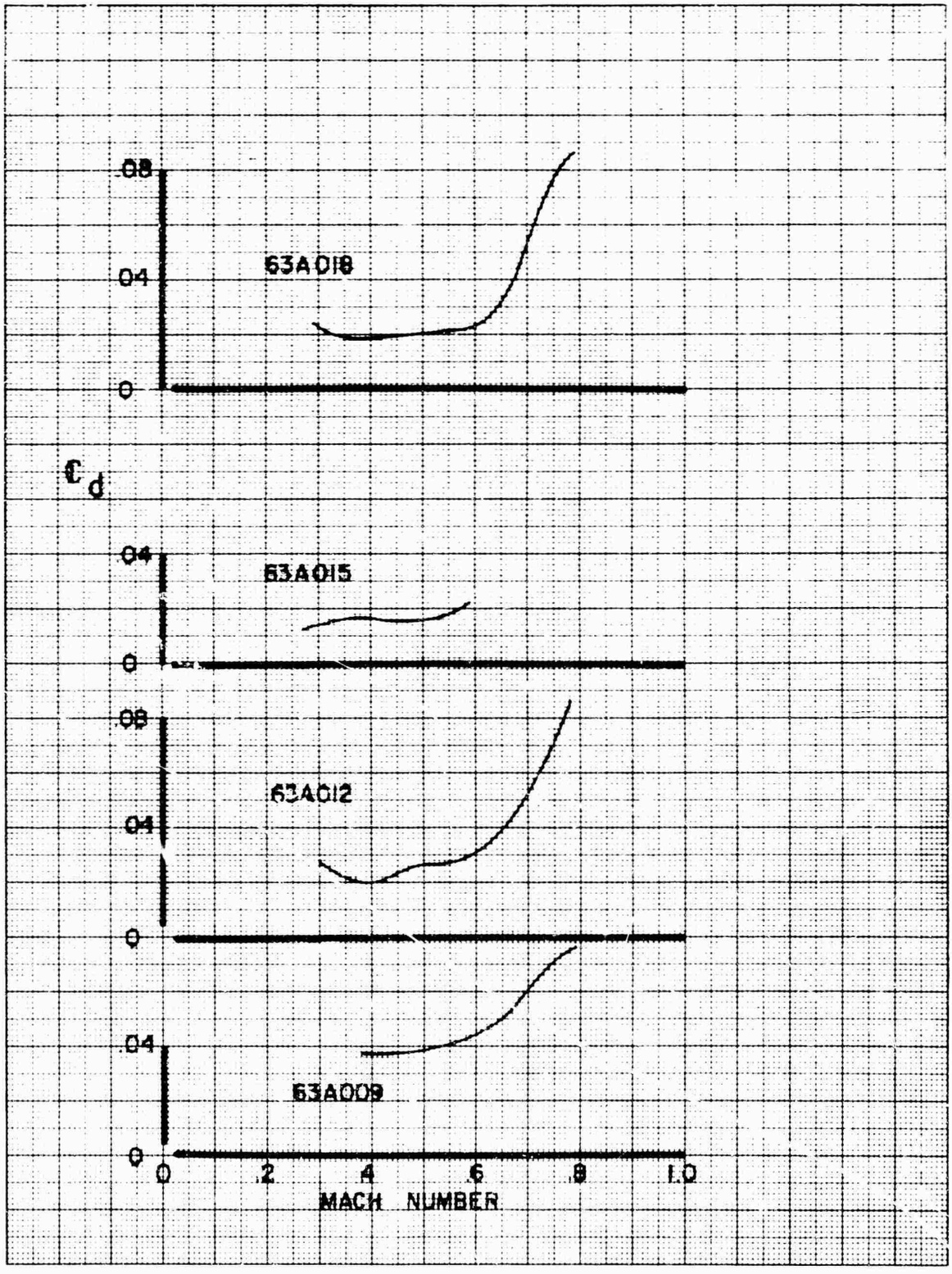


Figure 25L. Section Drag Coefficient Comparison for Various Thickness Ratios, $R = 3.5 \times 10^6$, $\alpha = 7$ Degrees

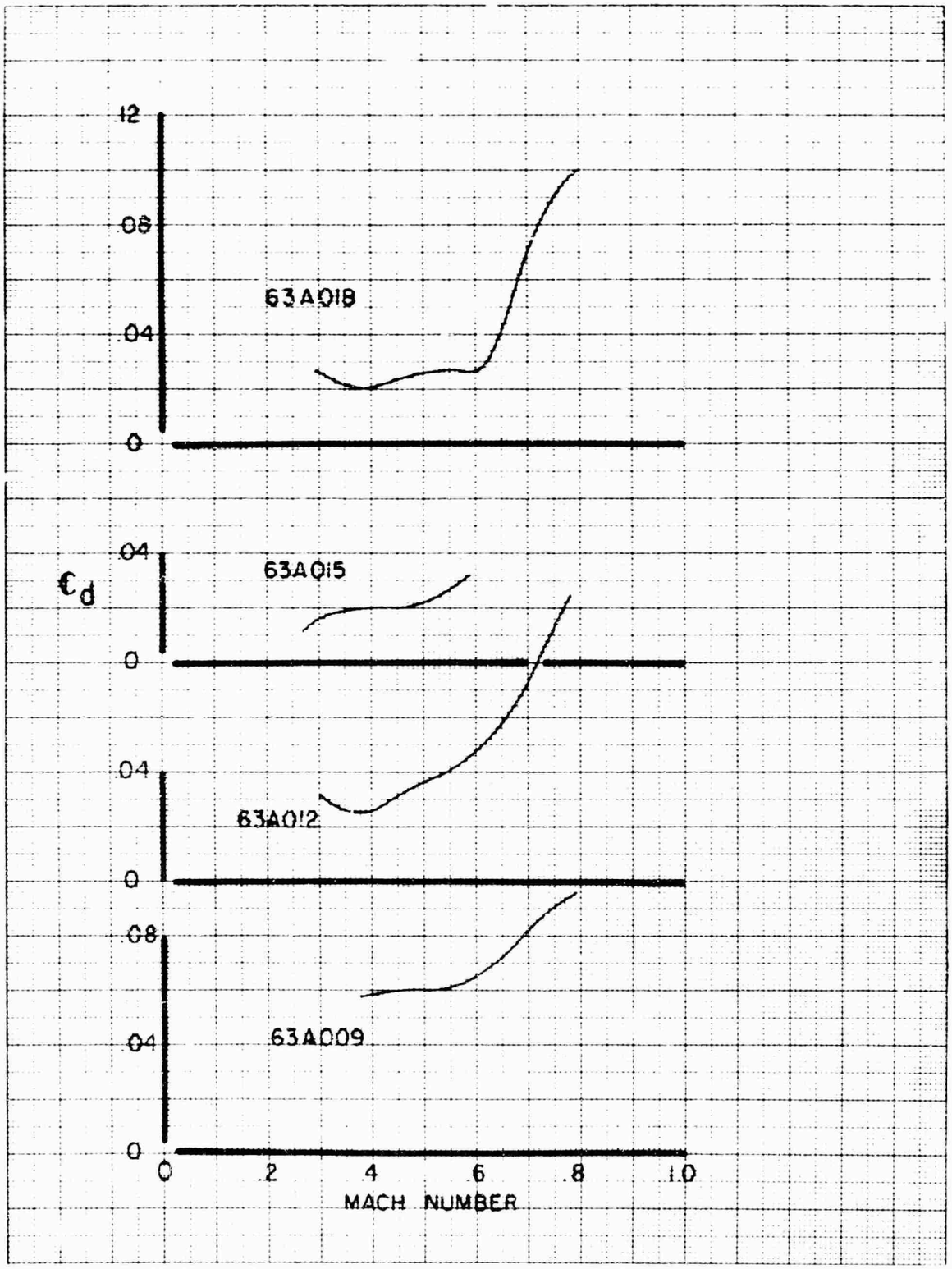


Figure 25M. Section Drag Coefficient Comparison for Various Thickness Ratios, $R = 3.5 \times 10^6$, $\alpha = 8$ Degrees

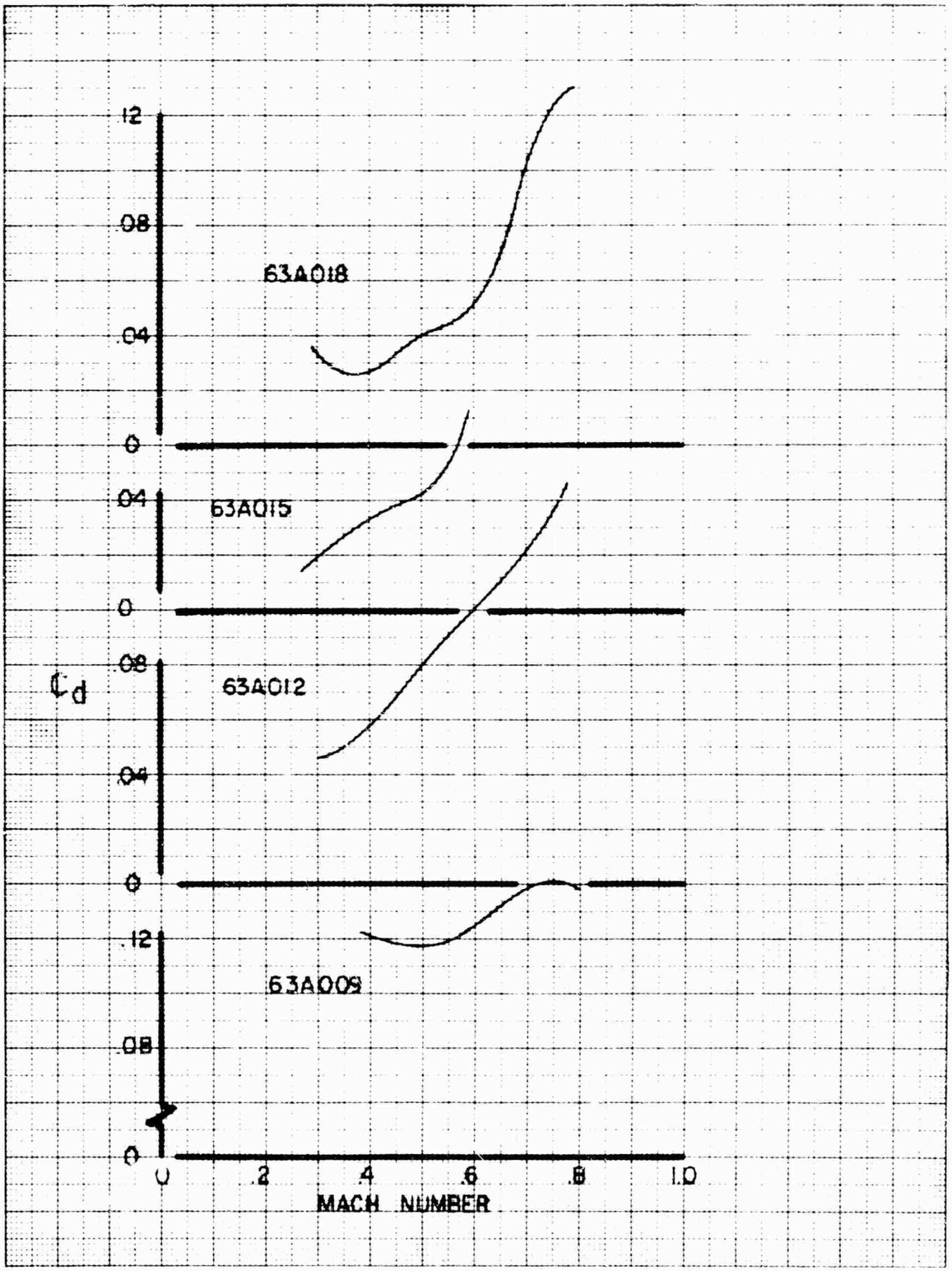


Figure 25N. Section Drag Coefficient Comparison for Various Thickness Ratios, $R = 3.5 \times 10^6$, $\alpha = 10$ Degrees

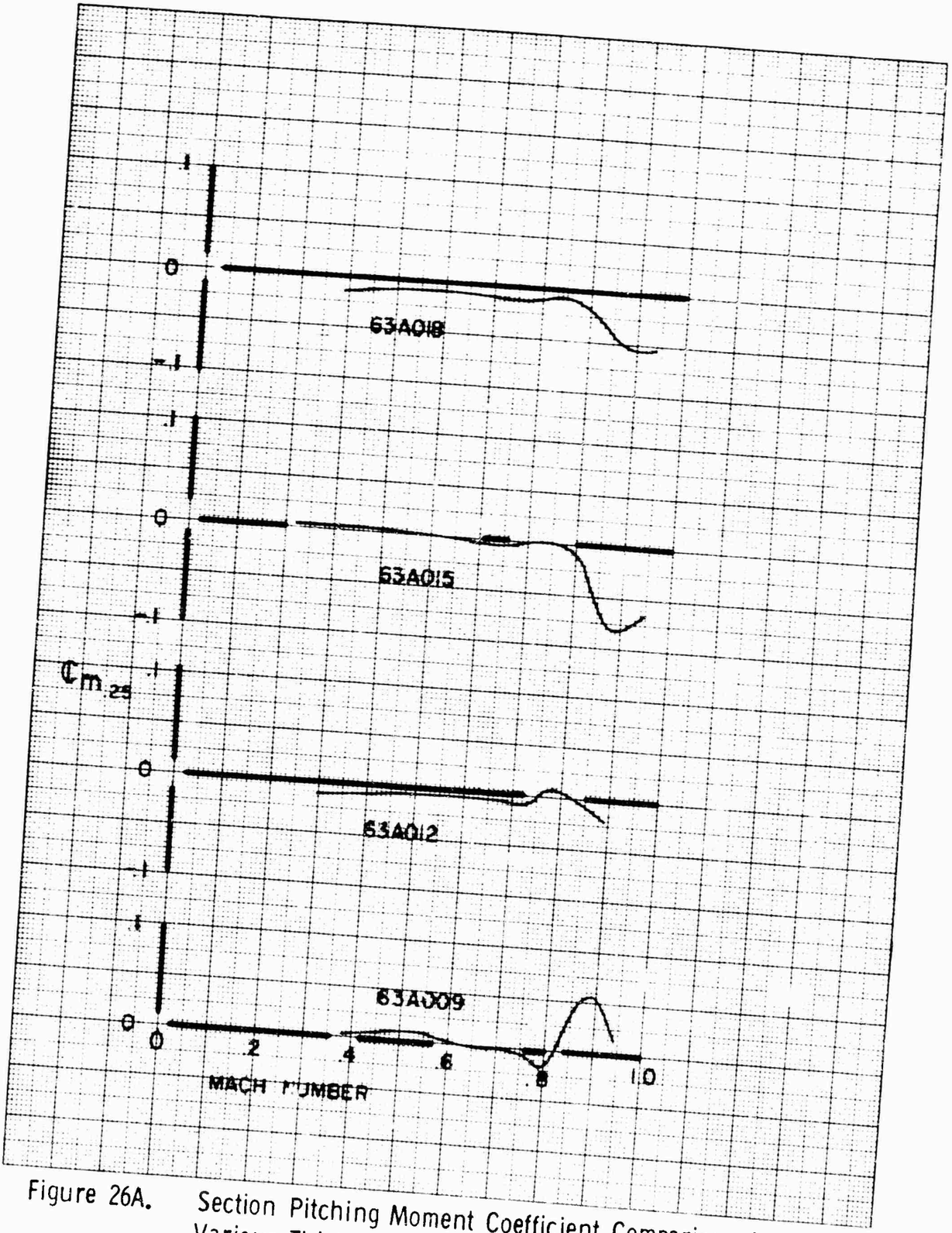


Figure 26A. Section Pitching Moment Coefficient Comparison for Various Thickness Ratios, $R = 3.5 \times 10^6$, $\alpha = -4$ Degrees

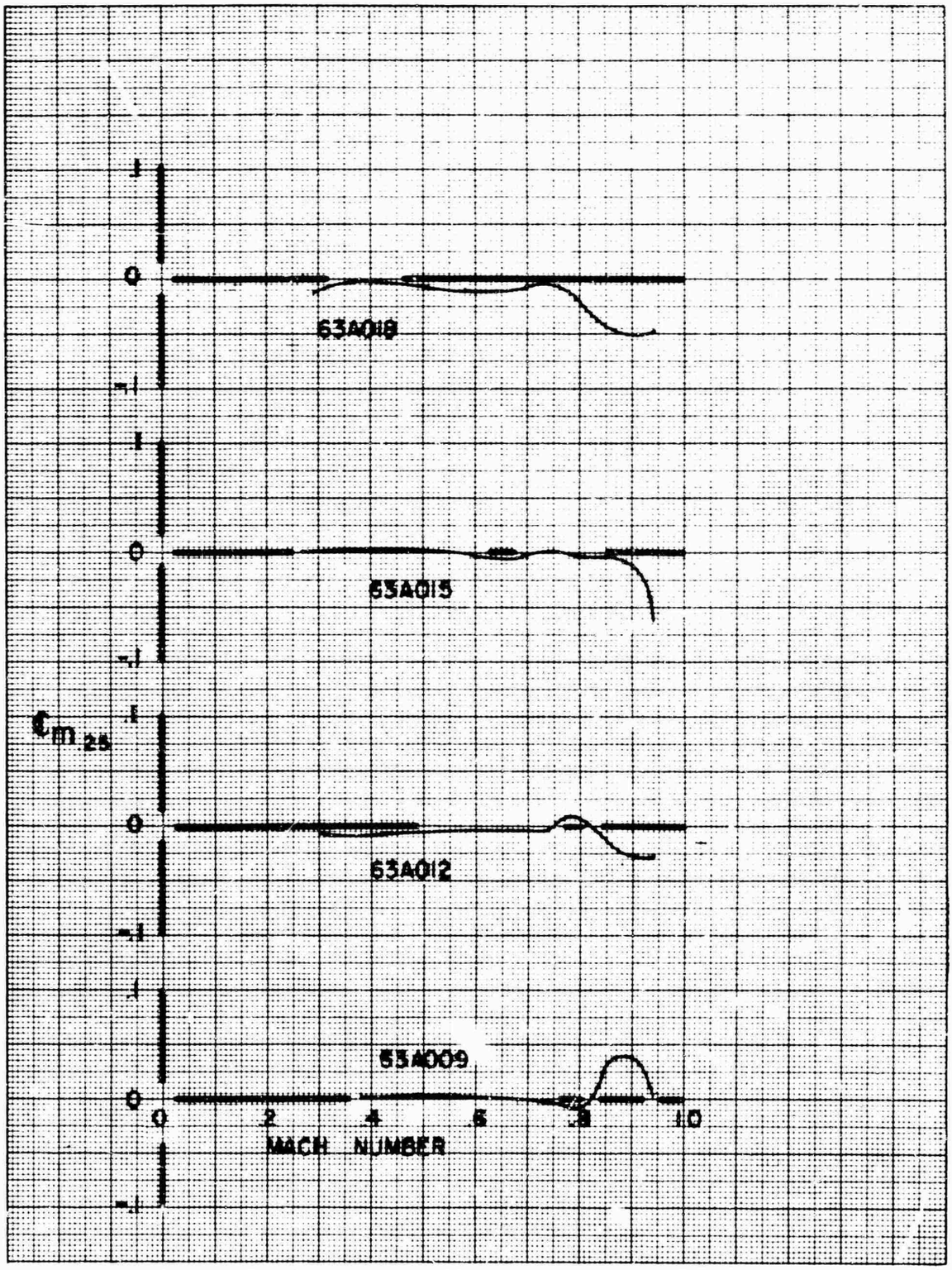


Figure 26B. Section Pitching Moment Coefficient Comparison for Various Thickness Ratios, $R = 3.5 \times 10^6$, $\alpha = -3$ Degrees

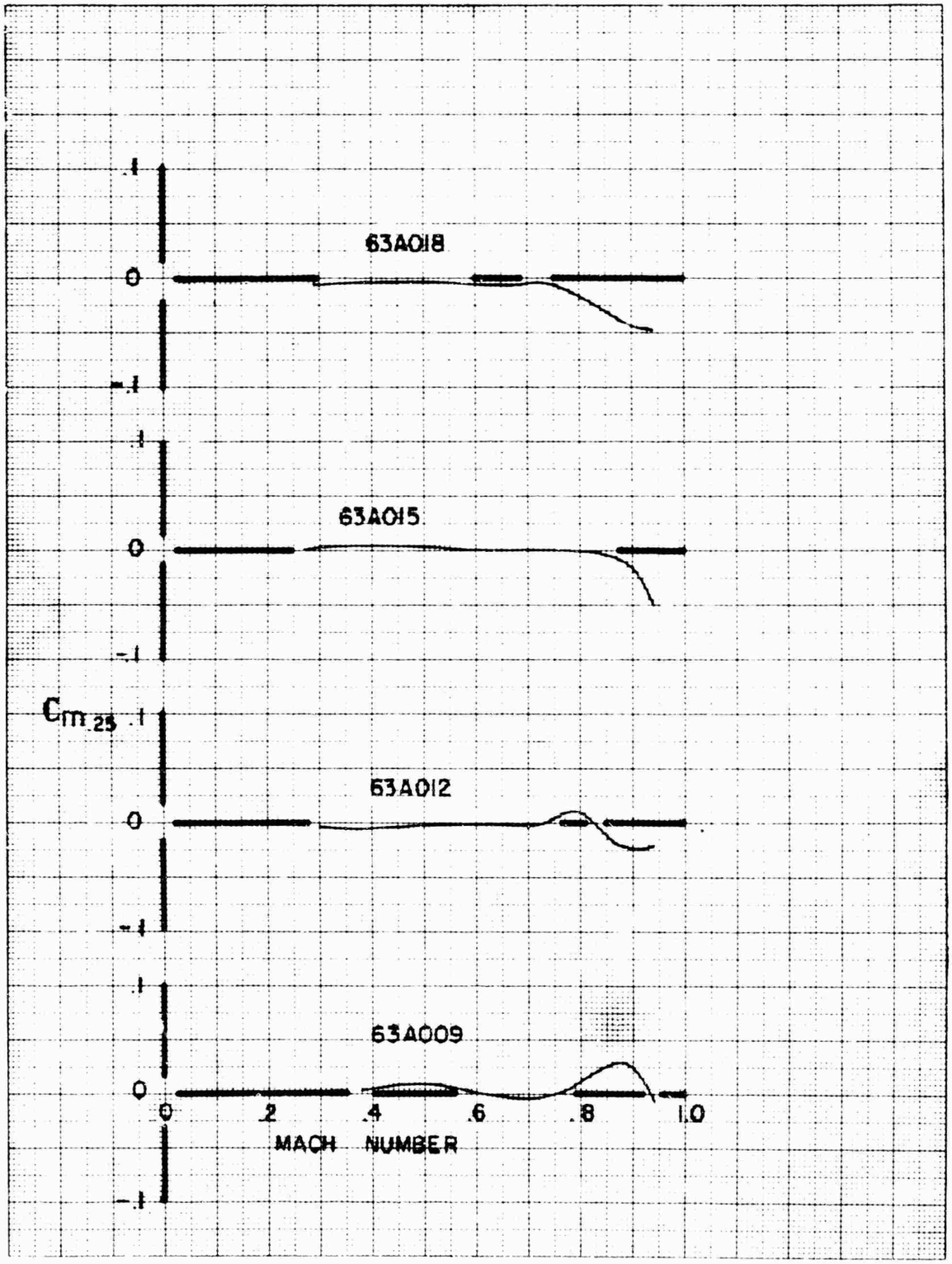


Figure 26C. Section Pitching Moment Coefficient Comparison for Various Thickness Ratios, $R = 3.5 \times 10^6$, $\alpha = -2$ Degrees

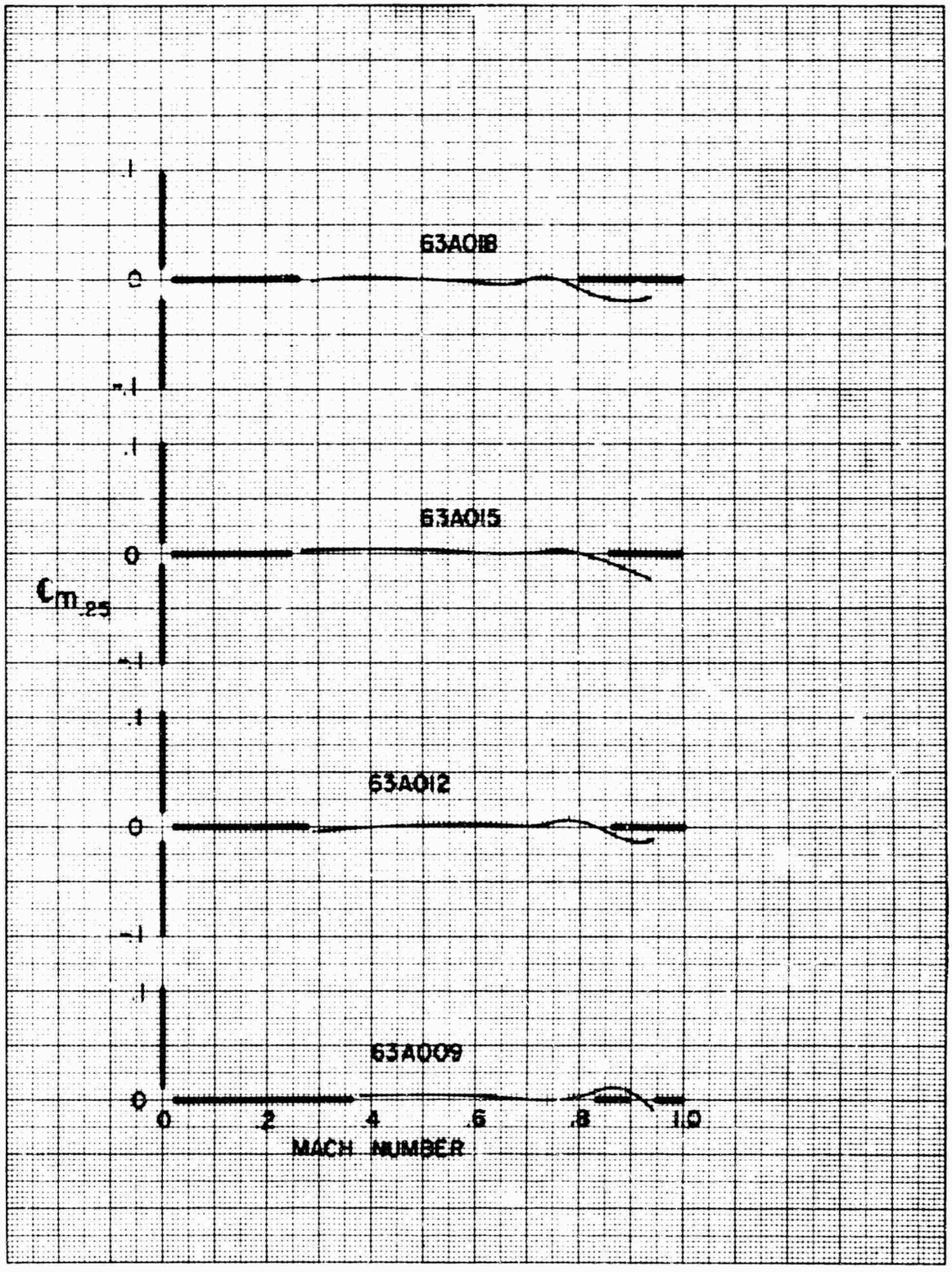


Figure 26D. Section Pitching Moment Coefficient Comparison for Various Thickness Ratios, $R = 3.5 \times 10^6$, $\alpha = -1$ Degree

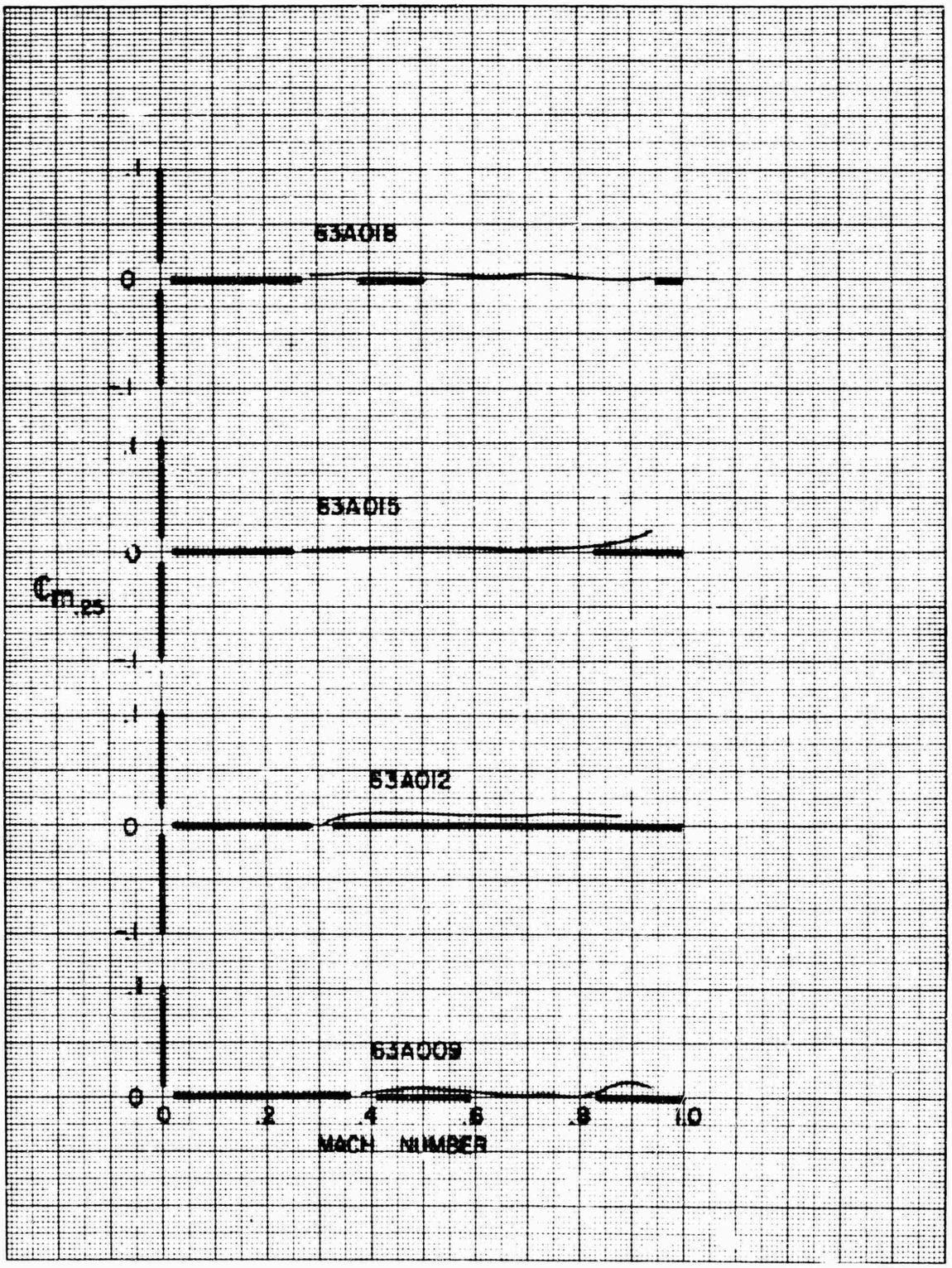


Figure 26E. Section Pitching Moment Coefficient Comparison for Various Thickness Ratios, $R = 3.5 \times 10^6$, $\alpha = 0$ Degrees

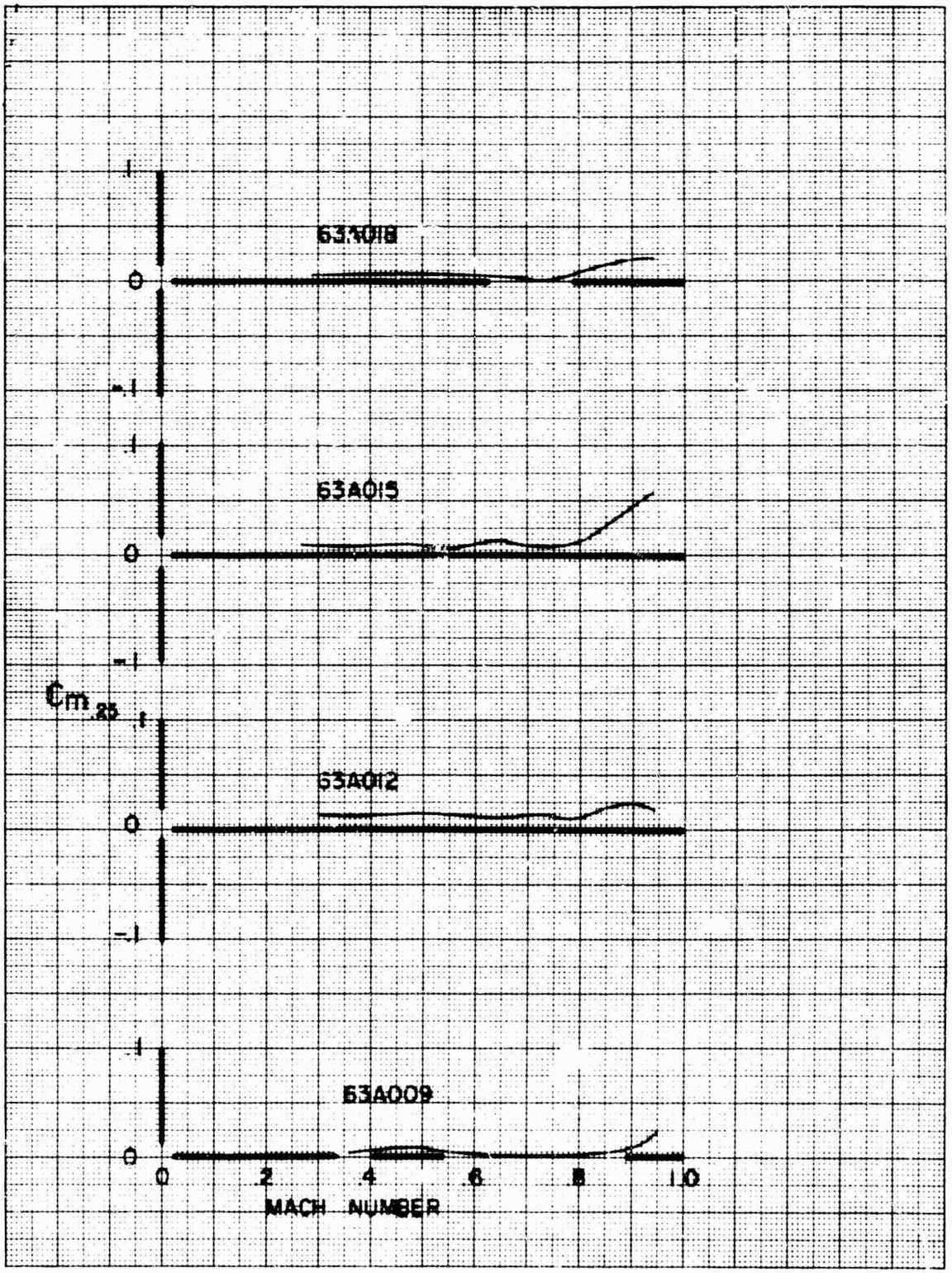


Figure 26F. Section Pitching Moment Coefficient Comparison for Various Thickness Ratios, $R = 3.5 \times 10^6$, $\alpha = 1$ Degree

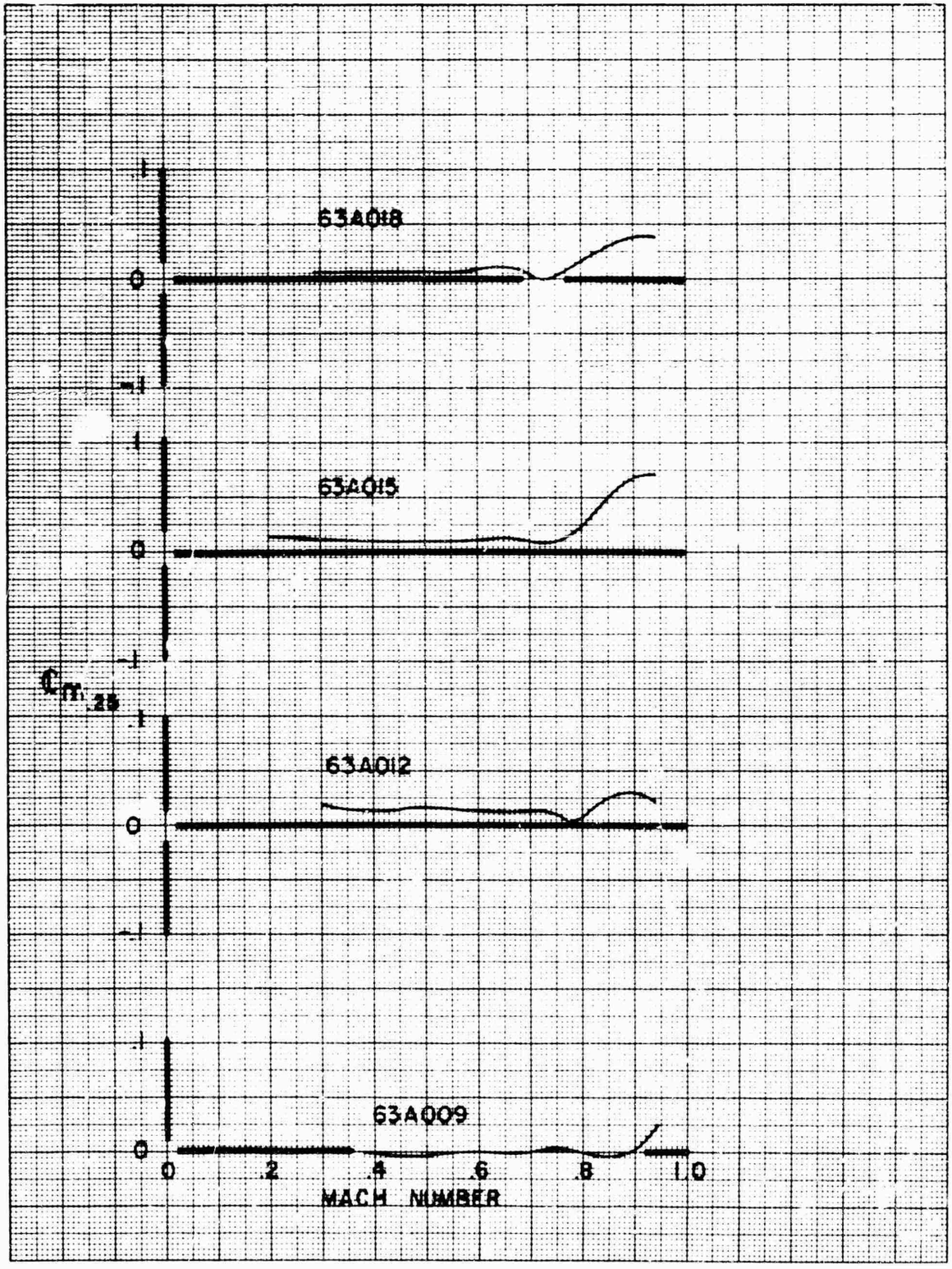


Figure 26G. Section Pitching Moment Coefficient Comparison for Various Thickness Ratios, $R = 3.5 \times 10^6$, $\alpha = 2$ Degrees

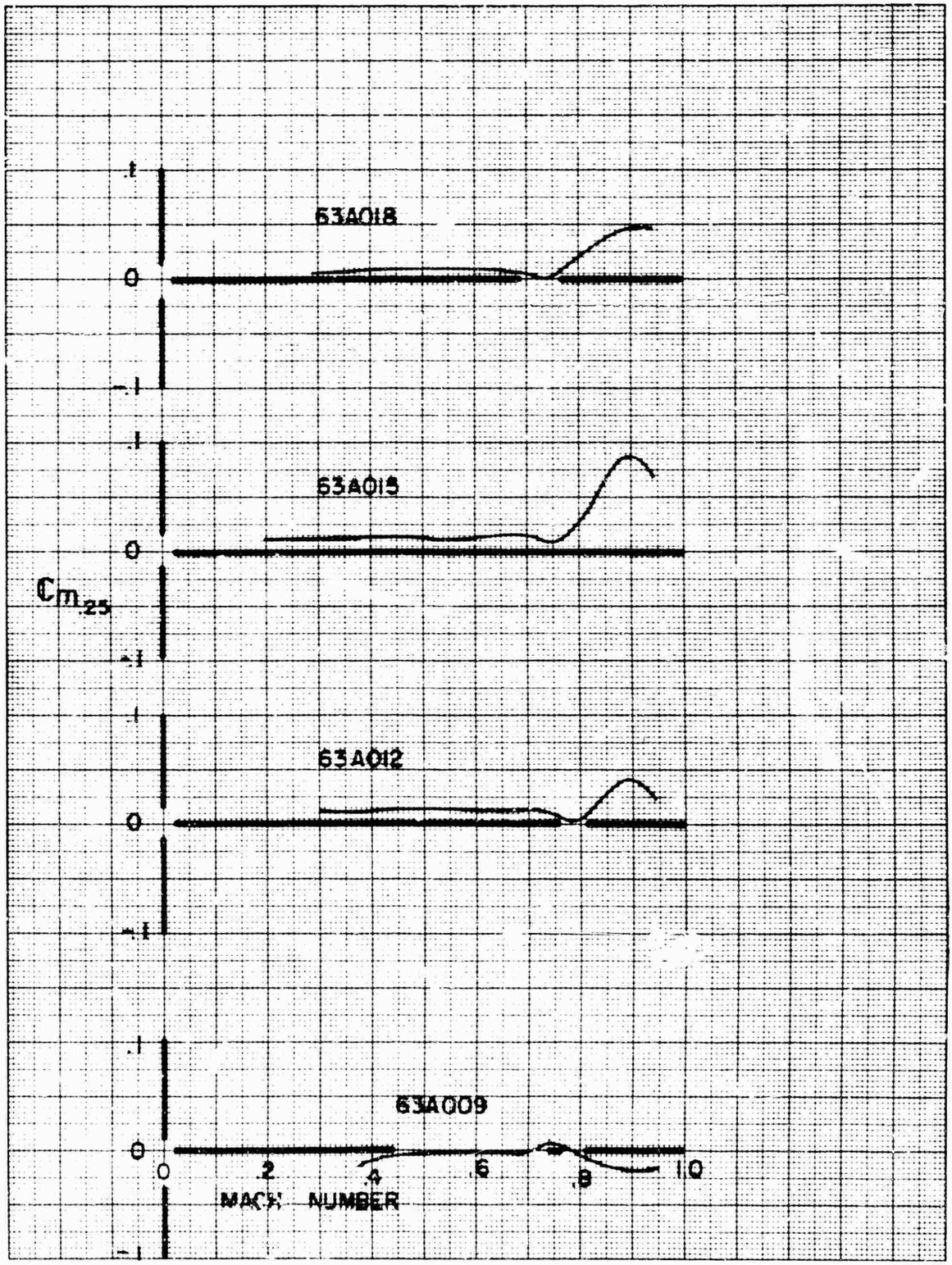


Figure 26H. Section Pitching Moment Coefficient Comparison for Various Thickness Ratios, $R = 3.5 \times 10^6$, $\alpha = 3$ Degrees

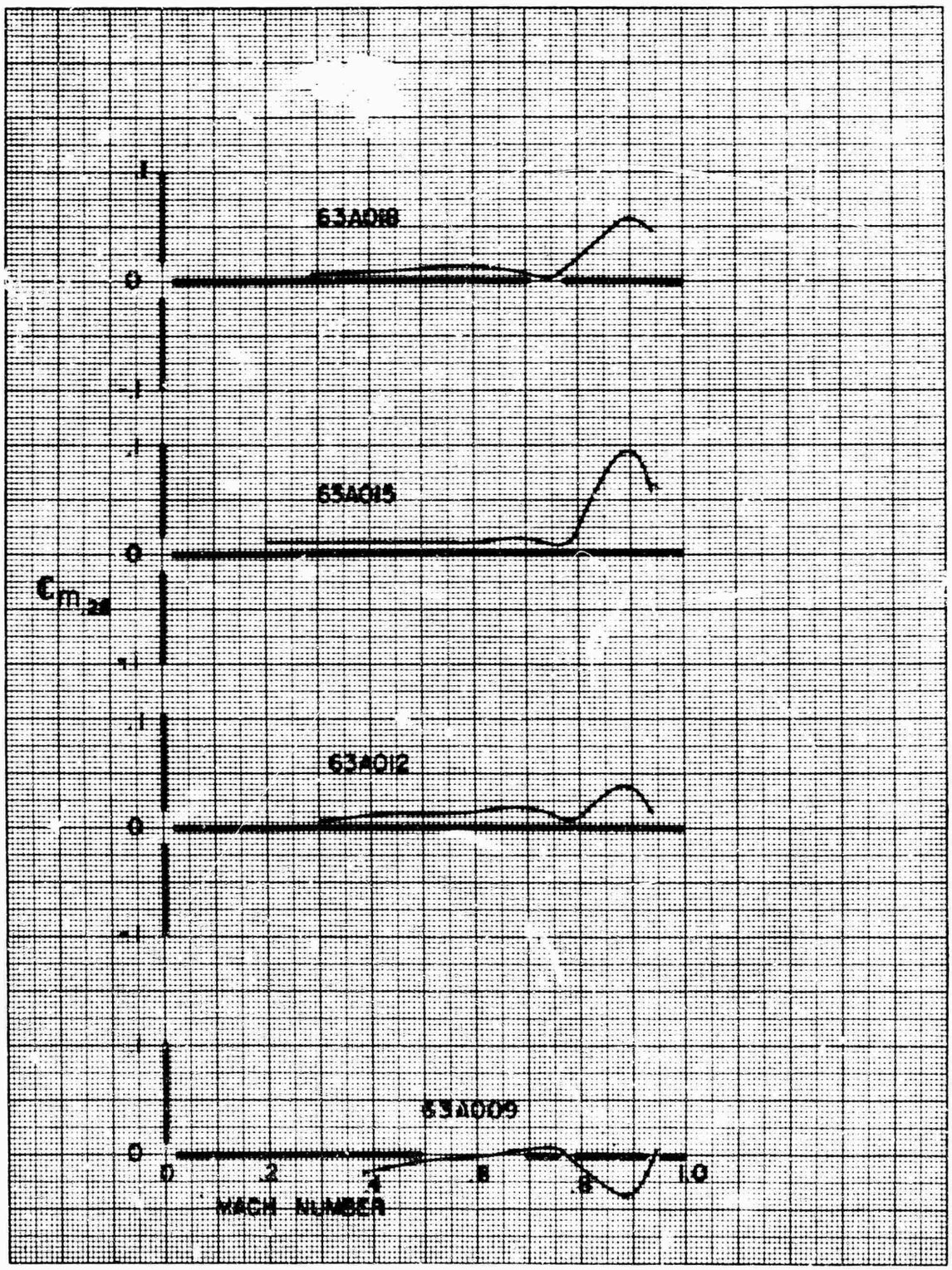


Figure 261. Section Pitching Moment Coefficient Comparison for Various Thickness Ratios, $R = 3.5 \times 10^6$, $\alpha = 4$ Degrees

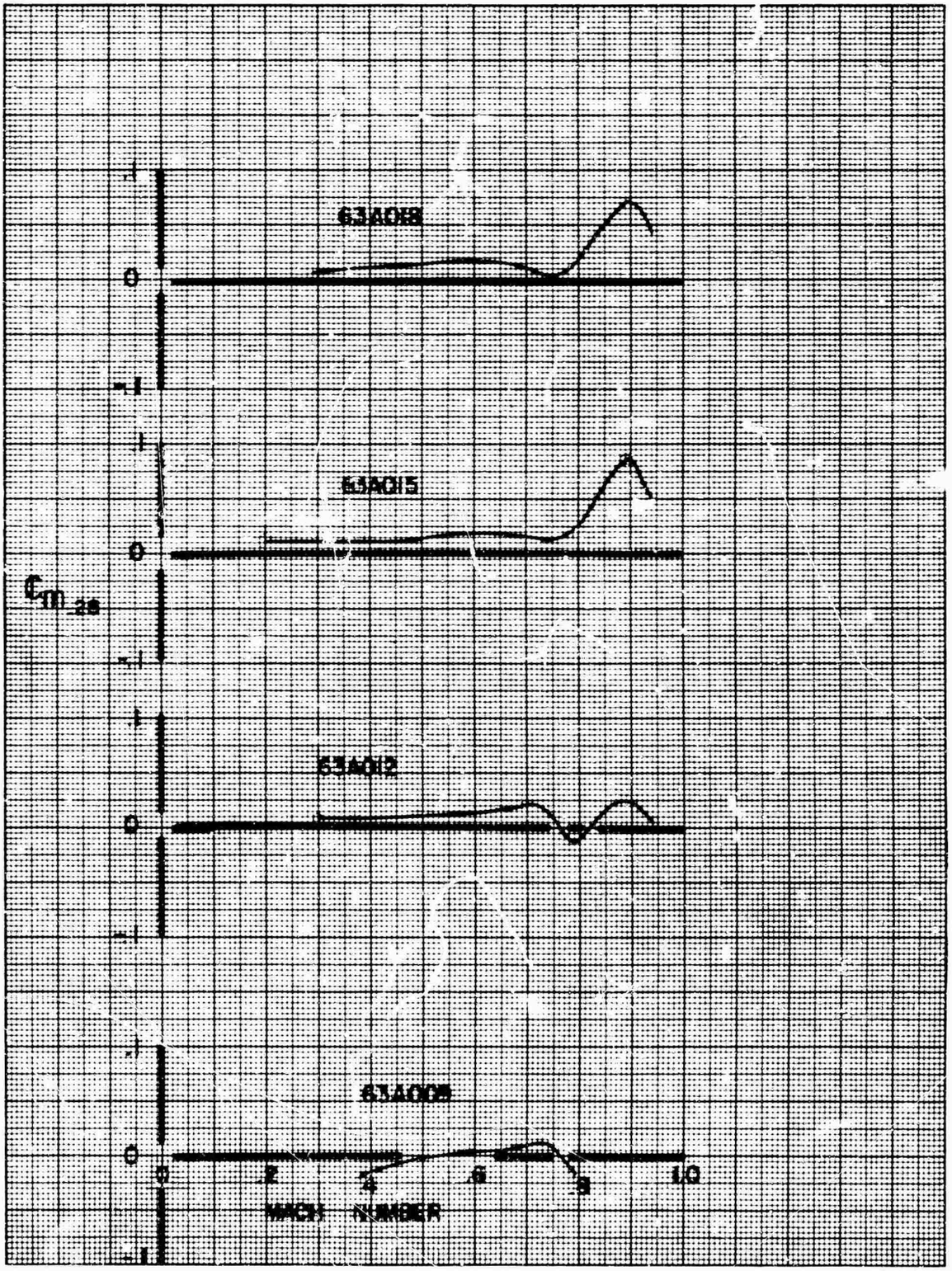


Figure 26J. Section Pitching Moment Coefficient Comparison for Various Thickness Ratios, R = 3.5 x 10^6, α = 5 Degrees

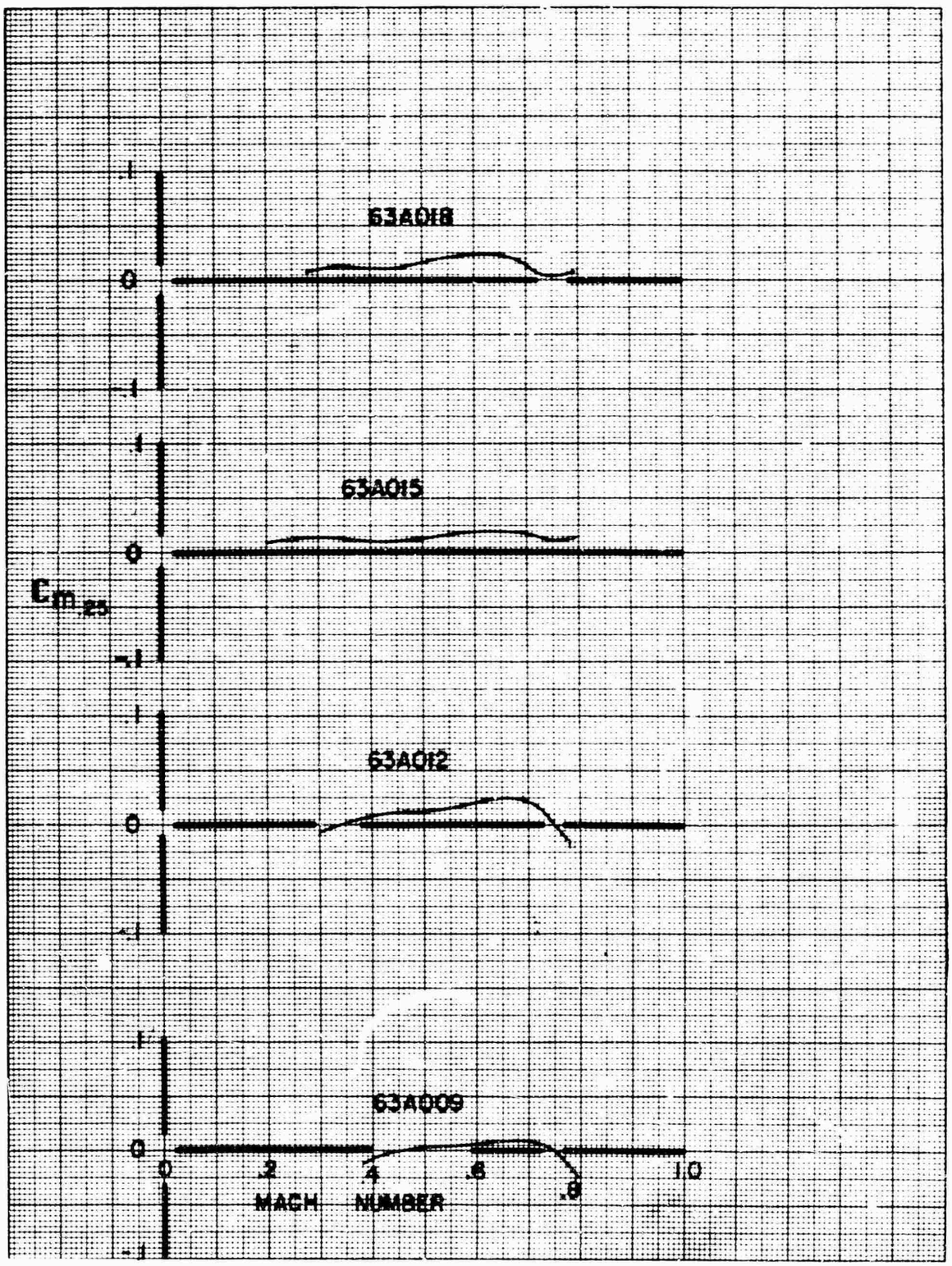


Figure 26K. Section Pitching Moment Coefficient Comparison for Various Thickness Ratios, $R = 3.5 \times 10^6$, $\alpha = 6$ Degrees

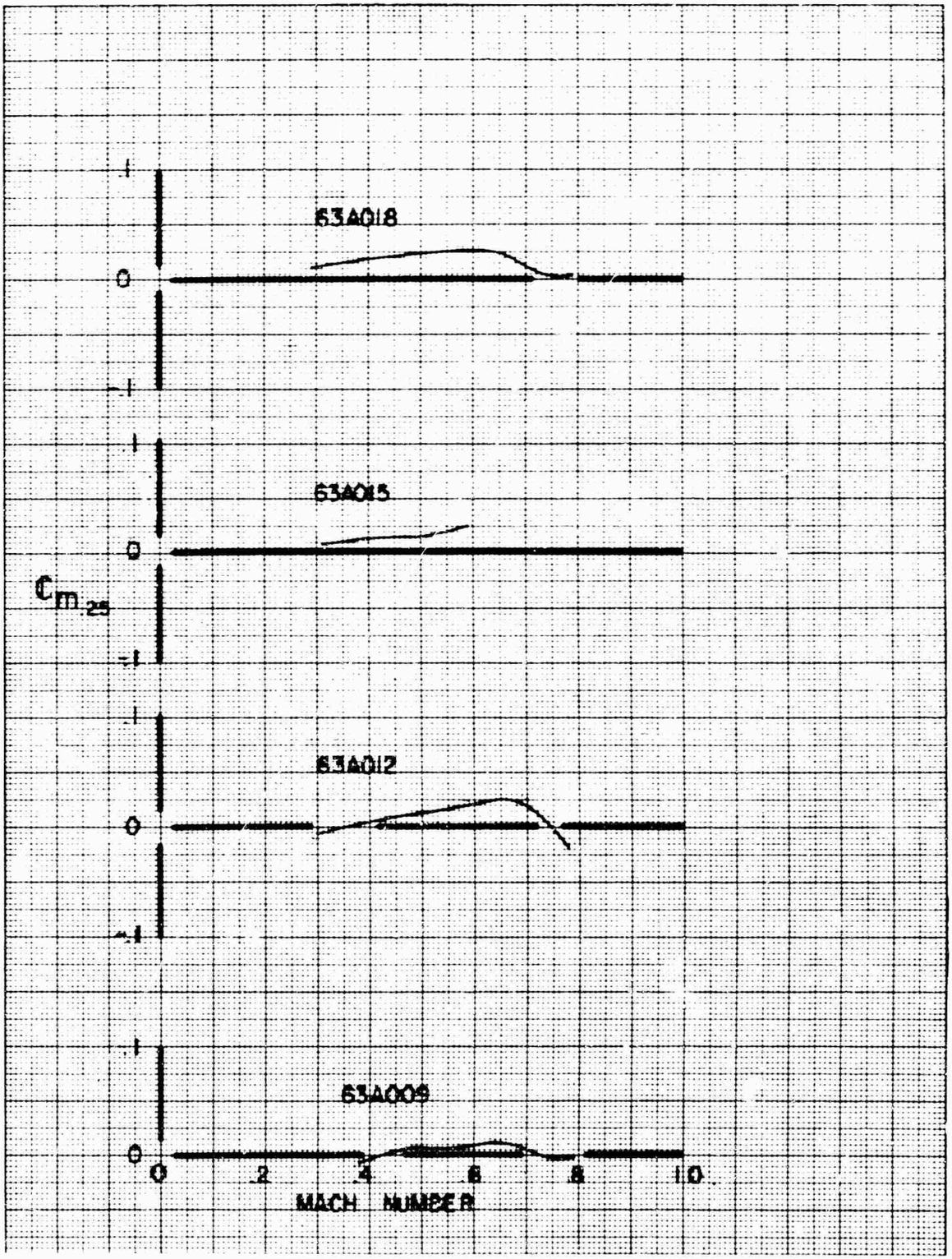


Figure 26L. Section Pitching Moment Coefficient Comparison for Various Thickness Ratios, $R = 3.5 \times 10^6$, $\alpha = 7$ Degrees

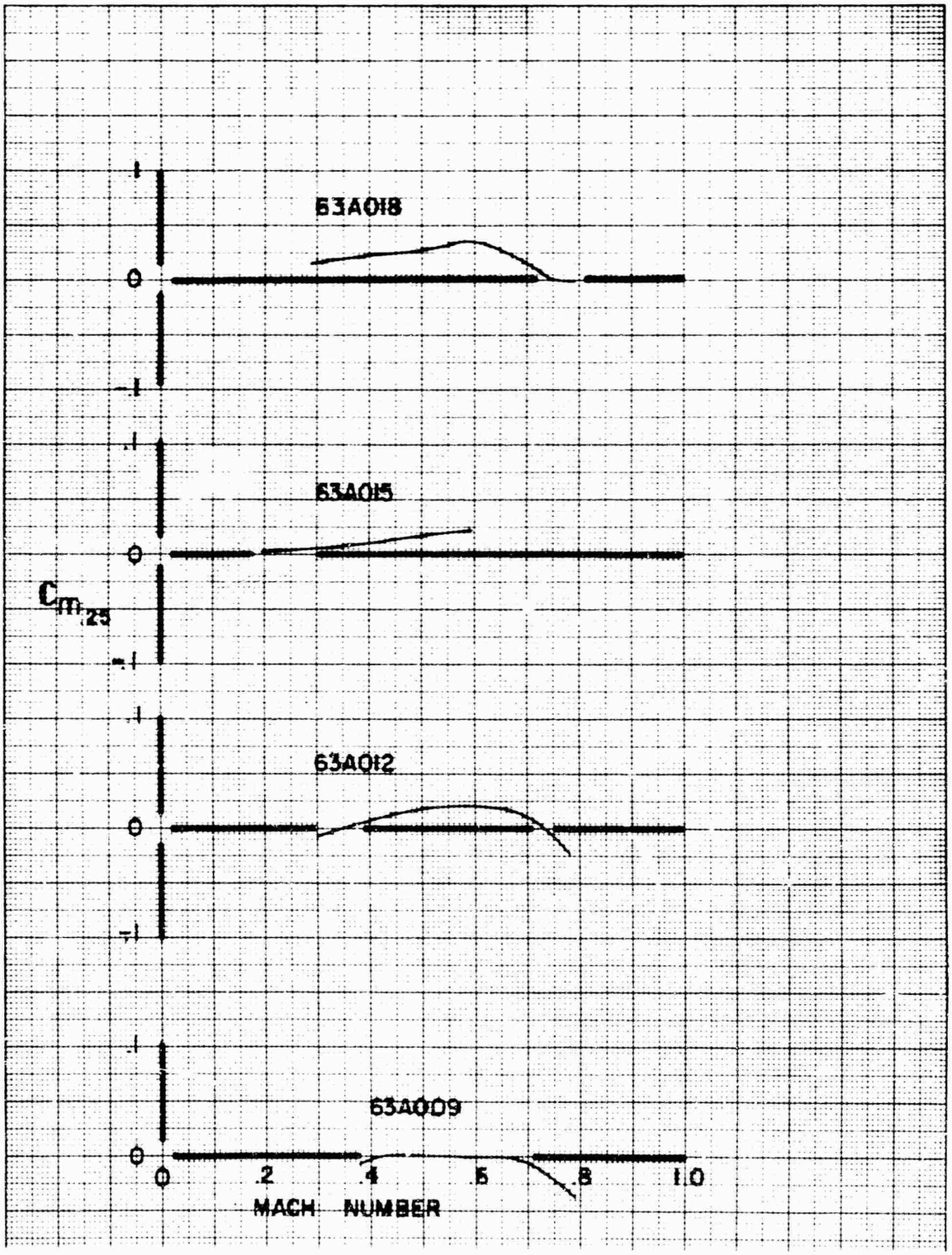


Figure 26M. Section Pitching Moment Coefficient Comparison for Various Thickness Ratios, $R = 3.5 \times 10^6$, $\alpha = 8$ Degrees

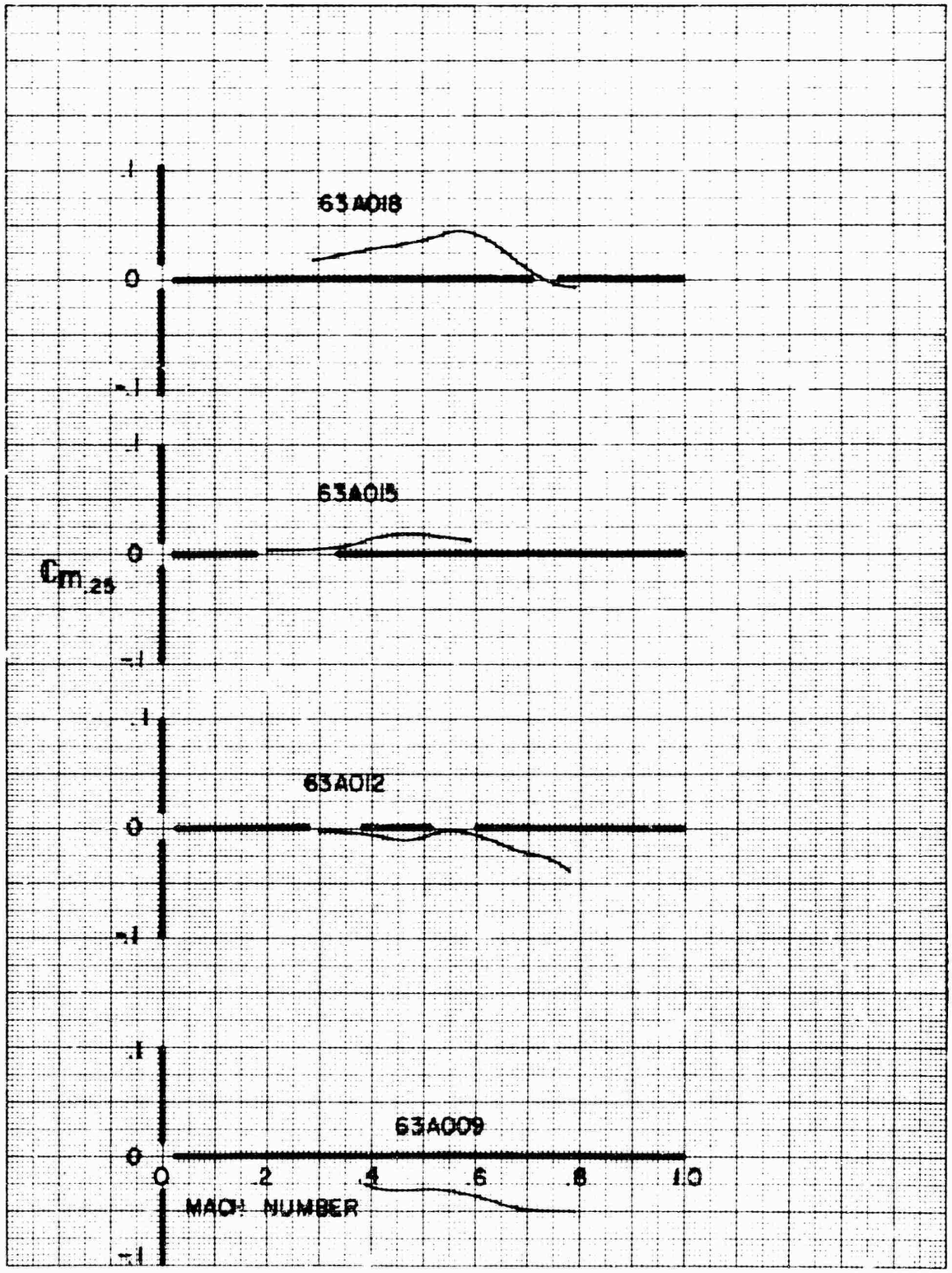


Figure 26N. Section Pitching Moment Coefficient Comparison for Various Thickness Ratios, $R = 3.5 \times 10^6$, $\alpha = 10^0$ Degrees

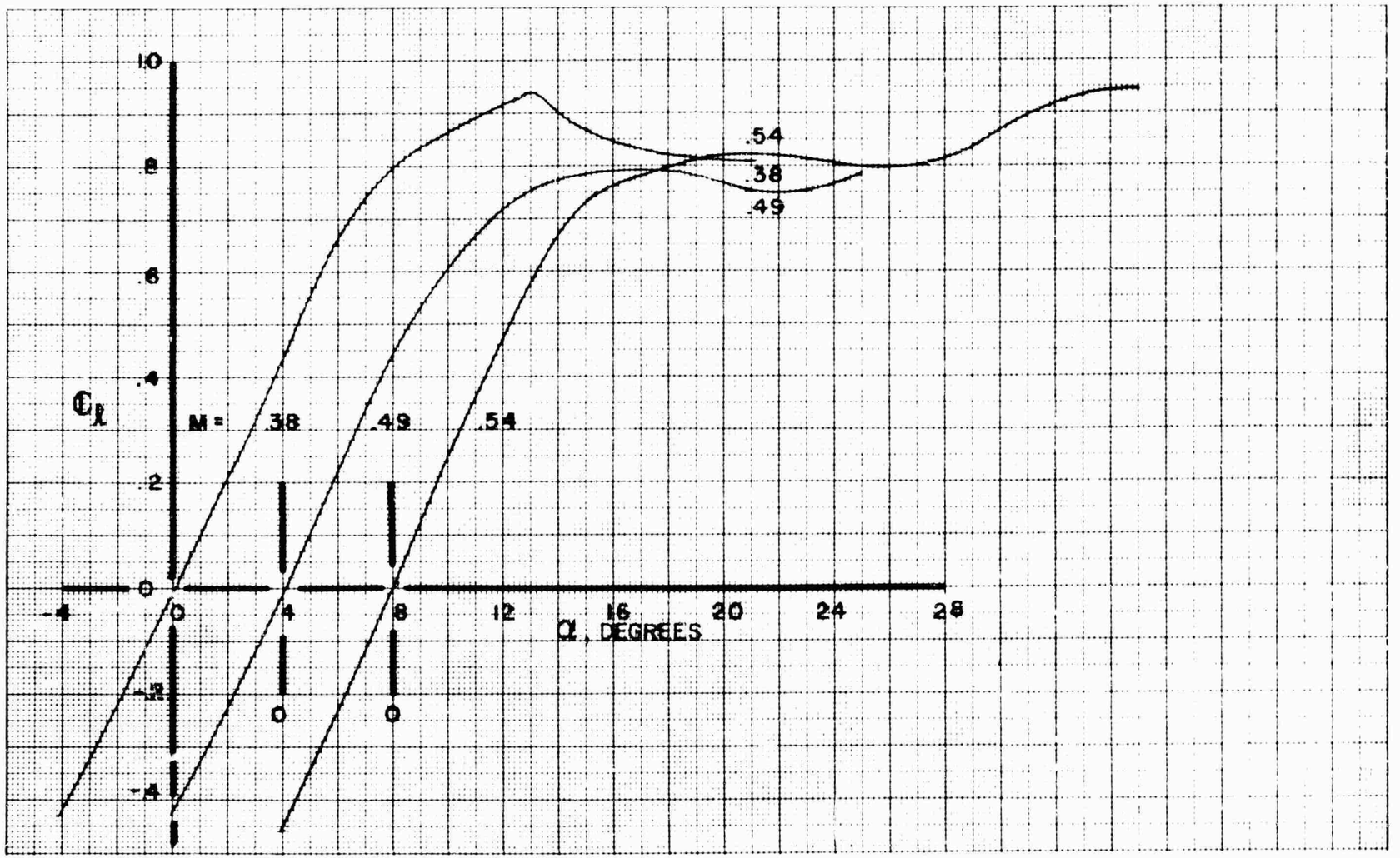


Figure 27A. Variation of Section Lift Coefficient With Angle of Attack at Constant Mach Number, NACA Section 63A009, $R = 2.0 \times 10^6$

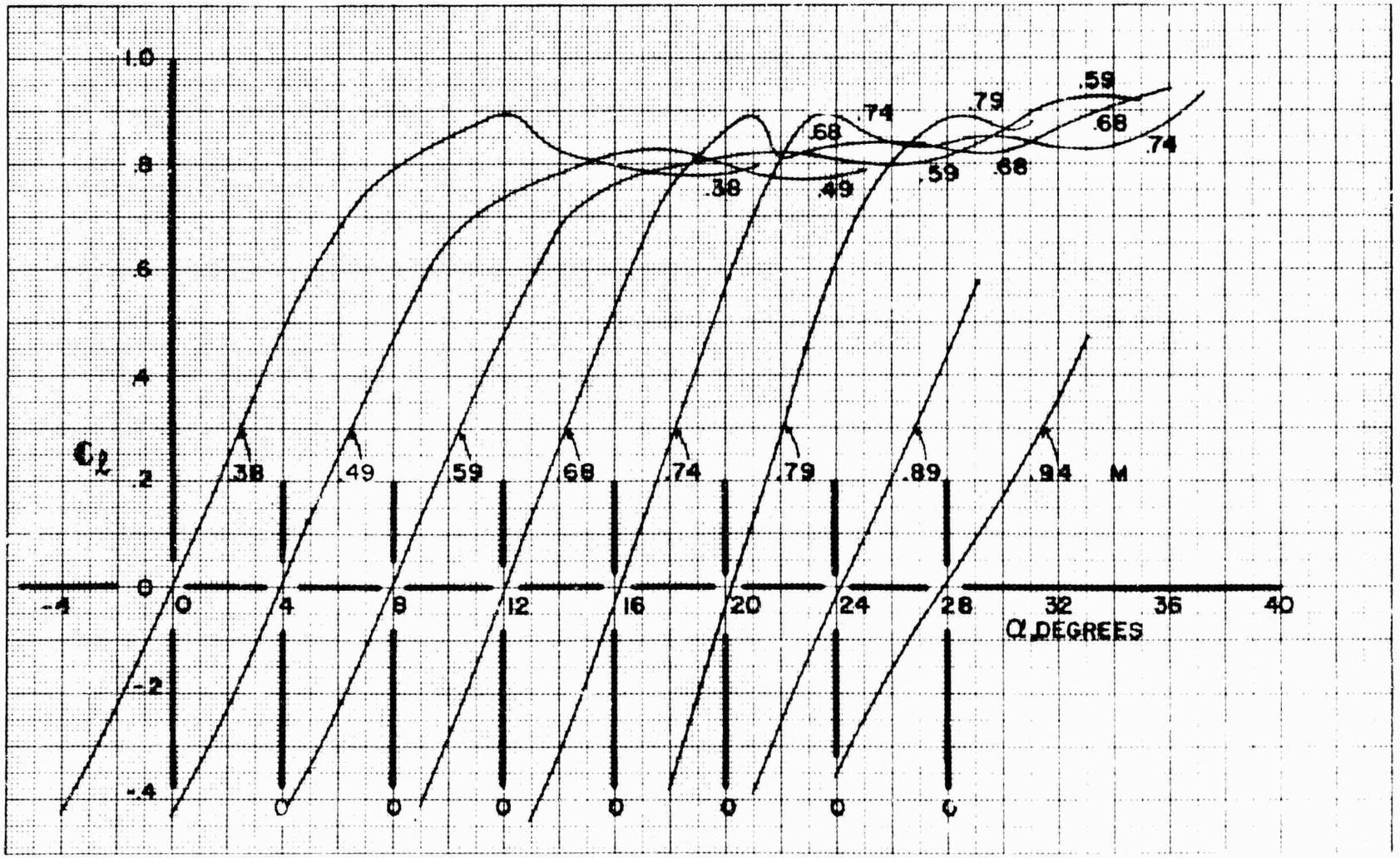


Figure 27B. Variation of Section Lift Coefficient With Angle of Attack at Constant Mach Number, NACA Section 63A009, R = 3.5 x 10^6

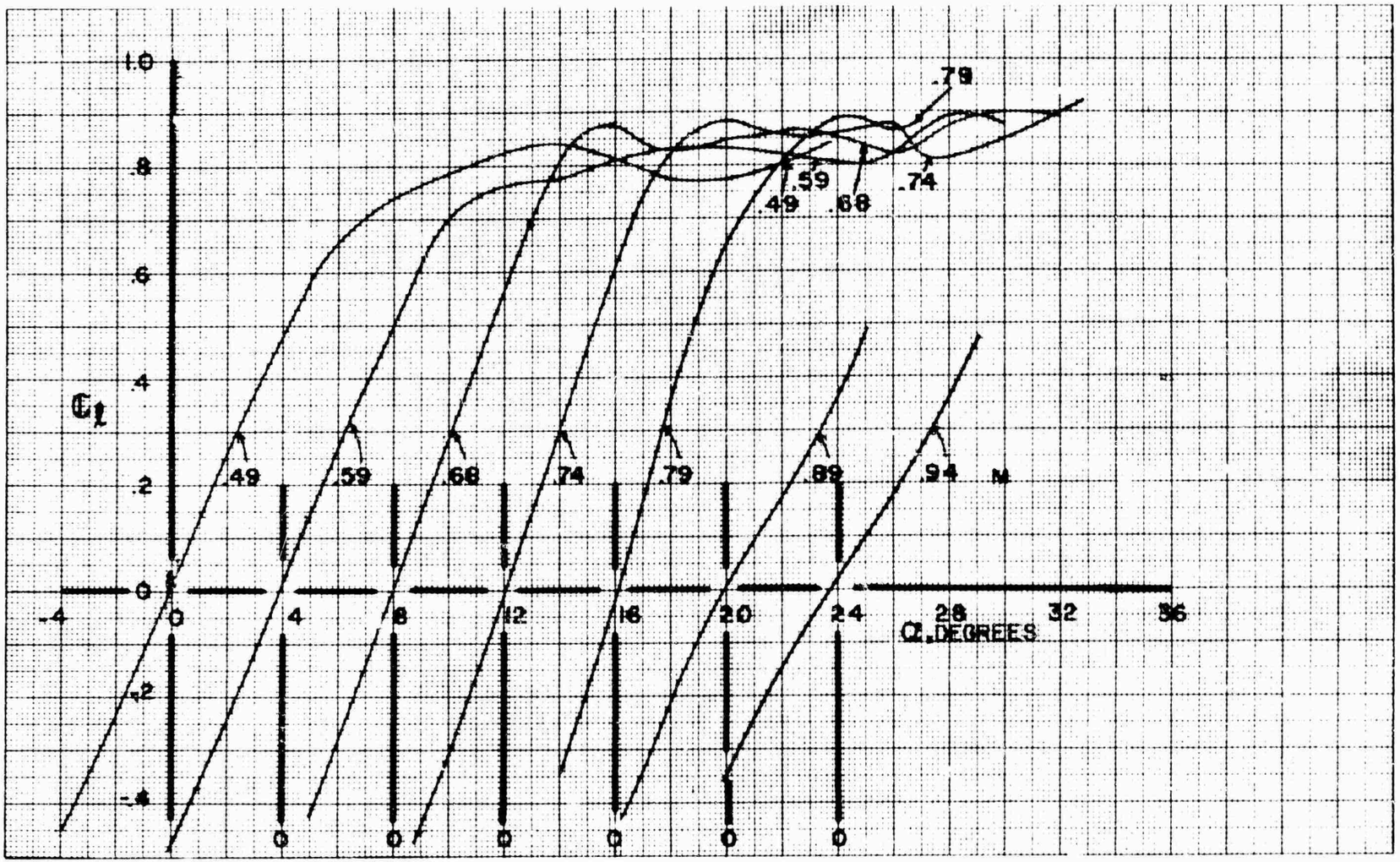


Figure 27C. Variation of Section Lift Coefficient With Angle of Attack at Constant Mach Number, NACA Section 63A009, $R = 5.0 \times 10^6$

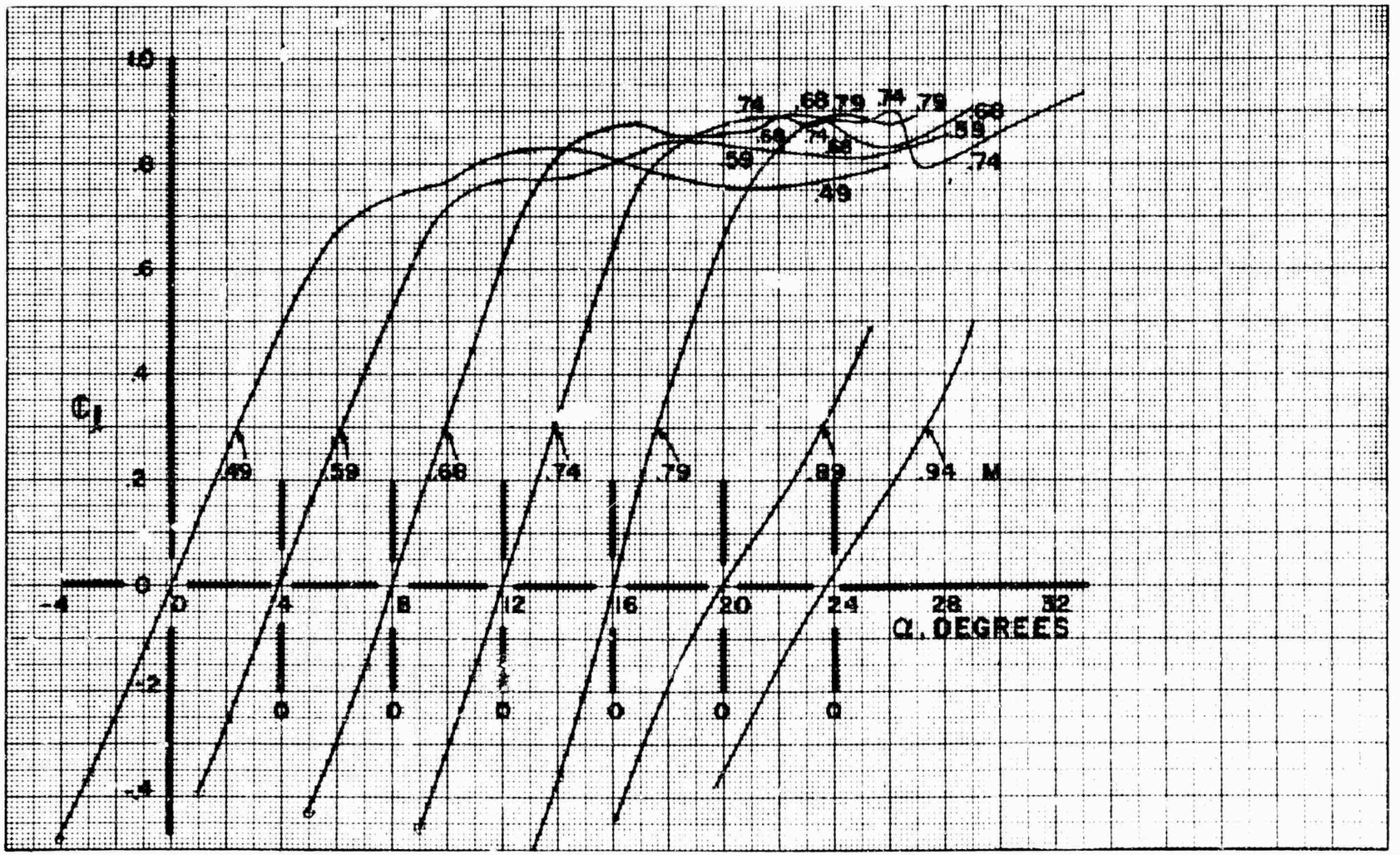


Figure 27D. Variation of Section Lift Coefficient With Angle of Attack at Constant Mach Number, NACA Section 63A009, $R = 6.5 \times 10^6$

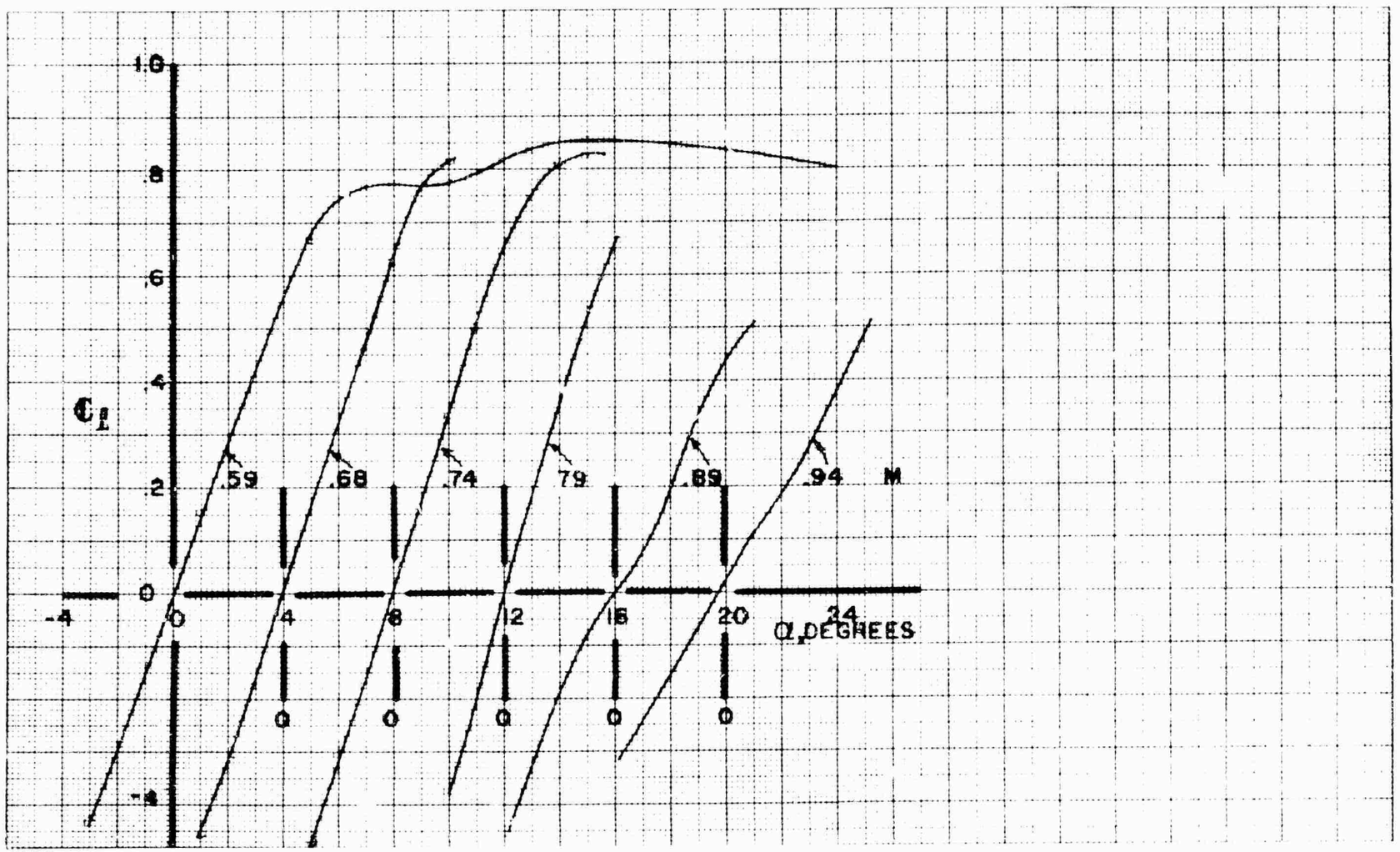


Figure 27E. Variation of Section Lift Coefficient With Angle of Attack at Constant Mach Number, NACA Section 63A009, $R = 8.0 \times 10^6$

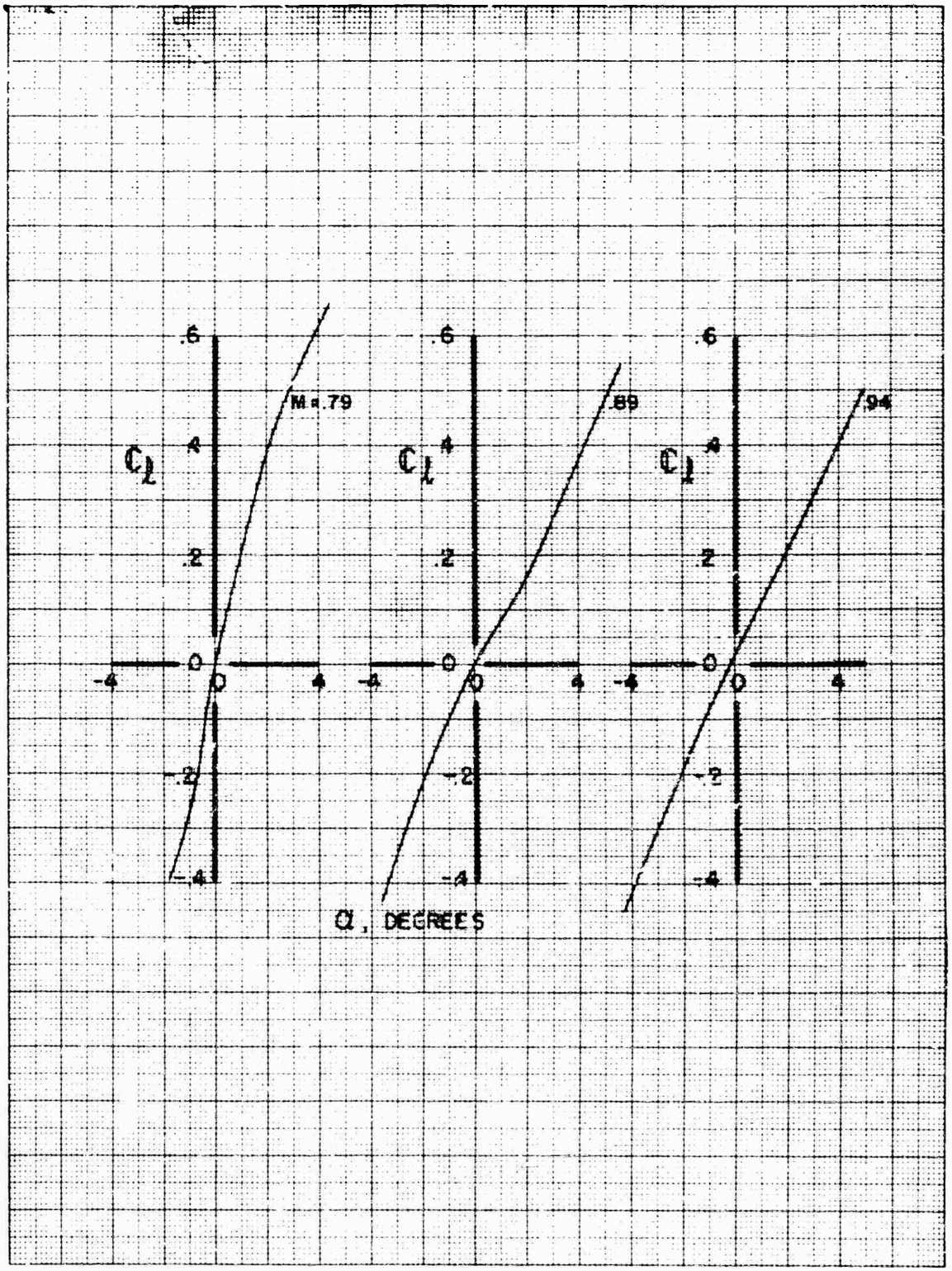


Figure 27F. Variation of Section Lift Coefficient With Angle of Attack at Constant Mach Number, NACA Section 63A009 - $R = 9.5 \times 10^6$

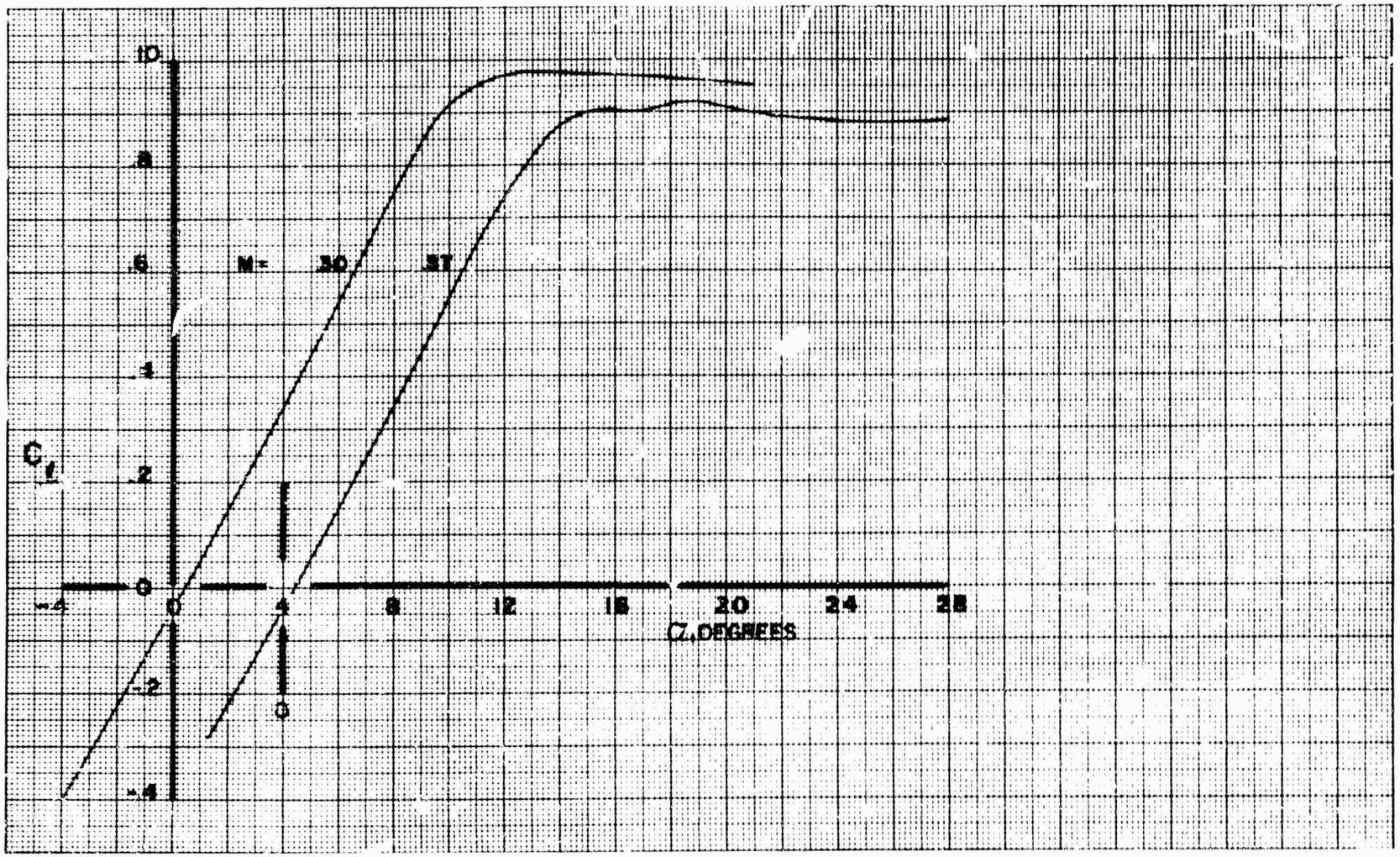


Figure 28A. Variation of Section Lift Coefficient With Angle of Attack at Constant Mach Number, NACA Section 63A012 - R = 2.0 x 10^6

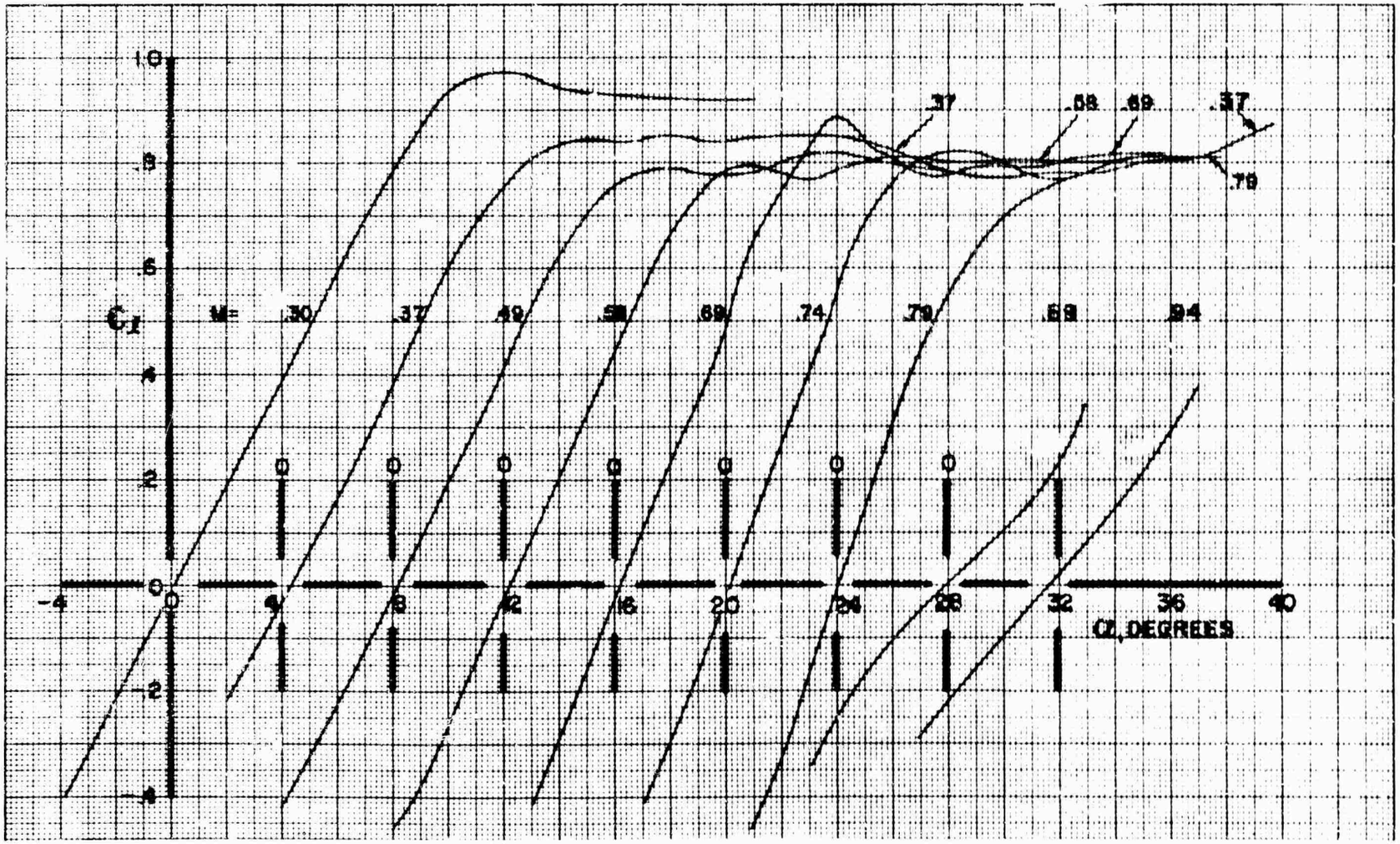


Figure 28B. Variation of Section Lift Coefficient With Angle of Attack at Constant Mach Number, NACA Section 63A012, R = 3.5 x 10^6

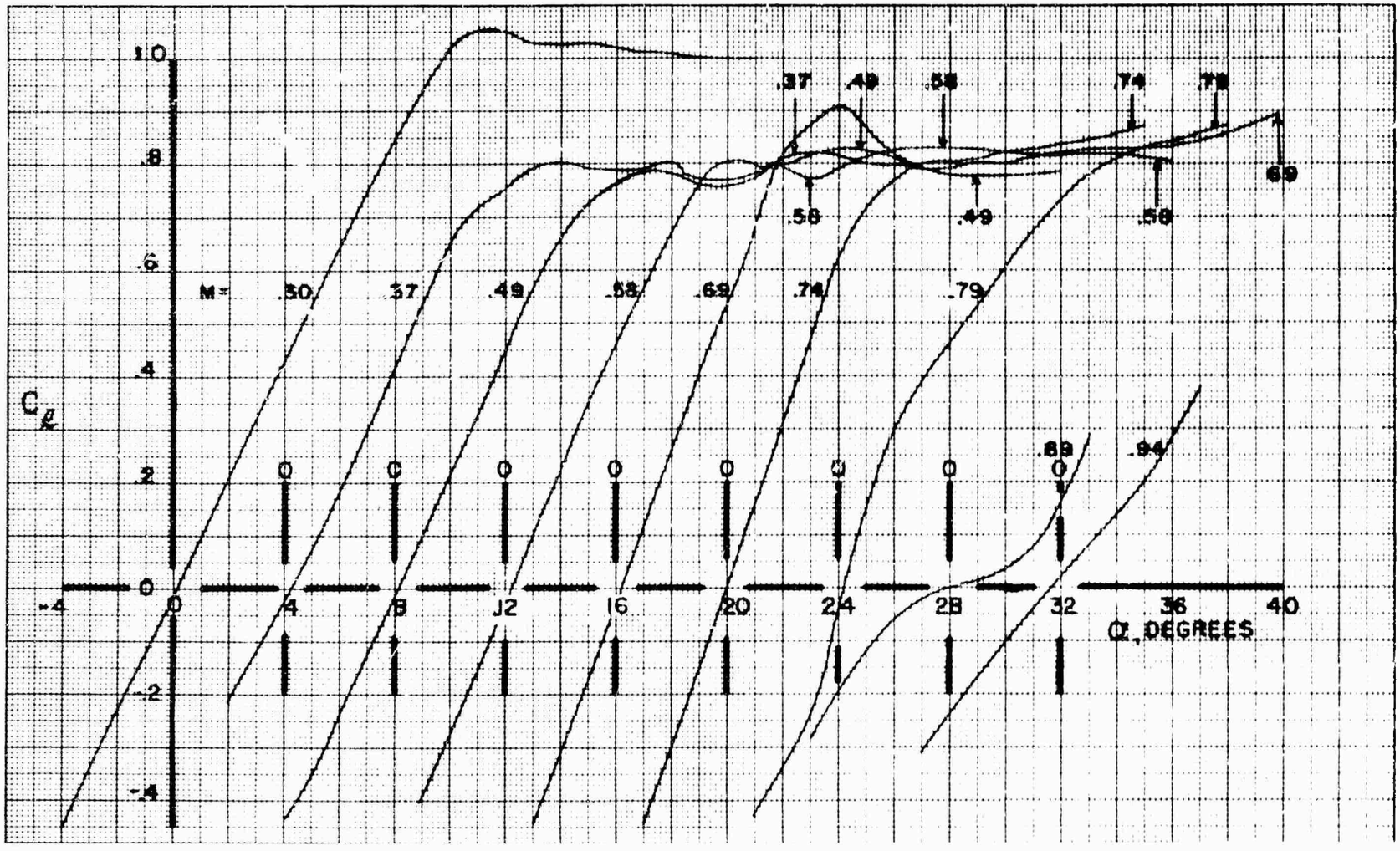


Figure 28C. Variation of Section Lift Coefficient With Angle of Attack at Constant Mach Number, NACA Section 63A012, $R = 5.0 \times 10^6$

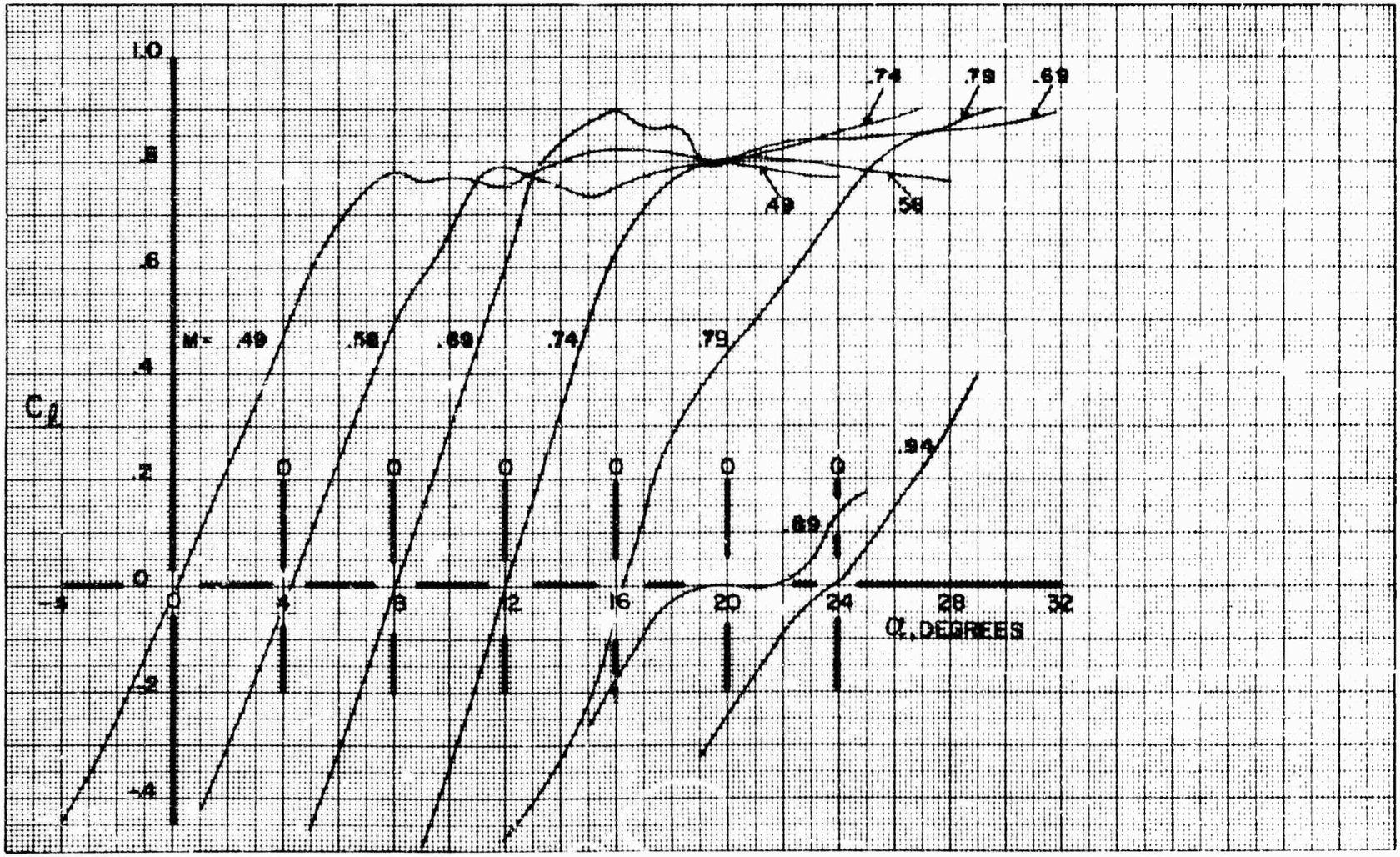


Figure 28D. Variation of Section Lift Coefficient With Angle of Attack at Constant Mach Number, NACA Section 63A012, R = 6.5 x 10^6

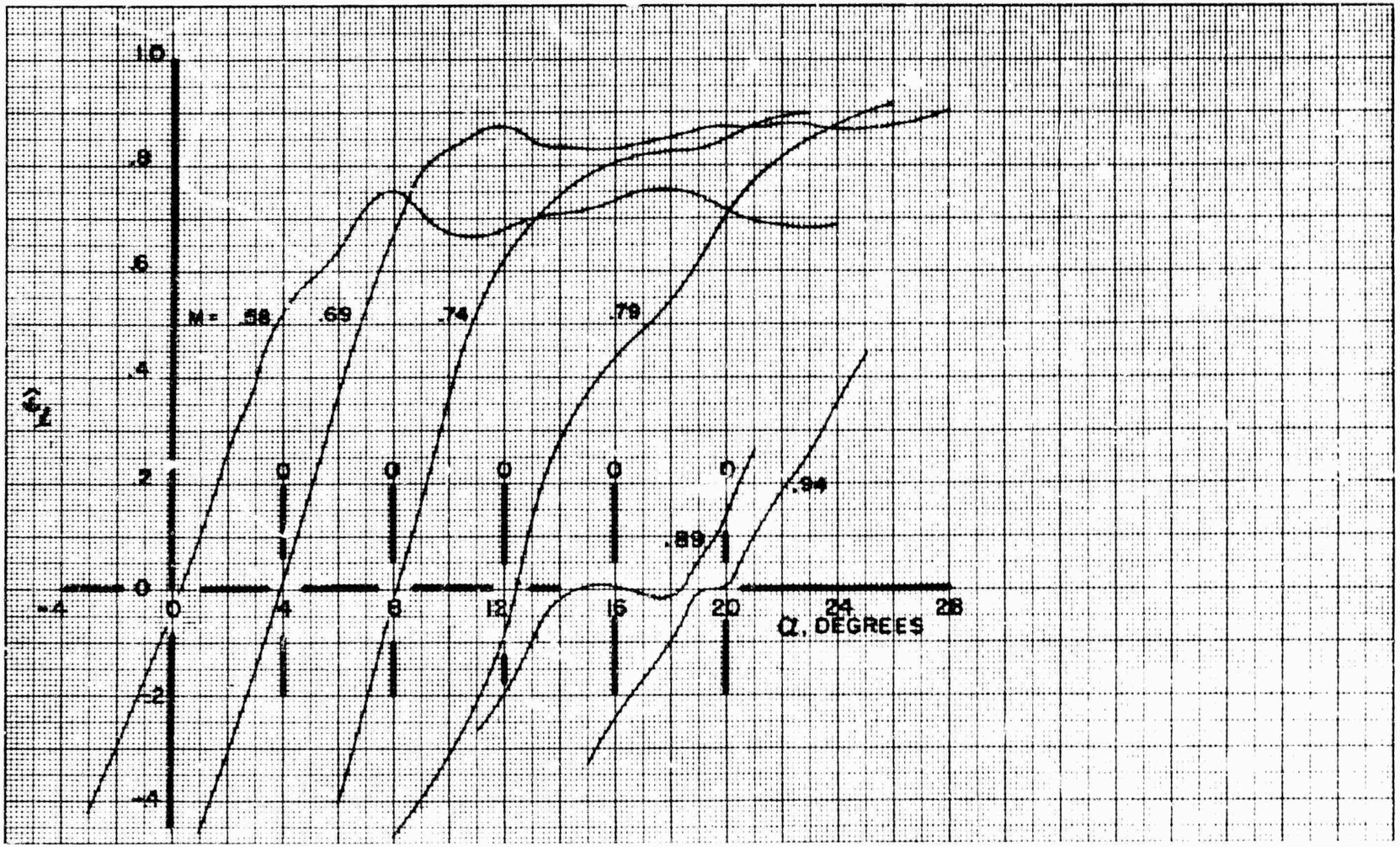


Figure 28E. Variation of Section Lift Coefficient With Angle of Attack at Constant Mach Number, NACA Section 63A012, R = 8.0 x 10^6

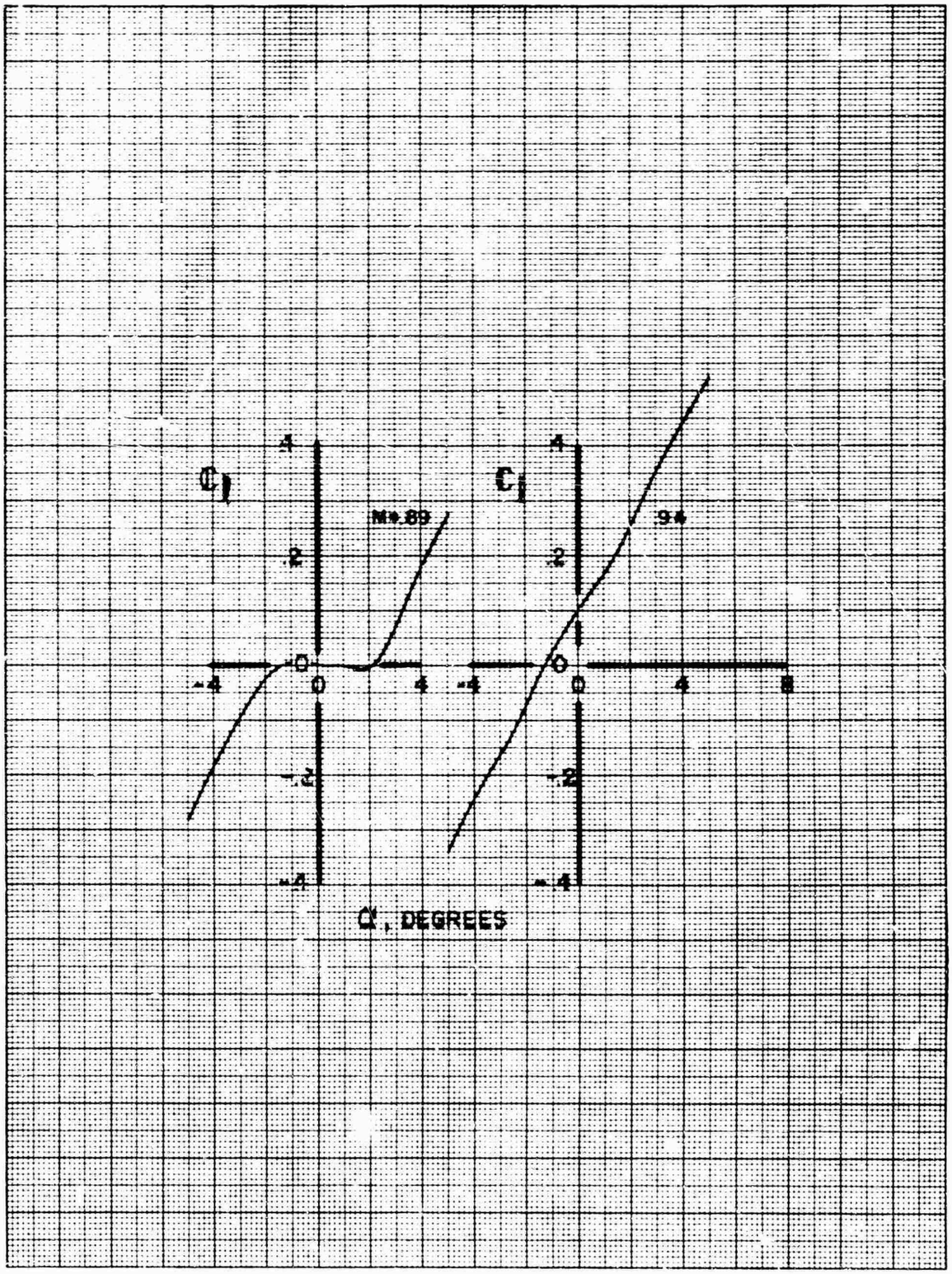


Figure 28F. Variation of Section Lift Coefficient With Angle of Attack at Constant Mach Number, NACA Section 63A012 - $R = 9.5 \times 10^6$

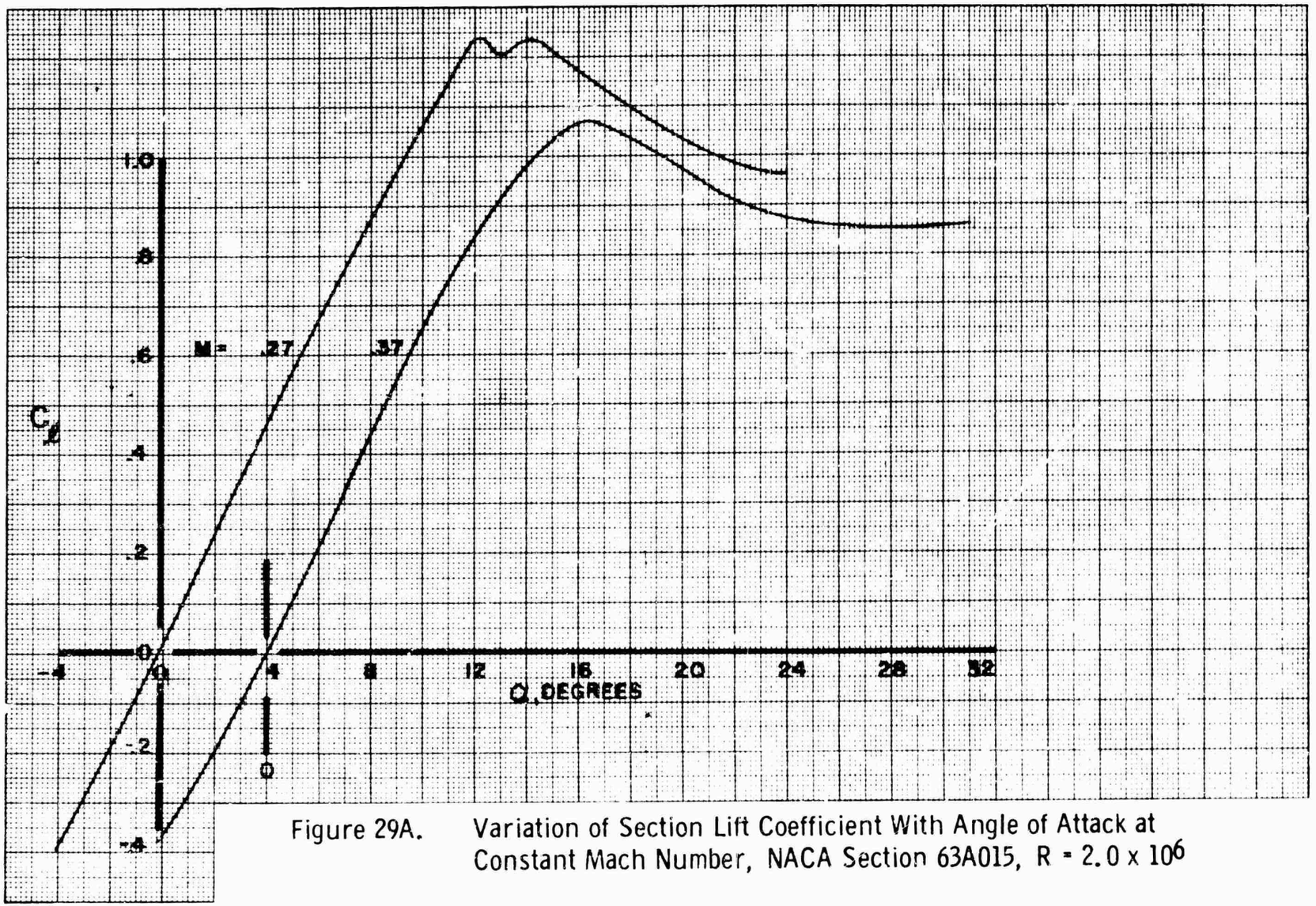


Figure 29A. Variation of Section Lift Coefficient With Angle of Attack at Constant Mach Number, NACA Section 63A015, R = 2.0 x 10^6

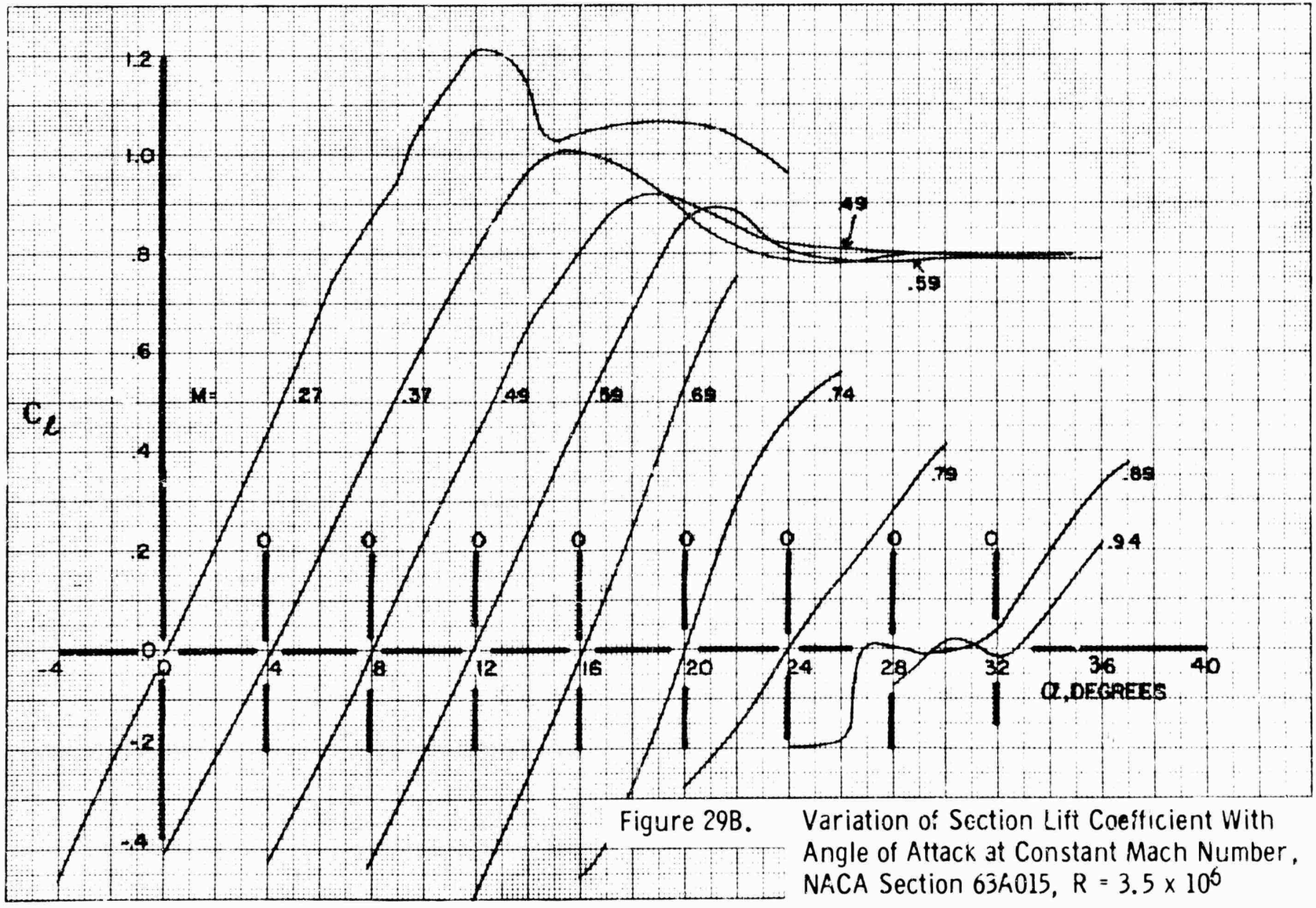


Figure 29B. Variation of Section Lift Coefficient With Angle of Attack at Constant Mach Number, NACA Section 63A015, $R = 3.5 \times 10^6$

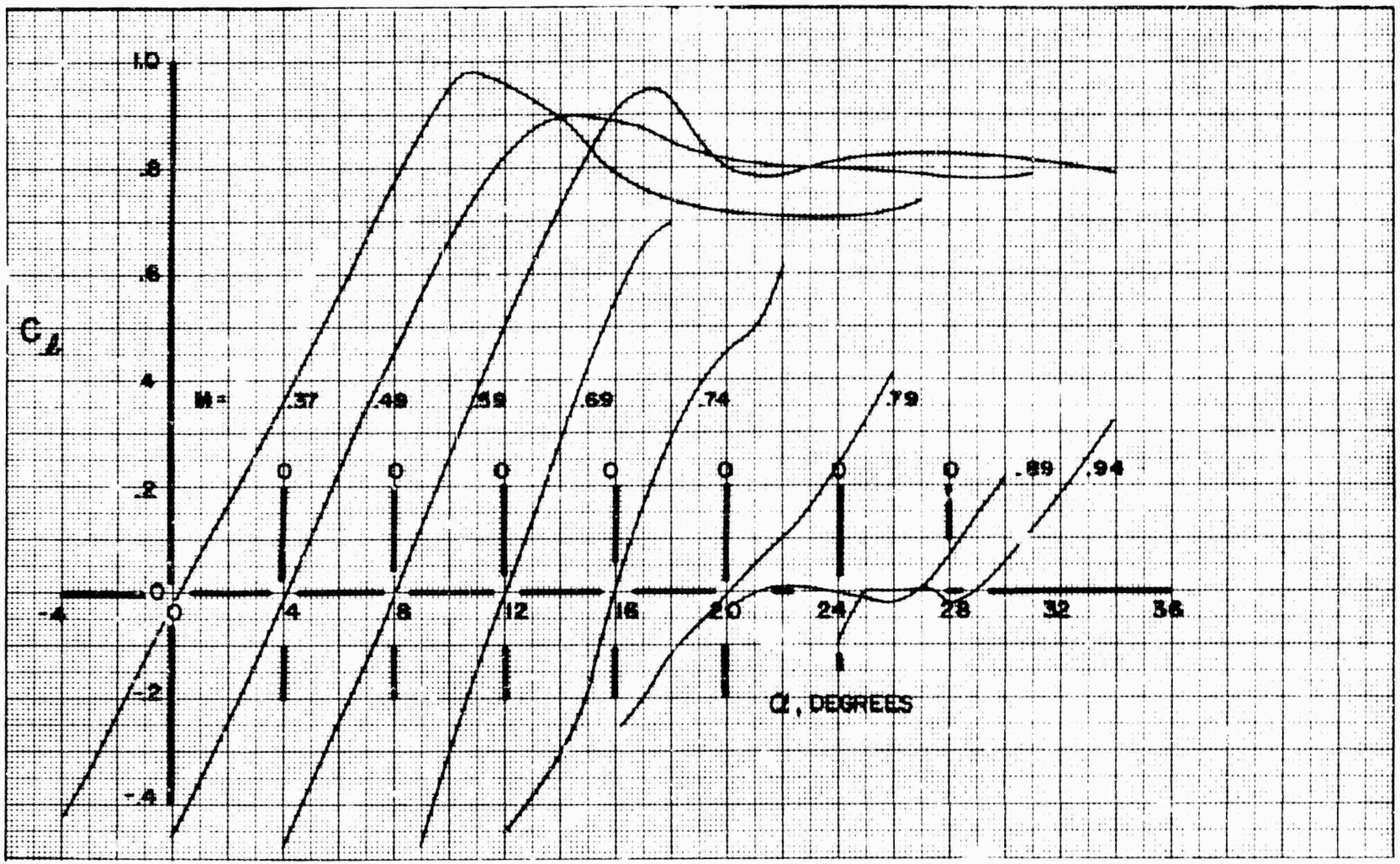


Figure 29C. Variation of Section Lift Coefficient With Angle of Attack at Constant Mach Number, NACA Section 63A015, $R = 5.0 \times 10^6$

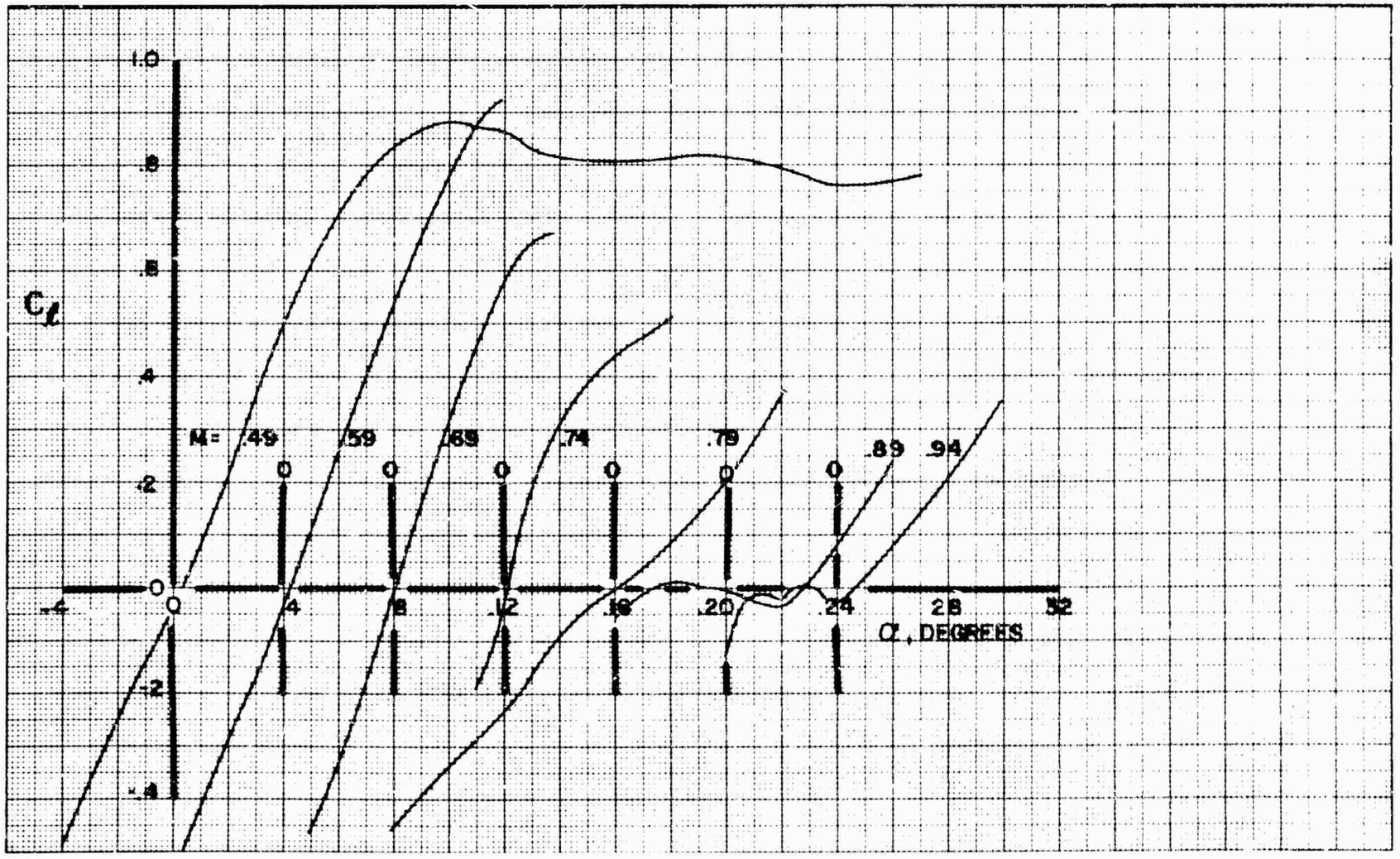


Figure 29D. Variation of Section Lift Coefficient With Angle of Attack at Constant Mach Number, NACA Section 63A015, $R = 6.5 \times 10^6$

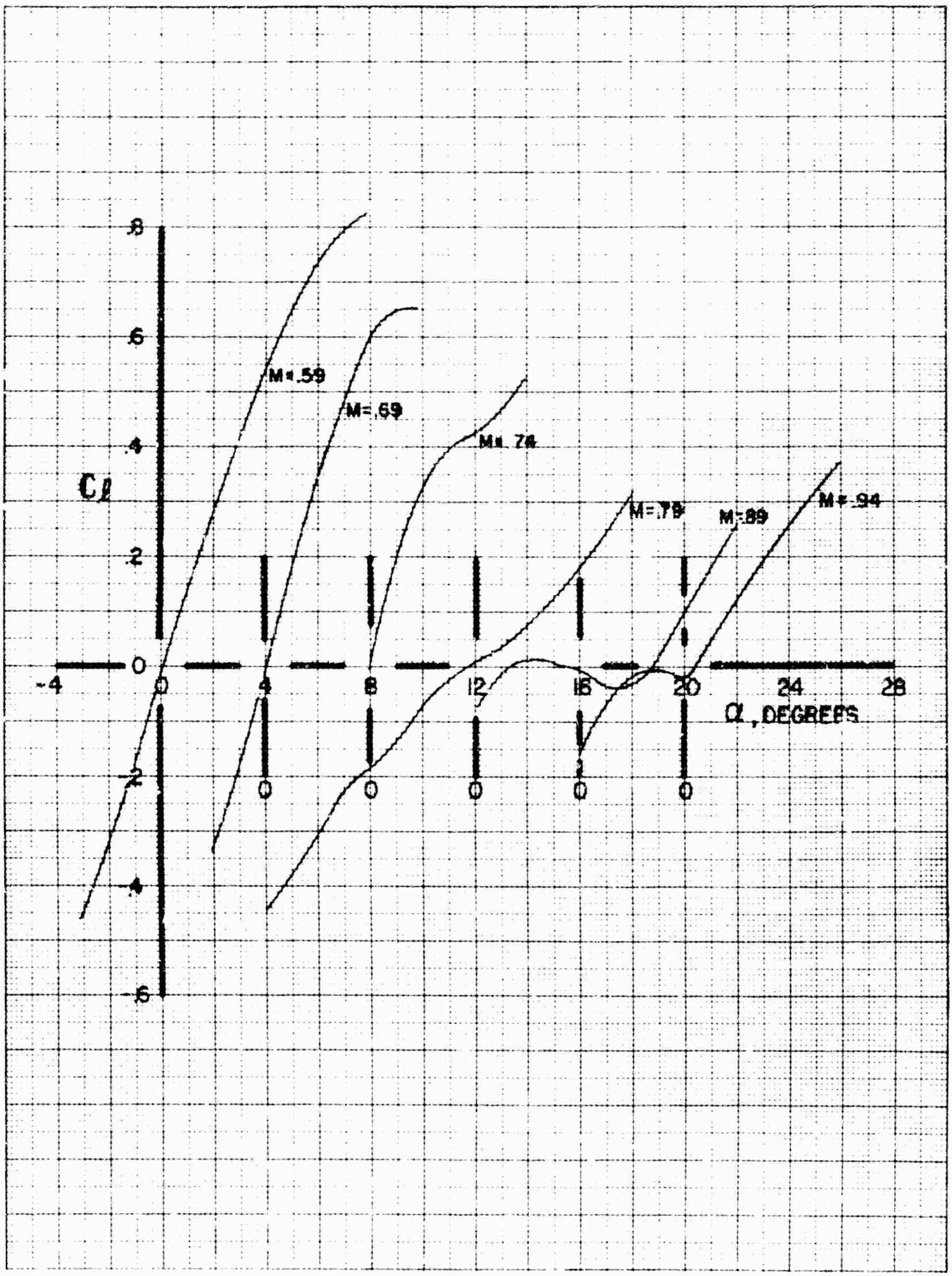


Figure 29E. Variation of Section Lift Coefficient With Angle of Attack at Constant Mach Number, NACA Section 63A015, $R = 8.0 \times 10^6$

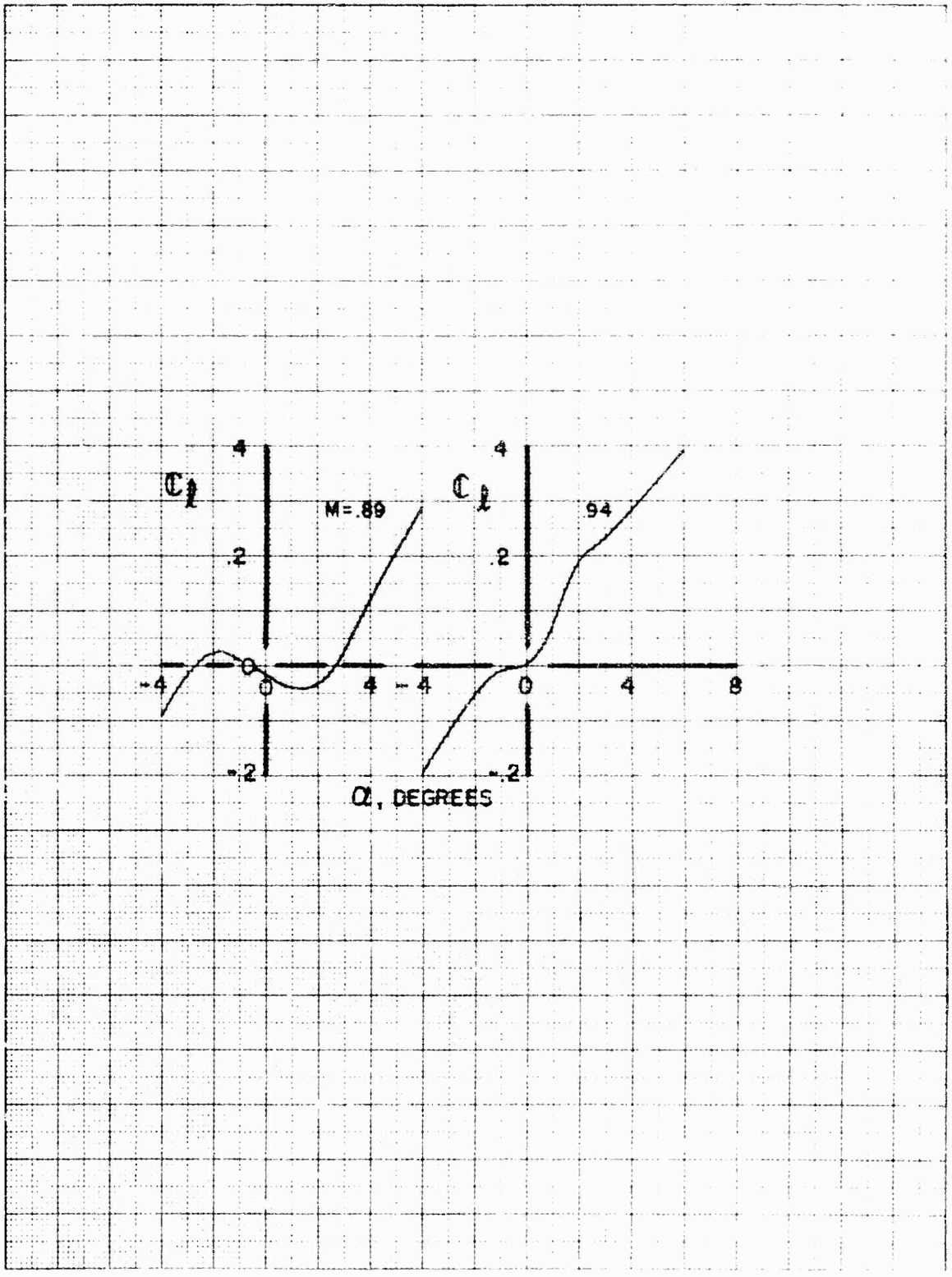


Figure 29F. Variation of Section Lift Coefficient With Angle of Attack at Constant Mach Number, NACA Section 63A015 - $R = 9.5 \times 10^6$

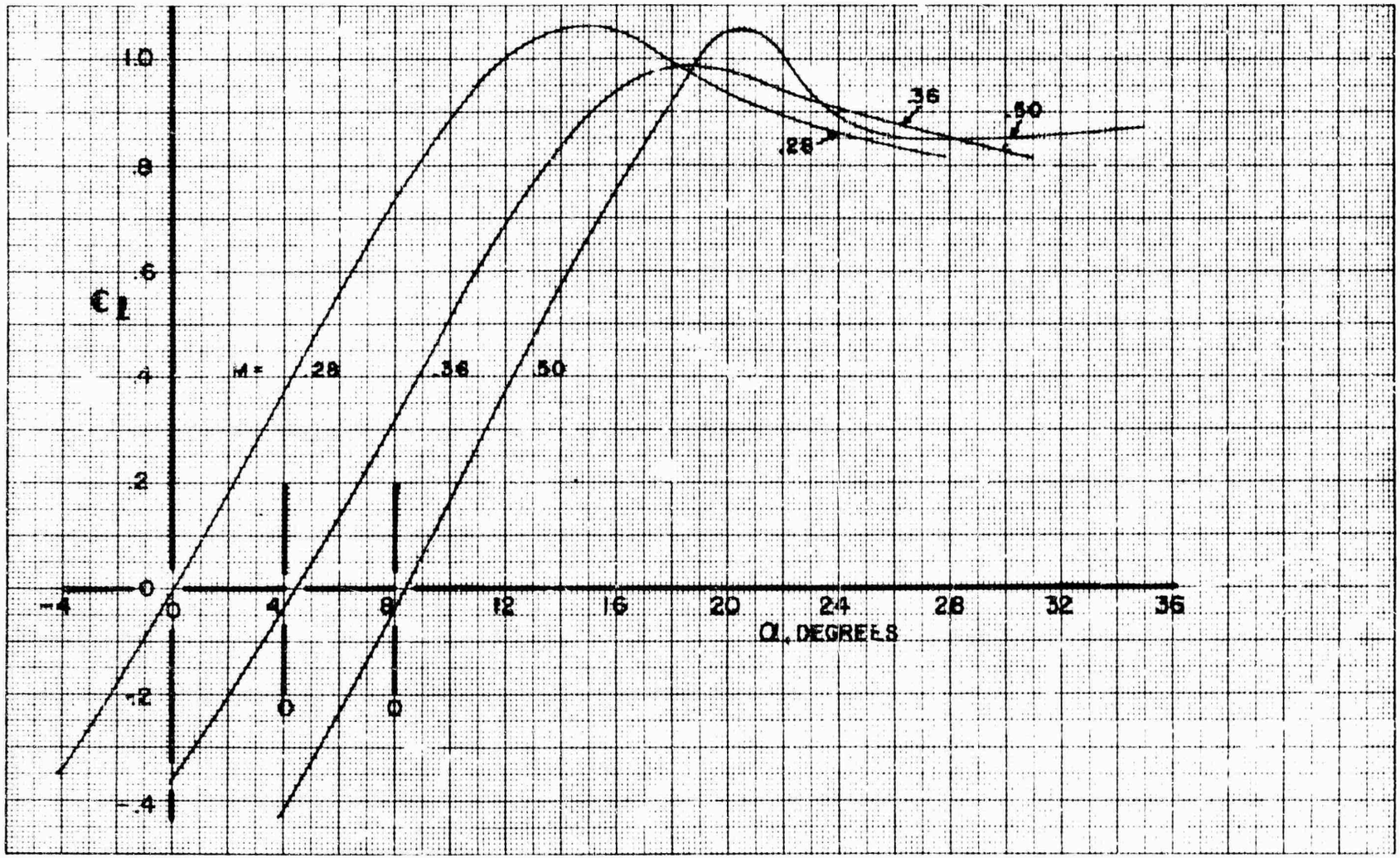


Figure 30A. Variation of Section Lift Coefficient With Angle of Attack at Constant Mach Number, NACA Section 63A018 - R = 2.0 x 10^6

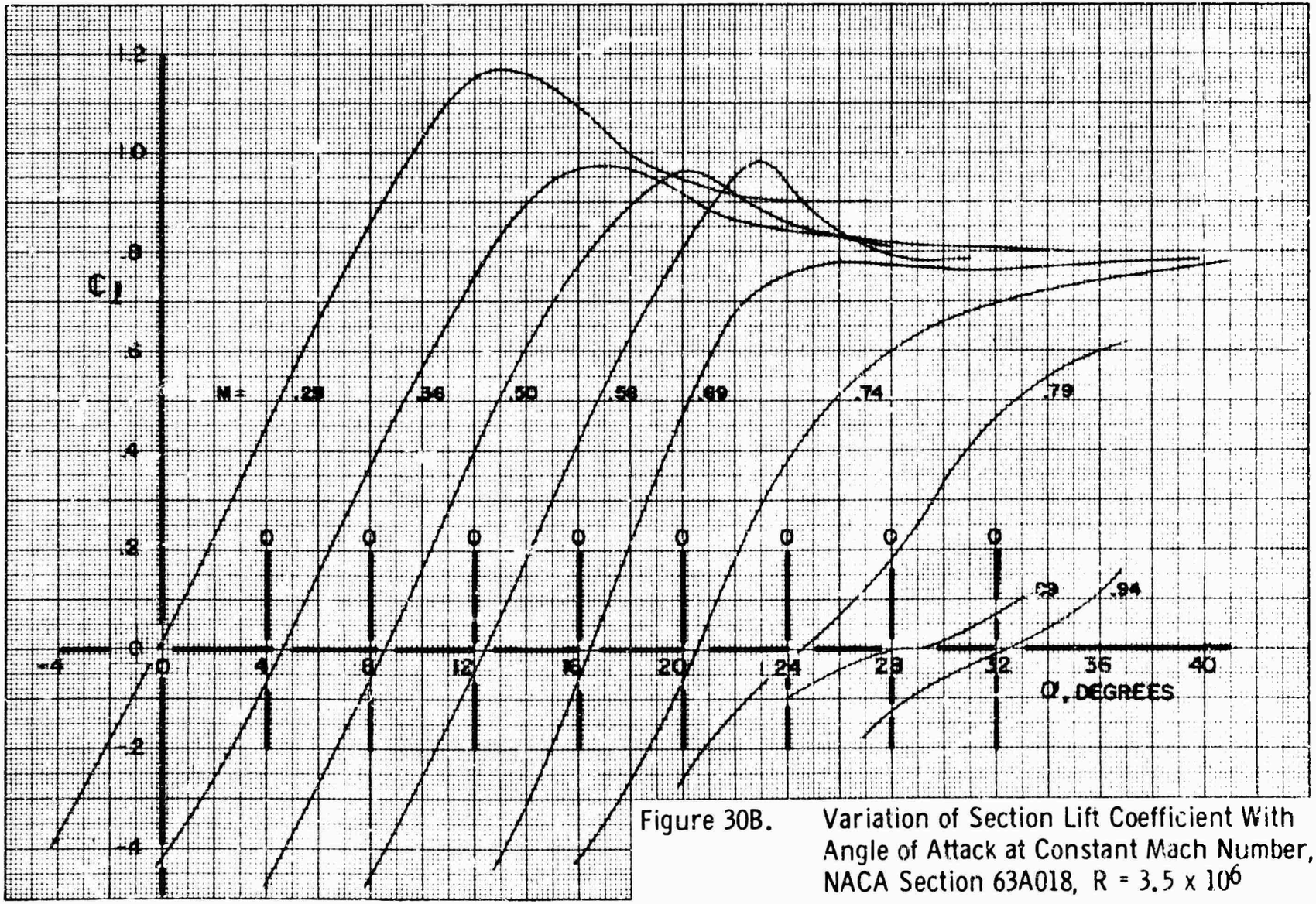


Figure 30B. Variation of Section Lift Coefficient With Angle of Attack at Constant Mach Number, NACA Section 63A018, $R = 3.5 \times 10^6$

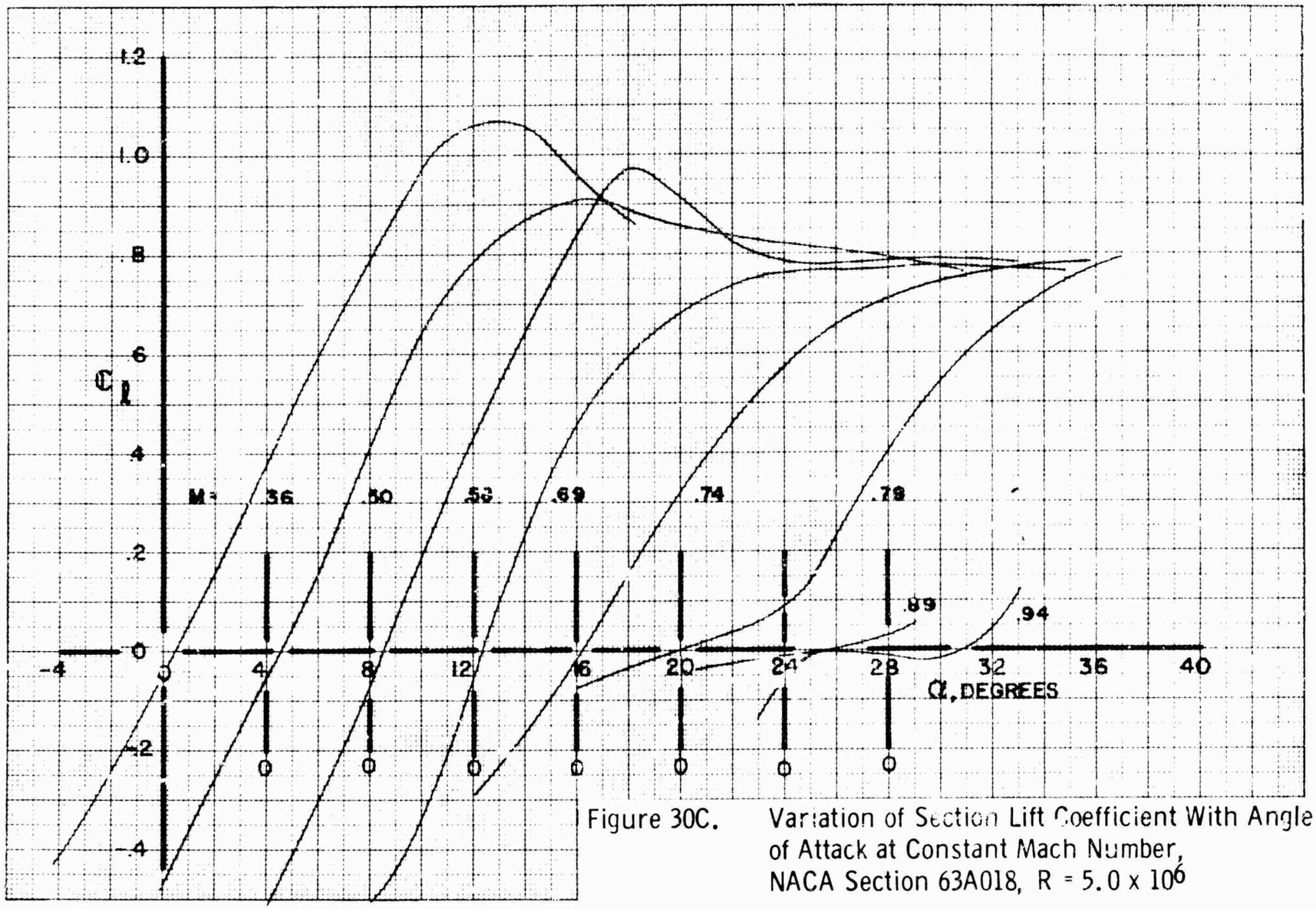


Figure 30C. Variation of Section Lift Coefficient With Angle of Attack at Constant Mach Number, NACA Section 63A018, $R = 5.0 \times 10^6$

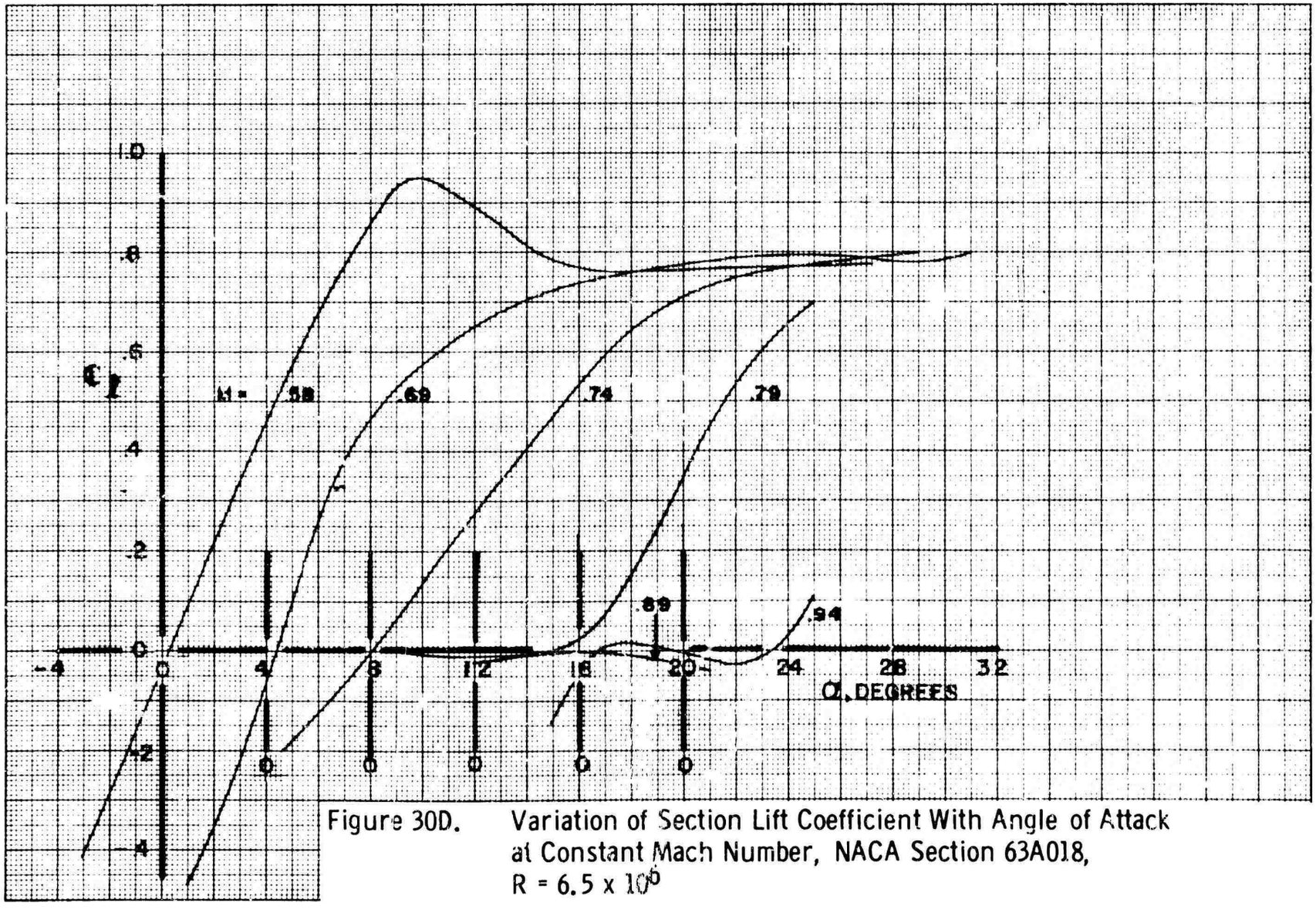


Figure 30D. Variation of Section Lift Coefficient With Angle of Attack at Constant Mach Number, NACA Section 63A018, $R = 6.5 \times 10^6$

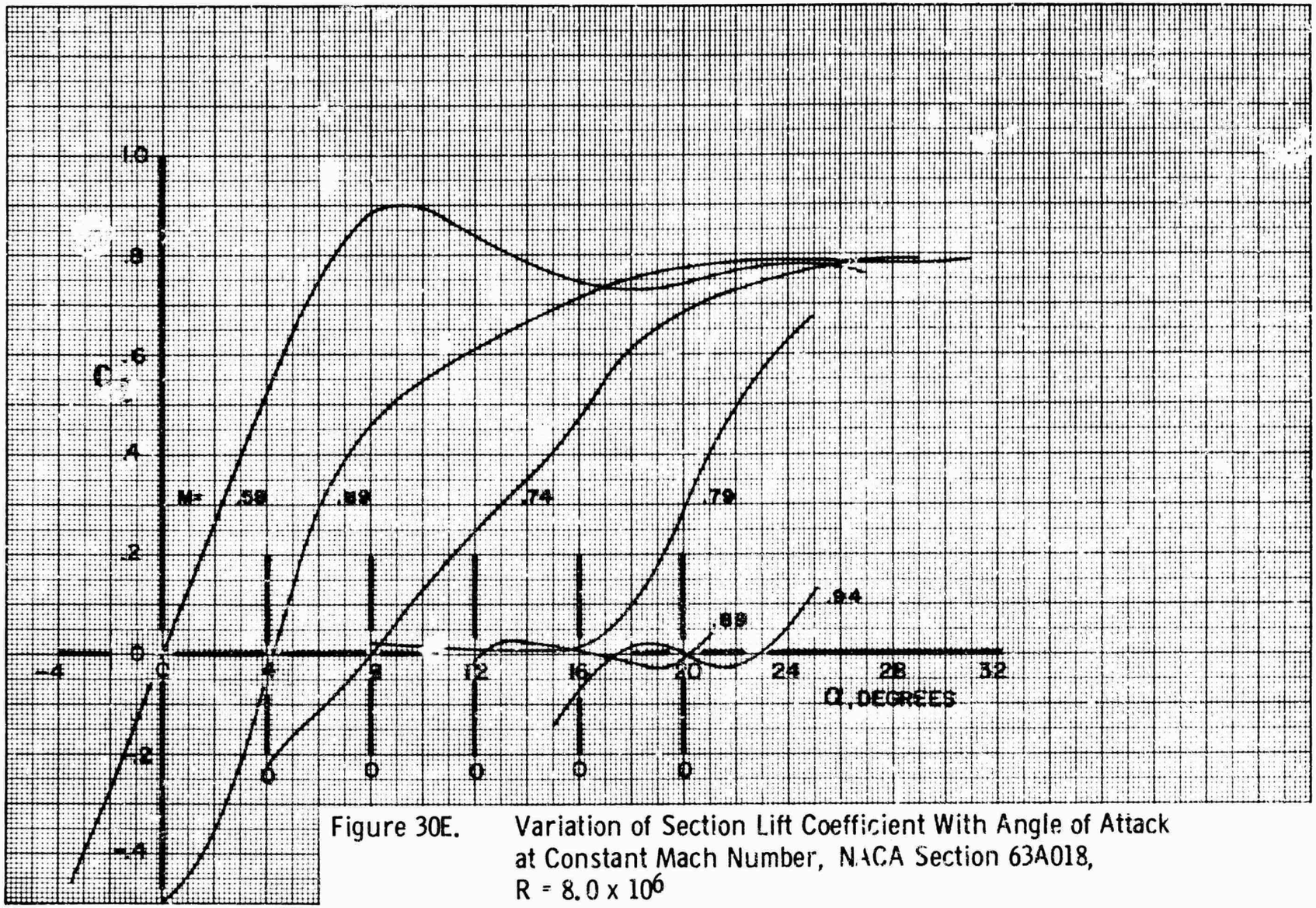


Figure 30E. Variation of Section Lift Coefficient With Angle of Attack at Constant Mach Number, NACA Section 63A018, $R = 8.0 \times 10^6$

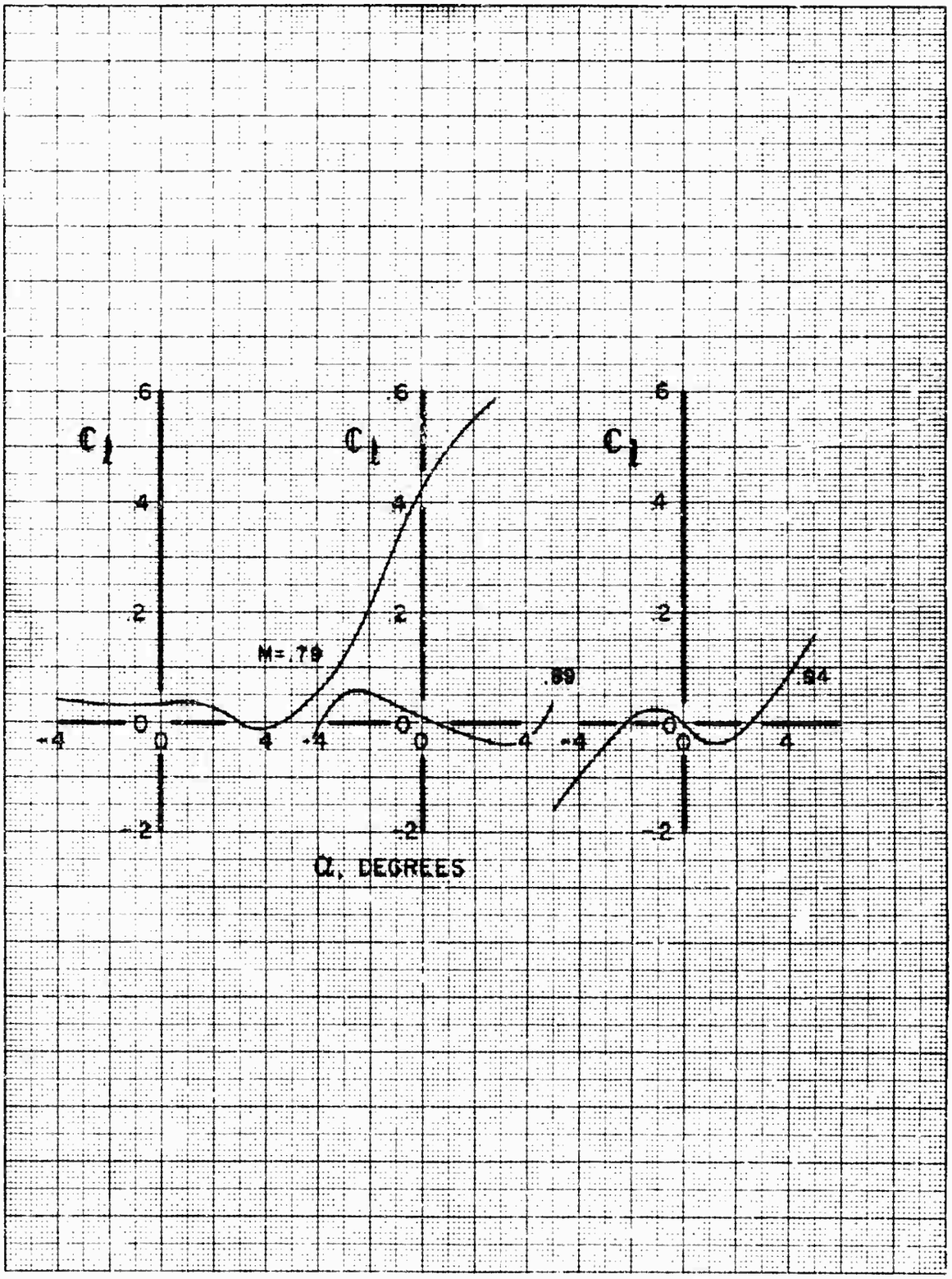


Figure 30F. Variation of Section Lift Coefficient With Angle of Attack at Constant Mach Number, NACA Section 63A018 - $R = 9.5 \times 10^6$

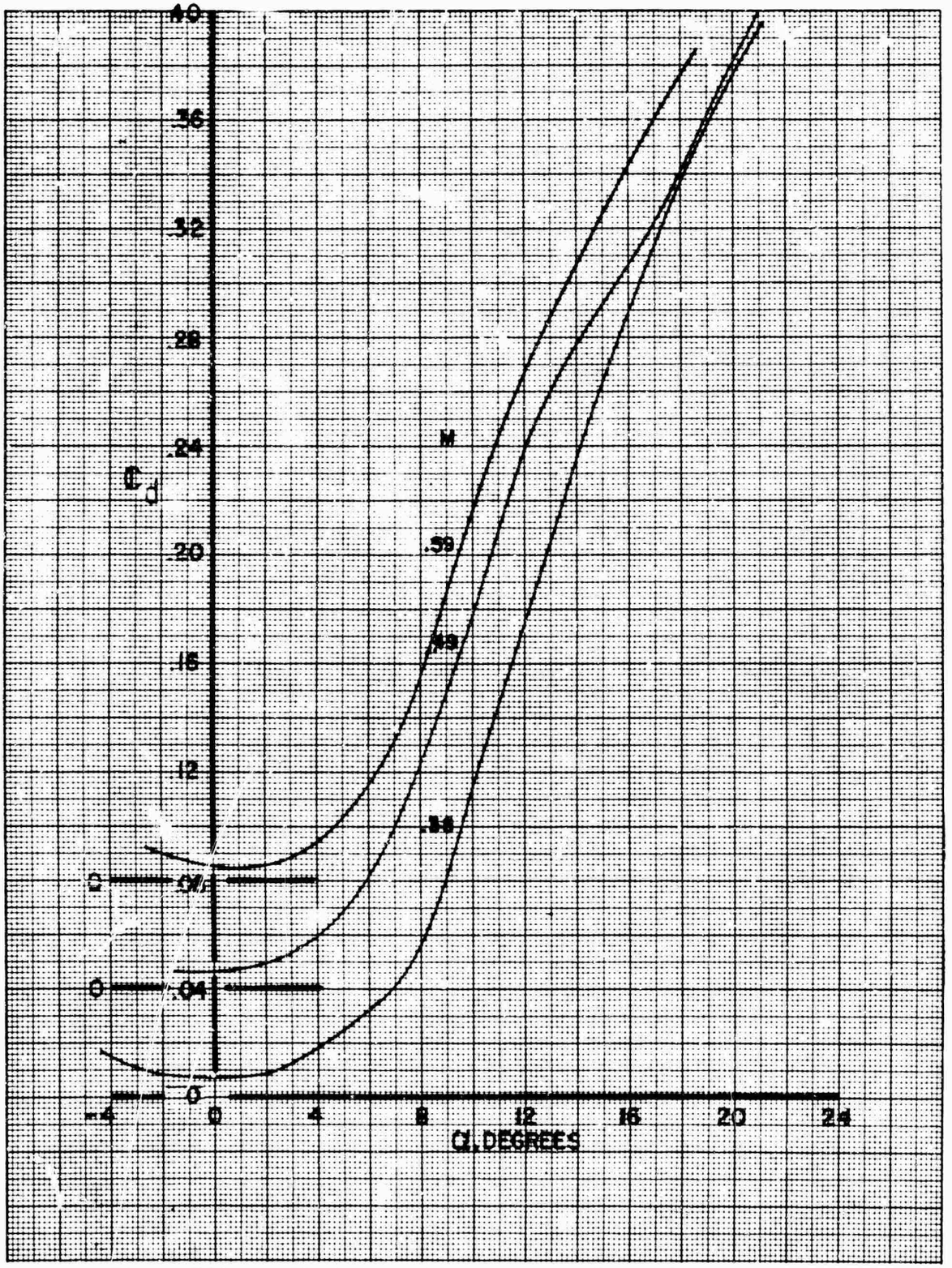


Figure 31A. Variation of Section Drag Coefficient With Angle of Attack at Constant Mach Number, NACA Section 63A009, $R = 2.0 \times 10^6$

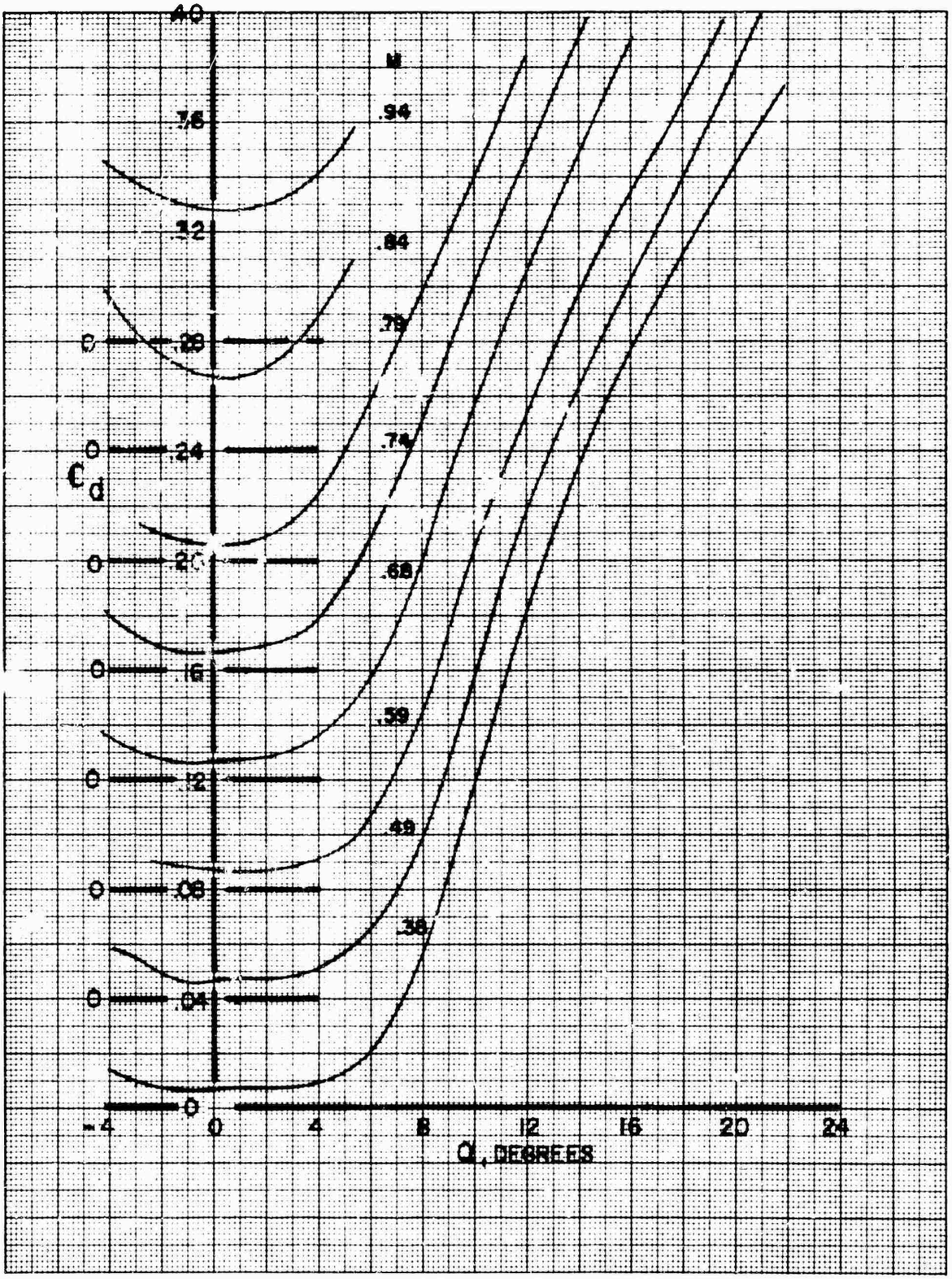


Figure 31B. Variation of Section Drag Coefficient With Angle of Attack at Constant Mach Number, NACA Section 63A009, R = 3.5 x 10^6

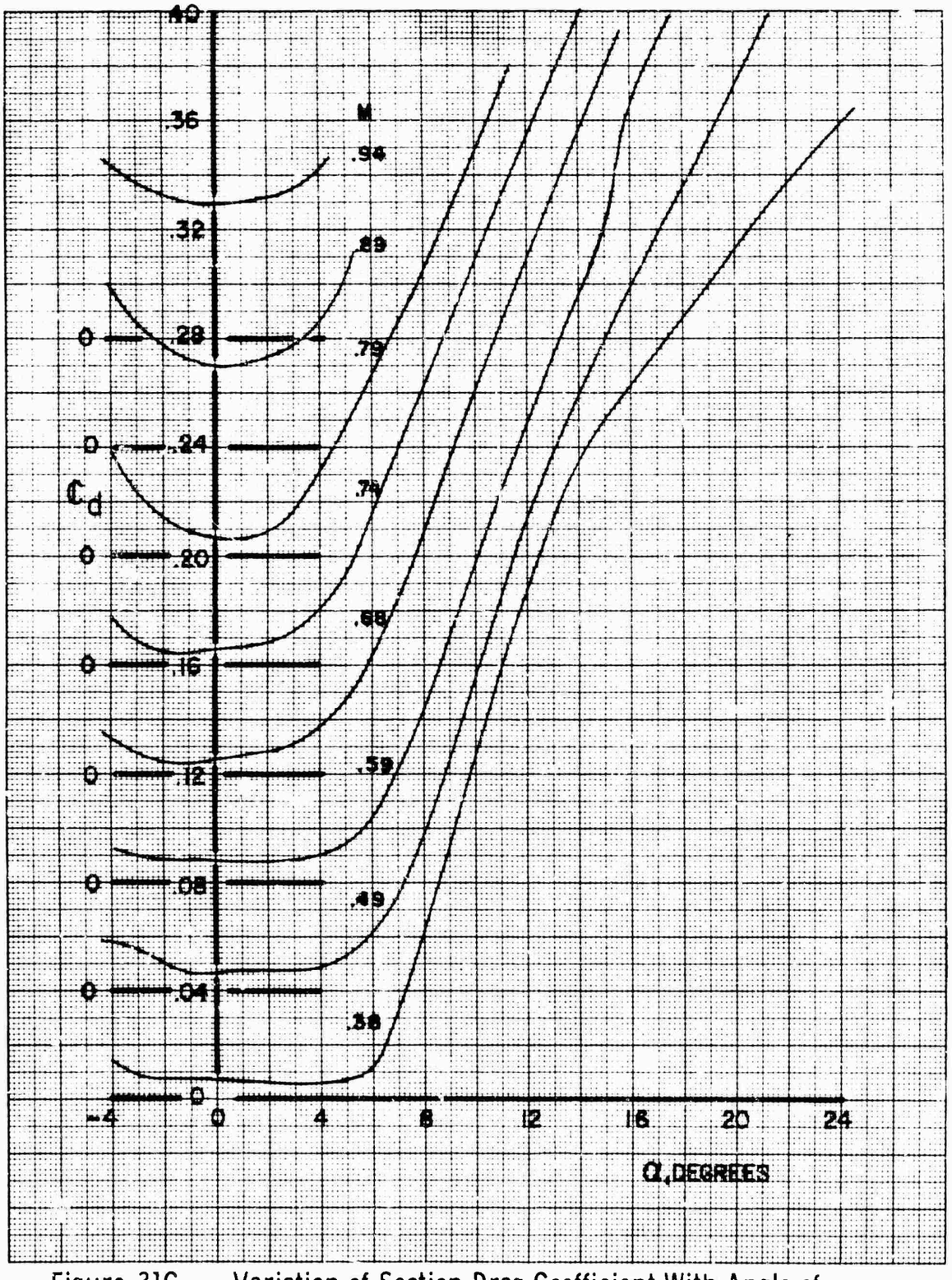


Figure 31C. Variation of Section Drag Coefficient With Angle of Attack at Constant Mach Number, NACA Section 63A009, $R = 5.0 \times 10^6$

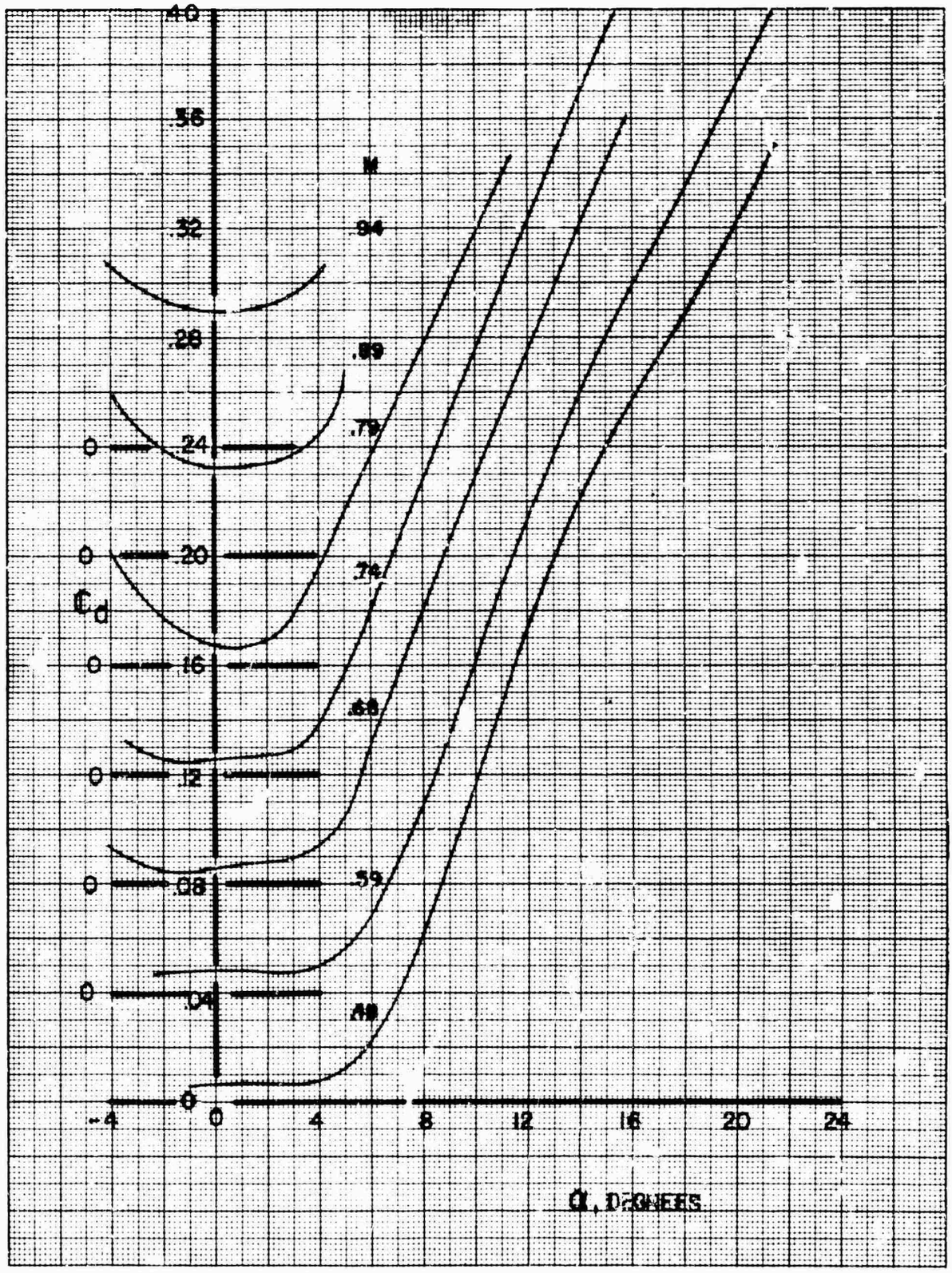


Figure 31D. Variation of Section Drag Coefficient With Angle of Attack at Constant Mach Number, NACA Section 63A009, $R = 6.5 \times 10^6$

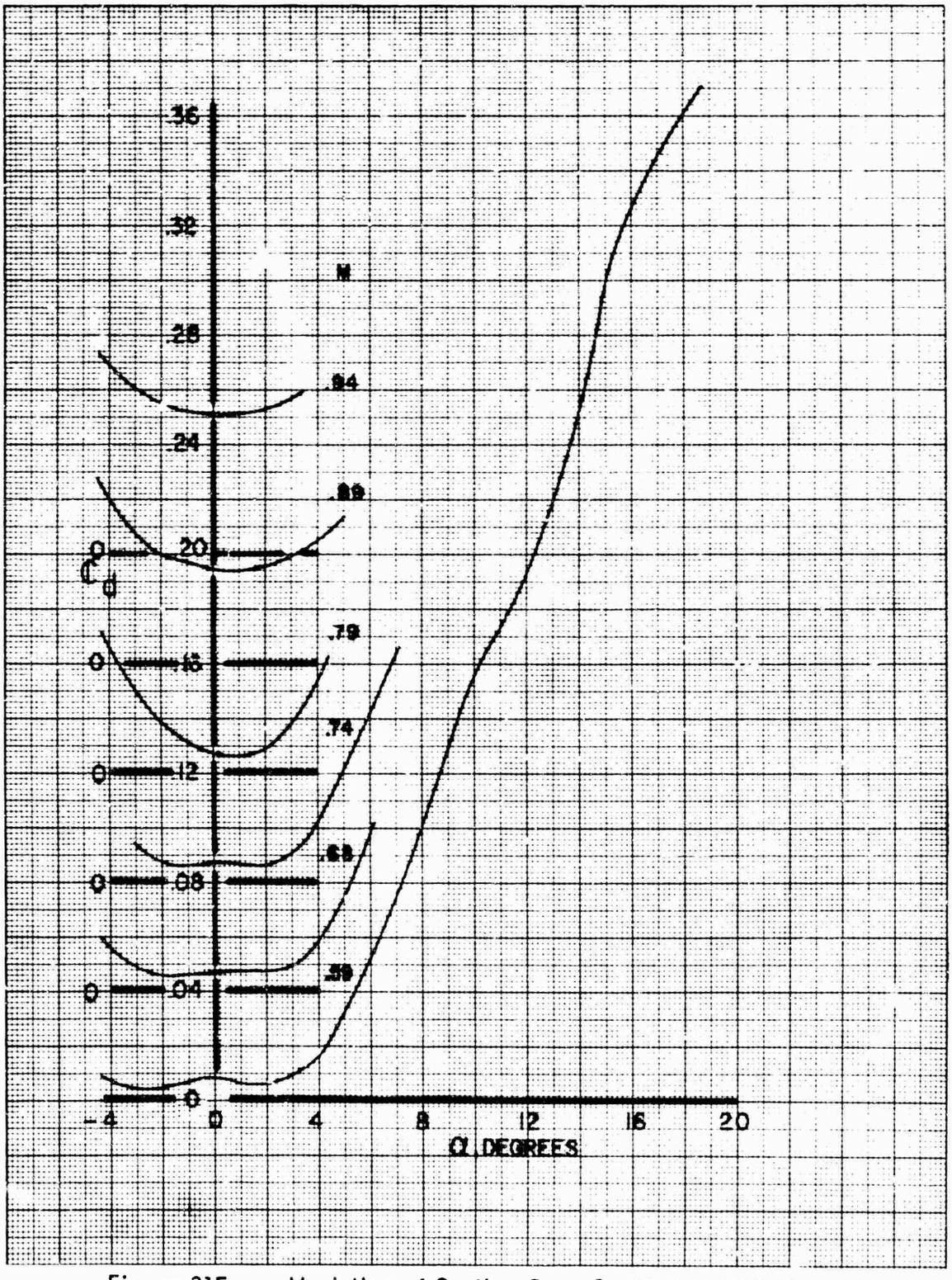


Figure 31E. Variation of Section Drag Coefficient With Angle of Attack at Constant Mach Number, NACA Section 63A009, $R = 8.0 \times 10^6$

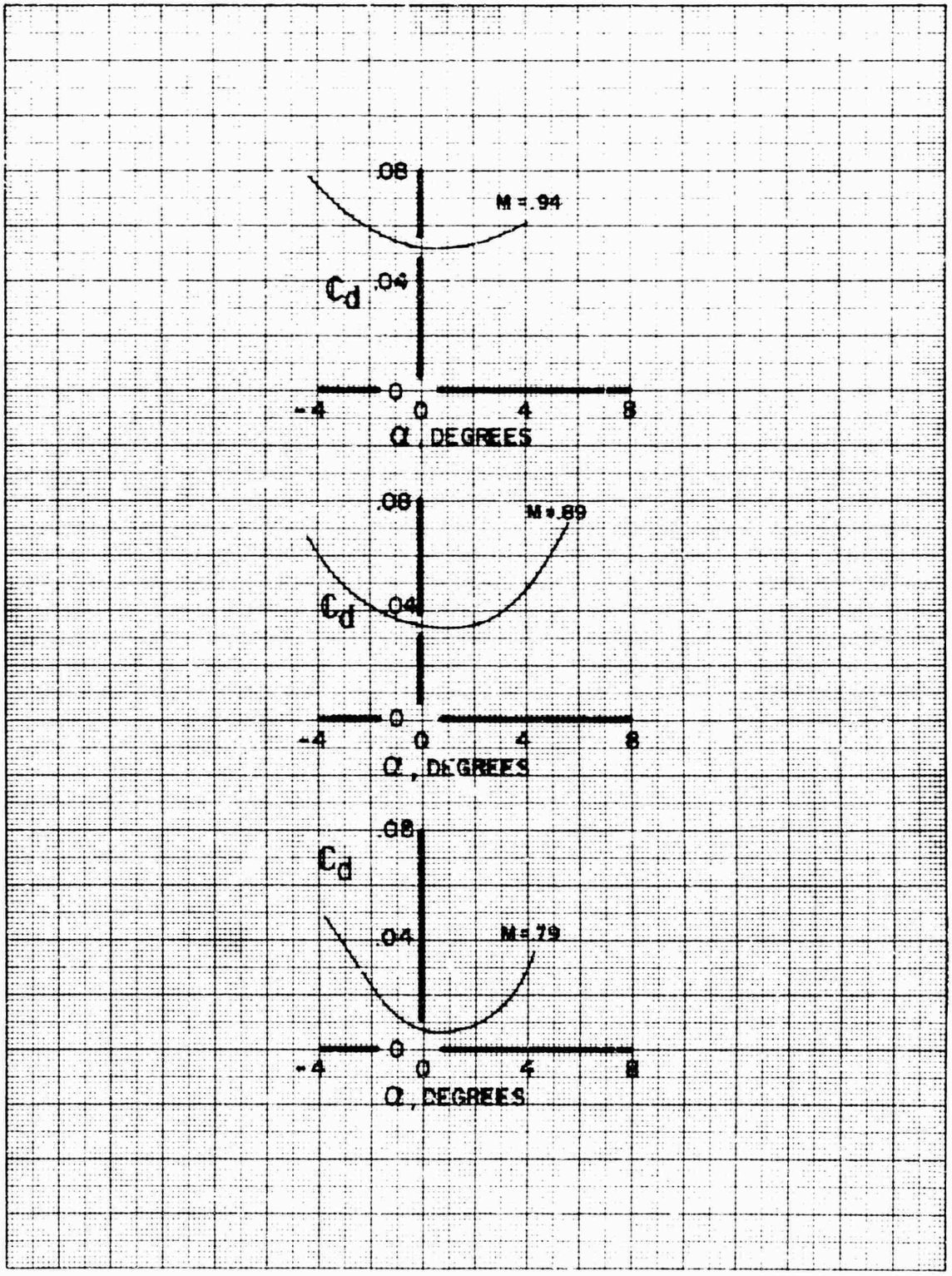


Figure 31F. Variation of Section Drag Coefficient With Angle of Attack at Constant Mach Number, NACA Section 63A009, $R = 9.5 \times 10^6$

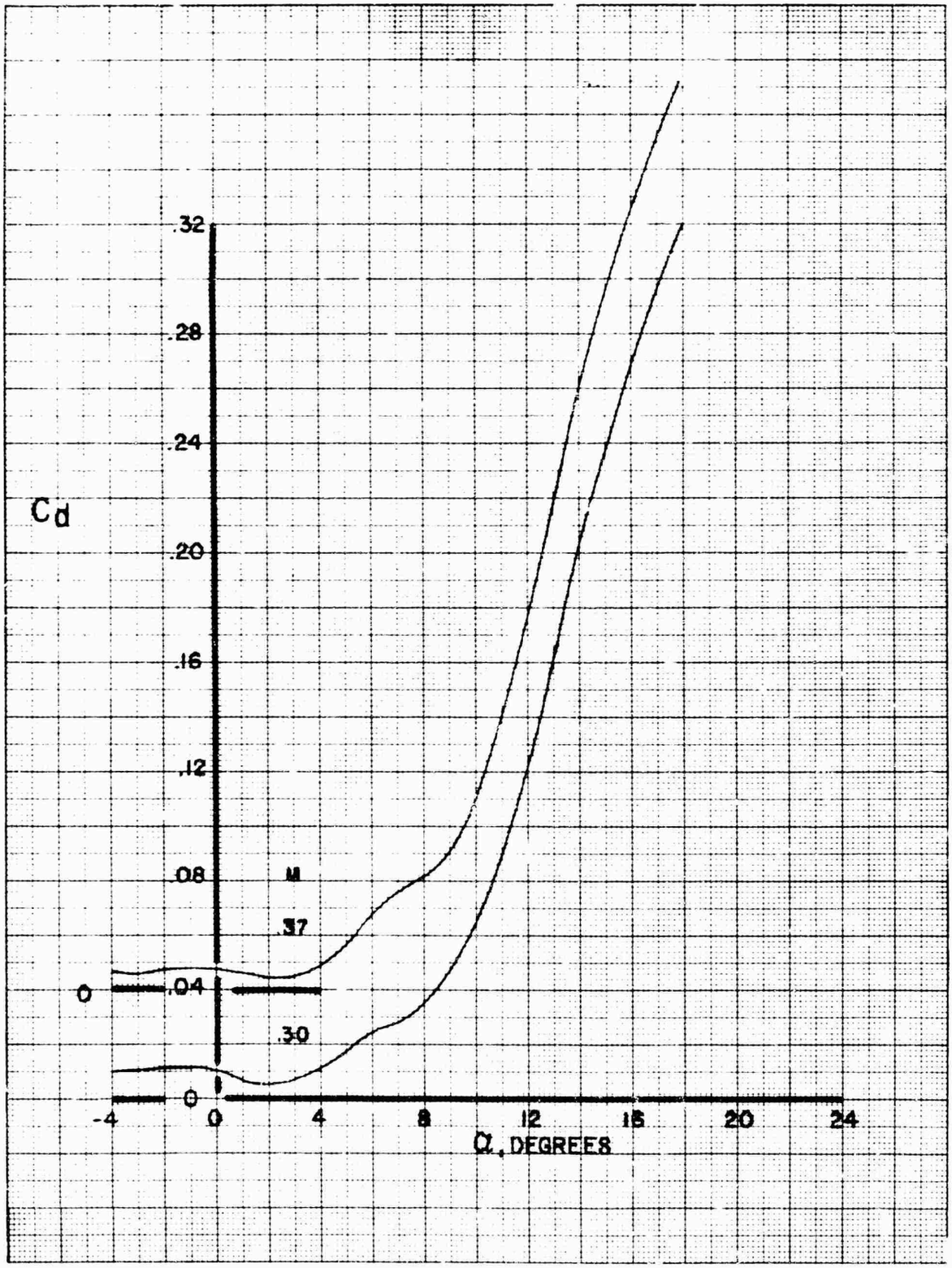


Figure 32A. Variation of Section Drag Coefficient With Angle of Attack at Constant Mach Number, NACA Section 63A012, $R = 2.0 \times 10^6$

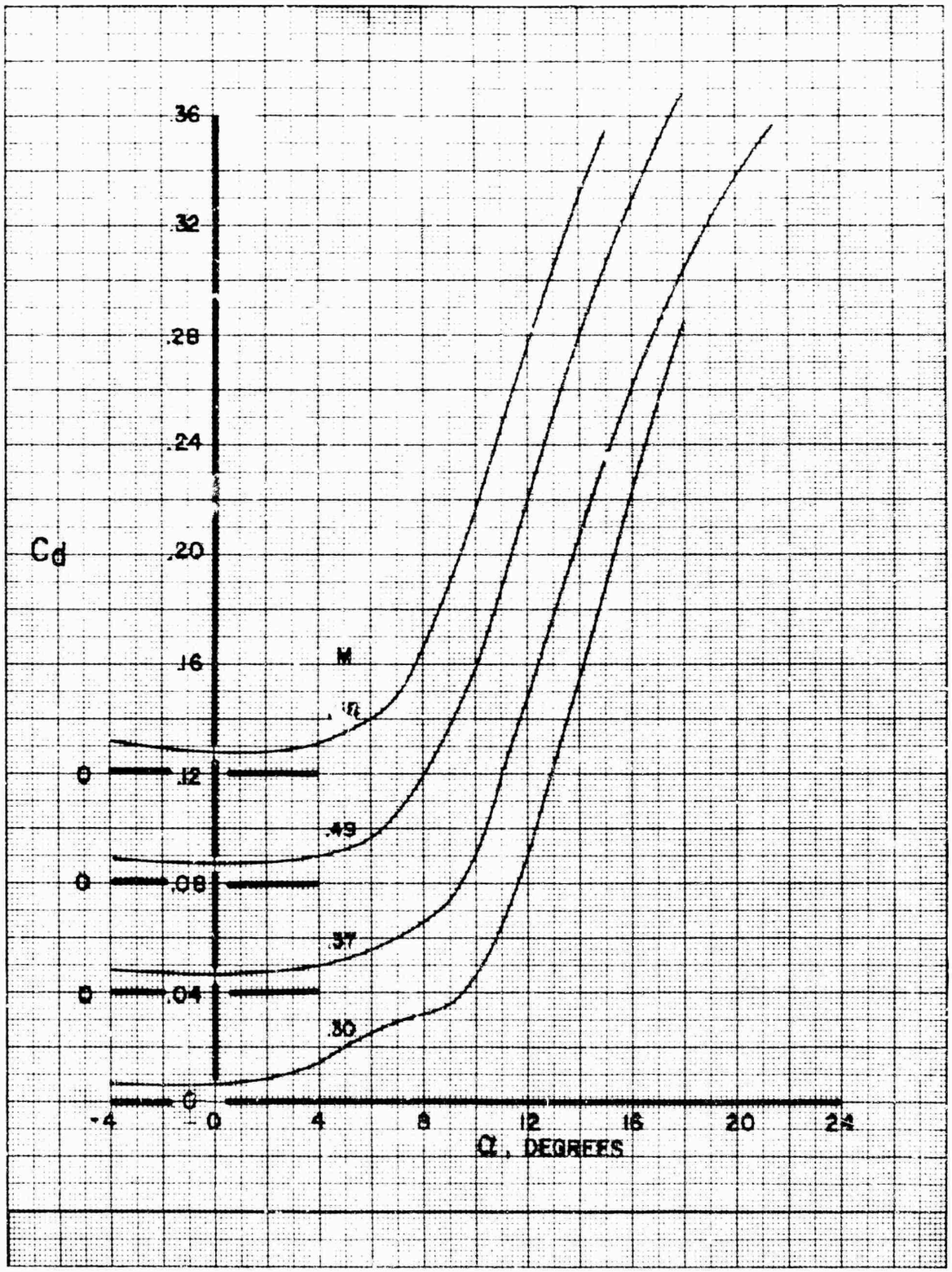


Figure 32B-1. Variation of Section Drag Coefficient With Angle of Attack at Constant Mach Number, NACA Section 63A012, $R = 3.5 \times 10^6$

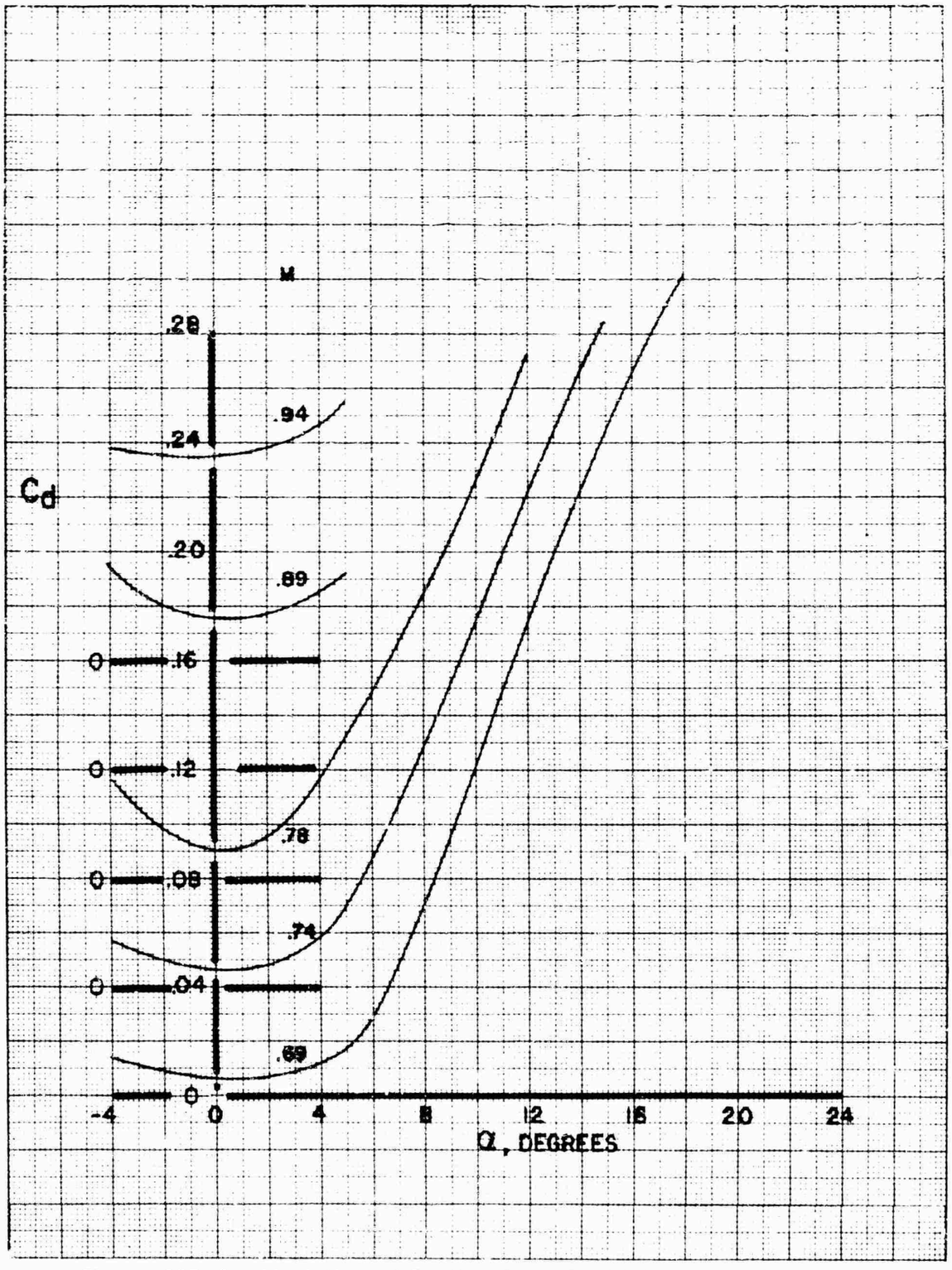


Figure 32B-2. Variation of Section Drag Coefficient With Angle of Attack at Constant Mach Number, NACA Section 63A012, $R = 3.5 \times 10^6$

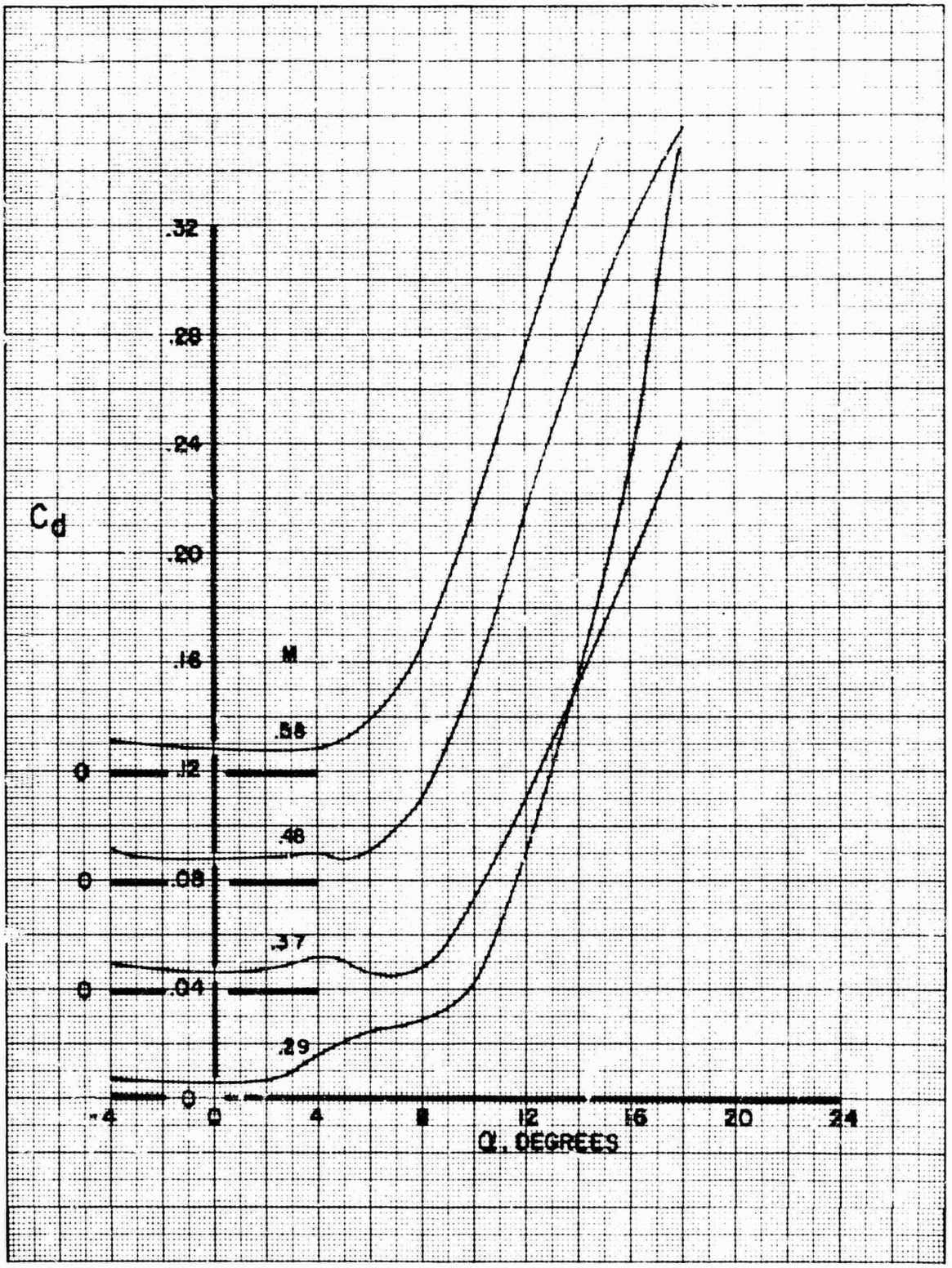


Figure 32C-1. Variation of Section Drag Coefficient With Angle of Attack at Constant Mach Number, NACA Section 63A012, $R = 5.0 \times 10^6$

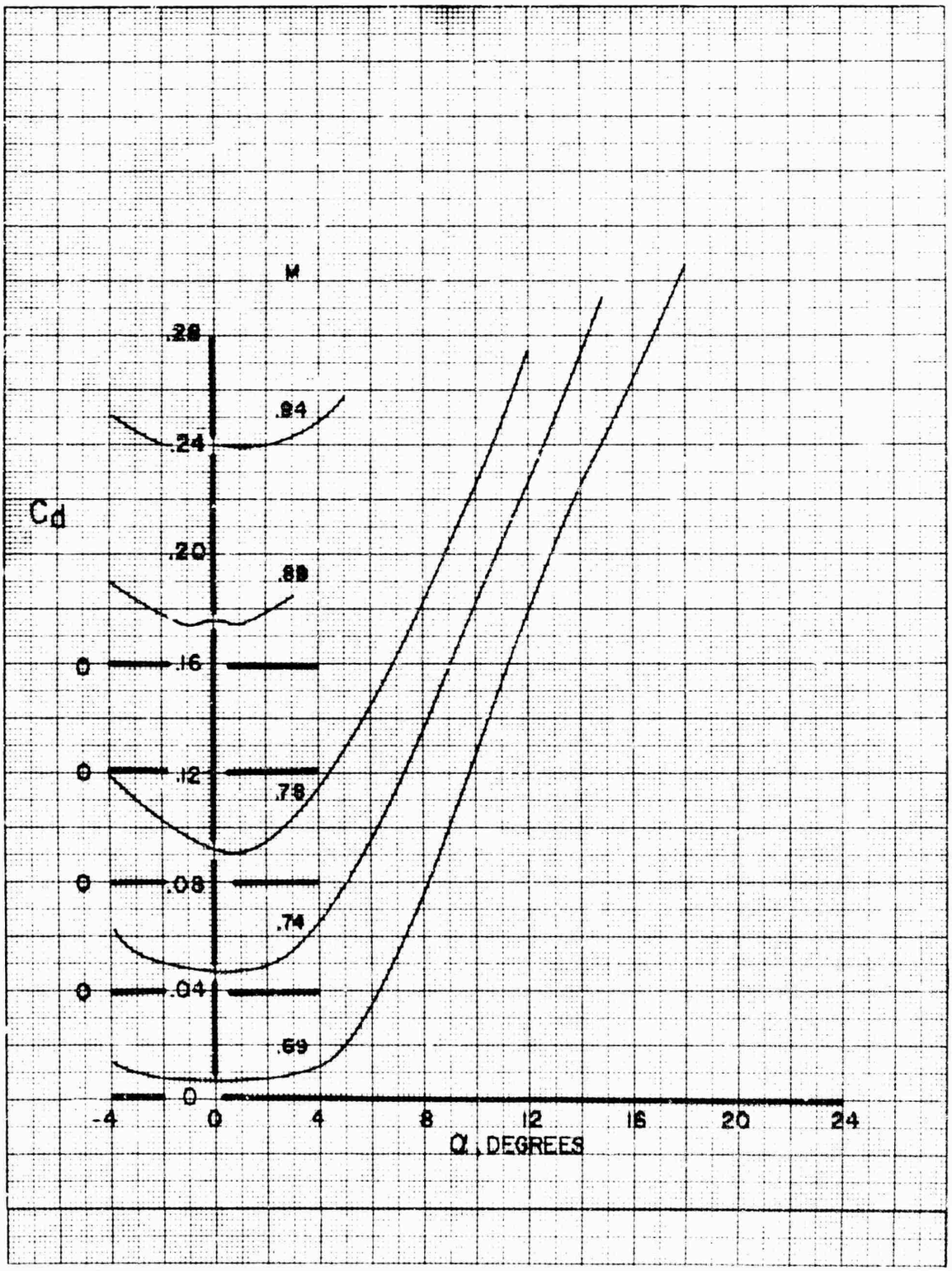


Figure 32C-2. Variation of Section Drag Coefficient With Angle of Attack at Constant Mach Number, NACA Section 63A012, $R = 5.0 \times 10^6$

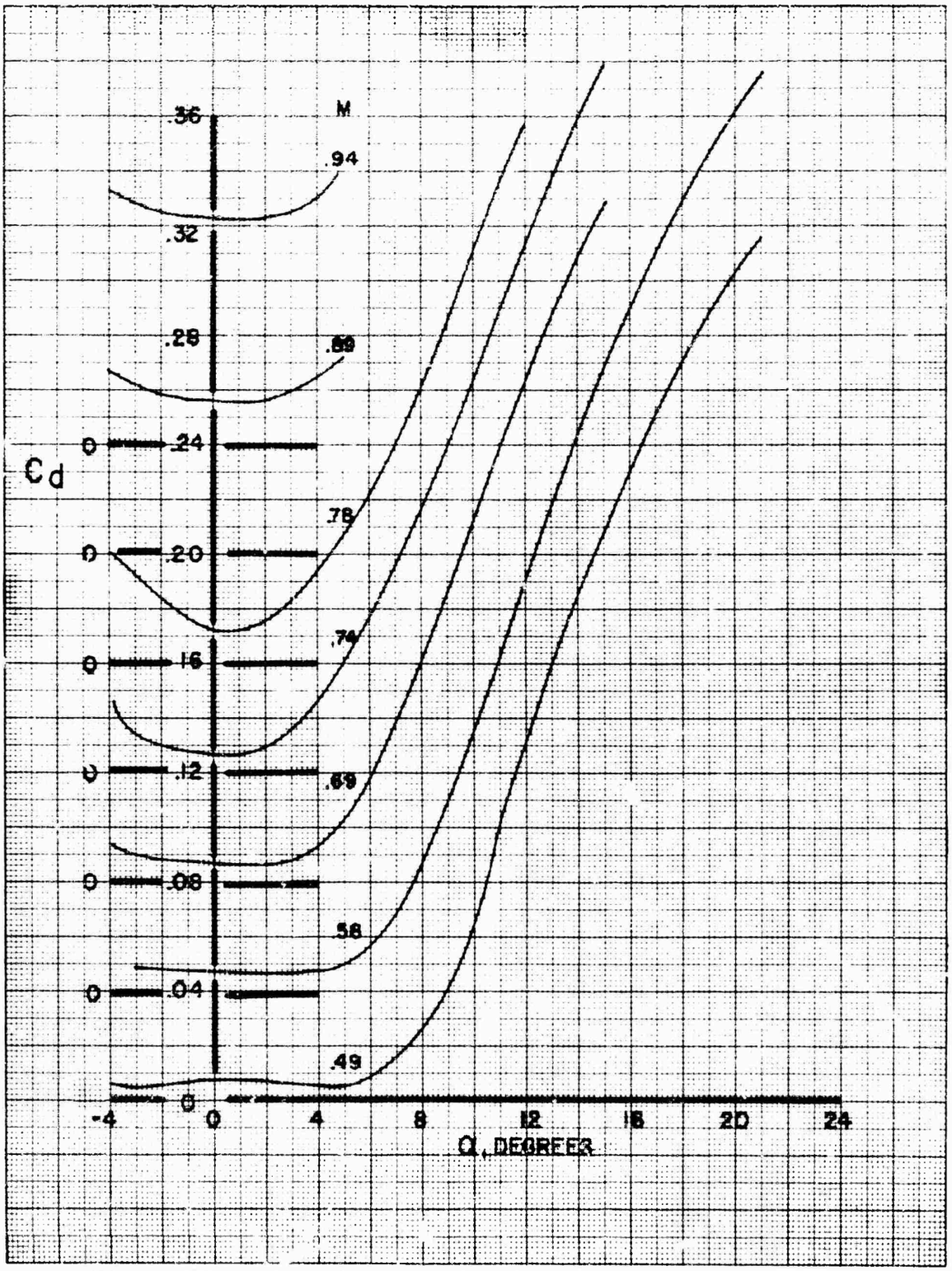


Figure 32D. Variation of Section Drag Coefficient With Angle of Attack at Constant Mach Number, NACA Section 63A012, $R = 6.5 \times 10^6$

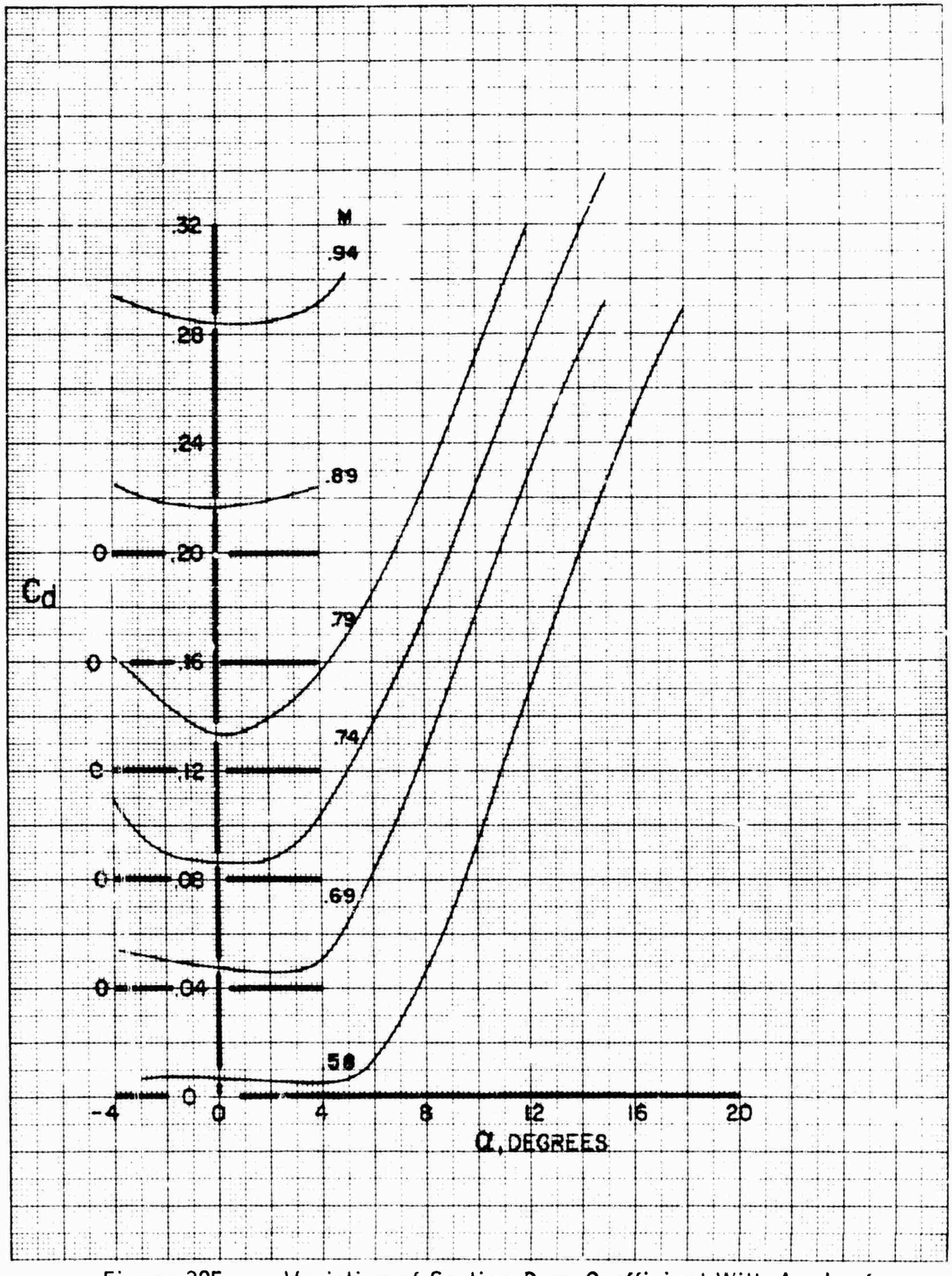


Figure 32E. Variation of Section Drag Coefficient With Angle of Attack at Constant Mach Number, NACA Section 63A012, $R = 8.0 \times 10^6$

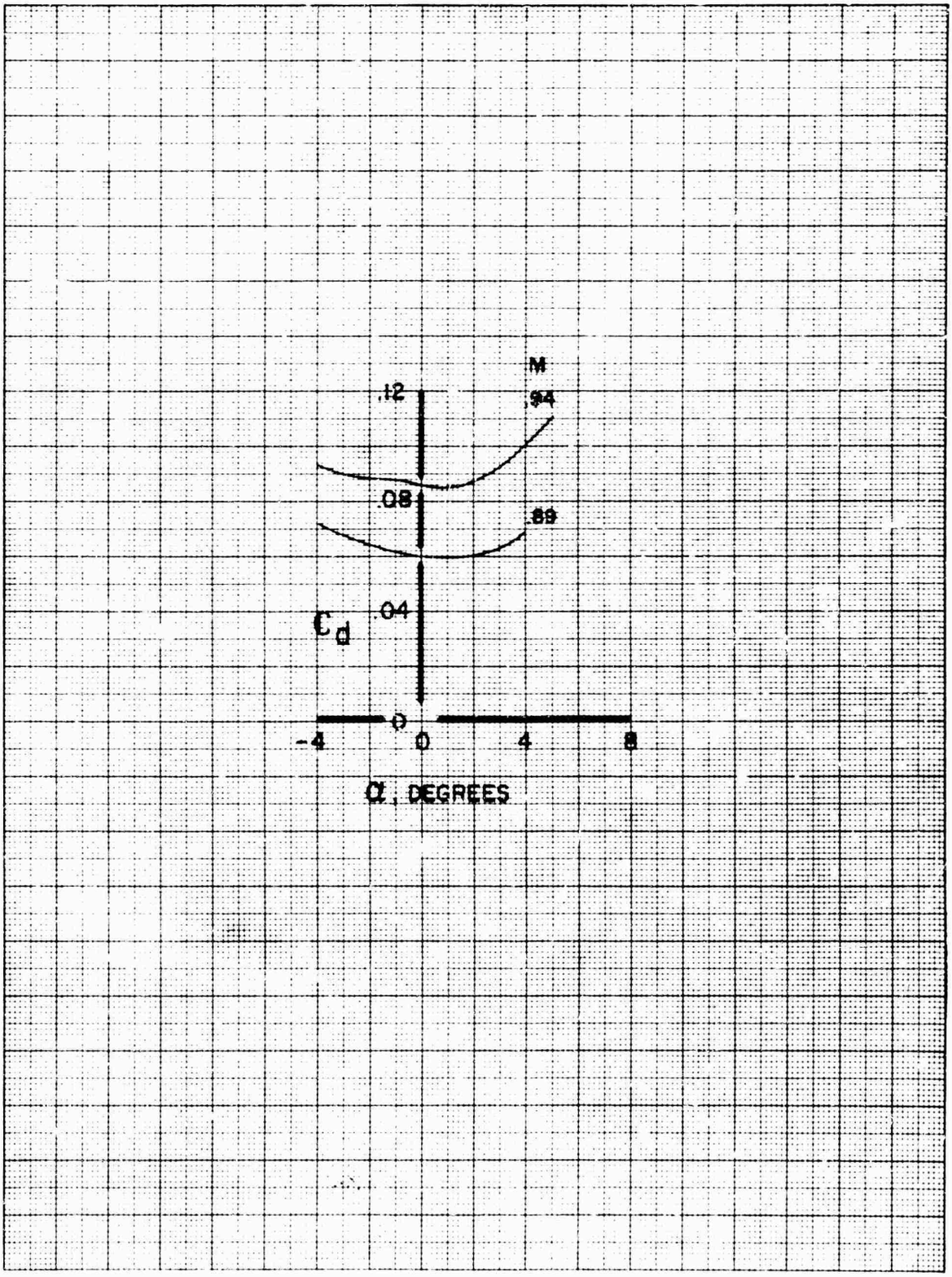


Figure 32F. Variation of Section Drag Coefficient With Angle of Attack at Constant Mach Number, NACA Section 63A012 - $R = 9.5 \times 10^6$

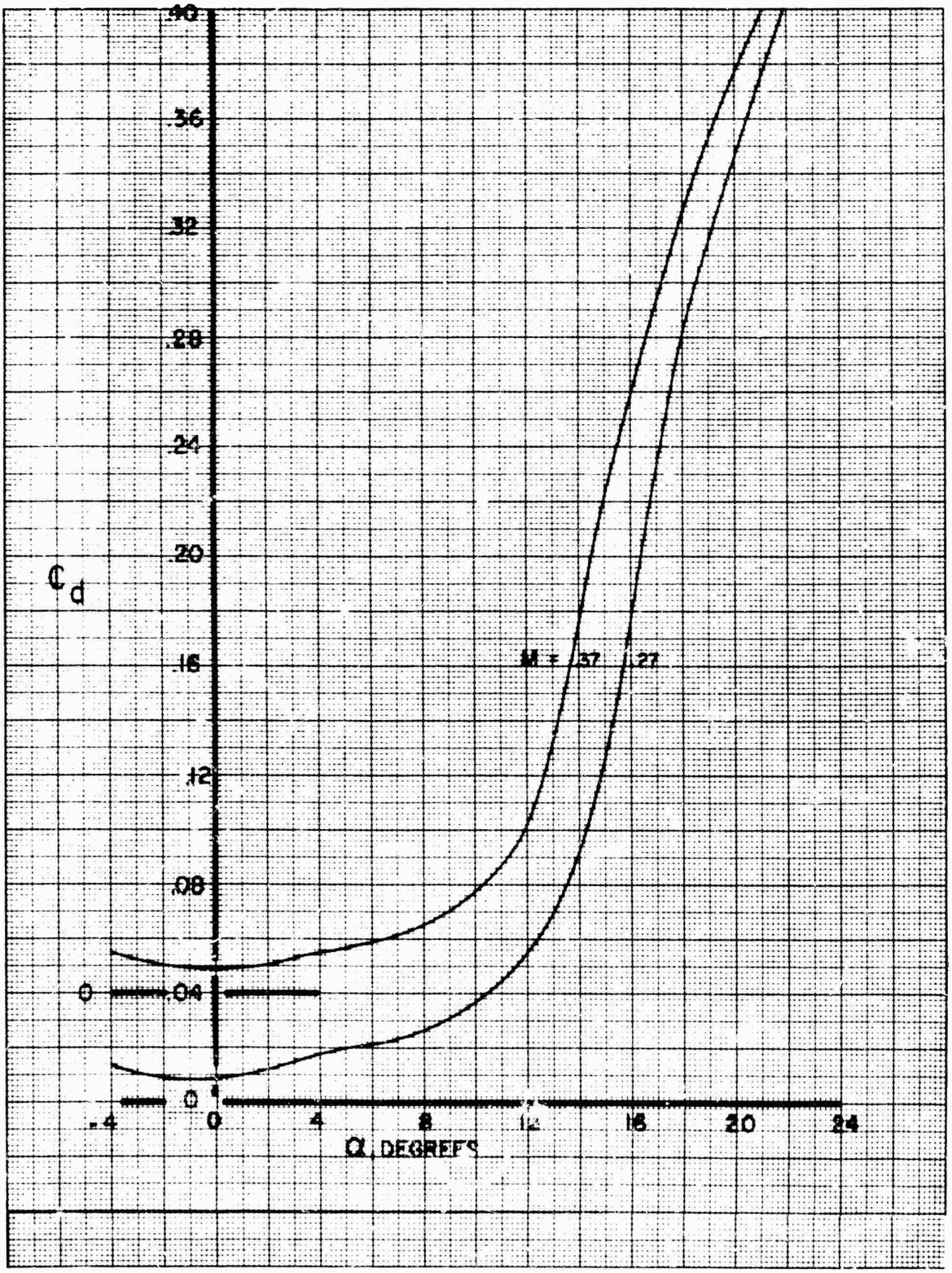


Figure 33A. Variation of Section Drag Coefficient With Angle of Attack at Constant Mach Number, NACA Section 63A015, $R = 2.0 \times 10^6$

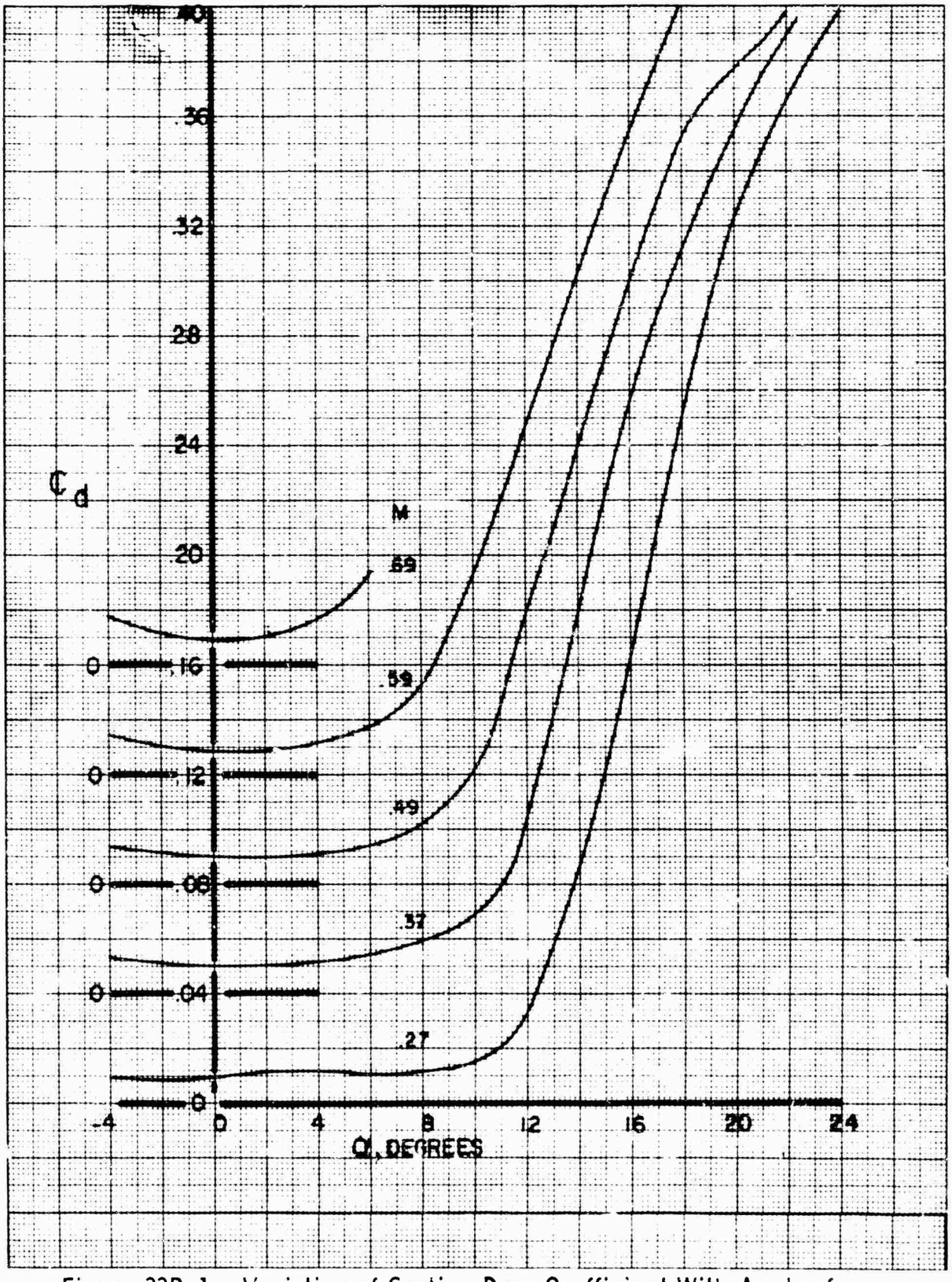


Figure 33B-1. Variation of Section Drag Coefficient With Angle of Attack at Constant Mach Number, NACA Section 63A015, $R = 3.5 \times 10^6$

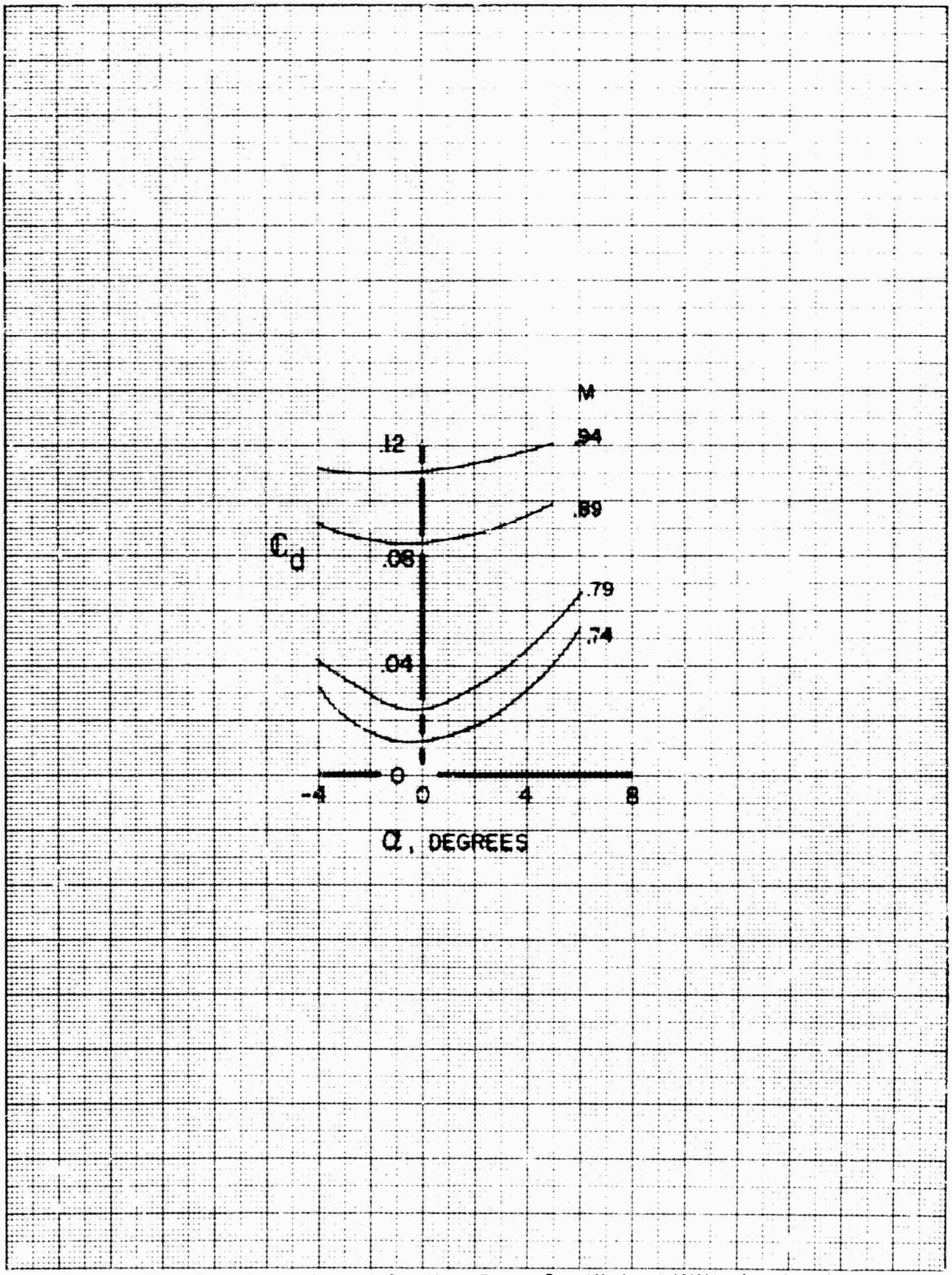


Figure 33B-2. Variation of Section Drag Coefficient With Angle of Attack at Constant Mach Number, NACA Section 63A015, $R = 3.5 \times 10^6$

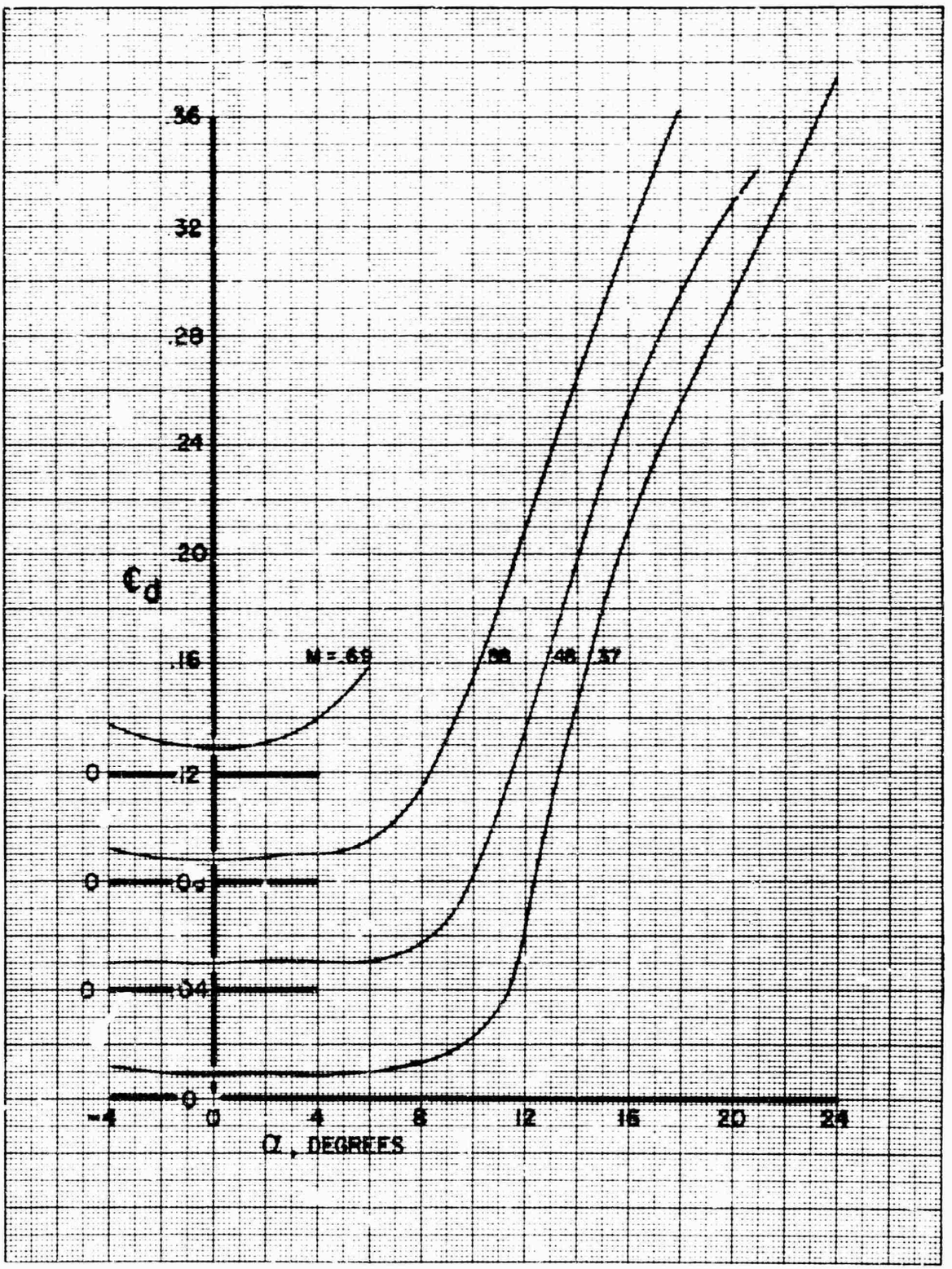


Figure 33C-1. Variation of Section Drag Coefficient With Angle of Attack at Constant Mach Number, NACA Section 63A015 - $R = 5.0 \times 10^6$

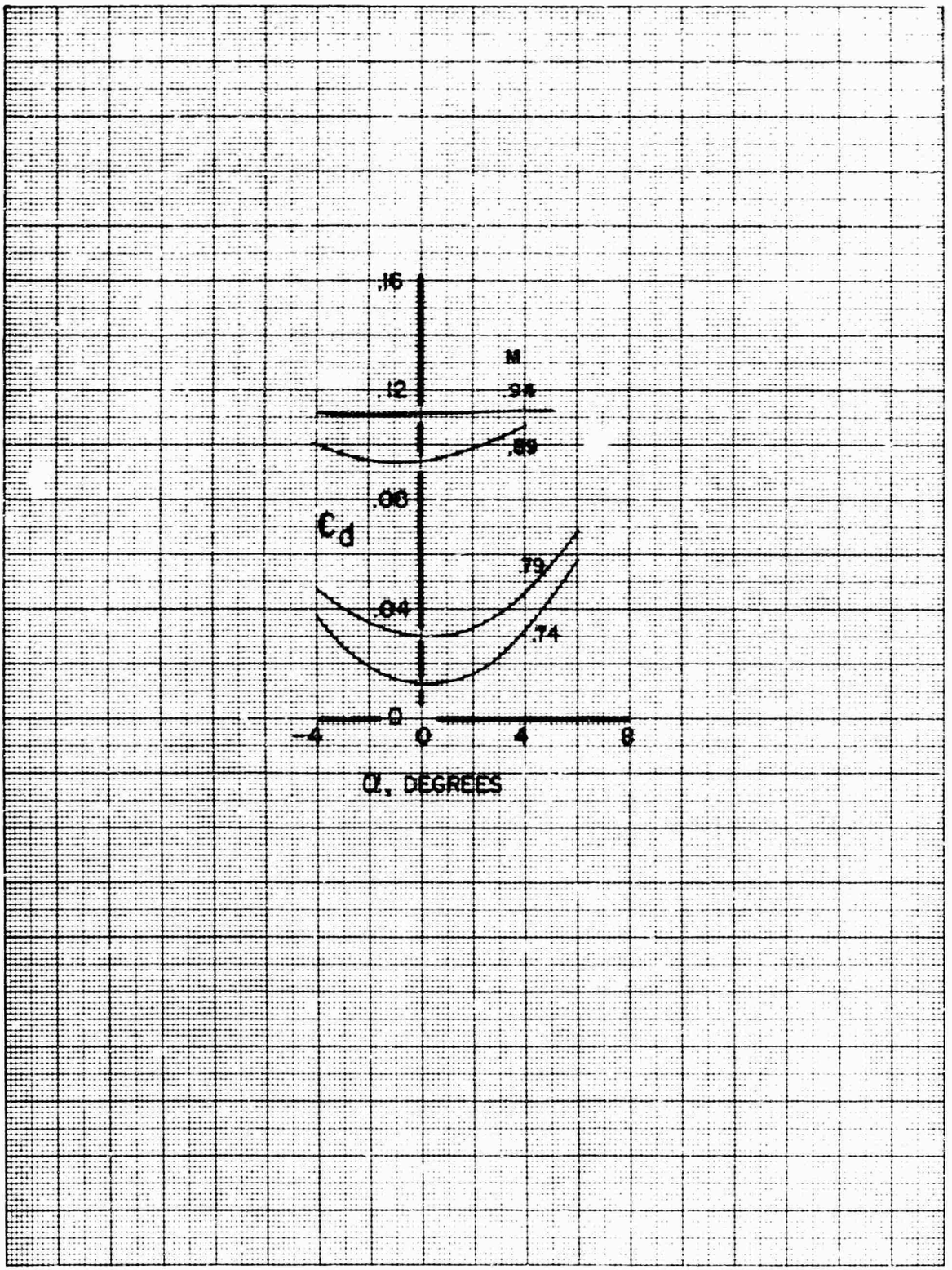


Figure 33C-2. Variation of Section Drag Coefficient With Angle of Attack at Constant Mach Number, NACA Section 63A015 - $R = 5.0 \times 10^6$

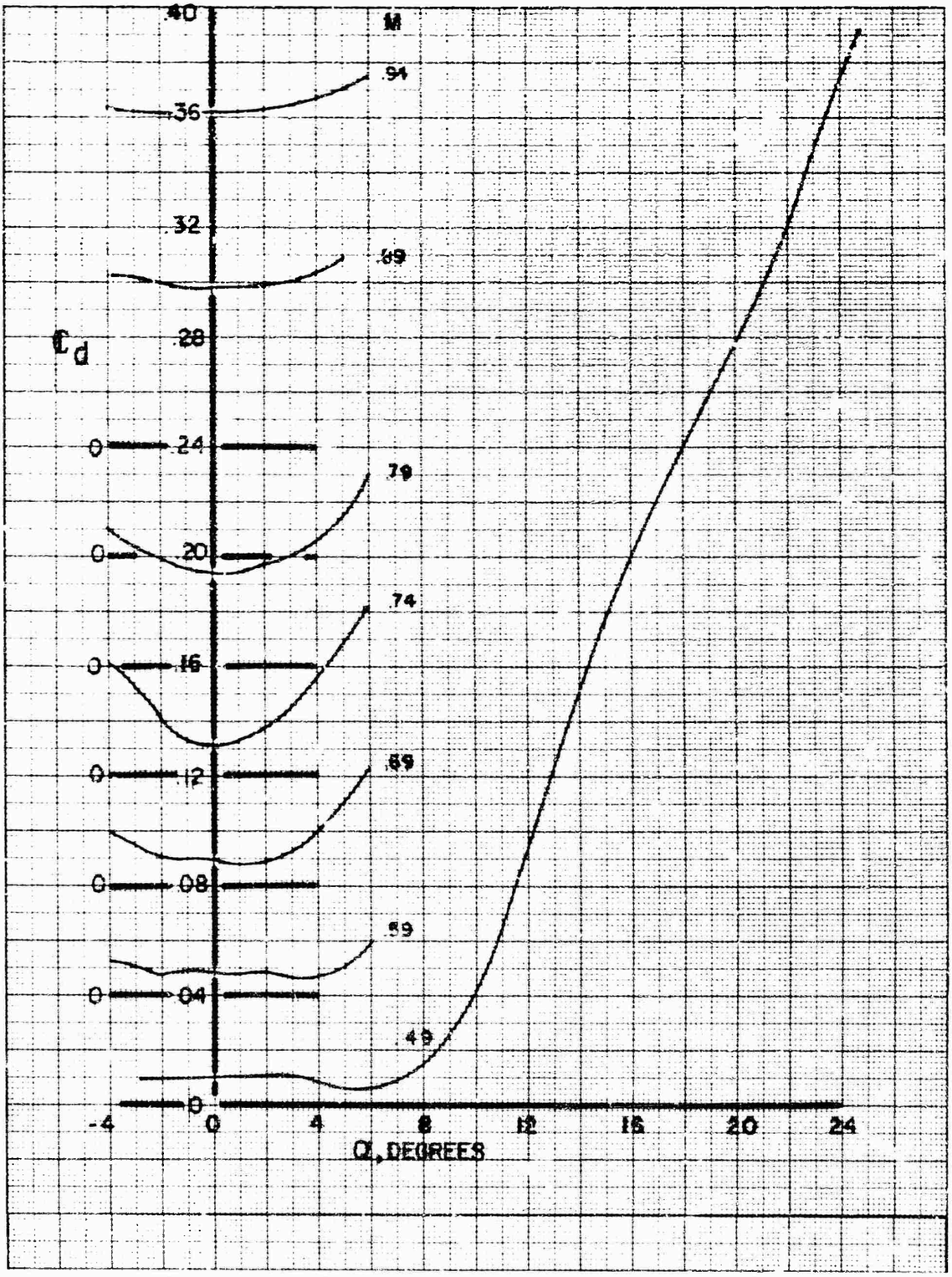


Figure 33D. Variation of Section Drag Coefficient With Angle of Attack at Constant Mach Number, NACA Section 63A015, $R = 6.5 \times 10^6$

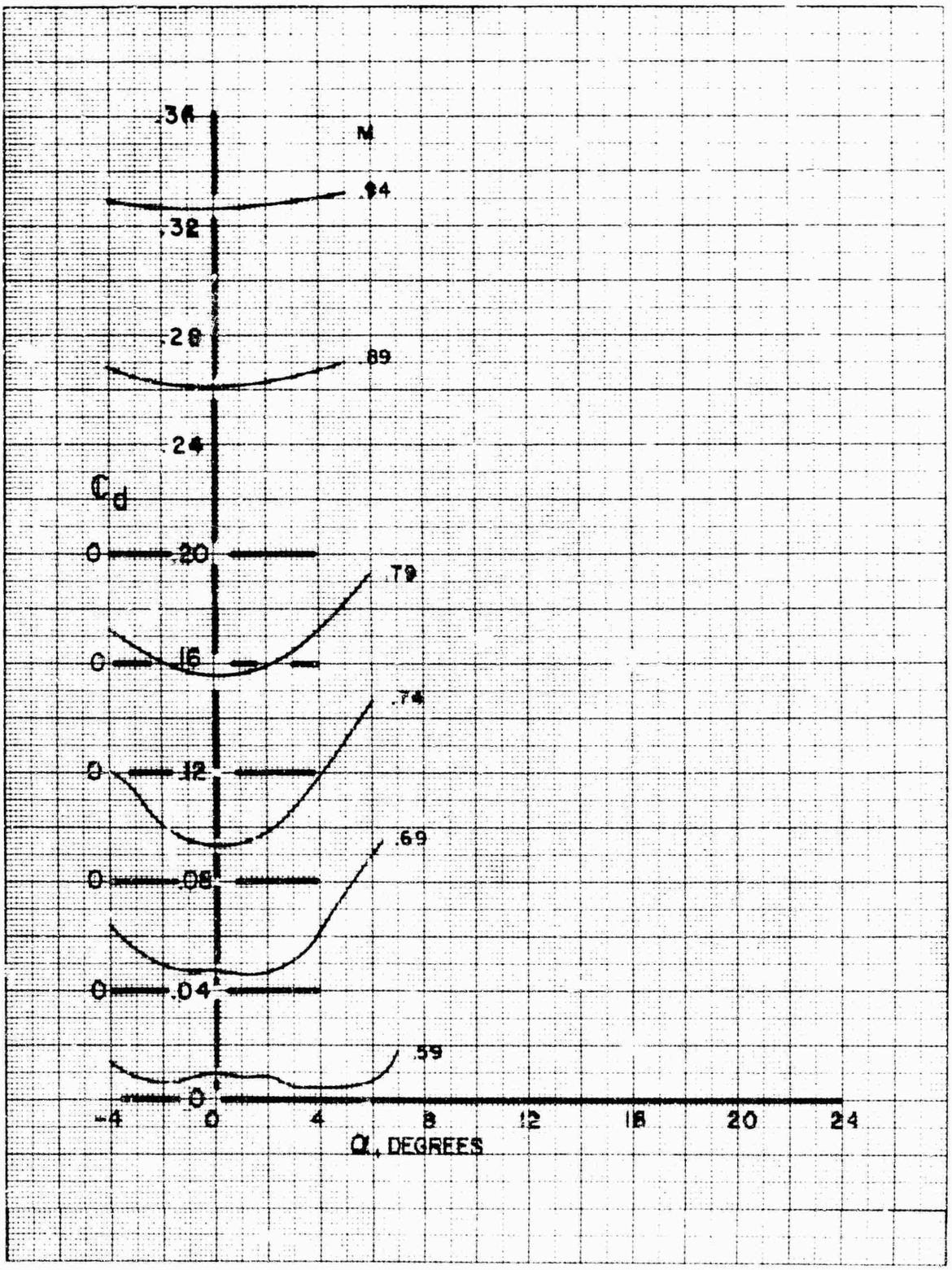


Figure 33E. Variation of Section Drag Coefficient With Angle of Attack at Constant Mach Number, NACA Section 63A015, $R = 8.0 \times 10^6$

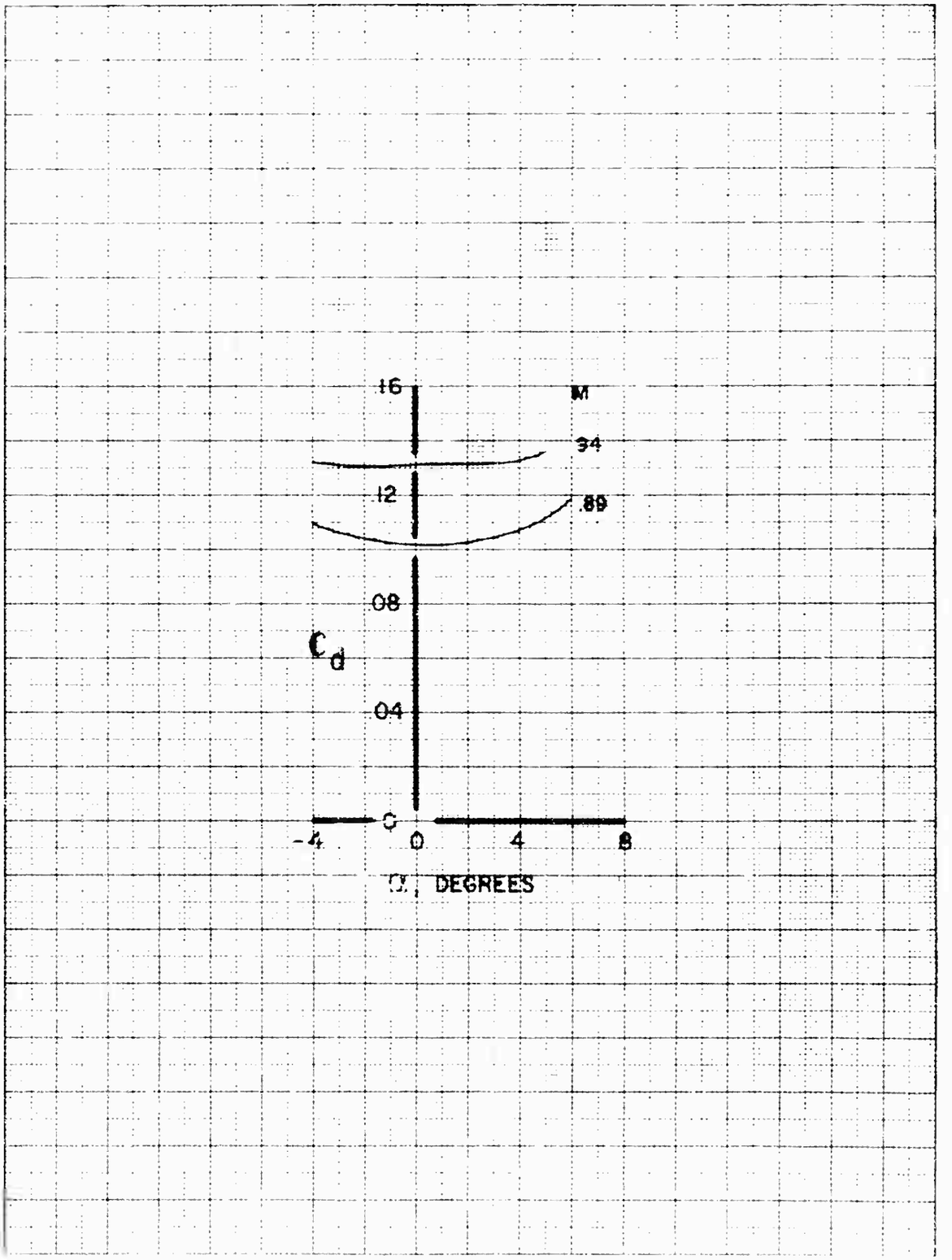


Figure 33F. Variation of Drag Coefficient With Angle of Attack at Constant Mach Number, NACA Section 63A015 - $R = 9.5 \times 10^6$

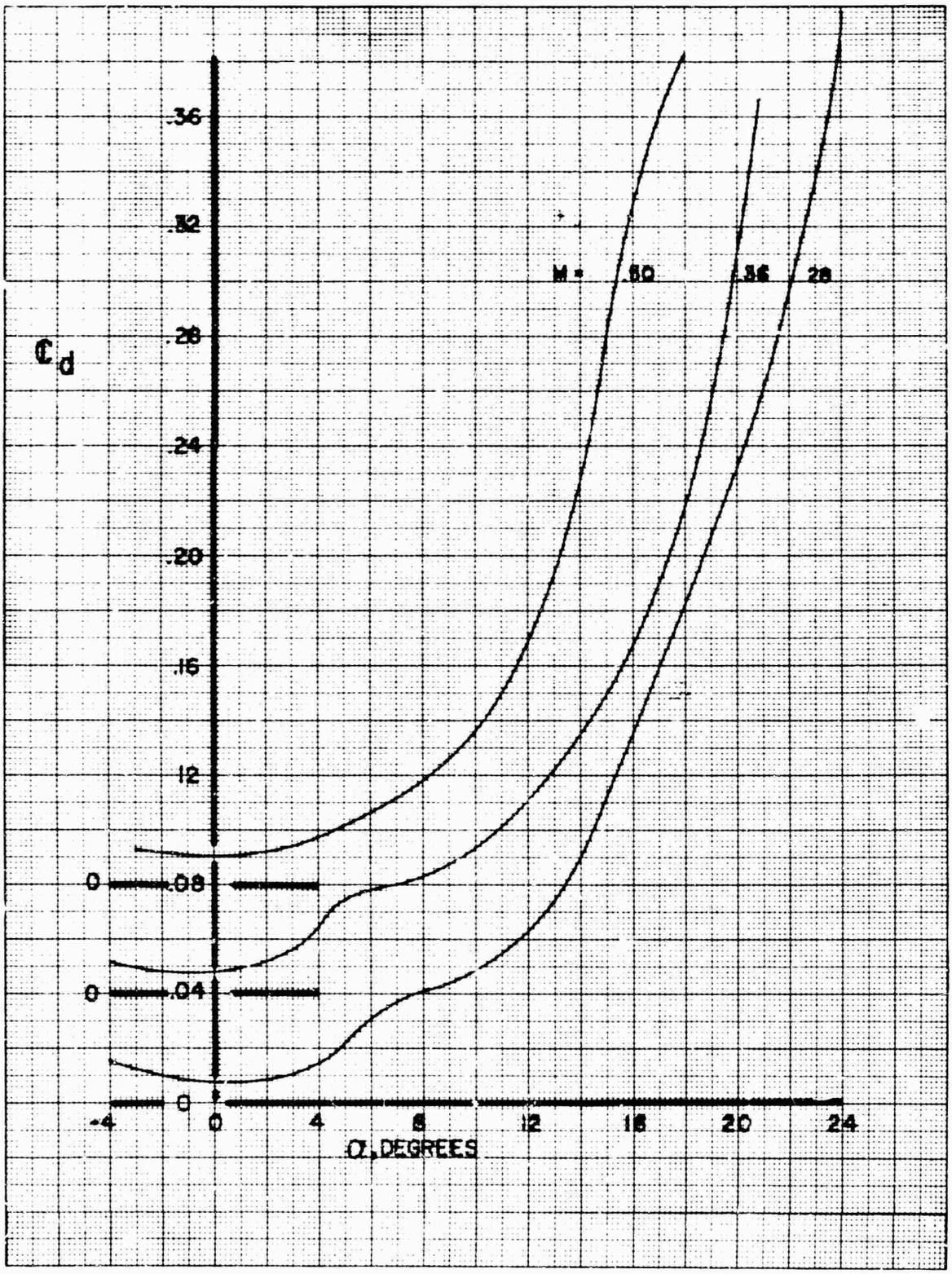


Figure 34A. Variation of Section Drag Coefficient With Angle of Attack at Constant Mach Number, NACA Section 63A018, $R = 2.0 \times 10^6$

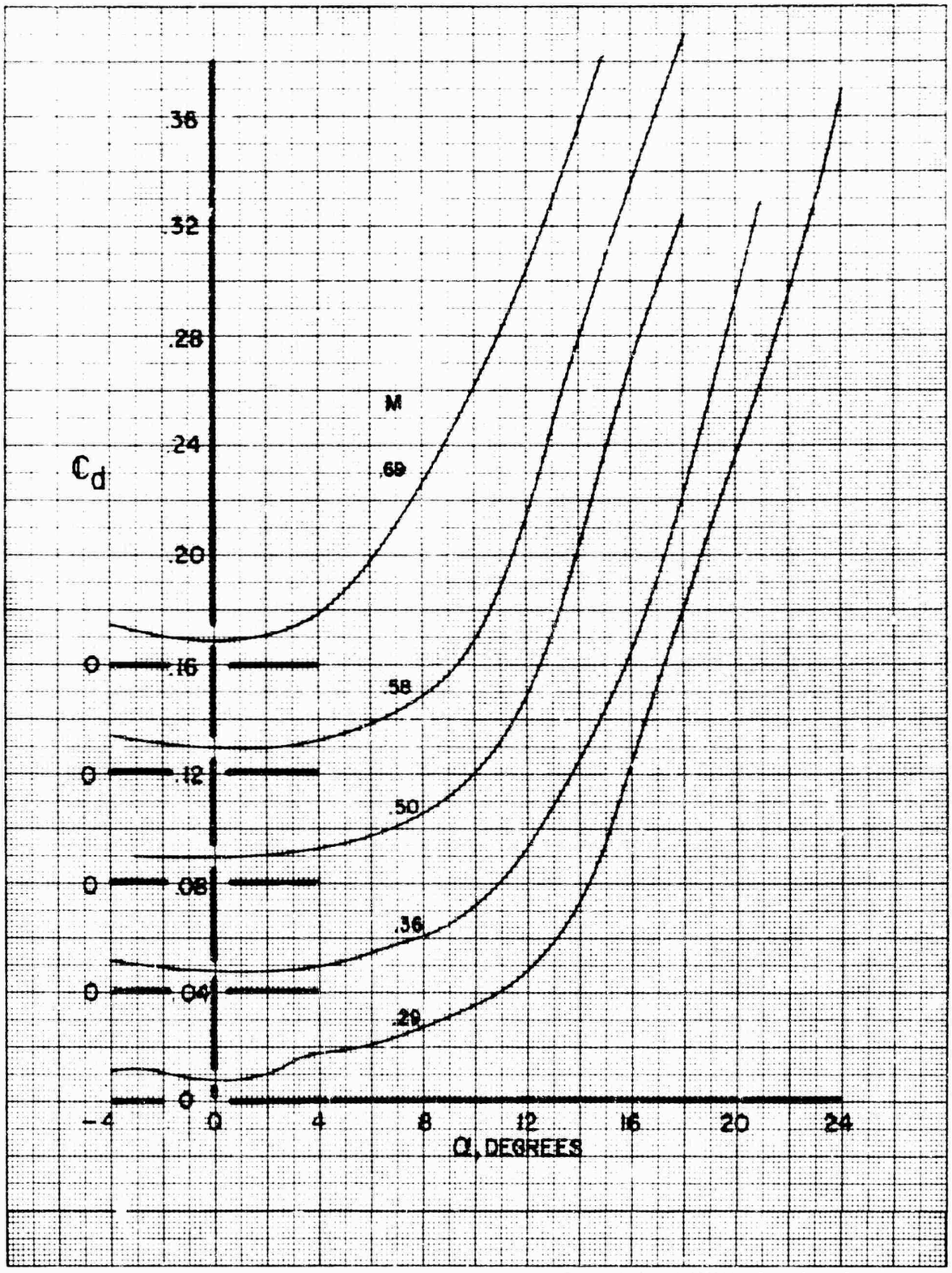


Figure 34B-1. Variation of Section Drag Coefficient With Angle of Attack at Constant Mach Number, NACA Section 63A018, $R = 3.5 \times 10^6$

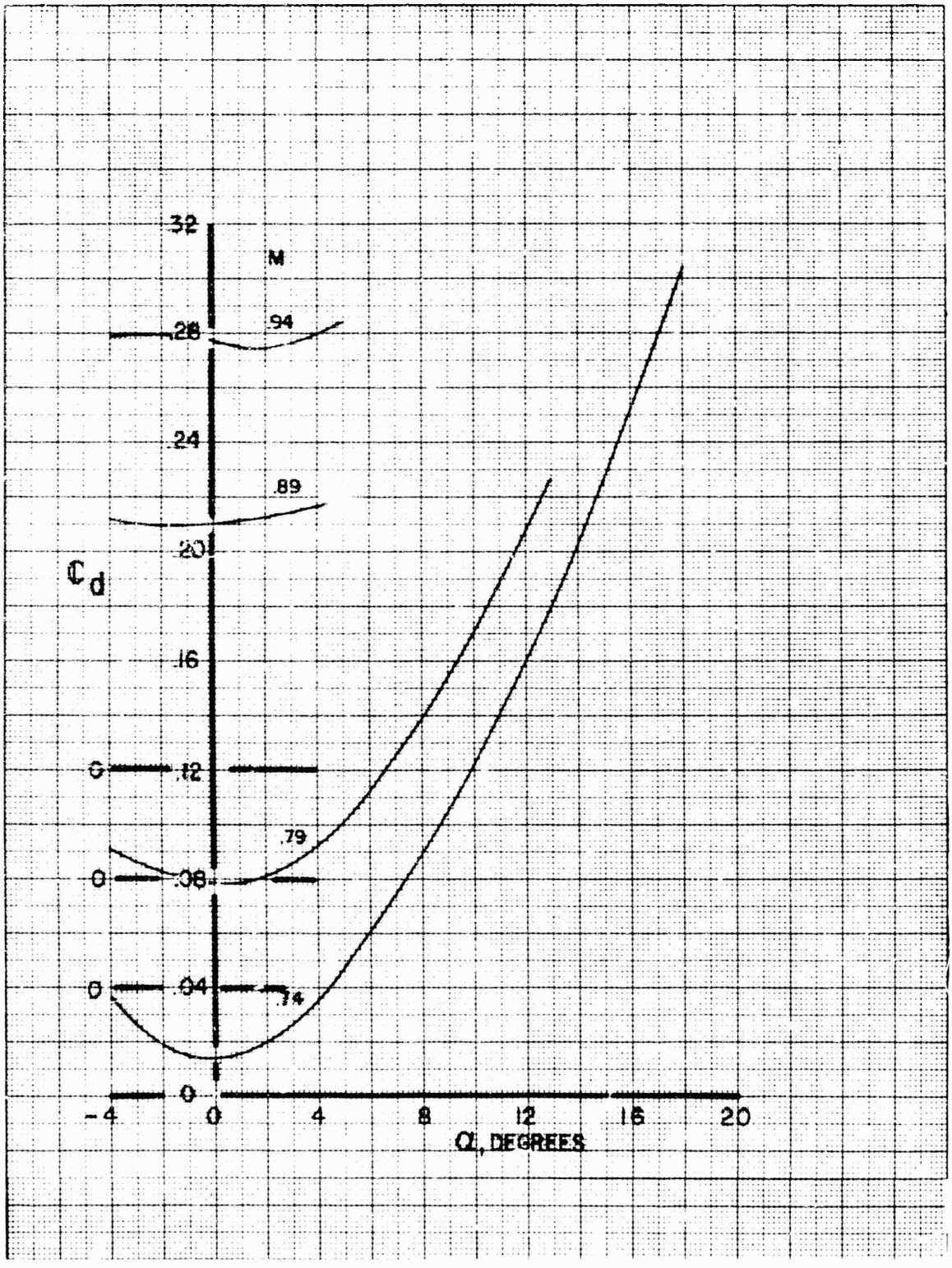


Figure 34B-2. Variation of Section Drag Coefficient With Angle of Attack at Constant Mach Number, NACA Section 63A018, $R = 3.5 \times 10^6$

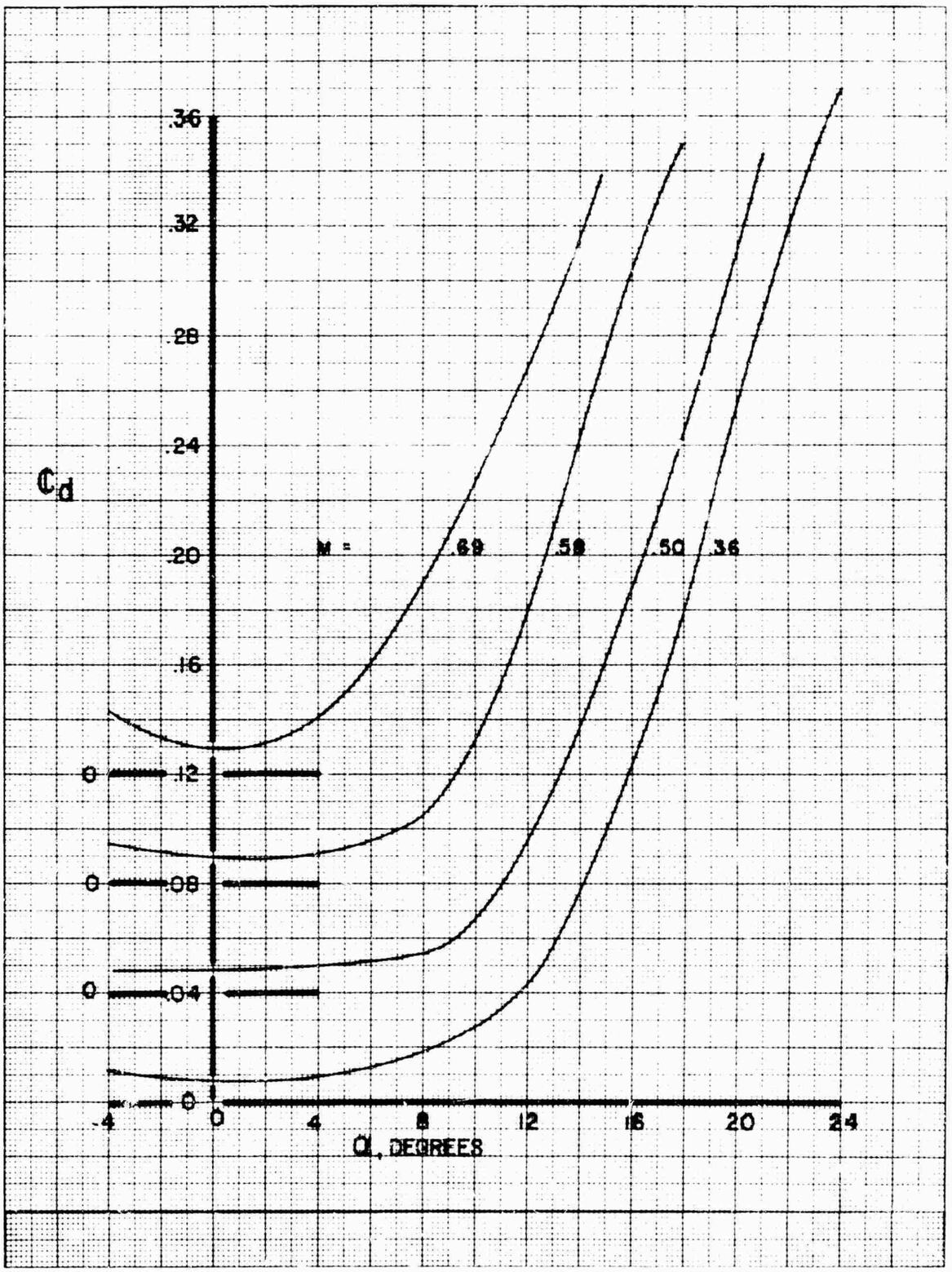


Figure 34C-1. Variation of Section Drag Coefficient With Angle of Attack at Constant Mach Number, NACA Section 63A018, $R = 5.0 \times 10^6$

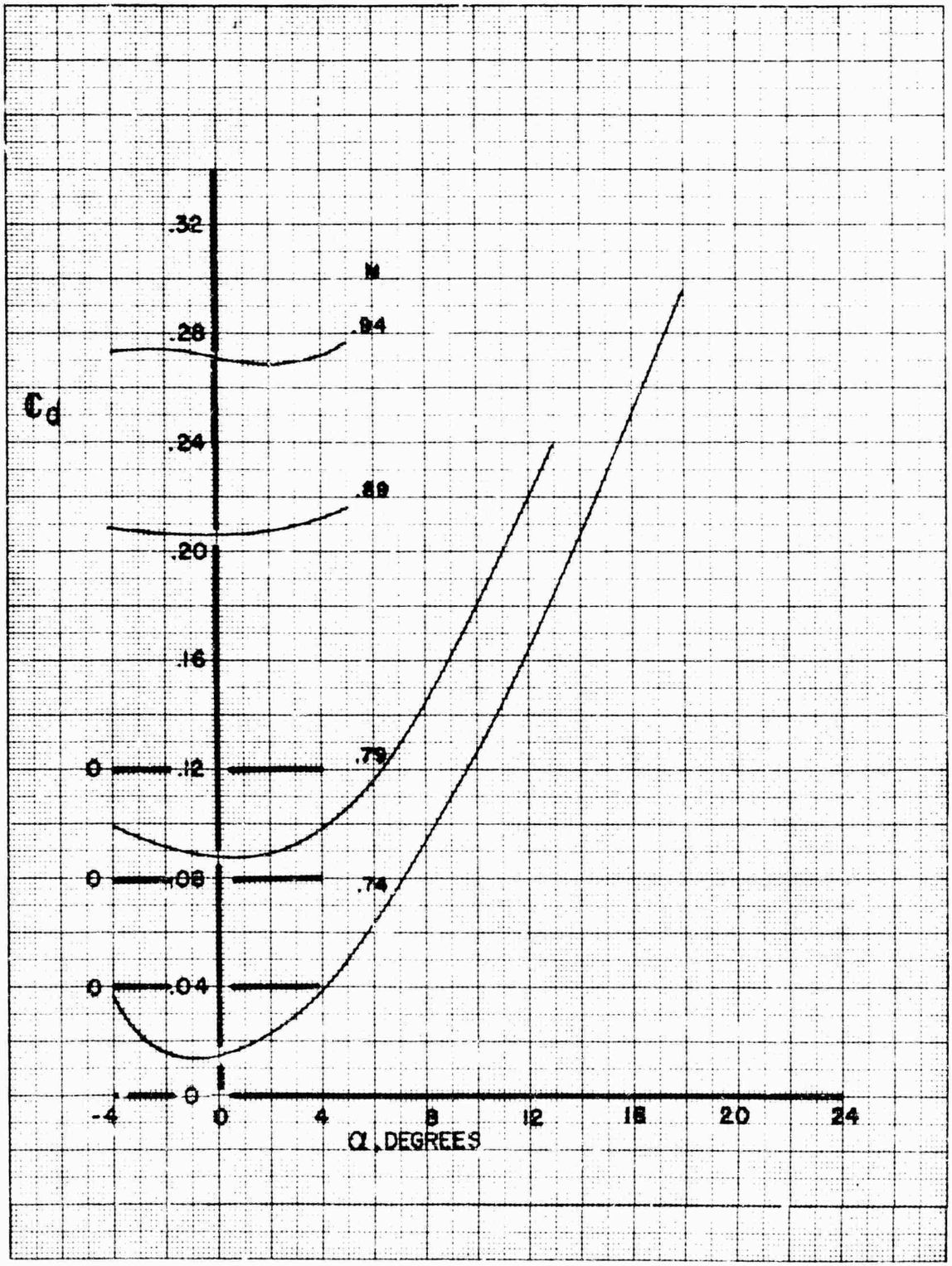


Figure 34C-2. Variation of Section Drag Coefficient With Angle of Attack at Constant Mach Number, NACA Section 63A018, $R = 5.0 \times 10^6$

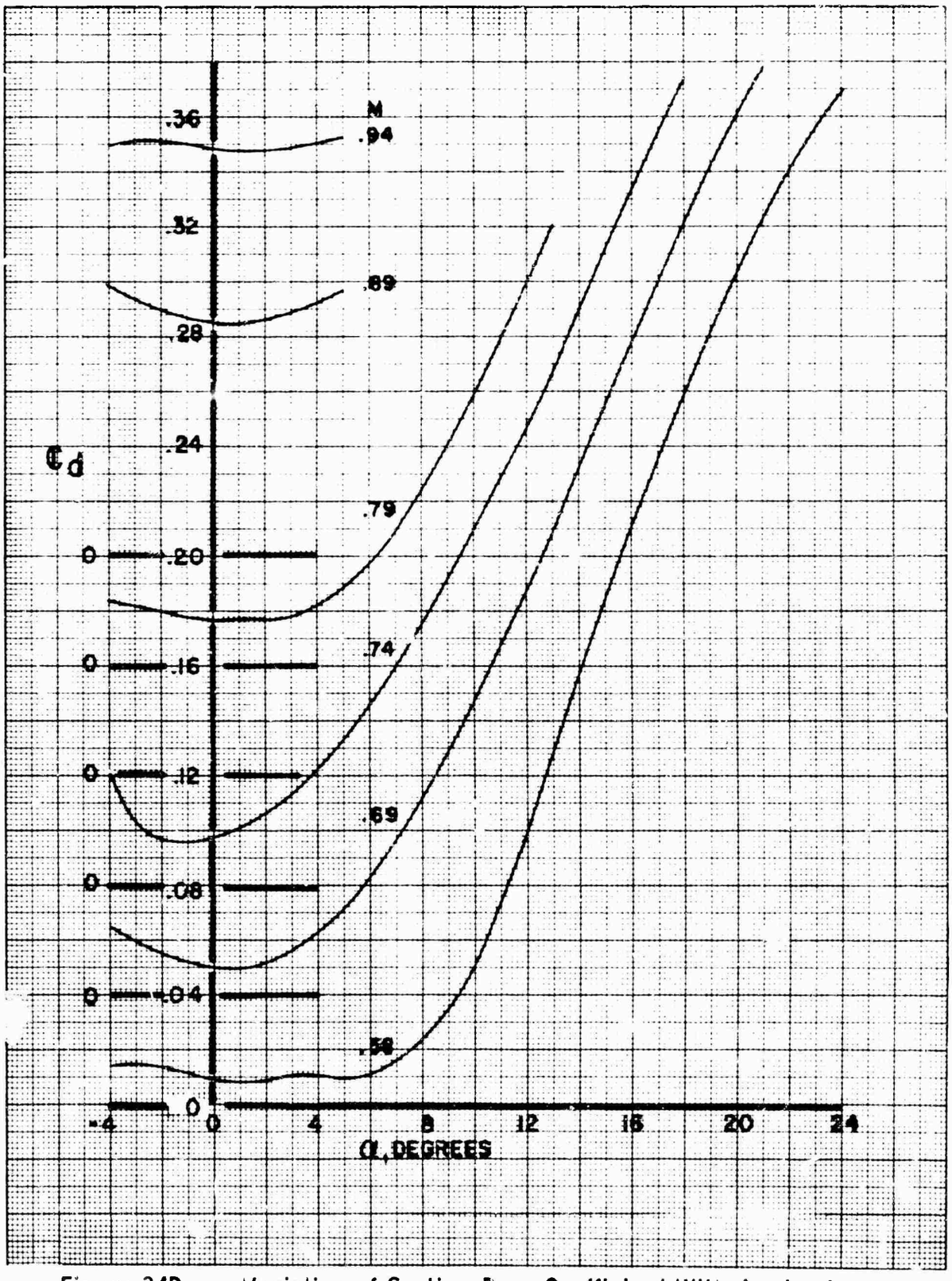


Figure 34D. Variation of Section Drag Coefficient With Angle of Attack at Constant Mach Number, NACA Section 63A018, $R = 6.5 \times 10^6$

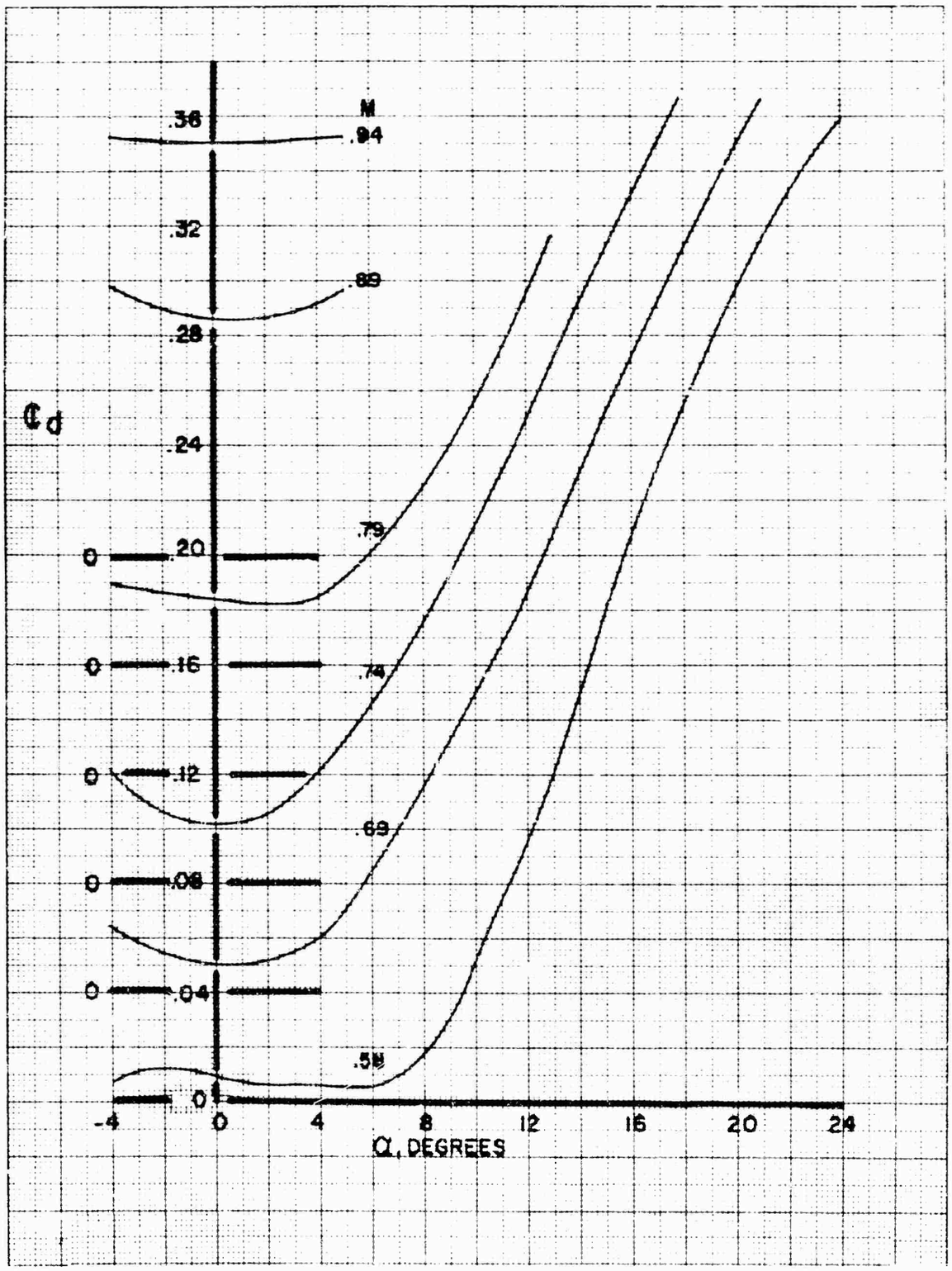


Figure 34E. Variation of Section Drag Coefficient With Angle of Attack at Constant Mach Number, NACA Section 63A018, $R = 8.0 \times 10^6$

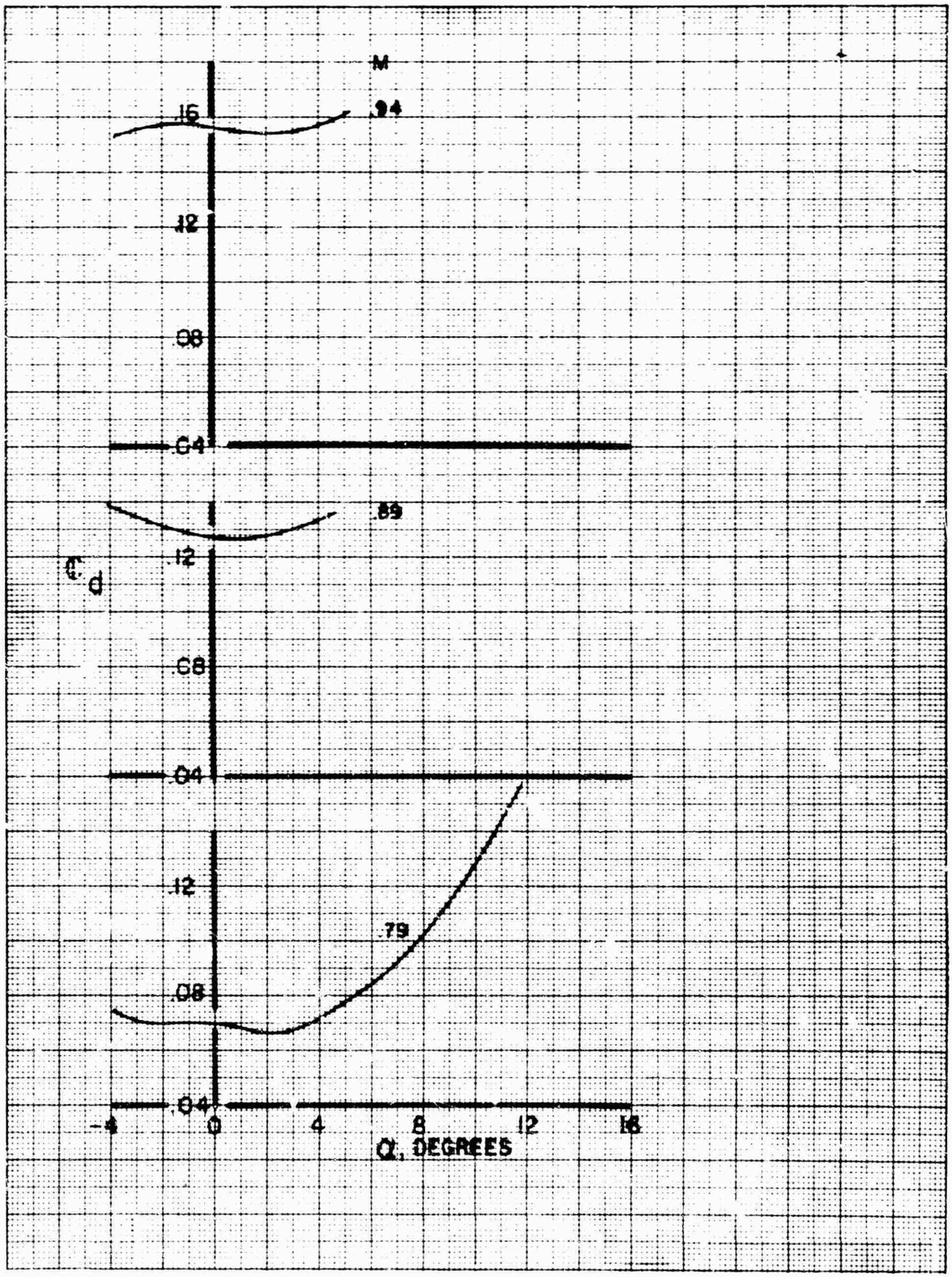


Figure 34F. Variation of Section Drag Coefficient With Angle of Attack at Constant Mach Number, NACA Section 63A018, $R = 9.5 \times 10^6$

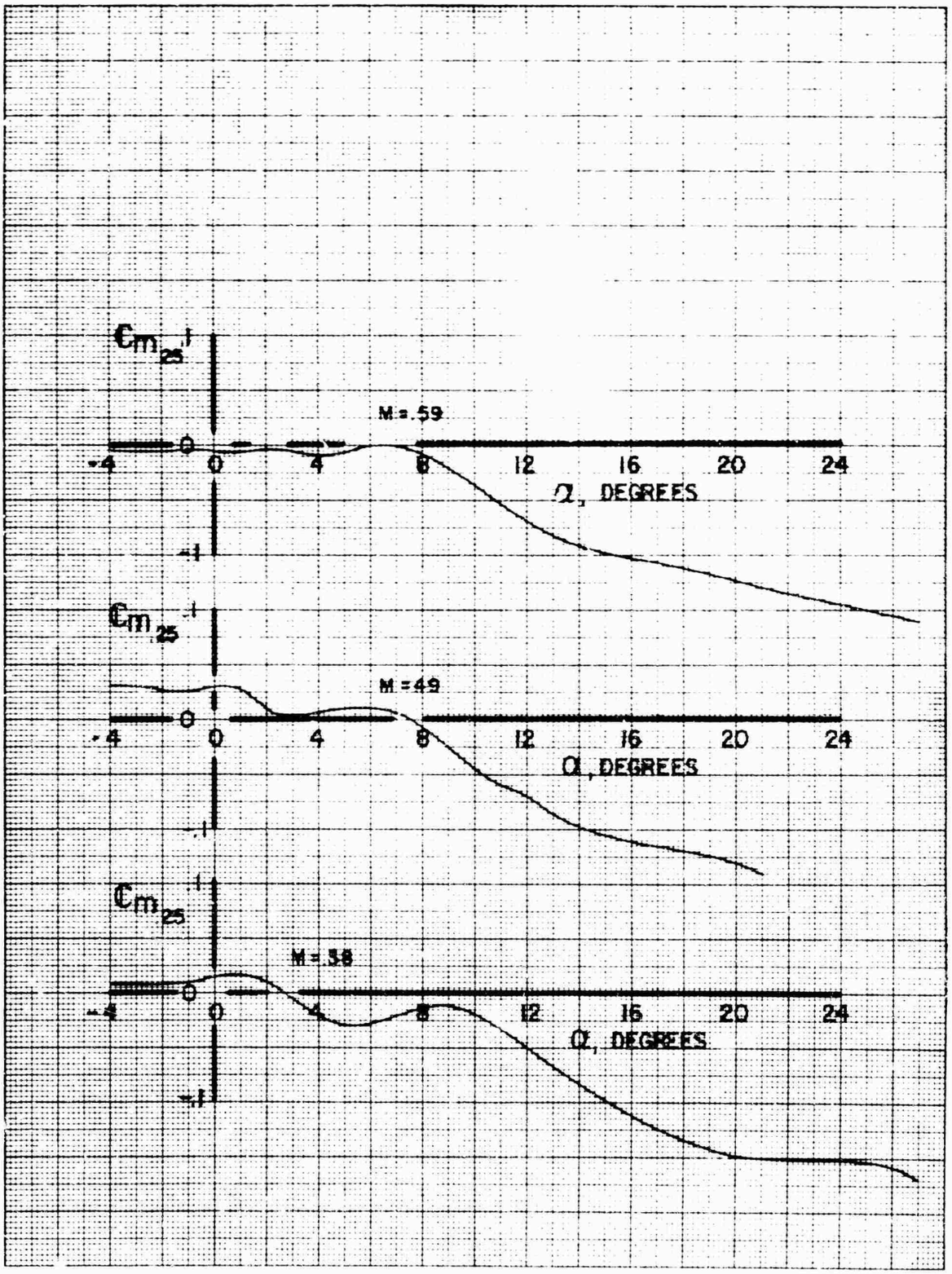


Figure 35A. Variation of Section Pitching Moment Coefficient With Angle of Attack at Constant Mach Number, NACA Section 63A009 - $R = 2.0 \times 10^6$

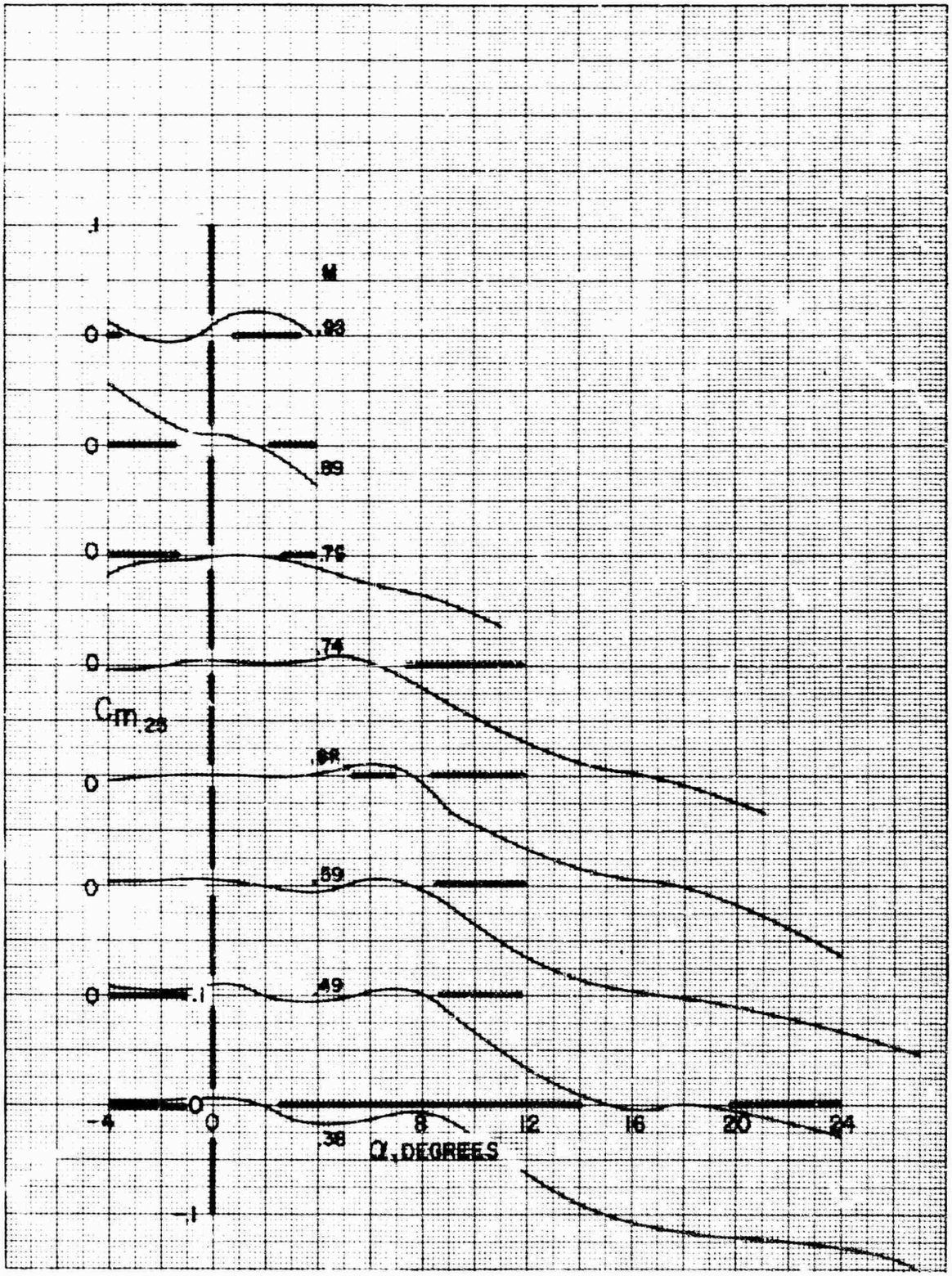


Figure 35B. Variation of Section Pitching Moment Coefficient With Angle of Attack at Constant Mach Number, NACA Section 63A009, $R = 3.5 \times 10^6$

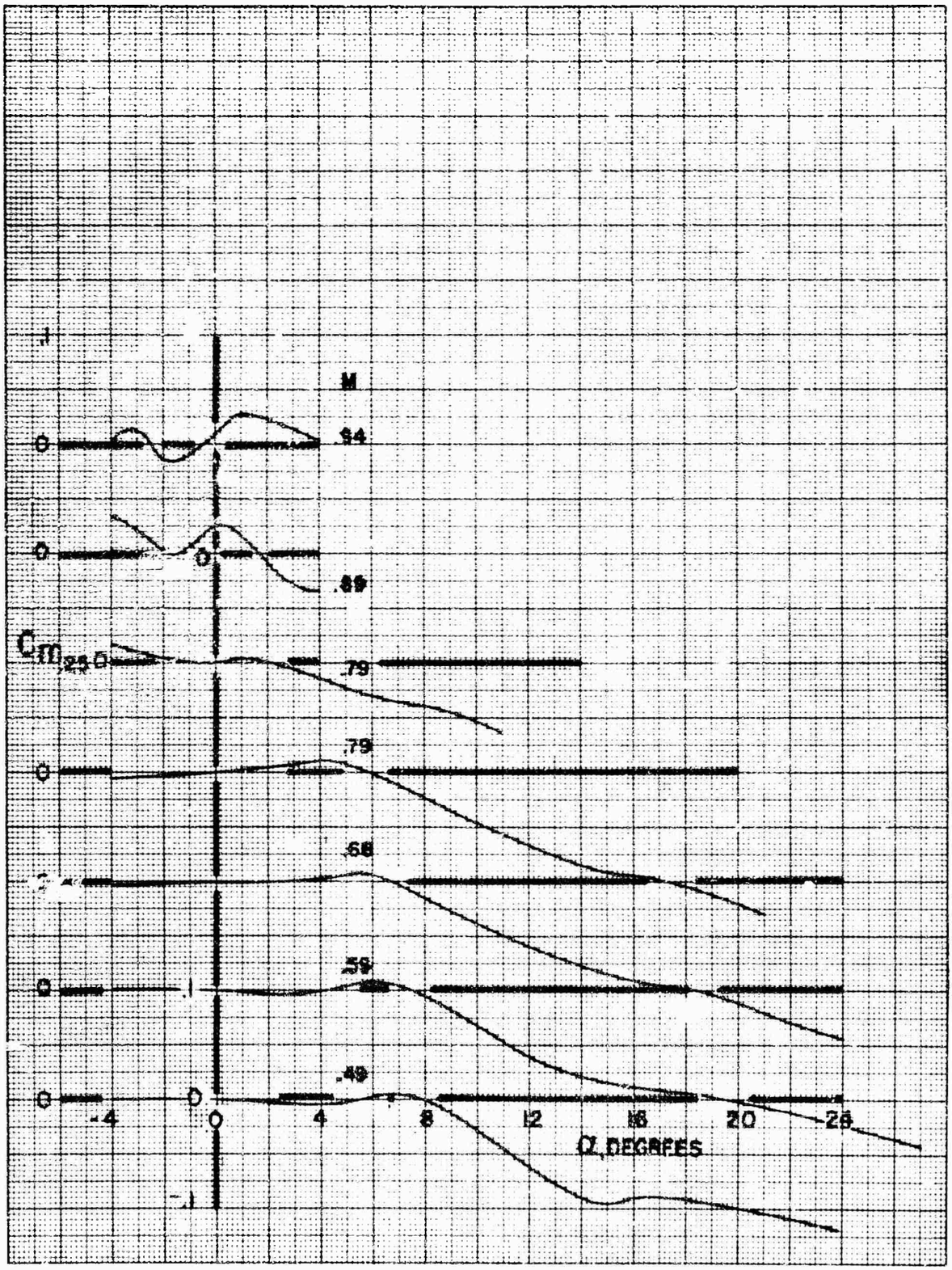


Figure 35C. Variation of Section Pitching Moment Coefficient With Angle of Attack at Constant Mach Number, NACA Section 63A009, $R = 5.0 \times 10^6$

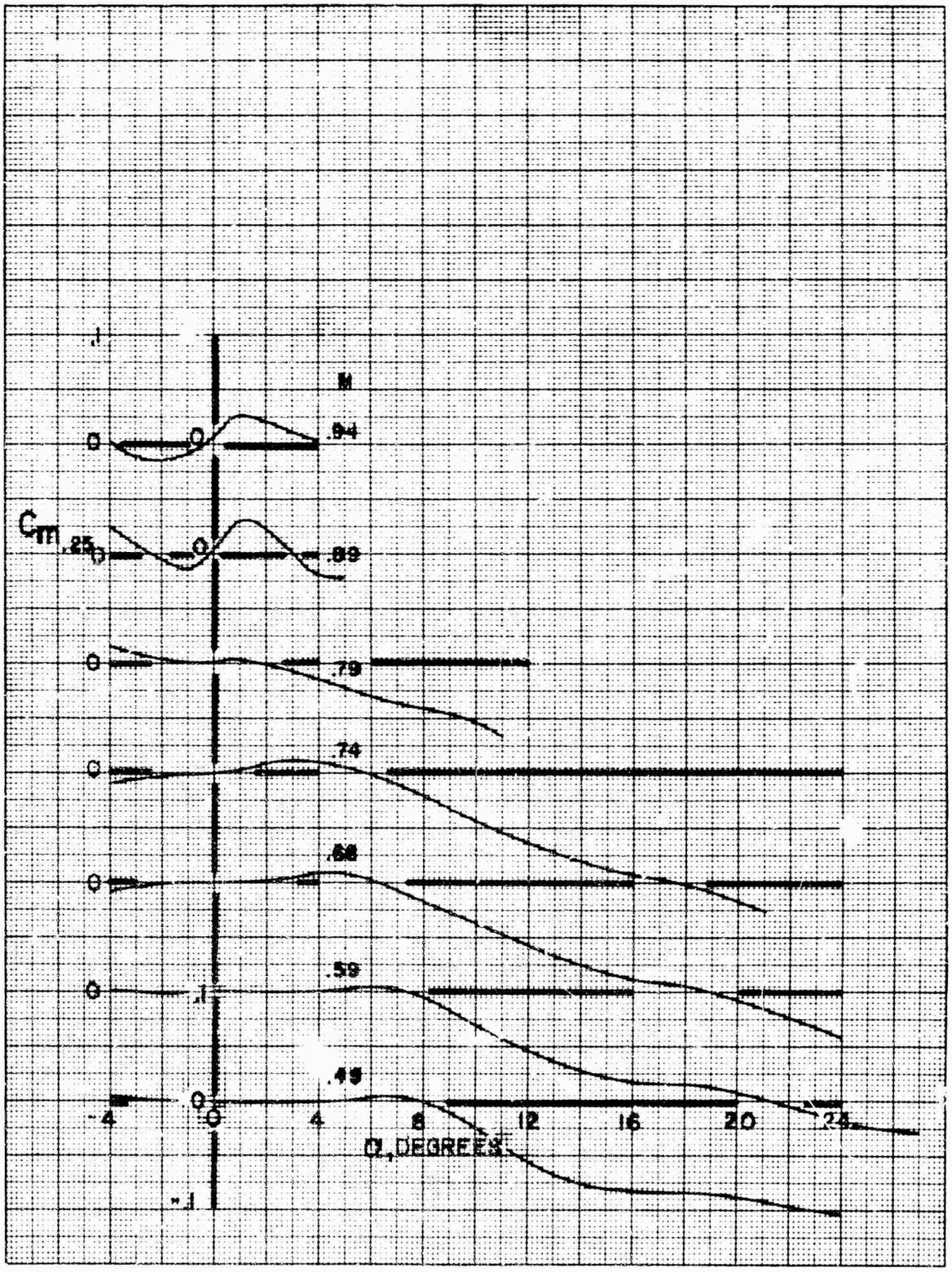


Figure 35D. Variation of Section Pitching Moment Coefficient With Angle of Attack at Constant Mach Number, NACA Section 63A009, $R = 6.5 \times 10^6$

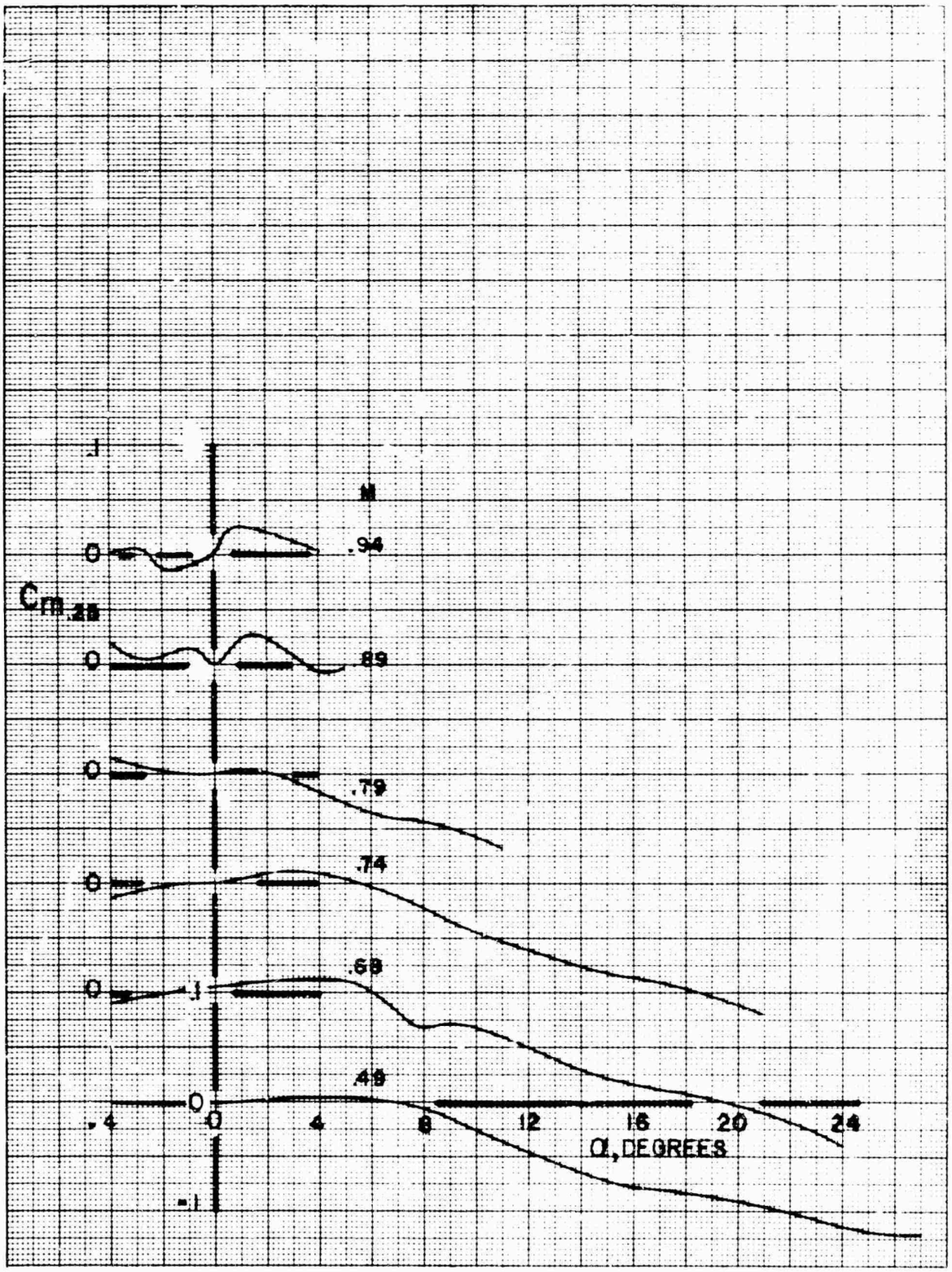


Figure 35E. Variation of Section Pitching Moment Coefficient With Angle of Attack at Constant Mach Number, NACA Section 63A009, $R = 8.0 \times 10^6$

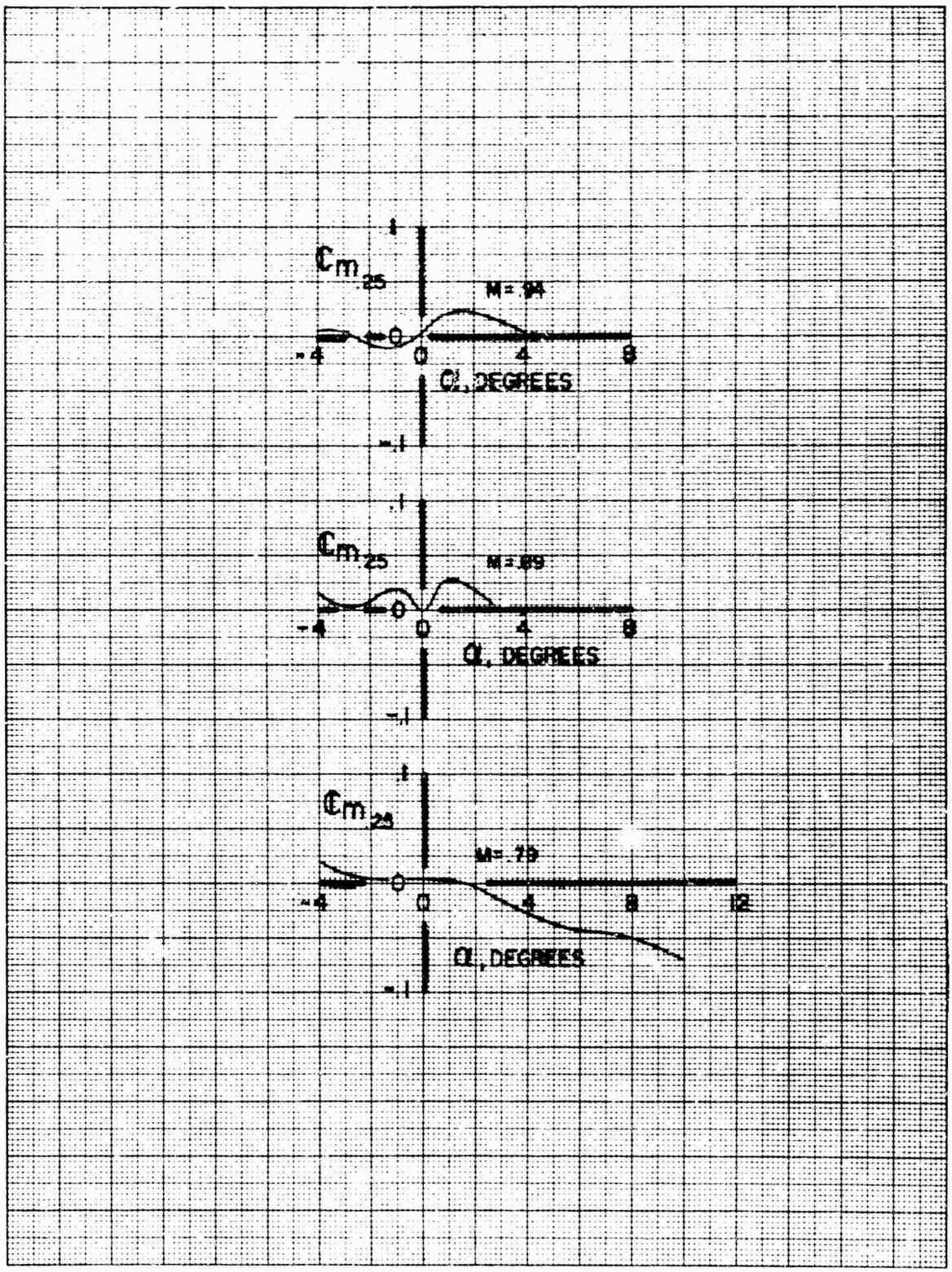


Figure 35F. Variation of Section Pitching Moment Coefficient With Angle of Attack at Constant Mach Number, NACA Section 63A009 - $R = 9.5 \times 10^6$

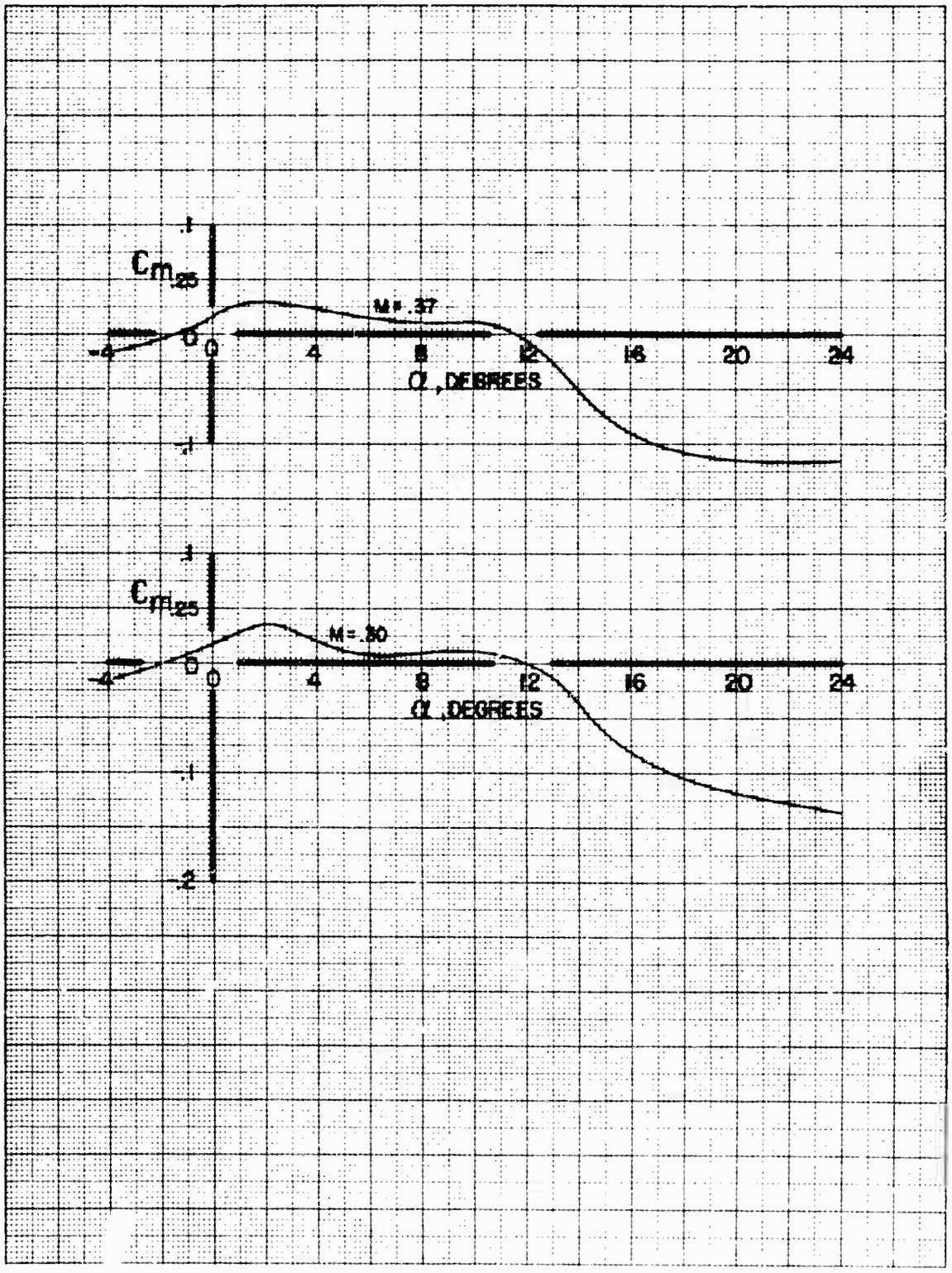


Figure 36A. Variation of Section Pitching Moment Coefficient With Angle of Attack at Constant Mach Number, NACA Section 63A012, $R = 2.0 \times 10^6$

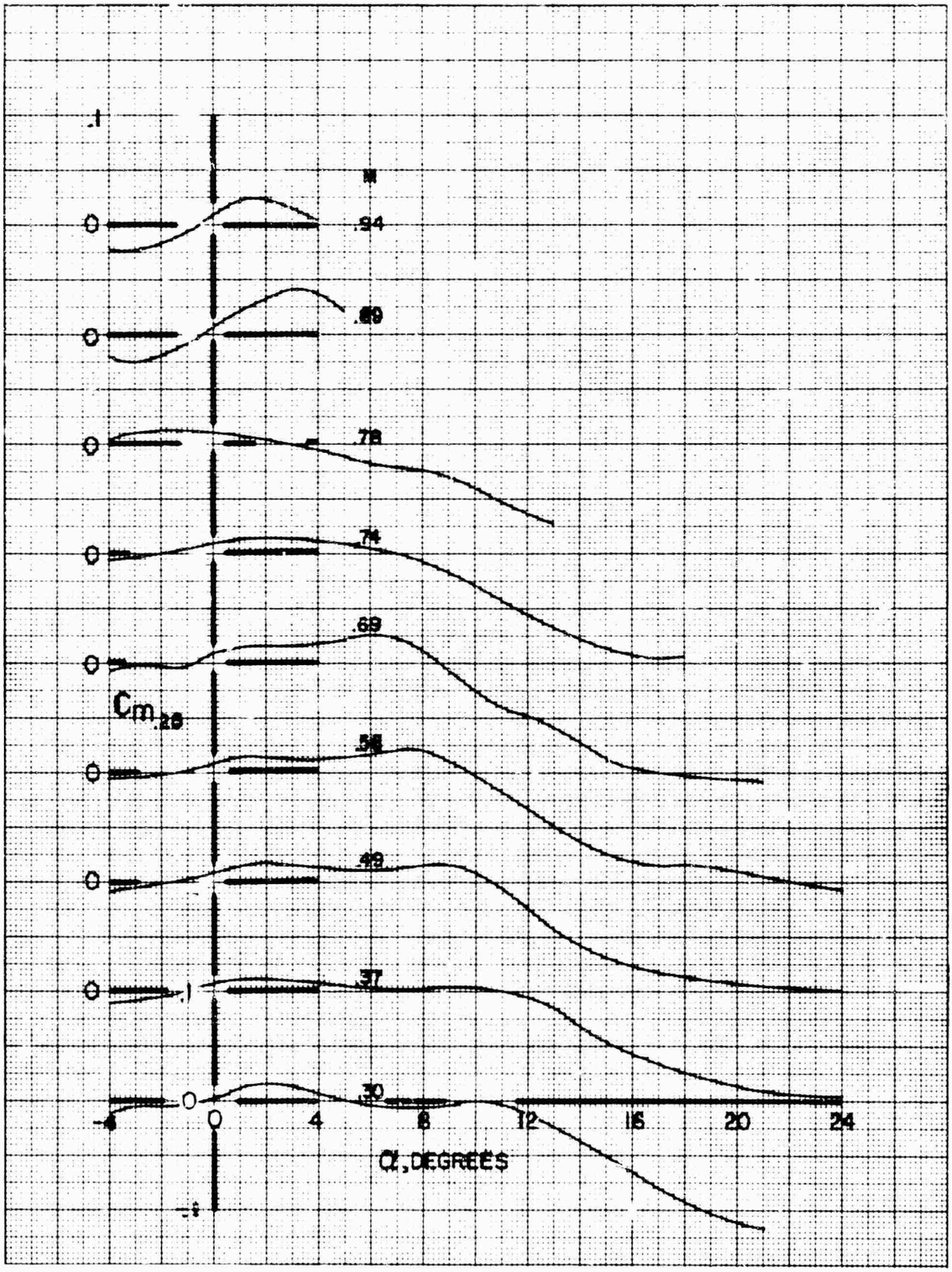


Figure 36B. Variation of Section Pitching Moment Coefficient With Angle of Attack at Constant Mach Number, NACA Section 63A012, $R = 3.5 \times 10^6$

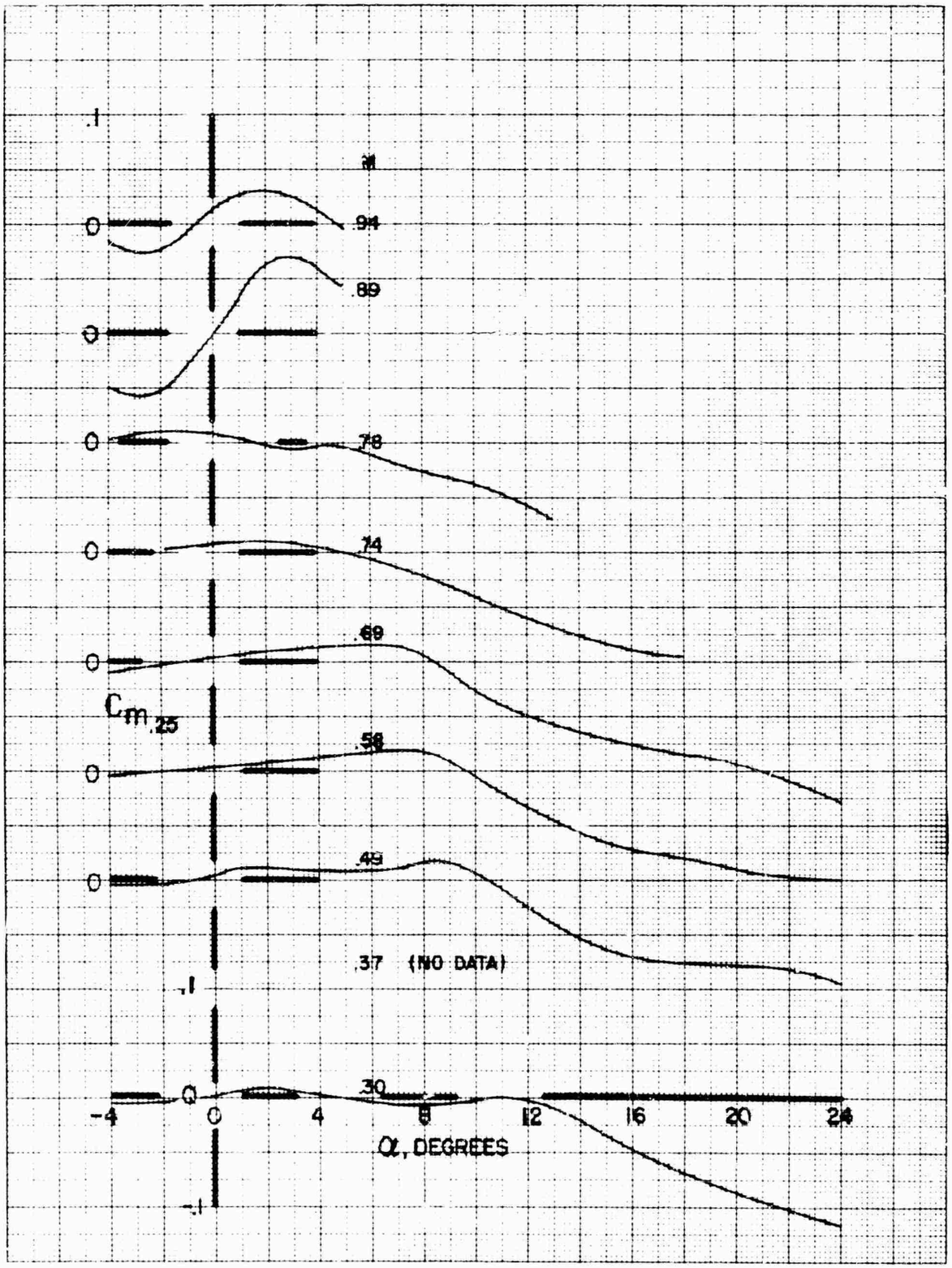


Figure 36C. Variation of Section Pitching Moment Coefficient With Angle of Attack at Constant Mach Number, NACA Section 63A012, $R = 5.0 \times 10^6$

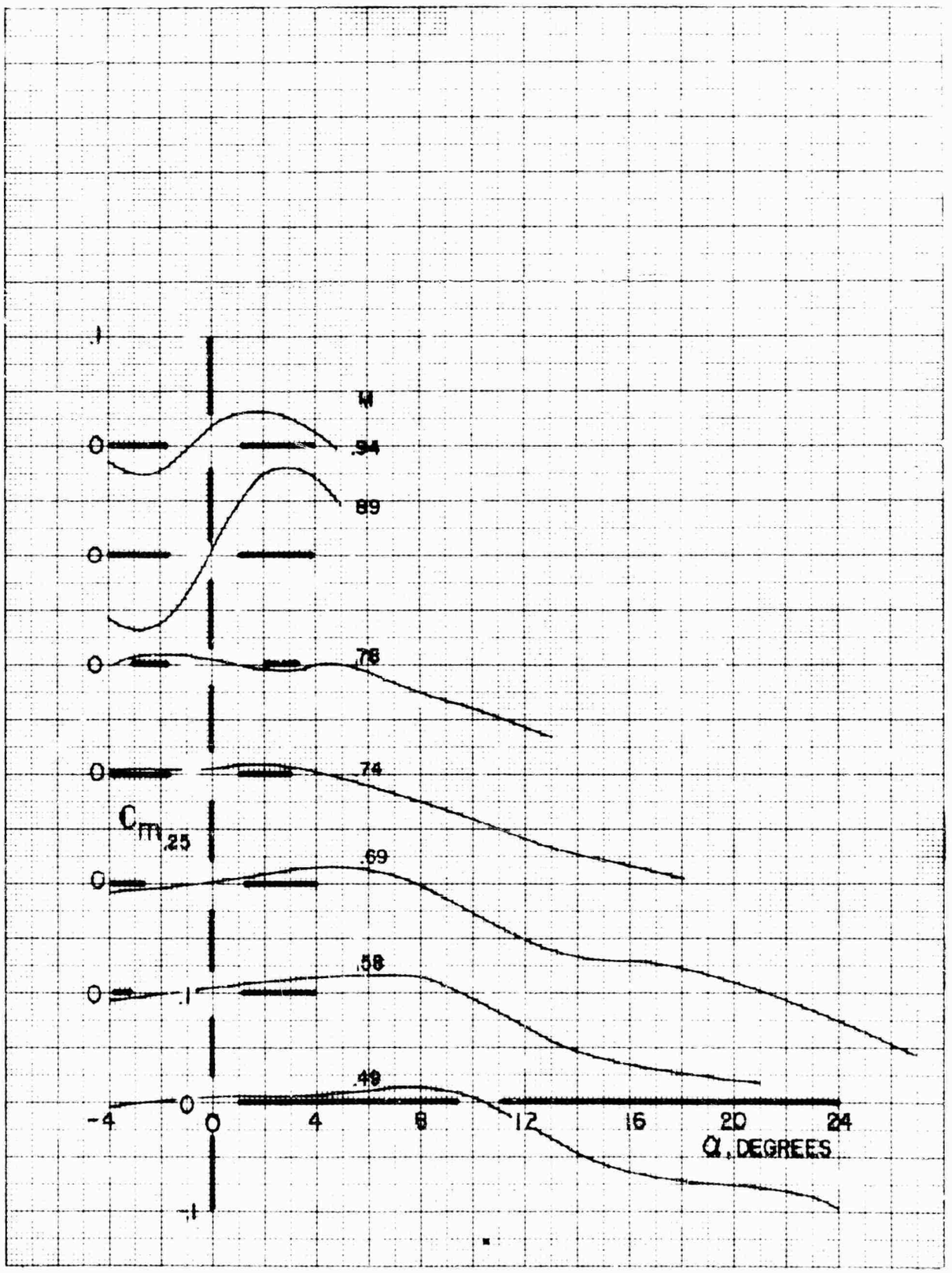


Figure 36D. Variation of Section Pitching Moment Coefficient With Angle of Attack at Constant Mach Number, NACA Section 63A012, $R = 6.5 \times 10^6$

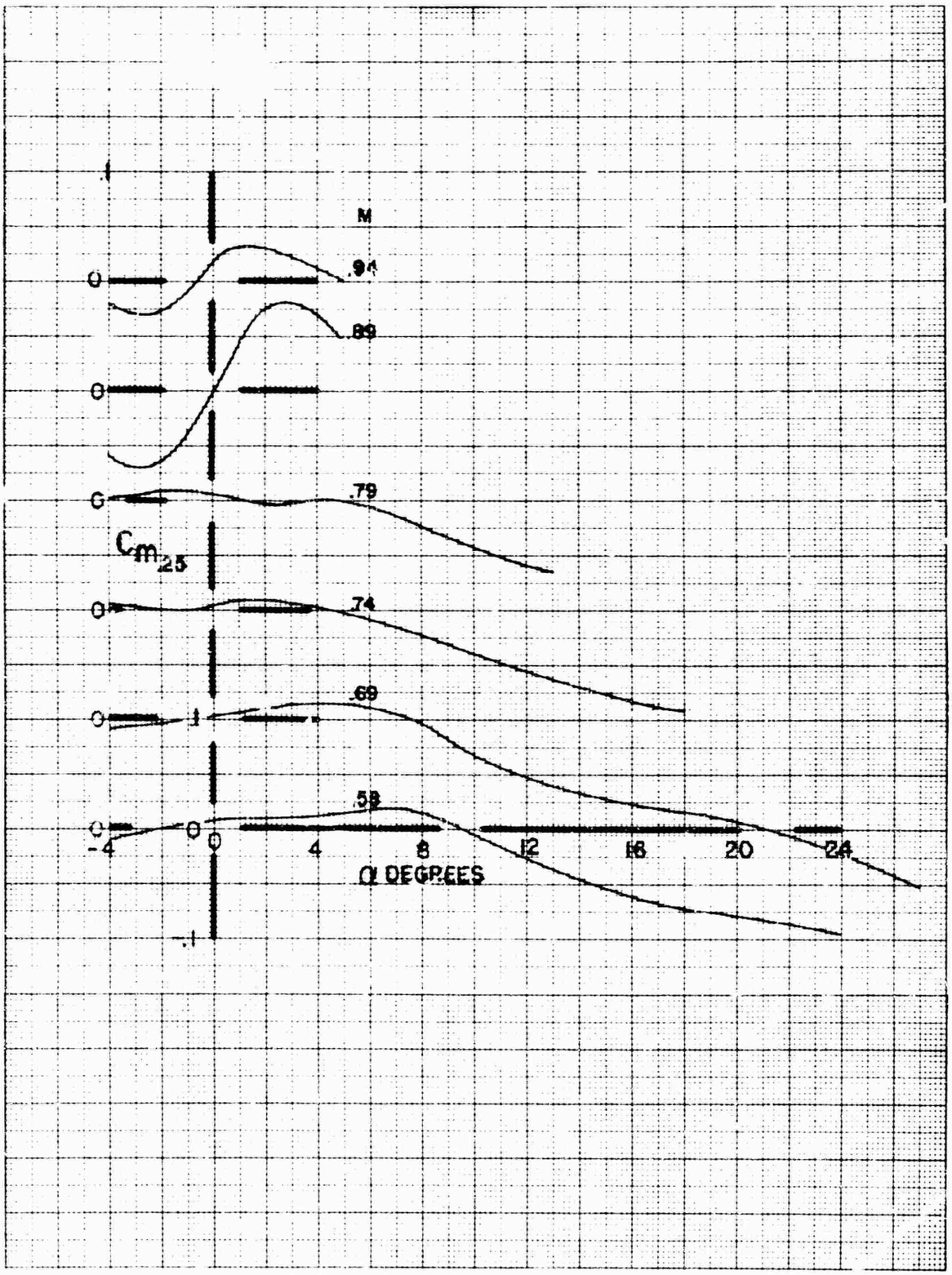


Figure 36E. Variation of Section Pitching Moment Coefficient With Angle of Attack at Constant Mach Number, NACA Section 63A012, $R = 8.0 \times 10^6$

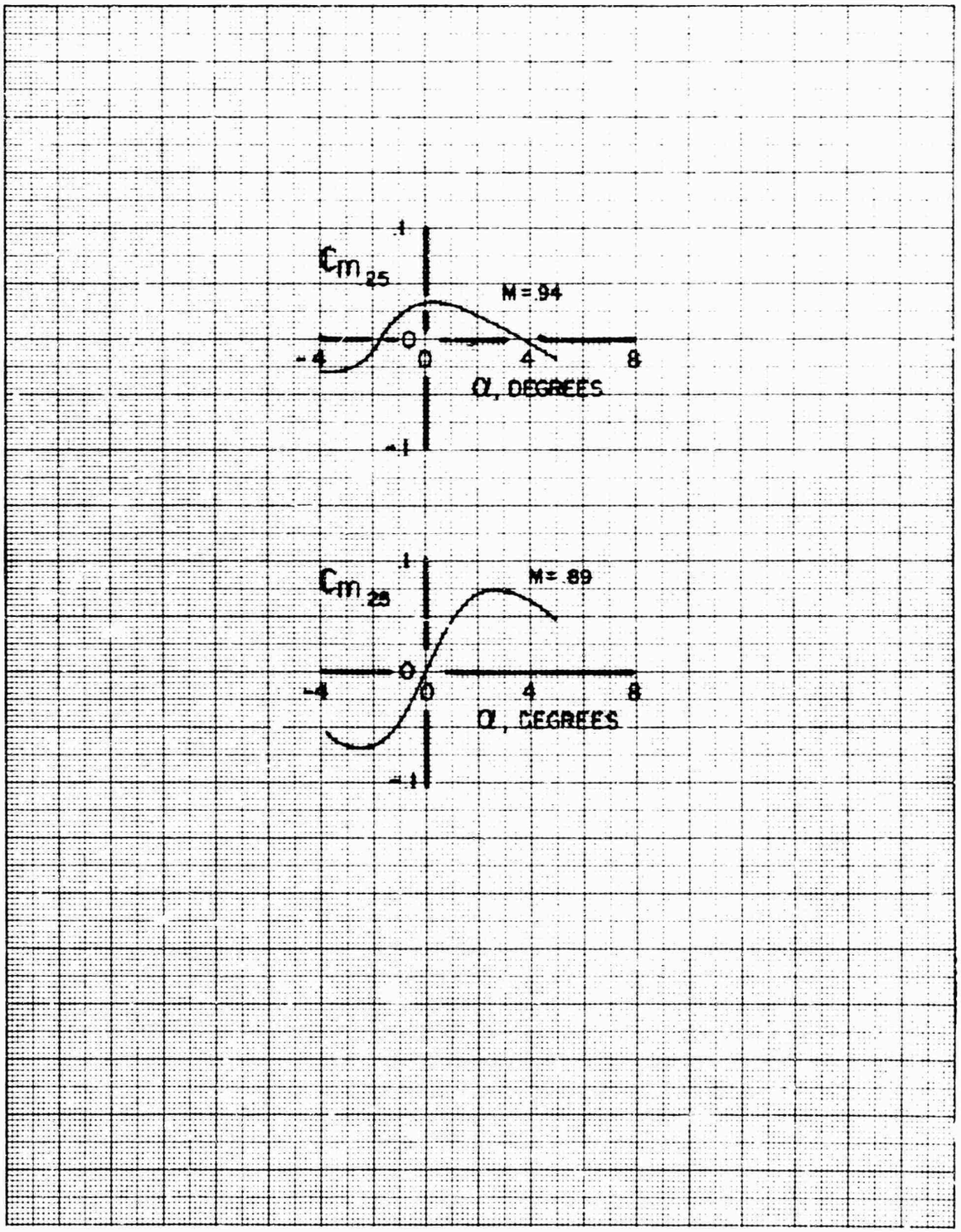


Figure 36F. Variation of Section Pitching Moment Coefficient With Angle of Attack at Constant Mach Number, NACA Section 63A012 - $R = 9.5 \times 10^6$

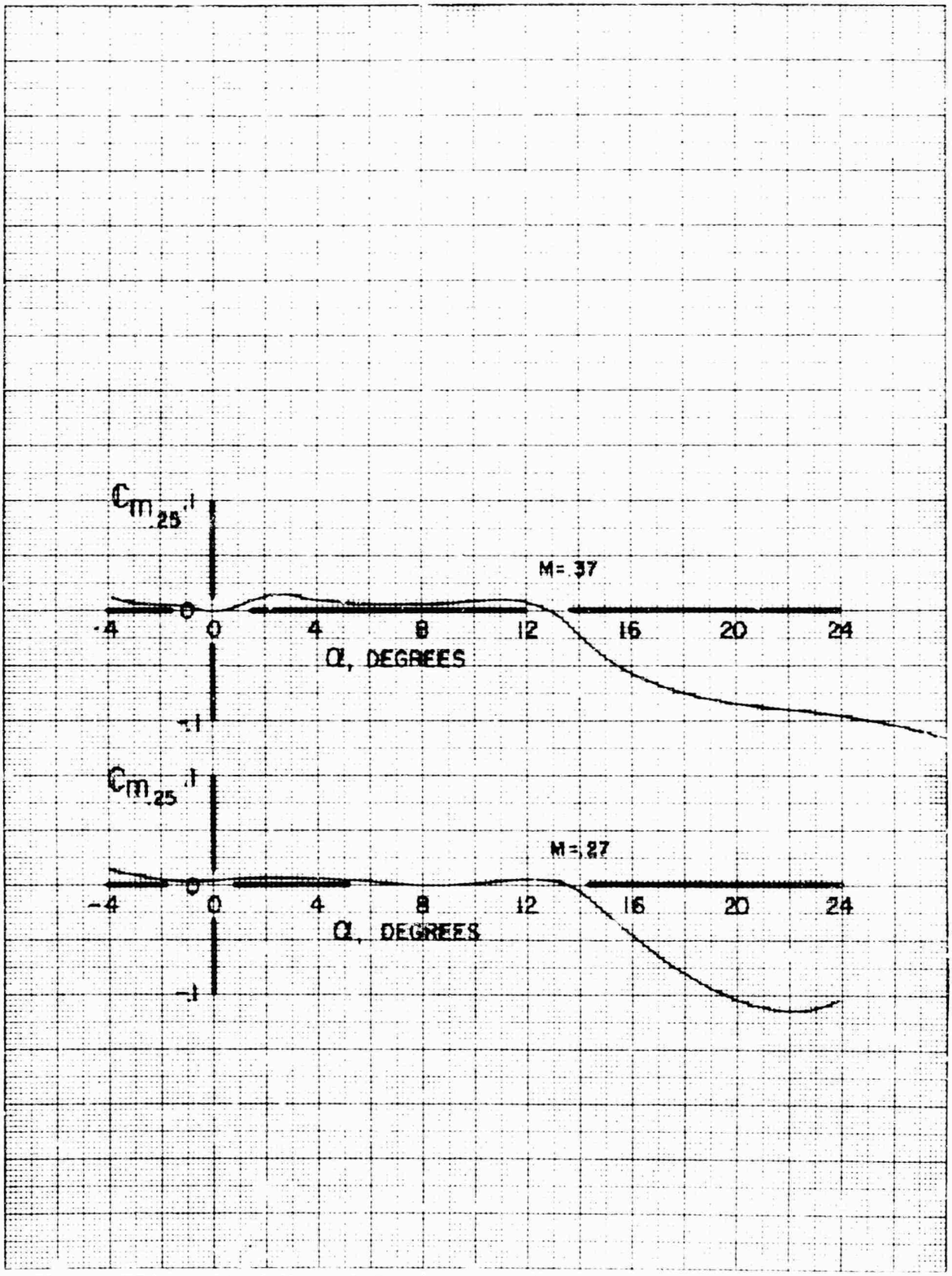


Figure 37A. Variation of Section Pitching Moment Coefficient With Angle of Attack at Constant Mach Number, NACA Section 63A015, $R = 2.0 \times 10^6$

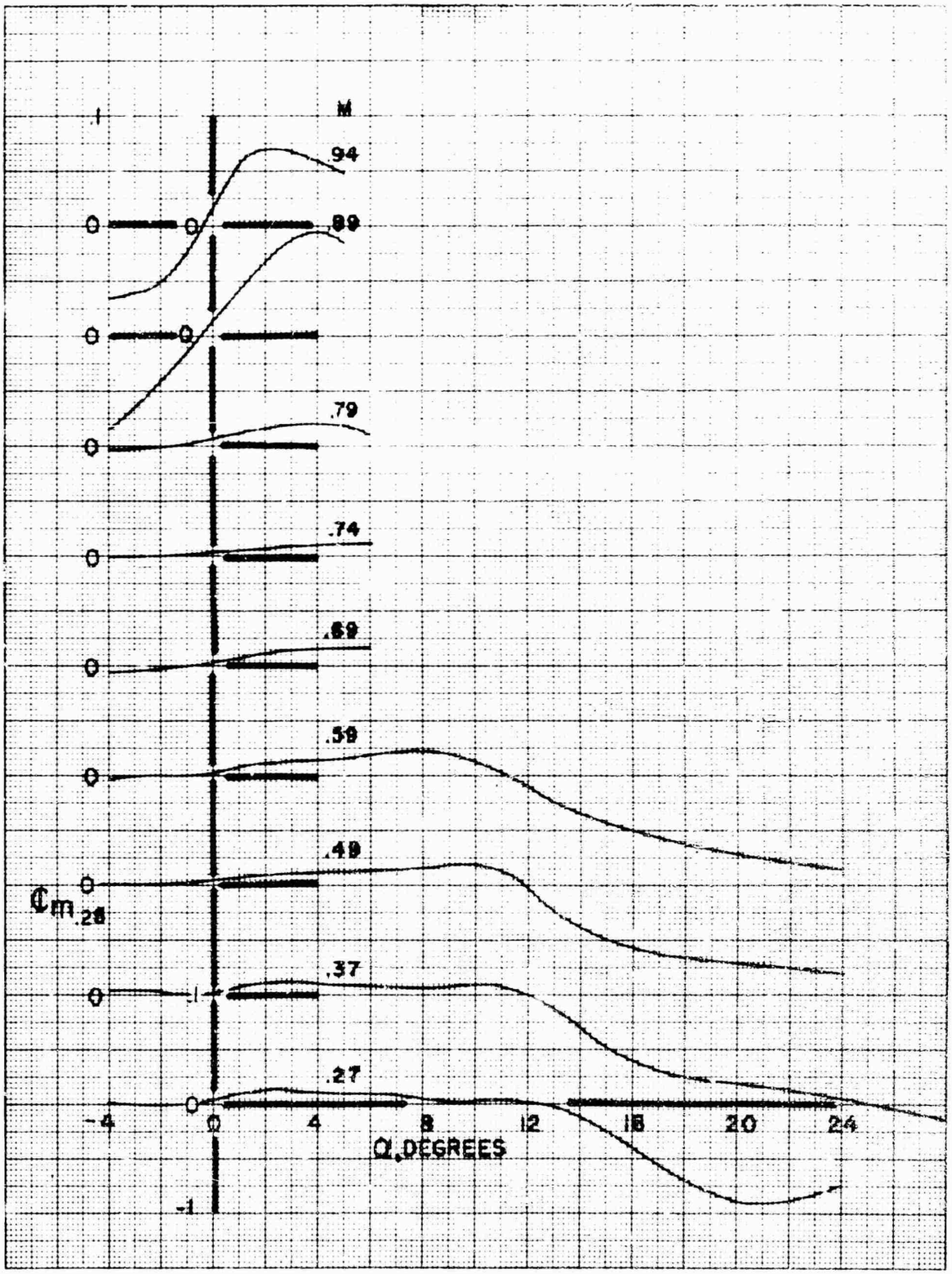


Figure 37B. Variation of Section Pitching Moment Coefficient With Angle of Attack at Constant Mach Number, NACA Section 63A015, $R = 3.5 \times 10^6$

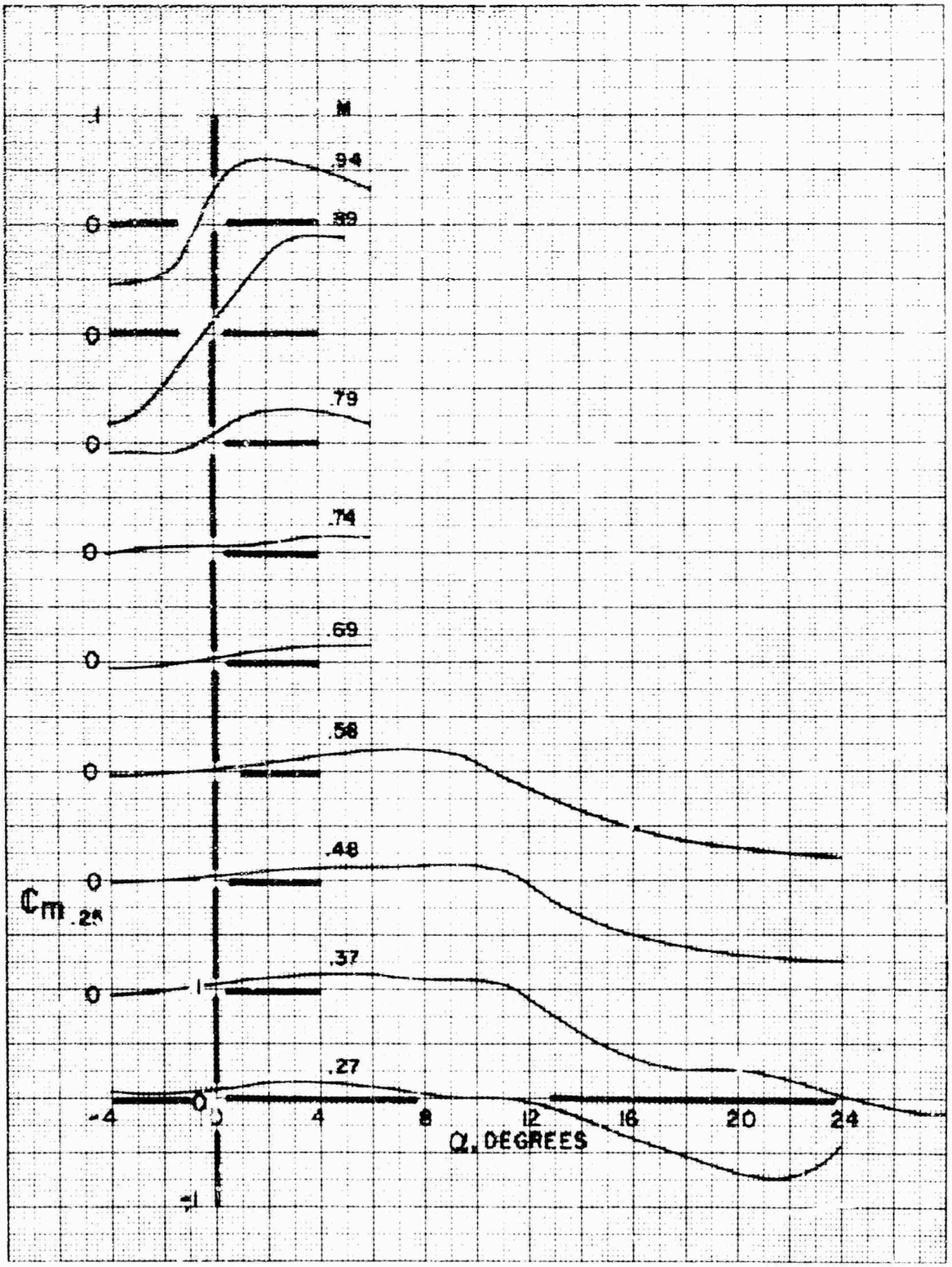


Figure 37C. Variation of Section Pitching Moment Coefficient With Angle of Attack at Constant Mach Number, NACA Section 63A015, $R = 5.0 \times 10^6$

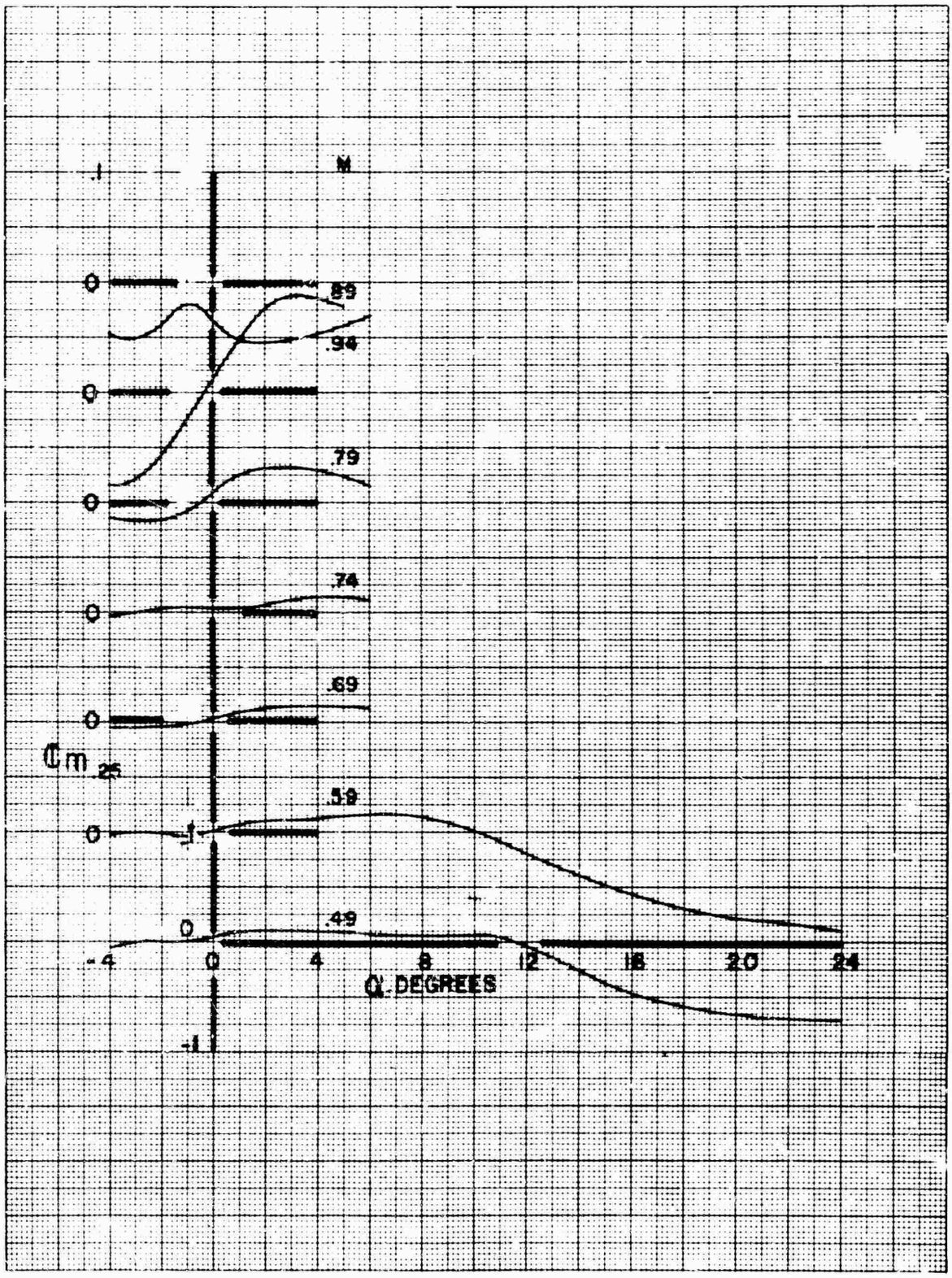


Figure 37D. Variation of Section Pitching Moment Coefficient With Angle of Attack at Constant Mach Number, NACA Section 63A015, $R = 6.5 \times 10^6$

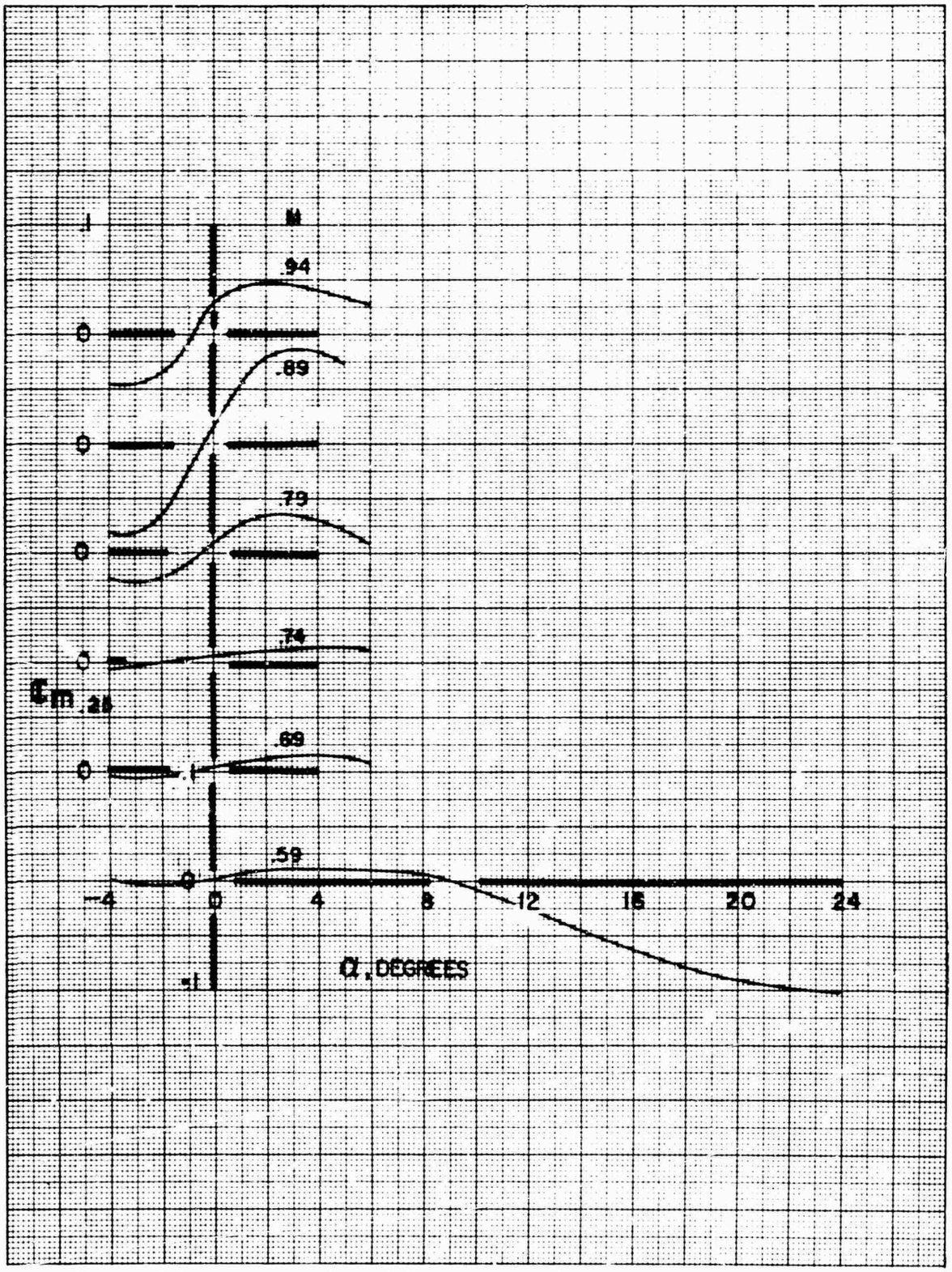


Figure 37E. Variation of Section Pitching Moment Coefficient With Angle of Attack at Constant Mach Number, NACA Section 63A015, R = 8.0 x 10^6

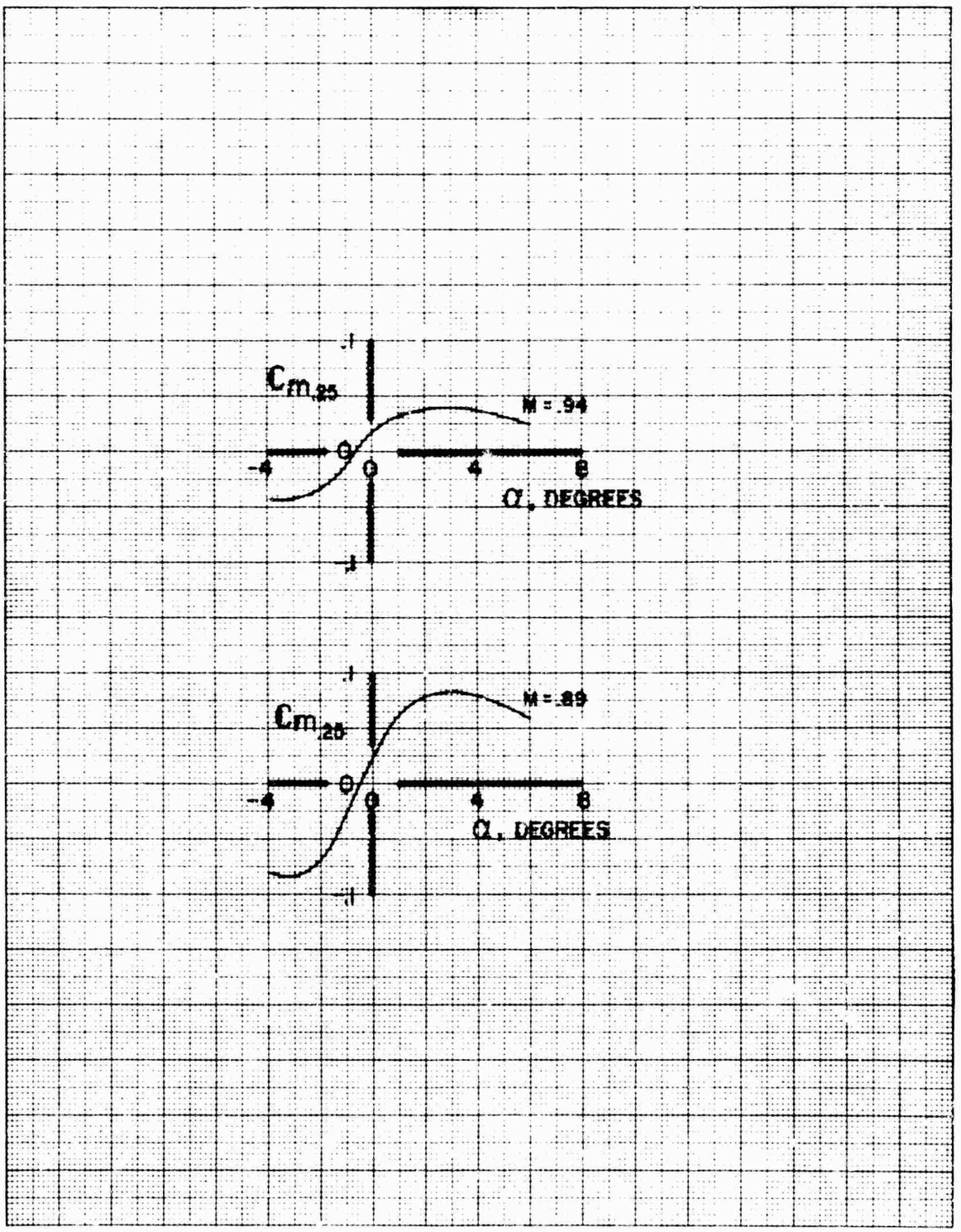


Figure 37F. Variation of Section Pitching Moment Coefficient With Angle of Attack at Constant Mach Number, NACA Section 63A015, $R = 9.5 \times 10^6$

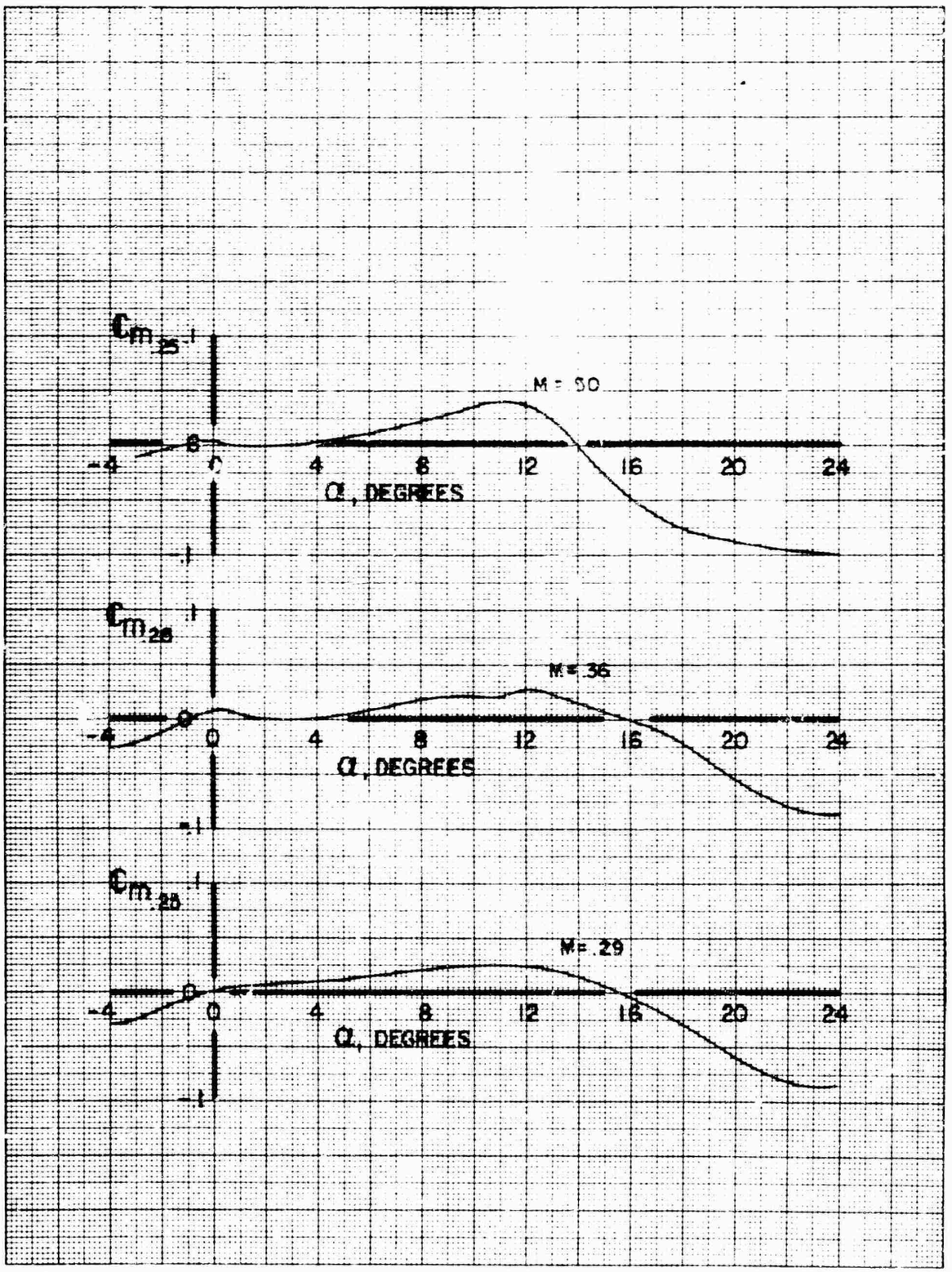


Figure 38A. Variation of Section Pitching Moment Coefficient With Angle of Attack at Constant Mach Number, NACA Section 63A018 - $R = 2.0 \times 10^6$

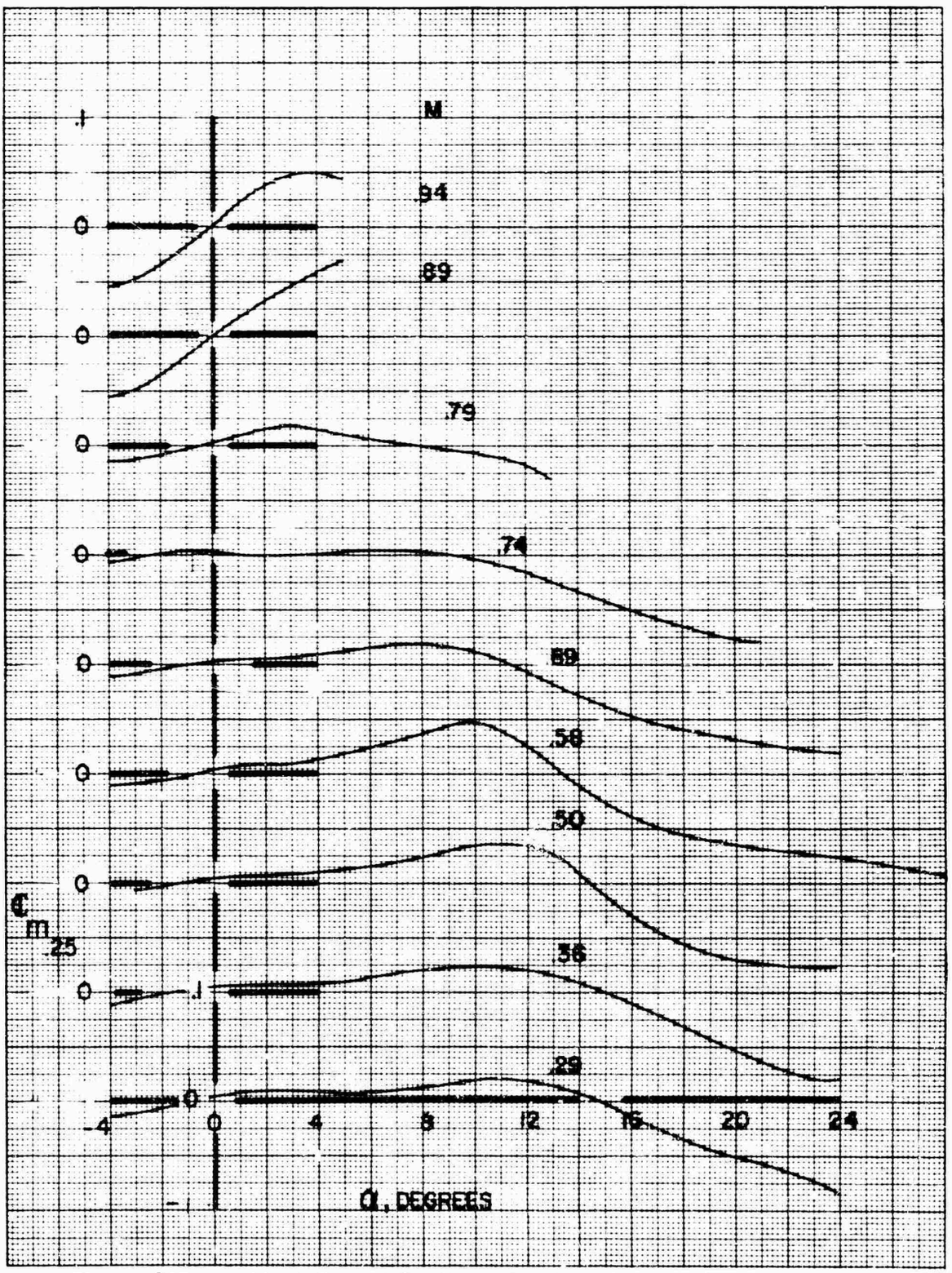


Figure 38B. Variation of Section Pitching Moment Coefficient With Angle of Attack at Constant Mach Number, NACA Section 63A018, R = 3.5 x 10^6

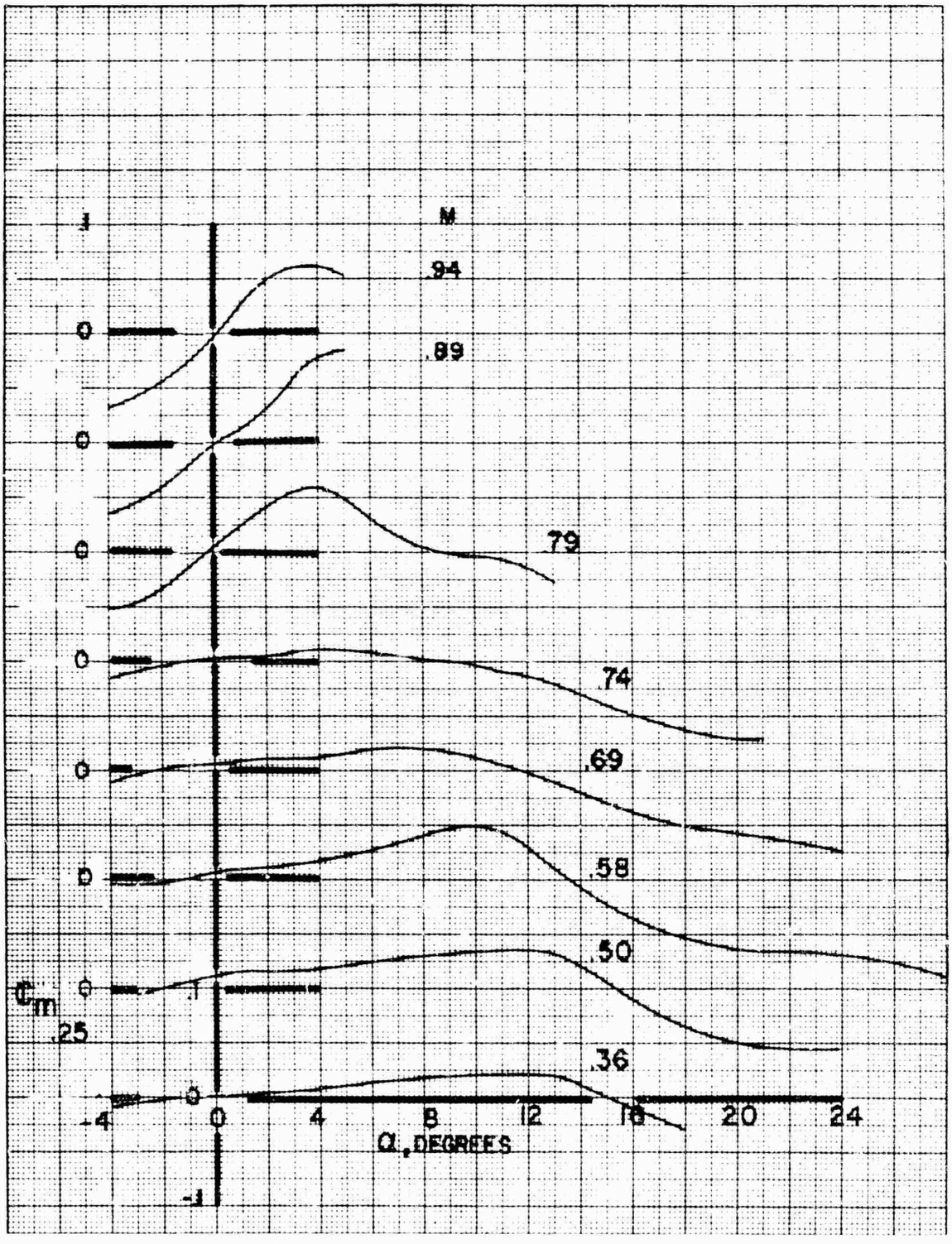


Figure 38C. Variation of Section Pitching Moment Coefficient With Angle of Attack at Constant Mach Number, NACA Section 63A018, $R = 5.0 \times 10^6$

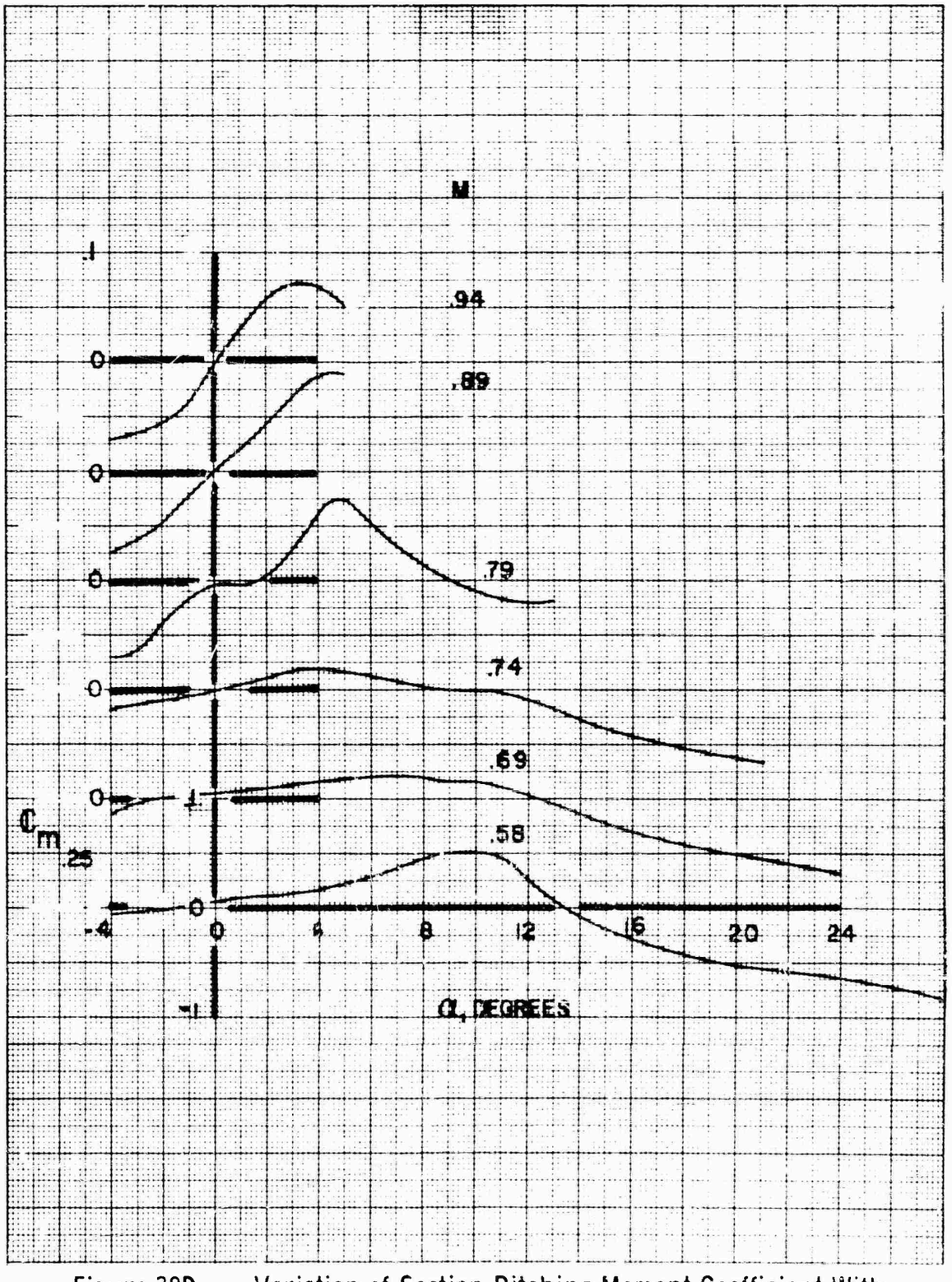


Figure 38D. Variation of Section Pitching Moment Coefficient With Angle of Attack at Constant Mach Number, NACA Section 63A018, $R = 6.5 \times 10^6$

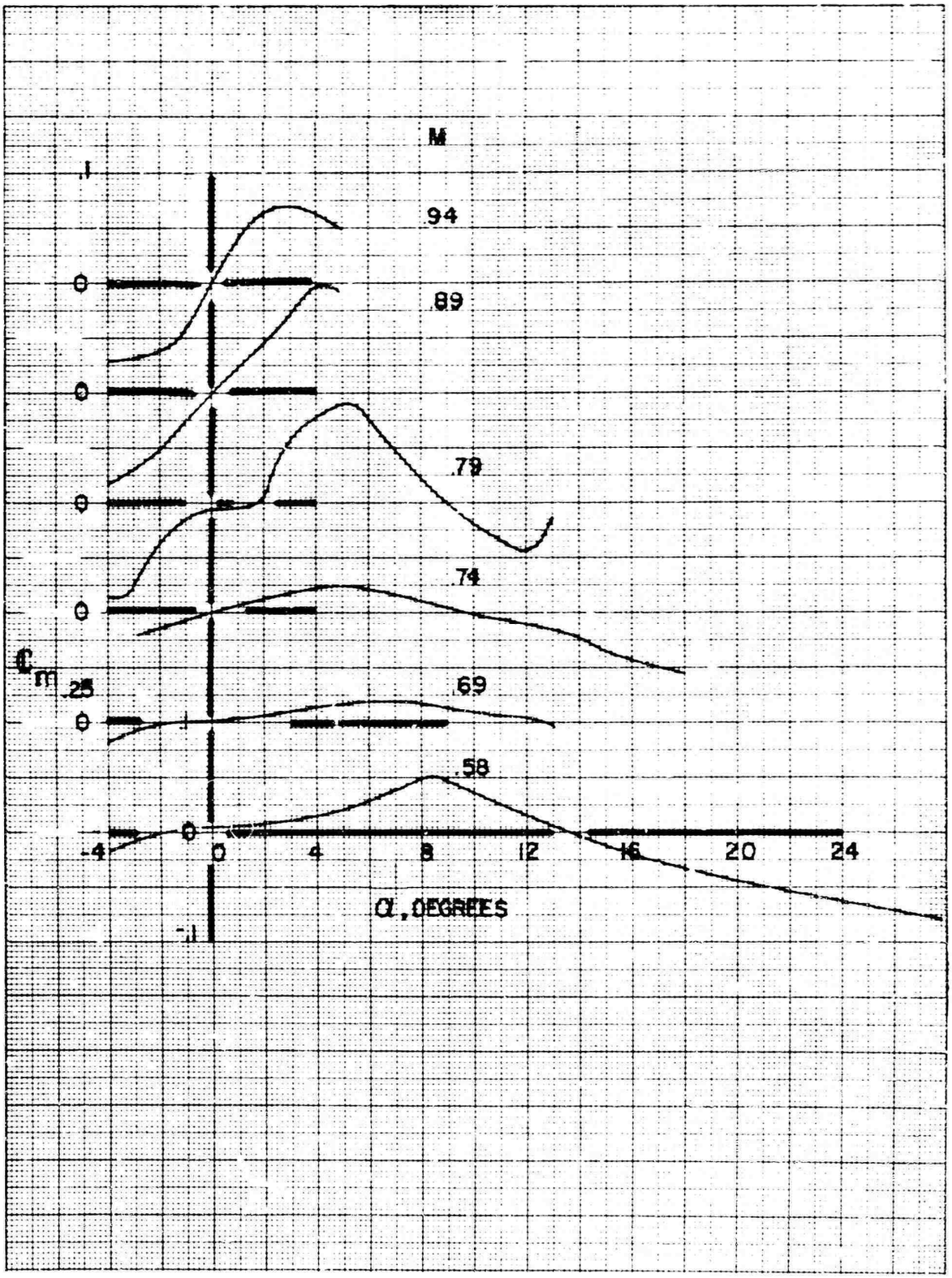


Figure 38E. Variation of Section Pitching Moment Coefficient With Angle of Attack at Constant Mach Number, NACA Section 63A018, R = 8.0 x 10^6

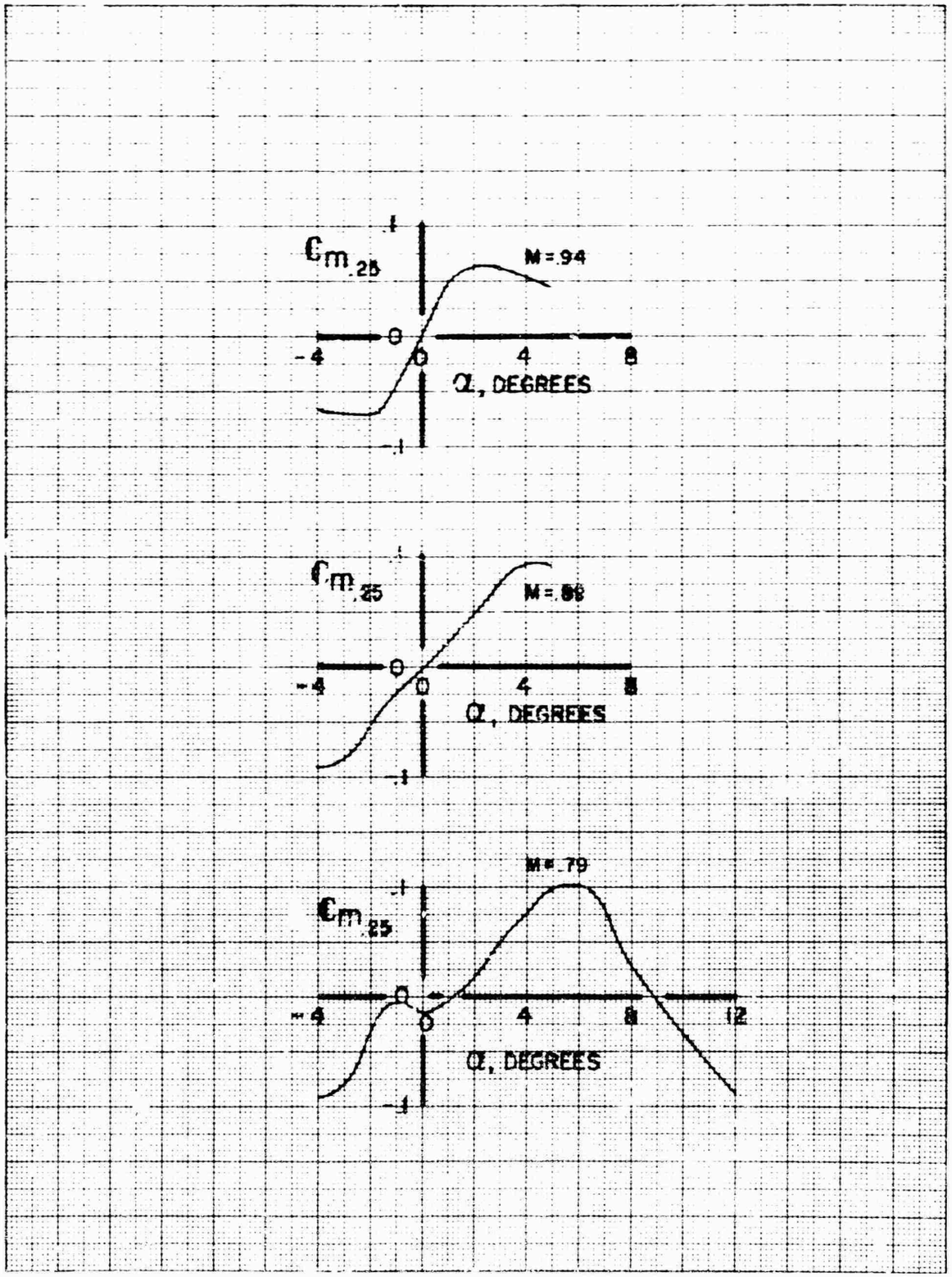


Figure 38F. Variation of Section Pitching Moment Coefficient With Angle of Attack at Constant Mach Number, NACA Section 63A018, $R = 9.5 \times 10^6$

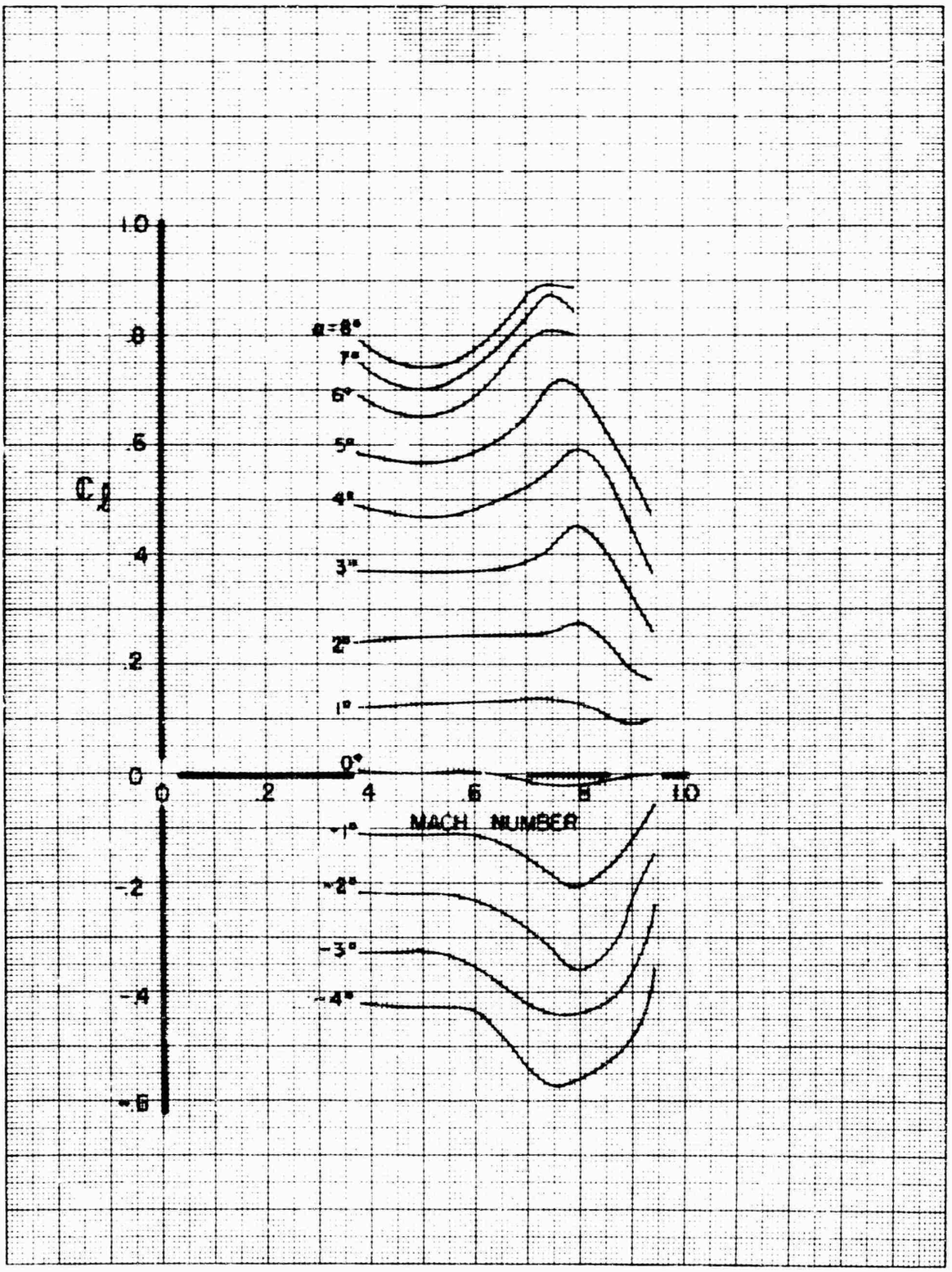


Figure 39A-1. Variation of Section Lift Coefficient With Mach Number at Constant Angle of Attack, $R = 3.5 \times 10^6$, NACA Section 63A009

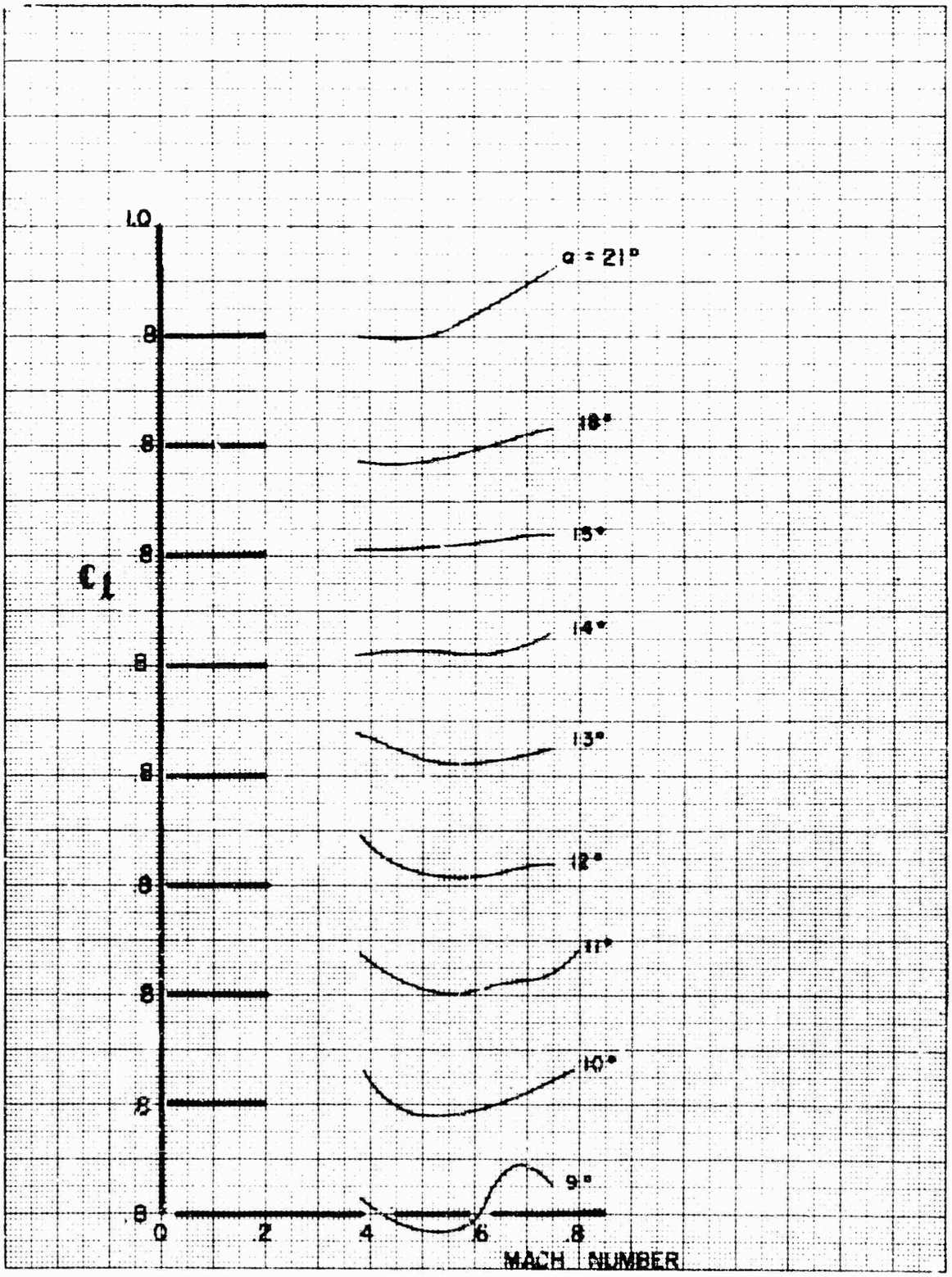


Figure 39A-2. Variation of Section Lift Coefficient With Mach Number at Constant Angle of Attack, R = 3.5 x 10^6, NACA Section 63A009

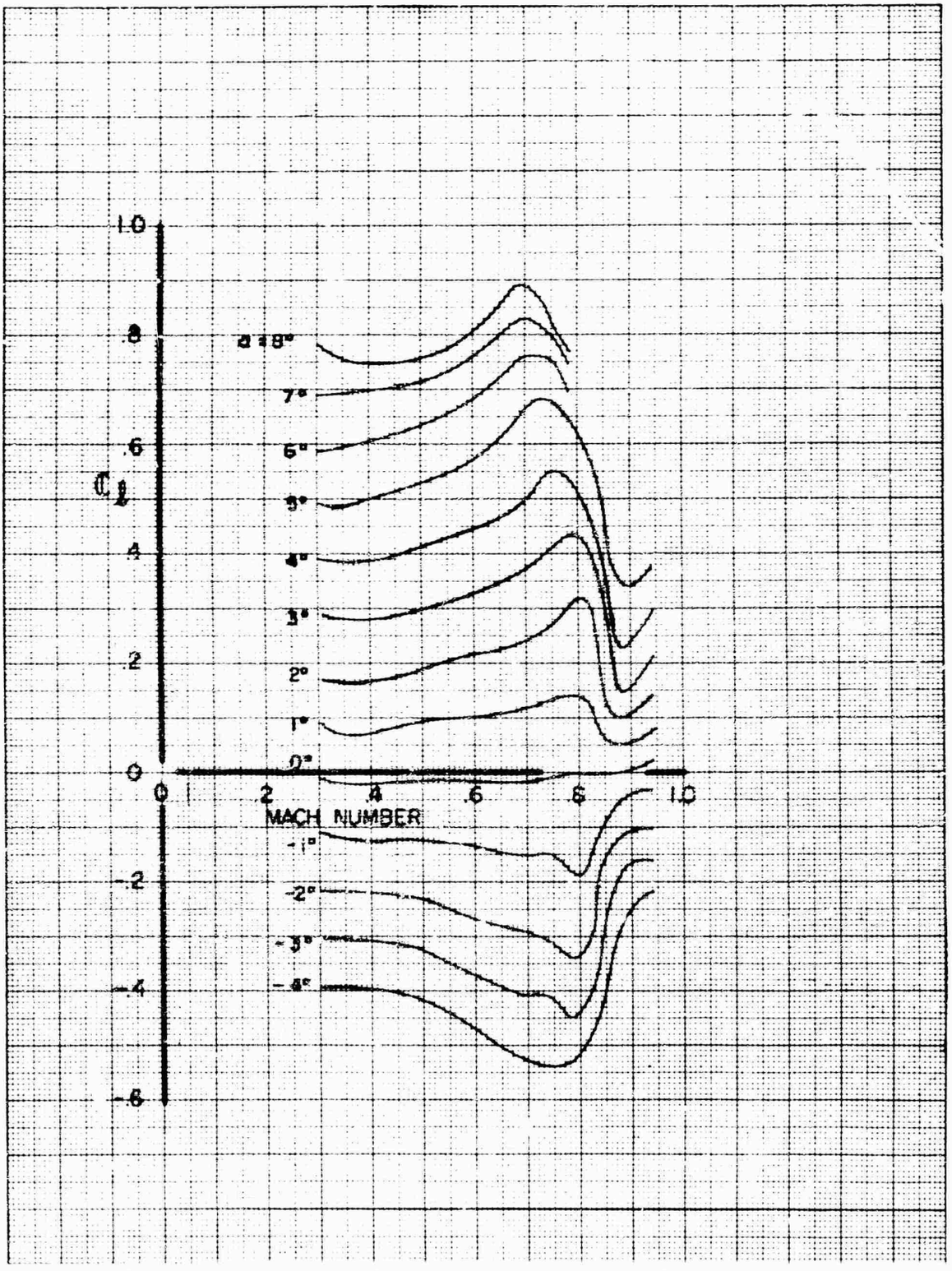


Figure 39B-1. Variation of Section Lift Coefficient With Mach Number at Constant Angle of Attack, R = 3.5 x 10^6, NACA Section 63A012

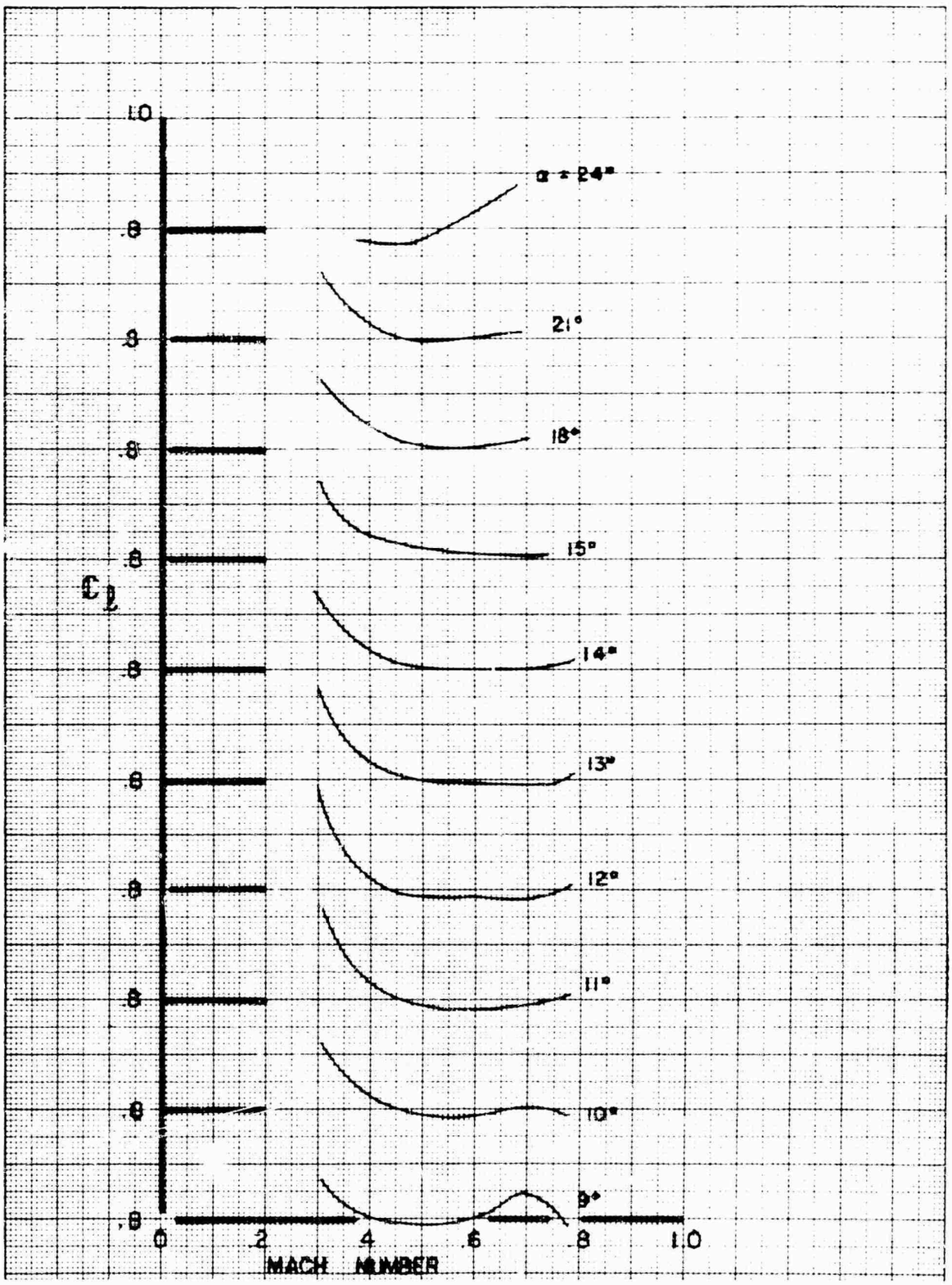


Figure 39B-2. Variation of Section Lift Coefficient With Mach Number at Constant Angle of Attack, $R = 3.5 \times 10^6$, NACA Section 63A012

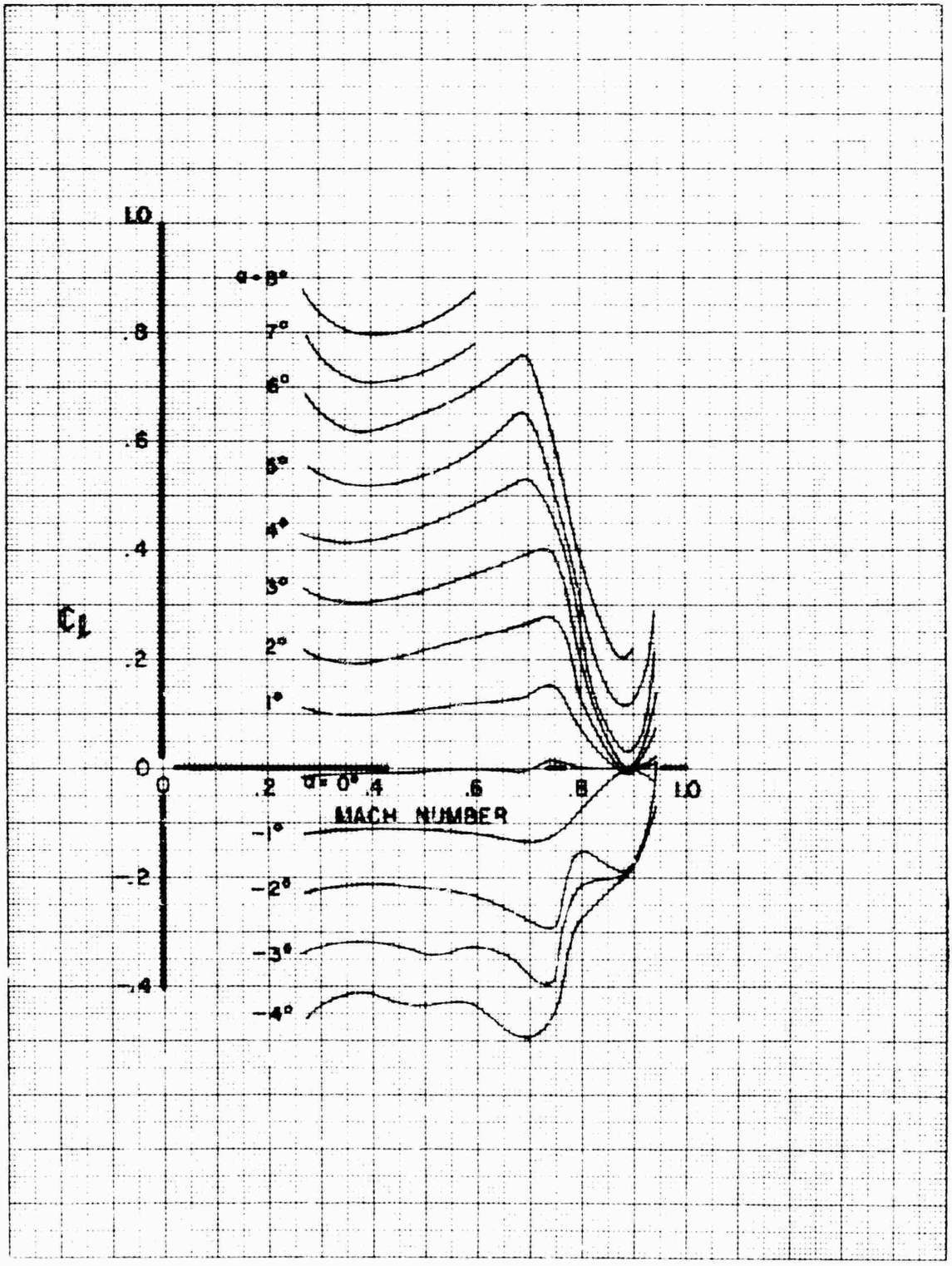


Figure 39C-1. Variation of Section Lift Coefficient With Mach Number at Constant Angle of Attack, R = 3.5×10^6, NACA Section 63A015

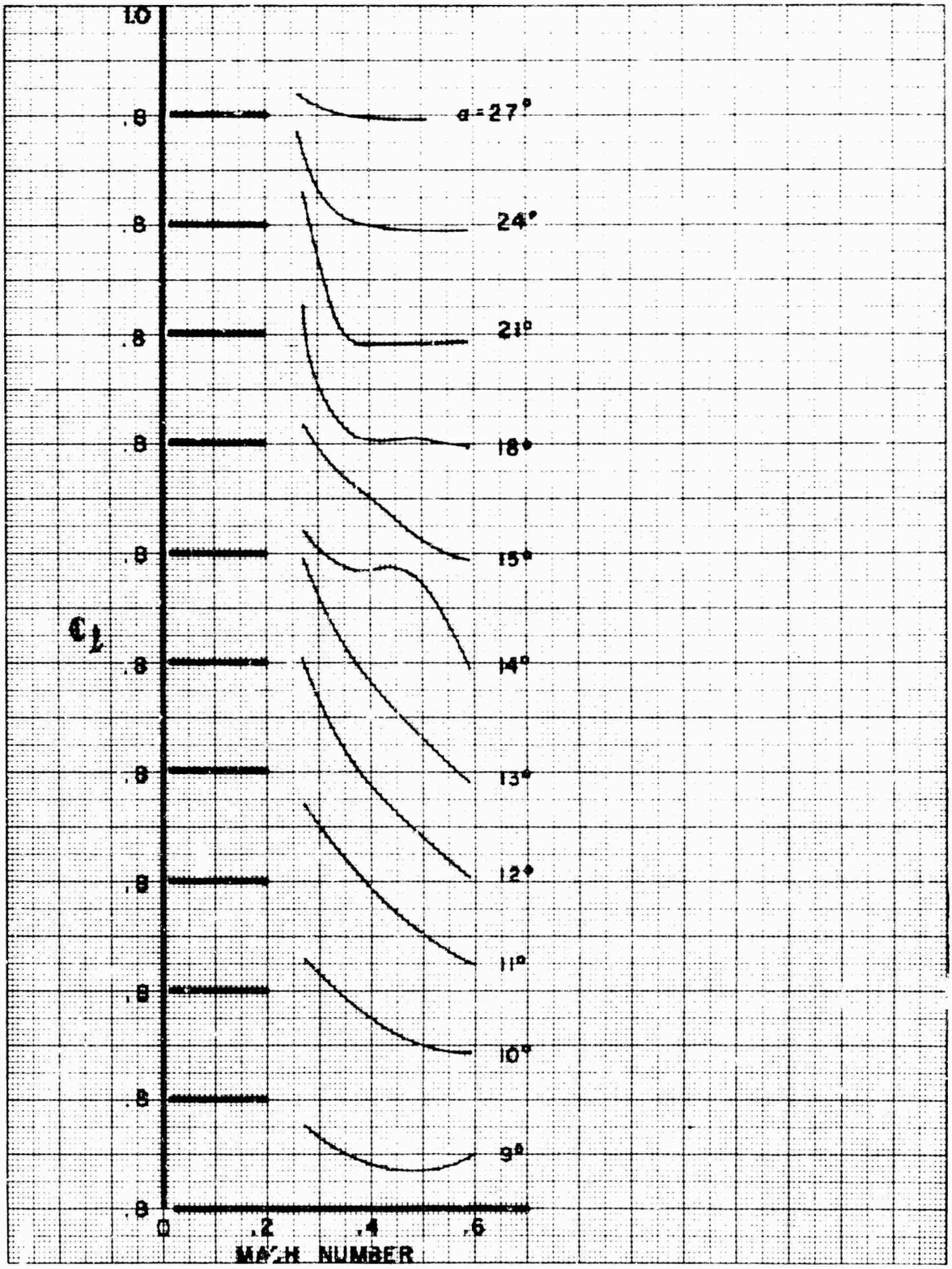


Figure 39C-2. Variation of Section Lift Coefficient With Mach Number at Constant Angle of Attack, R = 3.5 x 10^6, NACA Section 63A015

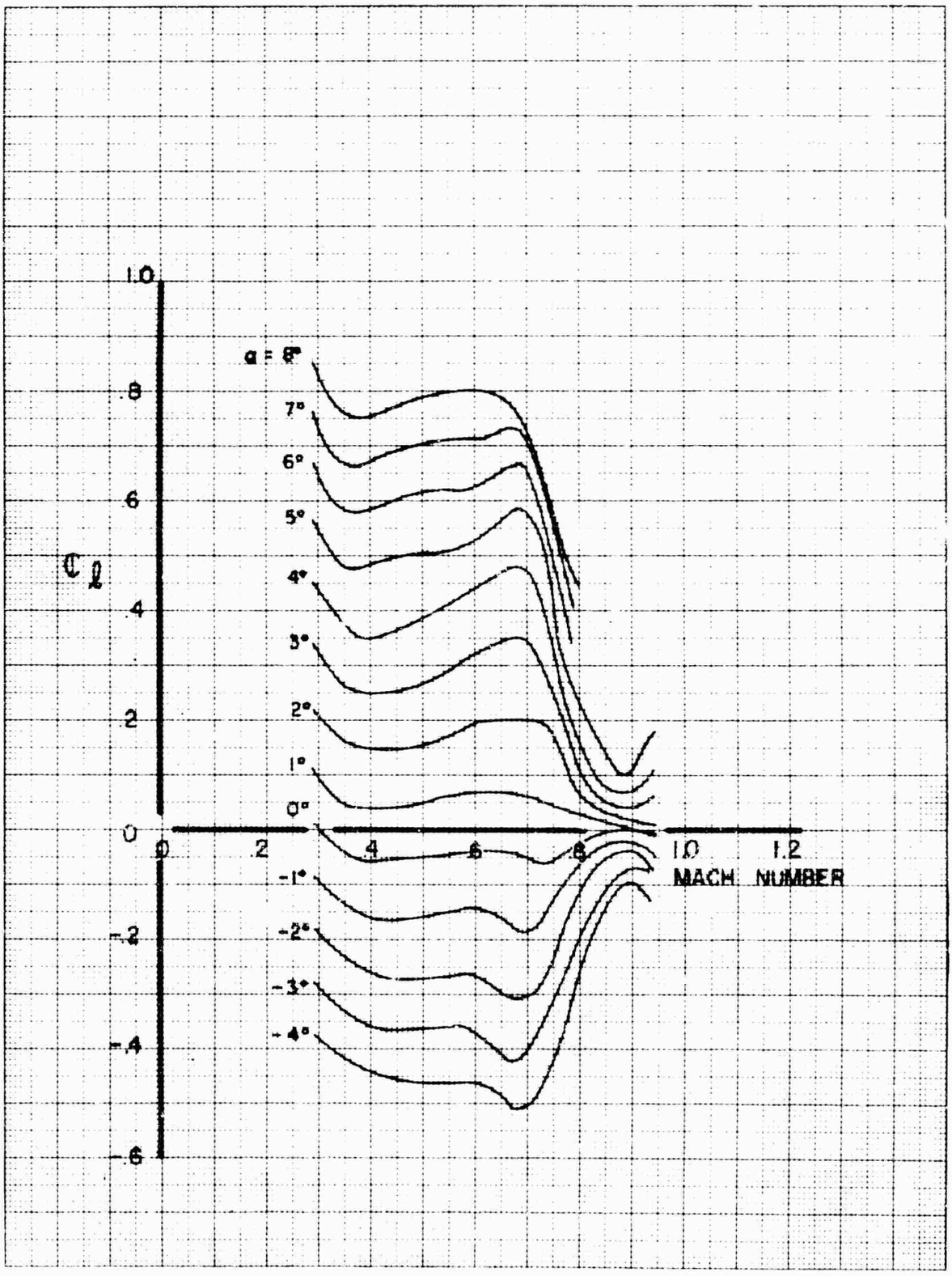


Figure 39D-1. Variation of Section Lift Coefficient With Mach Number at Constant Angle of Attack, $R = 3.5 \times 10^6$, NACA Section 63A018

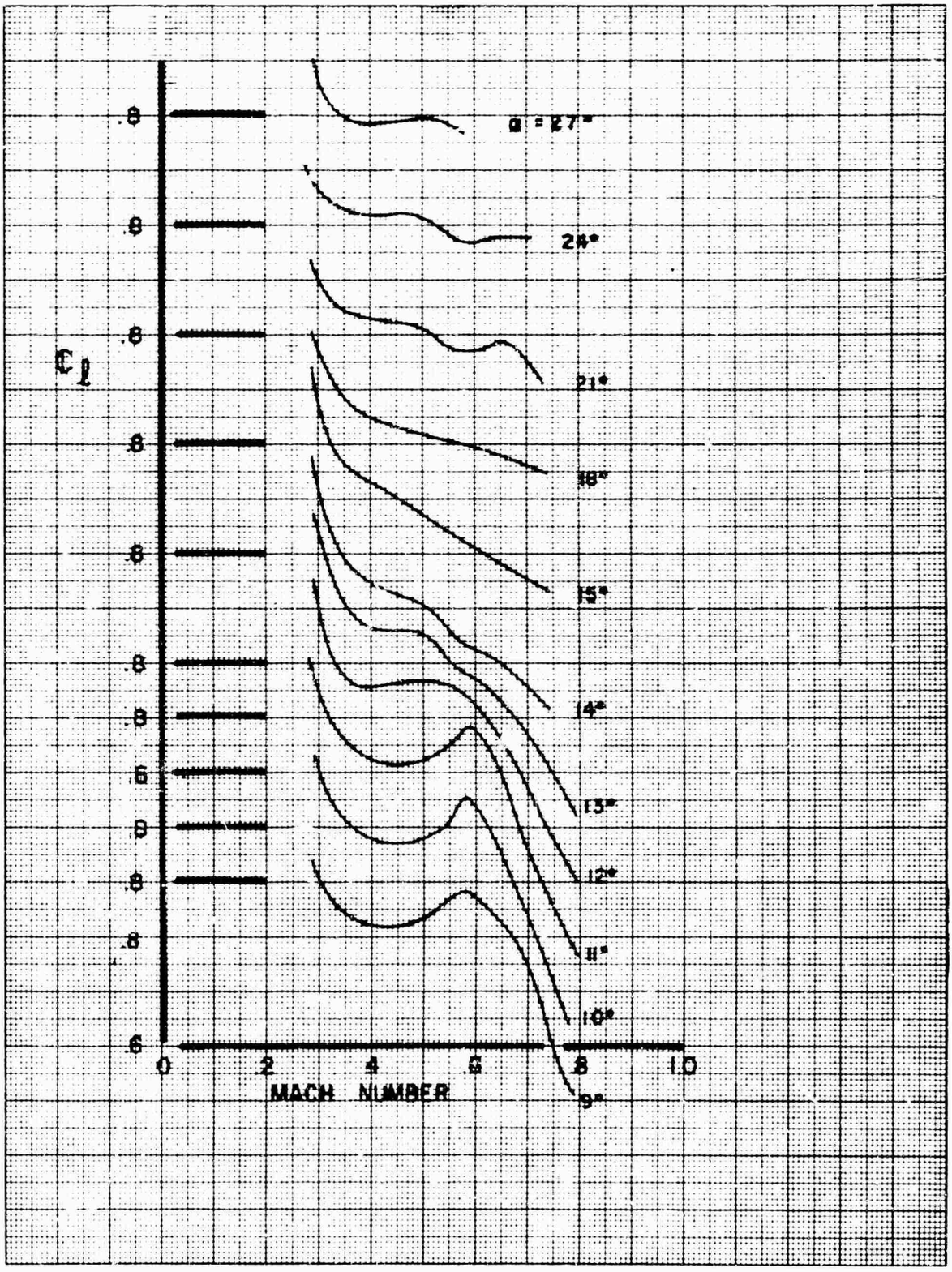


Figure 39D-2. Variation of Section Lift Coefficient With Mach Number at Constant Angle of Attack, R = 3.5×10^6, NACA Section 63A018

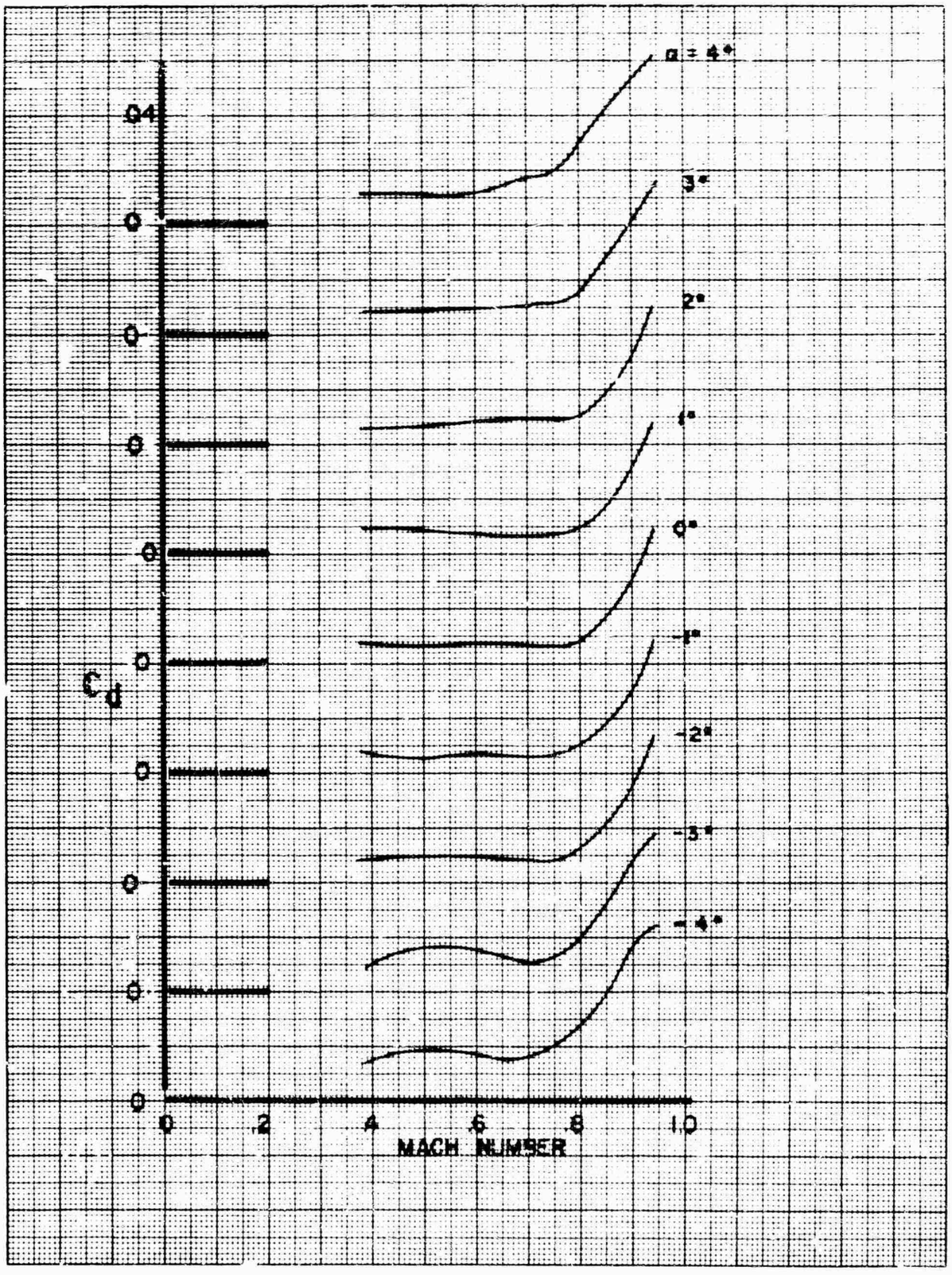


Figure 40A-1. Variation of Section Drag Coefficient With Mach Number at Constant Angle of Attack, R = 3.5 x 10^6, NACA Section 63A009

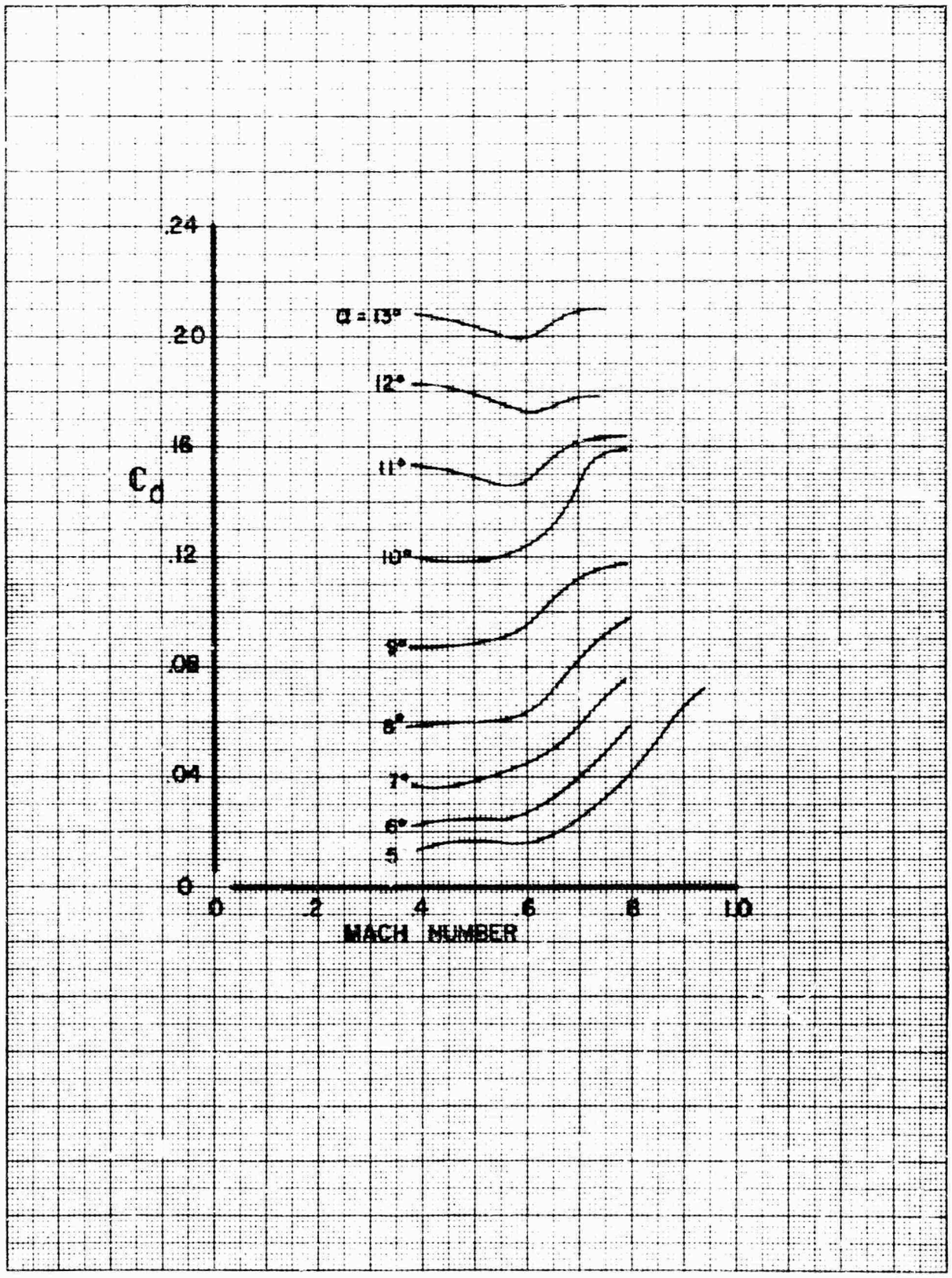


Figure 40A-2. Variation of Section Drag Coefficient With Mach Number at Constant Angle of Attack, R = 3.5×10^6 - NACA Section 63A009

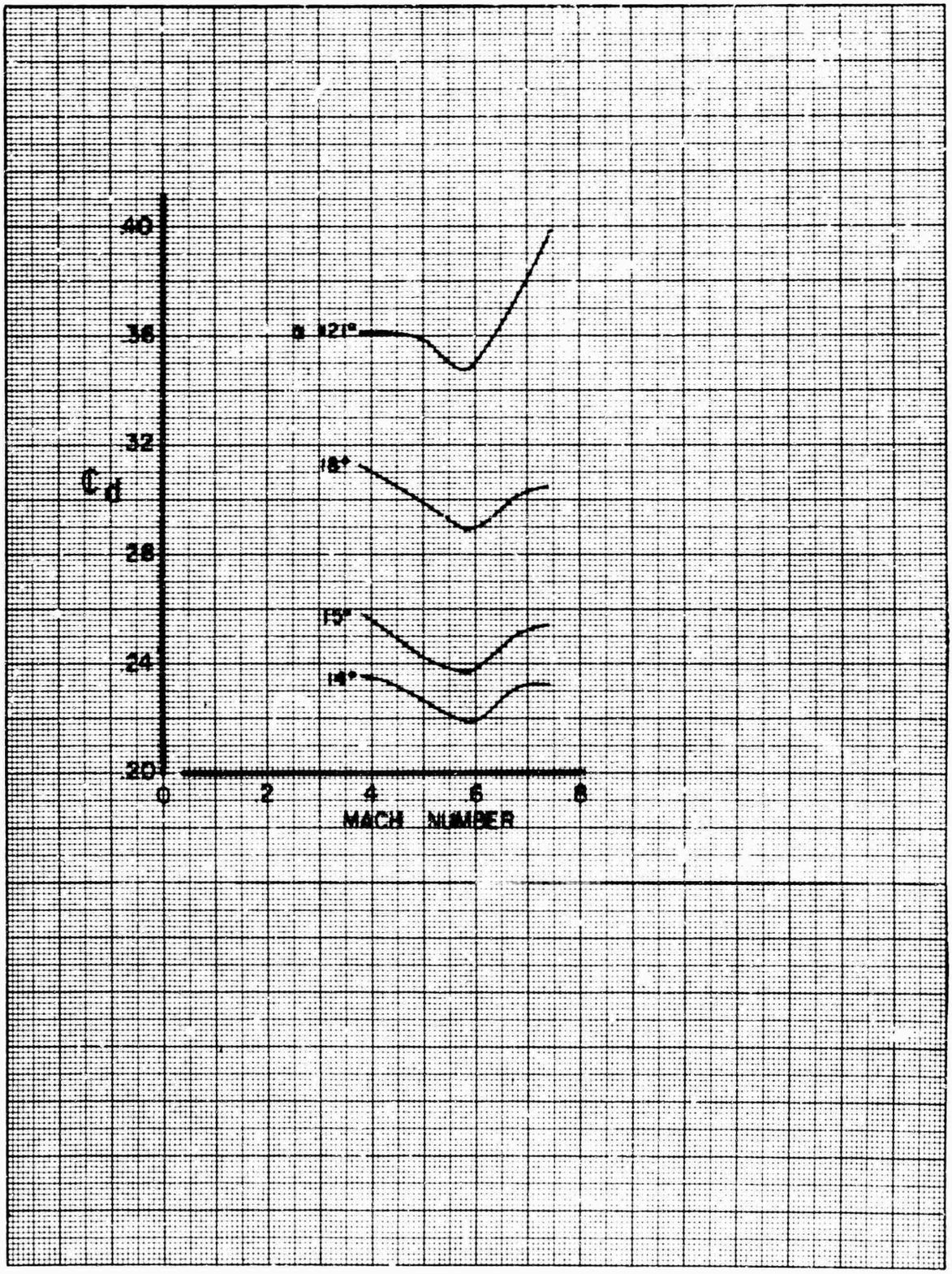


Figure 40A-3. Variation of Section Drag Coefficient With Mach Number at Constant Angle of Attack, R = 3.5×10^6, NACA Section 63A009

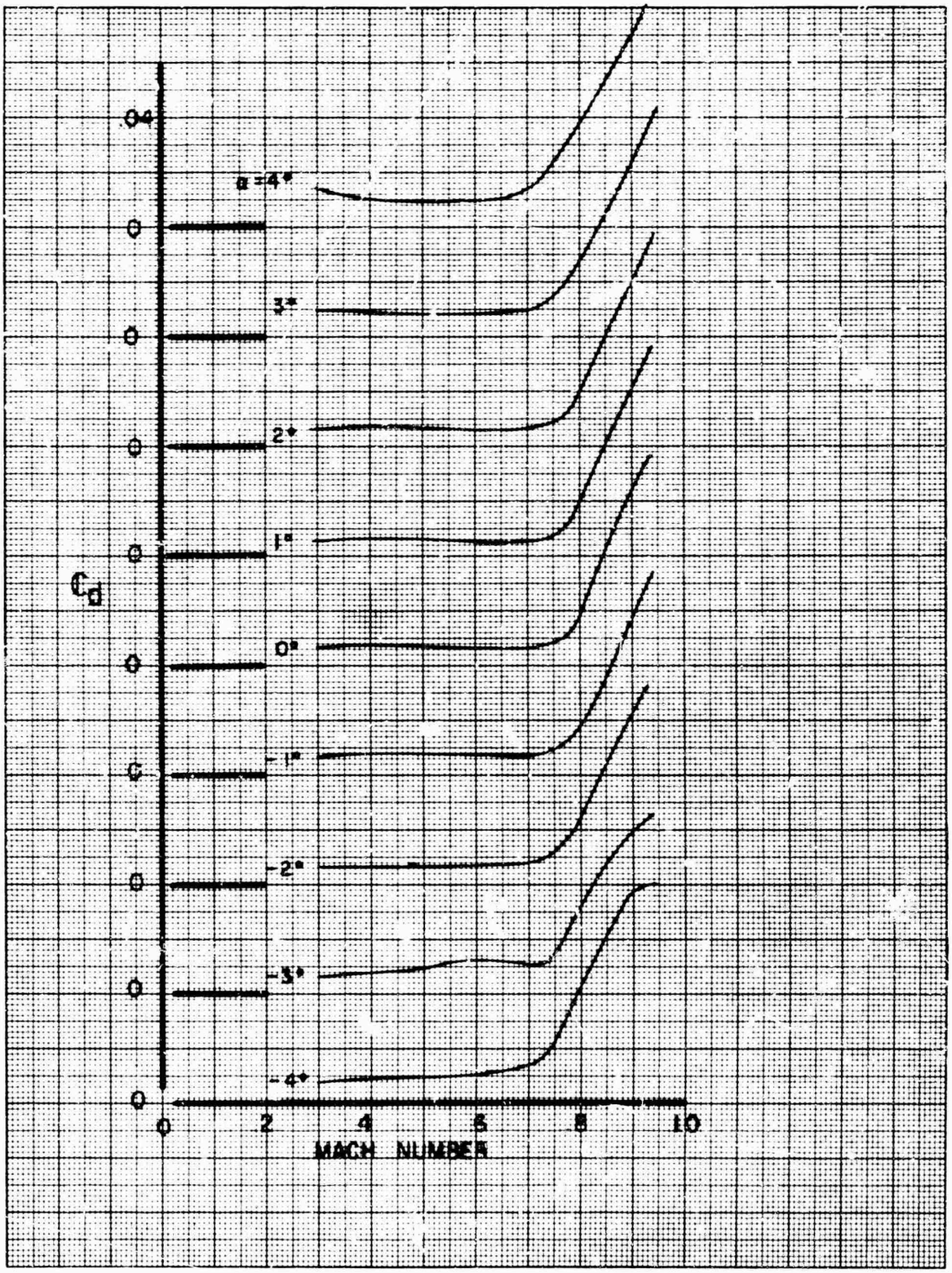


Figure 40B-1. Variation of Section Drag Coefficient With Mach Number at Constant Angle of Attack, R = 3.5×10^6, NACA Section 63A012

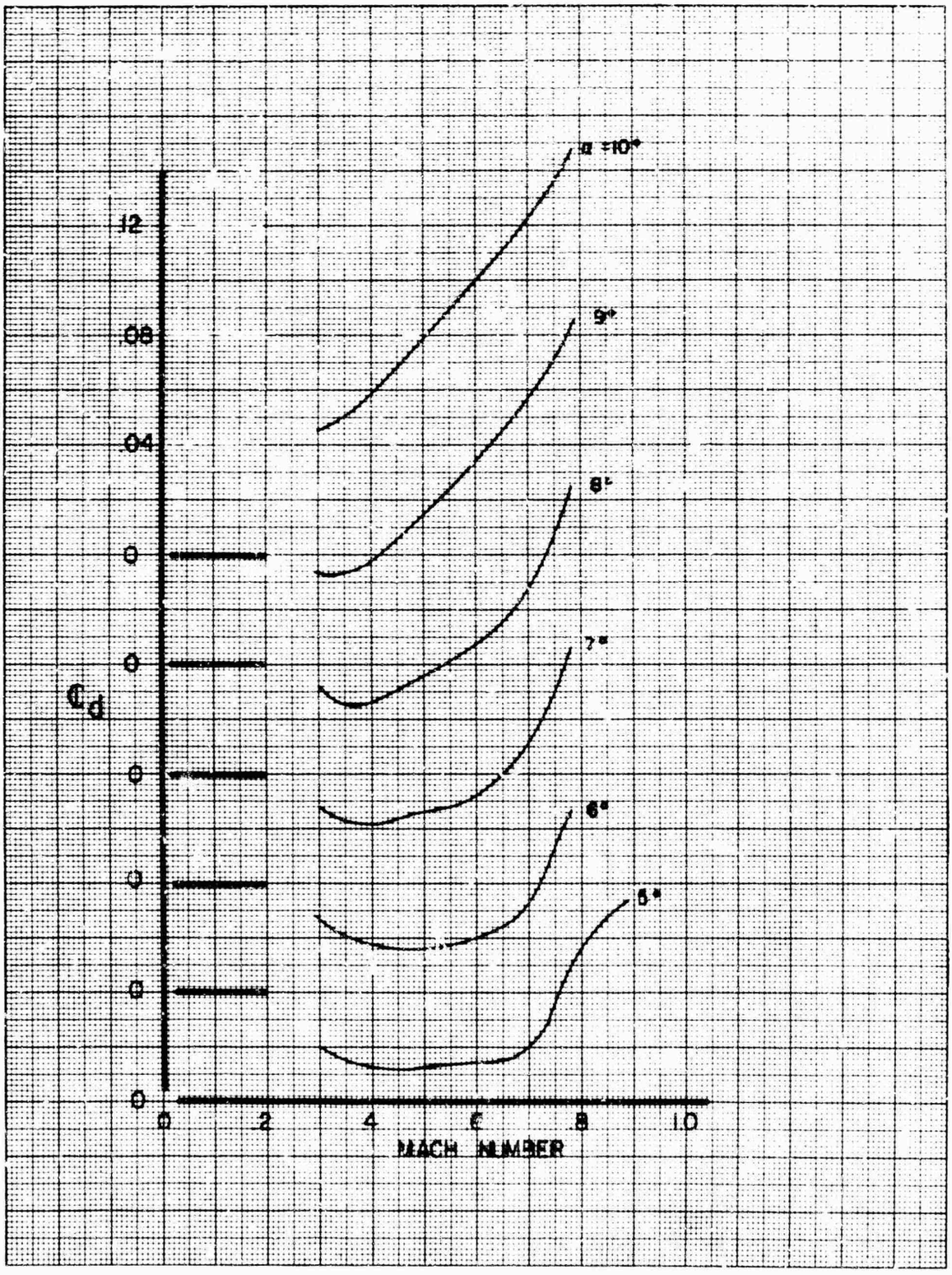


Figure 40B-2. Variation of Section Drag Coefficient With Mach Number at Constant Angle of Attack, R = 3.5 x 10^6, NACA Section 63A012

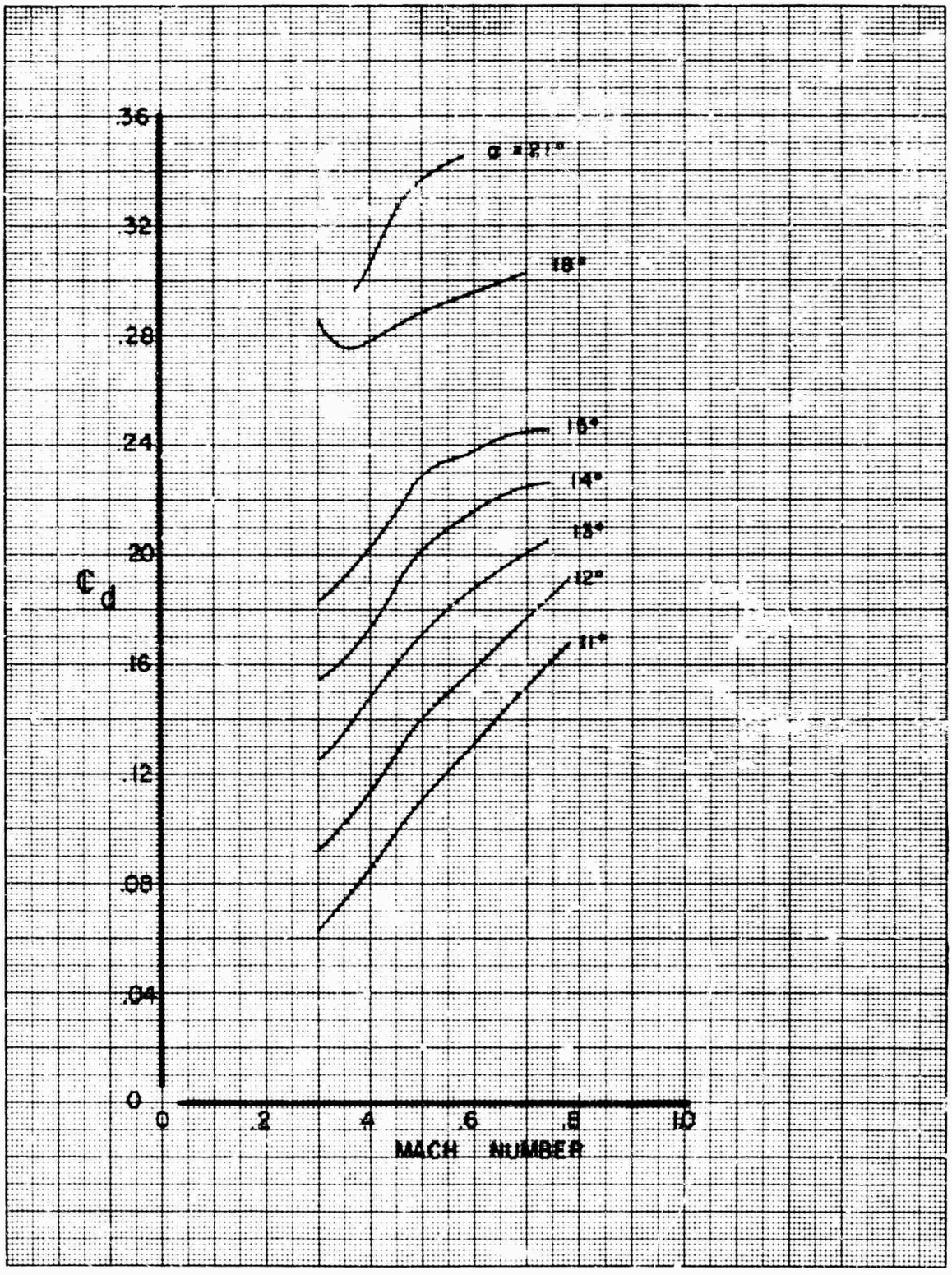


Figure 40B-3. Variation of Section Drag Coefficient With Mach Number at Constant Angle of Attack, R = 3.[illegible] x 10^6, NACA Section 63A012

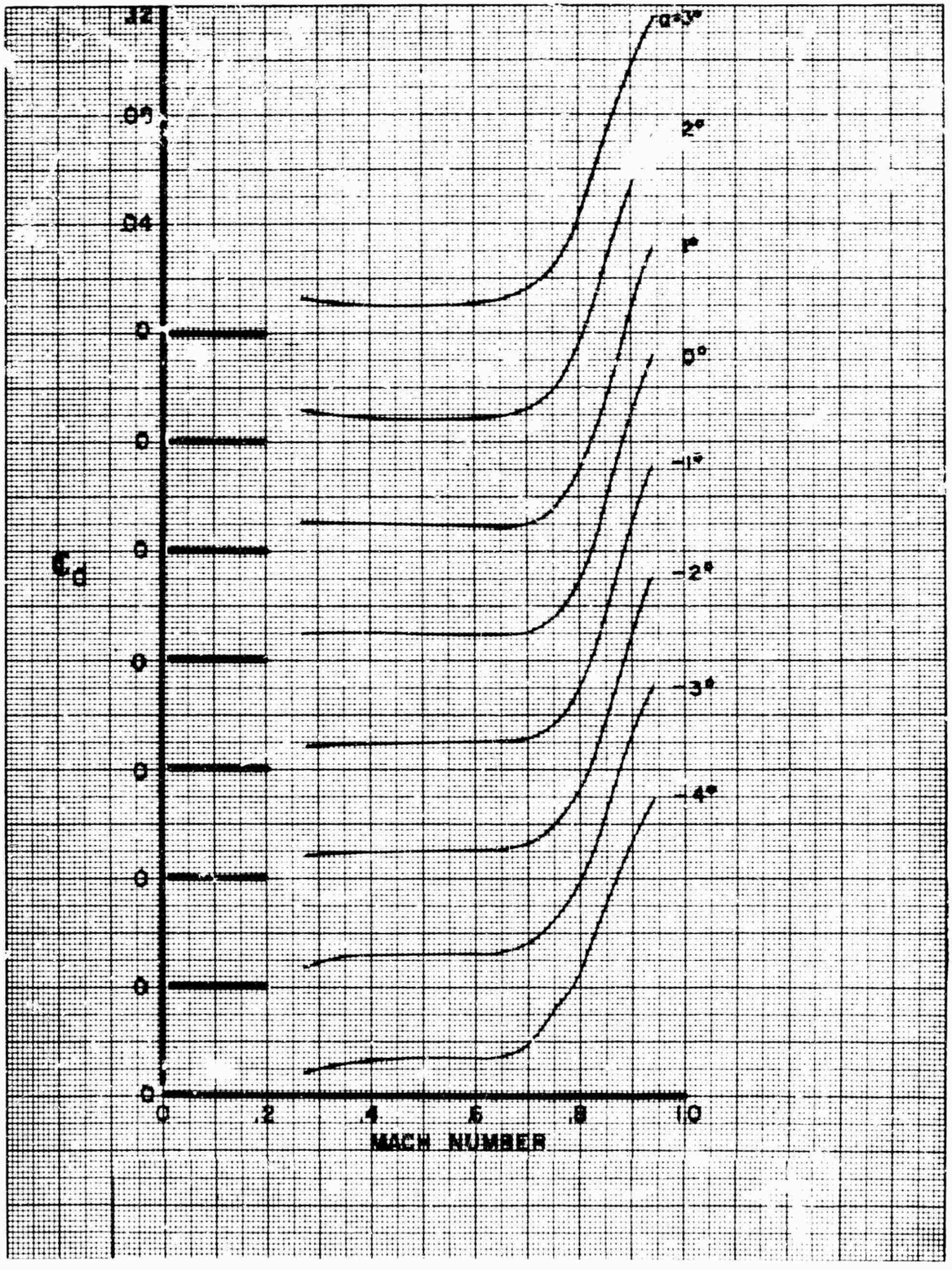


Figure 40C-1. Variation of Section Drag Coefficient With Mach Number at Constant Angle of Attack, R = 3.5 x 10^6, NACA Section 63A015

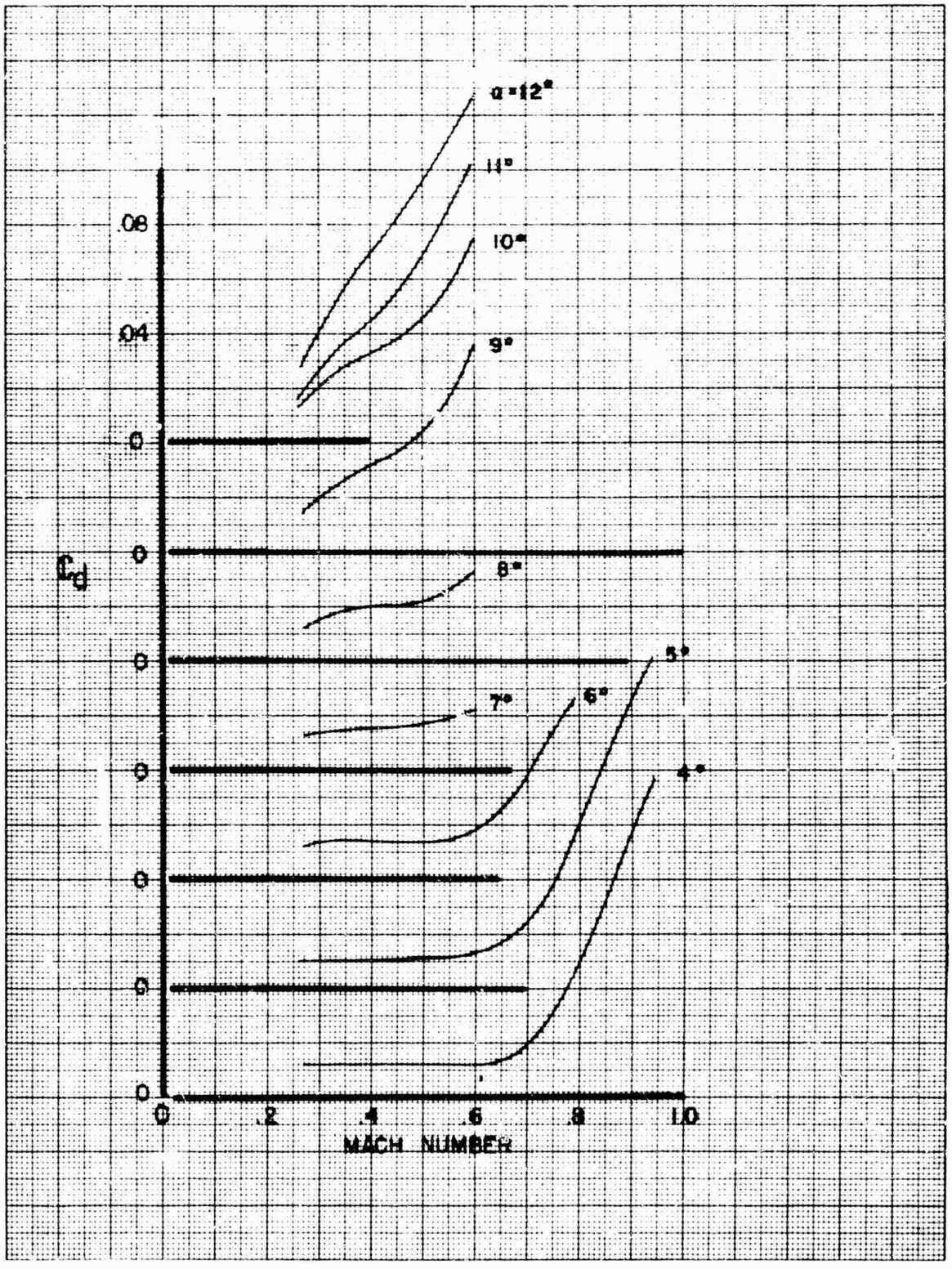


Figure 40C-2. Variation of Section Drag Coefficient With Mach Number at Constant Angle of Attack, R = 3.5 x 10^6, NACA Section 63A015

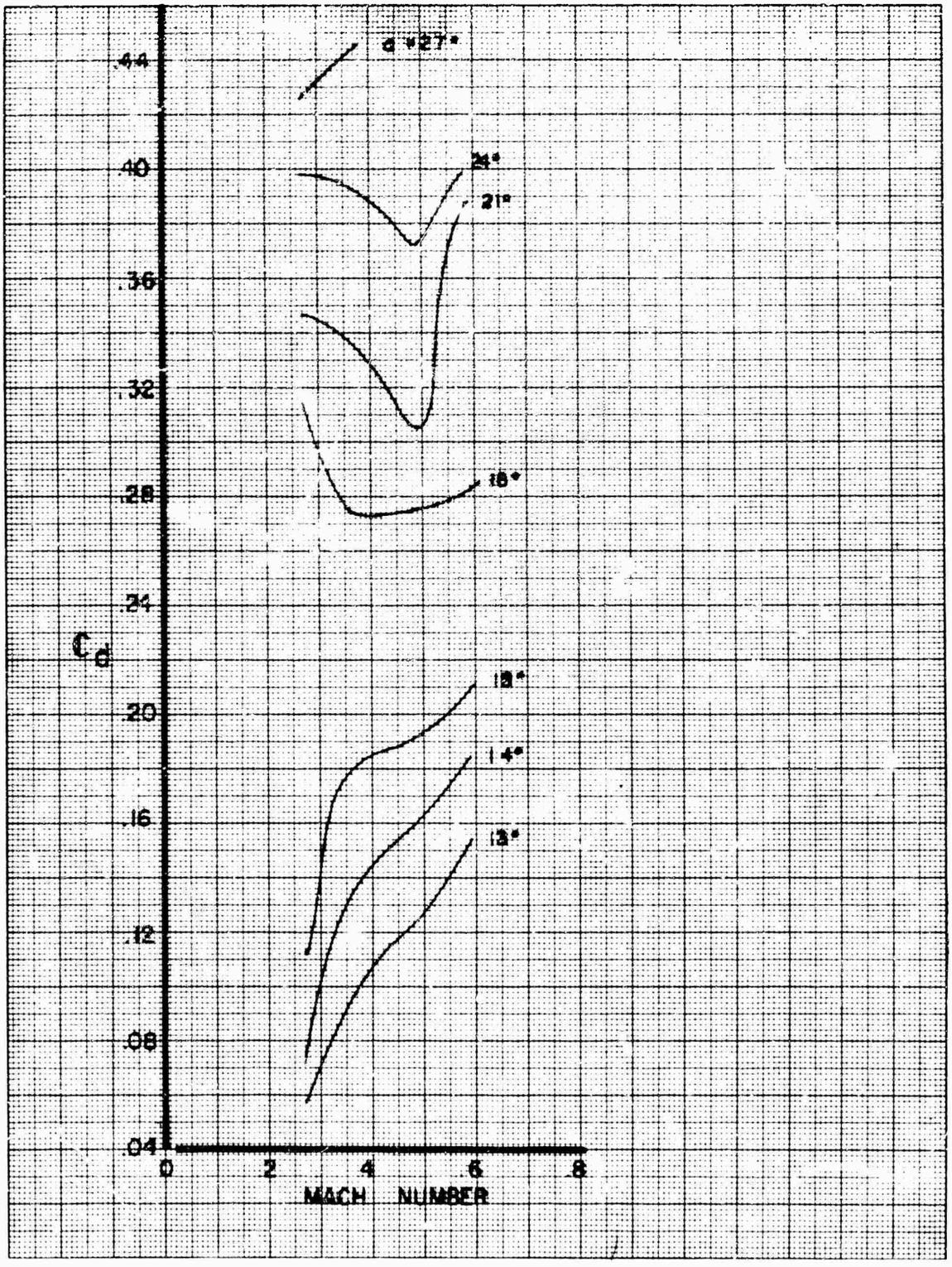


Figure 40C-3. Variation of Section Drag Coefficient With Mach Number at Constant Angle of Attack, R = 3.5 x 10^6, NACA Section 63A015

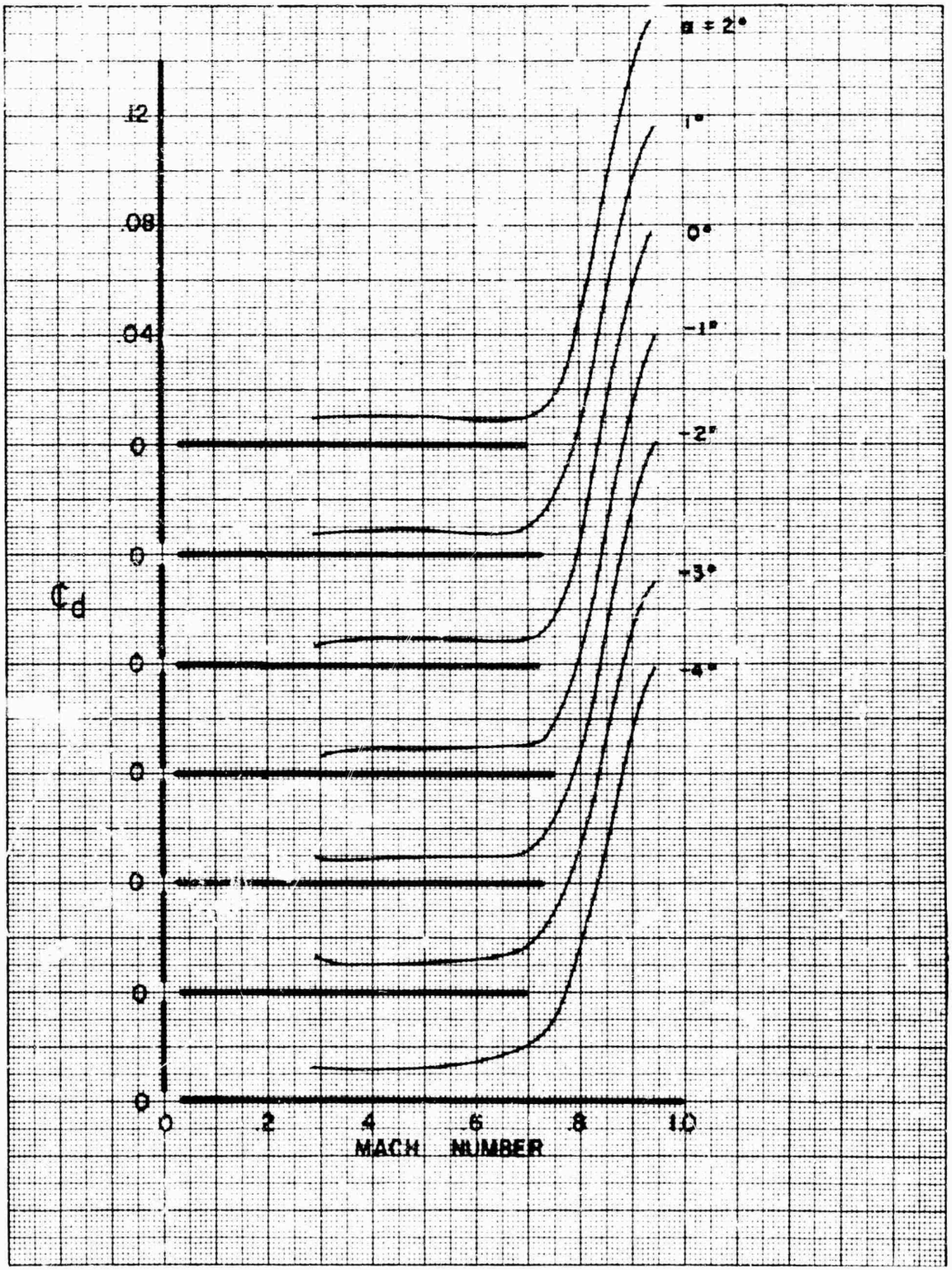


Figure 40D-1. Variation of Section Drag Coefficient With Mach Number at Constant Angle of Attack, R = 3.5 x 10^6, NACA Section 63A018

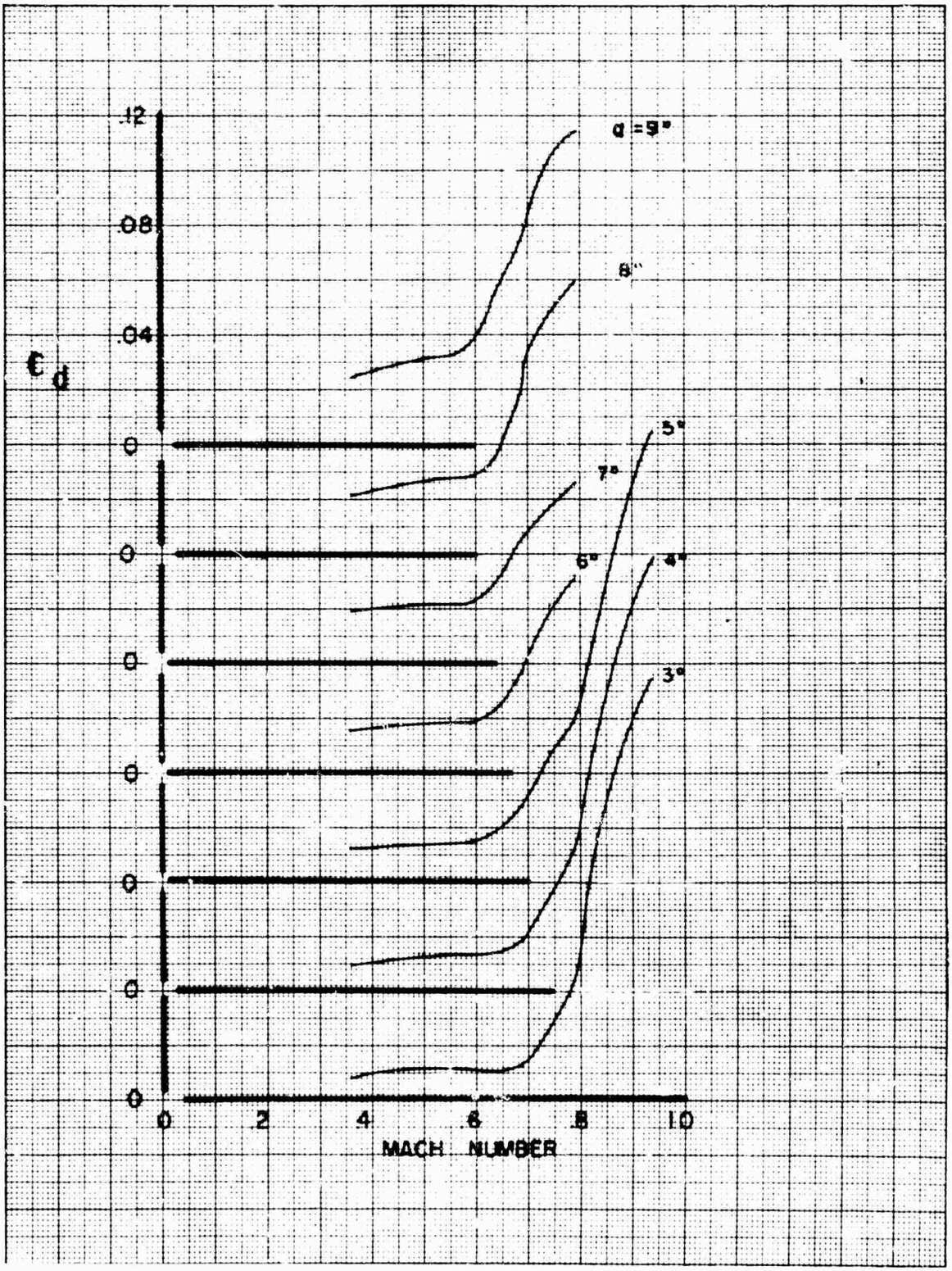


Figure 40D-2. Variation of Section Drag Coefficient With Mach Number at Constant Angle of Attack, R = 3.5 x 10^6, NACA Section 63A018

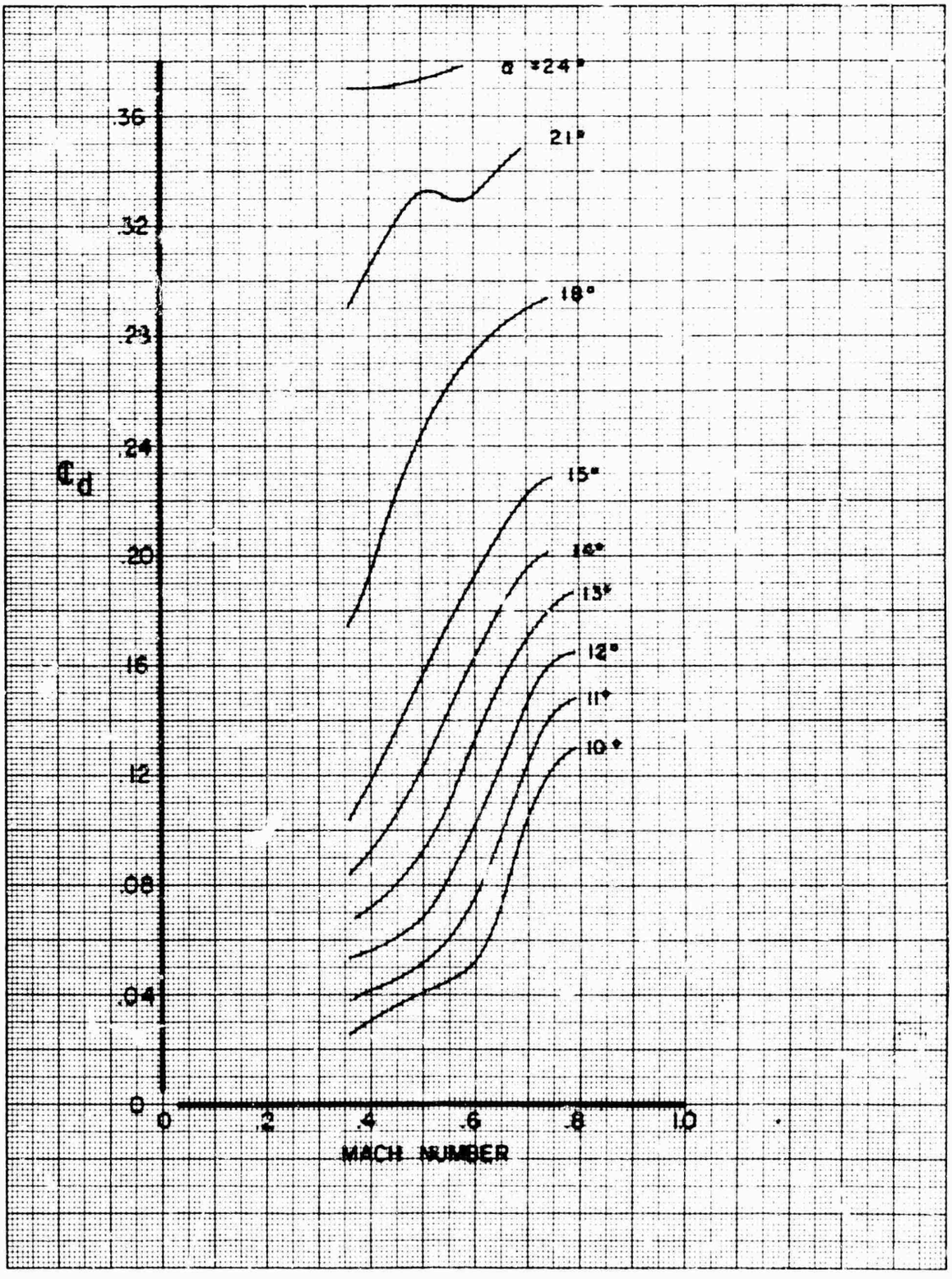


Figure 40D-3. Variation of Section Drag Coefficient With Mach Number at Constant Angle of Attack, R = 3.5 x 10^6, NACA Section 63A018

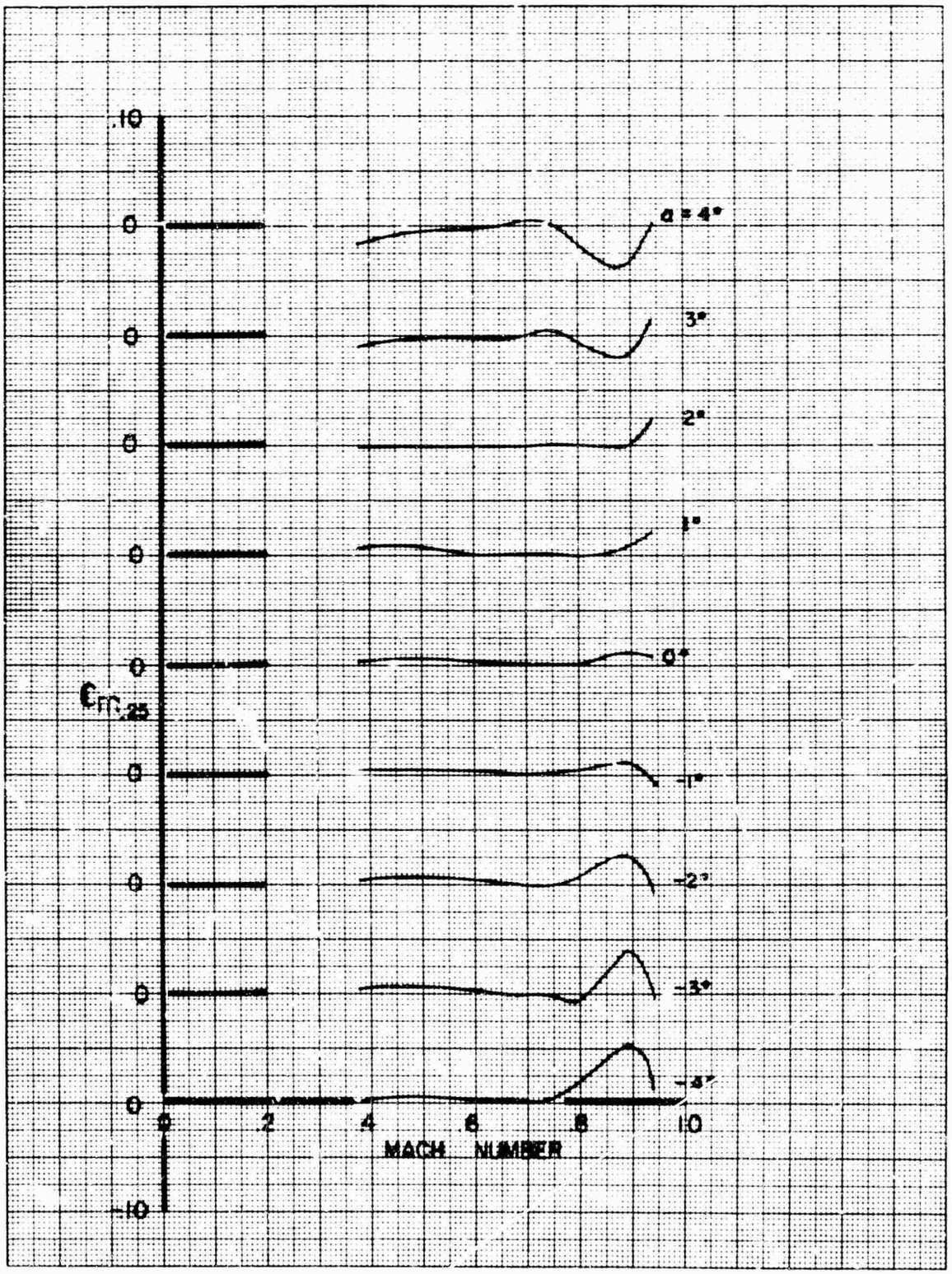


Figure 41A-1. Variation of Section Pitching Moment Coefficient With Mach Number at Constant Angle of Attack, $R = 3.5 \times 10^6$, NACA Section 63A009

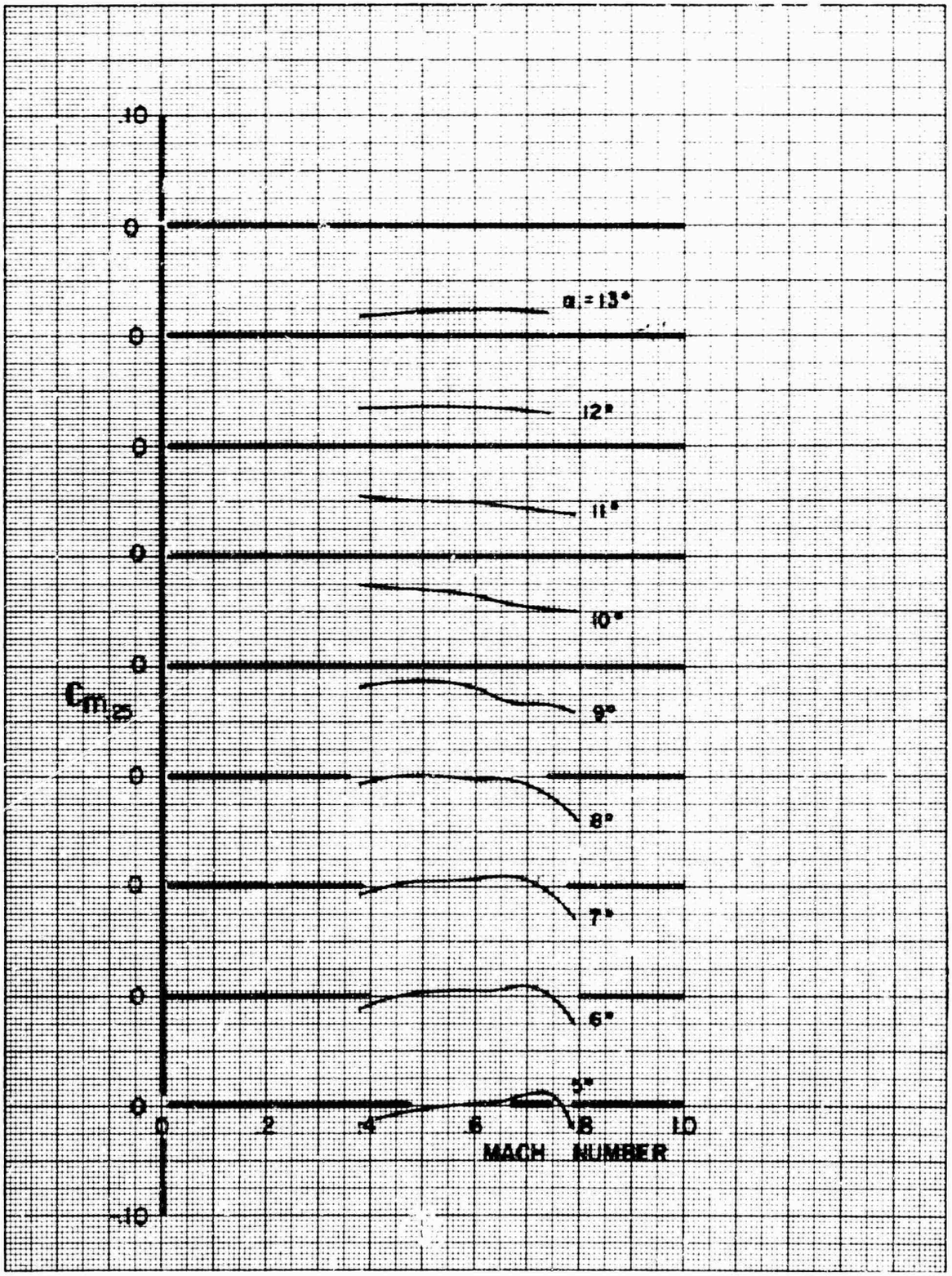


Figure 41A-2. Variation of Section Pitching Moment Coefficient With Mach Number at Constant Angle of Attack, R = 3.5 x 10^6, NACA Section 63A009

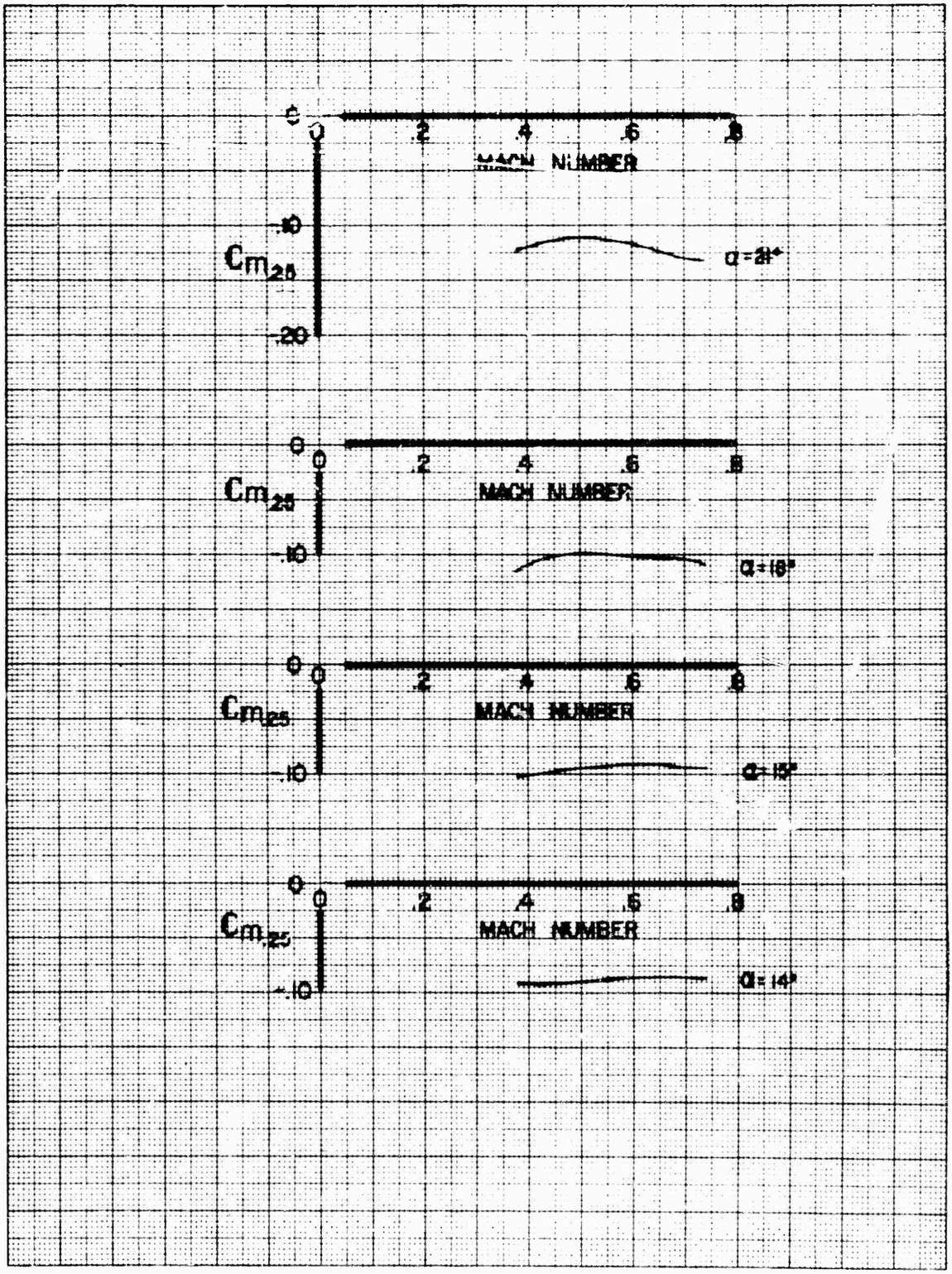


Figure 41A-3. Variation of Section Pitching Moment Coefficient With Mach Number at Constant Angle of Attack, R = 3.5 x 10^6, NACA Section 63A009

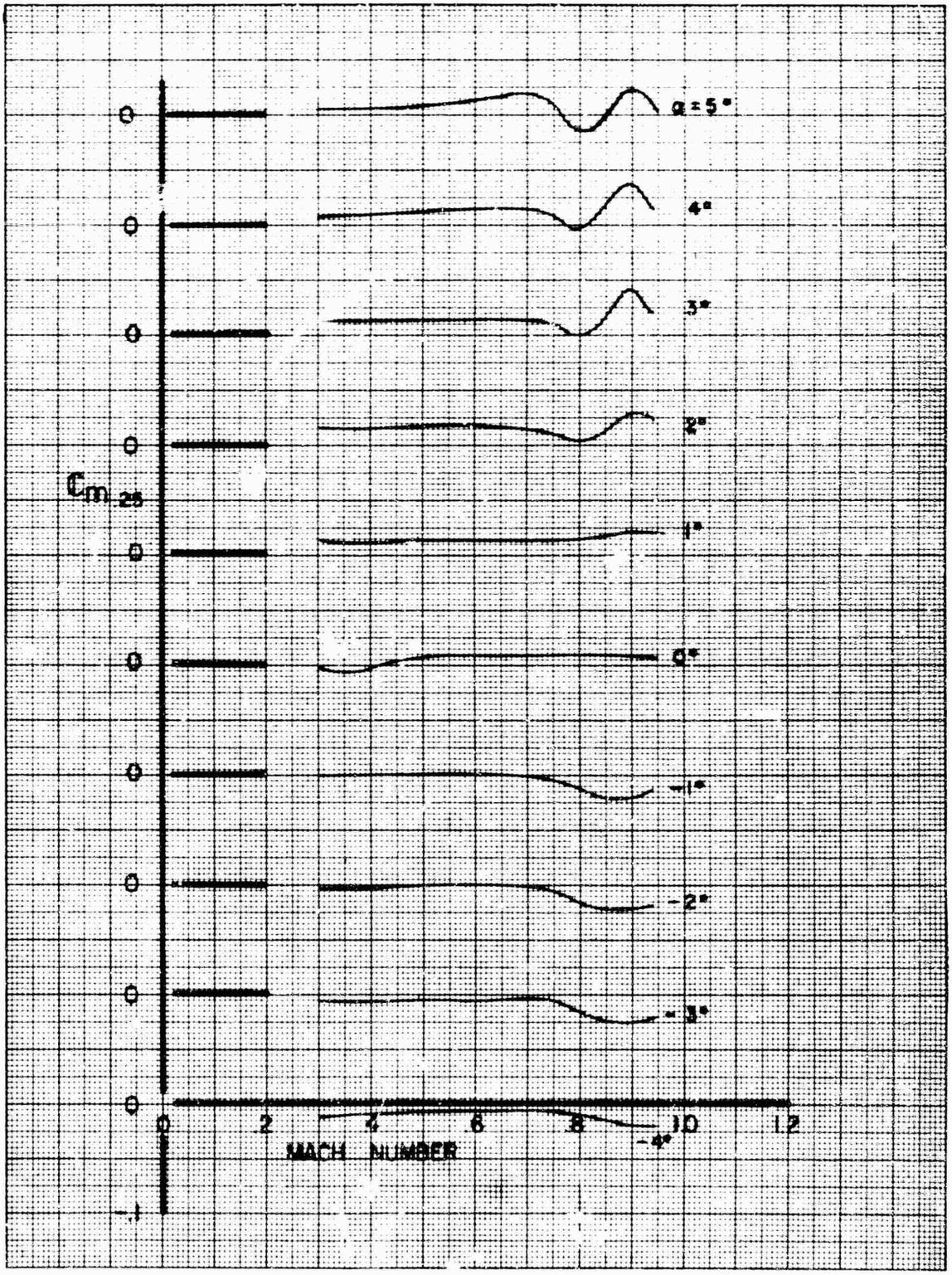


Figure 41B-1. Variation of Section Pitching Moment Coefficient With Mach Number at Constant Angle of Attack, R = 3.5 x 10^6, NACA Section 63A012

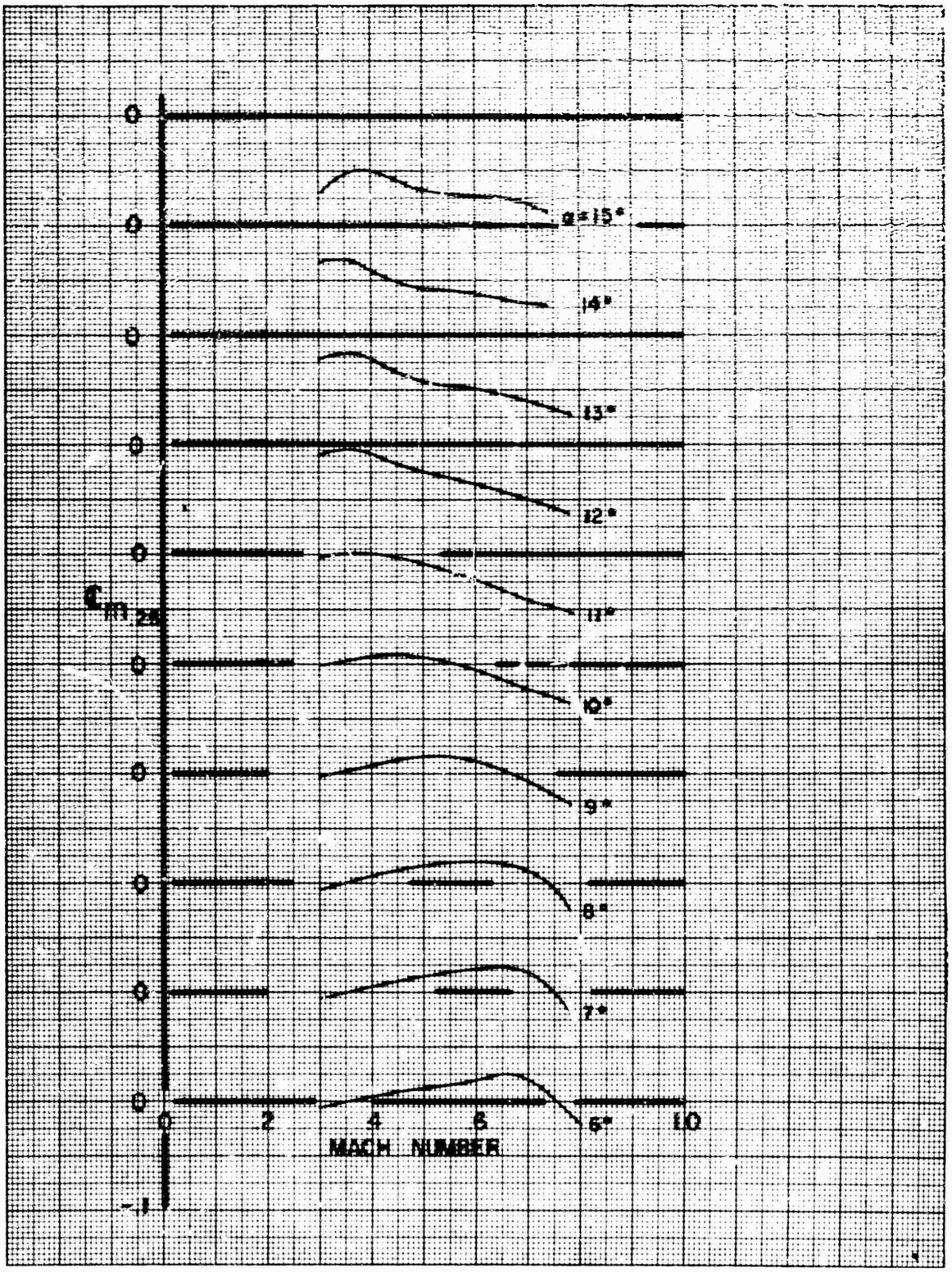


Figure 41B-2. Variation of Section Pitching Moment Coefficient With Mach Number at Constant Angle of Attack, R = 3.5×10^6, NACA Section 63A012

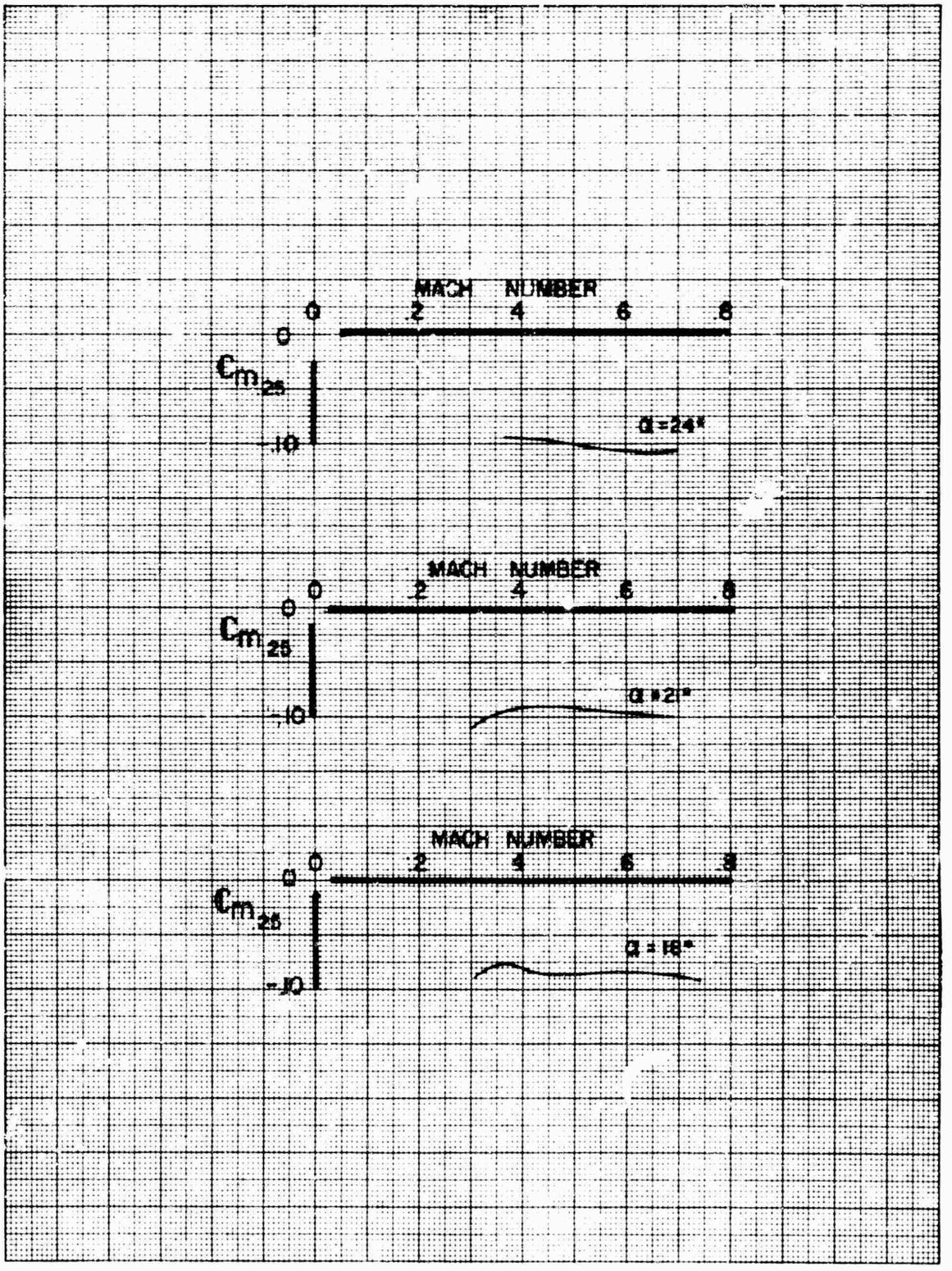


Figure 41B-3. Variation of Section Pitching Moment Coefficient With Mach Number at Constant Angle of Attack, R = 3.5 x 10^6 - NACA Section 63A012

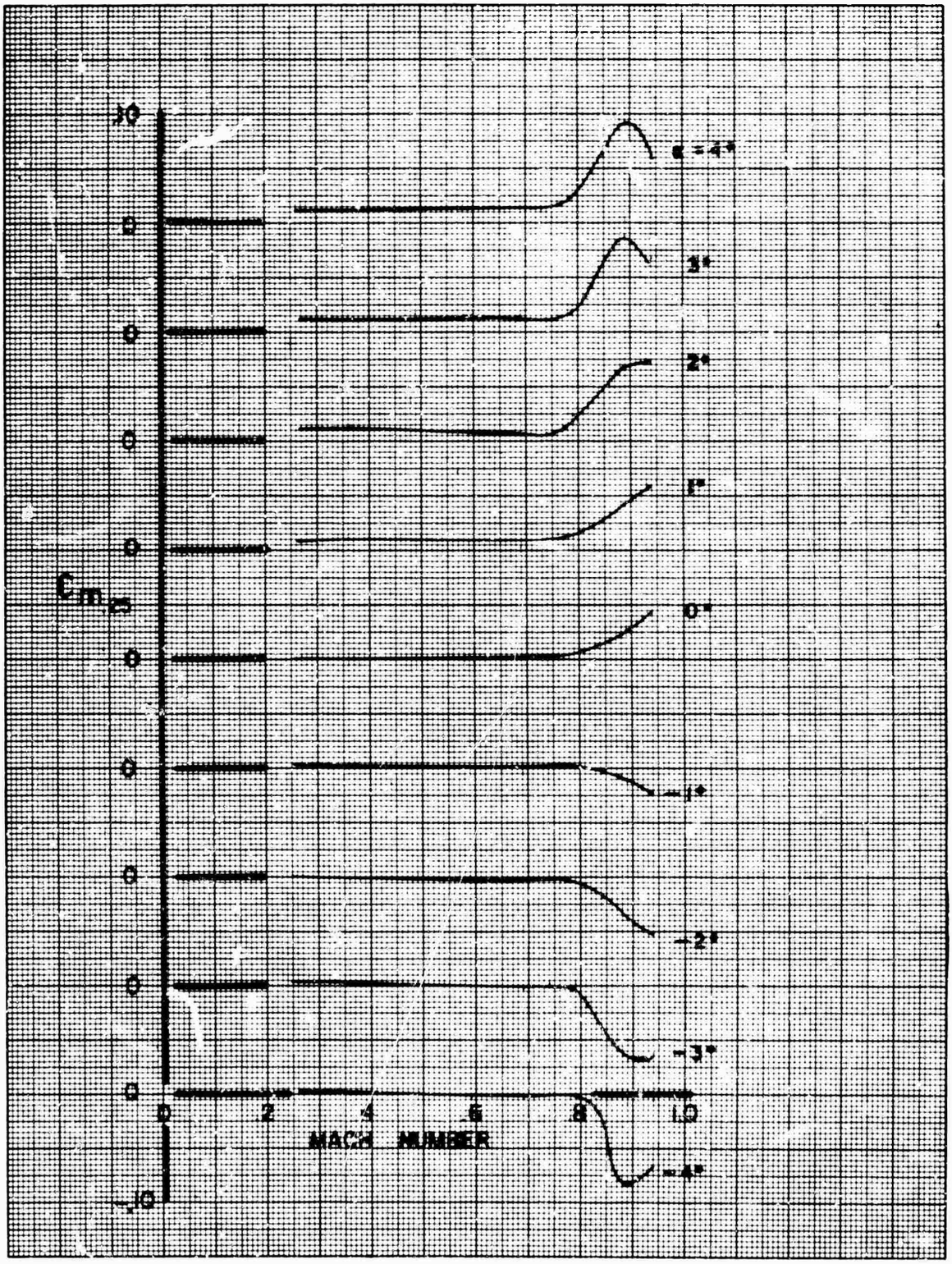


Figure 41C-1. Variation of Section Pitching Moment Coefficient With Mach Number at Constant Angle of Attack, R = 3.5 x 10^6, NACA Section 63A015

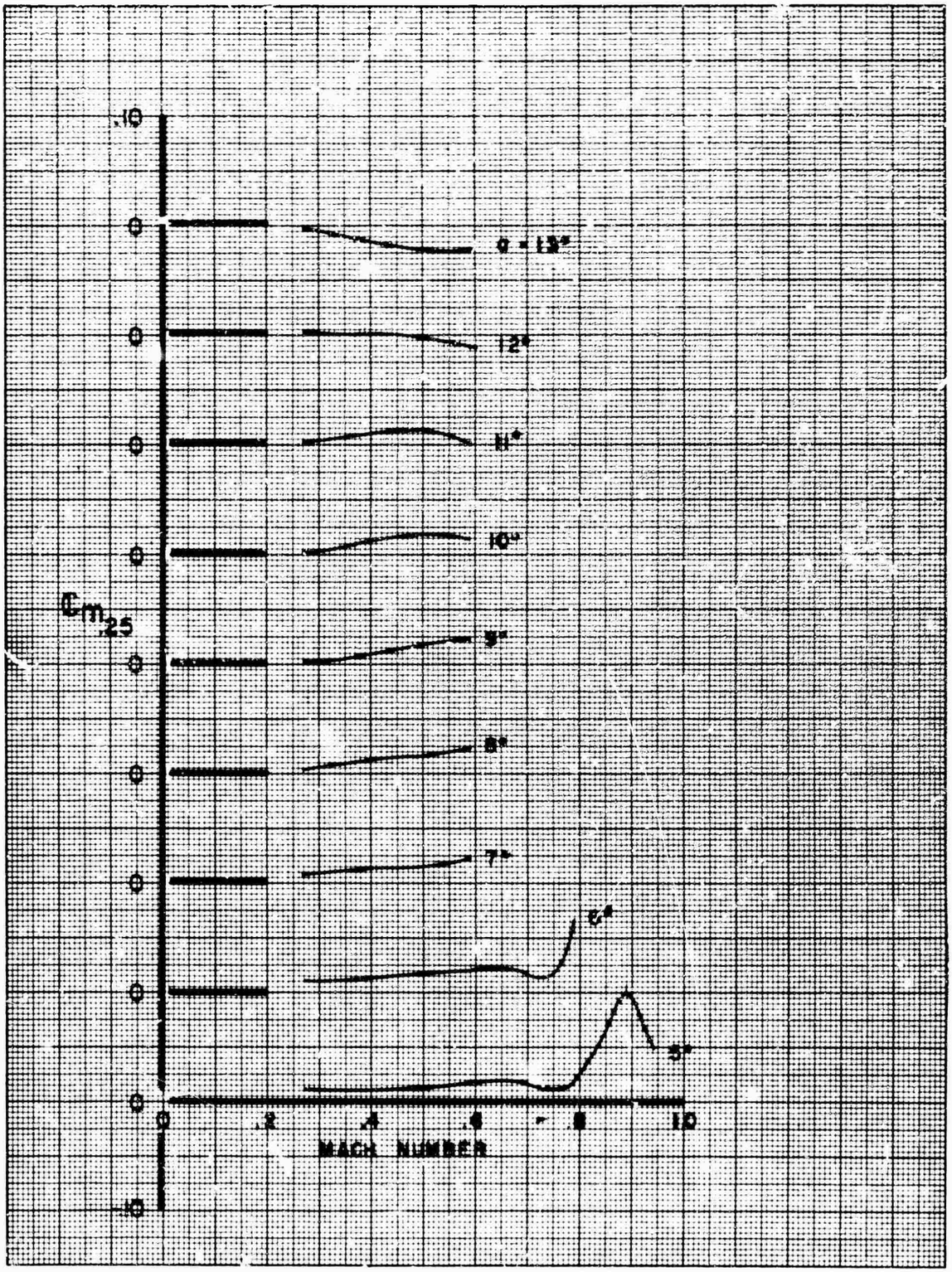


Figure 41C-2. Variation of Section Pitching Moment Coefficient With Mach Number at Constant Angle of Attack, R = 3.5 x 10^6, NACA Section 63A015

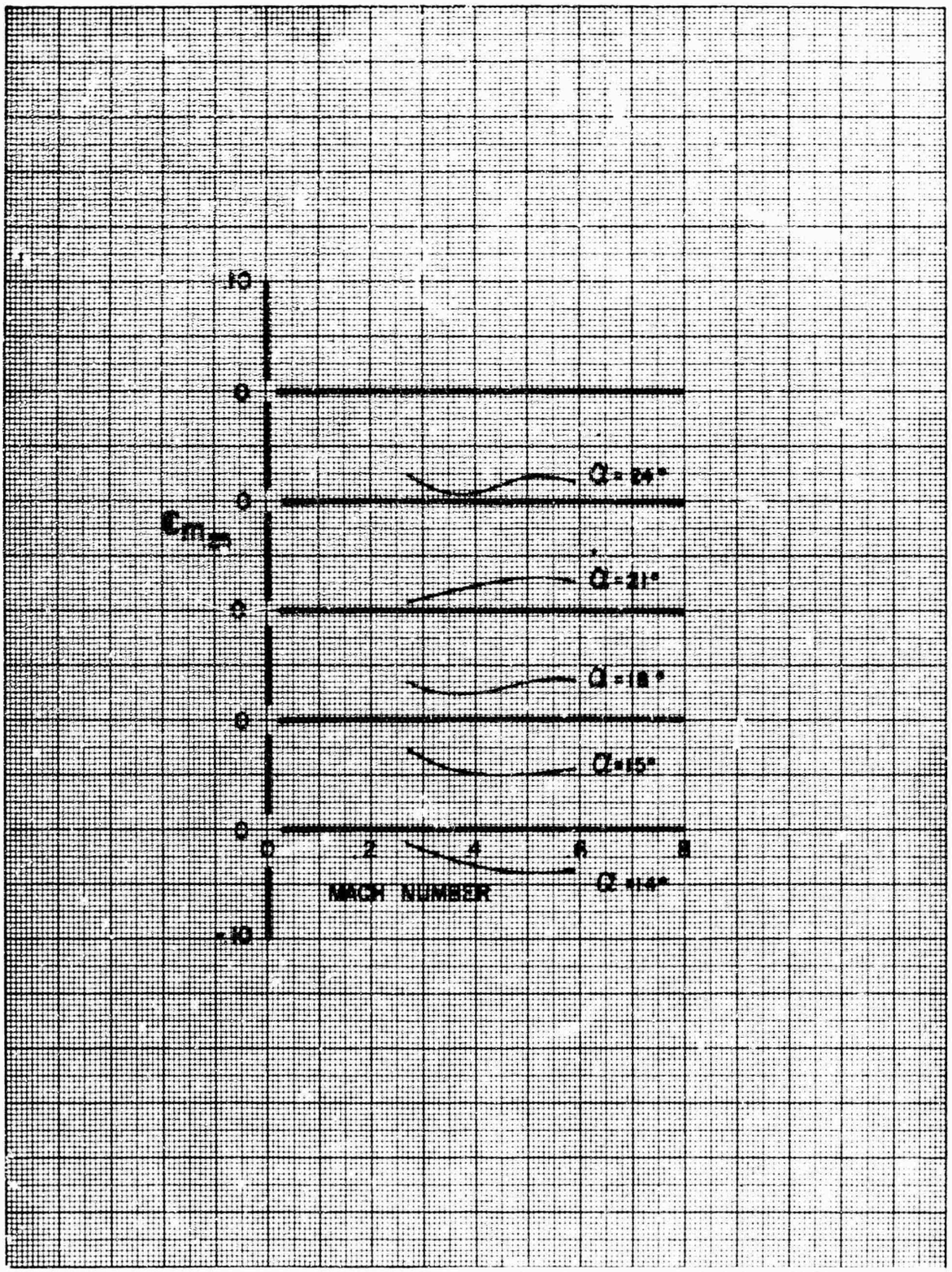


Figure 41C-3. Variation of Section Pitching Moment Coefficient With Mach Number at Constant Angle of Attack, $R = 3.5 \times 10^6$, NACA Section 63A015

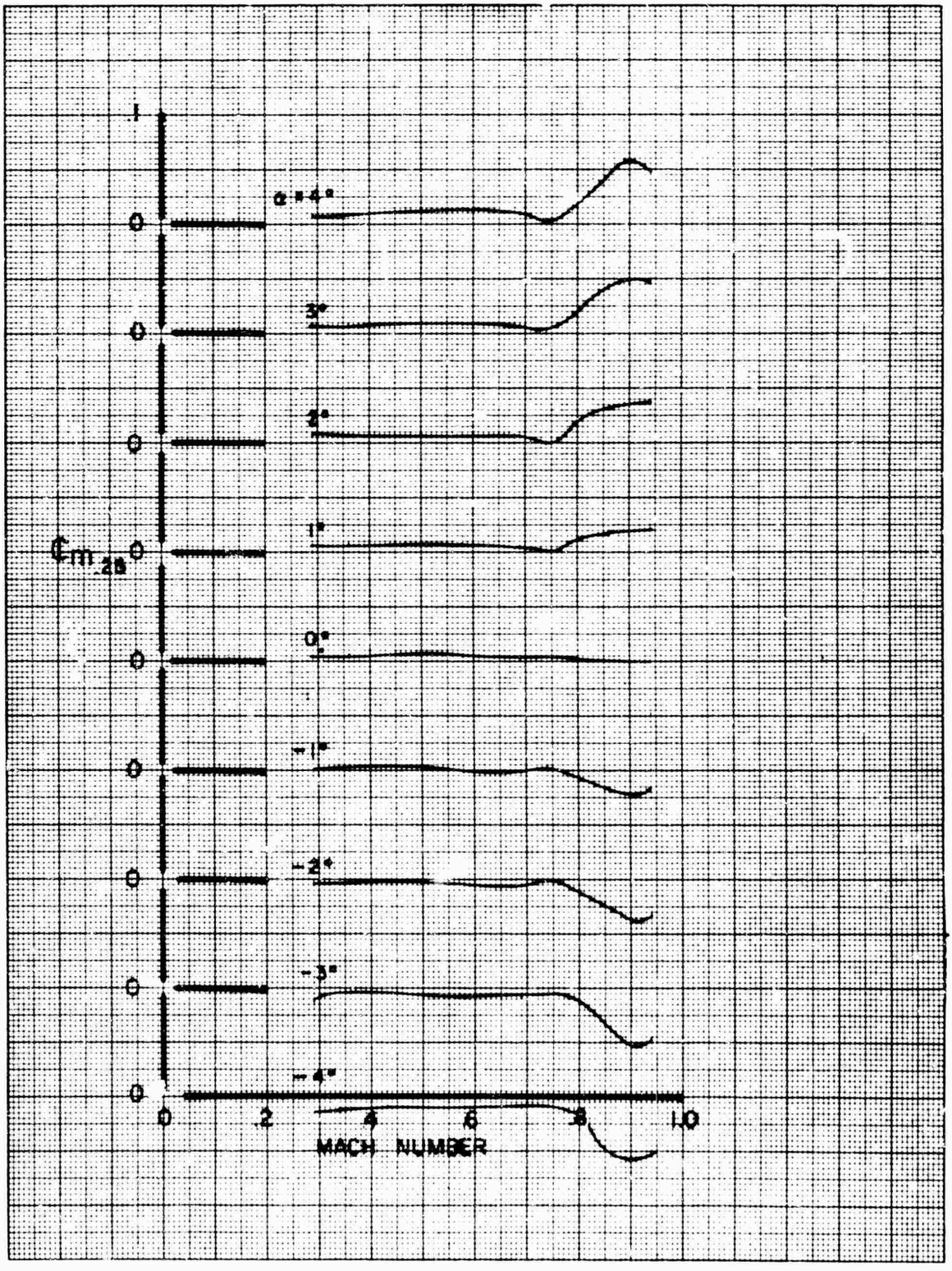


Figure 41D-1. Variation of Section Pitching Moment Coefficient With Mach Number at Constant Angle of Attack, R = 3.5 x 10^6, NACA Section 63A018

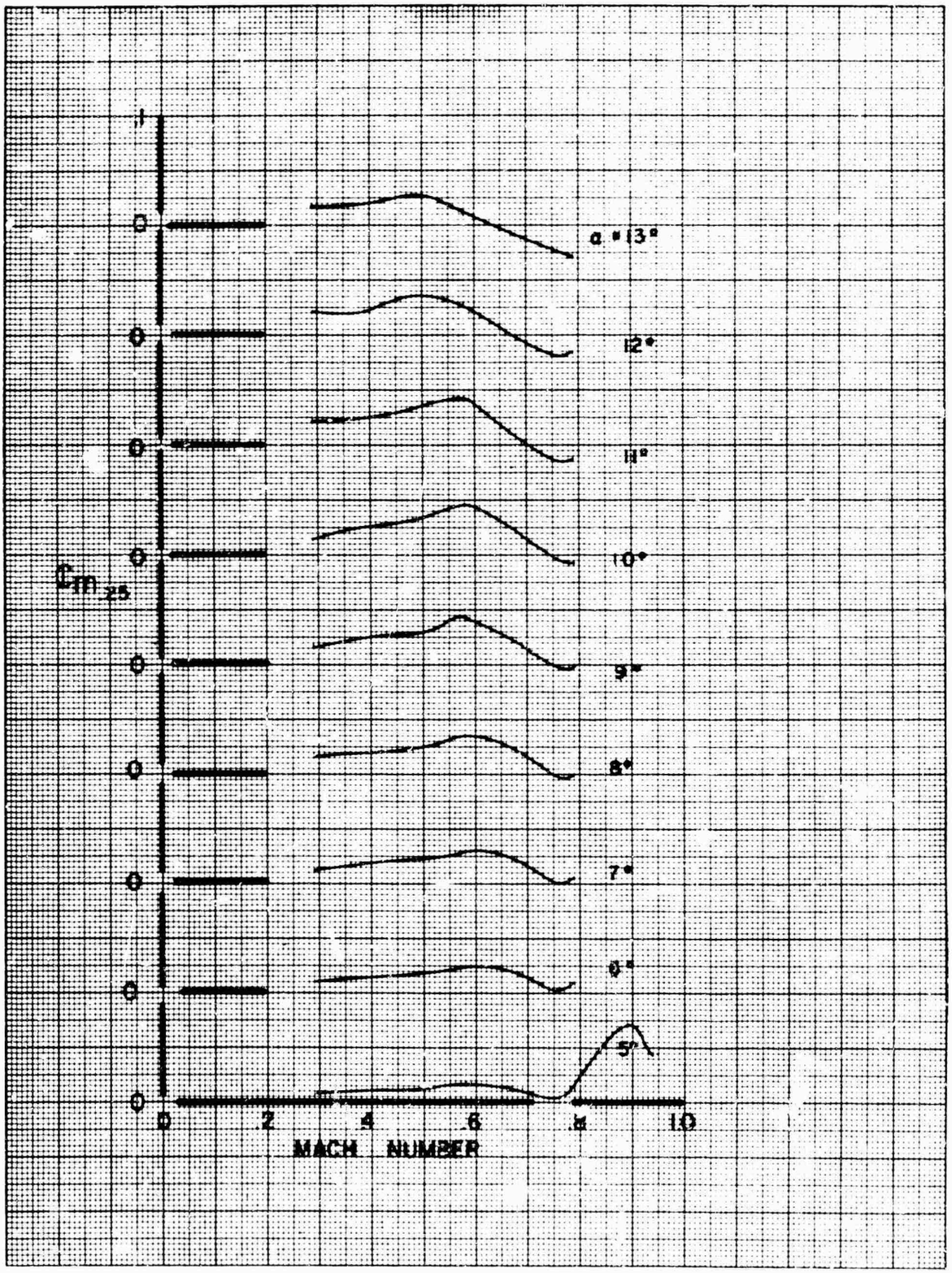


Figure 41D-2. Variation of Section Pitching Moment Coefficient With Mach Number at Constant Angle of Attack, $R = 3.5 \times 10^6$, NACA Section 63A018

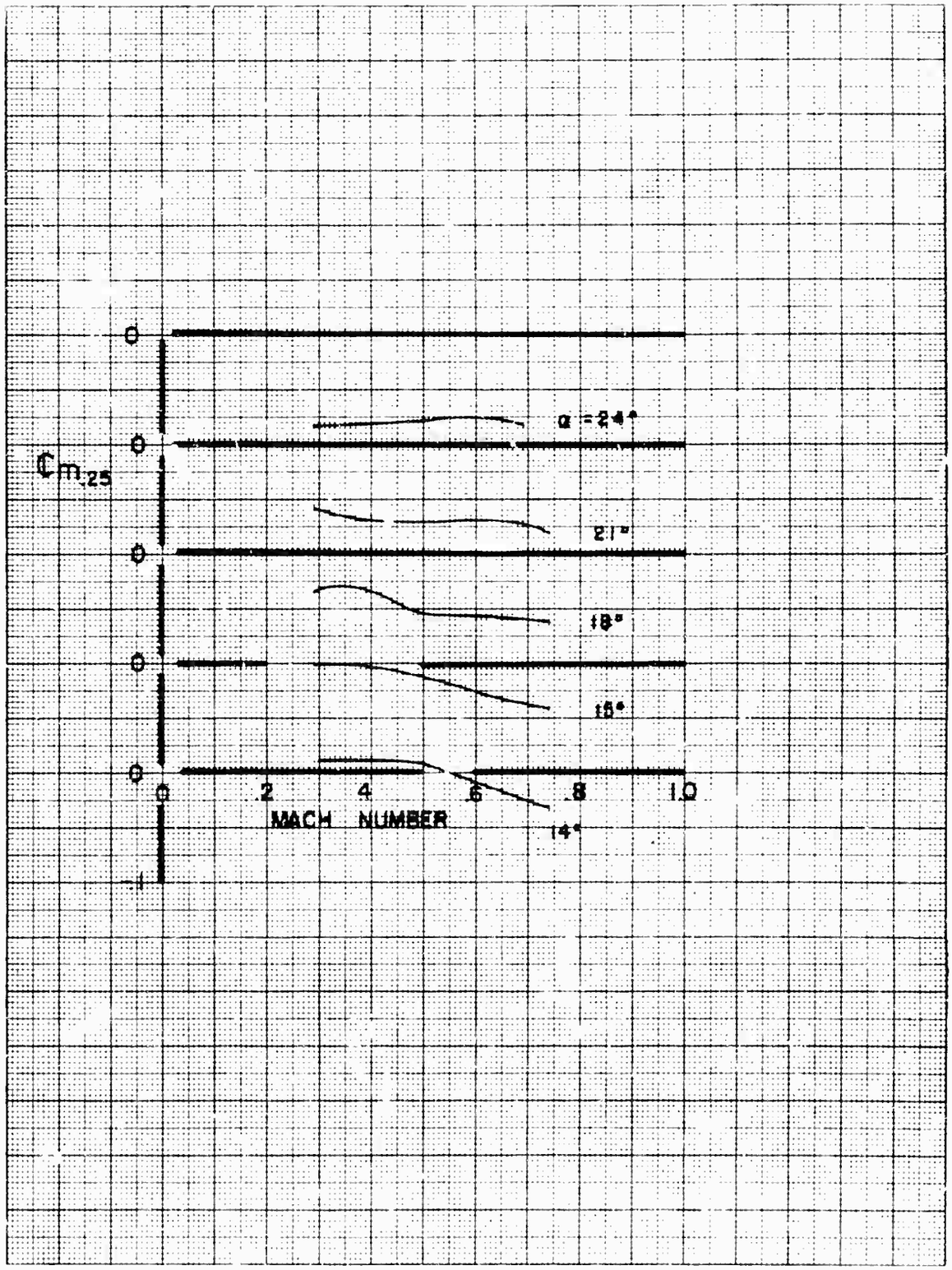


Figure 4!D-3. Variation of Section Pitching Moment Coefficient With Mach Number at Constant Angle of Attack, R = ² 5 x 10^6, NACA Section 63A018

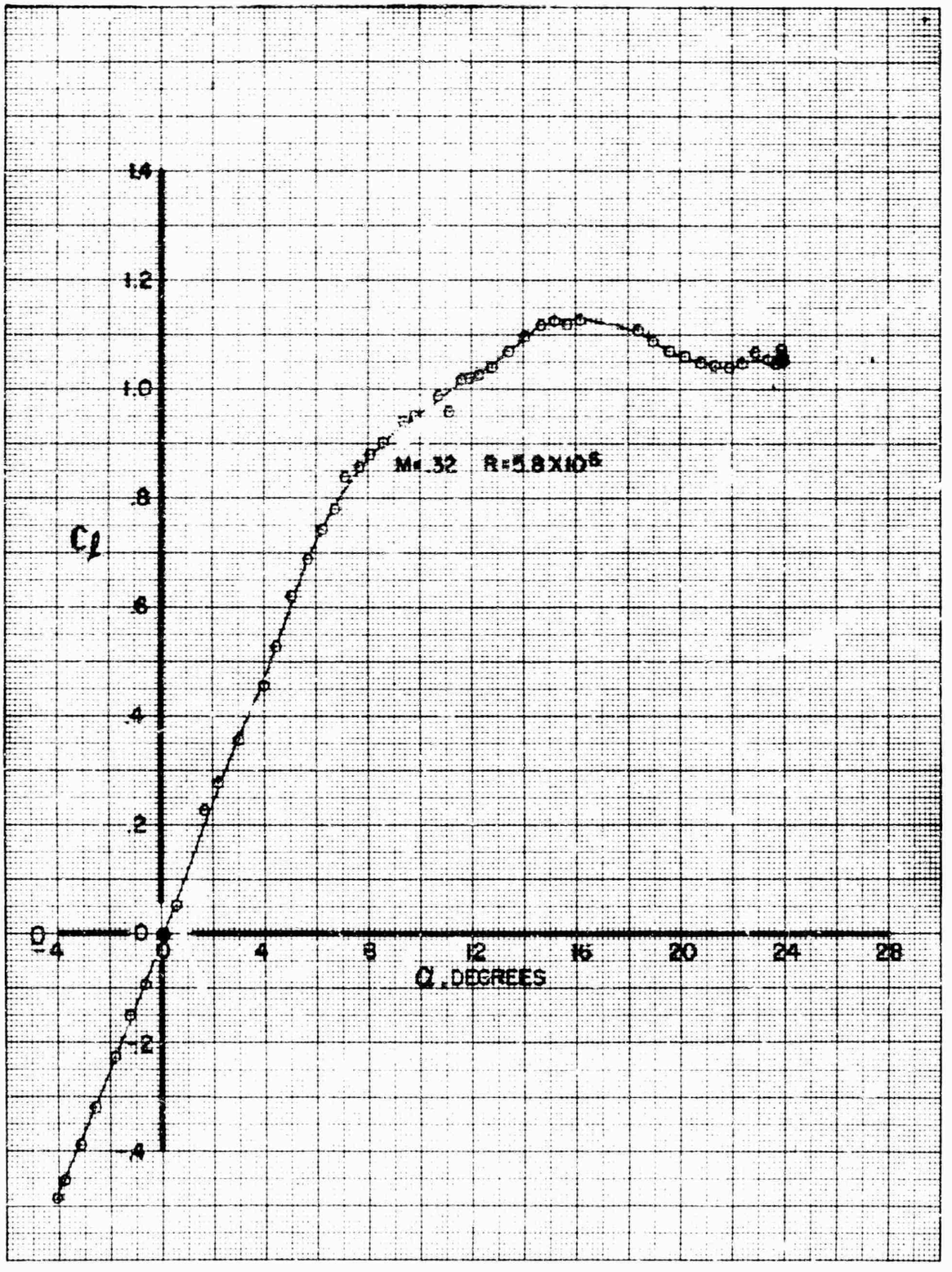


Figure 42A. Variation of Section Lift Coefficient With Angle of Attack, NACA Section 63A009

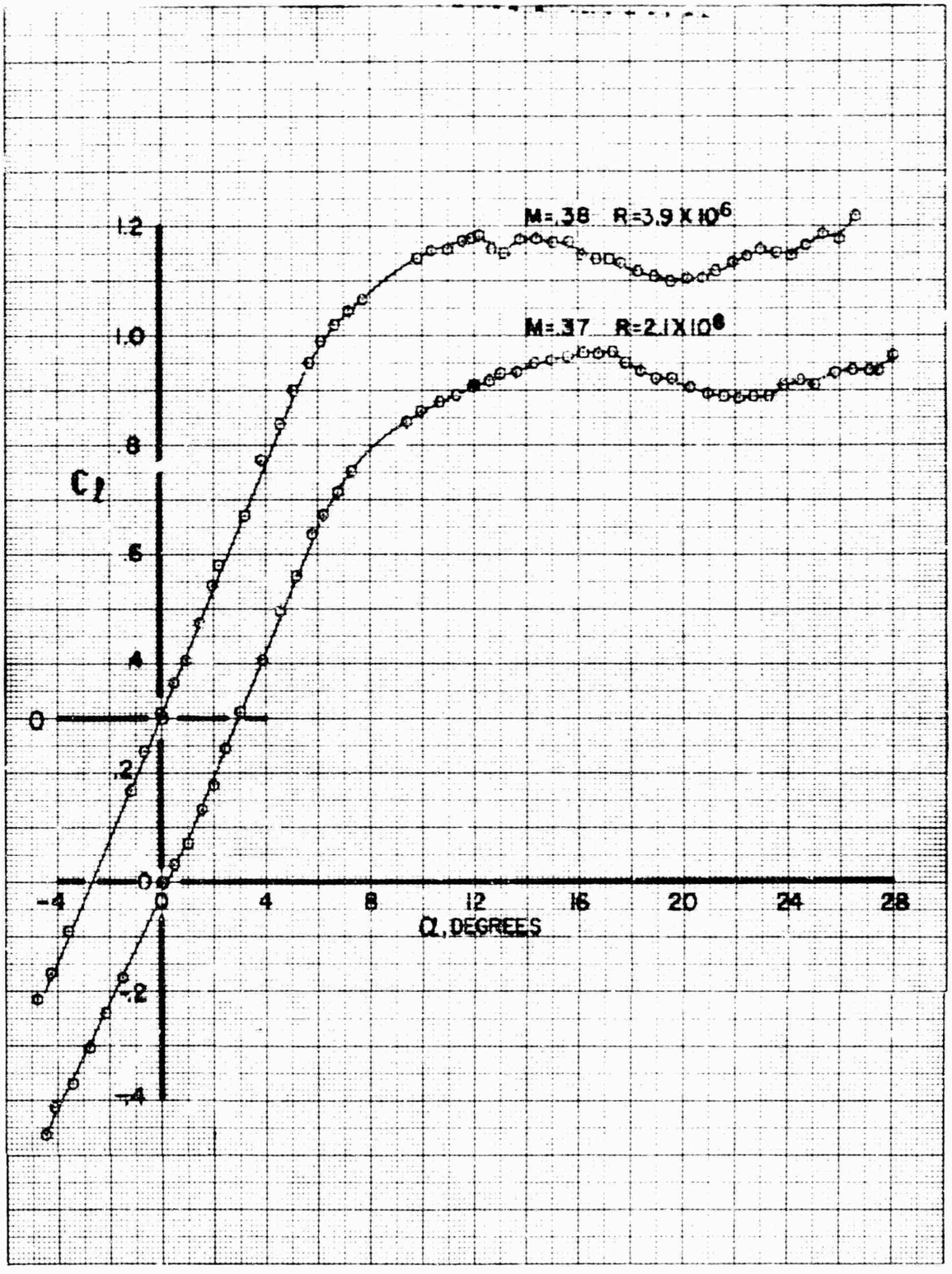


Figure 42B. Variation of Section Lift Coefficient With Angle of Attack, NACA Section 63A009

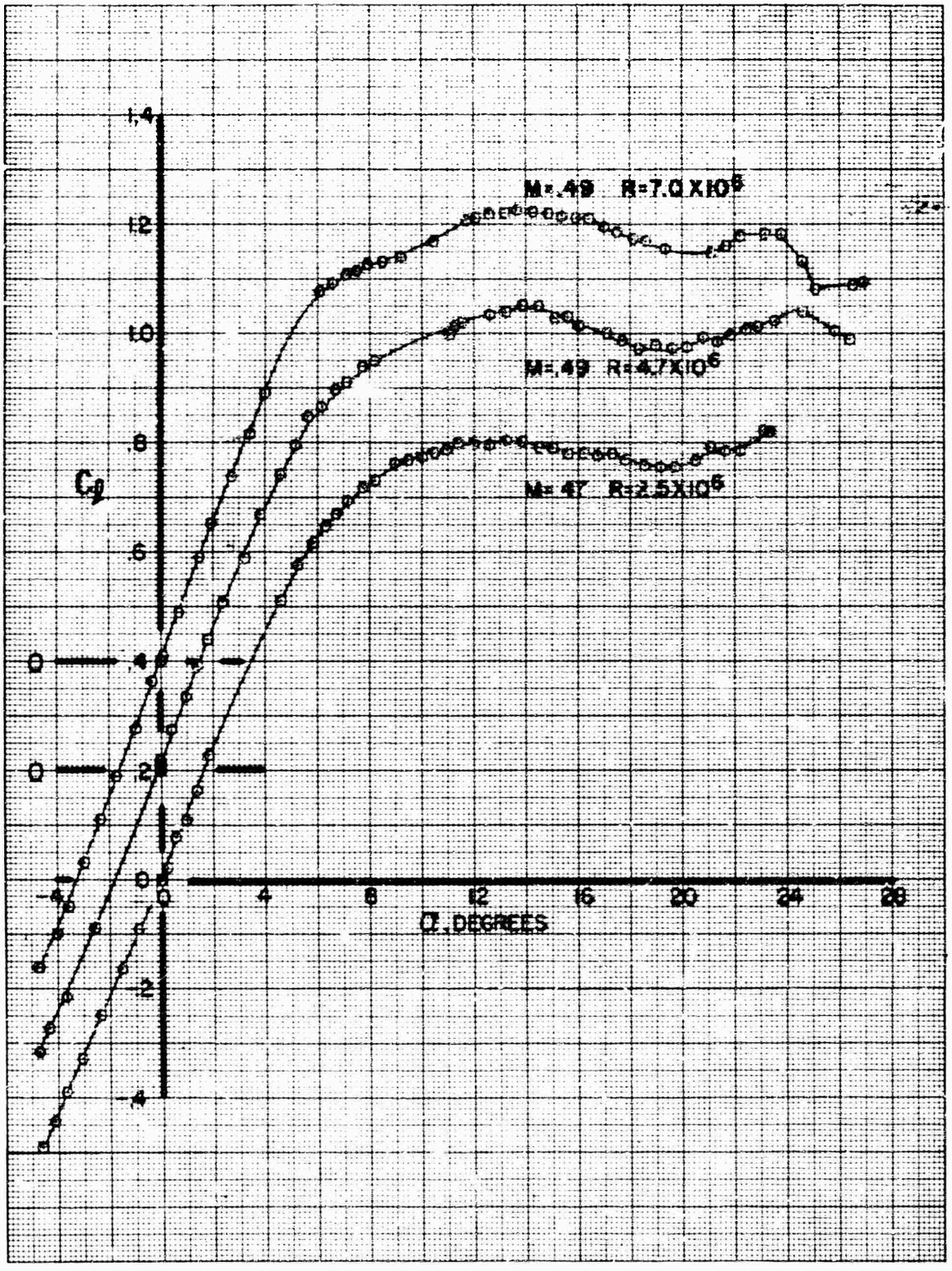


Figure 42C. Variation of Section Lift Coefficient With Angle of Attack, NACA Section 63A009

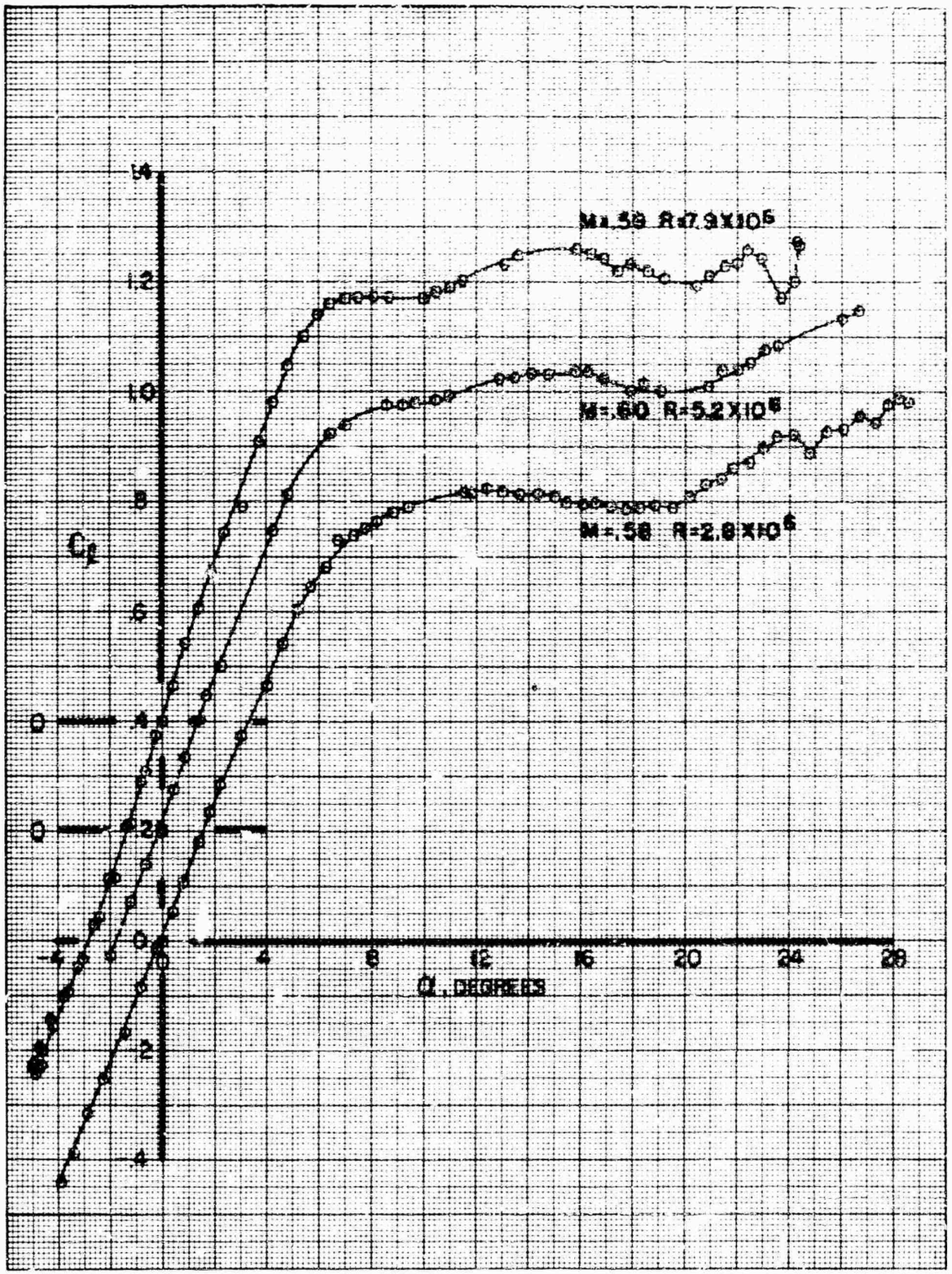


Figure 42D. Variation of Section Lift Coefficient With Angle of Attack, NACA Section 63A009

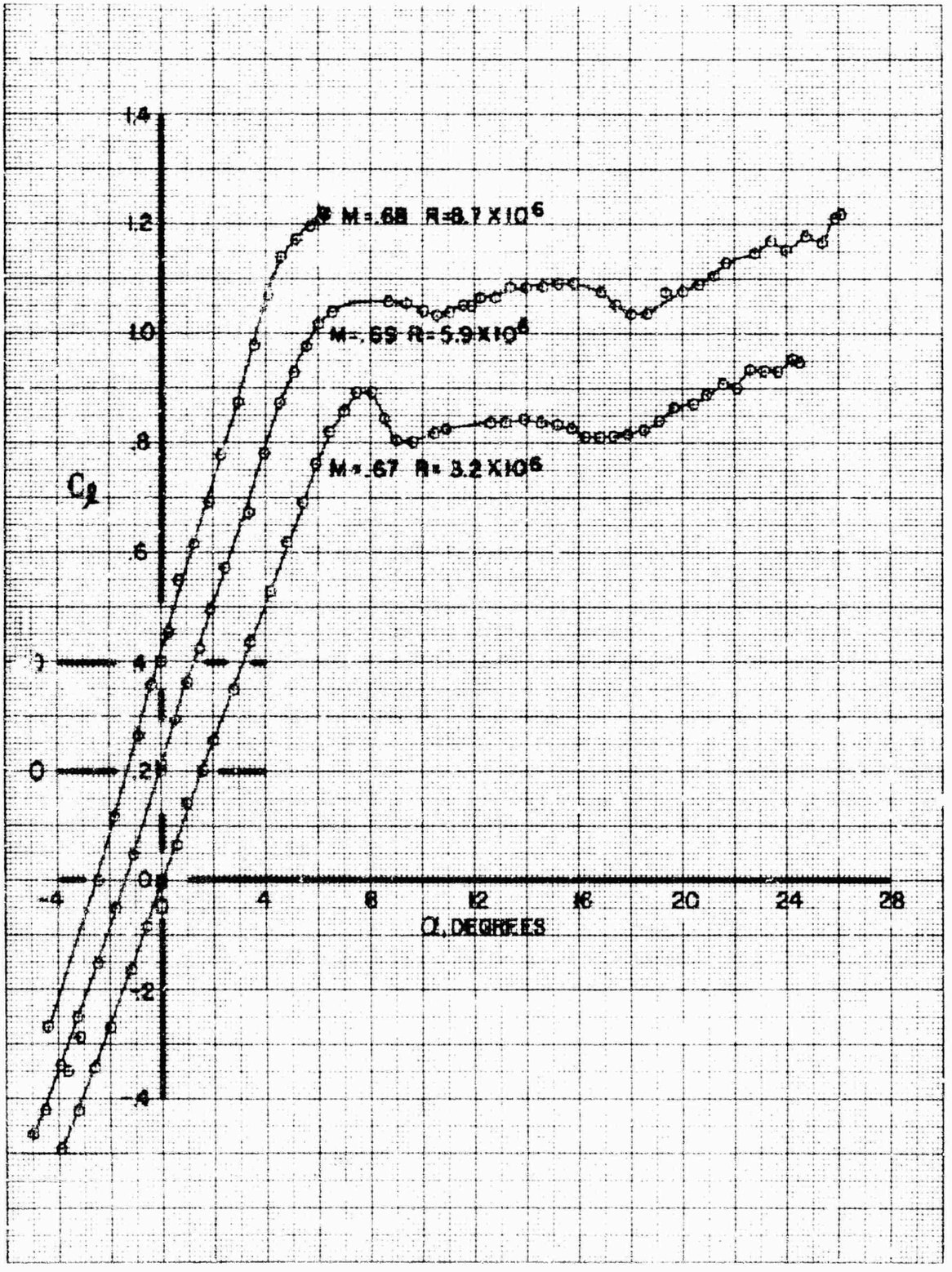


Figure 42E. Variation of Section Lift Coefficient With Angle of Attack, NACA Section 63A009

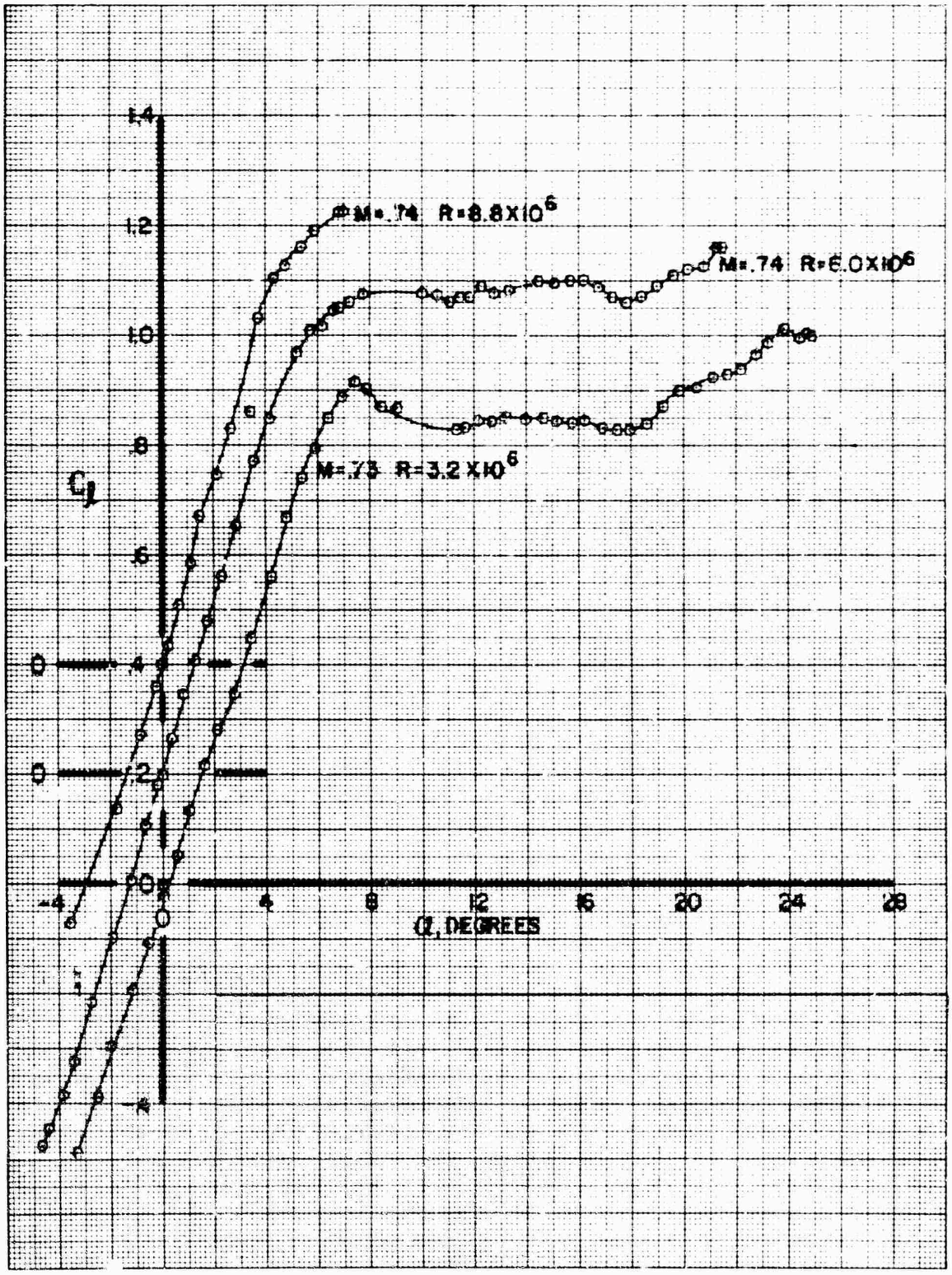


Figure 42F. Variation of Section Lift Coefficient With Angle of Attack, NACA Section 63A009

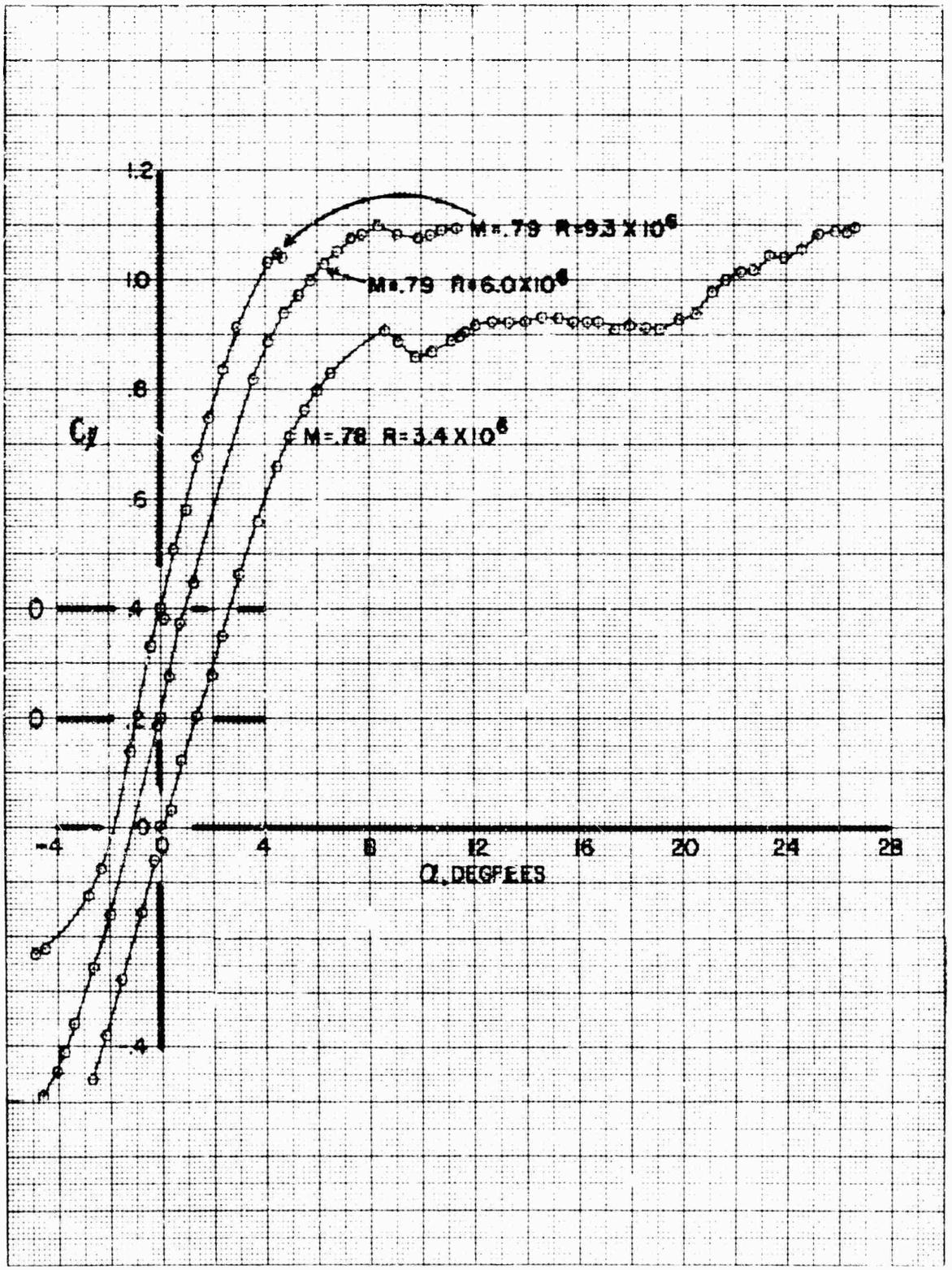


Figure 42G. Variation of Section Lift Coefficient With Angle of Attack, NACA Section 63A009

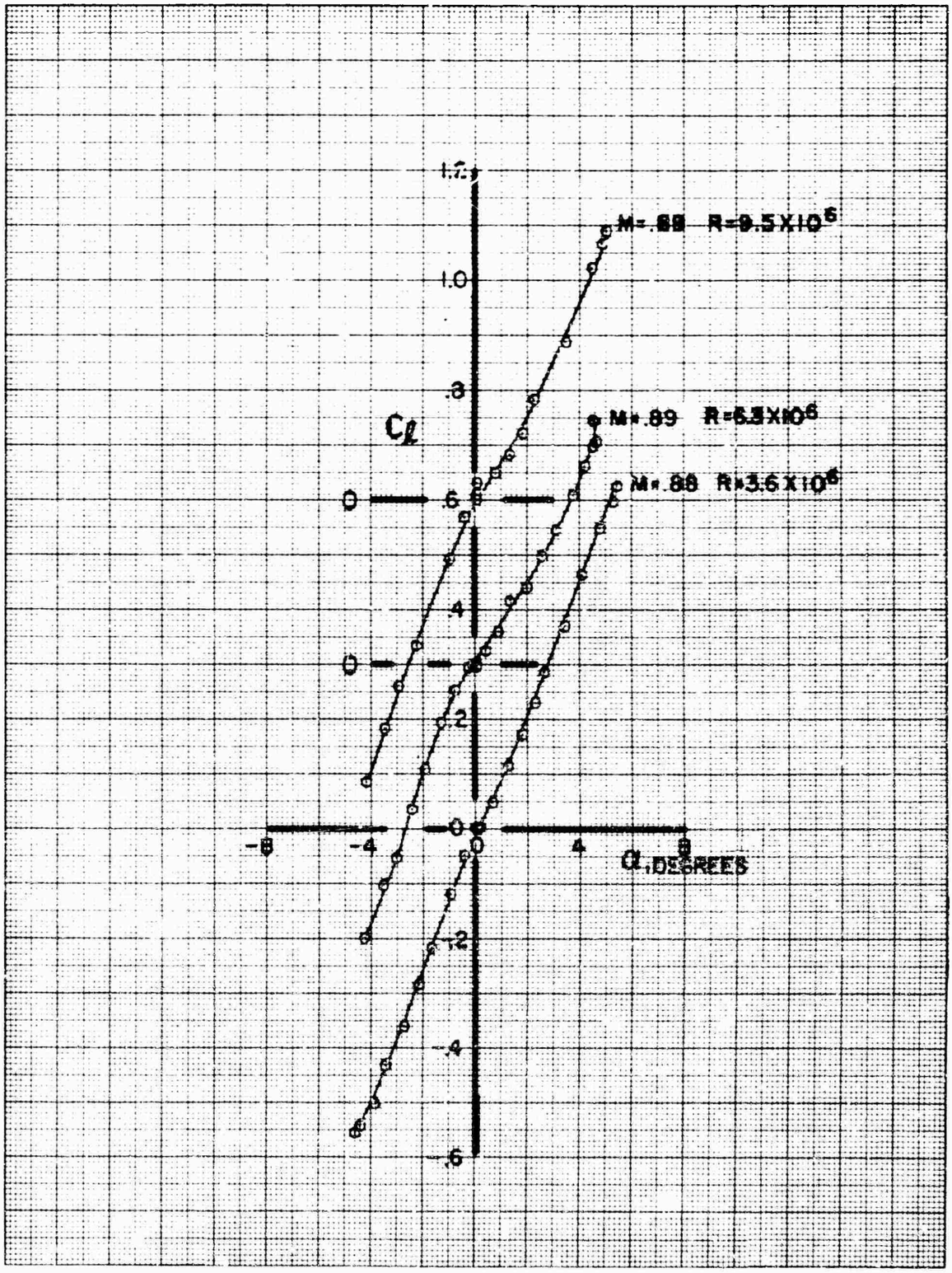


Figure 42H. Variation of Section Lift Coefficient With Angle of Attack, NACA Section 63A009

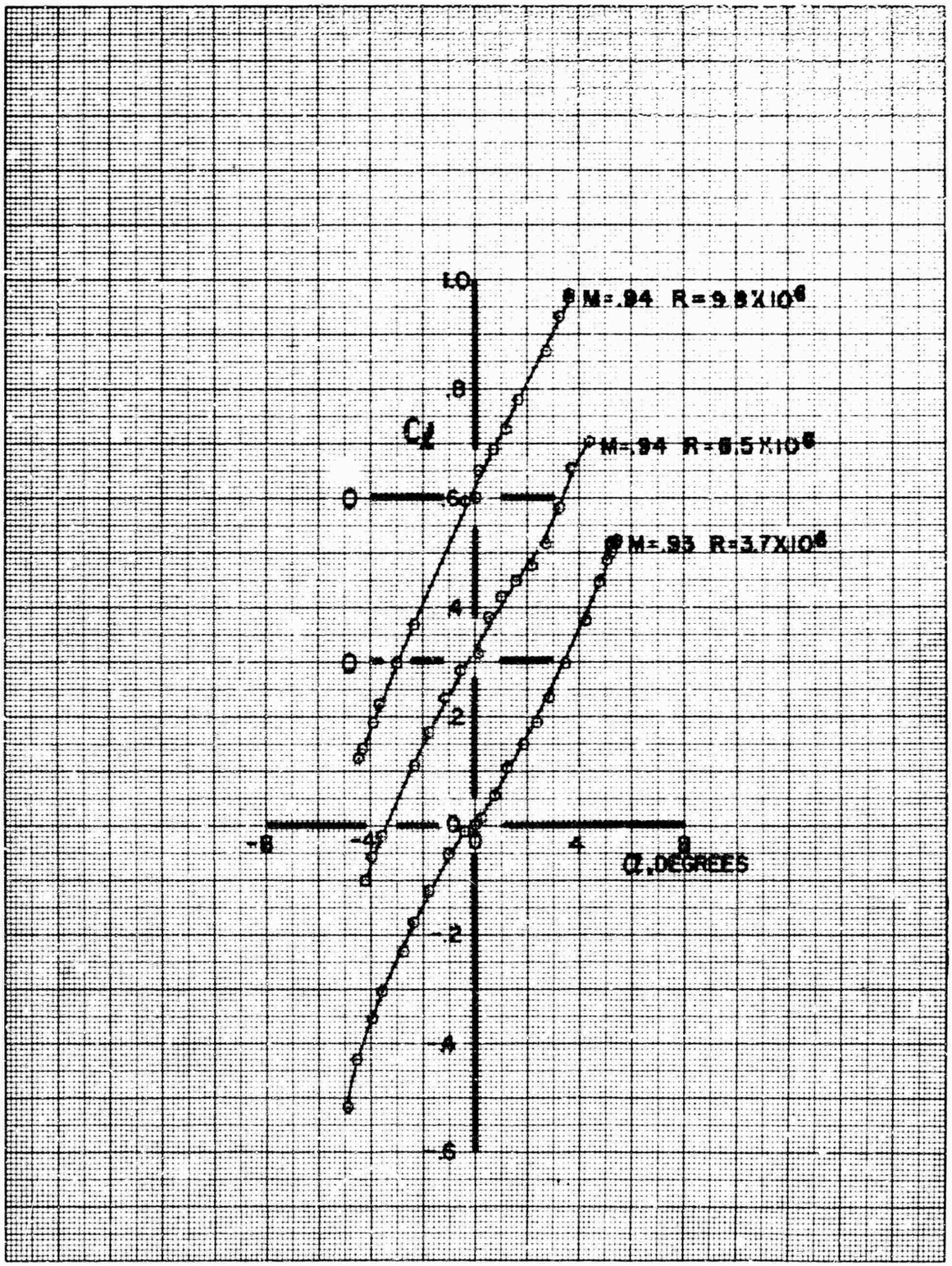


Figure 421. Variation of Section Lift Coefficient With Angle of Attack, NACA Section 63A009

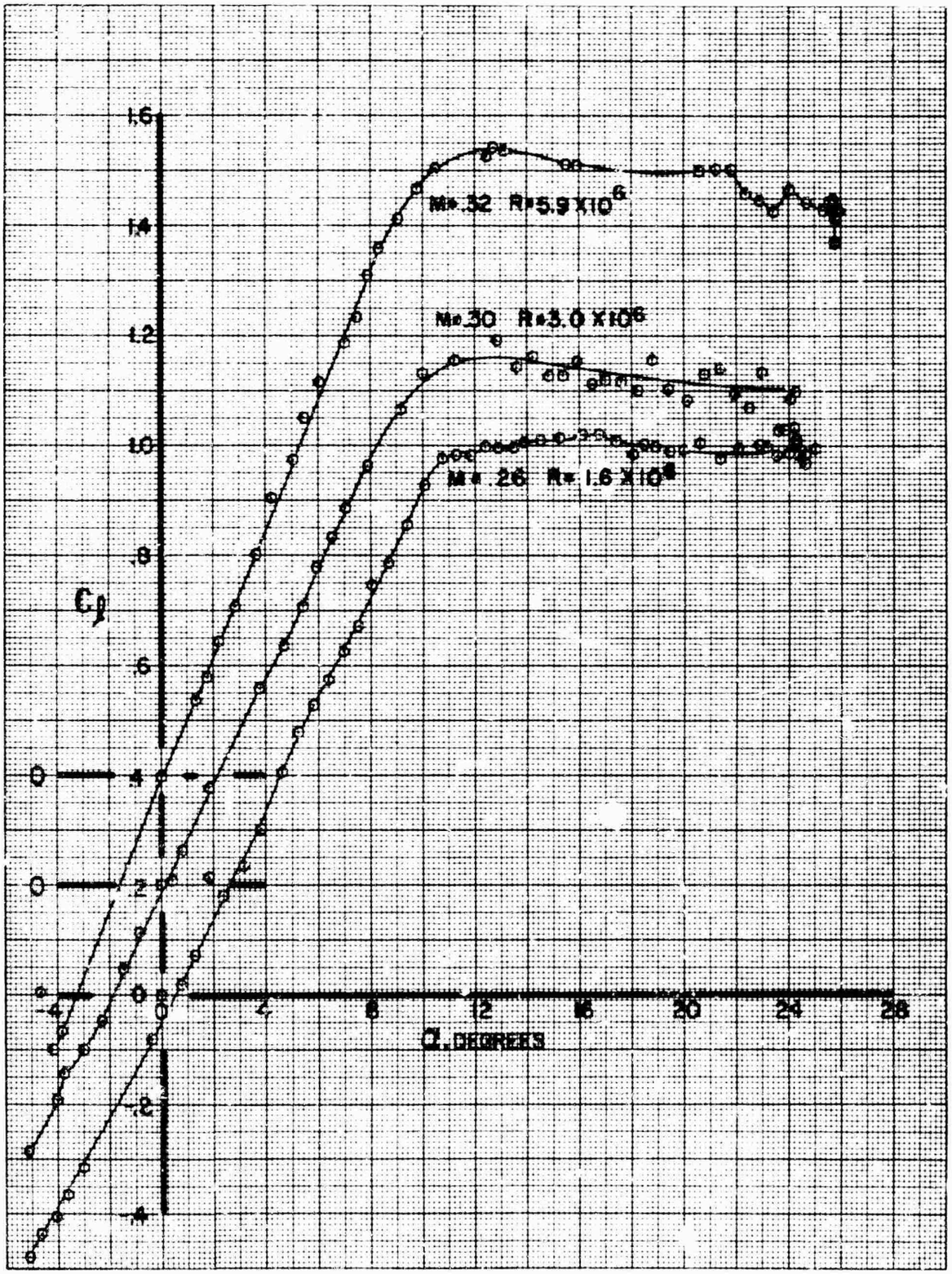


Figure 43A. Variation of Section Lift Coefficient With Angle of Attack, NACA Section 63A012

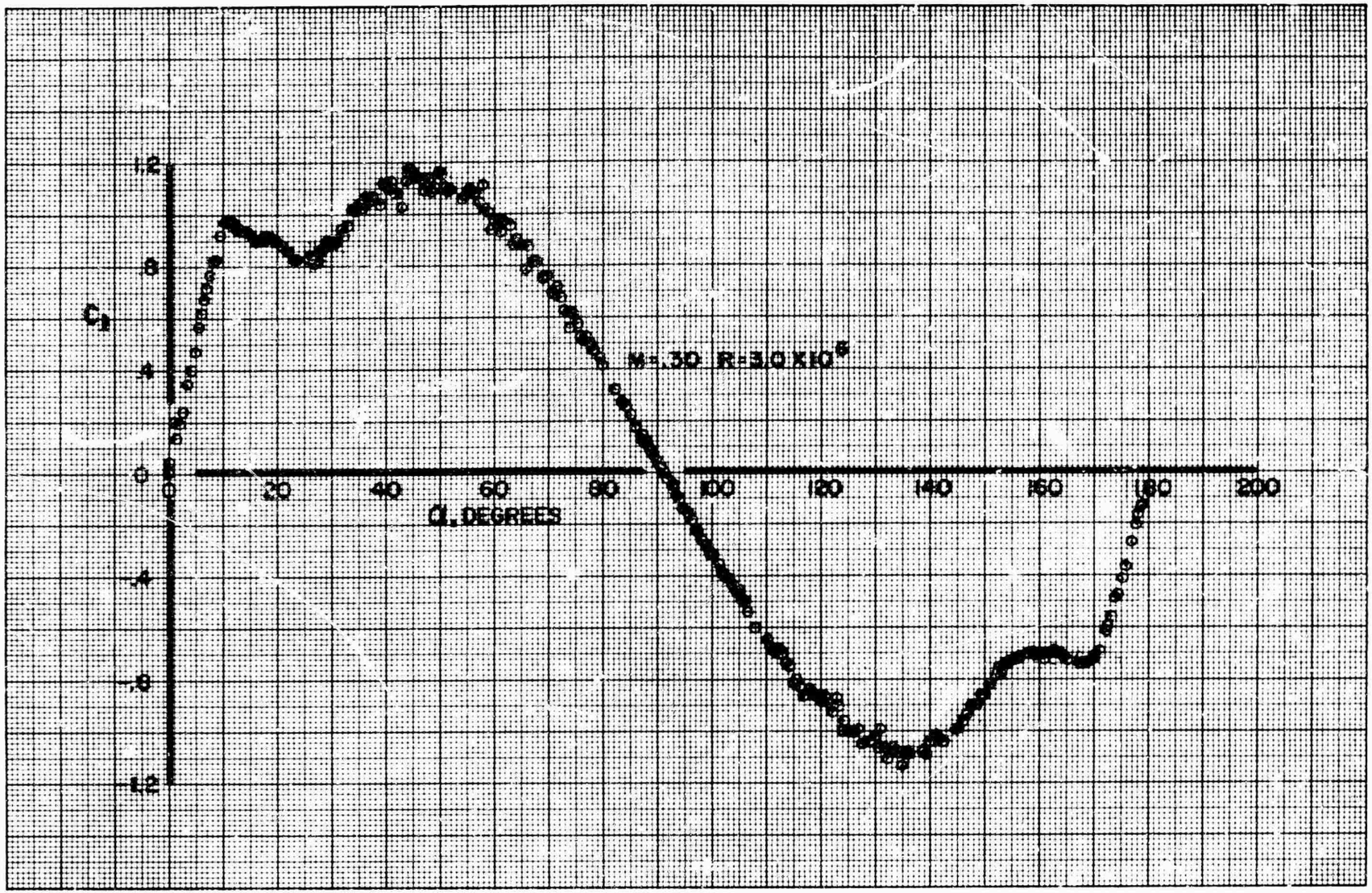


Figure 43B. Variation of Section Lift Coefficient With Angle of Attack, NACA Section 63A012

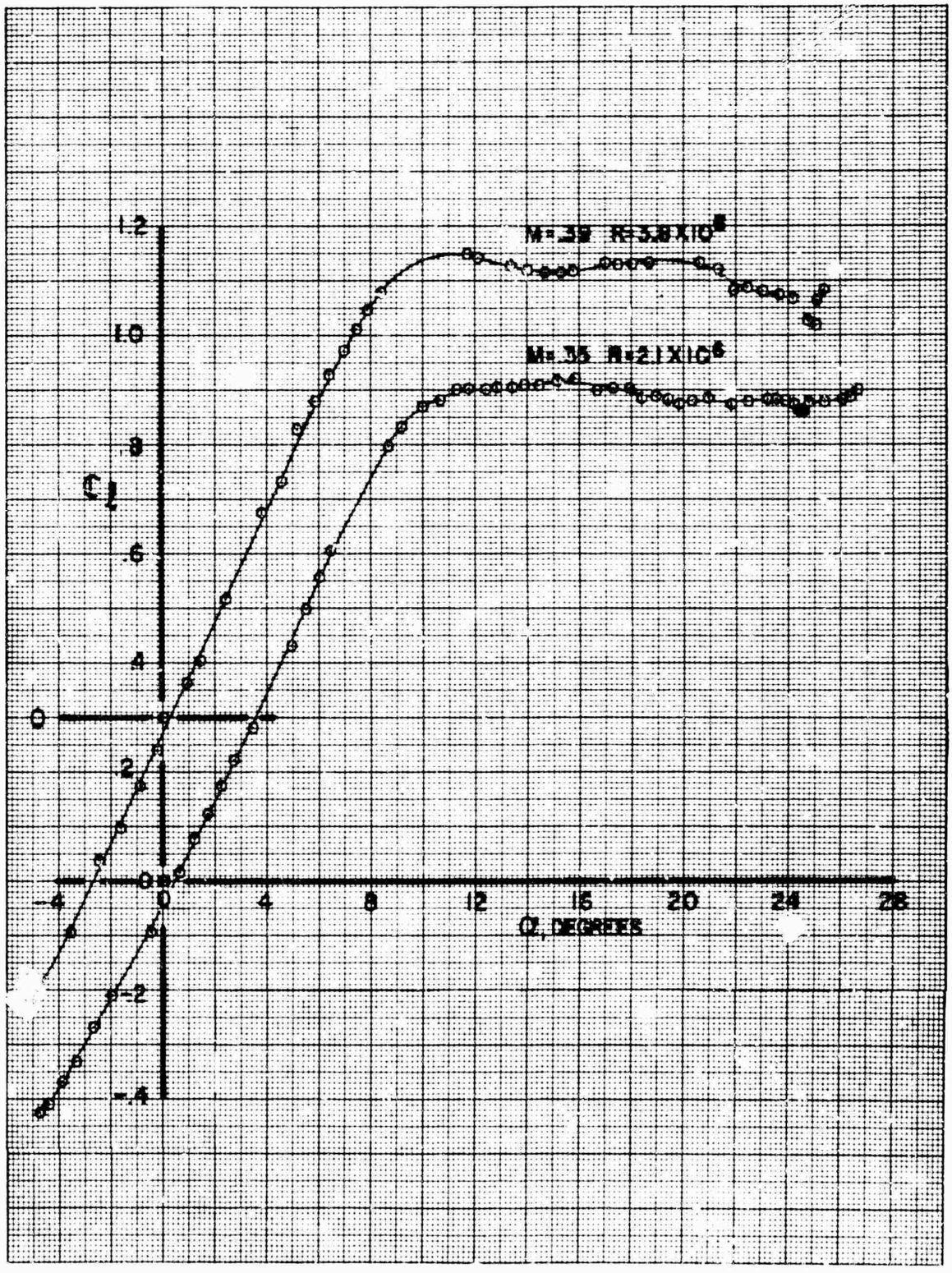


Figure 43C. Variation of Section Lift Coefficient With Angle of Attack, NACA Section 63A012

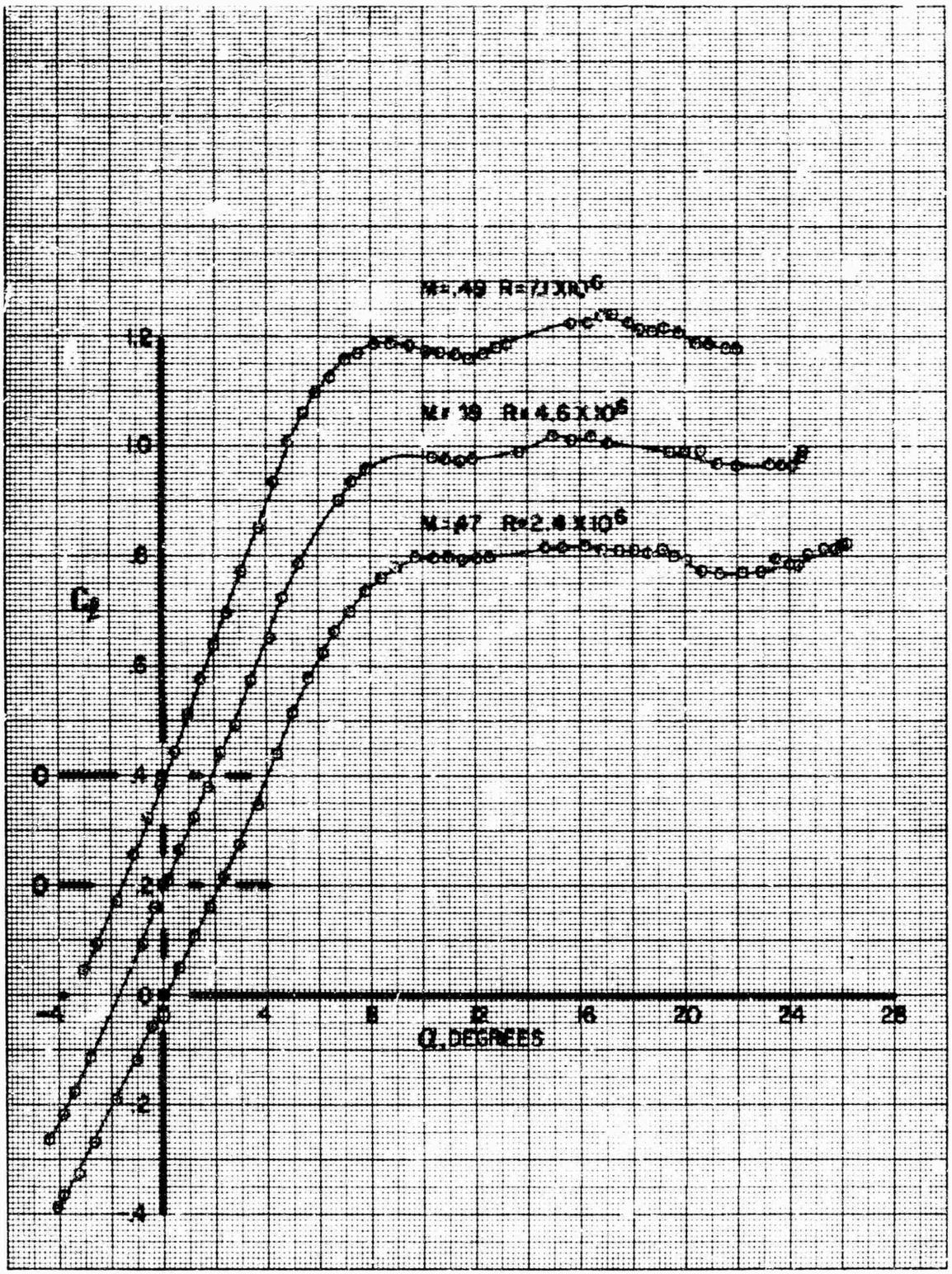


Figure 43D. Variation of Section Lift Coefficient With Angle of Attack, NACA Section 63A012

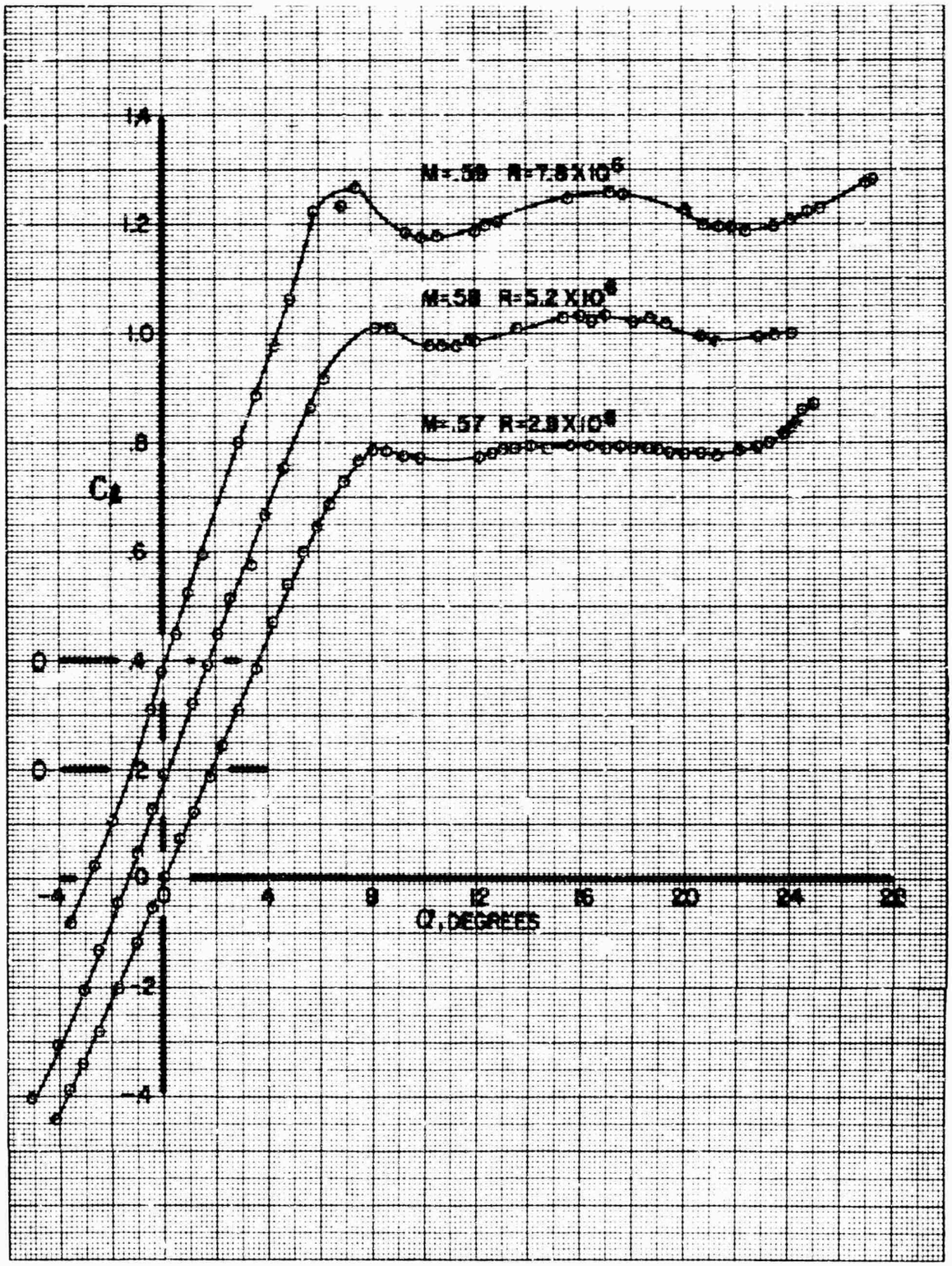


Figure 43E. Variation of Section Lift Coefficient With Angle of Attack, NACA Section 63A012

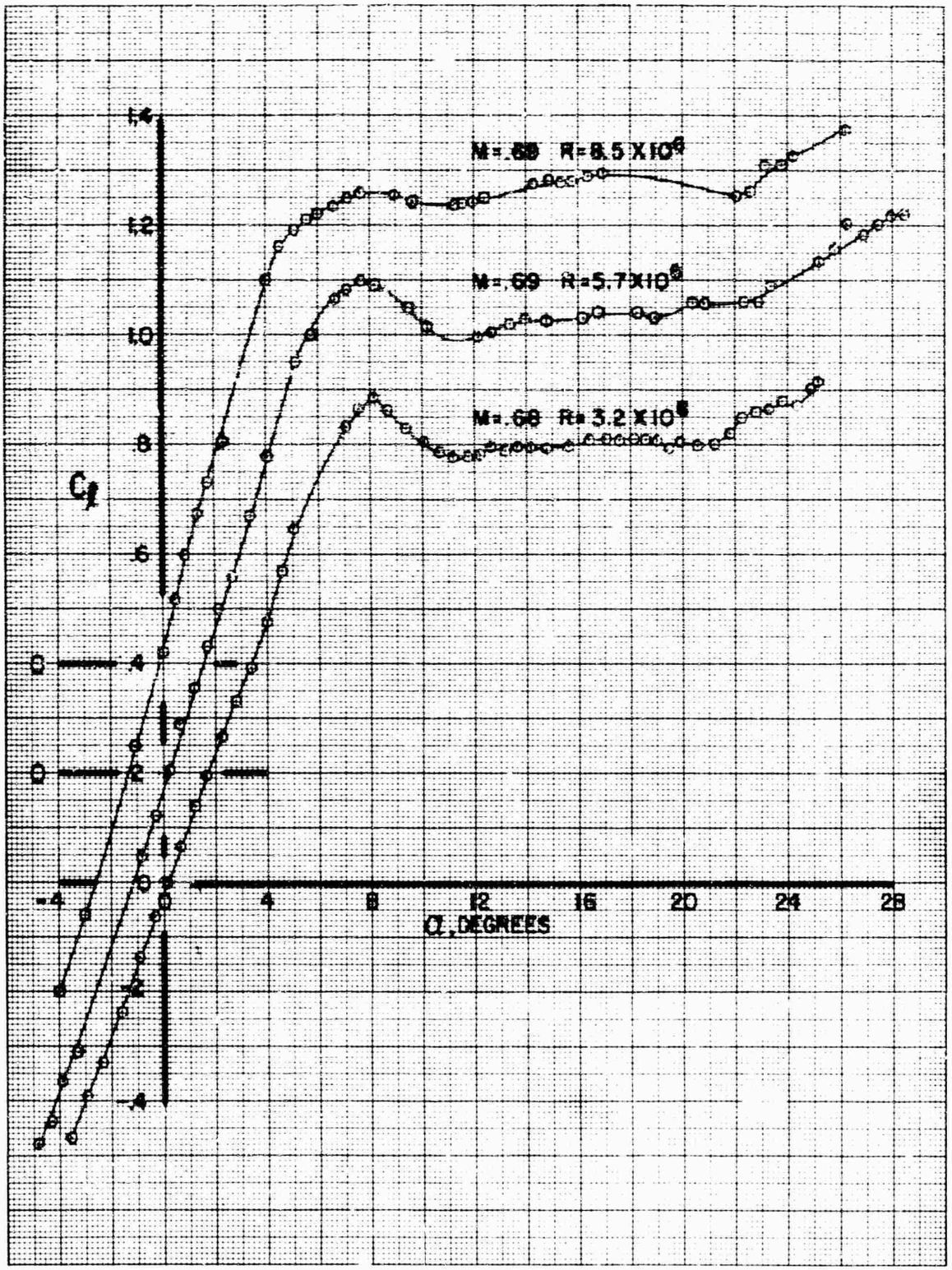


Figure 43F. Variation of Section Lift Coefficient With Angle of Attack, NACA Section 63A012

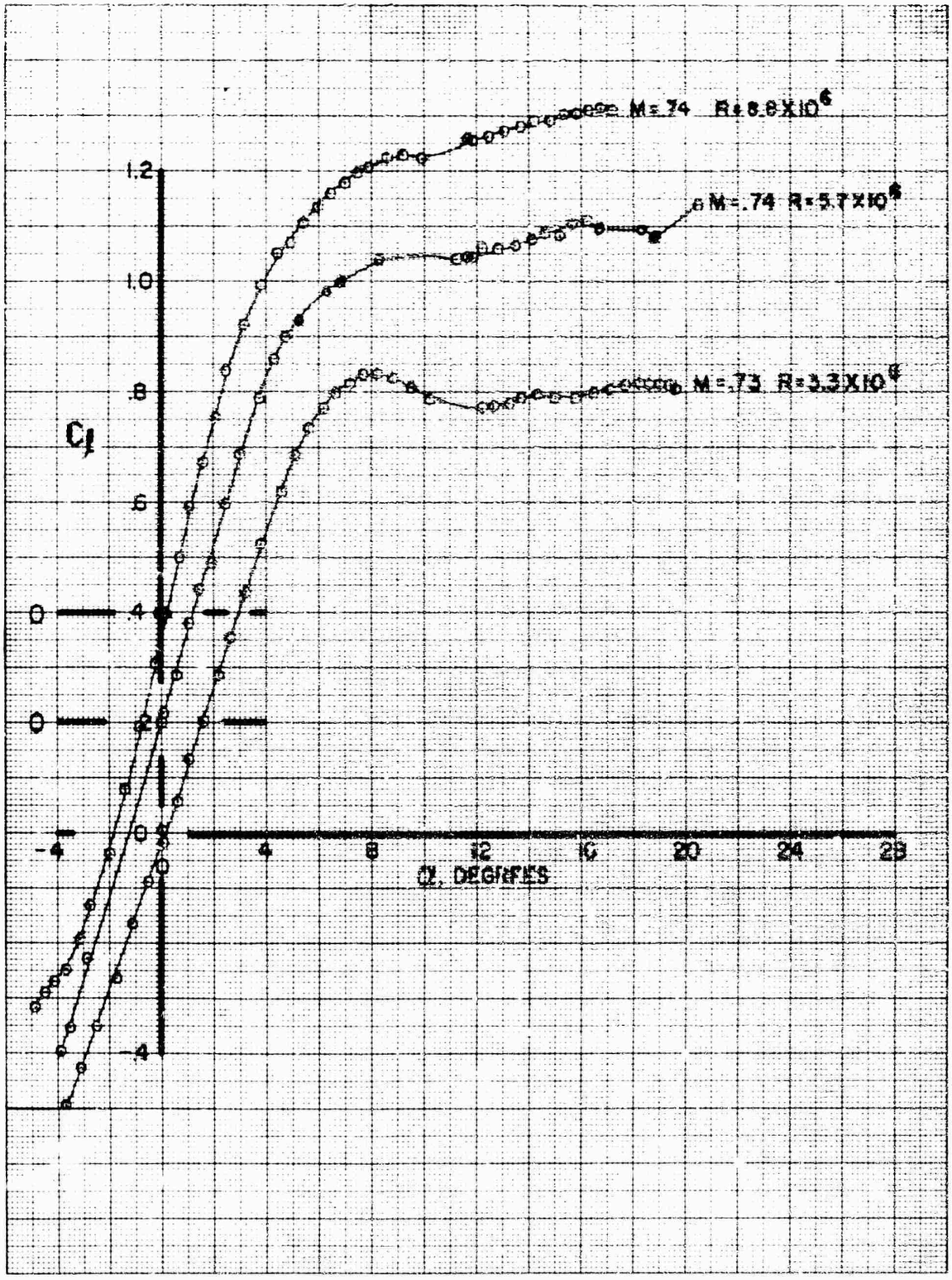


Figure 43G. Variation of Section Lift Coefficient With Angle of Attack, NACA Section 63A012

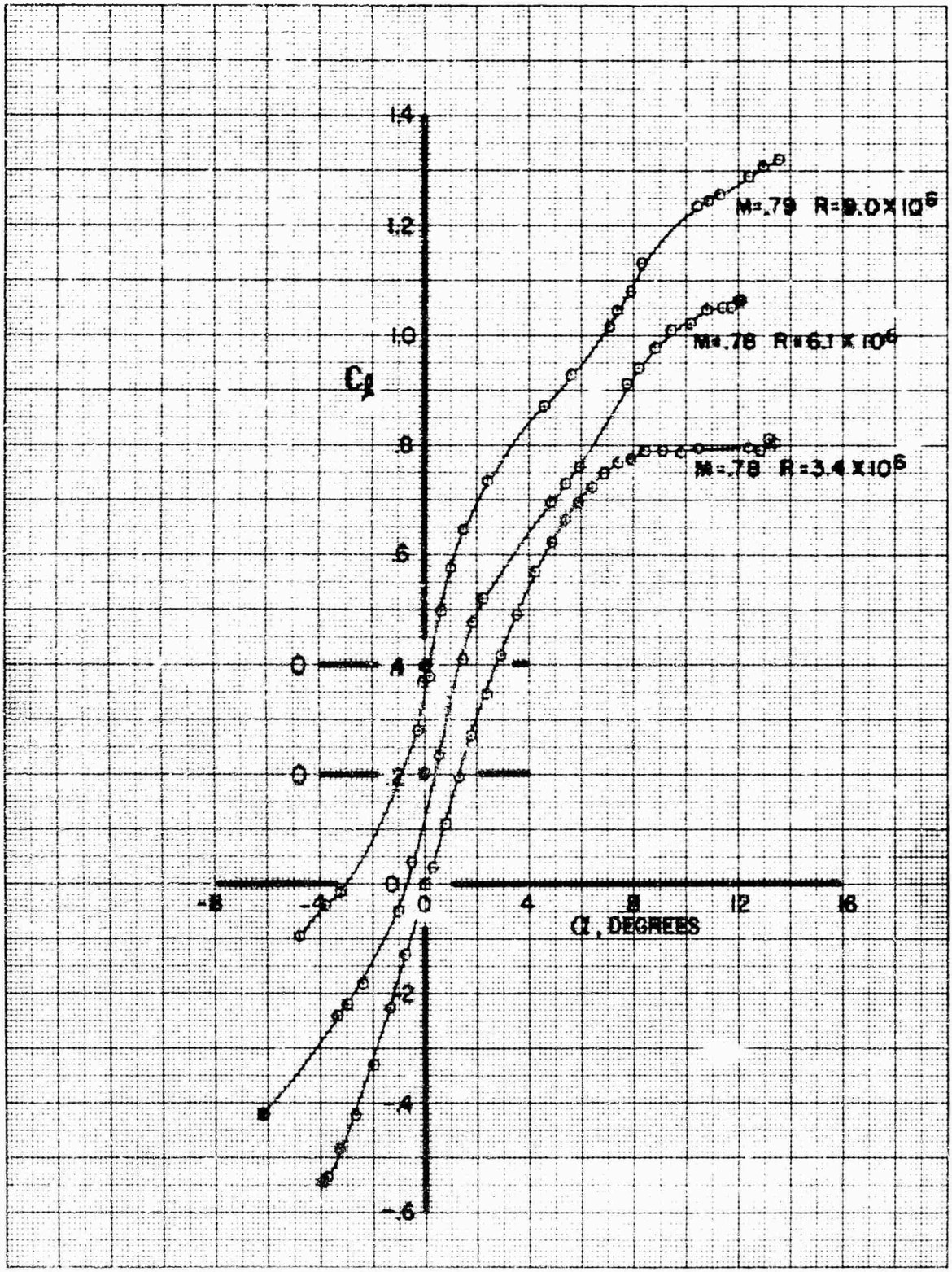


Figure 43H. Variation of Section Lift Coefficient With Angle of Attack, NACA Section 63A012

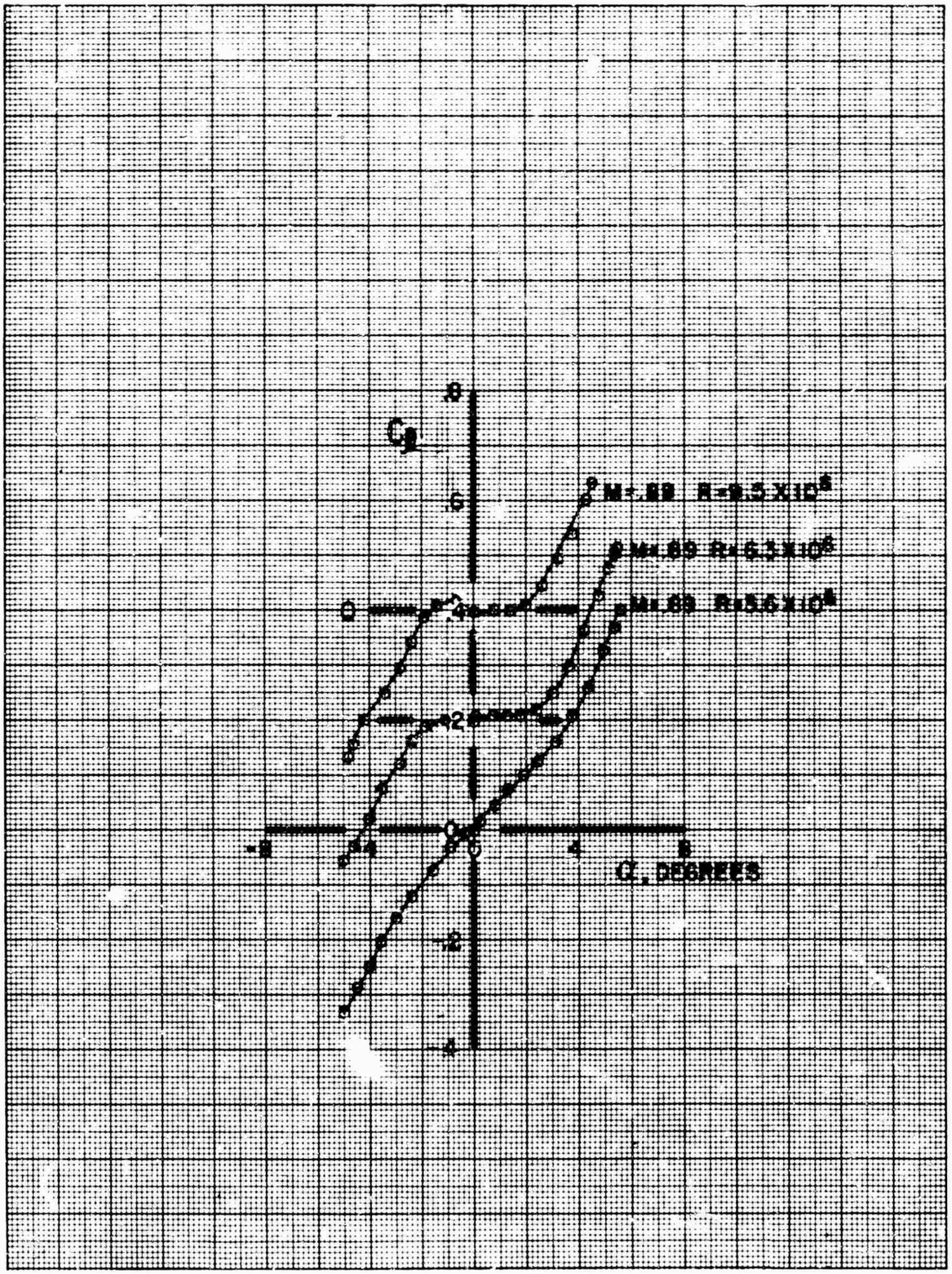


Figure 431. Variation of Section Lift Coefficient With Angle of Attack, NACA Section 63A012

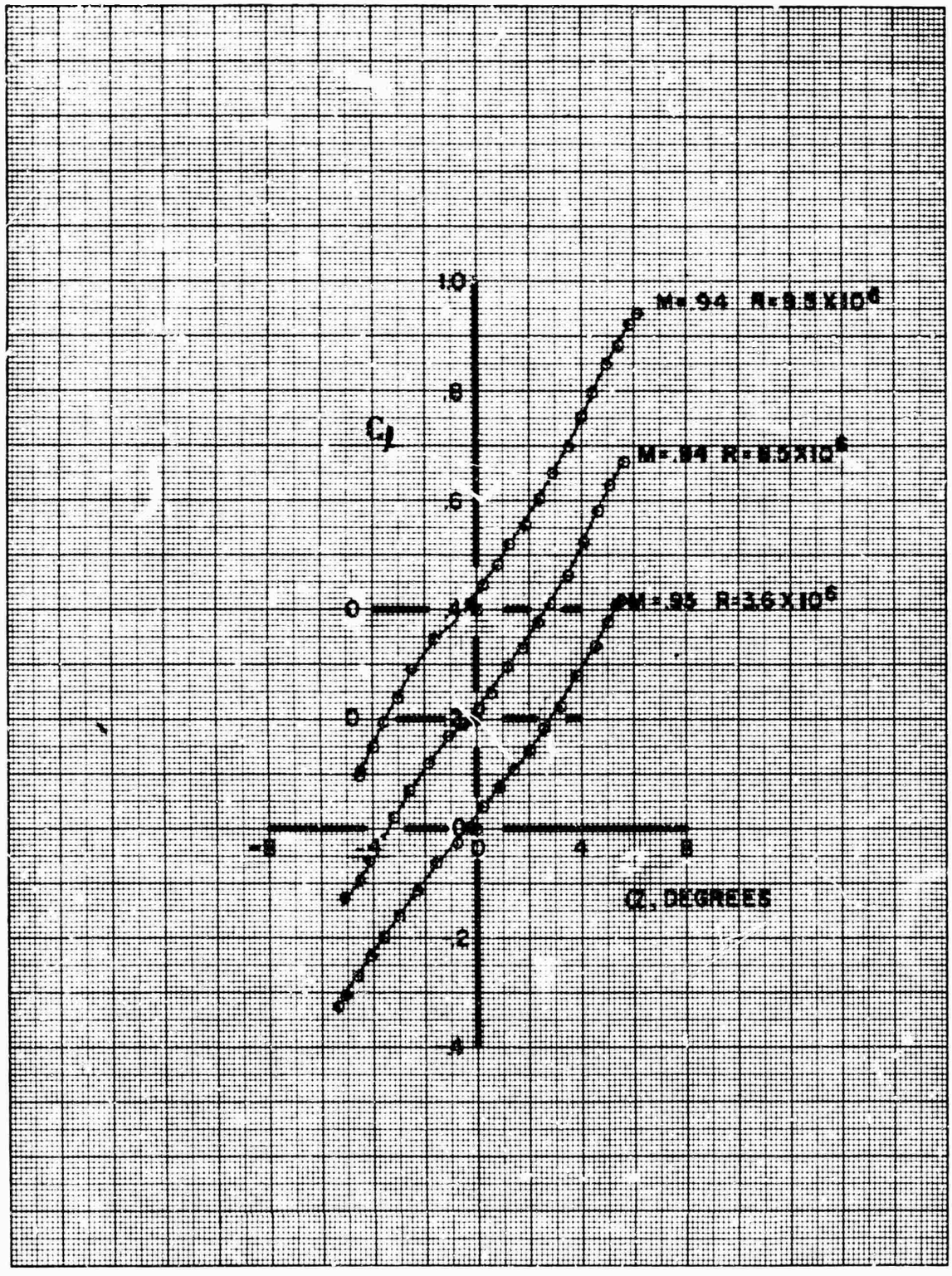


Figure 43J. Variation of Section Lift Coefficient With Angle of Attack, NACA Section 63A012

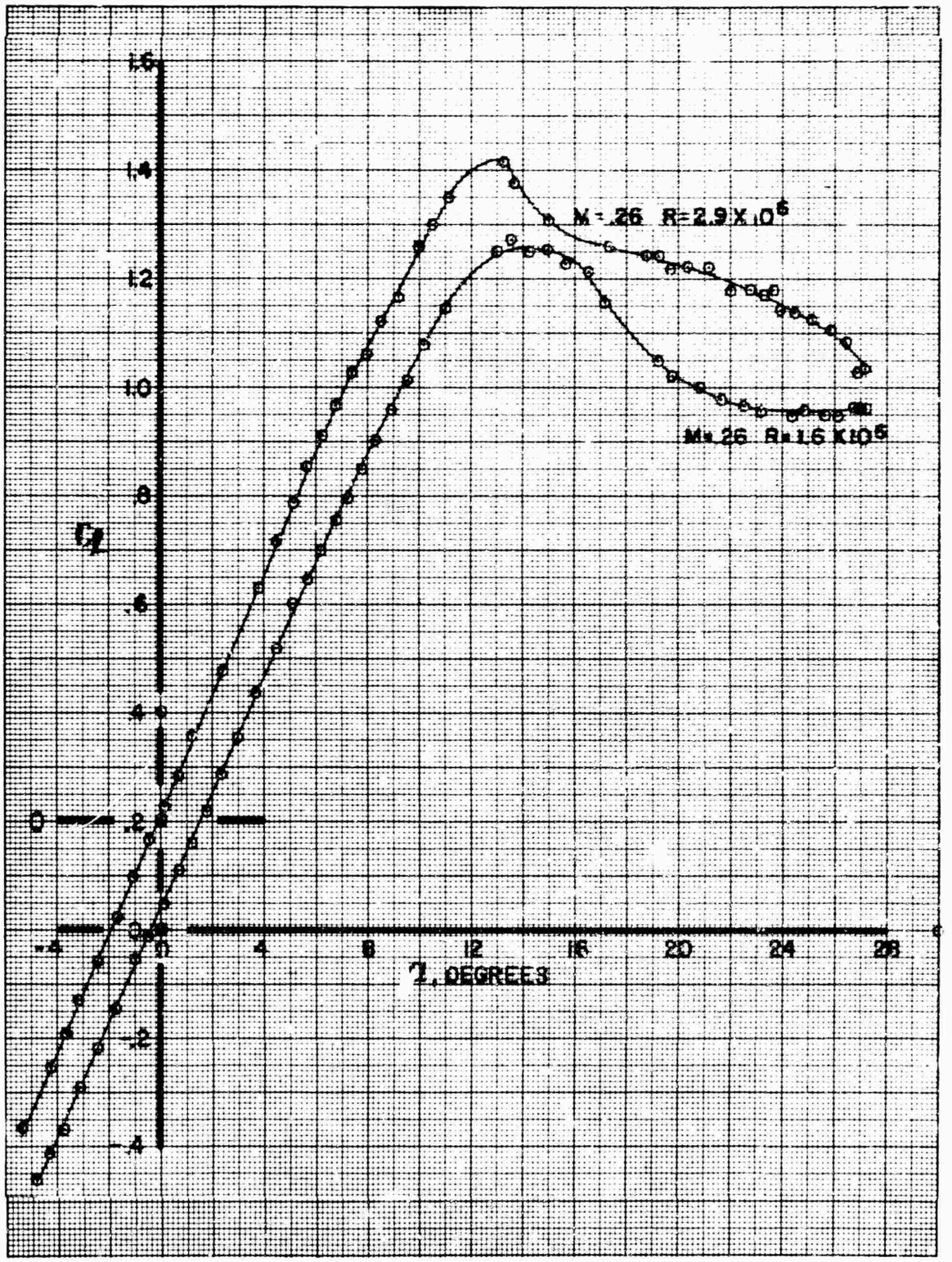


Figure 44A. Variation of Section Lift Coefficient With Angle of Attack, NACA Section 63A015

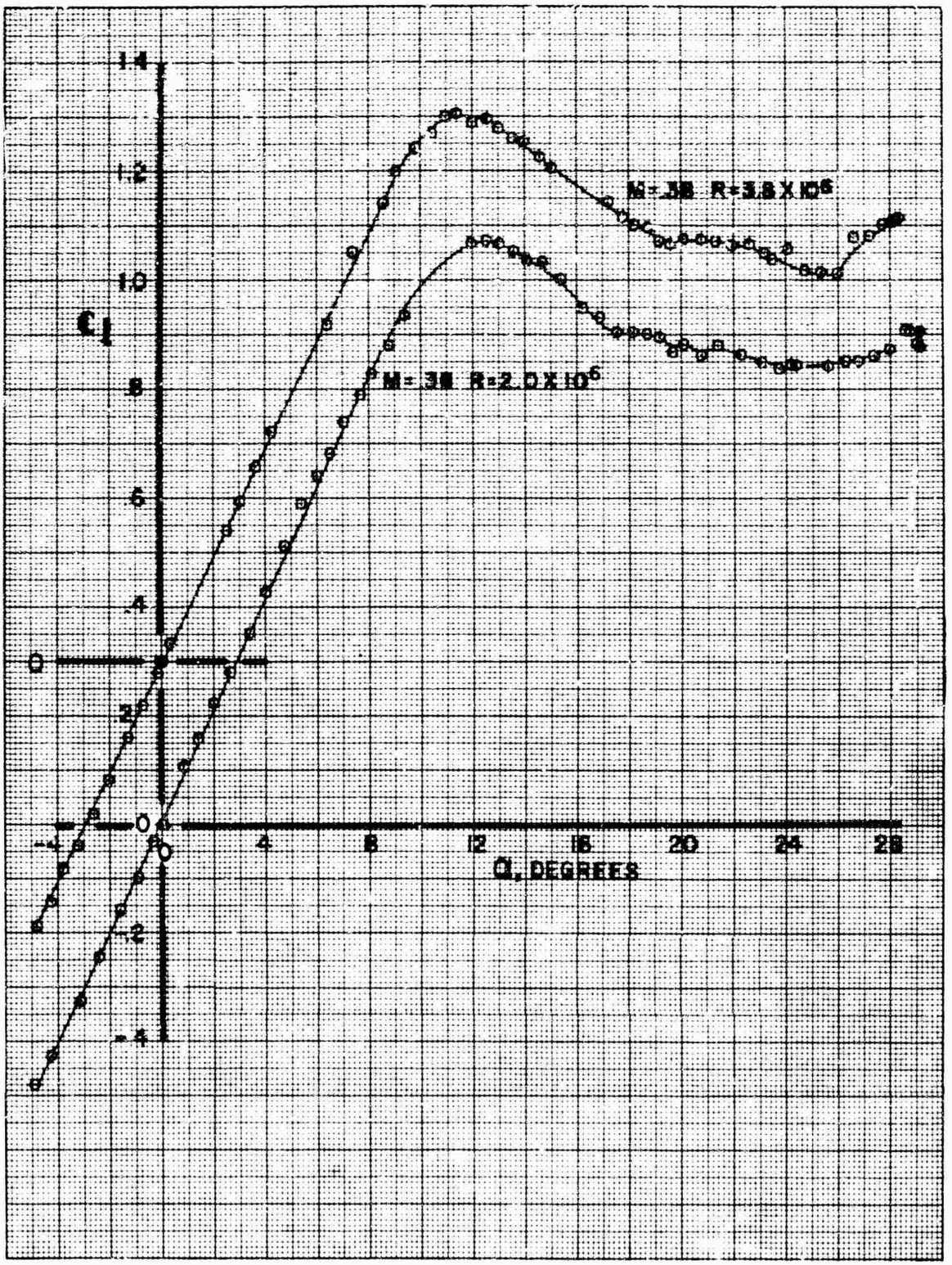


Figure 44B. Variation of Section Lift Coefficient With Angle of Attack, NACA Section 63A015

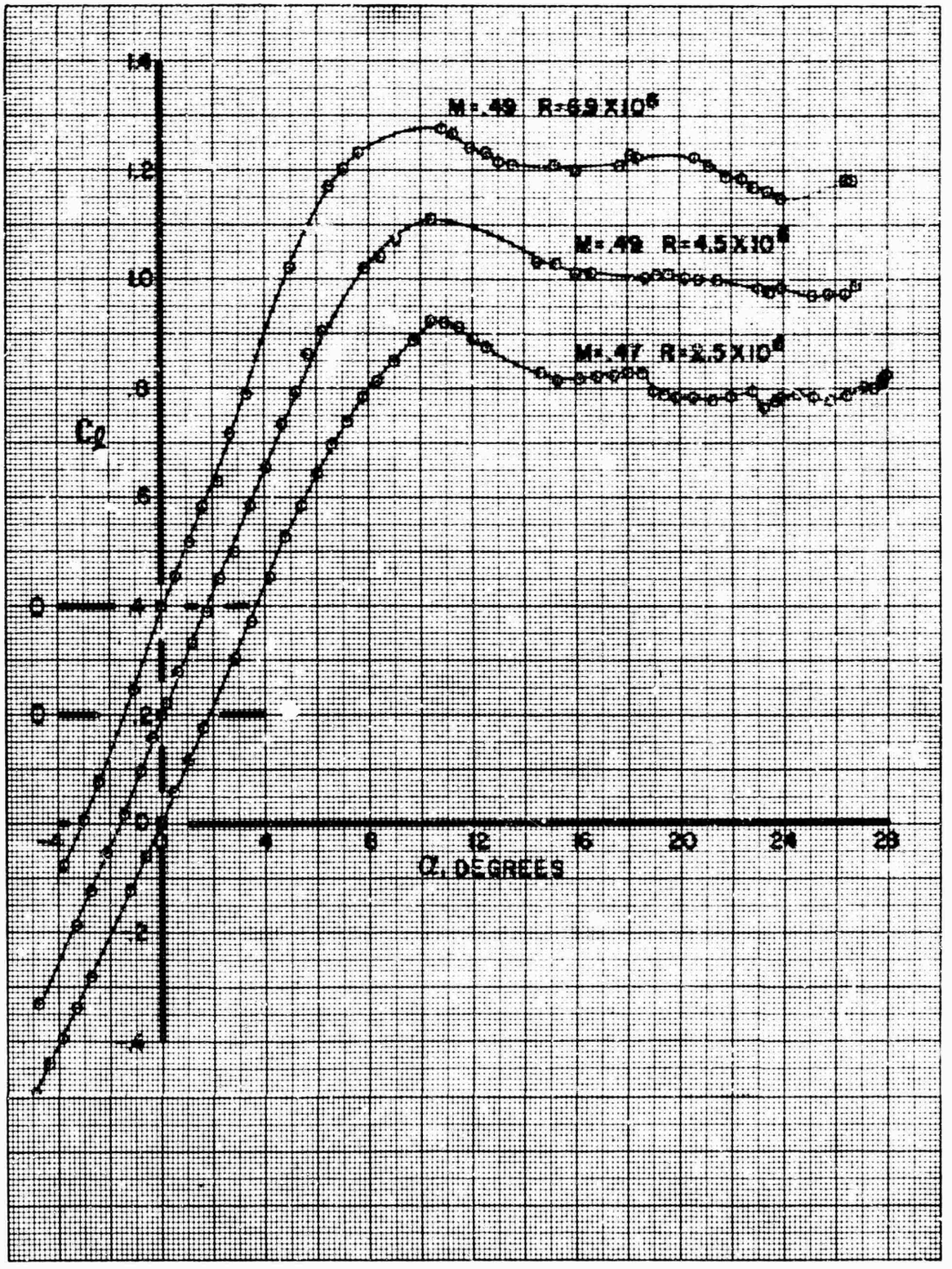


Figure 44C. Variation of Section Lift Coefficient With Angle of Attack, NACA Section 63A015

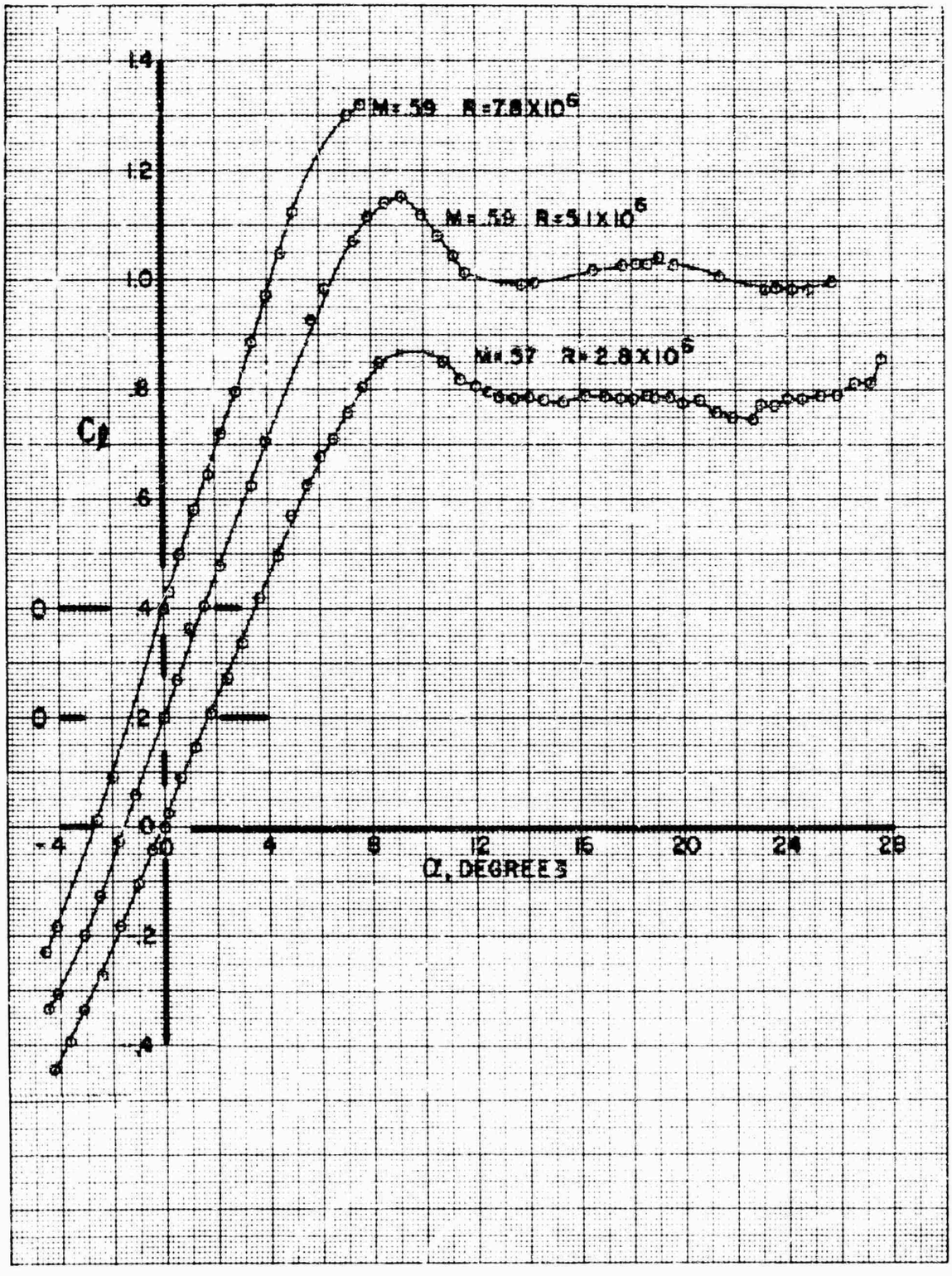


Figure 44D. Variation of Section Lift Coefficient With Angle of Attack, NACA Section 63A015

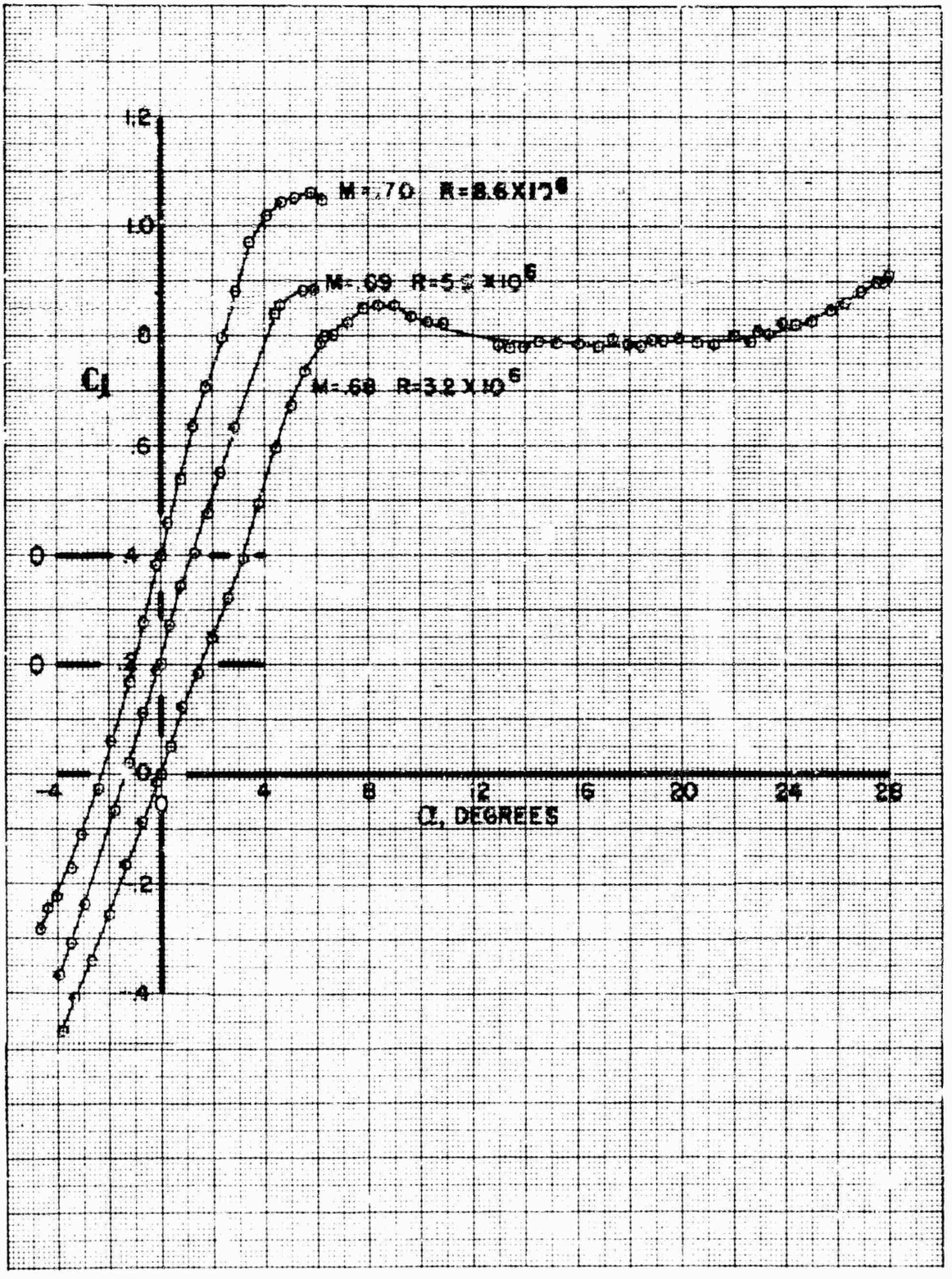


Figure 44E. Variation of Section Lift Coefficient With Angle of Attack NACA Section 63A015

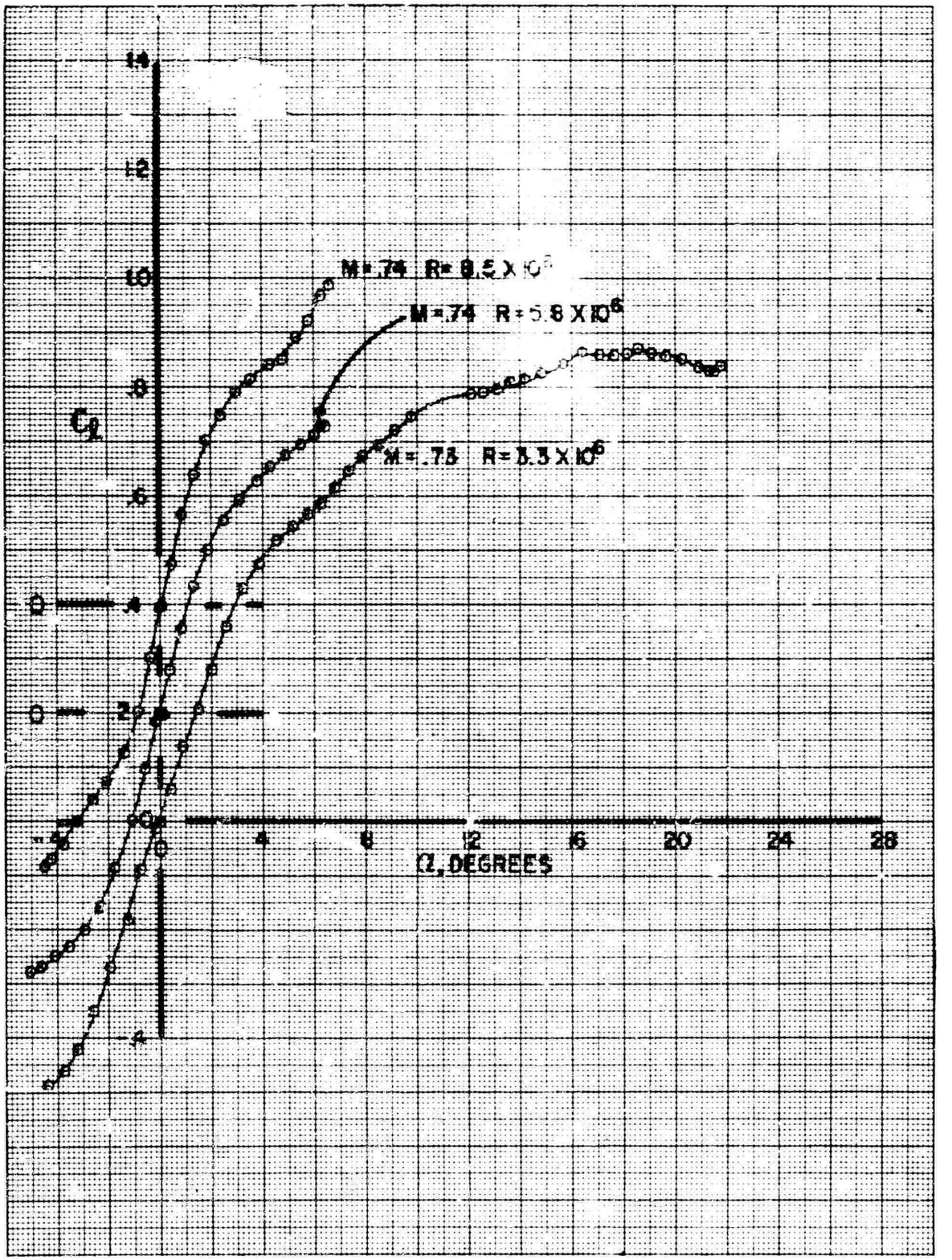


Figure 44F. Variation of Section Lift Coefficient With Angle of Attack, NACA Section 63A015

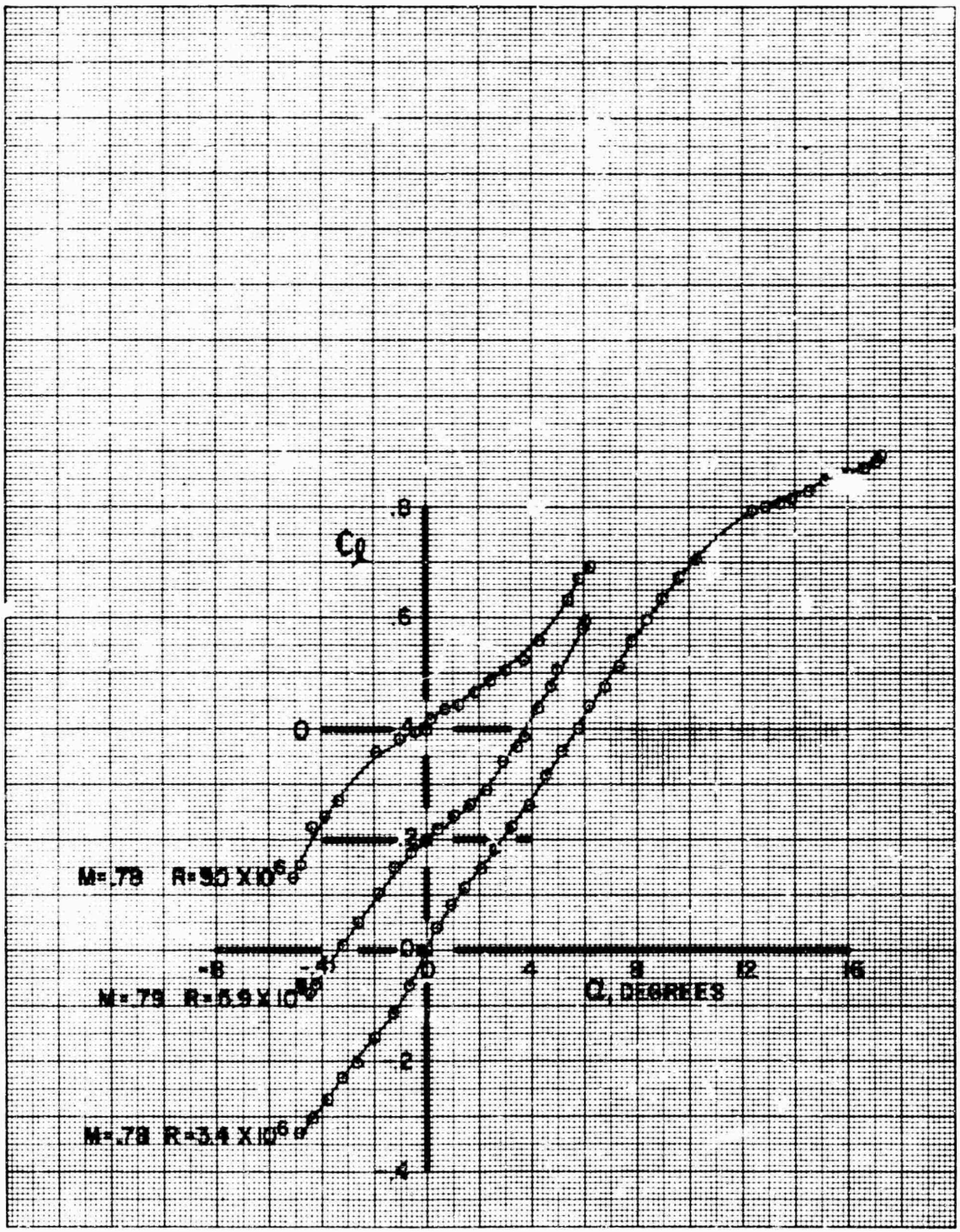


Figure 44G. Variation of Section Lift Coefficient With Angle of Attack, NACA Section 63A015

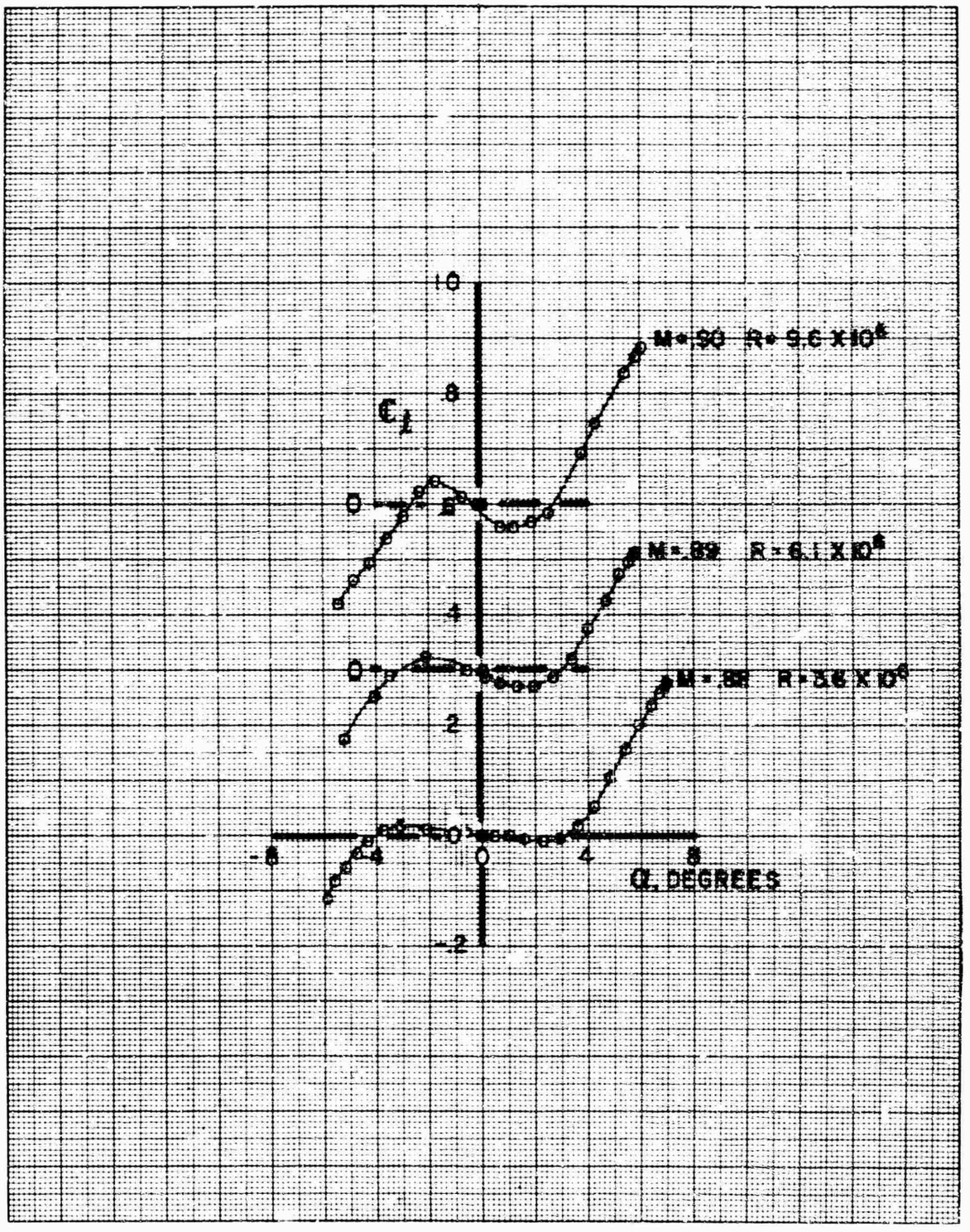


Figure 44H. Variation of Section Lift Coefficient With Angle of Attack, NACA Section 63A015

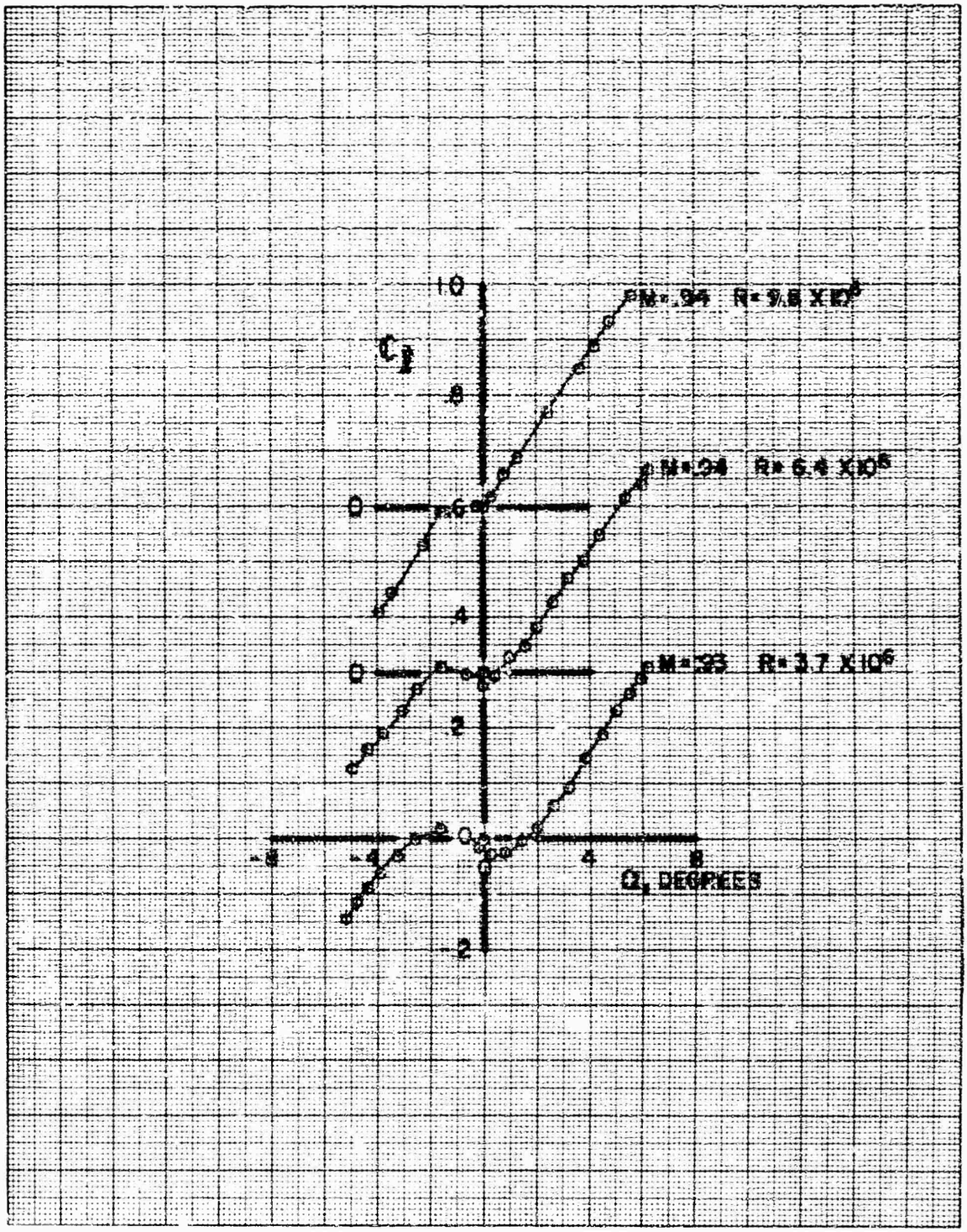


Figure 441. Variation of Section Lift Coefficient With Angle of Attack, NACA Section 63A015

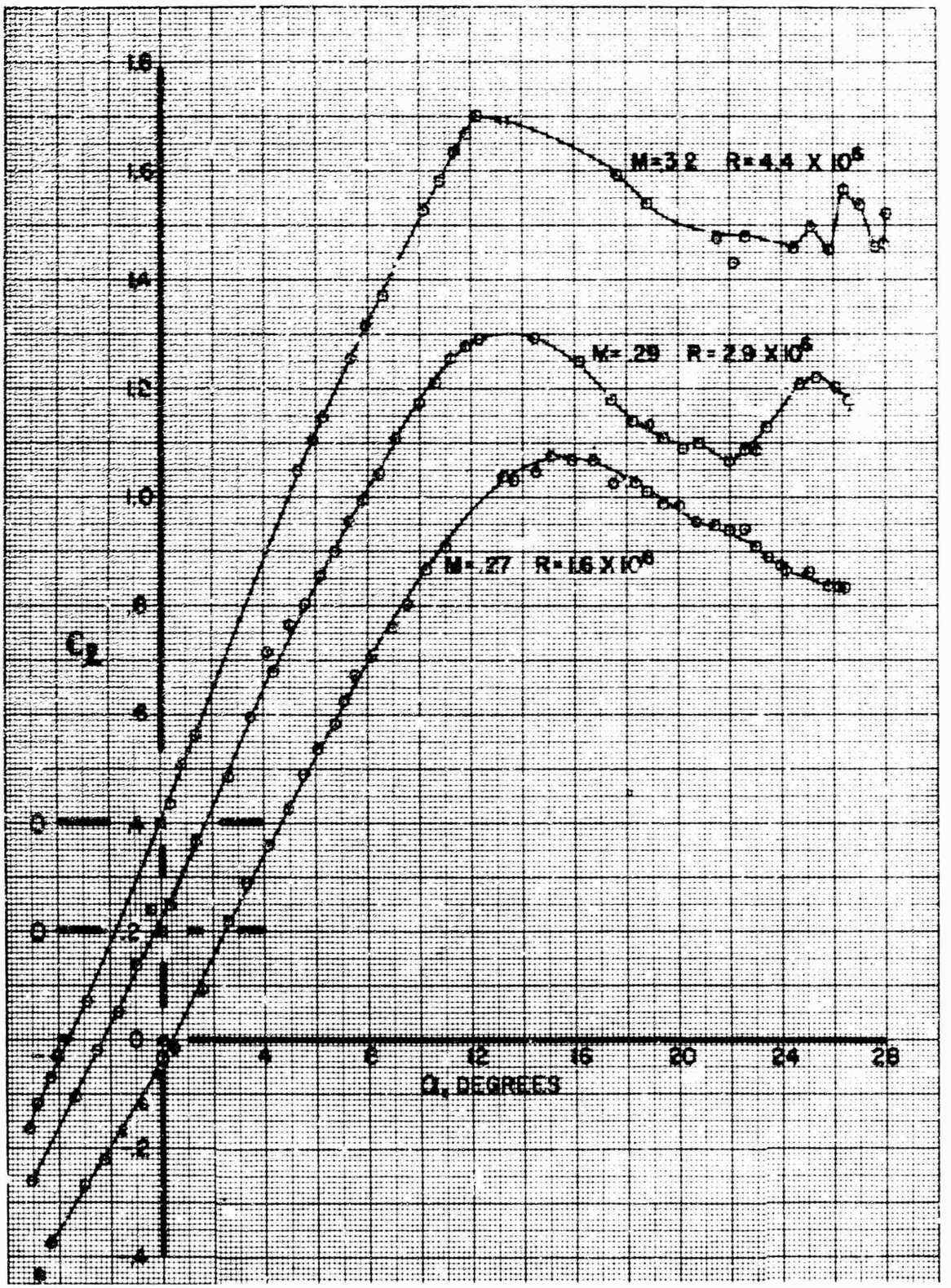


Figure 45A. Variation of Section Lift Coefficient With Angle of Attack, NACA Section 63A018

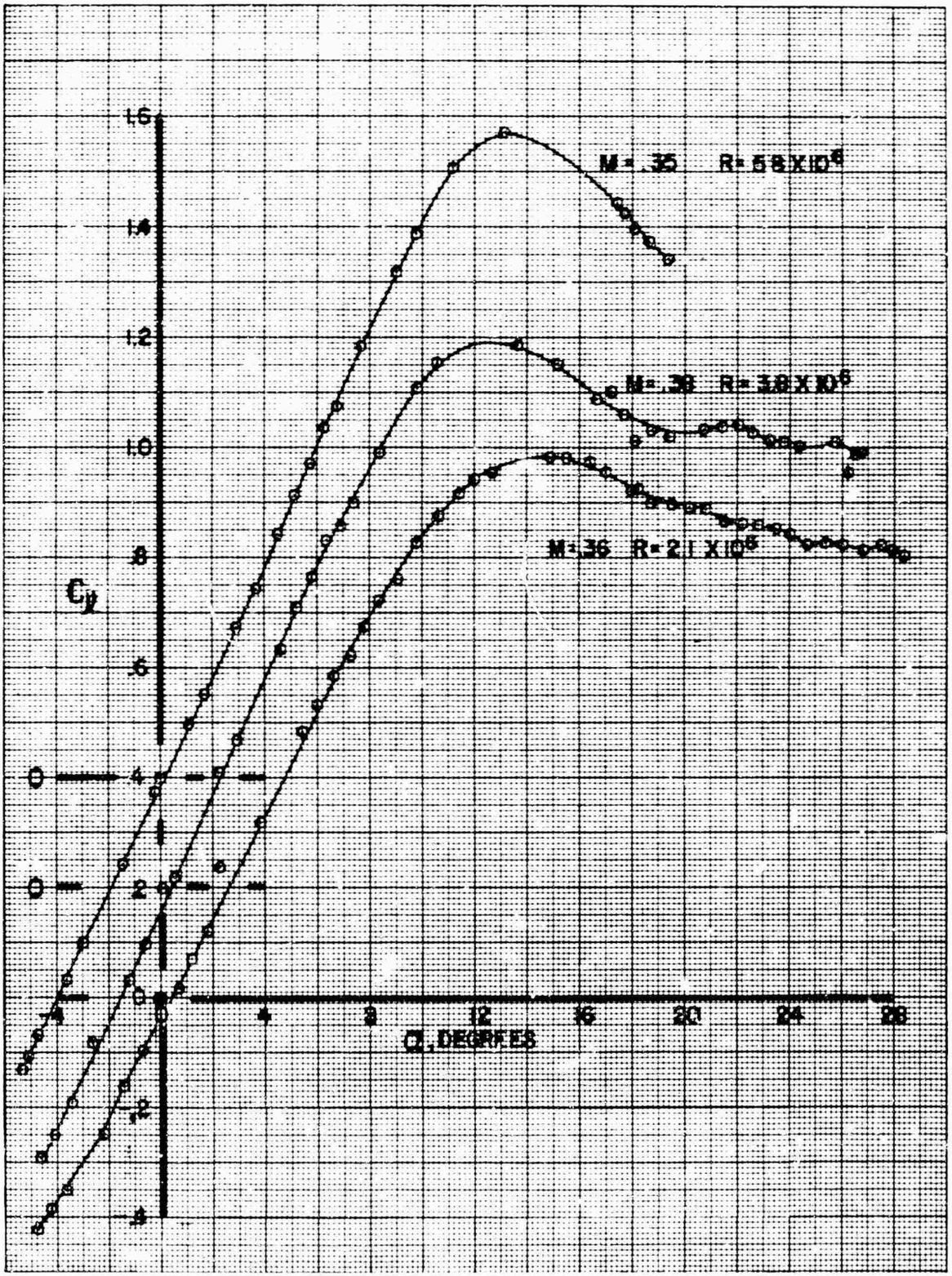


Figure 45B. Variation of Section Lift Coefficient With Angle of Attack, NACA Section 63A018

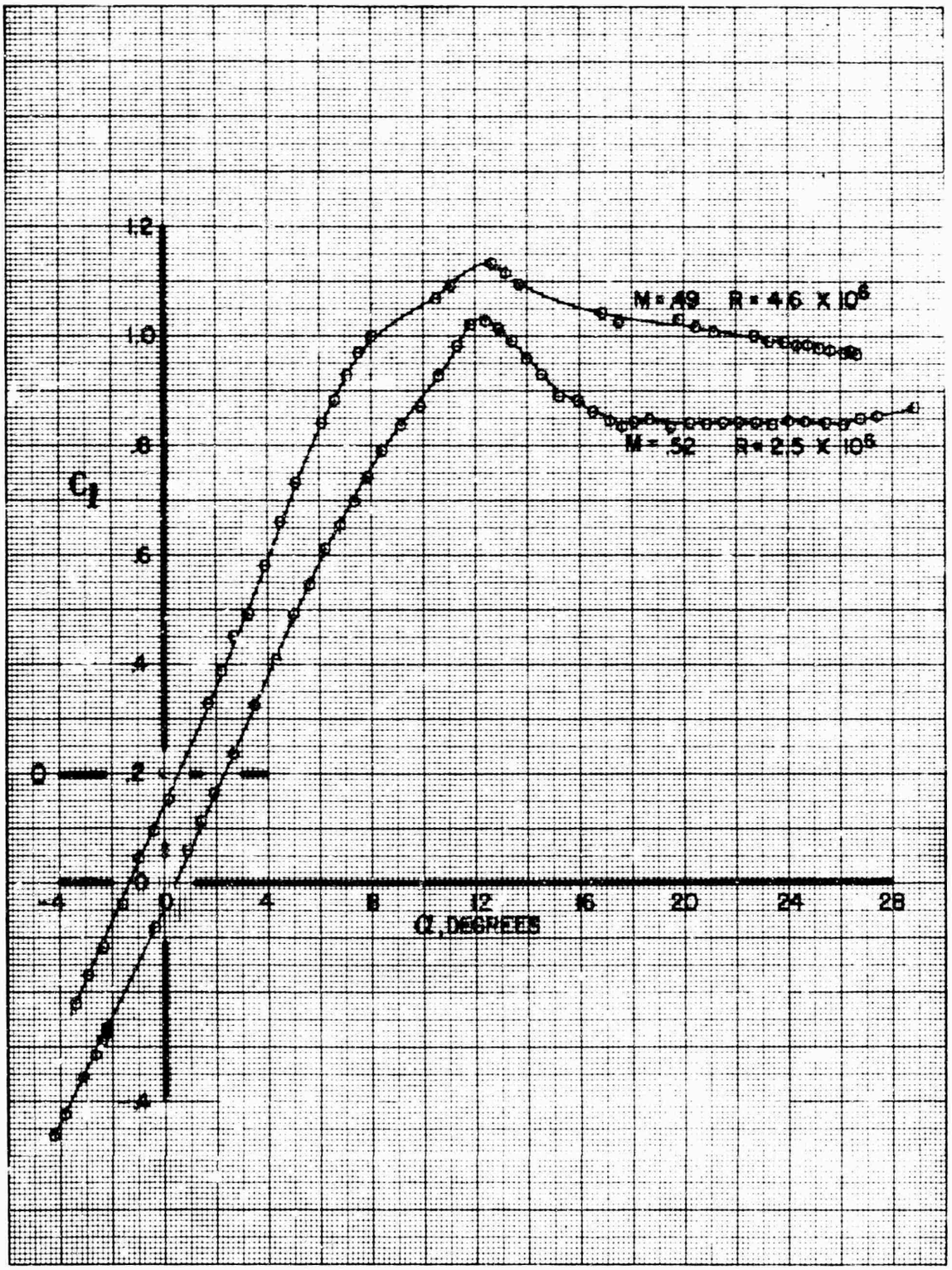


Figure 45C. Variation of Section Lift Coefficient With Angle of Attack, NACA Section 63A018

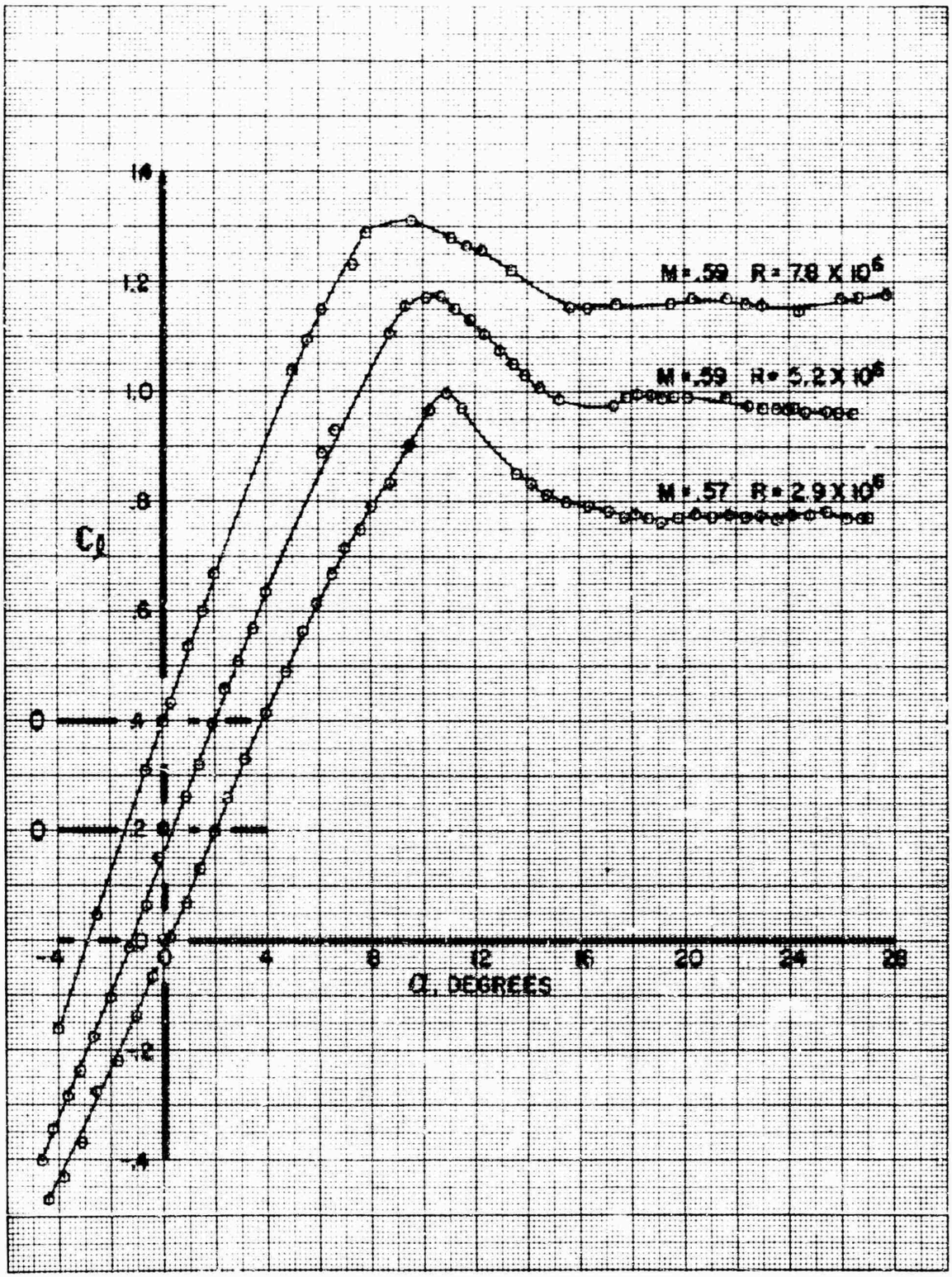


Figure 45D. Variation of Section Lift Coefficient With Angie of Attack, NACA Section 63A018

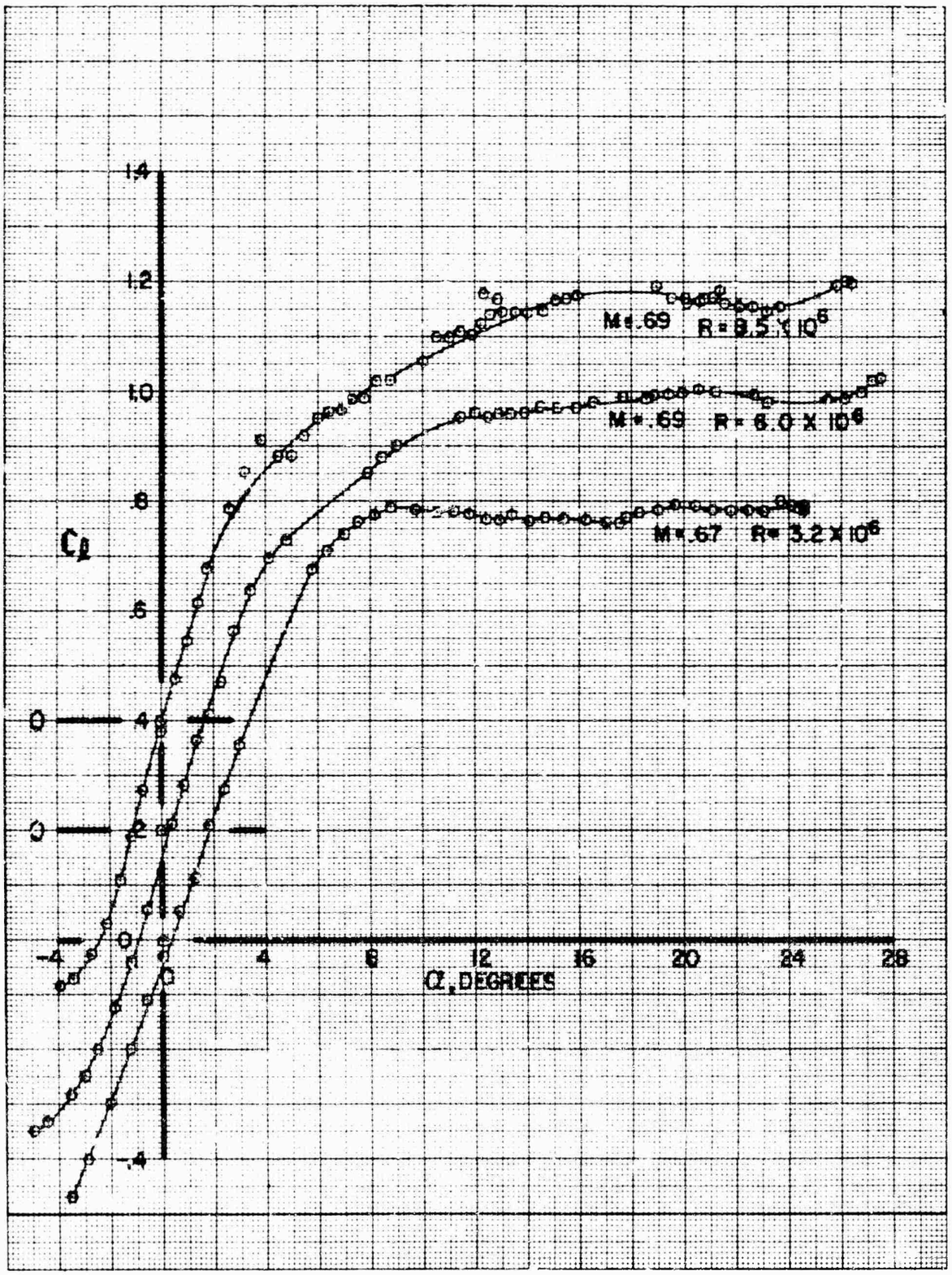


Figure 45E. Variation of Section Lift Coefficient With Angle of Attack, NACA Section 63A018

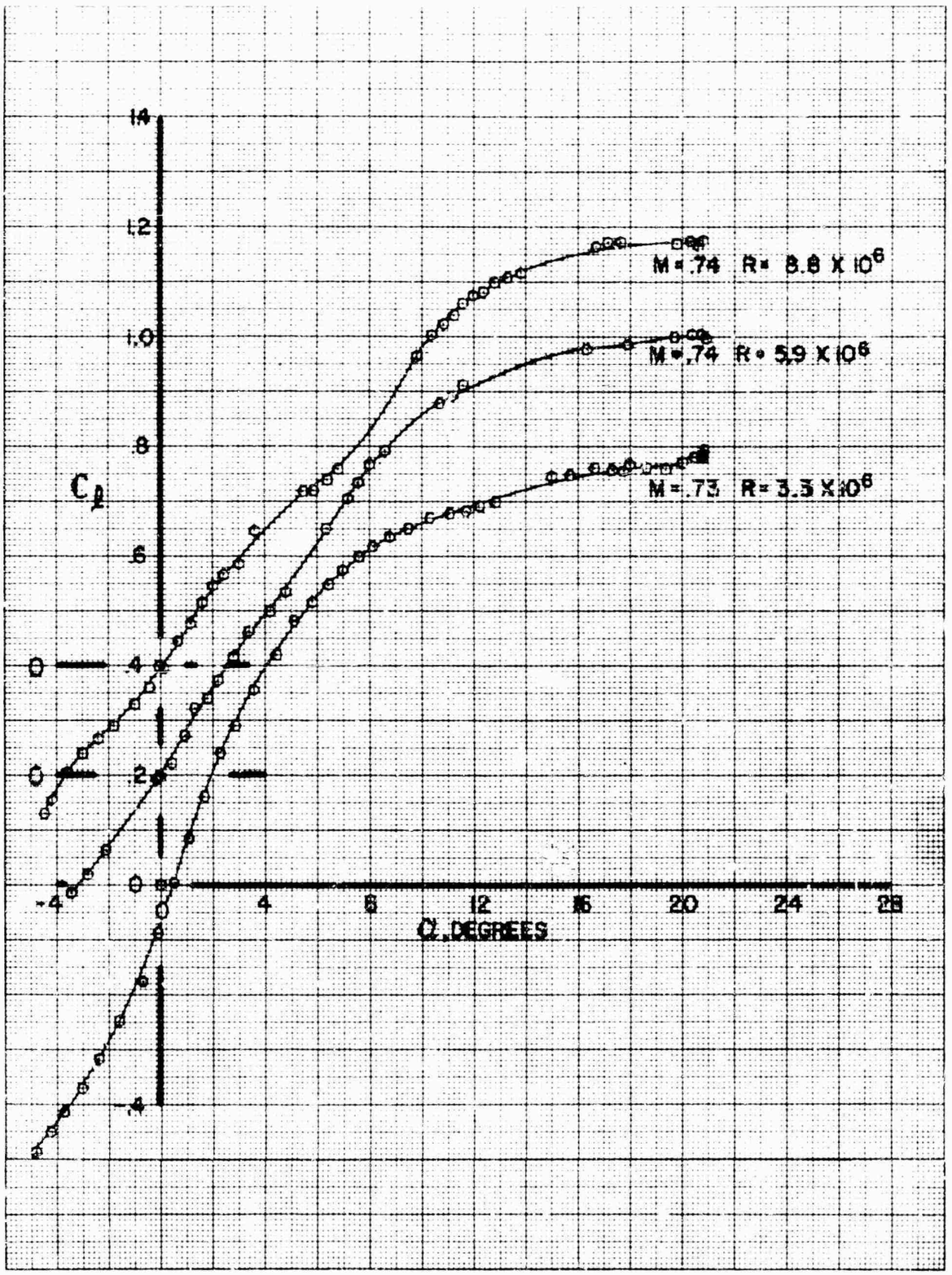


Figure 45F. Variation of Section Lift Coefficient With Angle of Attack, NACA Section 63A018

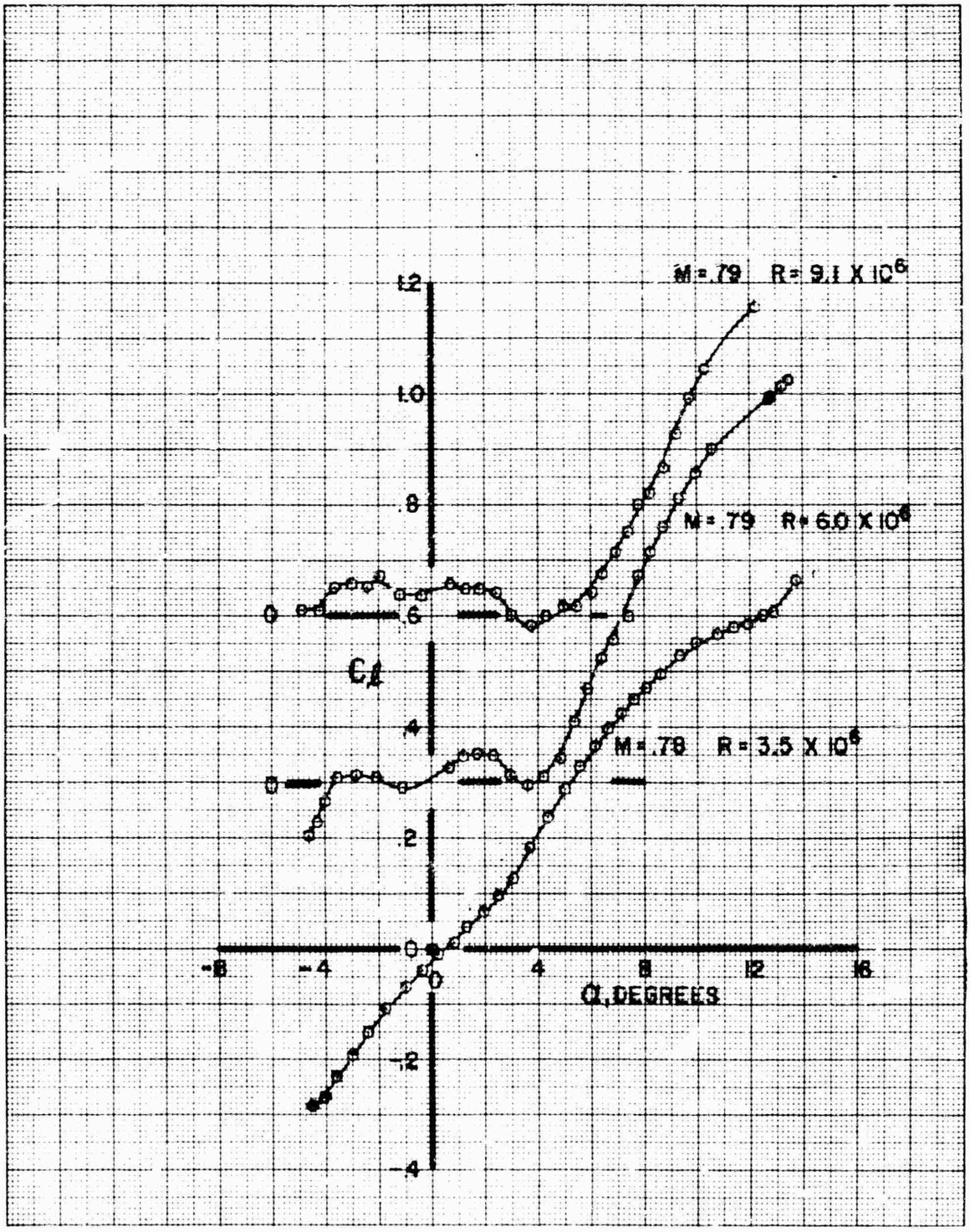


Figure 45G. Variation of Section Lift Coefficient With Angle of Attack, NACA Section 63A018

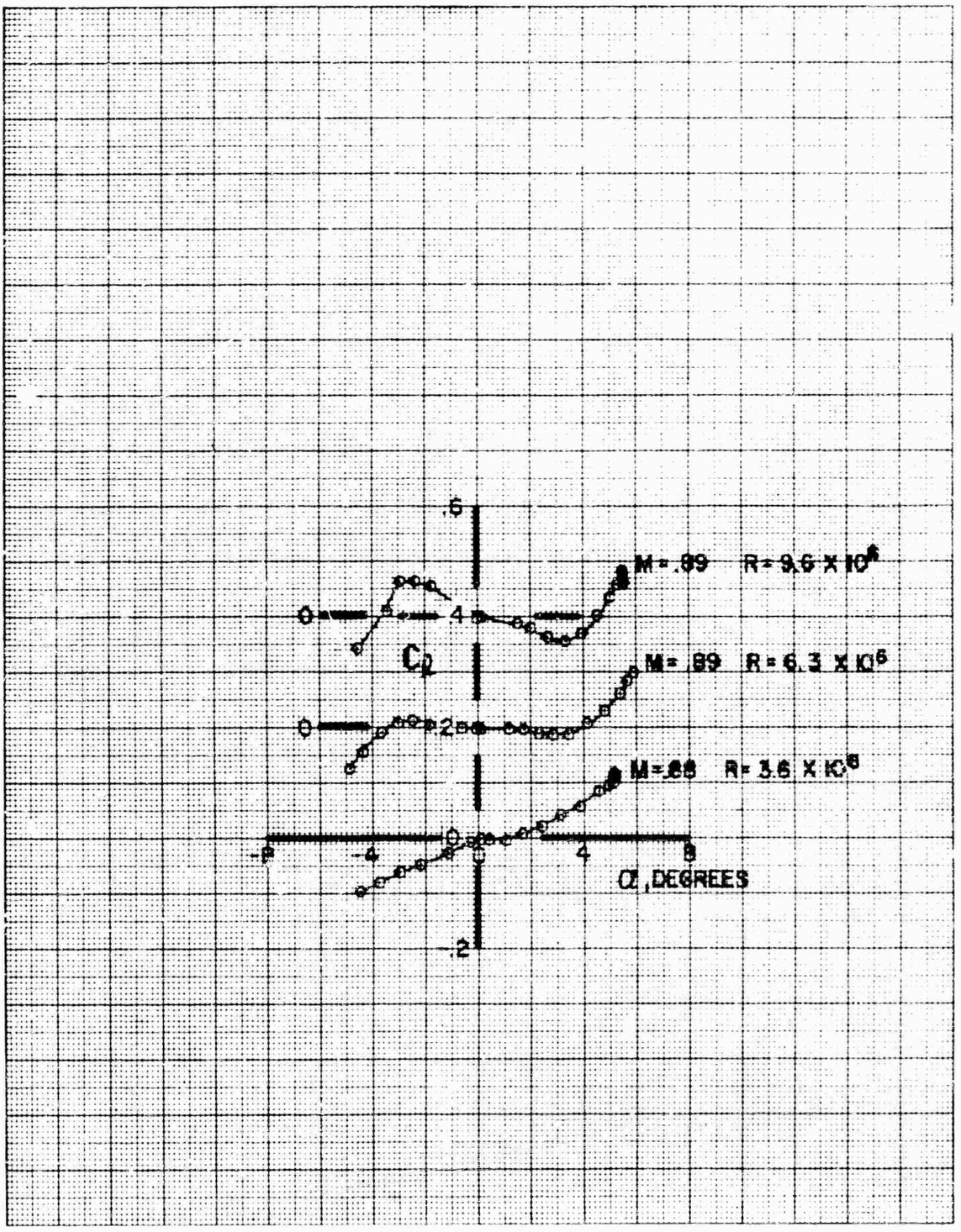


Figure 45H. Variation of Section Lift Coefficient With Angle of Attack, NACA Section 63A018

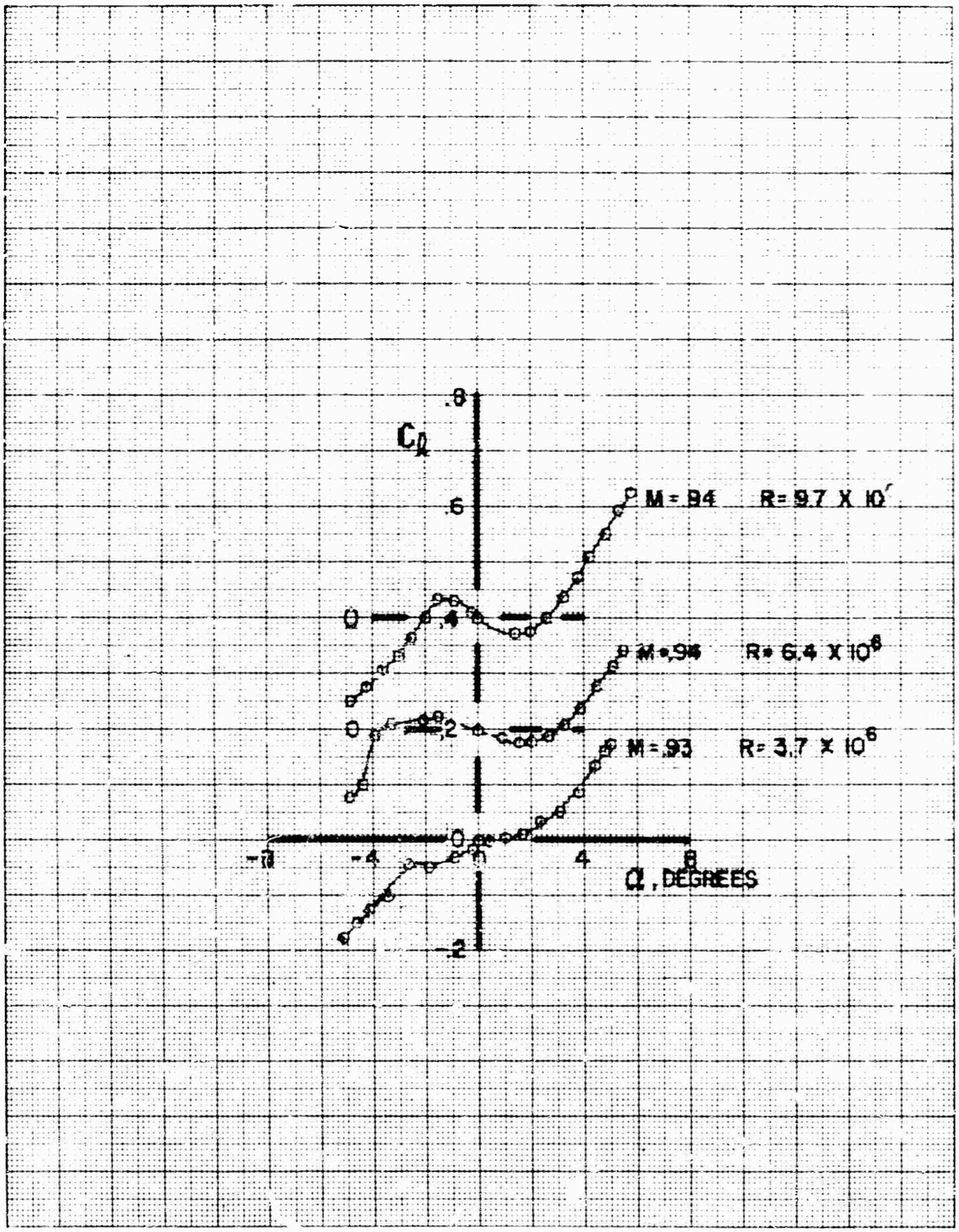


Figure 451. Variation of Section Lift Coefficient With Angle of Attack, NACA Section 63A018

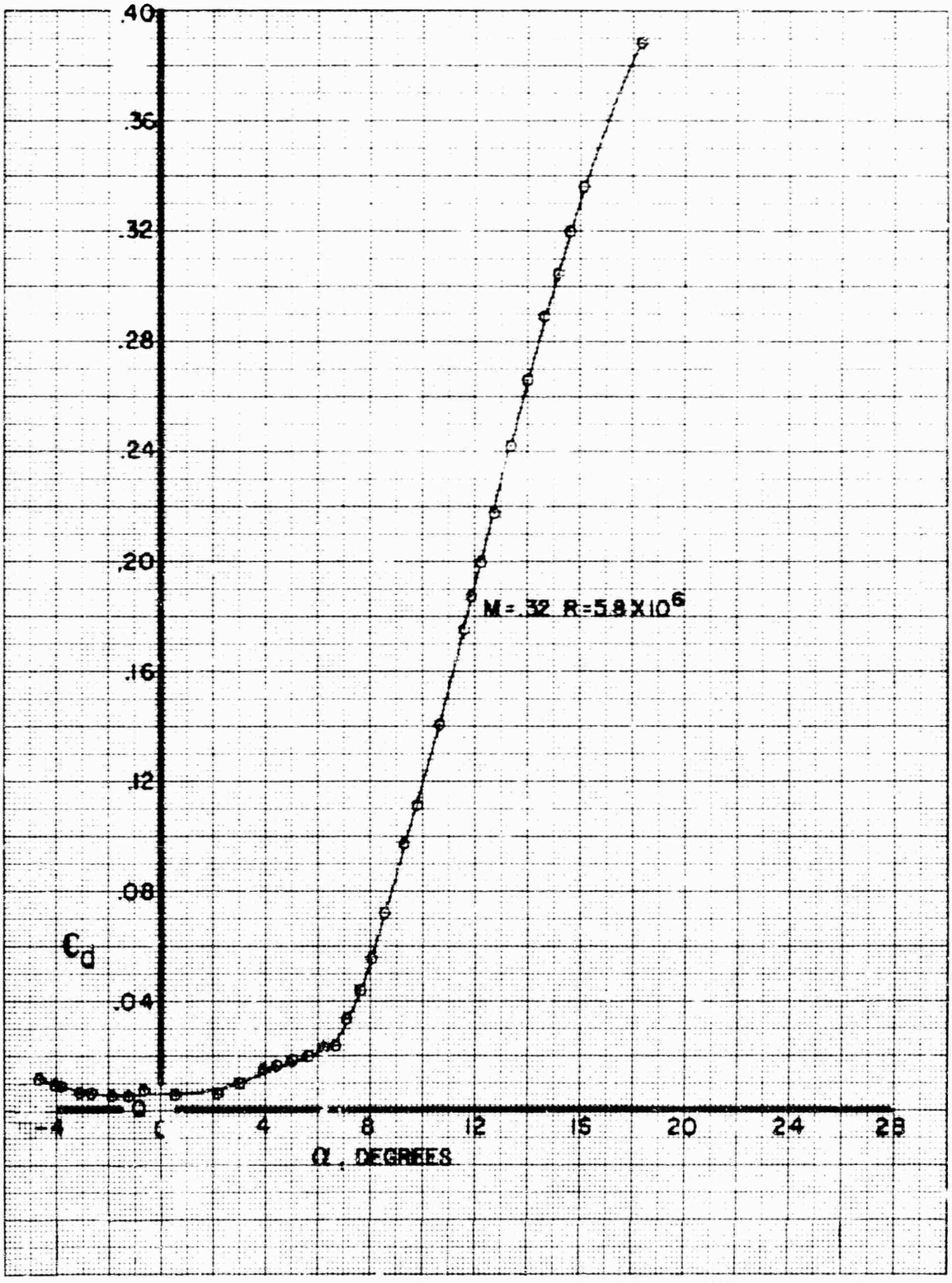


Figure 46A-1. Variation of Section Drag Coefficient With Angle of Attack, NACA Section 63A009

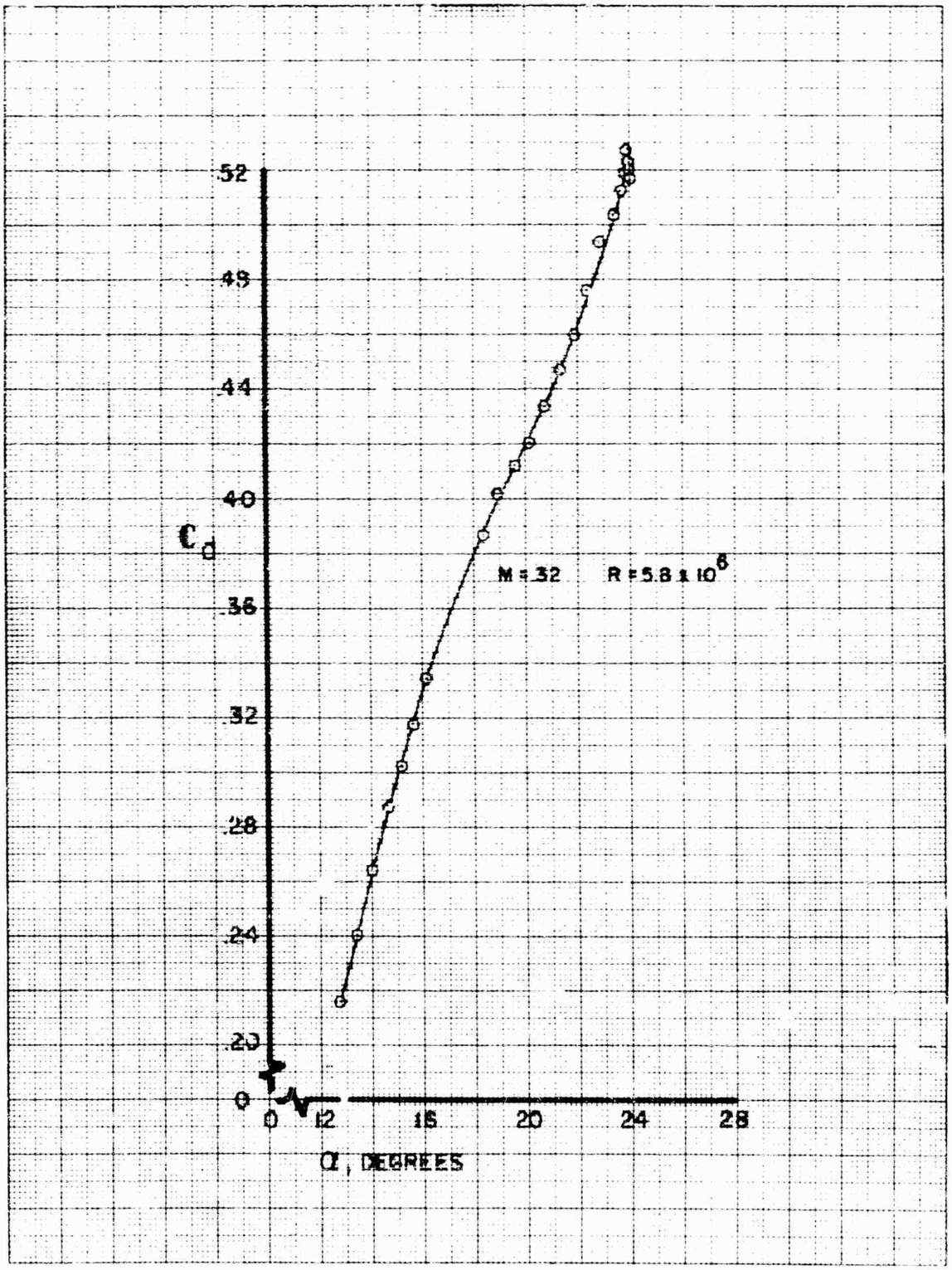


Figure 46A-2. Variation of Section Drag Coefficient With Angle of Attack, NACA Section 63A009

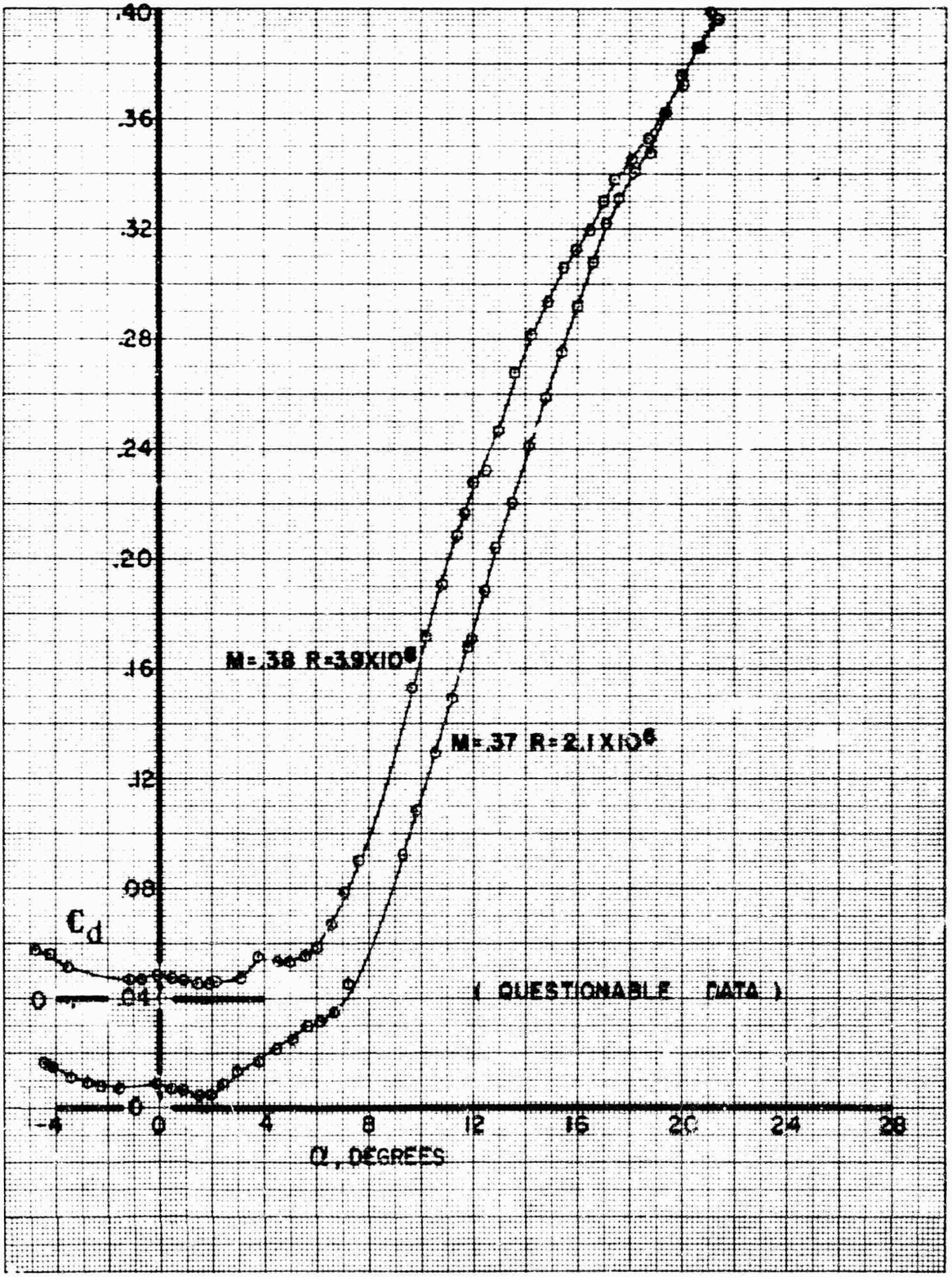


Figure 46B-1. Variation of Section Drag Coefficient With Angle of Attack, NACA Section 63A009

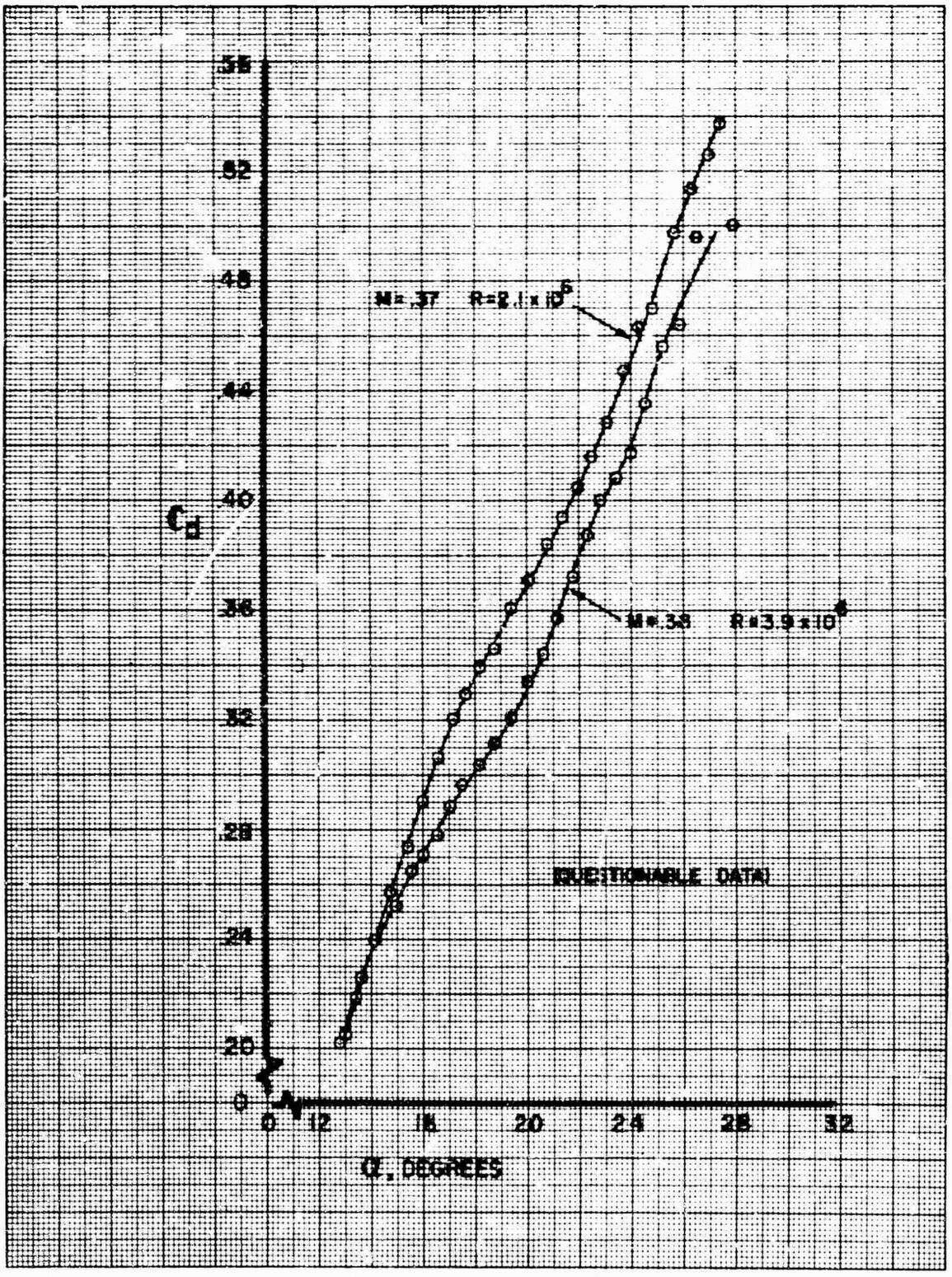


Figure 46B-2. Variation of Section Drag Coefficient With Angle of Attack, NACA Section 63A009

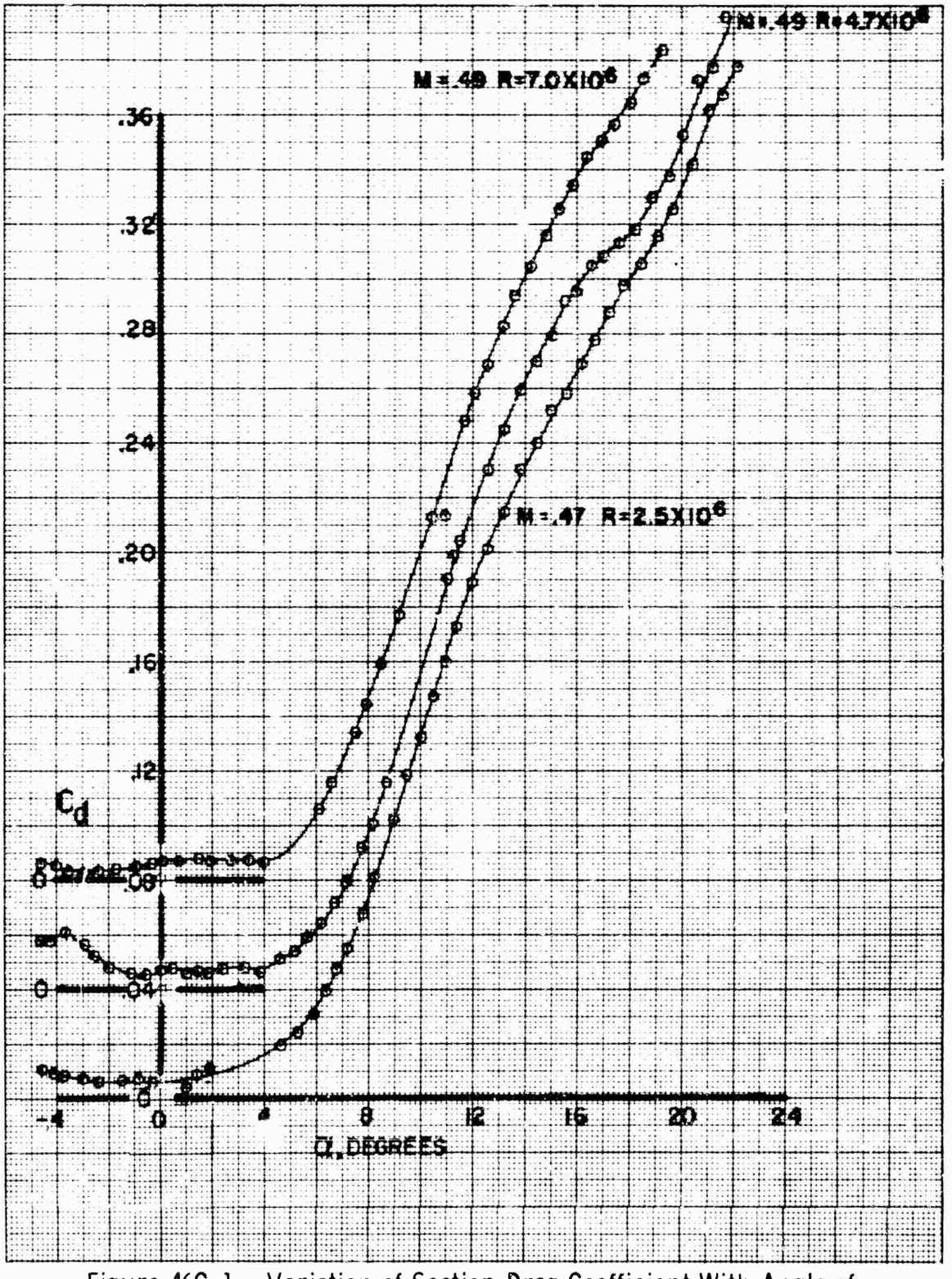


Figure 46C-1. Variation of Section Drag Coefficient With Angle of Attack, NACA Section 63A009

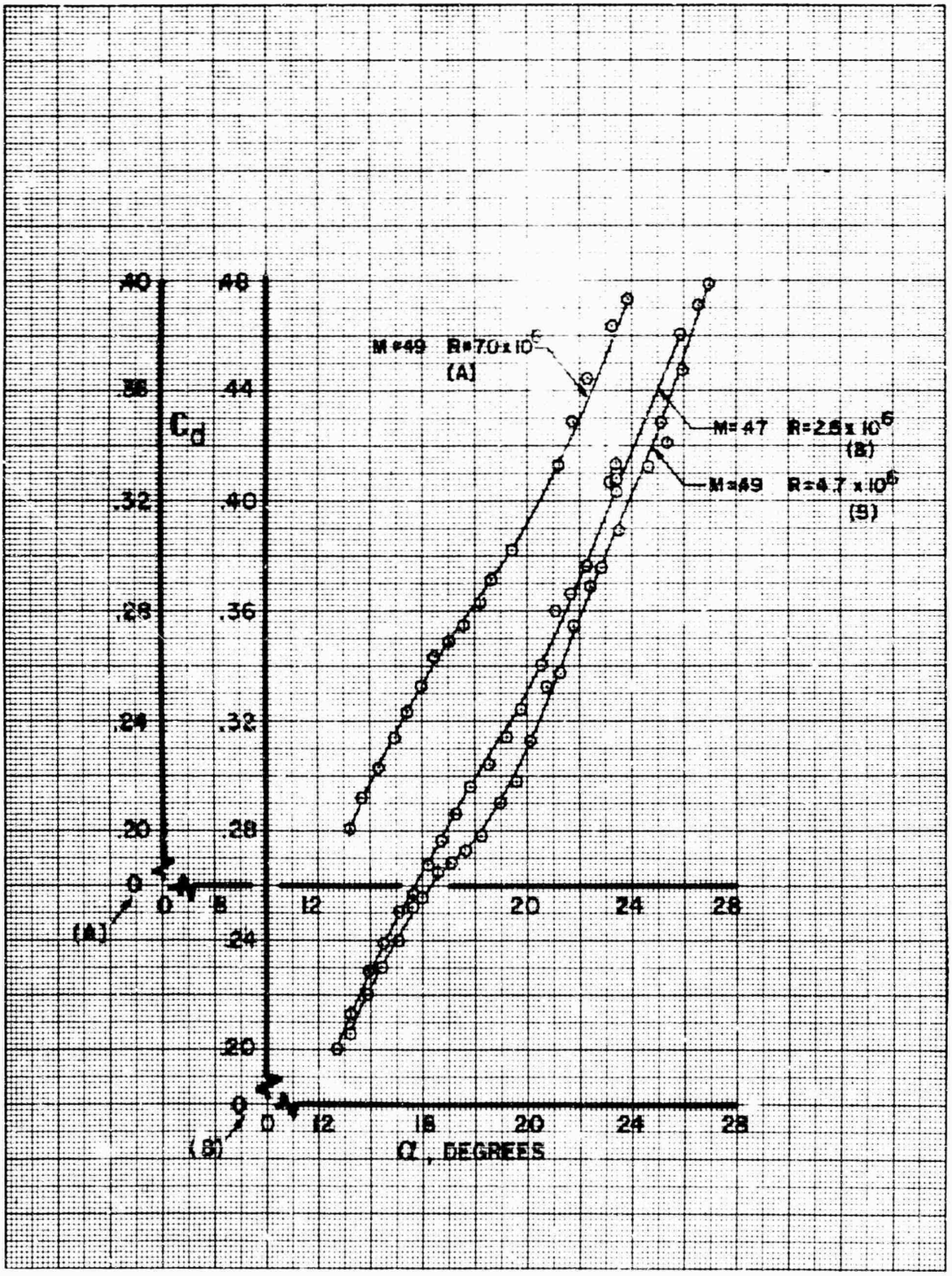


Figure 46C-2. Variation of Section Drag Coefficient With Angle of Attack, NACA Section 63A009

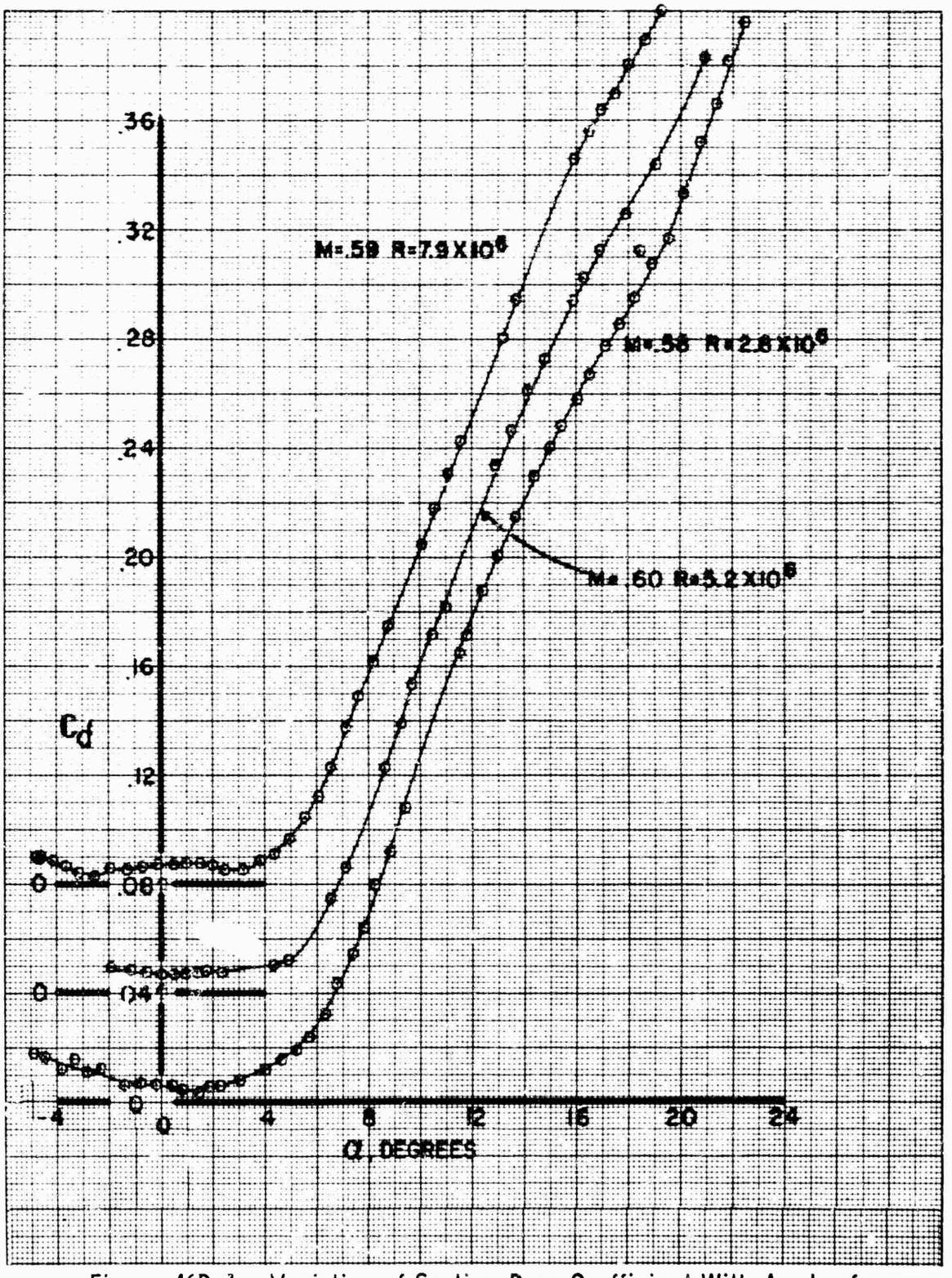


Figure 46D-1. Variation of Section Drag Coefficient With Angle of Attack, NACA Section 63A009

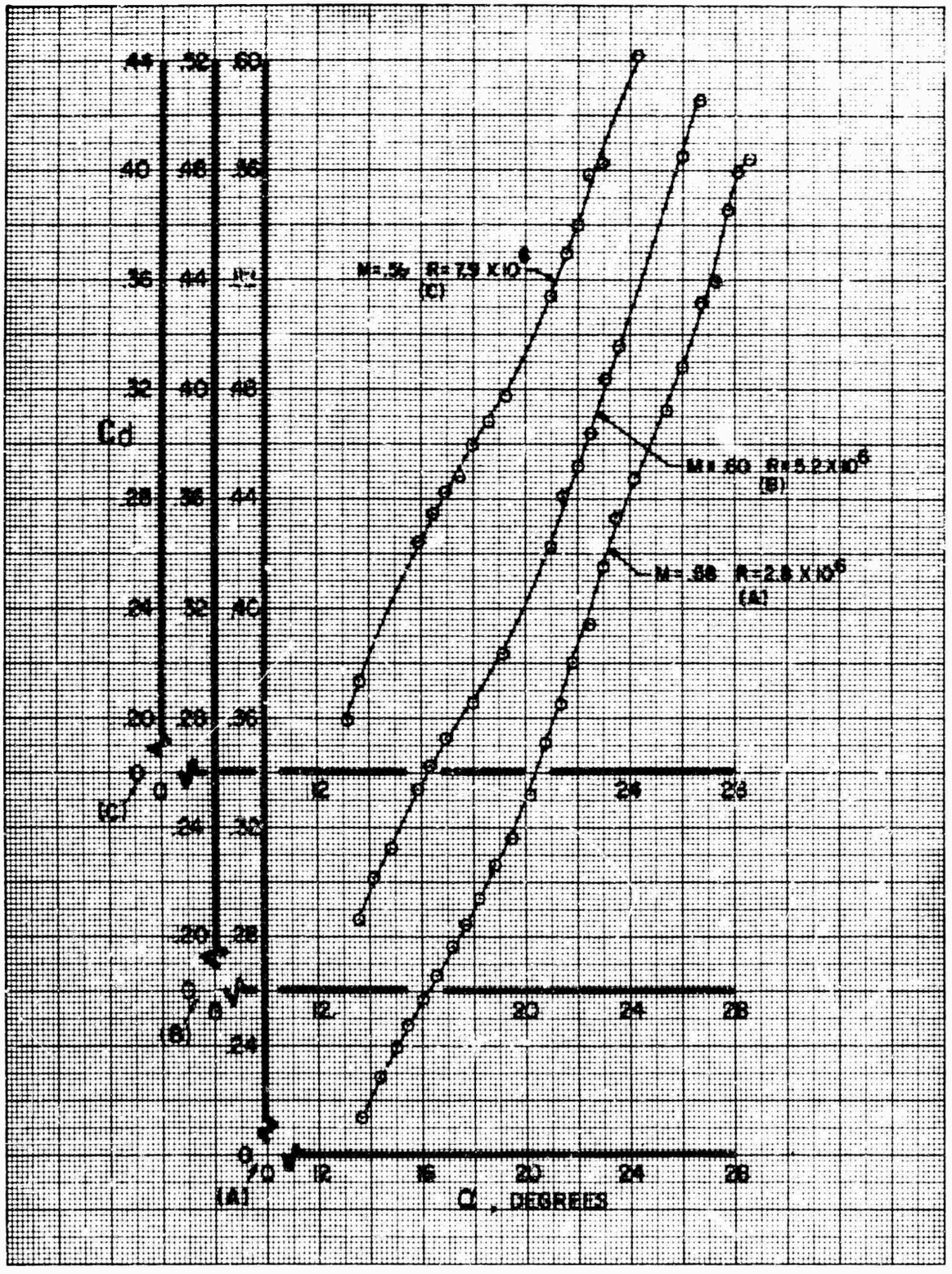


Figure 46D-2. Variation of Section Drag Coefficient With Angle of Attack, NACA Section 63A009

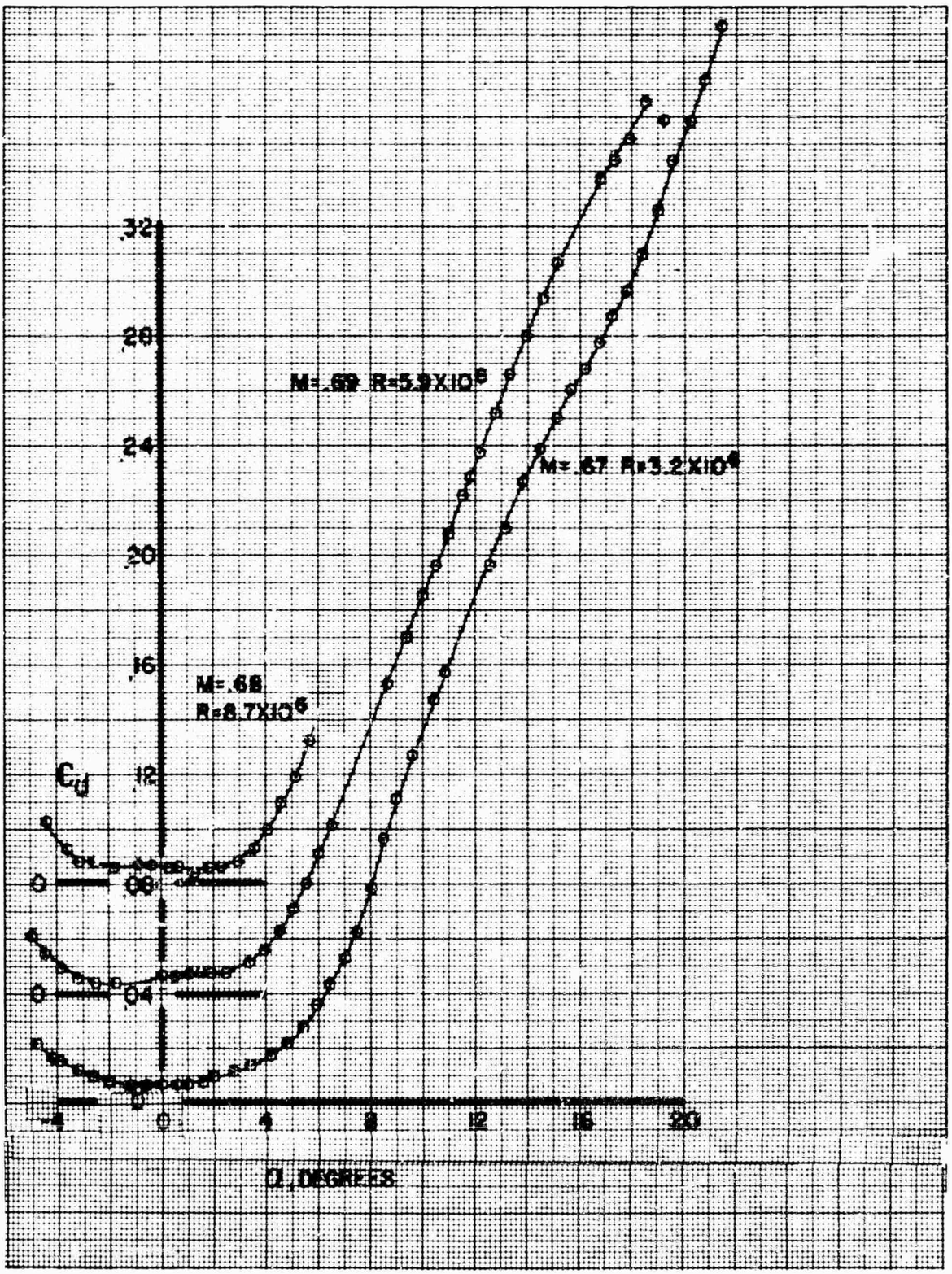


Figure 46E-1. Variation of Section Drag Coefficient With Angle of Attack, NACA Section 63A009

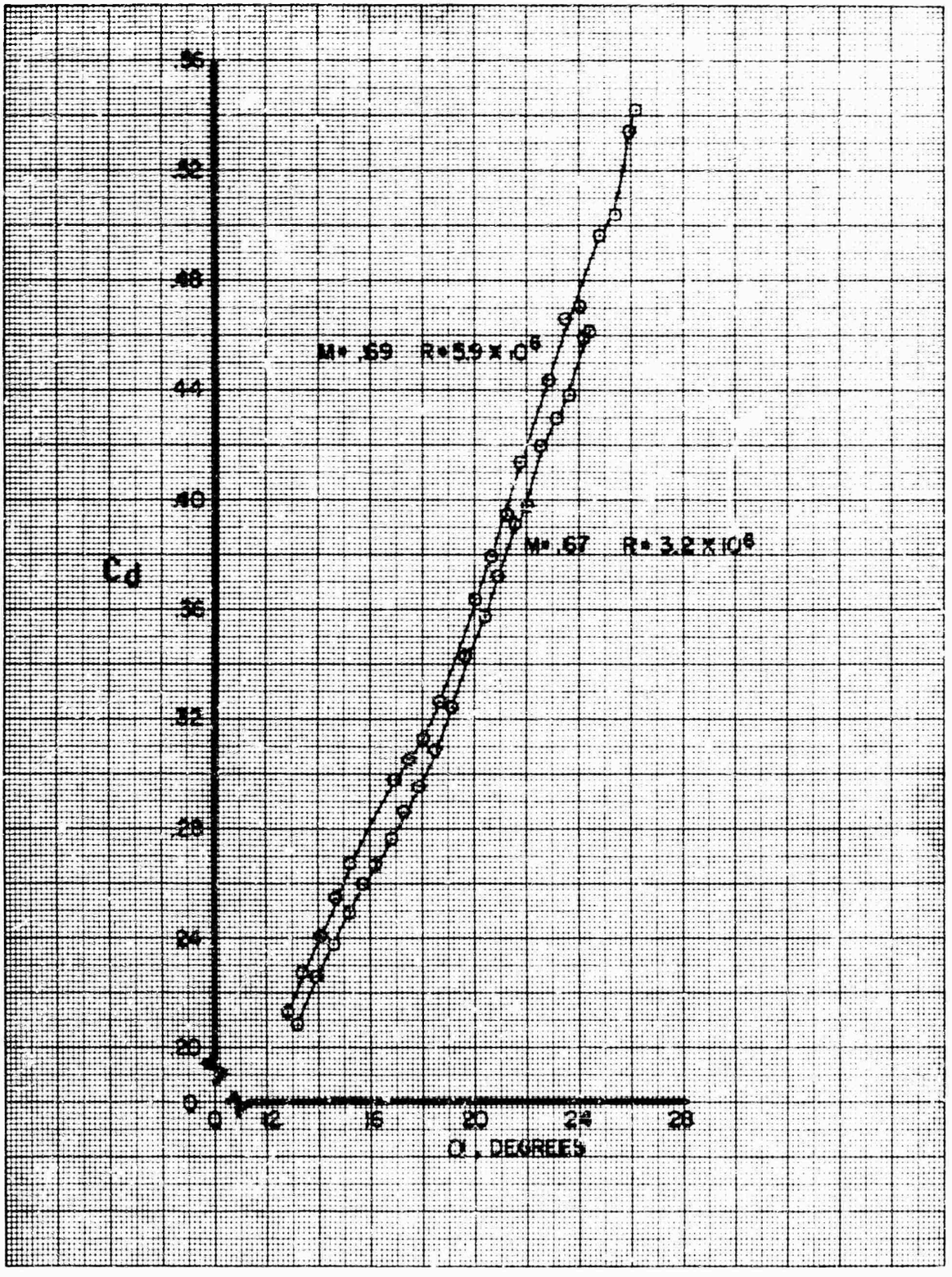


Figure 46E-2. Variation of Section Drag Coefficient With Angle of Attack, NACA Section 63A009

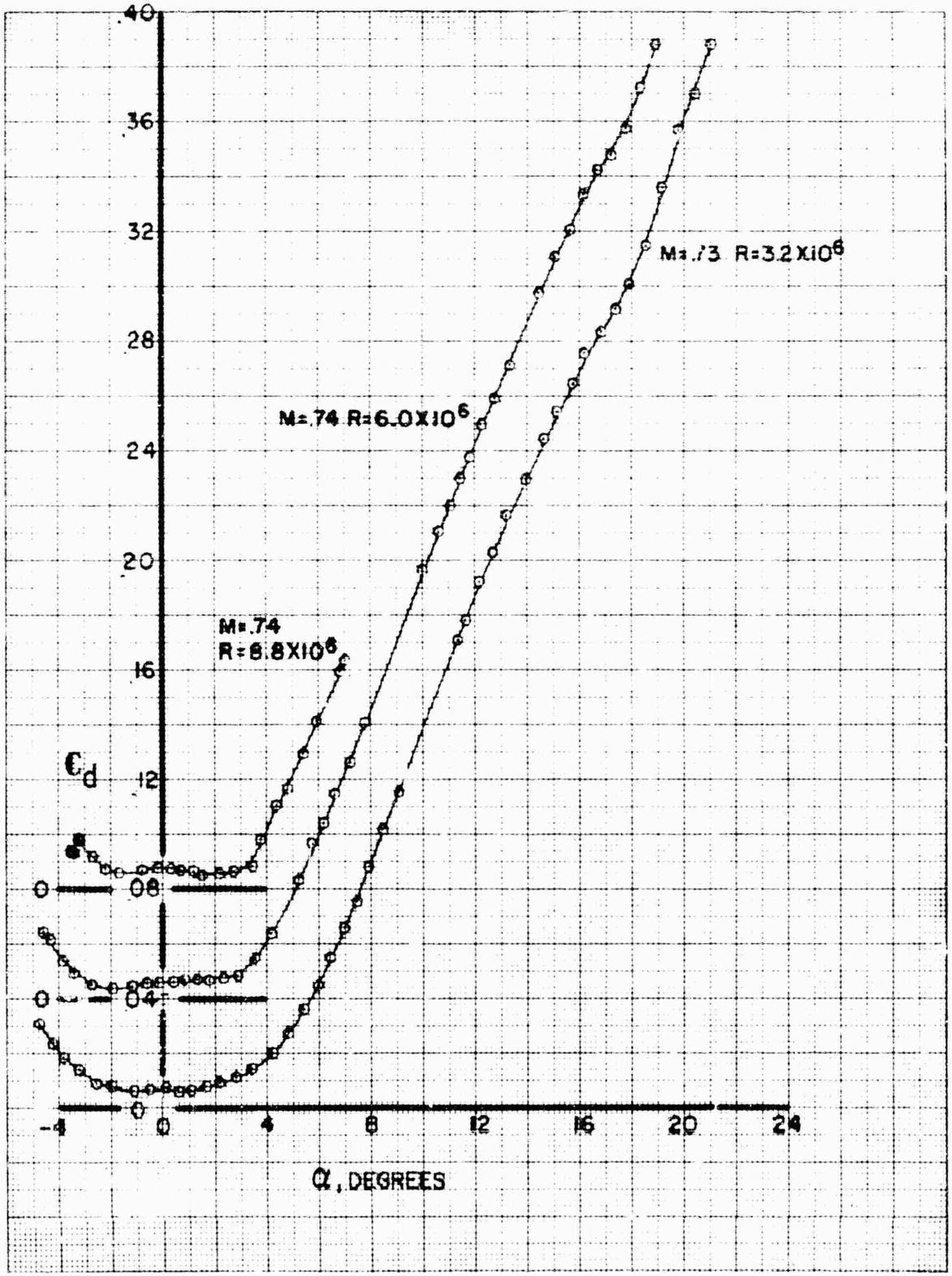


Figure 46F-1. Variation of Section Drag Coefficient With Angle of Attack, NACA Section 63A009

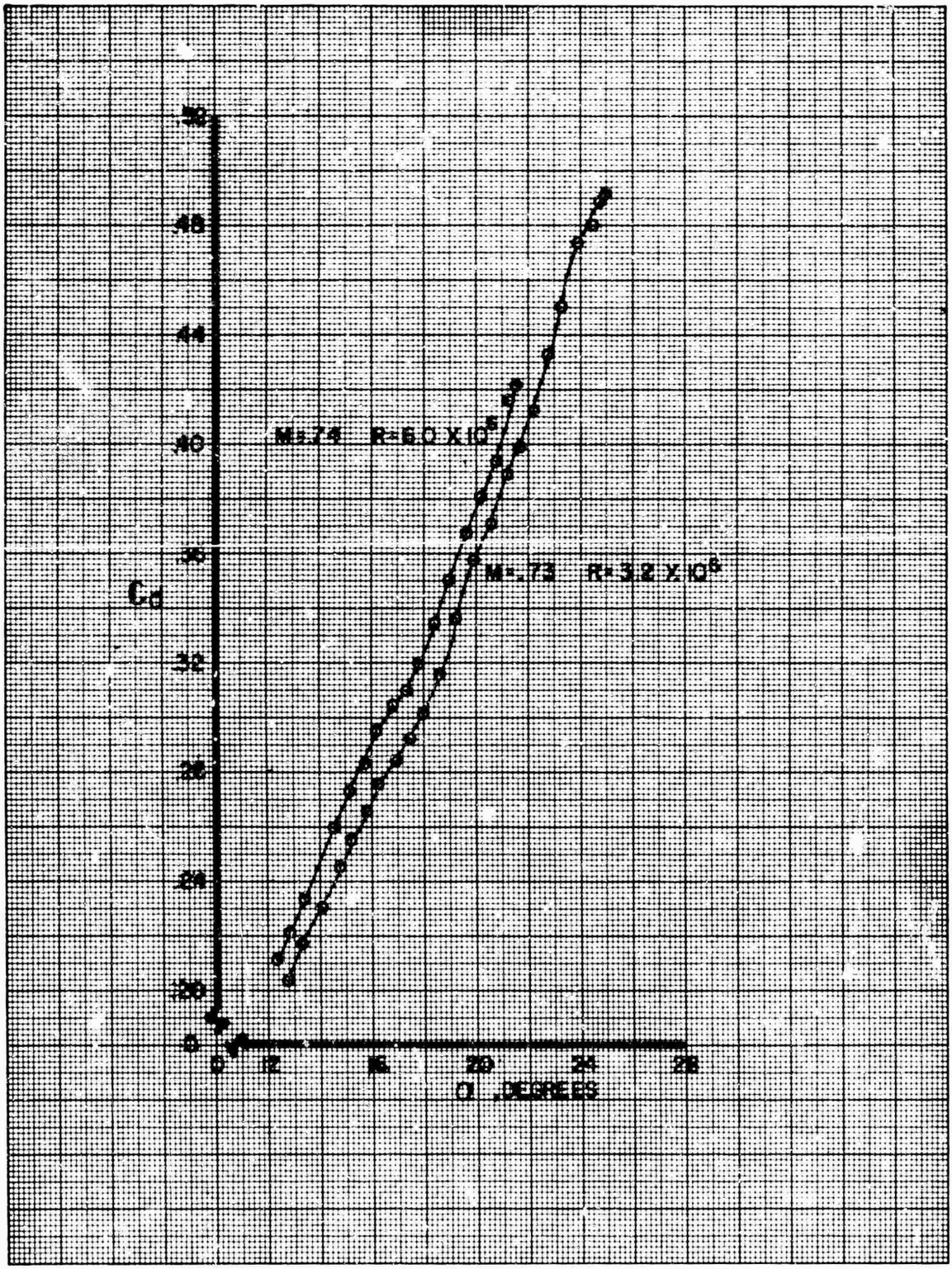


Figure 46F-2. Variation of Section Drag Coefficient With Angle of Attack, NACA Section 63A009

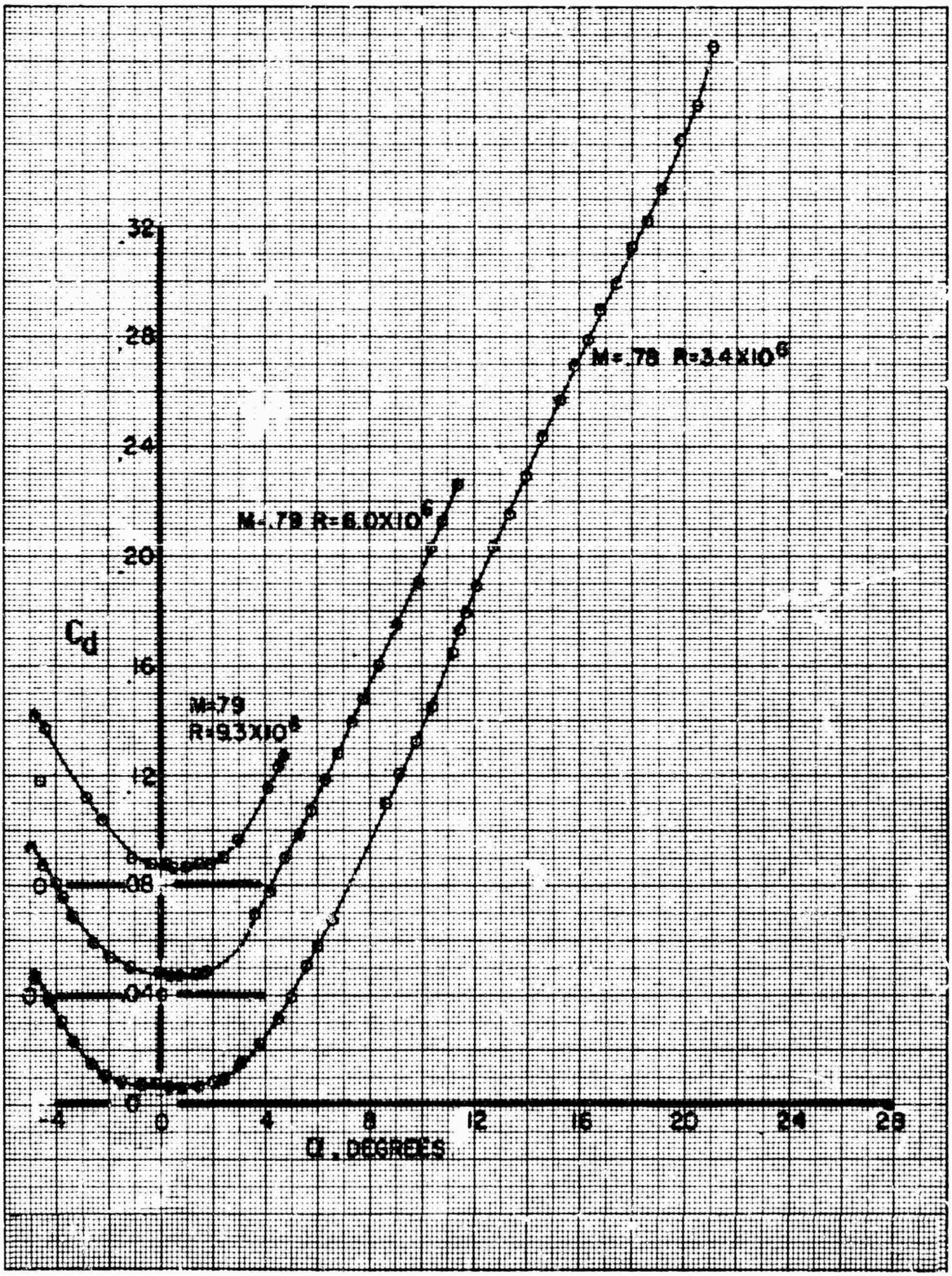


Figure 46G-1. Variation of Section Drag Coefficient With Angle of Attack, NACA Section 63A009 .

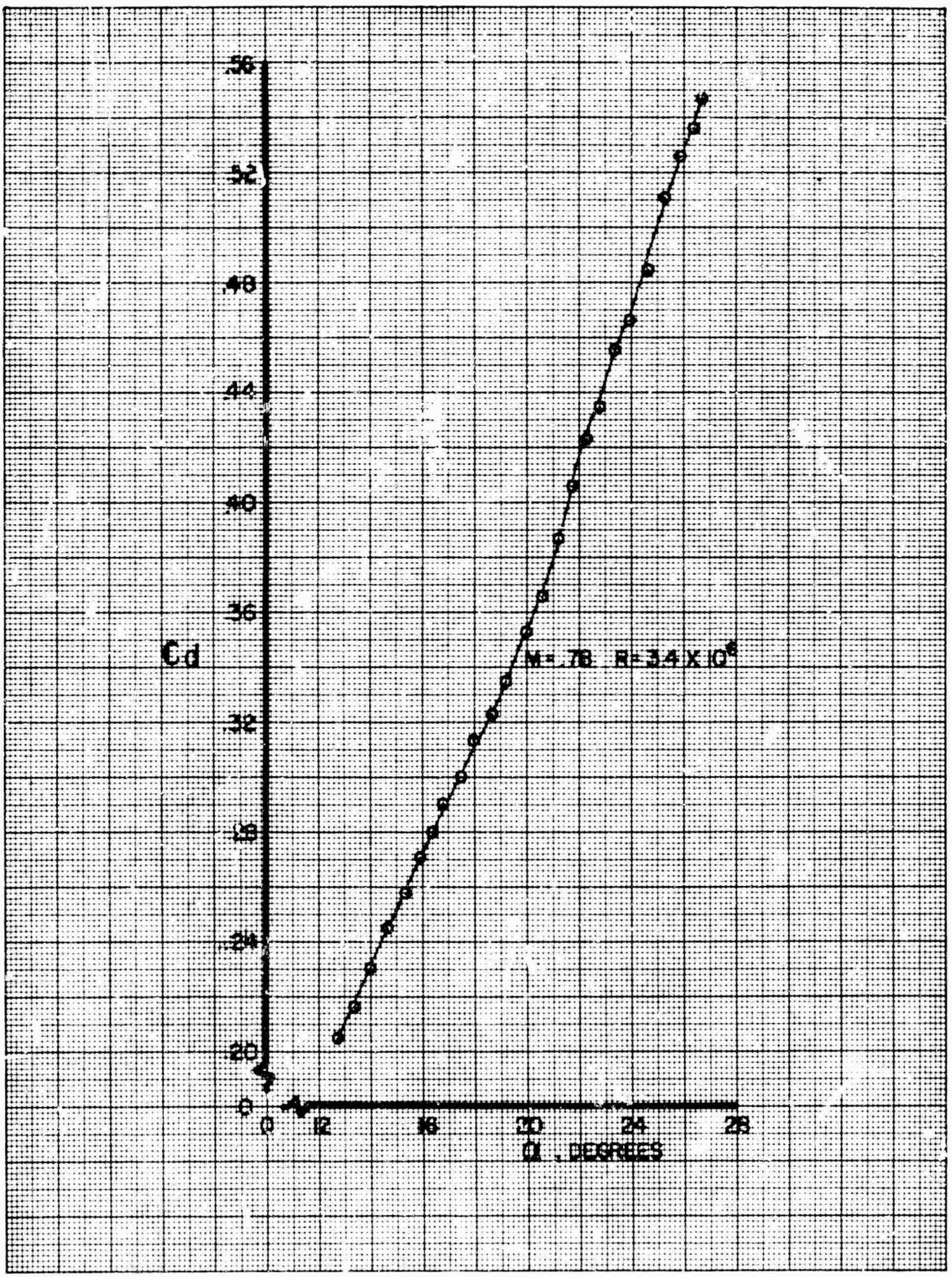


Figure 46G-2. Variation of Section Drag Coefficient With Angle of Attack, NACA Section 63A009

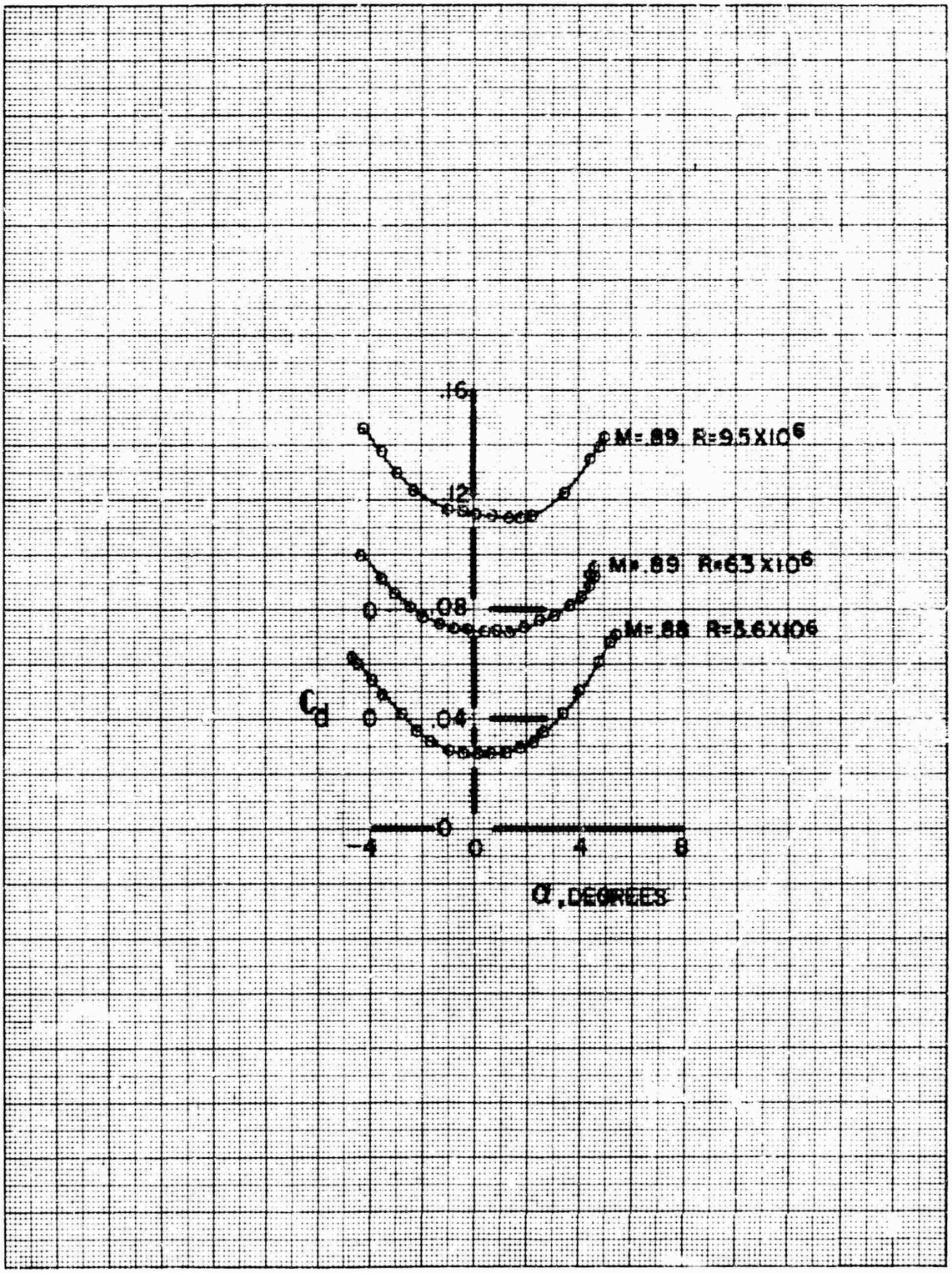


Figure 46H. Variation of Section Drag Coefficient With Angle of Attack, NACA Section 63A009

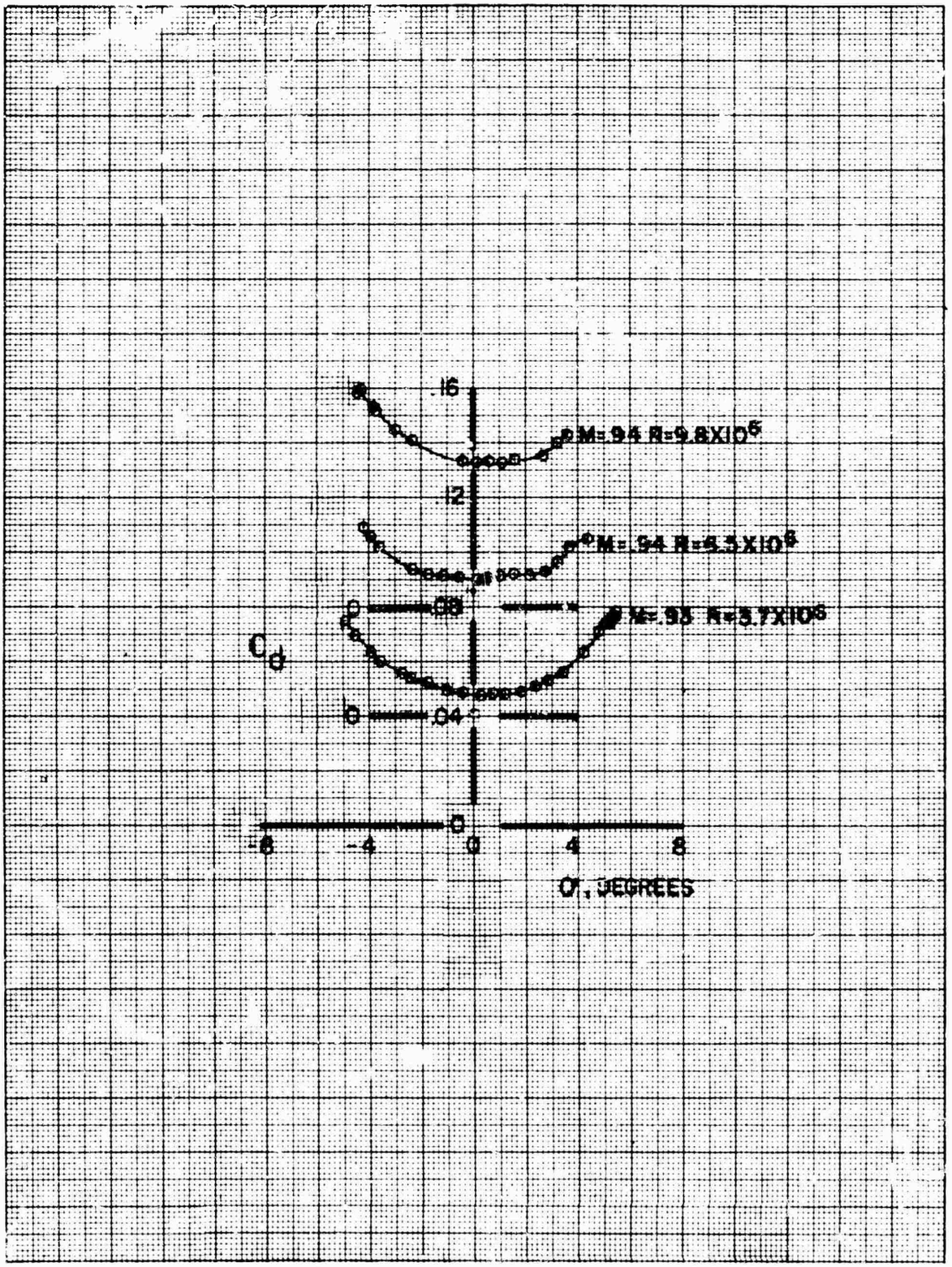


Figure 461. Variation of Section Drag Coefficient With Angle of Attack, NACA Section 63A009

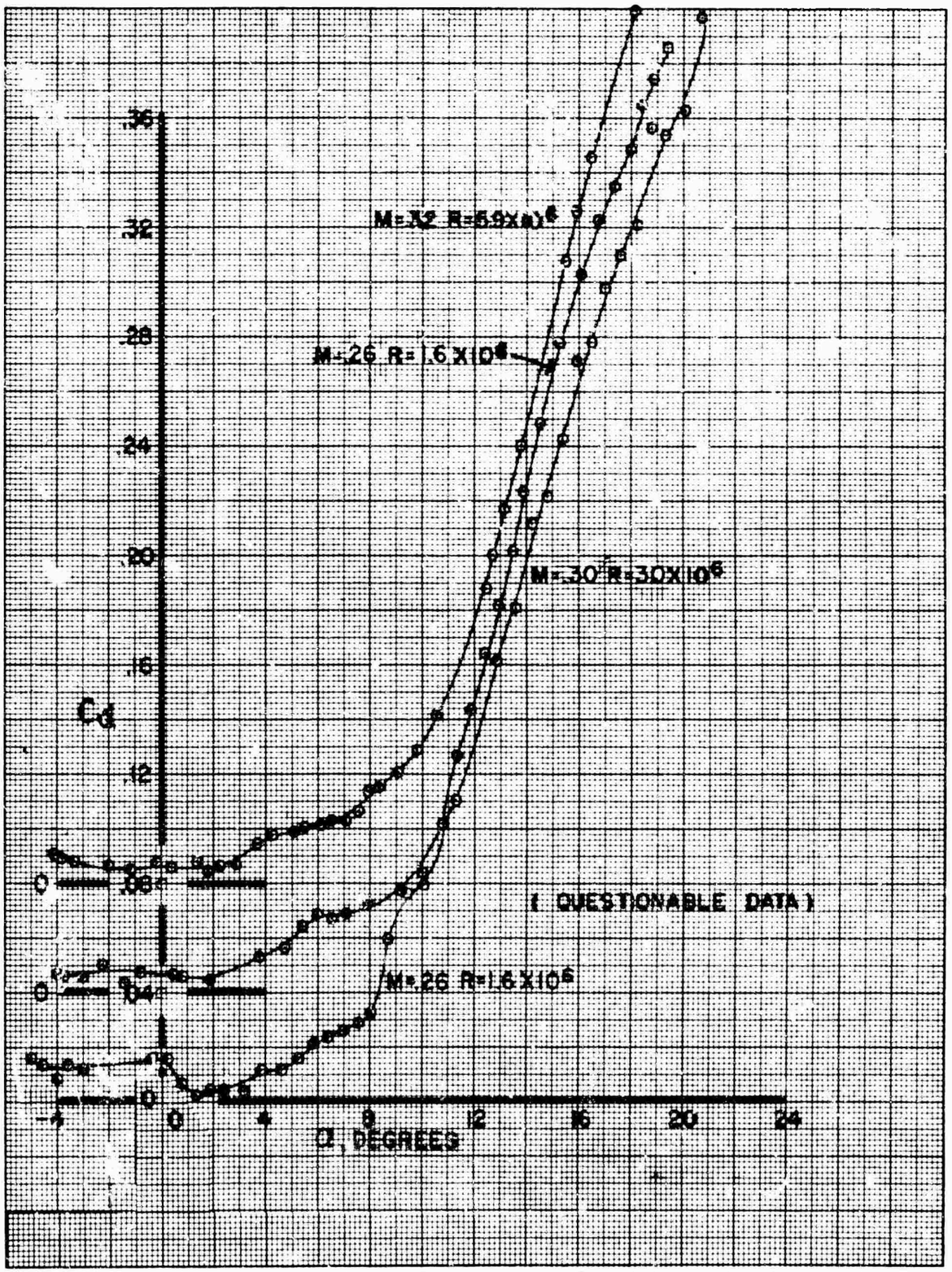


Figure 47A-1. Variation of Section Drag Coefficient With Angle of Attack, NACA Section 63A012

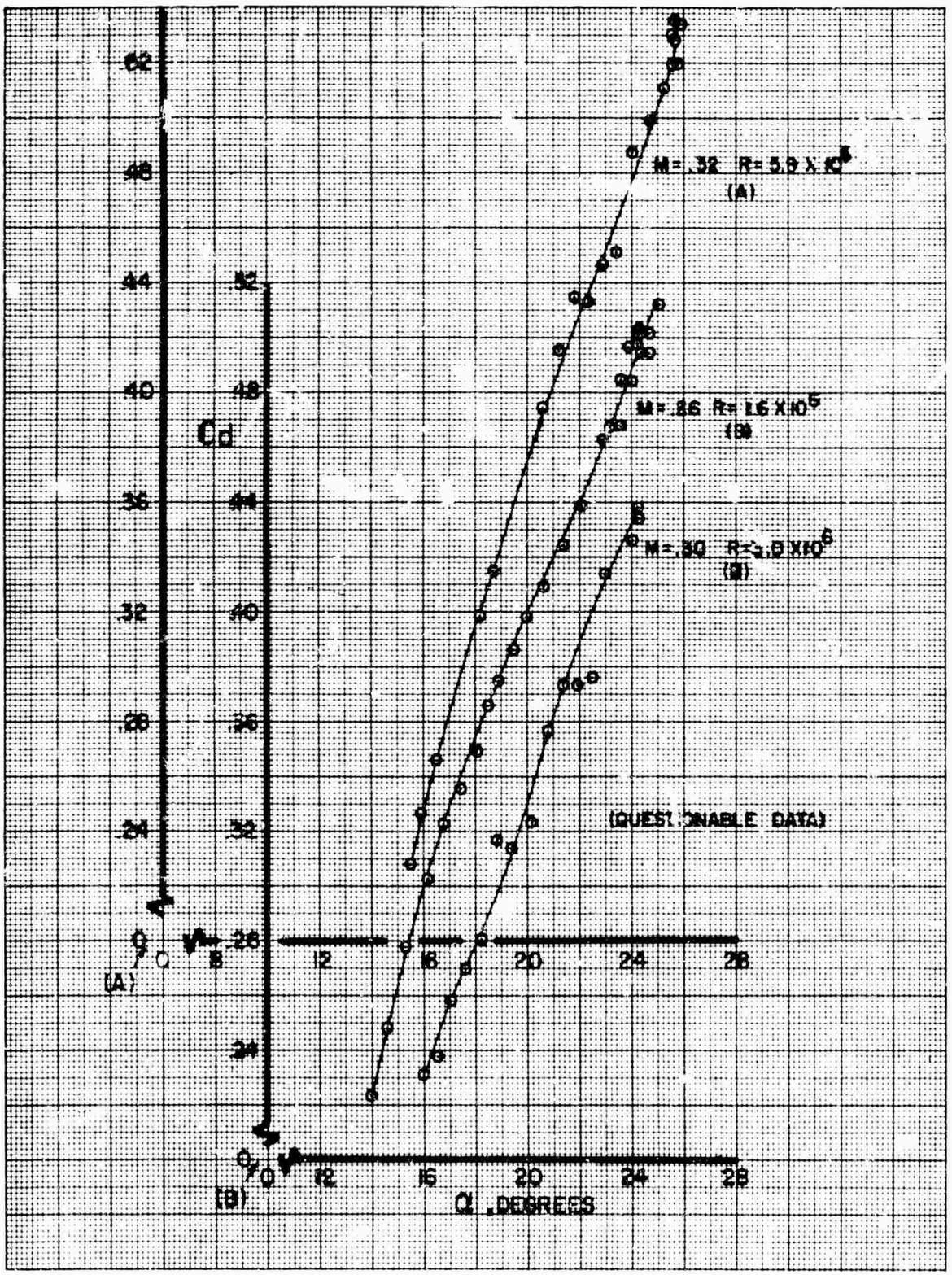


Figure 47A-2. Variation of Section Drag Coefficient With Angle of Attack, NACA Section 63A012

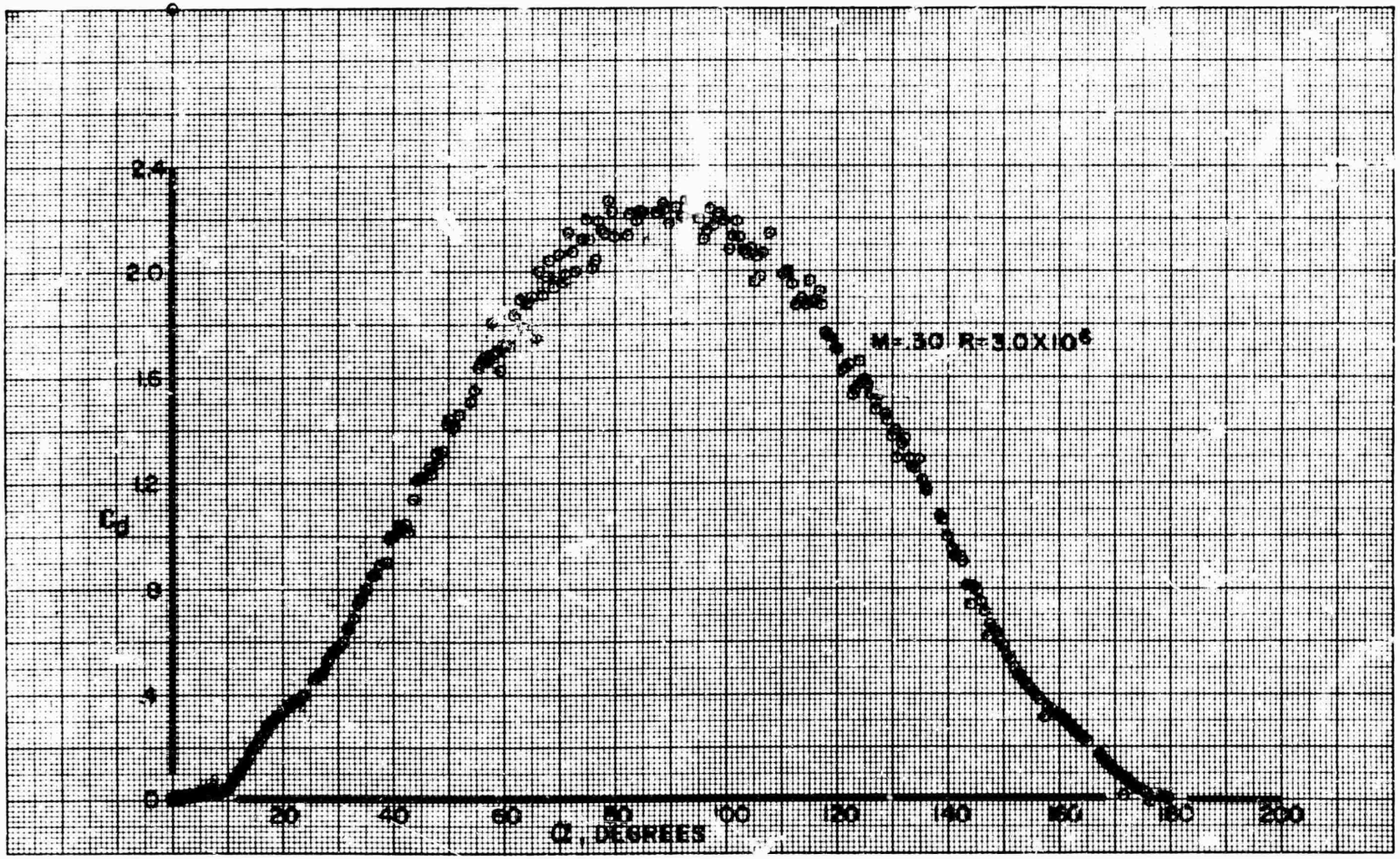


Figure 47B. Variation of Section Drag Coefficient With Angle of Attack, NACA Section 63A012

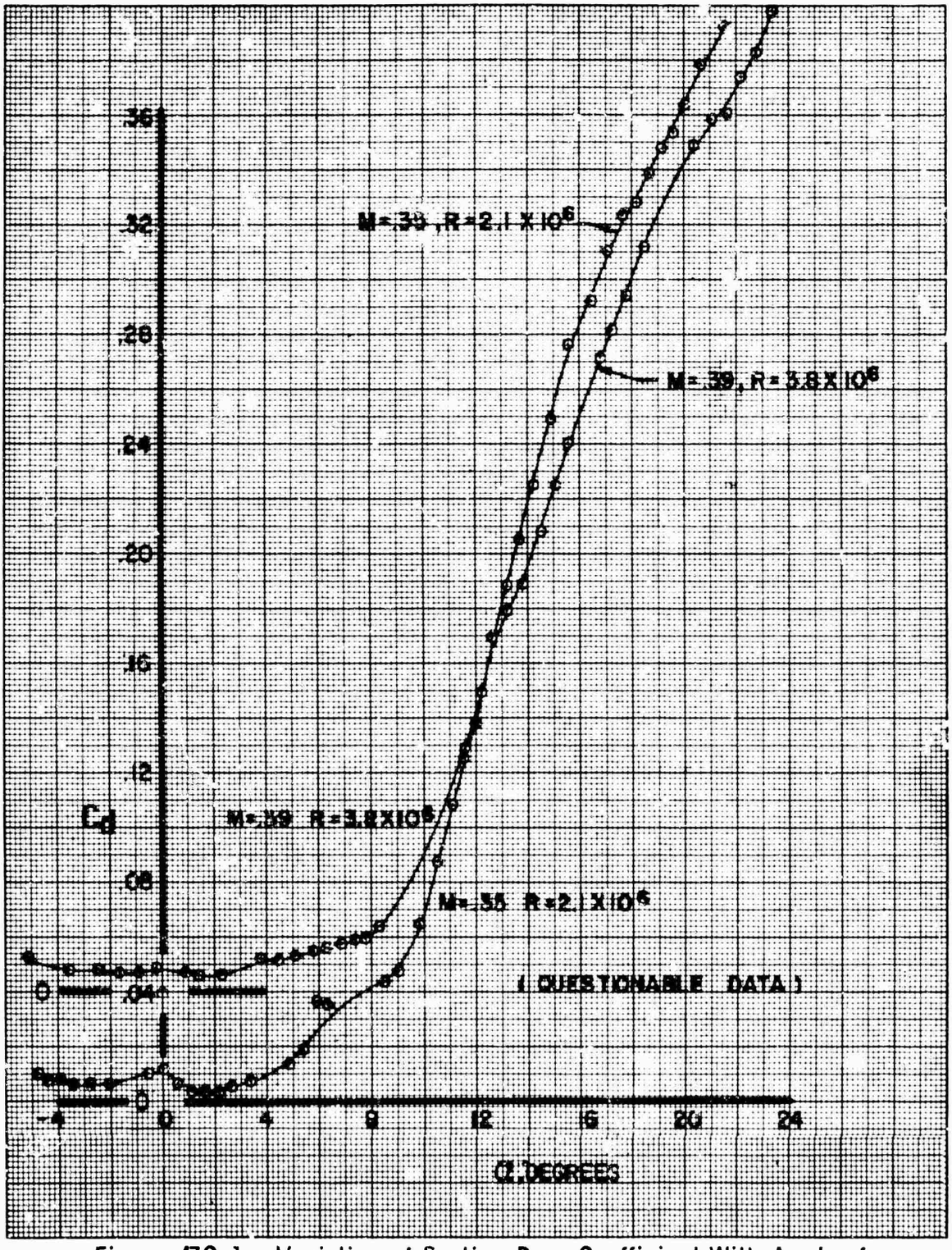


Figure 47C-1. Variation of Section Drag Coefficient With Angle of Attack, NACA Section 63A012

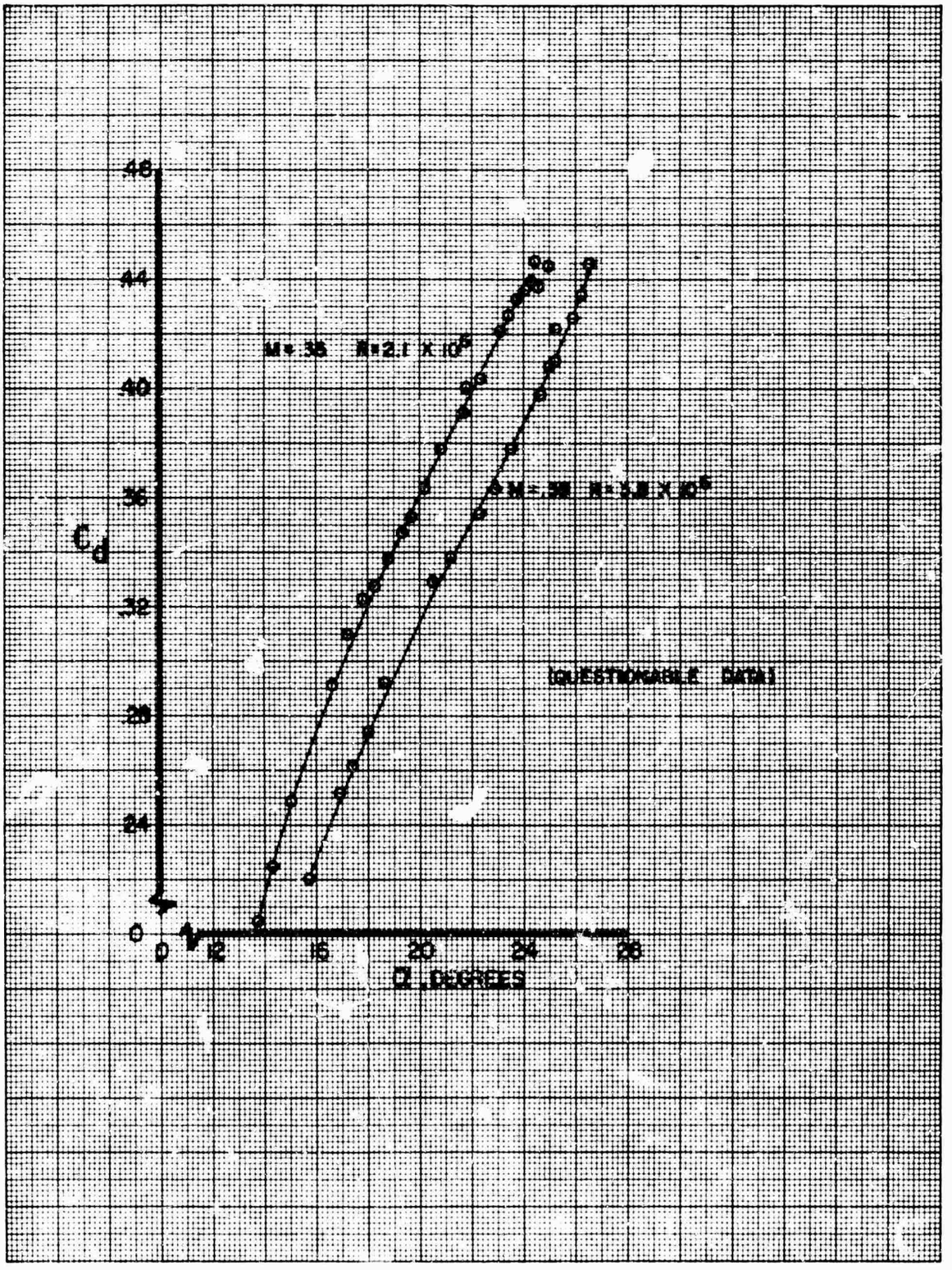


Figure 47C-2. Variation of Section Drag Coefficient With Angle of Attack, NACA Section 63A012

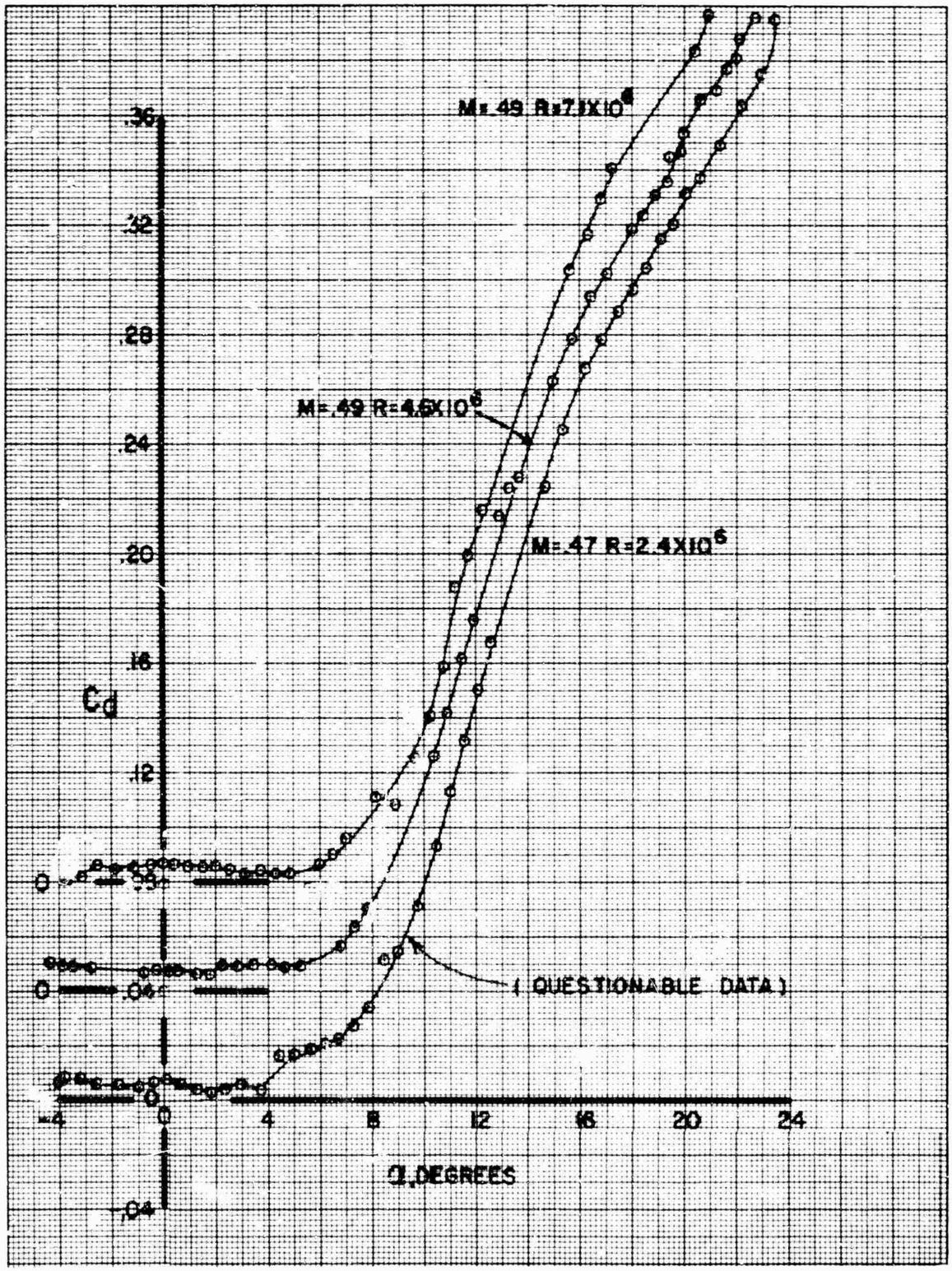


Figure 47D-1. Variation of Section Drag Coefficient With Angle of Attack, NACA Section 63A012

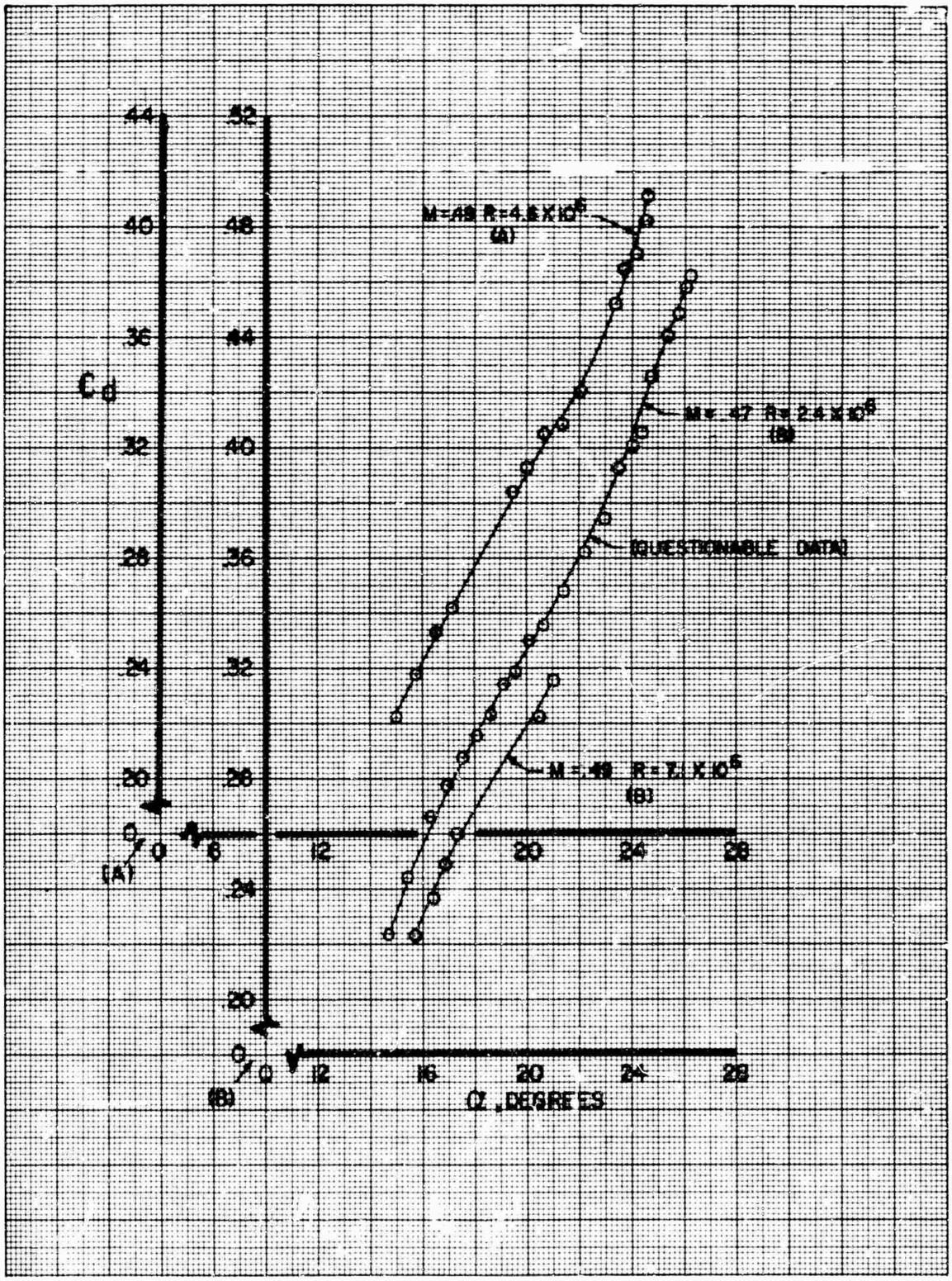


Figure 47D-2. Variation of Section Drag Coefficient With Angle of Attack, NACA Section 63A012

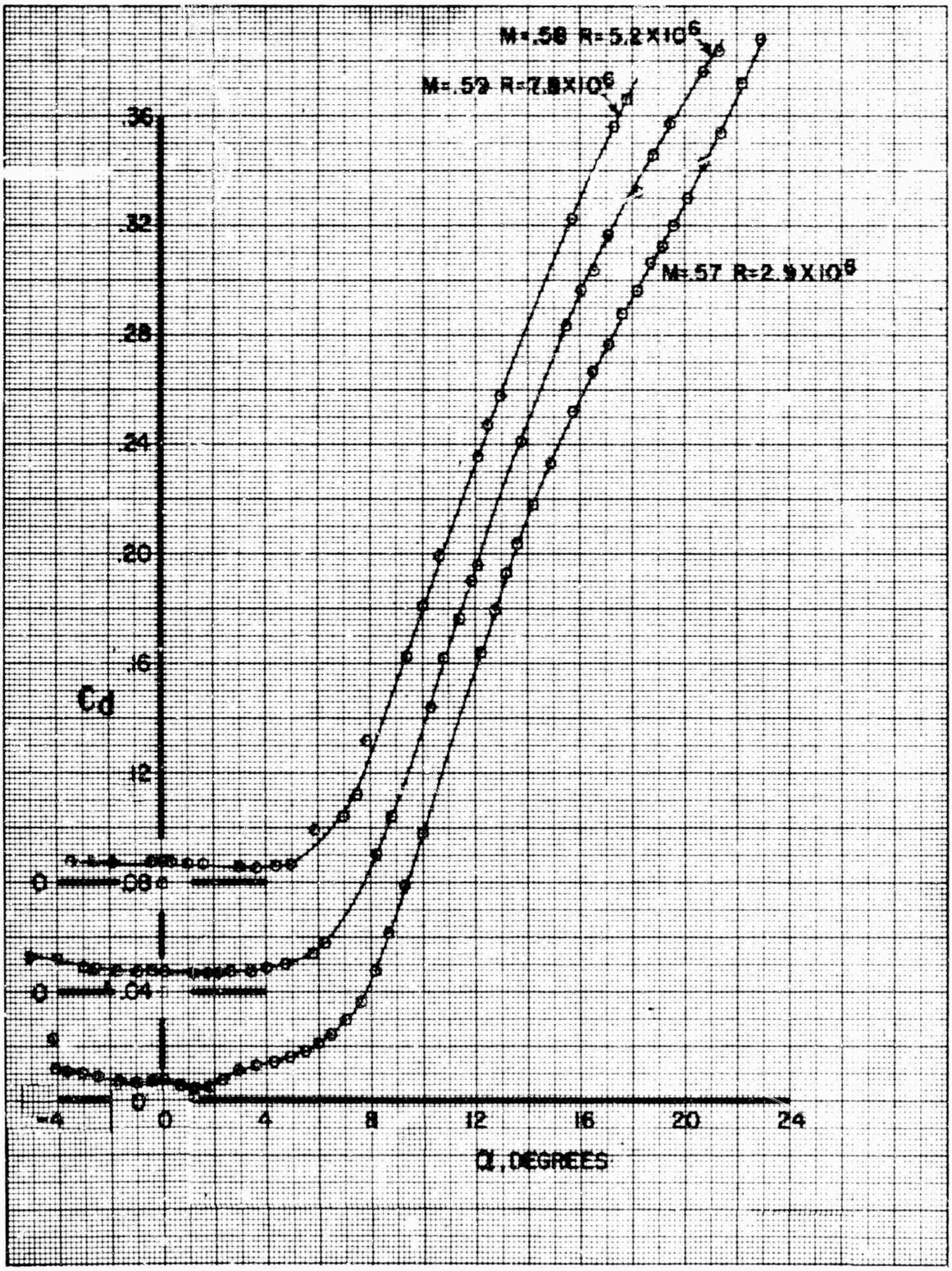


Figure 47E-1. Variation of Section Drag Coefficient With Angle of Attack, NACA Section 63A012

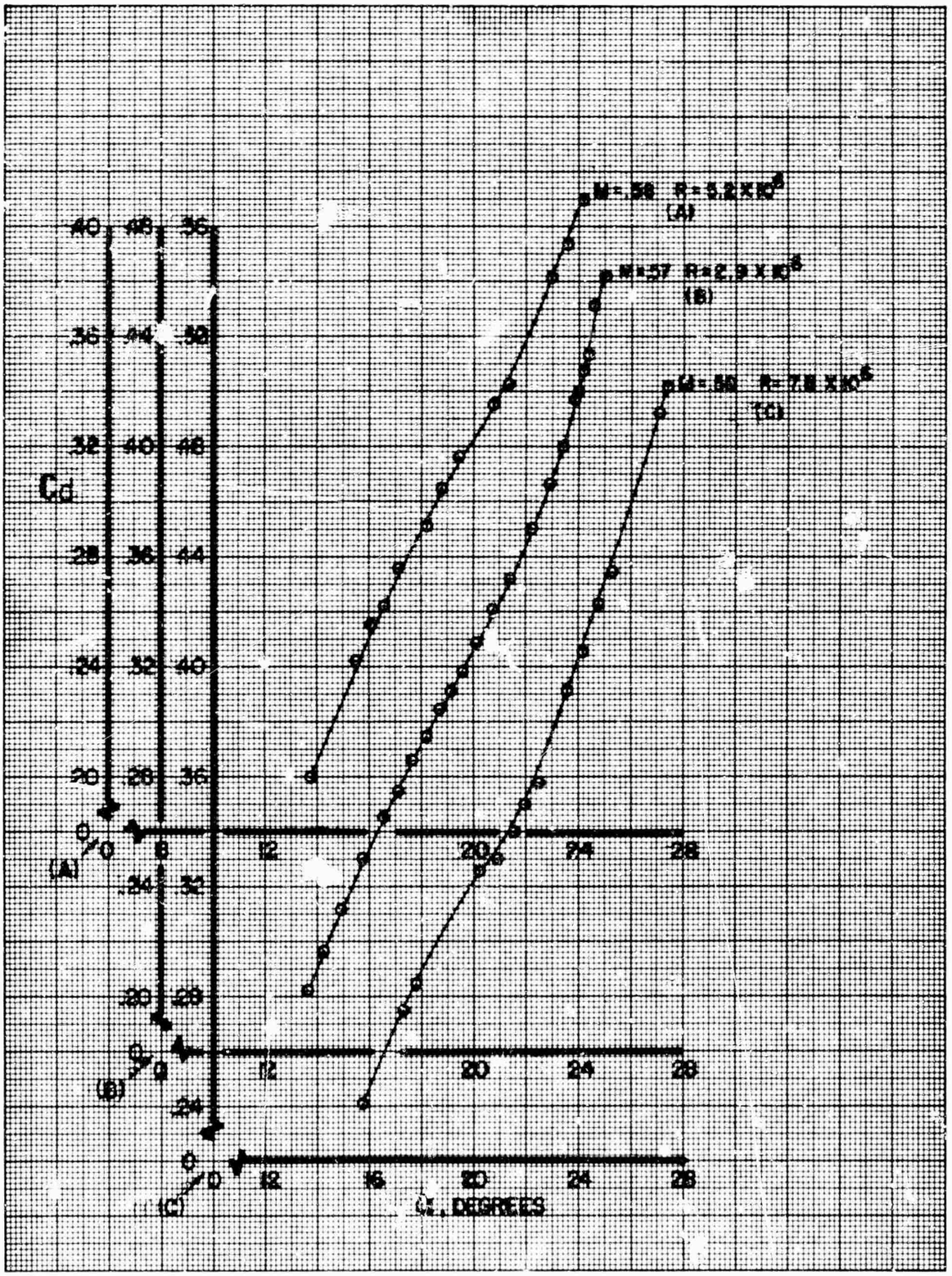


Figure 47E-2. Variation of Section Drag Coefficient With Angle of Attack, NACA Section 63A012

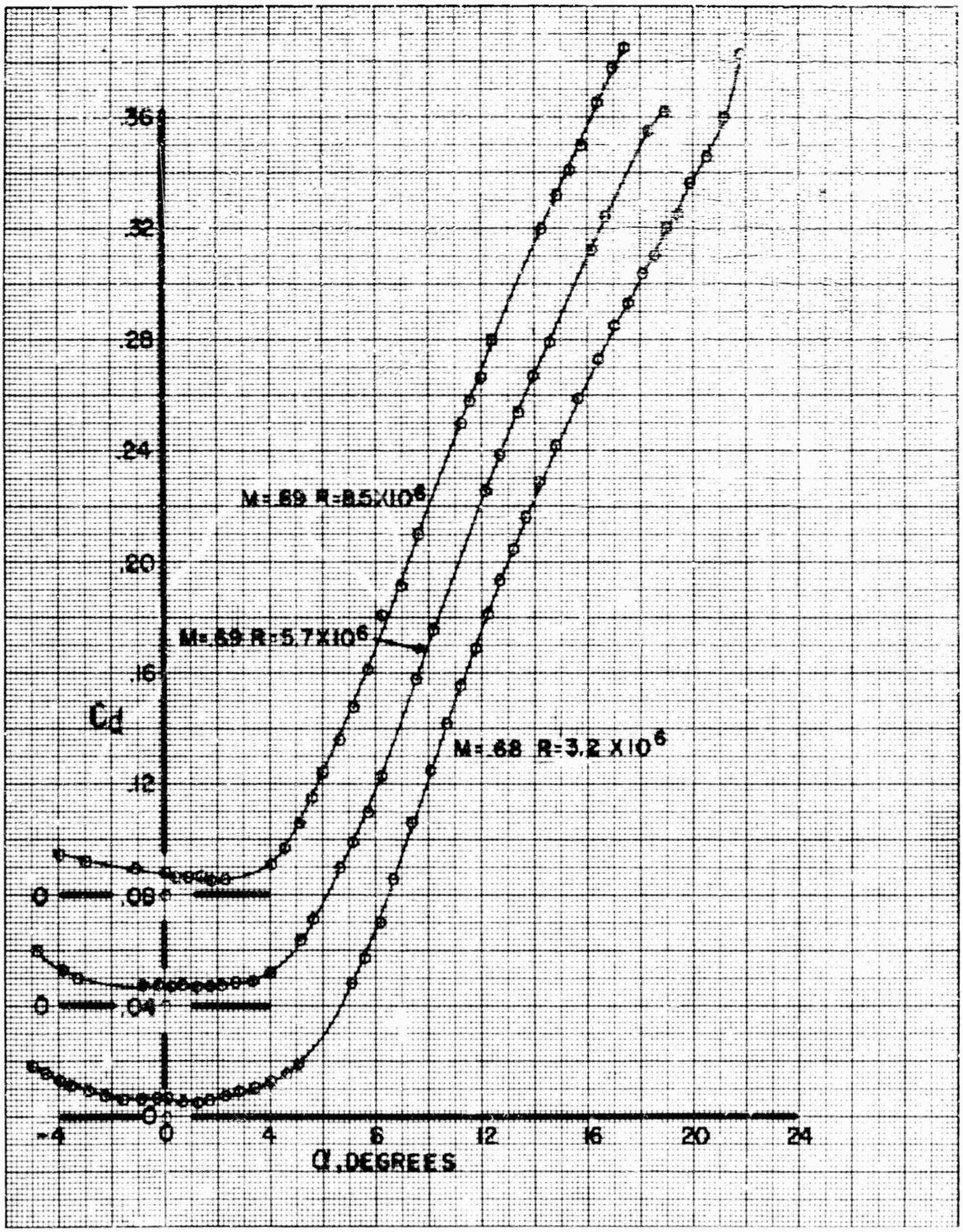


Figure 47F-1. Variation of Section Drag Coefficient With Angle of Attack, NACA Section 63A012

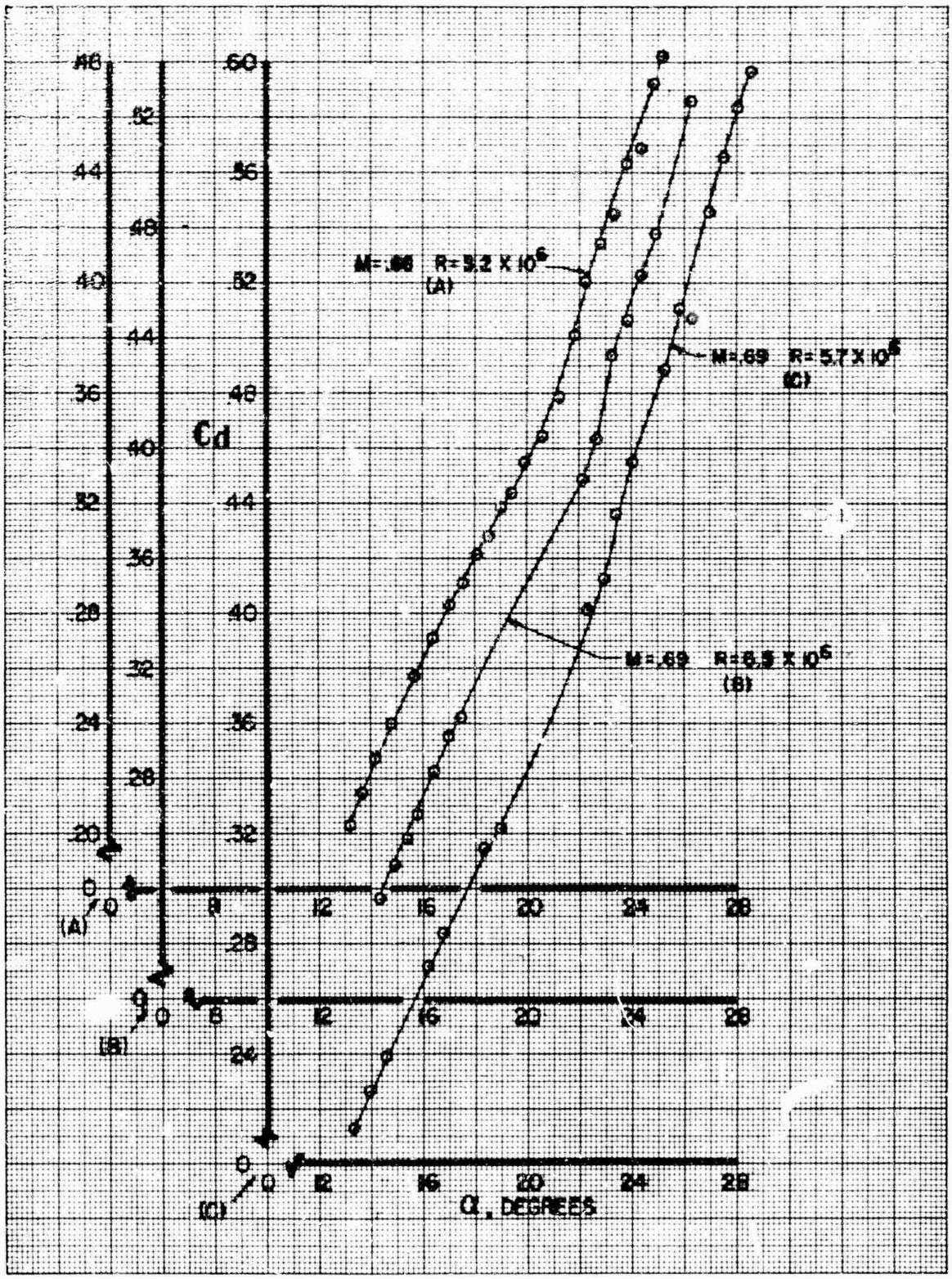


Figure 47F-2. Variation of Section Drag Coefficient With Angle of Attack, NACA Section 63A012

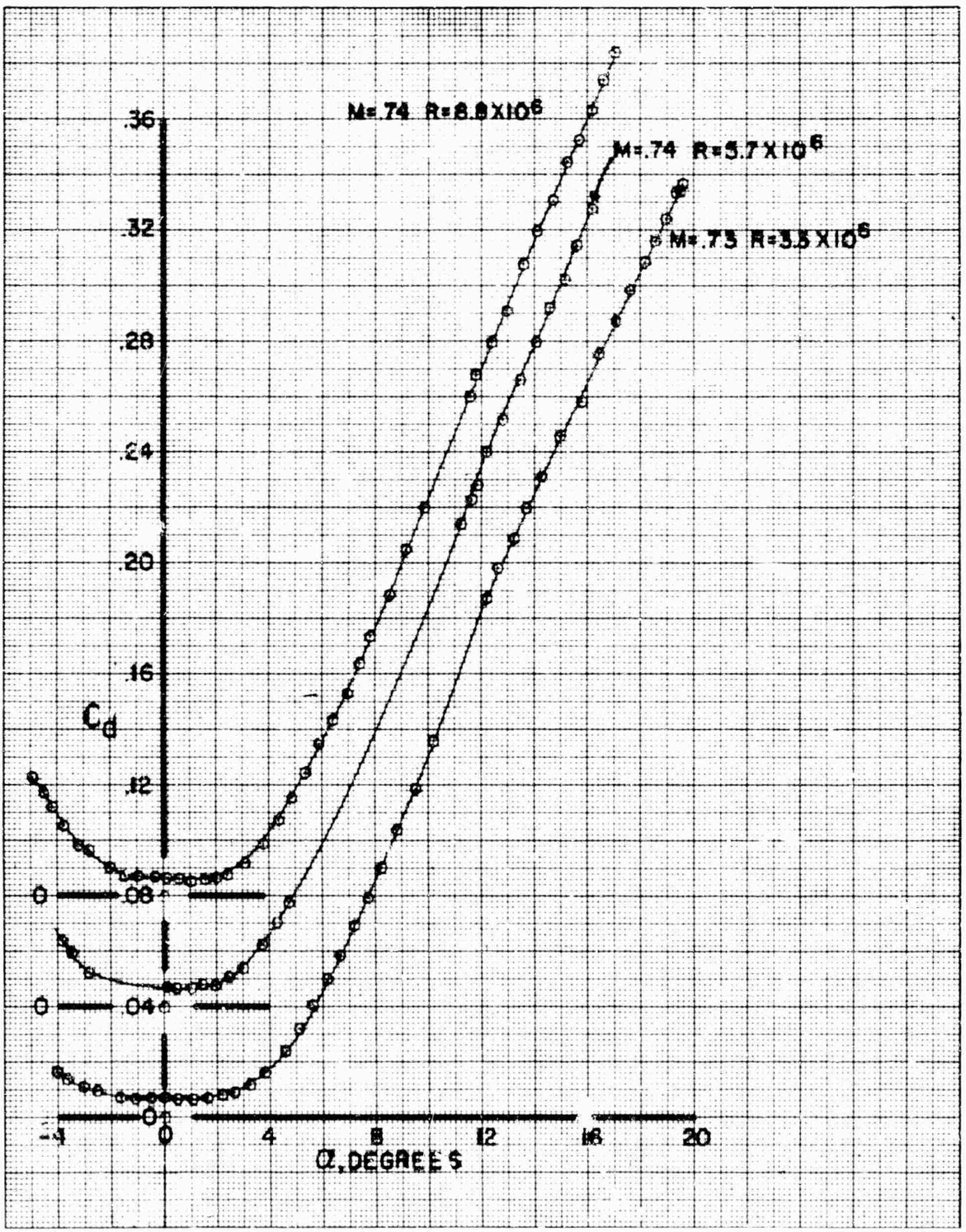


Figure 476. Variation of Section Drag Coefficient With Angle of Attack, NACA Section 63A012

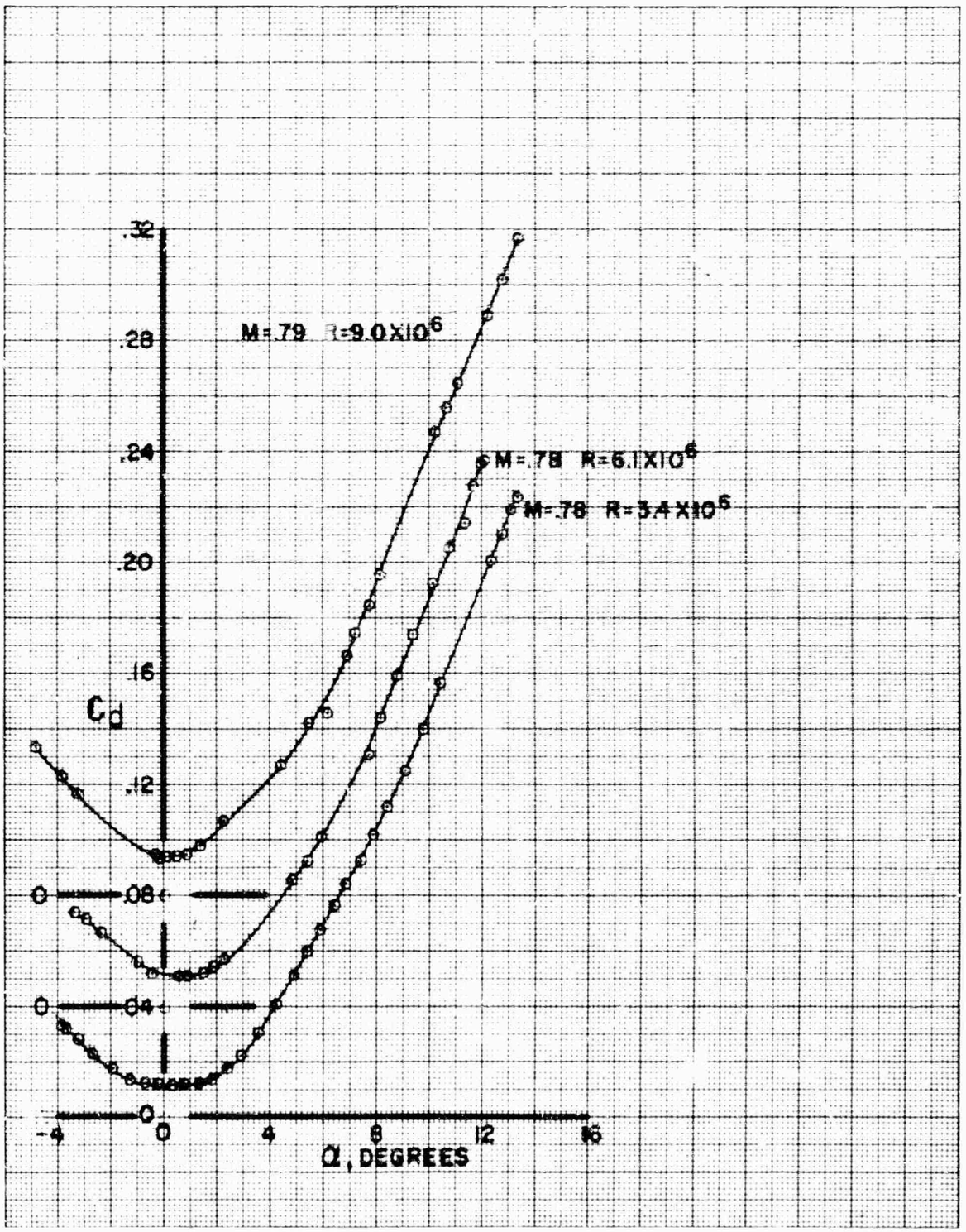


Figure 47H. Variation of Section Drag Coefficient With Angle of Attack, NACA Section 63A012

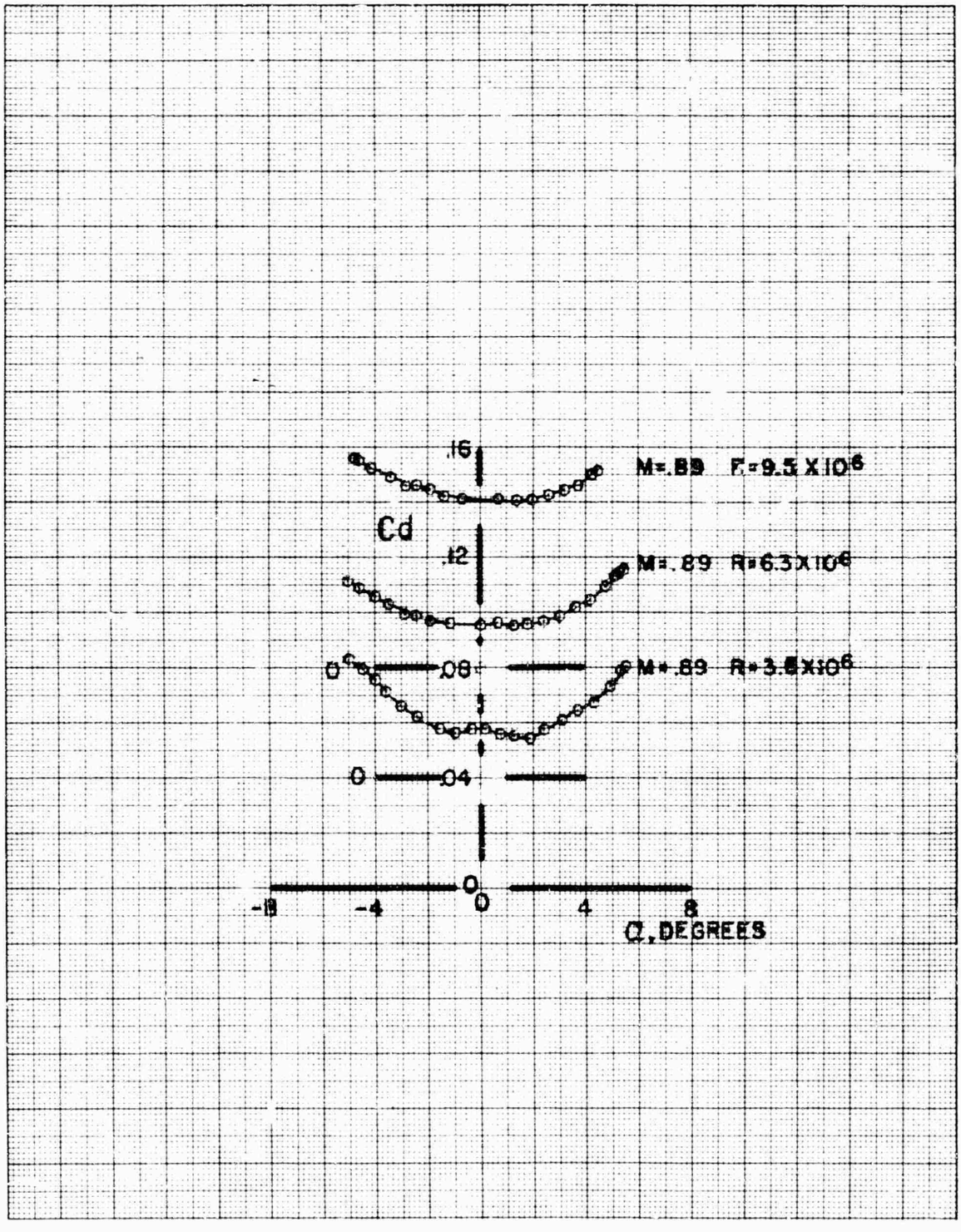


Figure 471. Variation of Section Drag Coefficient With Angle of Attack, NACA Section 63A012

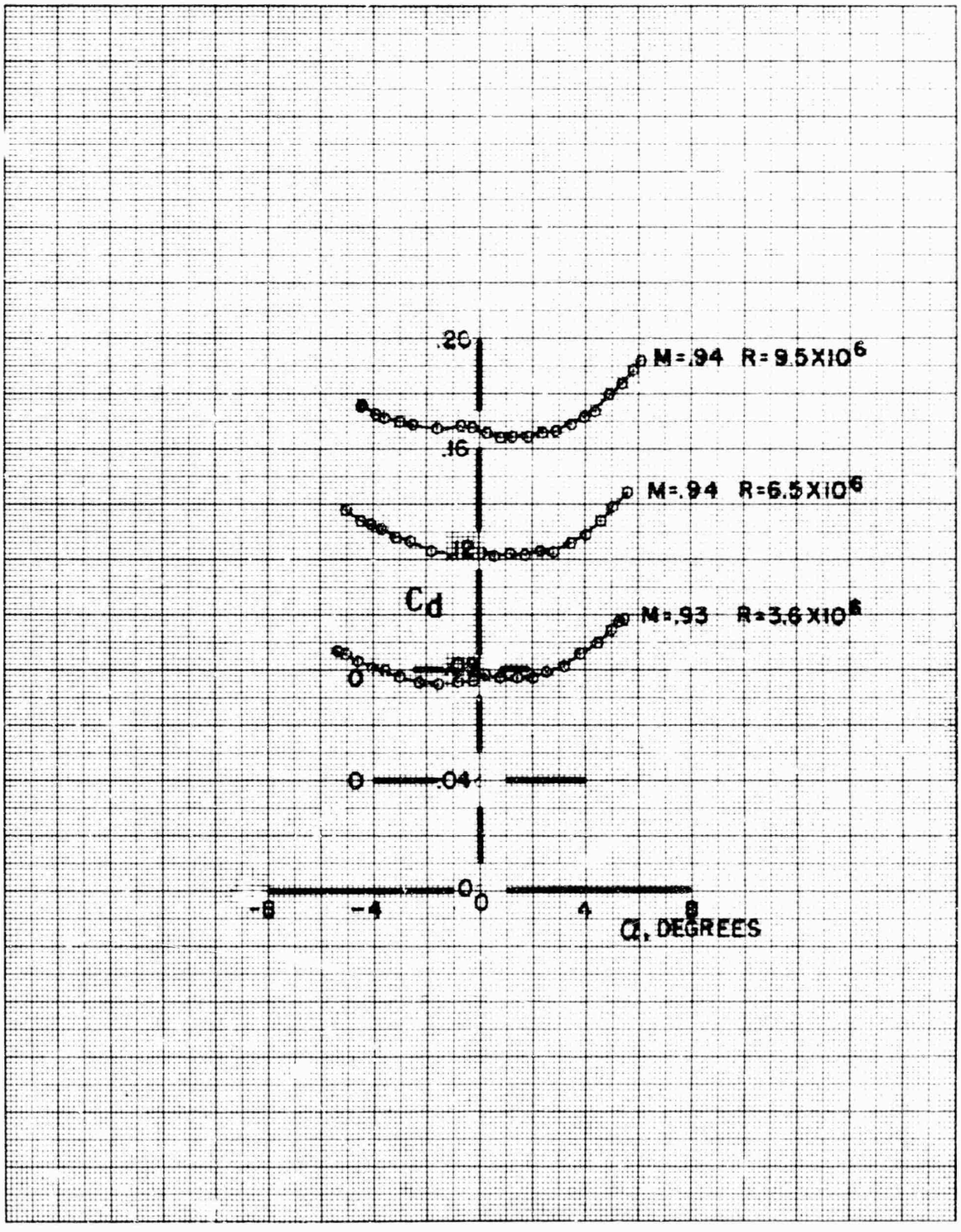


Figure 47j. Variation of Section Drag Coefficient With Angle of Attack, NACA Section 63A012

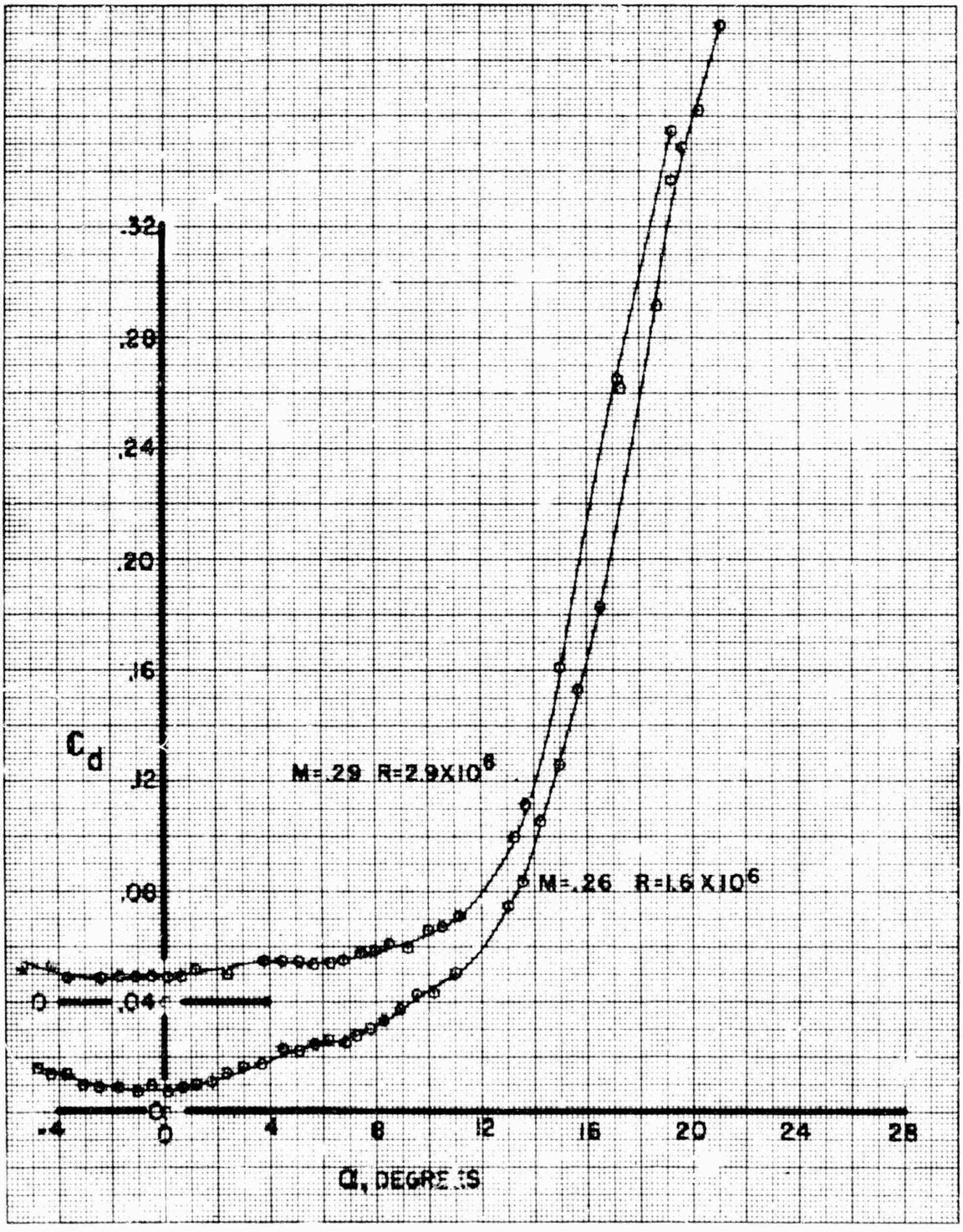


Figure 48A-1. Variation of Section Drag Coefficient With Angle of Attack, NACA Section 63A015

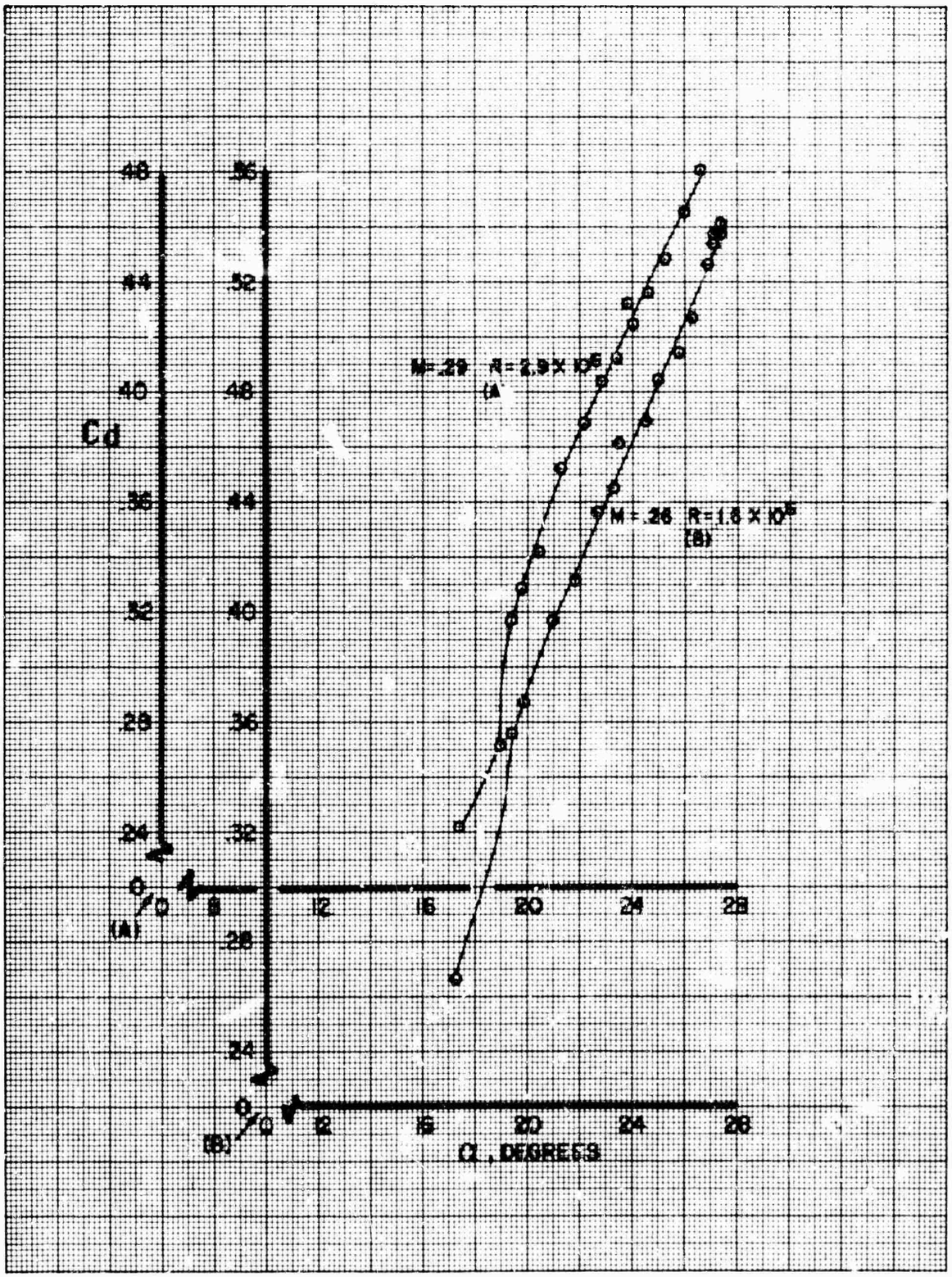


Figure 48A-2. Variation of Section Drag Coefficient With Angle of Attack, NACA Section 63A015

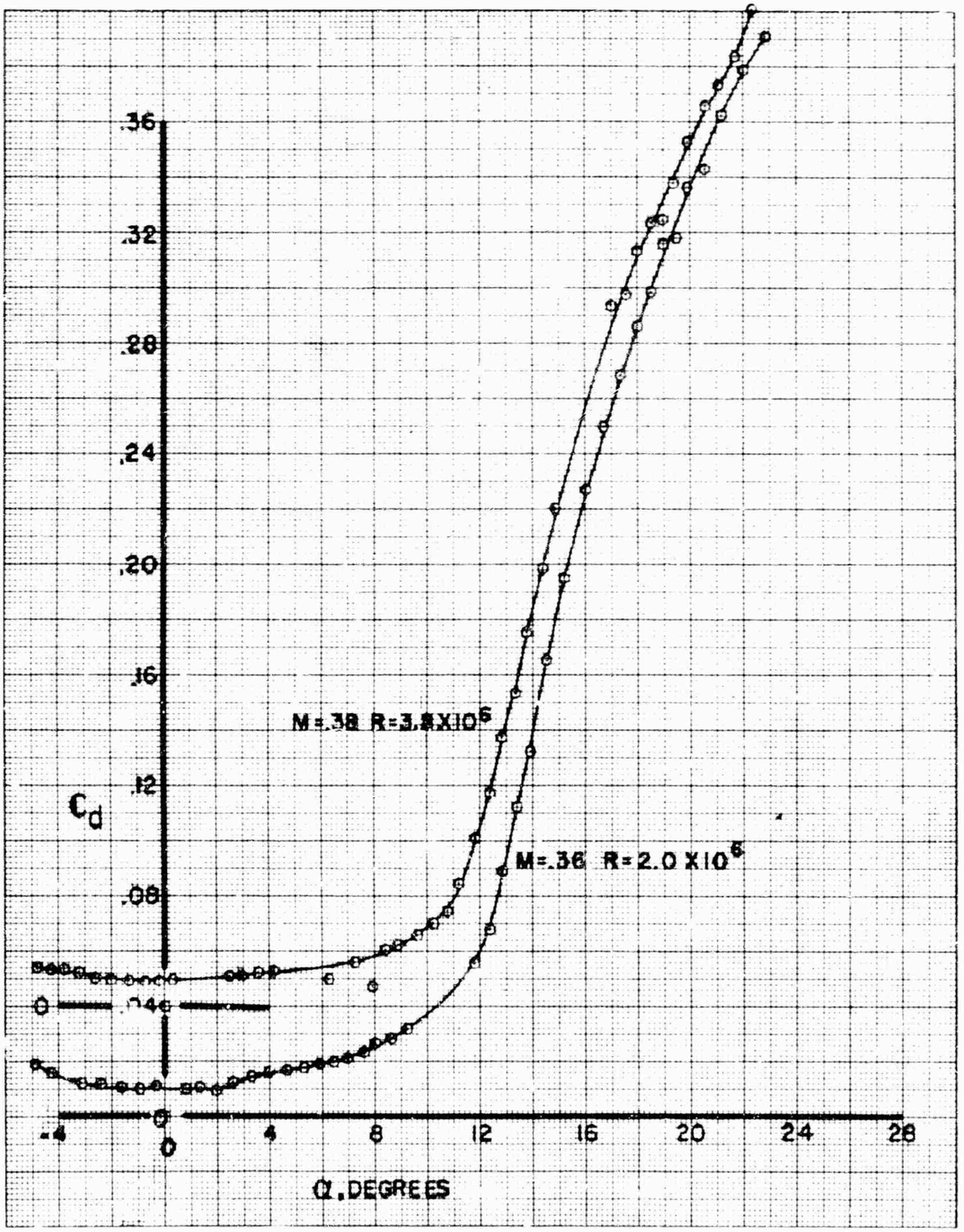


Figure 48B-1. Variation of Section Drag Coefficient With Angle of Attack, NACA Section 63A015

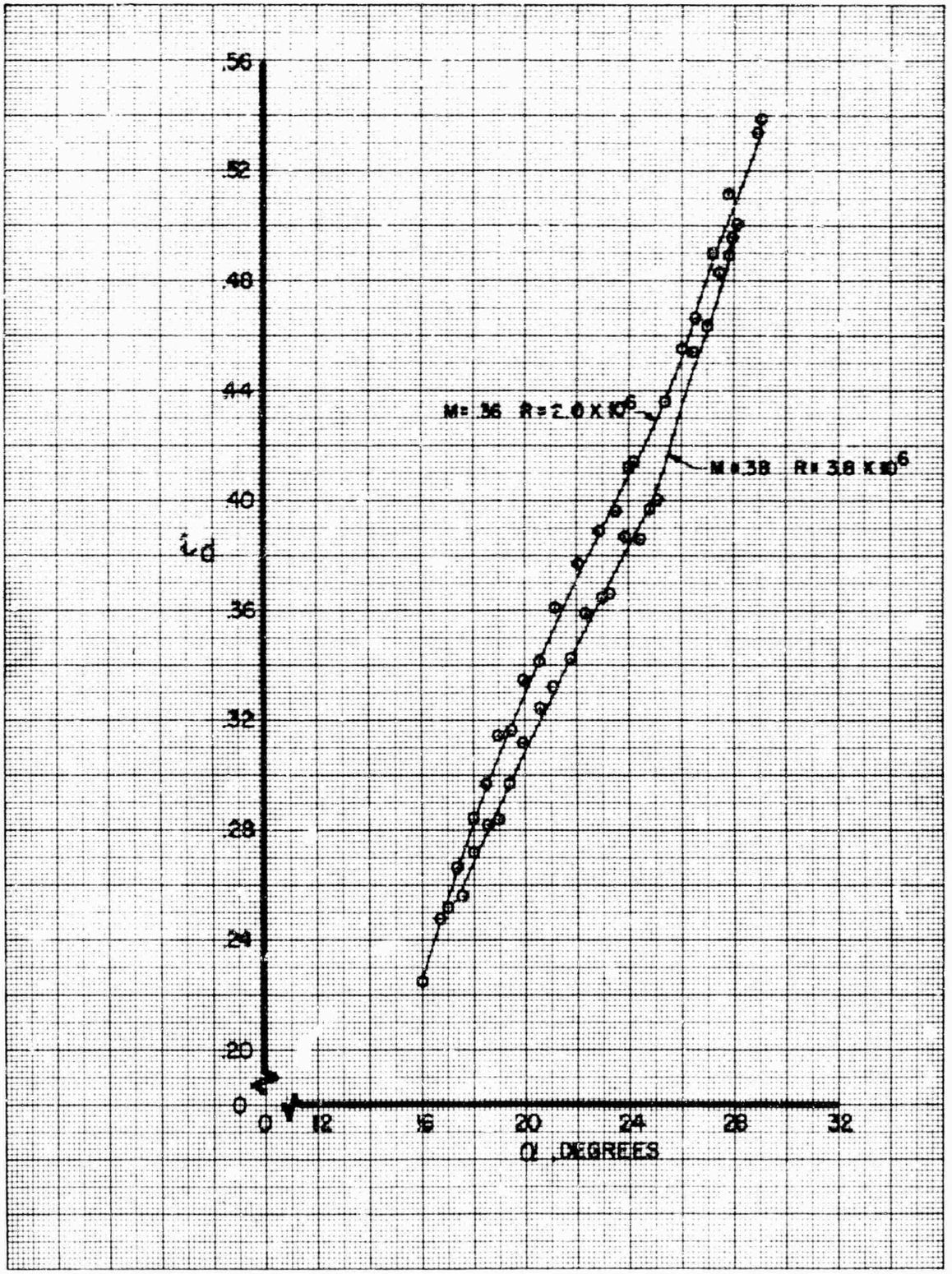


Figure 48B-2. Variation of Section Drag Coefficient With Angle of Attack, NACA Section 63$_1$015

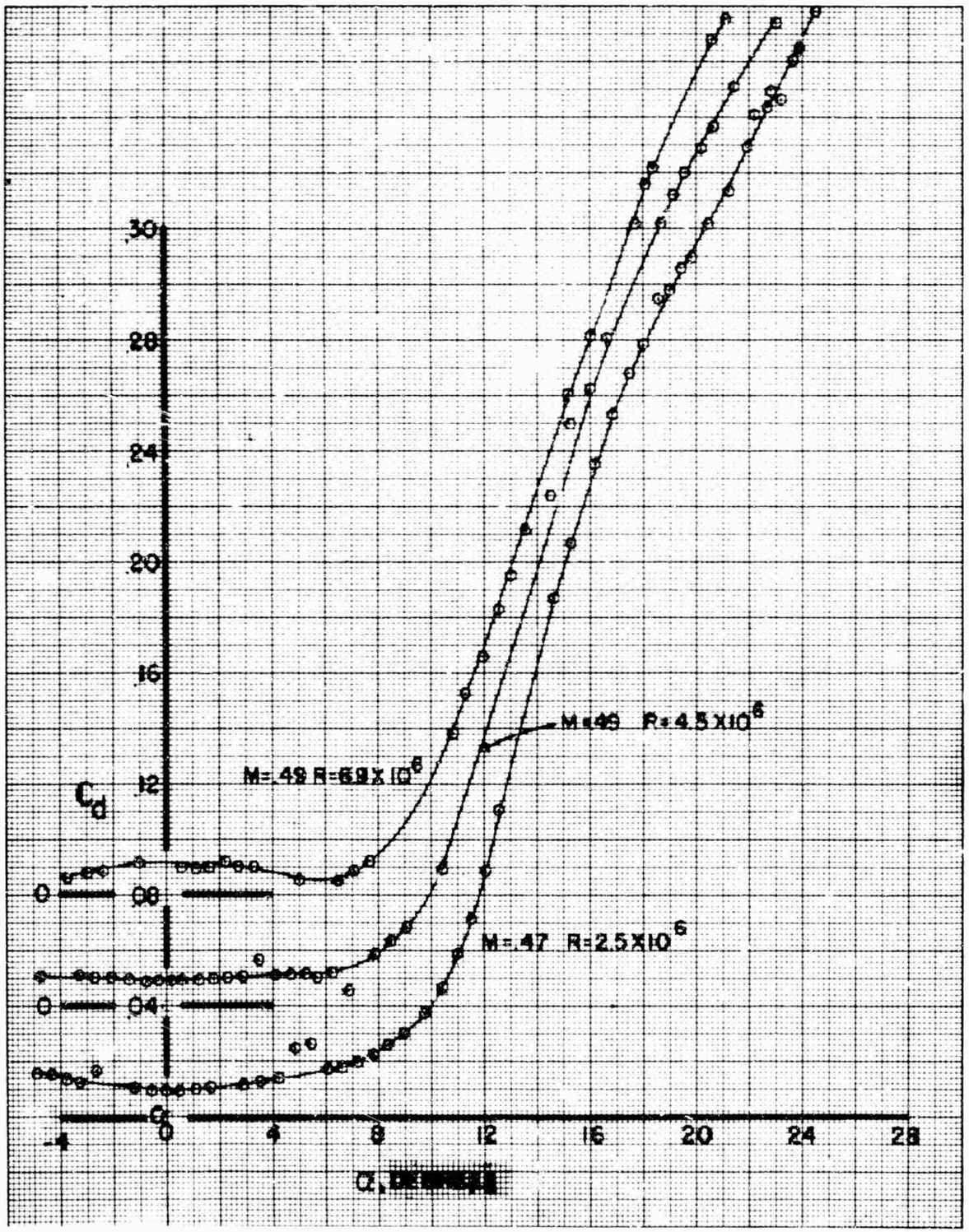


Figure 48C-1. Variation of Section Drag Coefficient With Angle of Attack, NACA Section 63A015

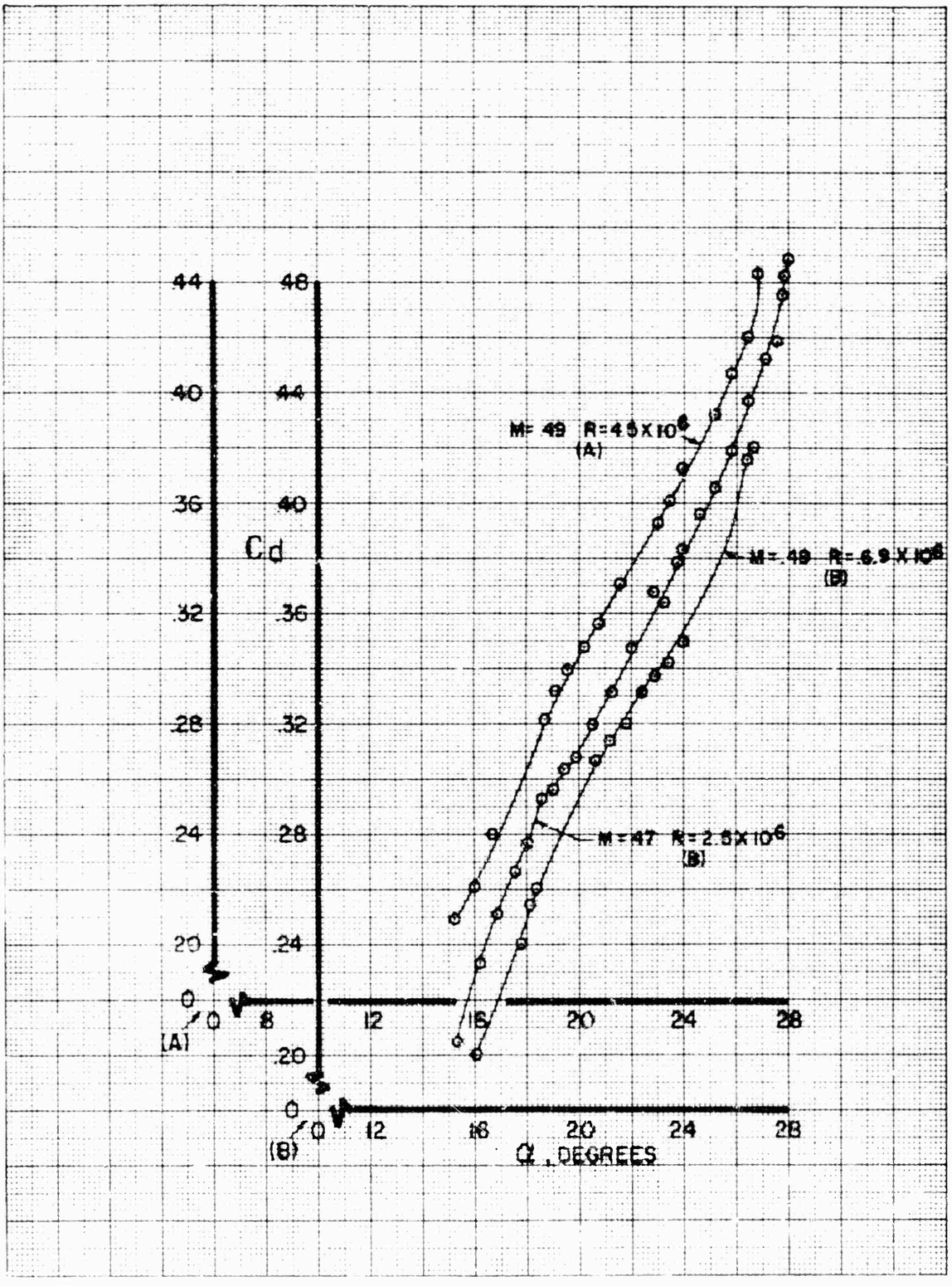


Figure 48C-2. Variation of Drag Coefficient With Angle of Attack, NACA Section 63A015

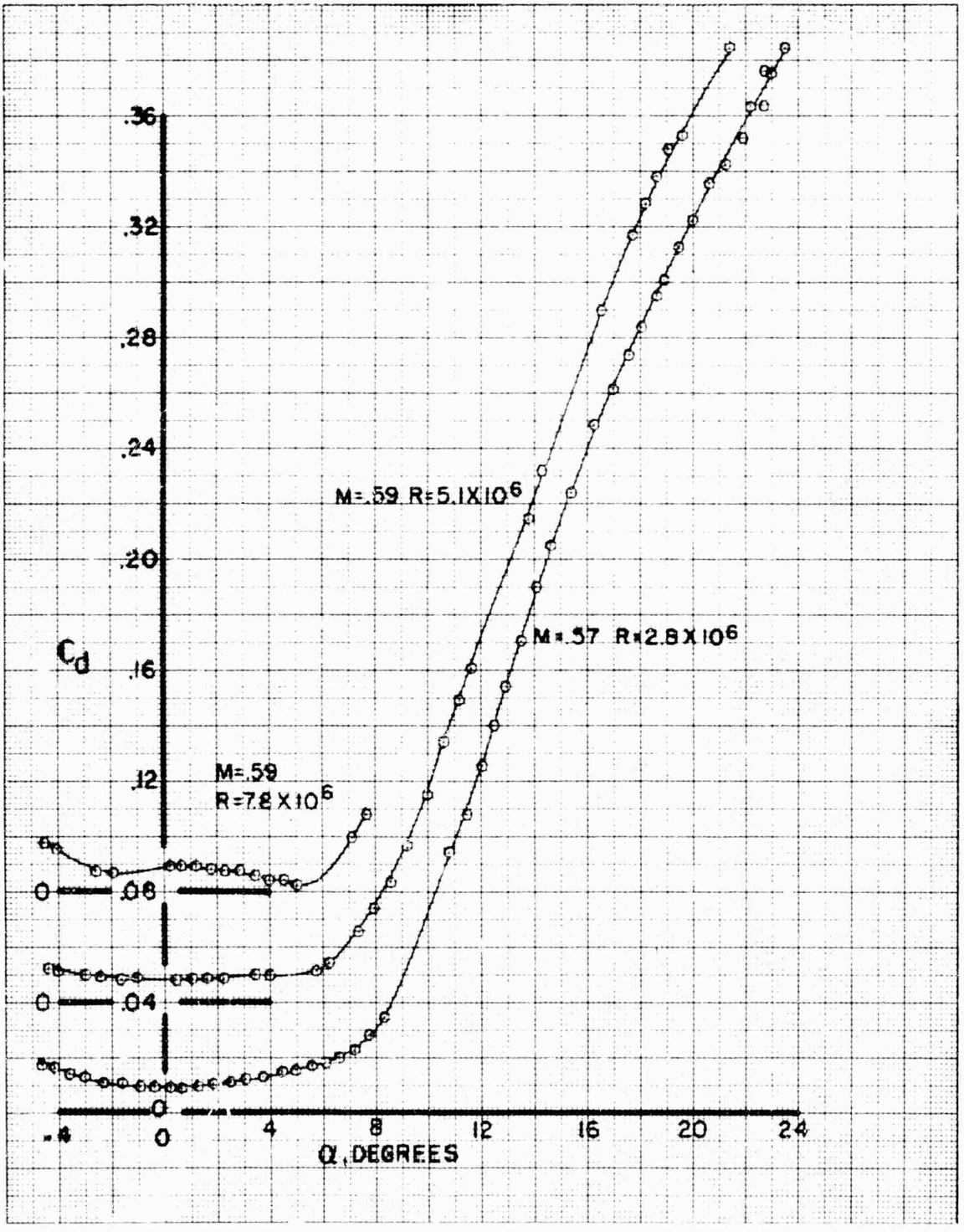


Figure 48D-1. Variation of Section Drag Coefficient With Angle of Attack, NACA Section 63A015

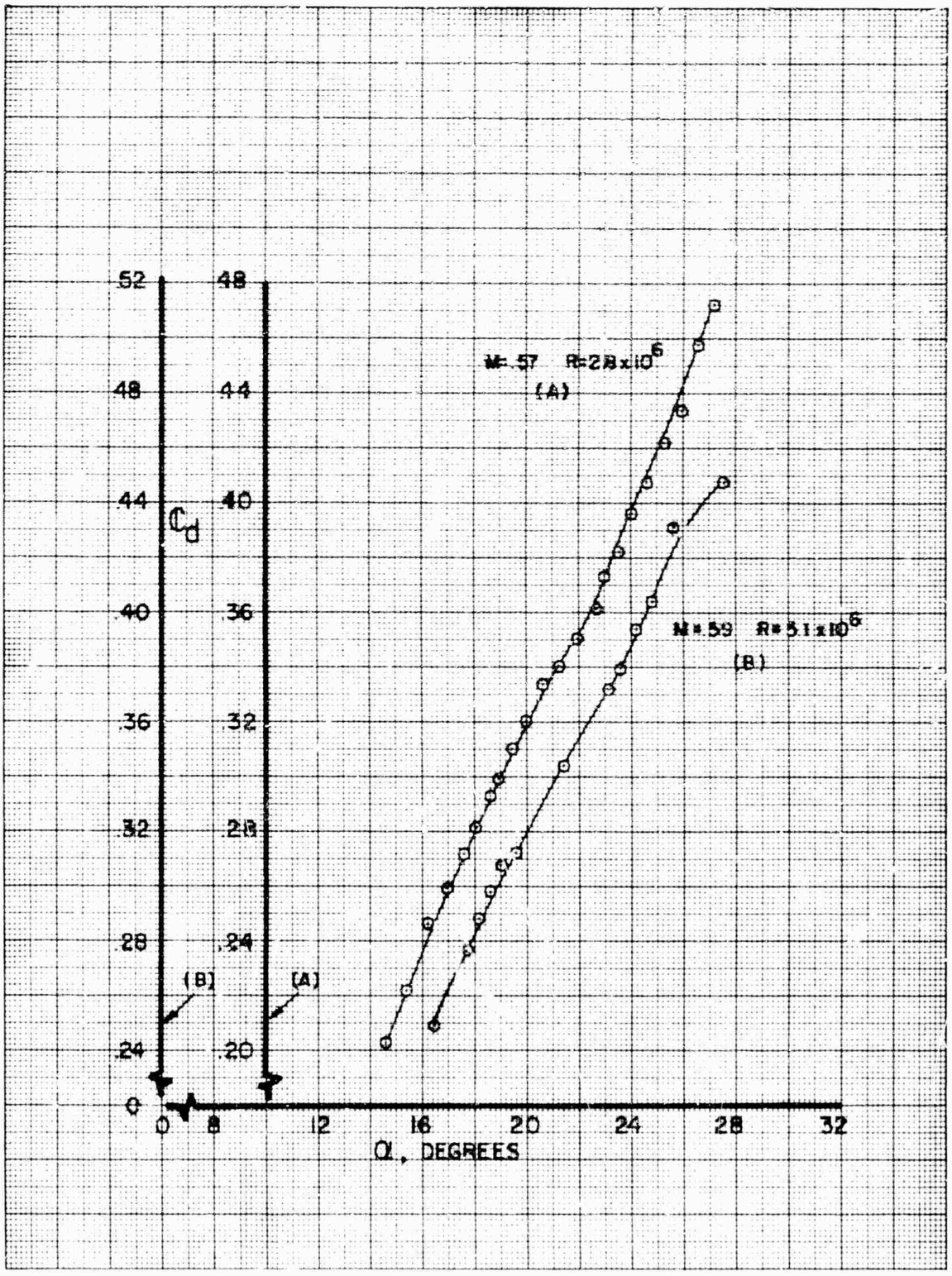


Figure 48D-2. Variation of Section Drag Coefficient With Angle of Attack, NACA Section 63A015

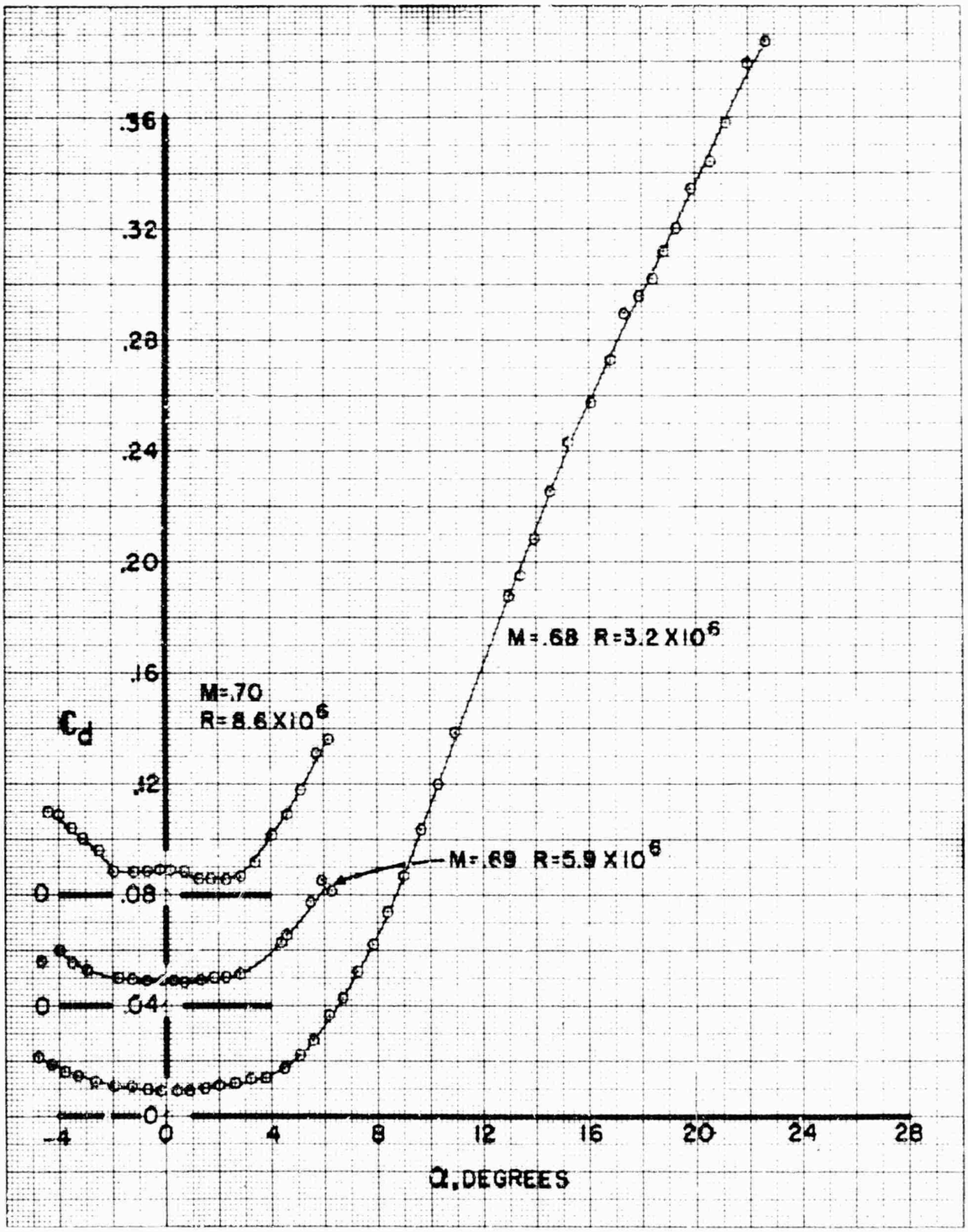


Figure 48E-1. Variation of Section Drag Coefficient With Angle of Attack, NACA Section 63A015

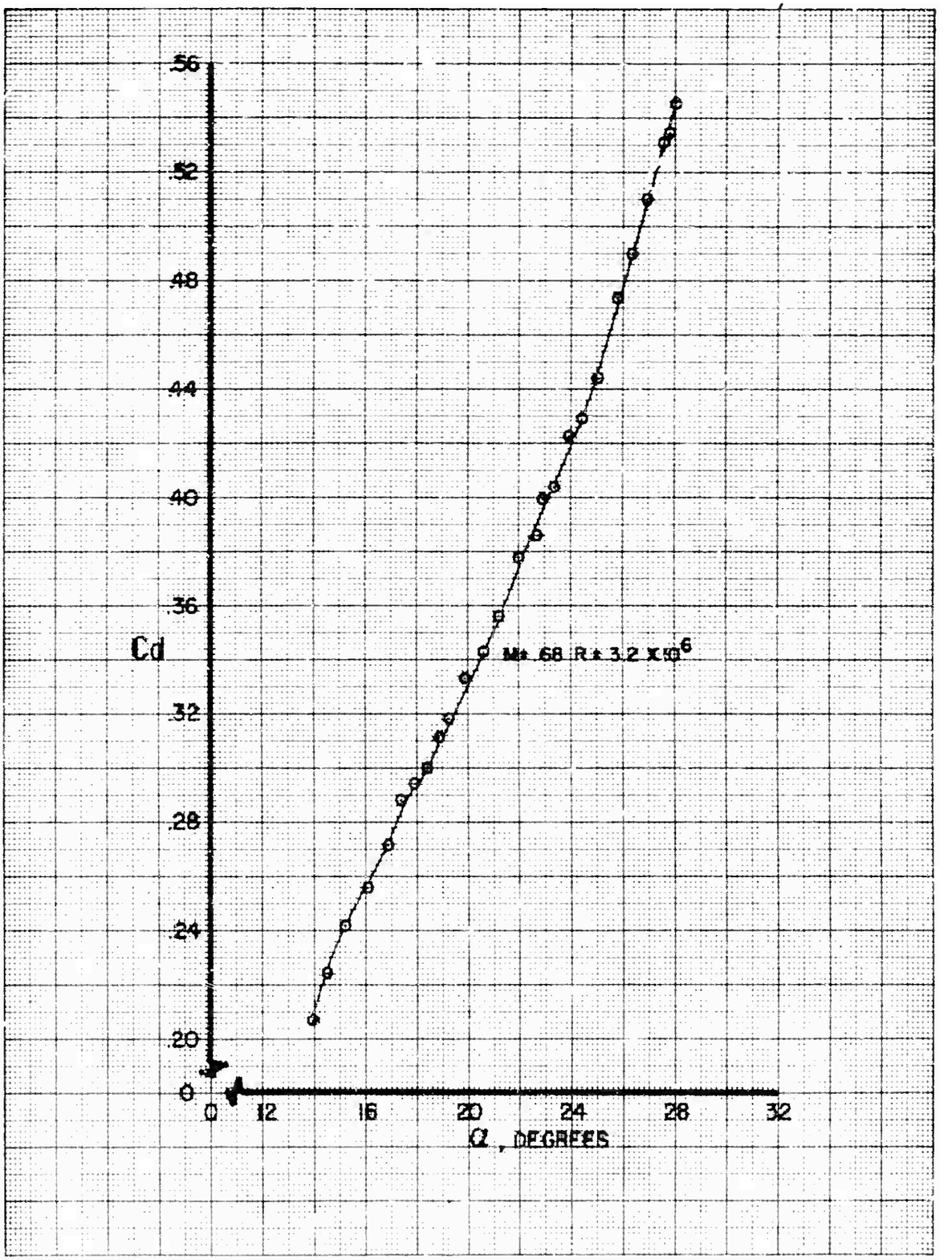


Figure 48E-2. Variation of Section Drag Coefficient With Angle of Attack, NACA Section 63A015

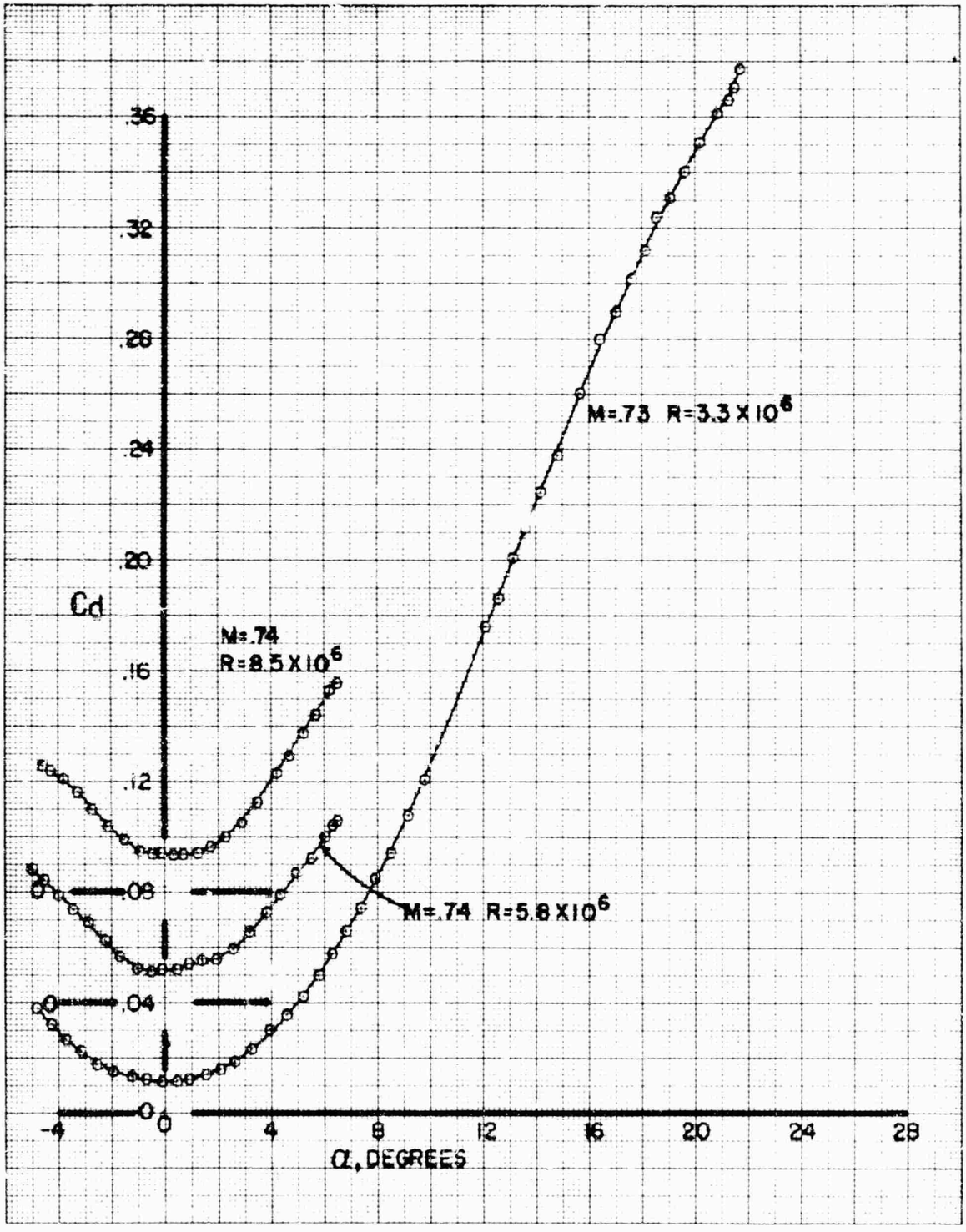


Figure 48F. Variation of Section Drag Coefficient With Angle of Attack, NACA Section 63A015

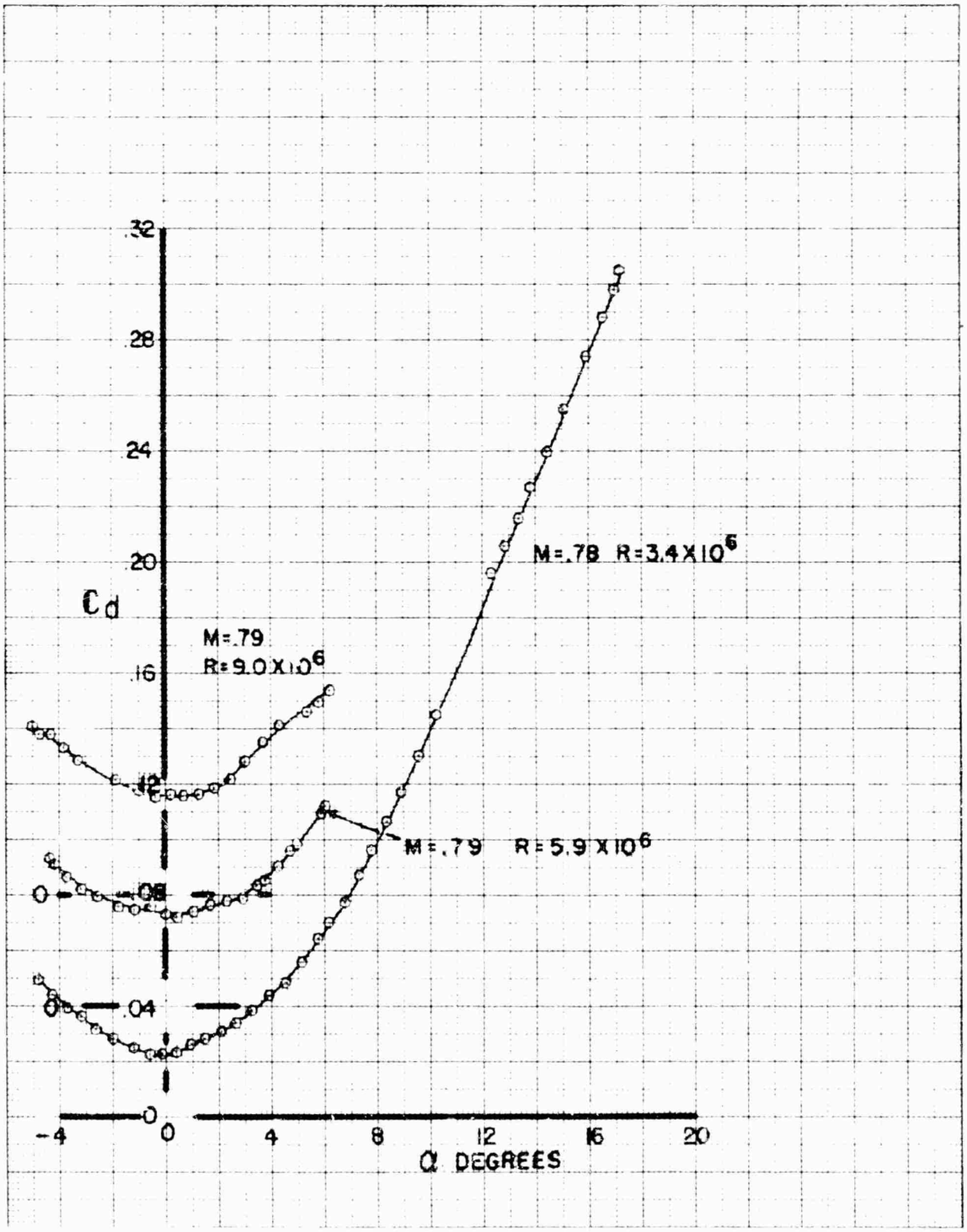


Figure 48G. Variation of Section Drag Coefficient With Angle of Attack, NACA Section 63A015

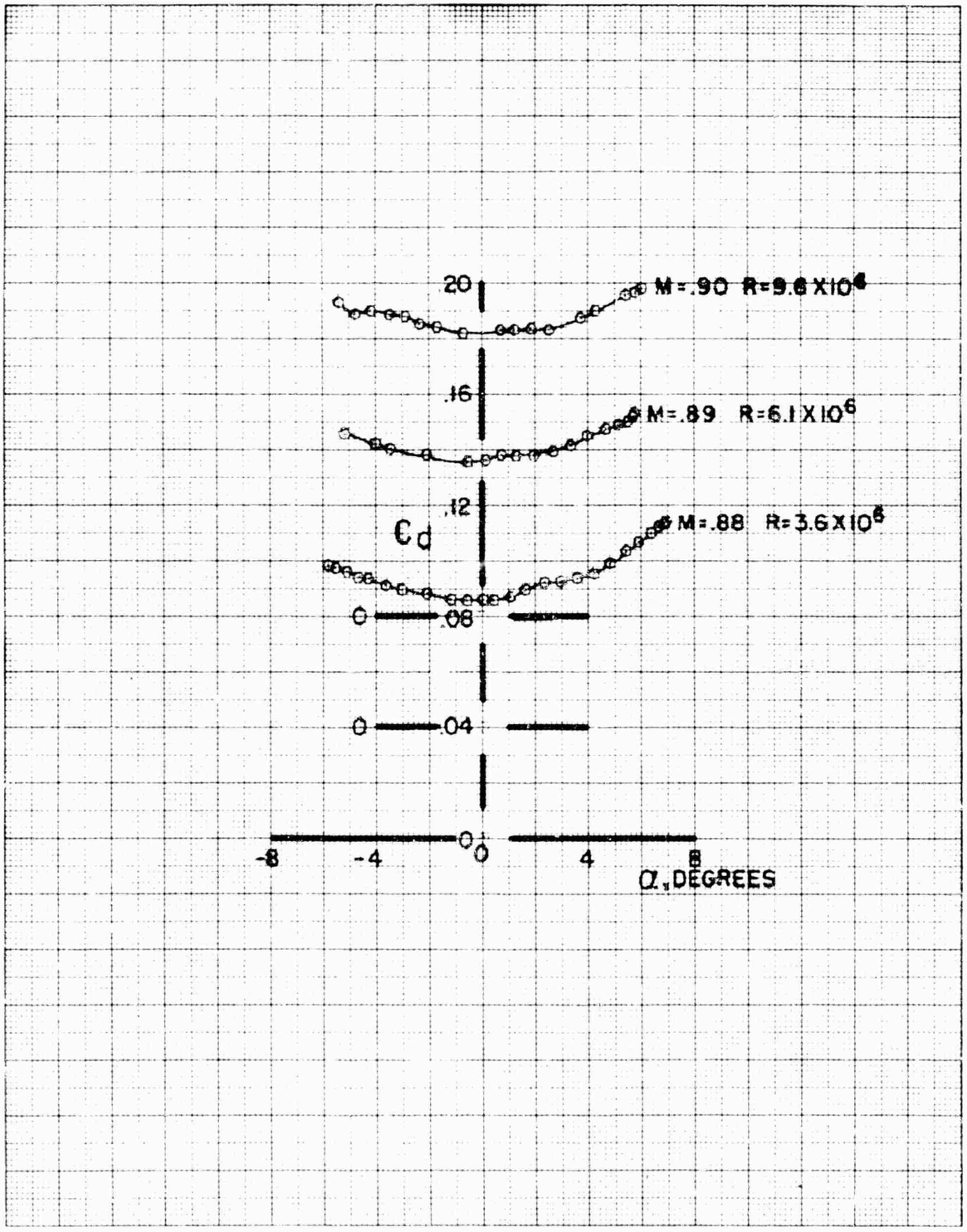


Figure 48H. Variation of Section Drag Coefficient With Angle of Attack, NACA Section 63A015

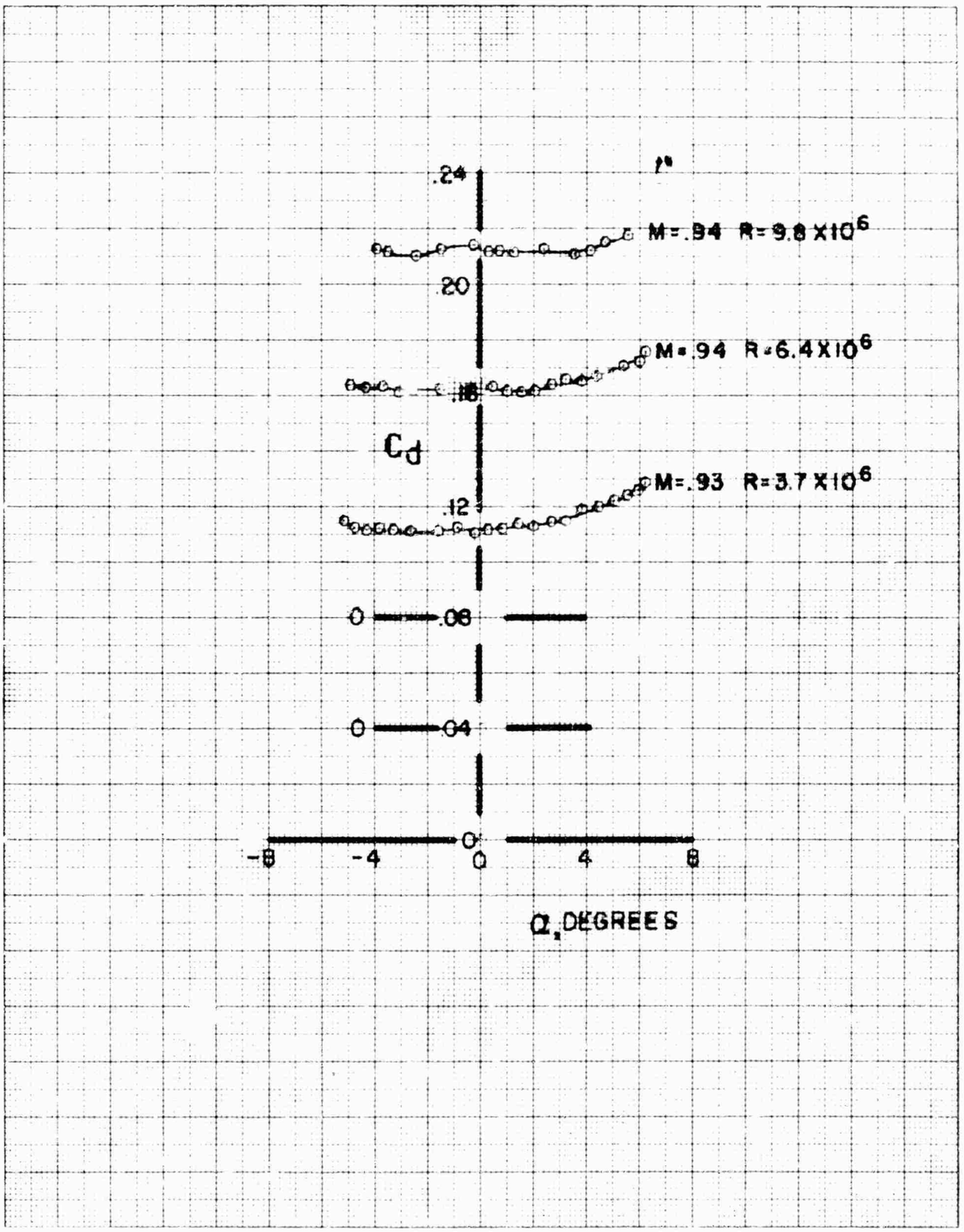


Figure 481. Variation of Section Drag Coefficient With Angle of Attack, NACA Section 63A015

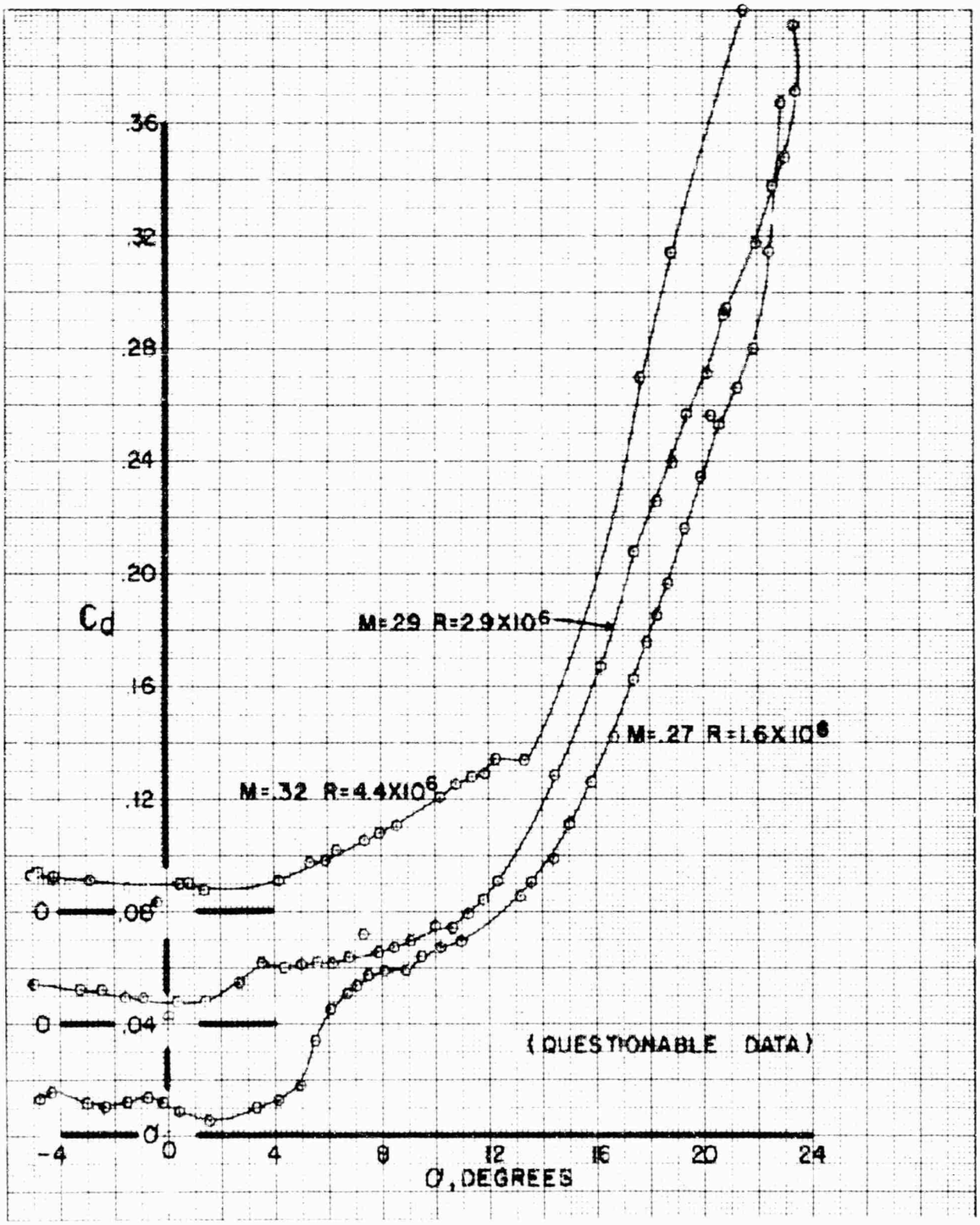


Figure 49A-1. Variation of Section Drag Coefficient With Angle of Attack, NACA Section 63A018

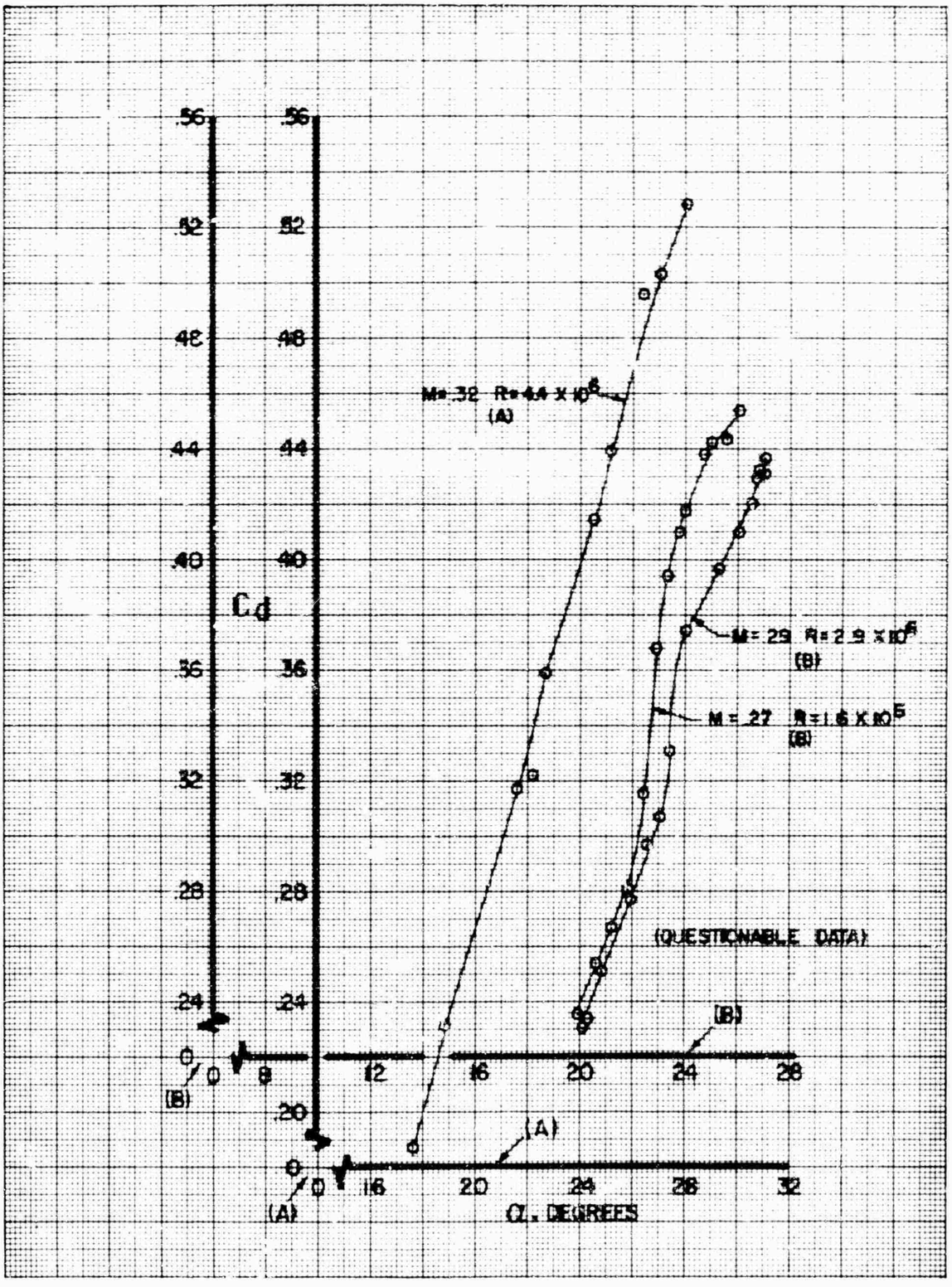


Figure 49A-2. Variation of Section Drag Coefficient With Angle of Attack, NACA Section 63A018

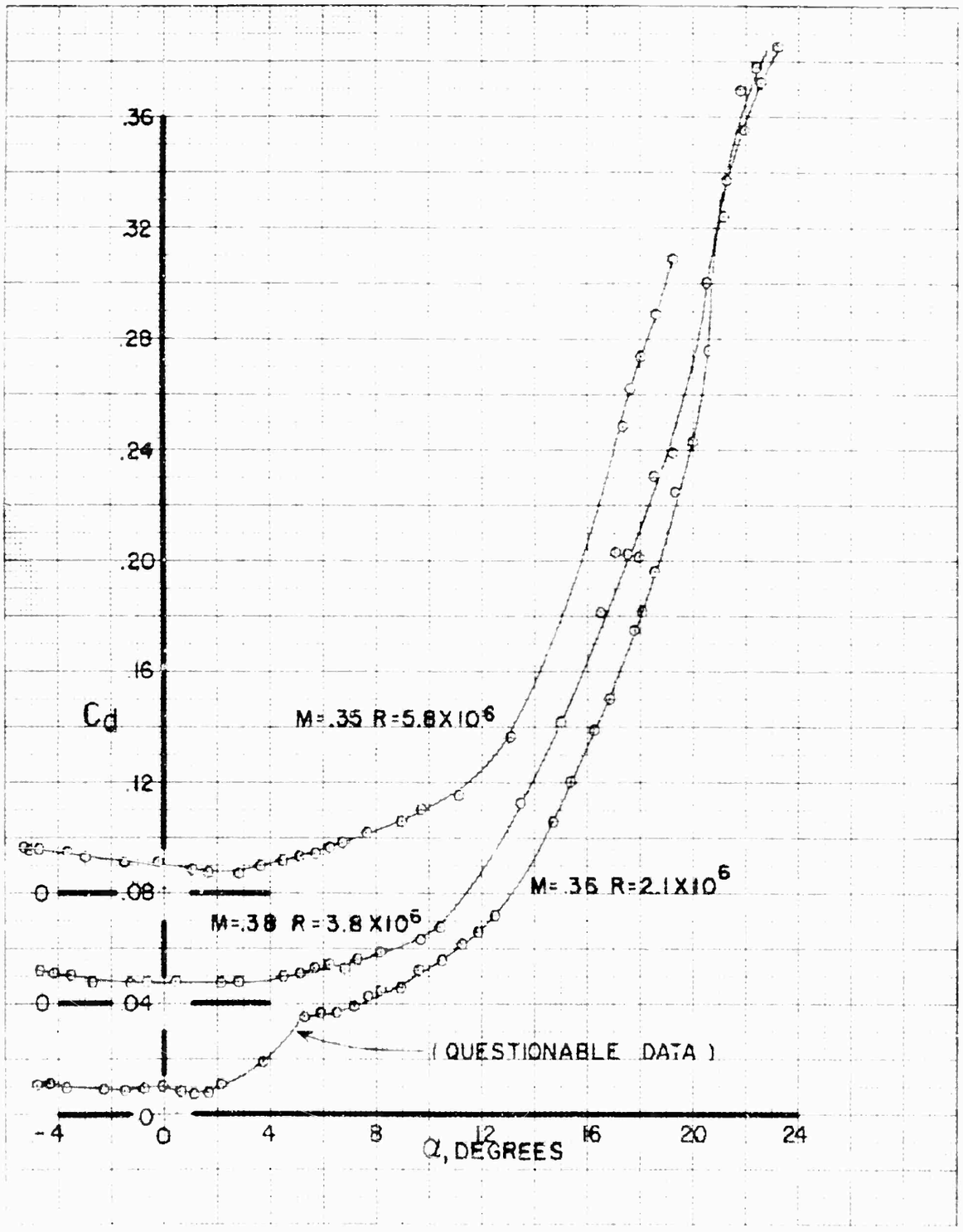


Figure 49B-1. Variation of Section Drag Coefficient With Angle of Attack, NACA Section 63A018

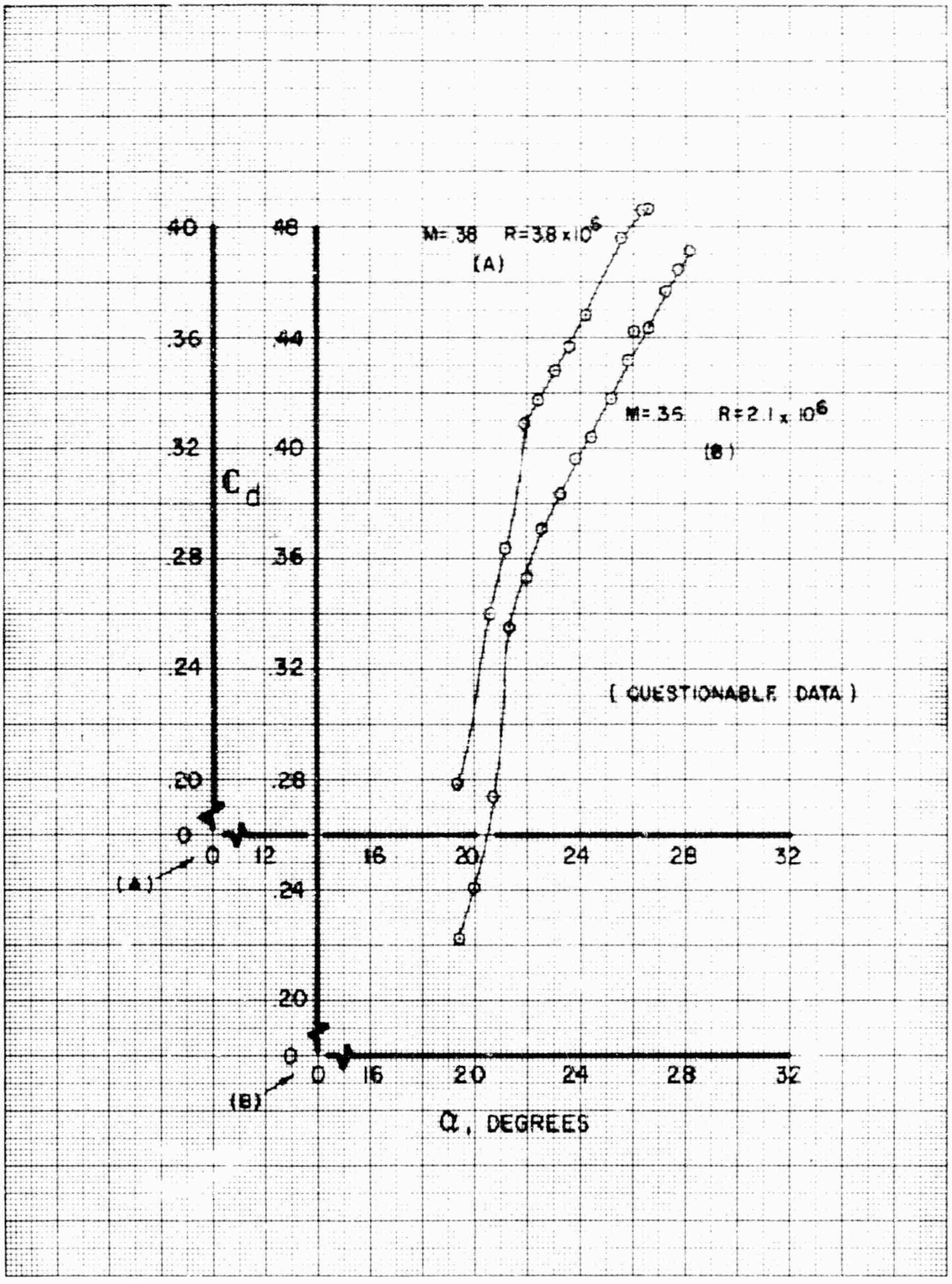


Figure 49B-2. Variation of Section Drag Coefficient With Angle of Attack, NACA Section 63018

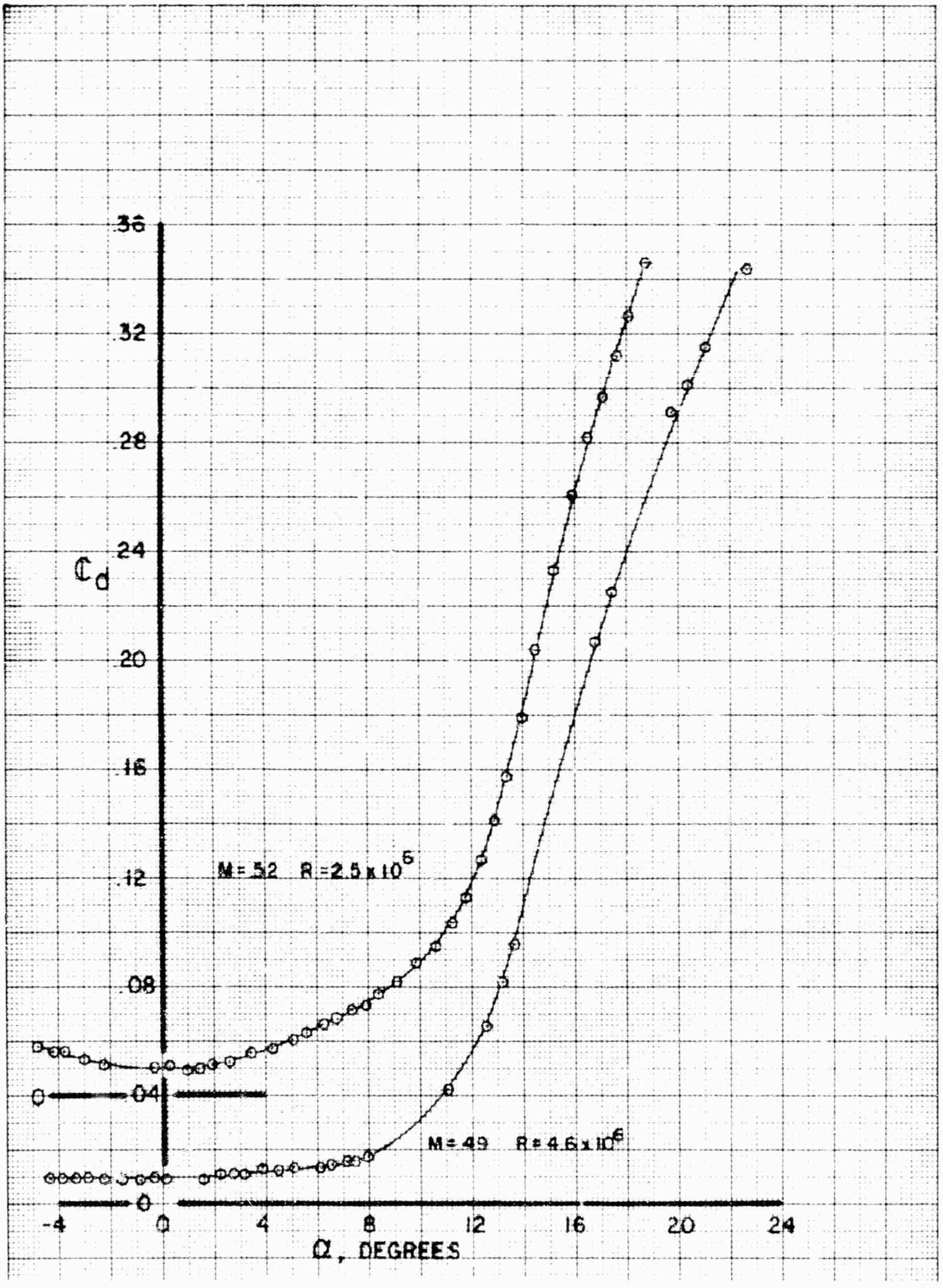


Figure 49C-1. Variation of Section Drag Coefficient With Angle of Attack, NACA Section 63A018

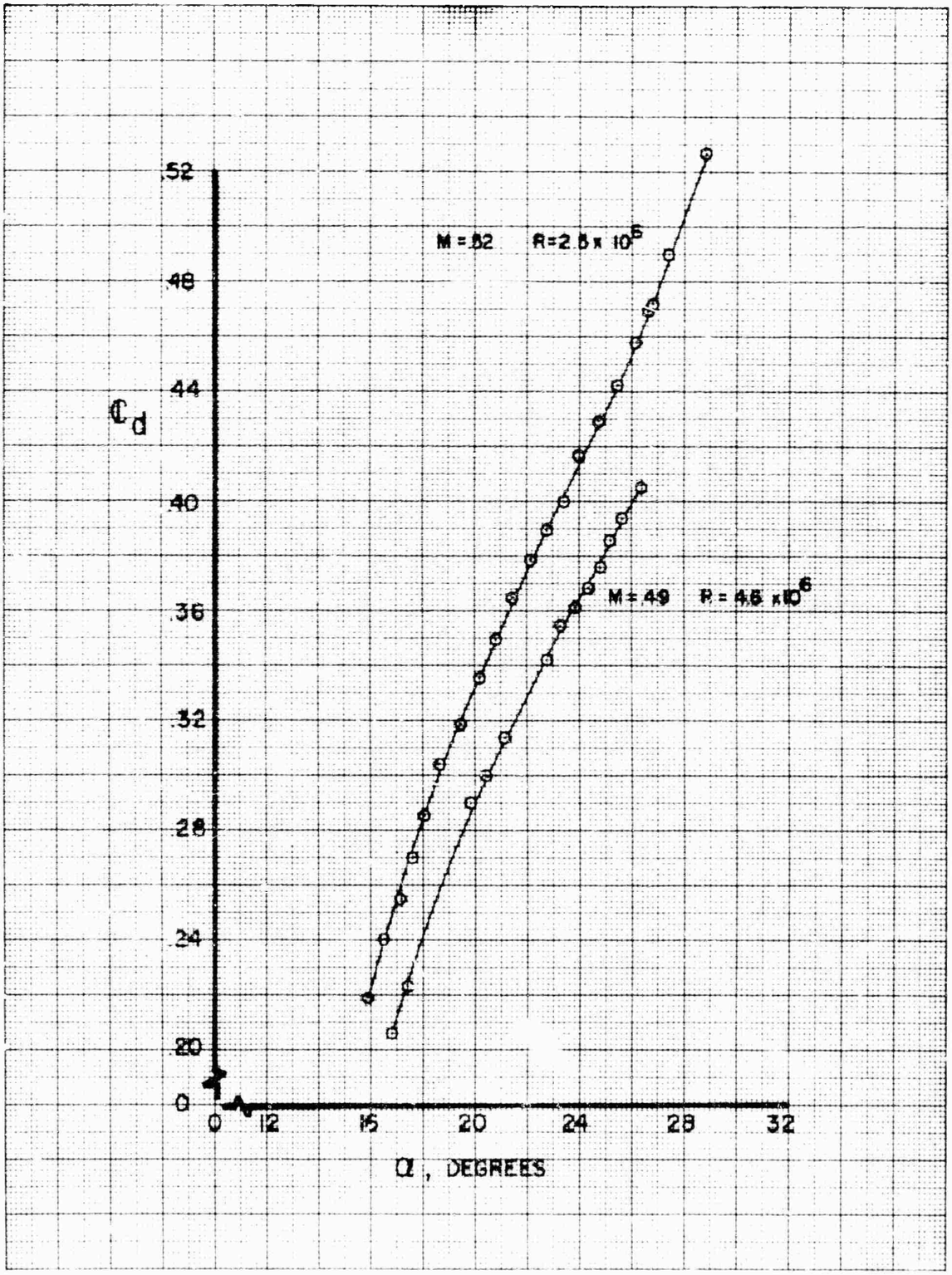


Figure 49C-2. Variation of Section Drag Coefficient With Angle of Attack, NACA Section 63A018

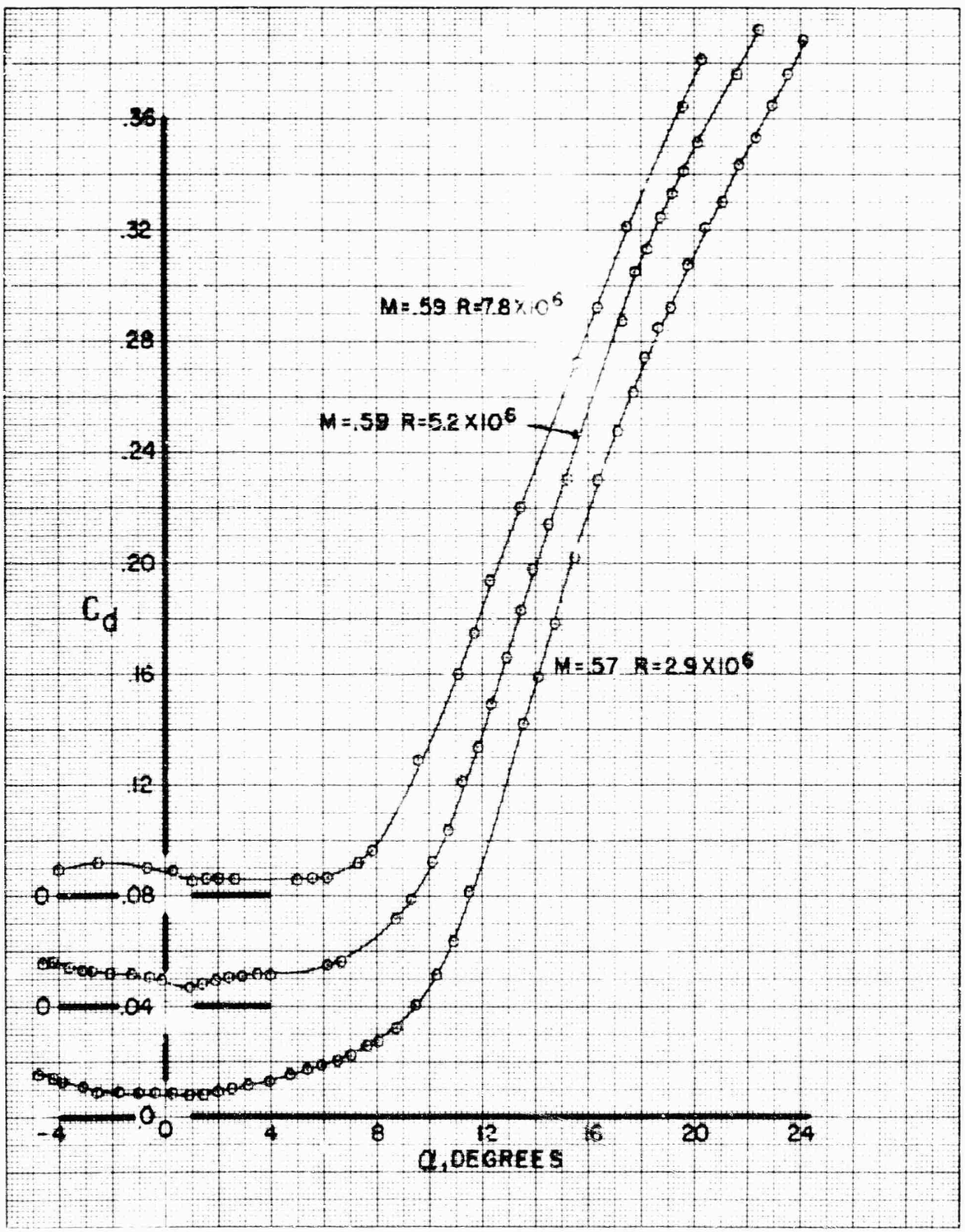


Figure 49D-1. Variation of Section Drag Coefficient With Angle of Attack, NACA Section 63A018

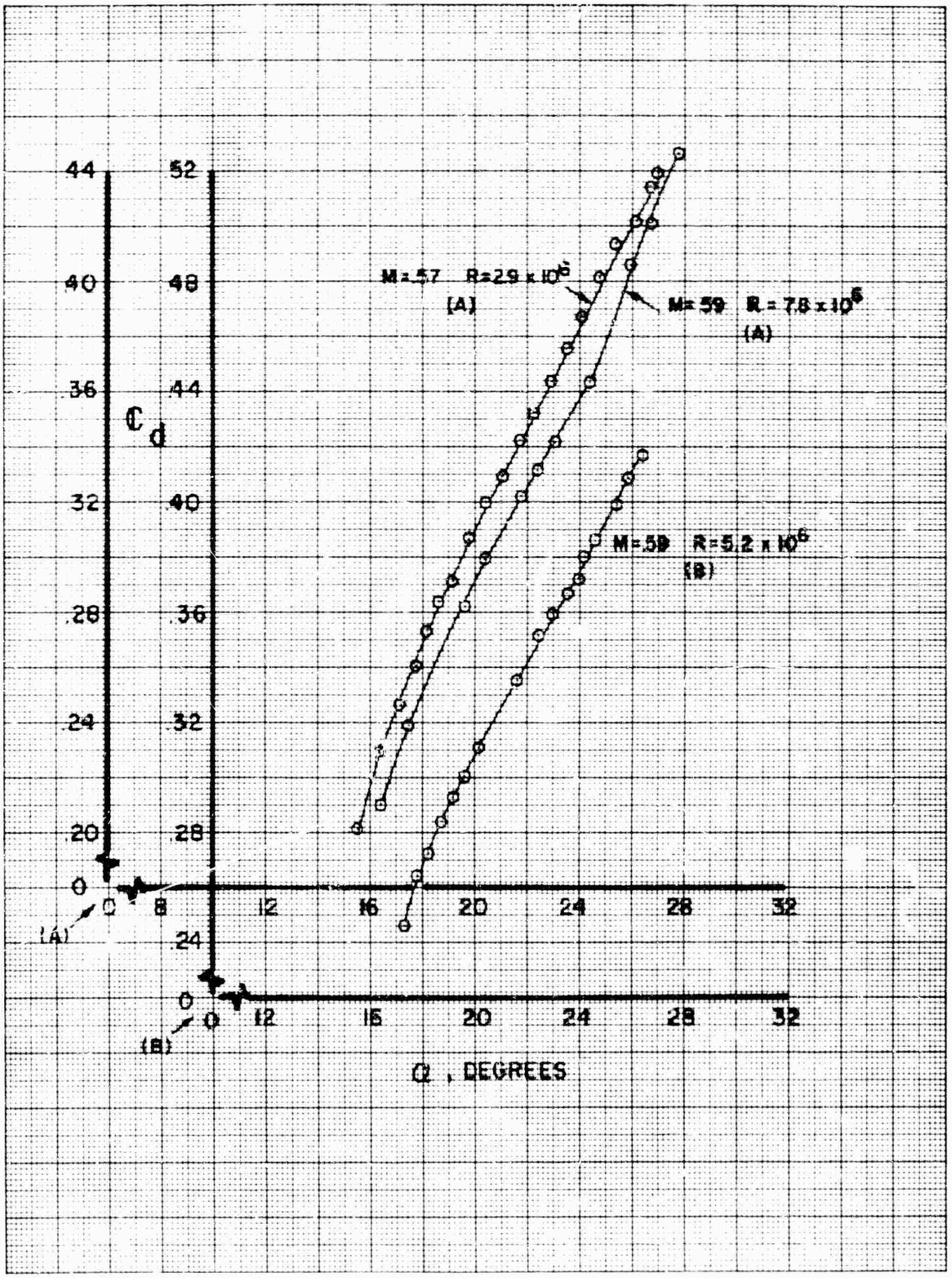


Figure 49D-2. Variation of Section Drag Coefficient With Angle of Attack, NACA Section 63A018

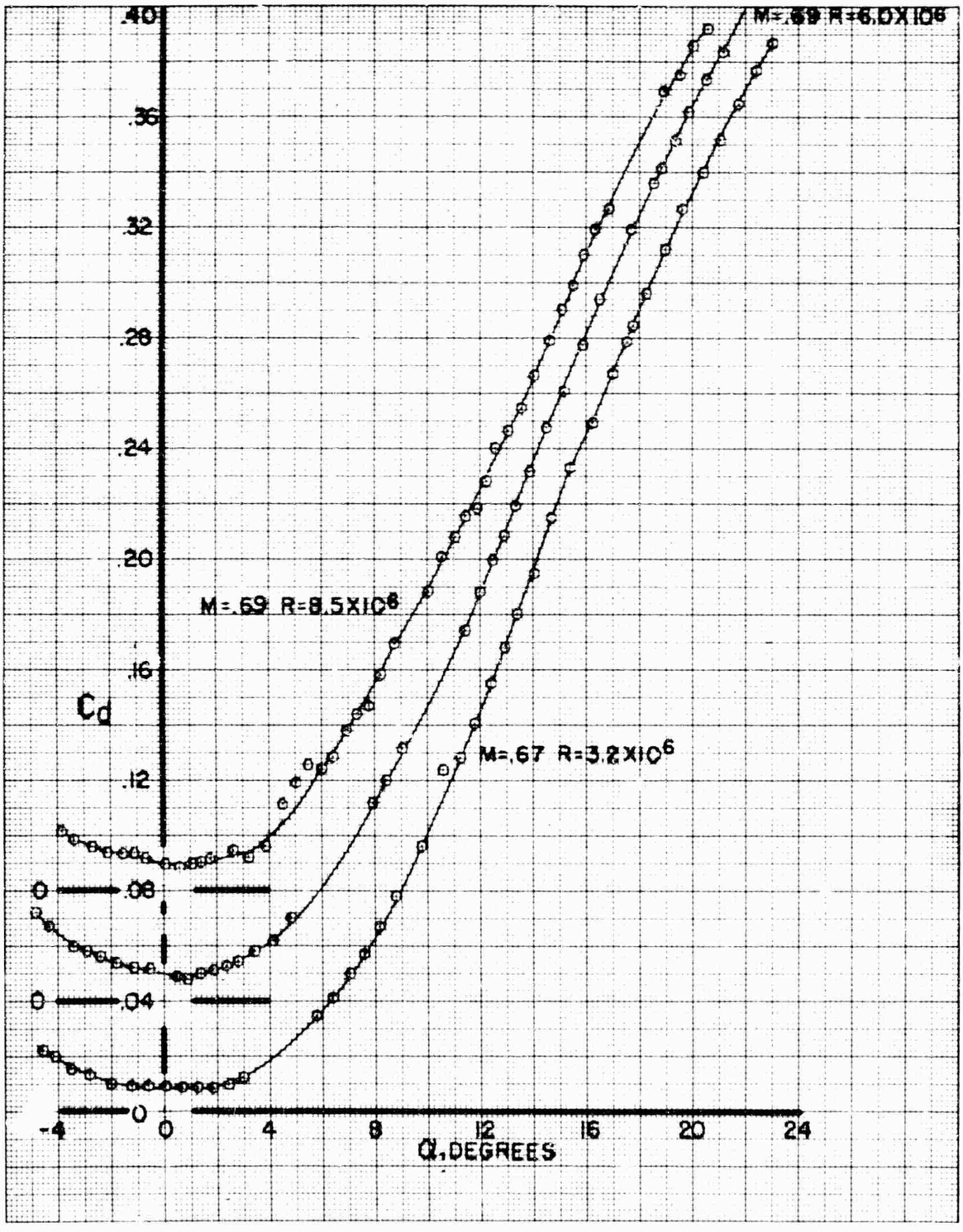


Figure 49E-1. Variation of Section Drag Coefficient With Angle of Attack, NACA Section 63A018

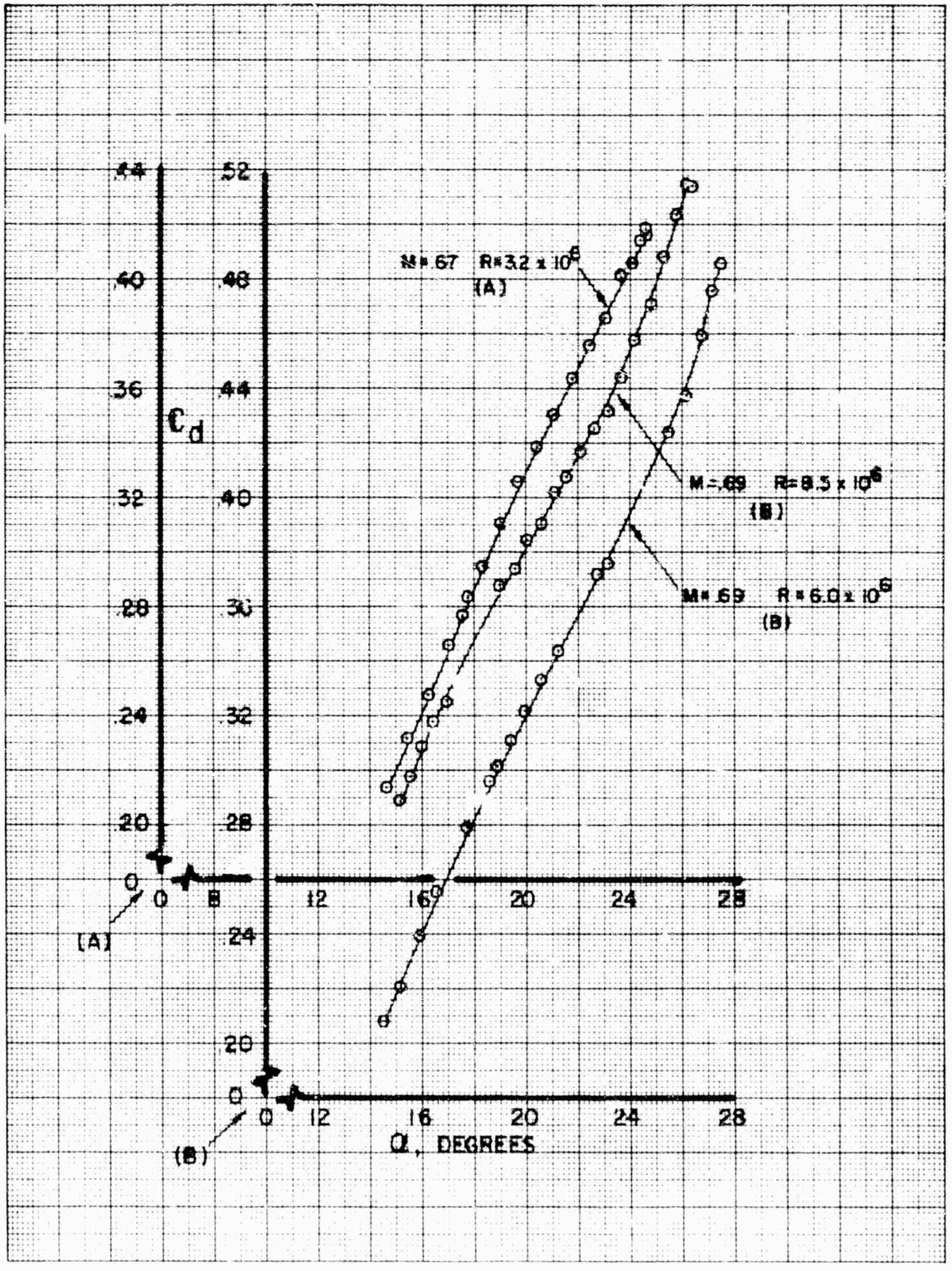


Figure 49E-2. Variation of Section Drag Coefficient With Angle of Attack, NACA Section 63A018

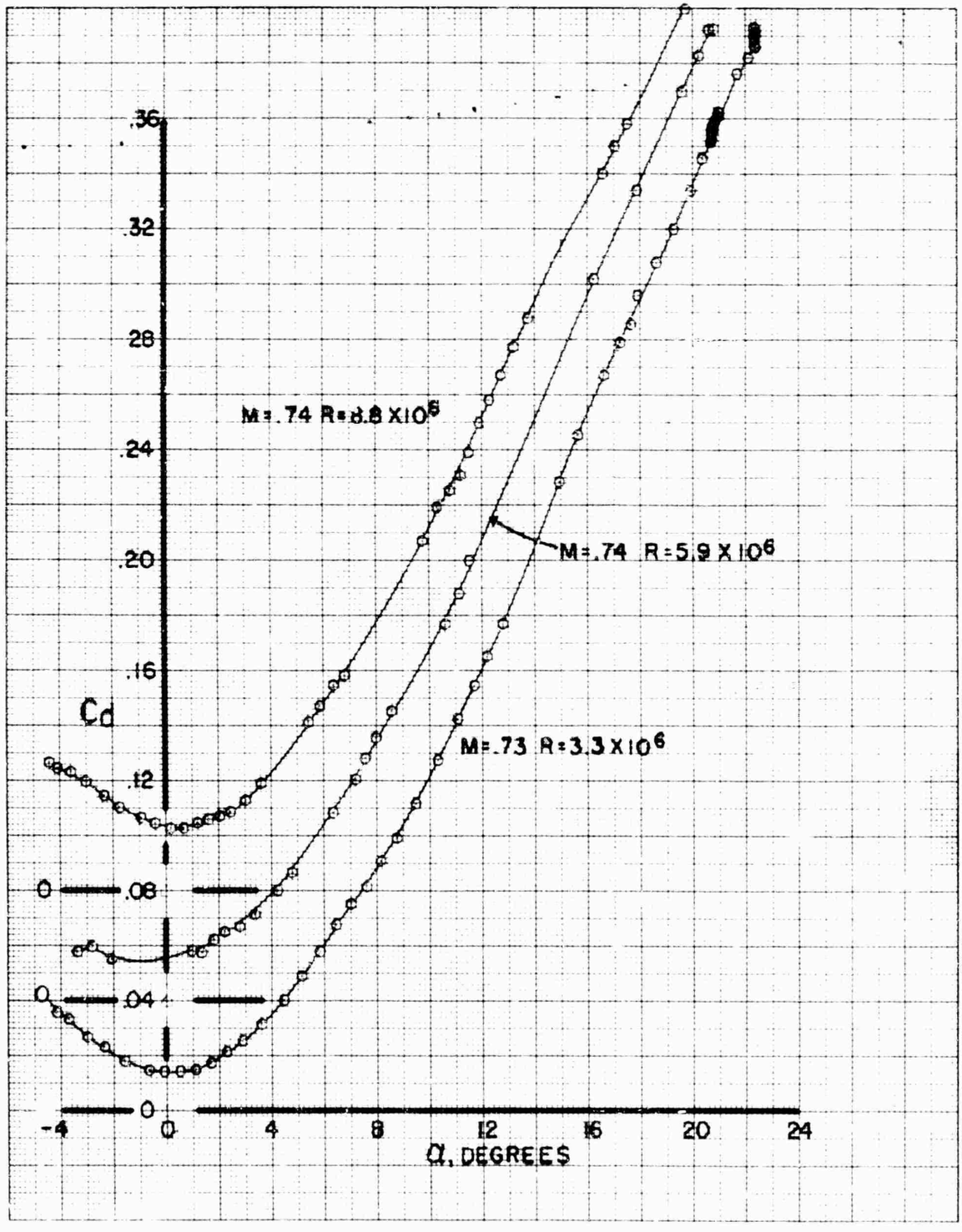


Figure 49F. Variation of Section Drag Coefficient With Angle of Attack, NACA Section 63A018

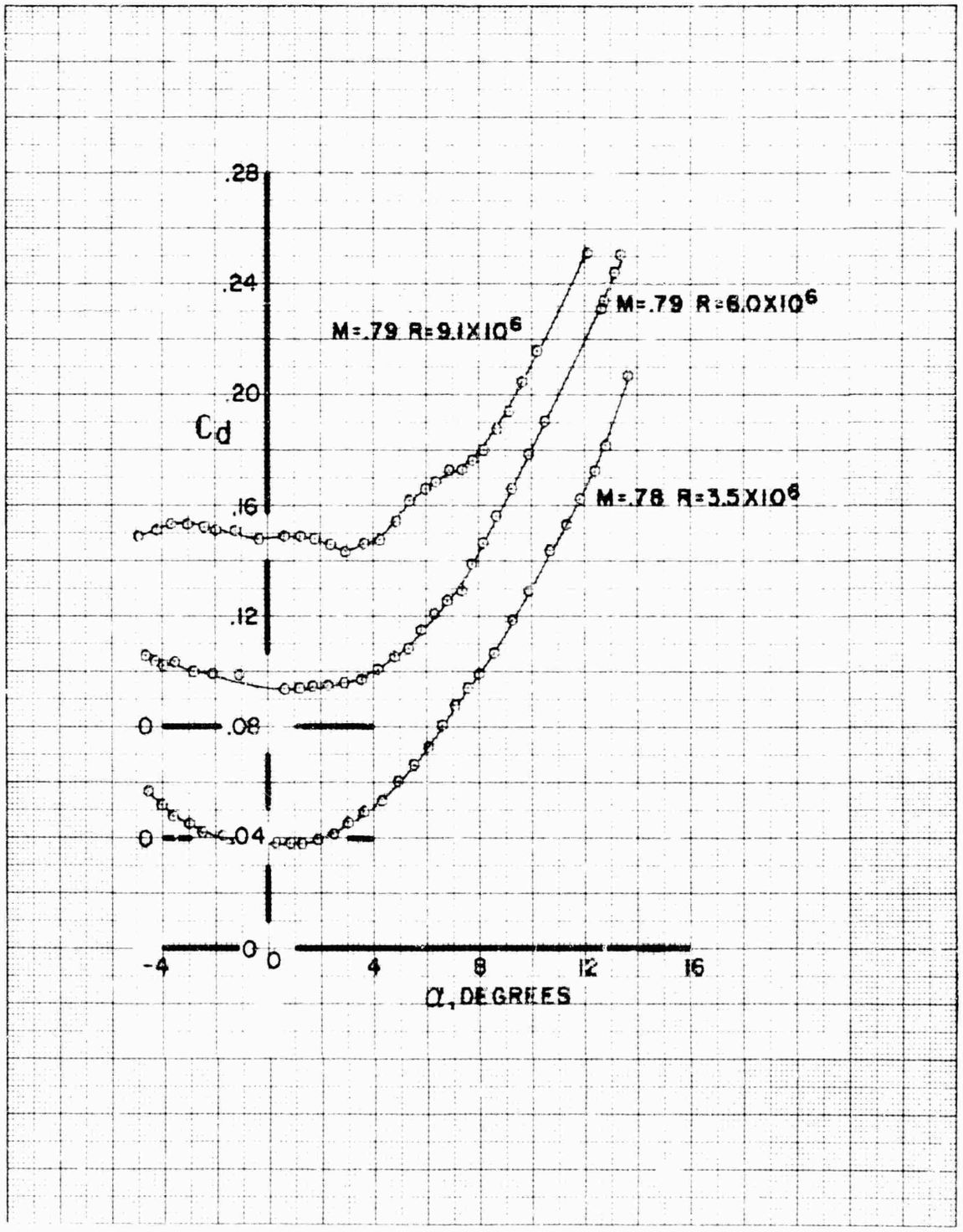


Figure 49G. Variation of Section Drag Coefficient With Angle of Attack, NACA Section 63A018

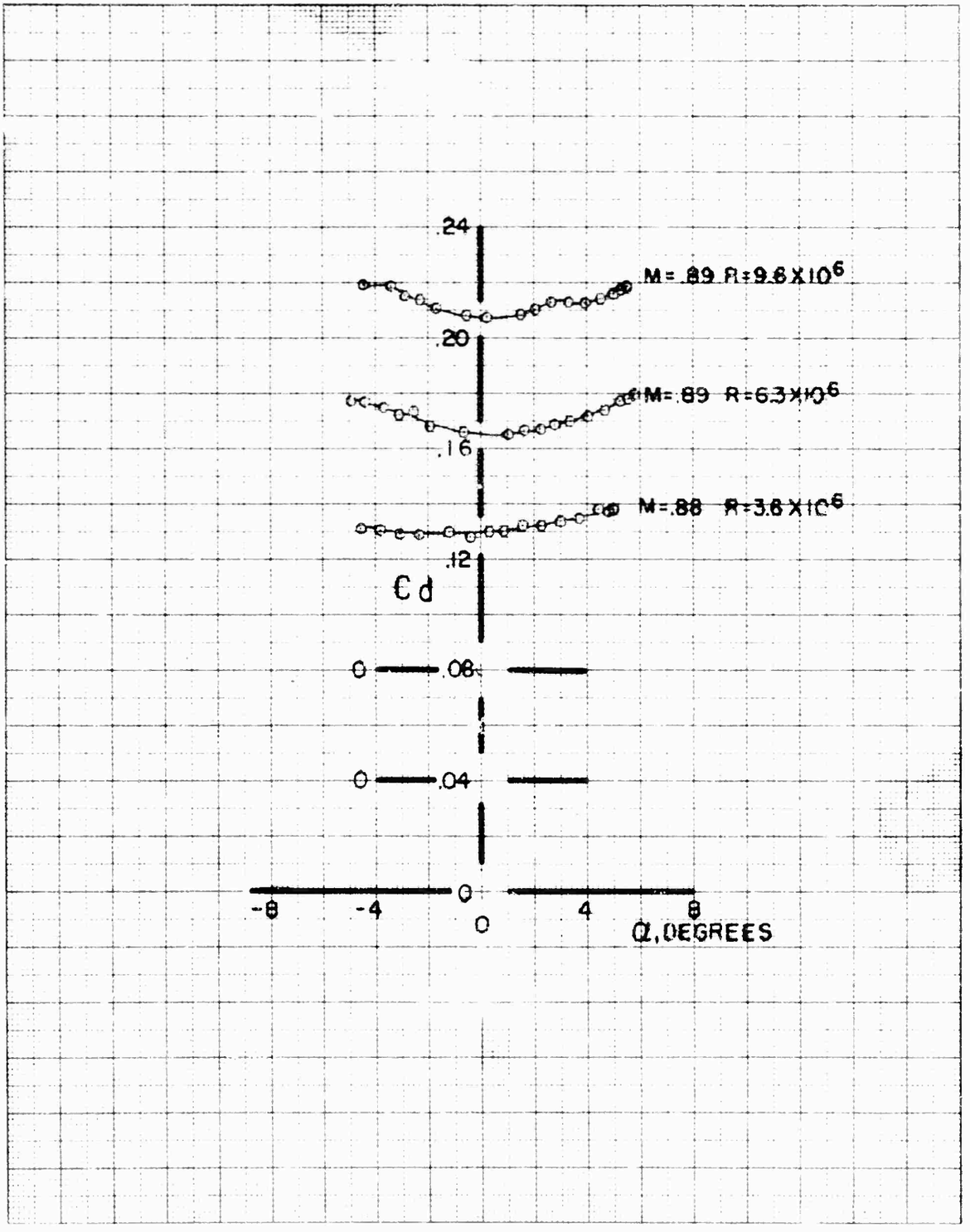


Figure 49H. Variation of Section Drag Coefficient With Angle of Attack, NACA Section 63A018

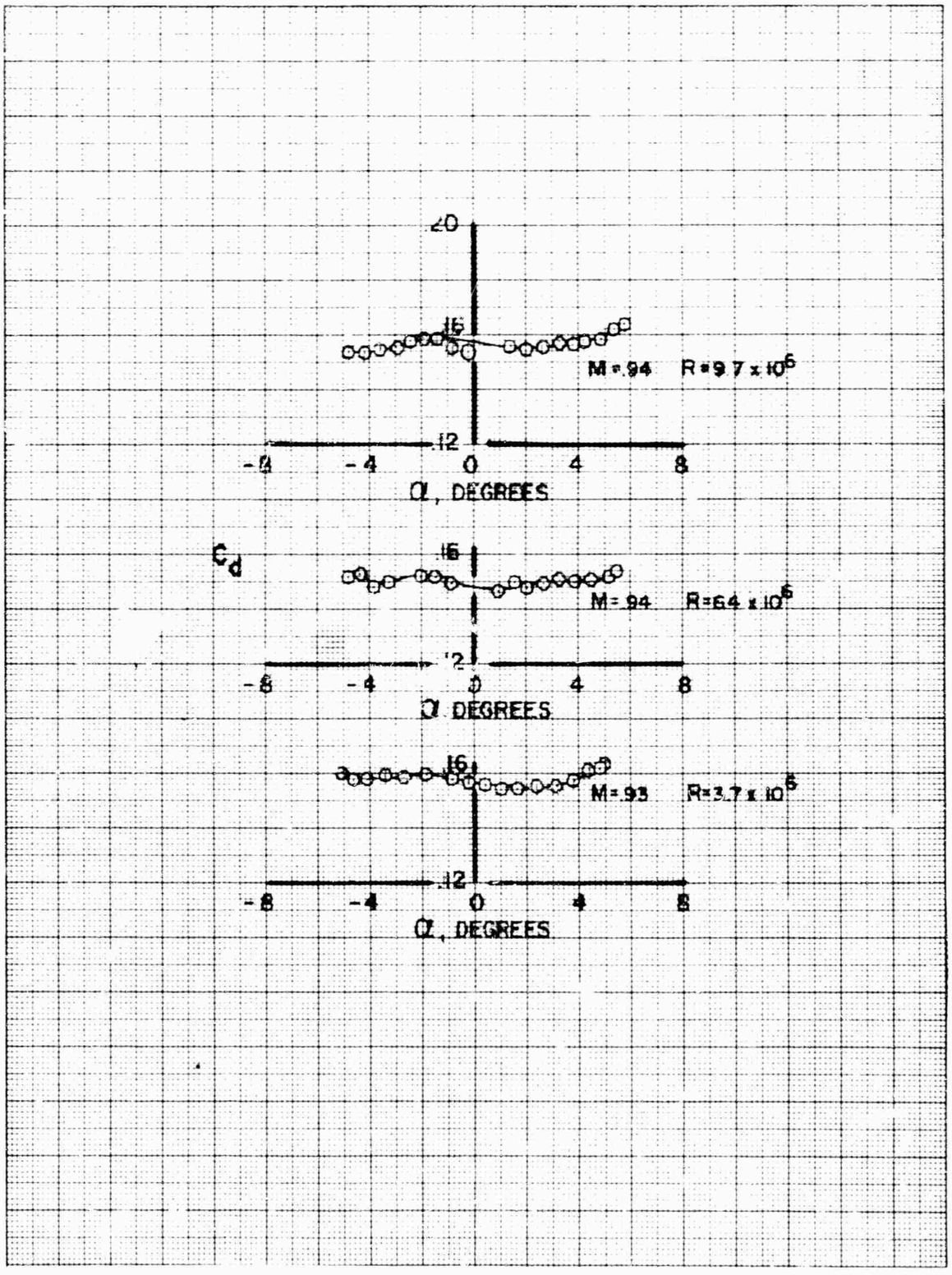


Figure 491. Variation of Section Drag Coefficient With Angle of Attack NACA Section 63A018

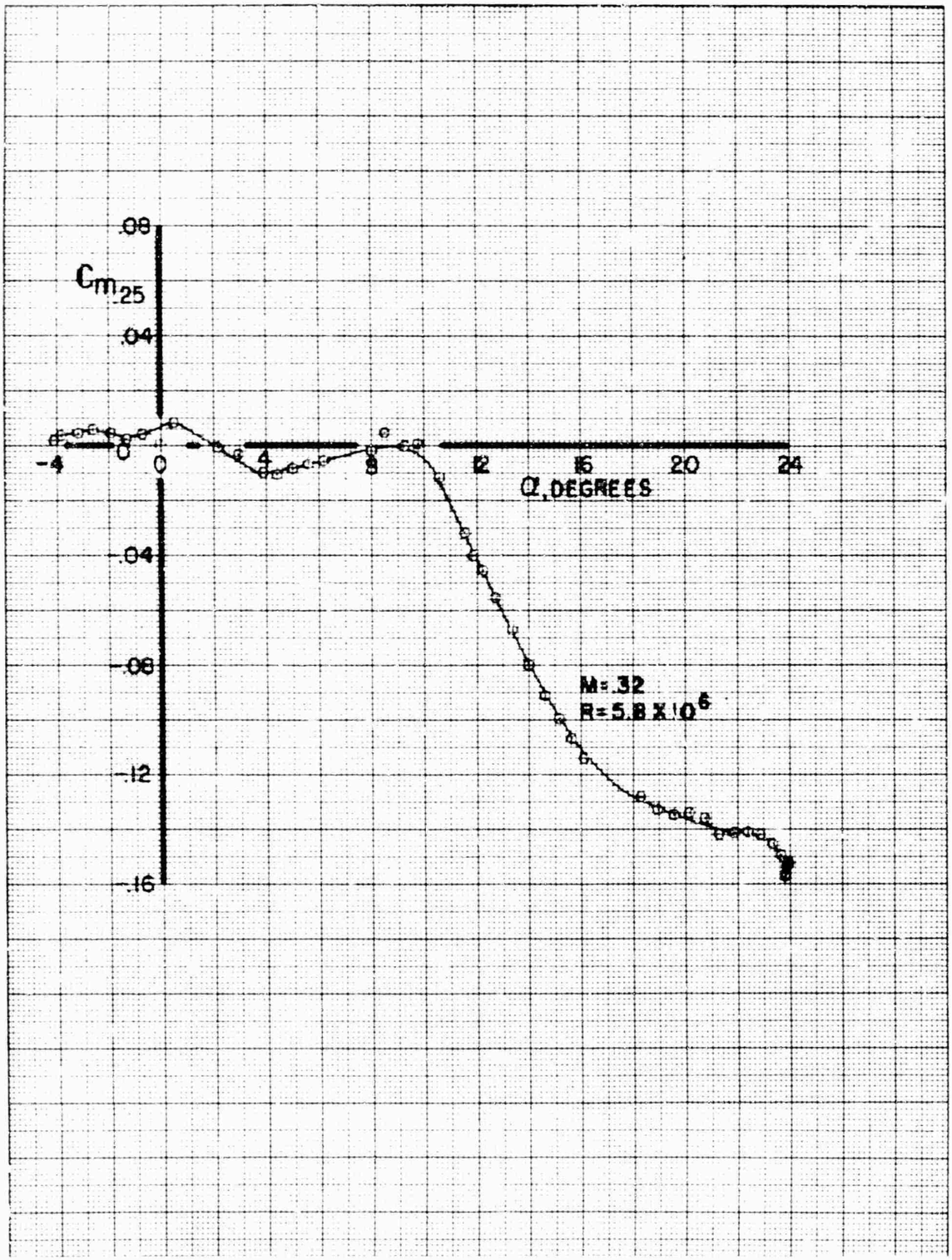


Figure 50A. Variation of Section Pitching Moment Coefficient With Angle of Attack, NACA Section 63A009

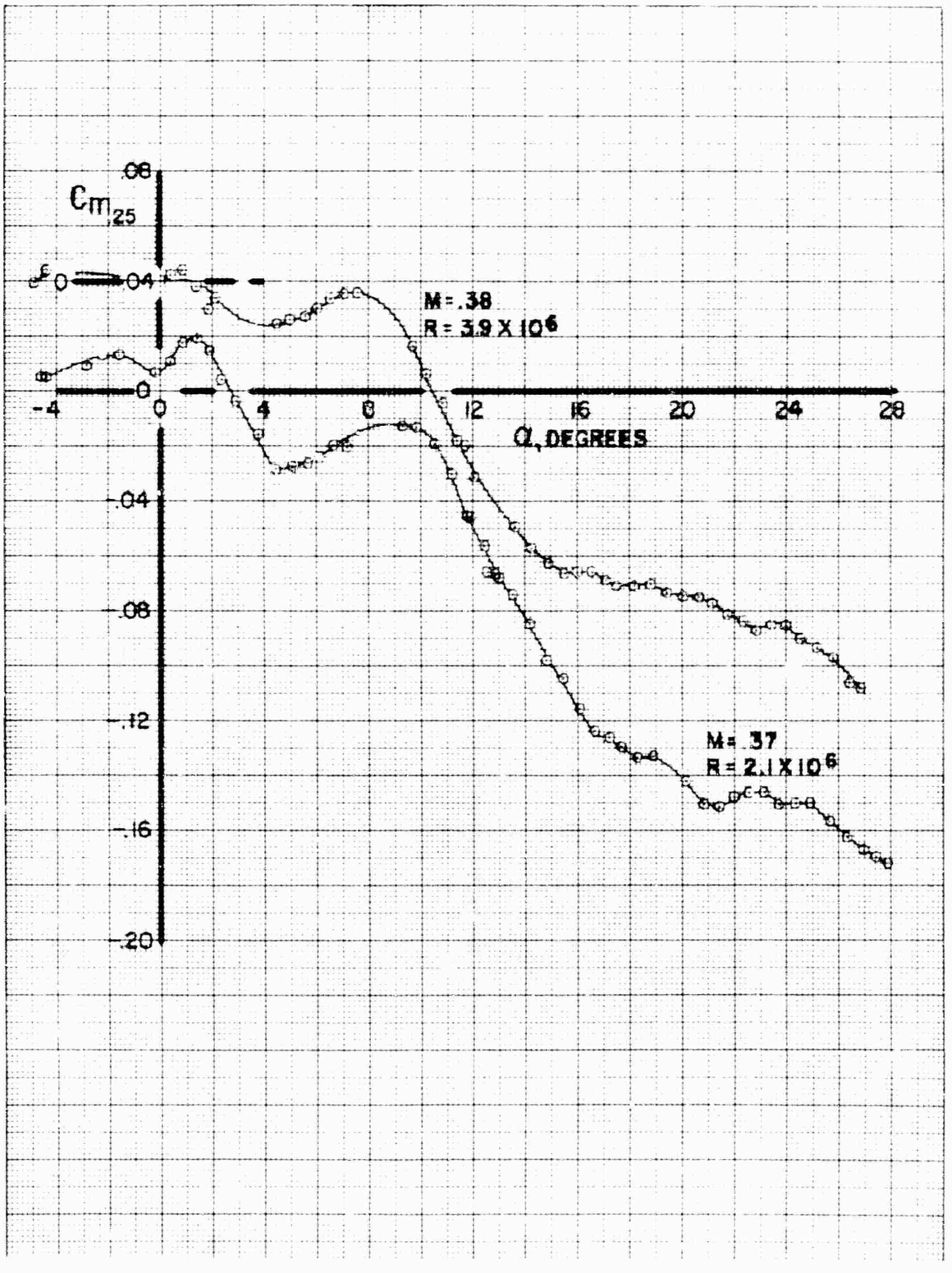


Figure 50B. Variation of Section Pitching Moment Coefficient With Angle of Attack, NACA Section 63A009

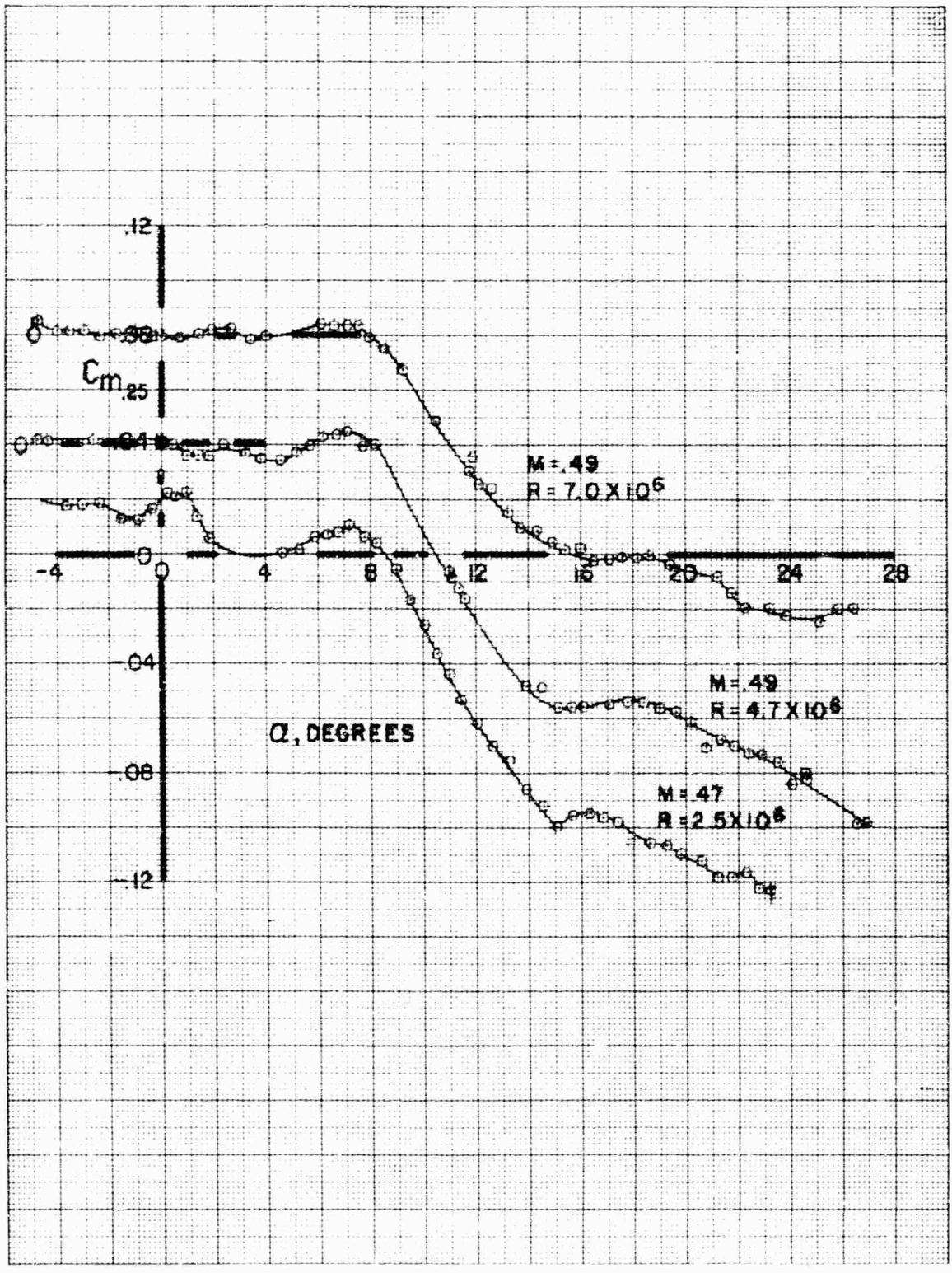


Figure 50C. Variation of Section Pitching Moment Coefficient With Angle of Attack, NACA Section 63A009.

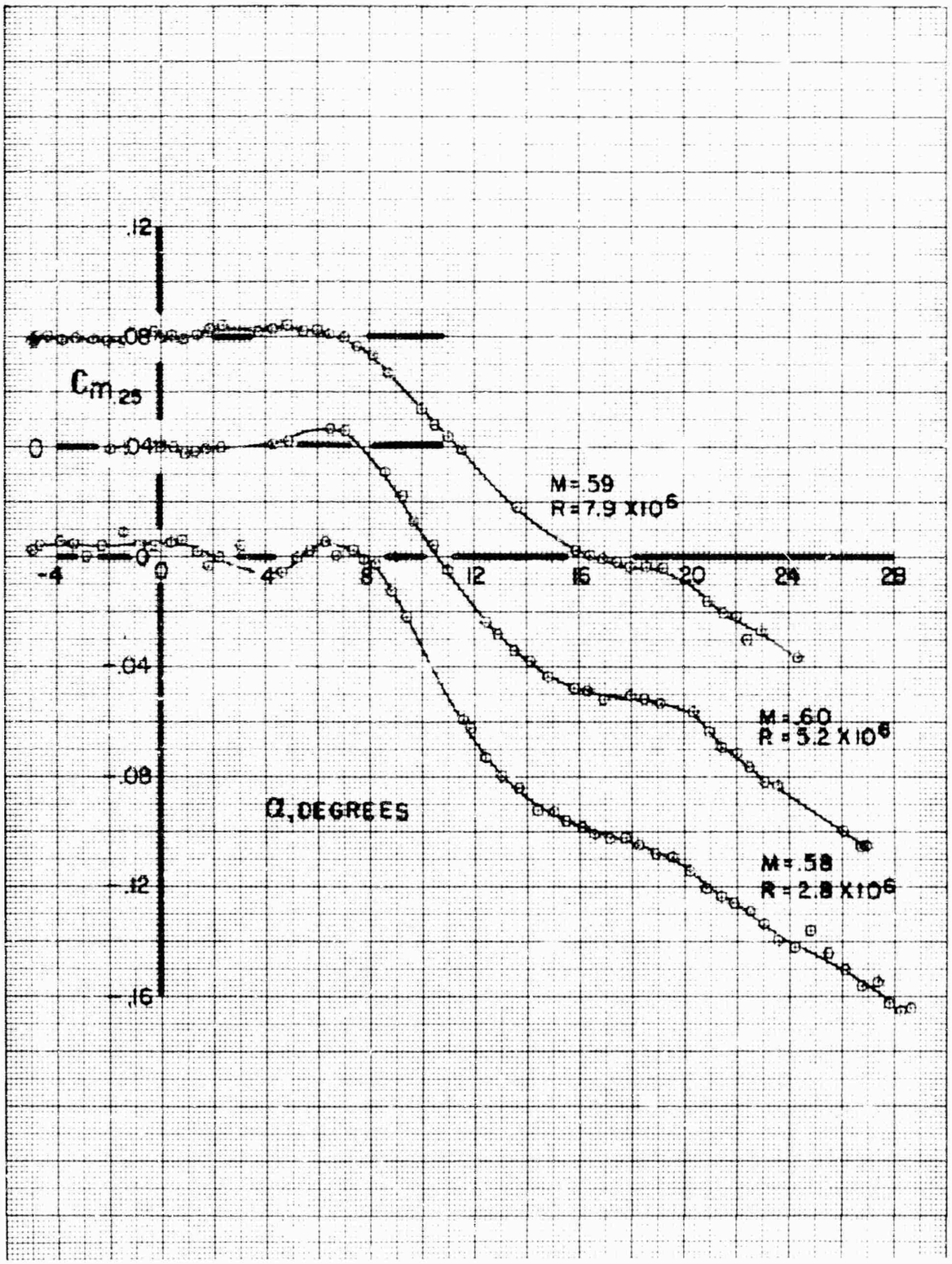


Figure 50D. Variation of Section Pitching Moment Coefficient With Angle of Attack, NACA Section 63A009

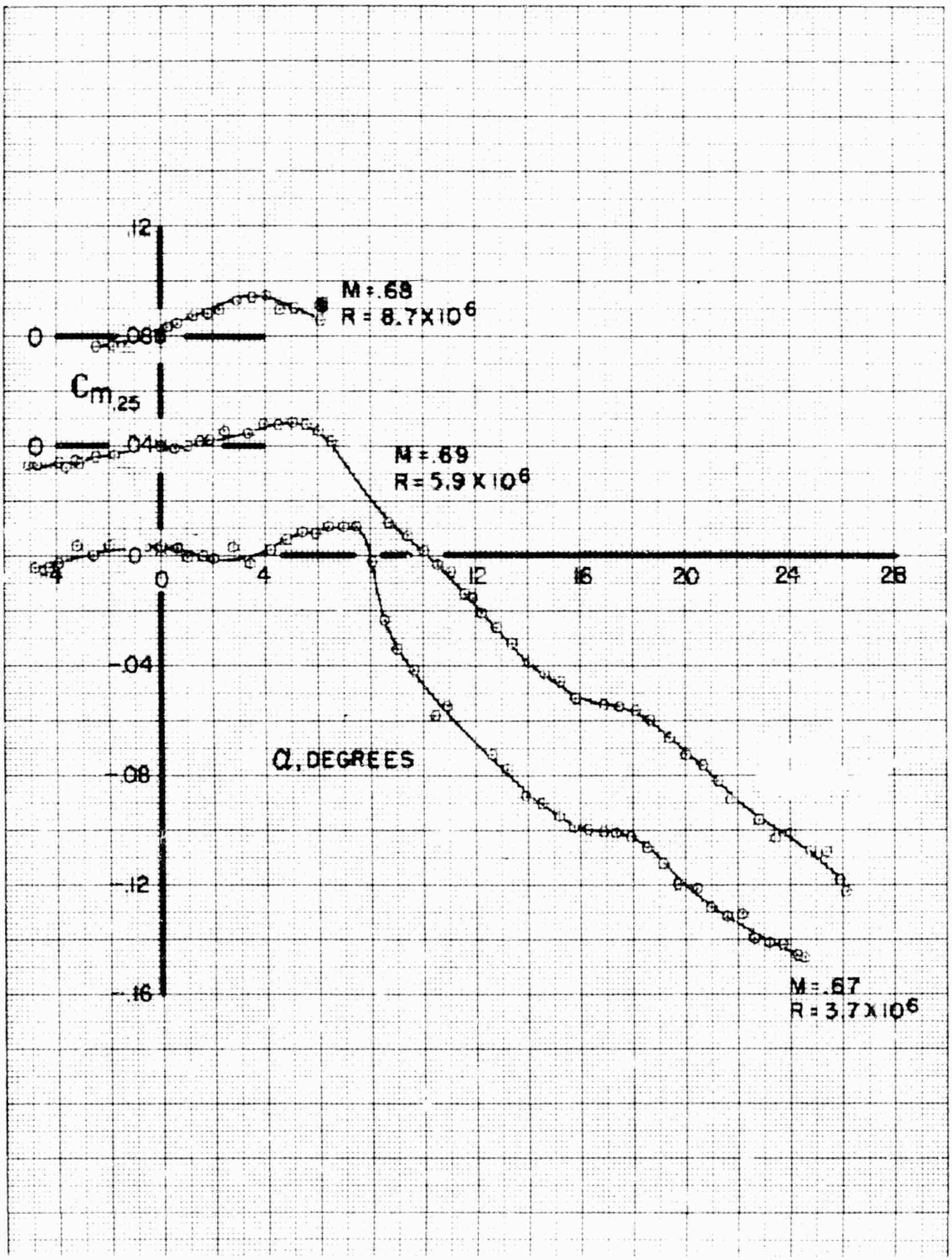


Figure 50E. Variation of Section Pitching Moment Coefficient With Angle of Attack, NACA Section 63A009

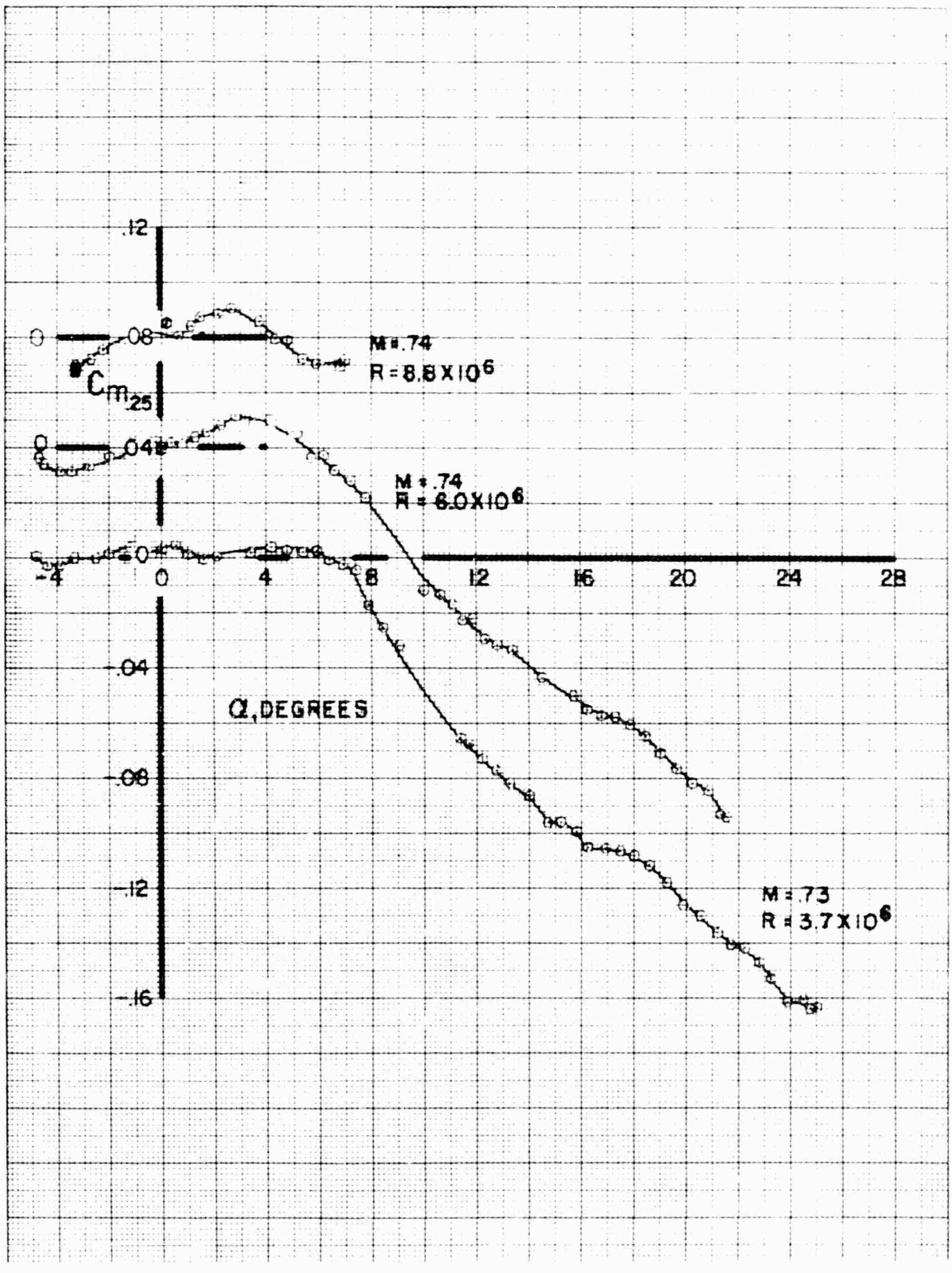


Figure 50F. Variation of Section Pitching Moment Coefficient With Angle of Attack, NACA Section 63A009

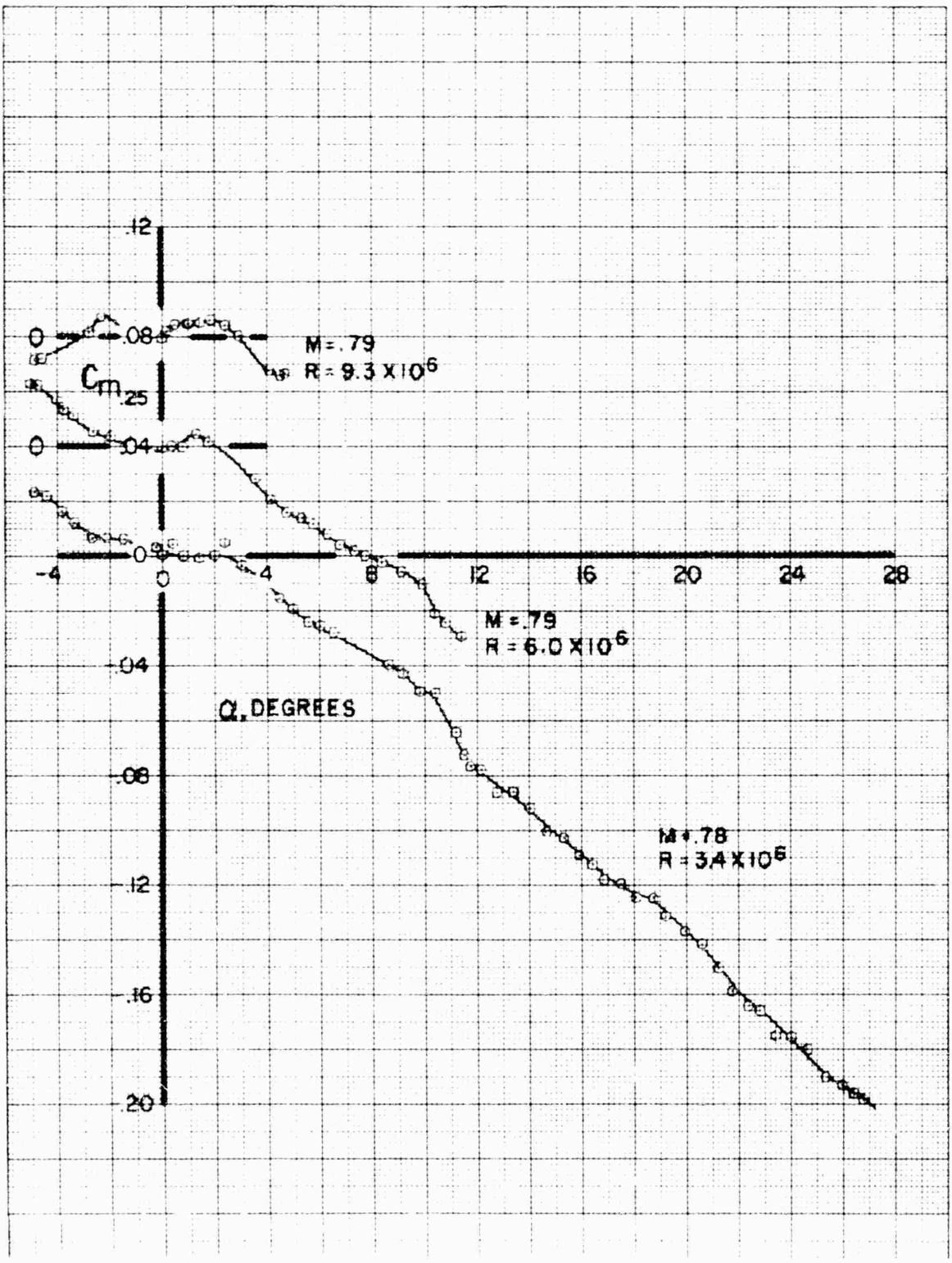


Figure 50G. Variation of Section Pitching Moment Coefficient With Angle of Attack, NACA Section 63A009

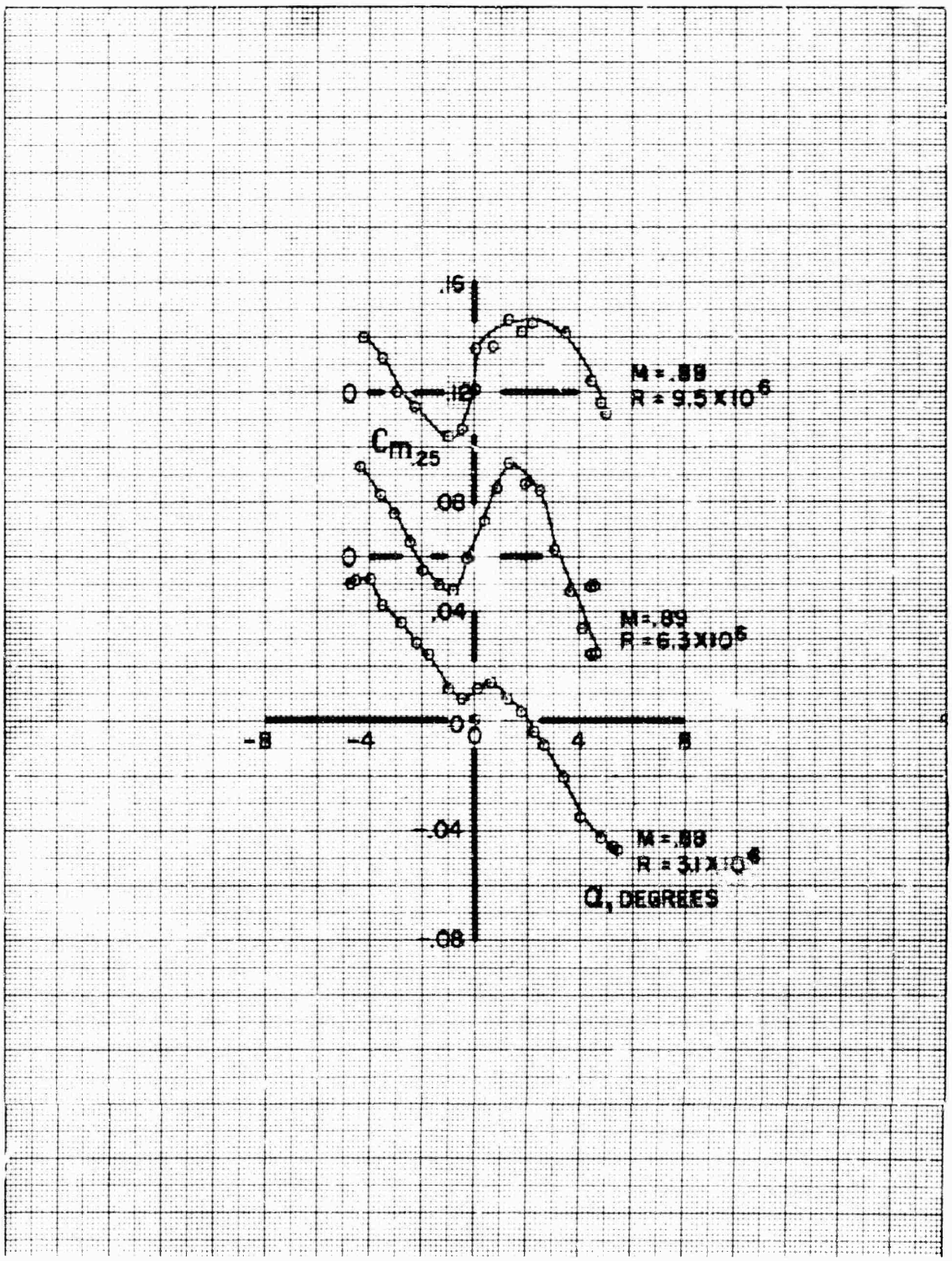


Figure 50H. Variation of Section Pitching Moment Coefficient With Angle of Attack, NACA Section 63A009

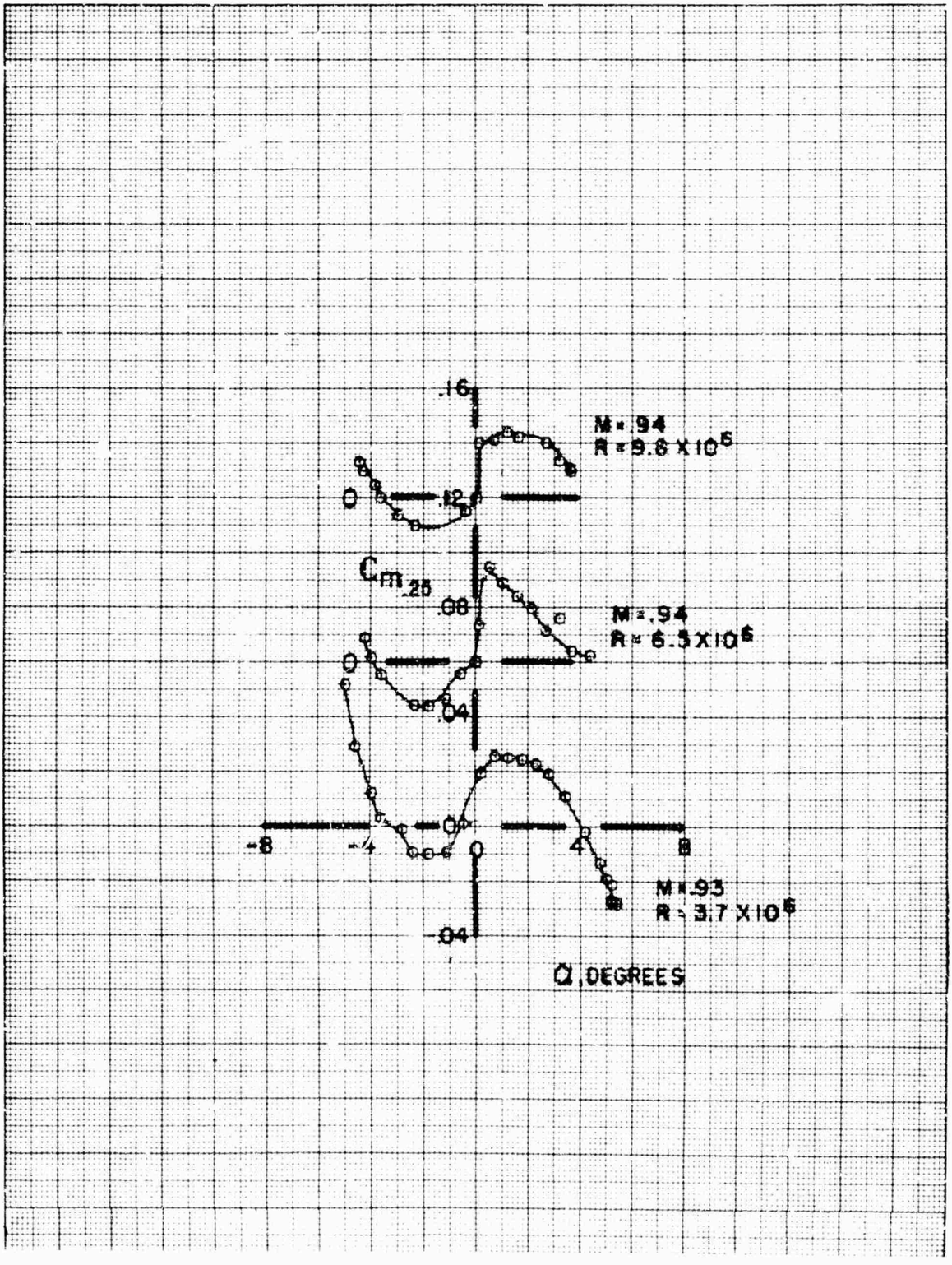


Figure 501. Variation of Section Pitching Moment Coefficient With Angle of Attack, NACA Section 63A009

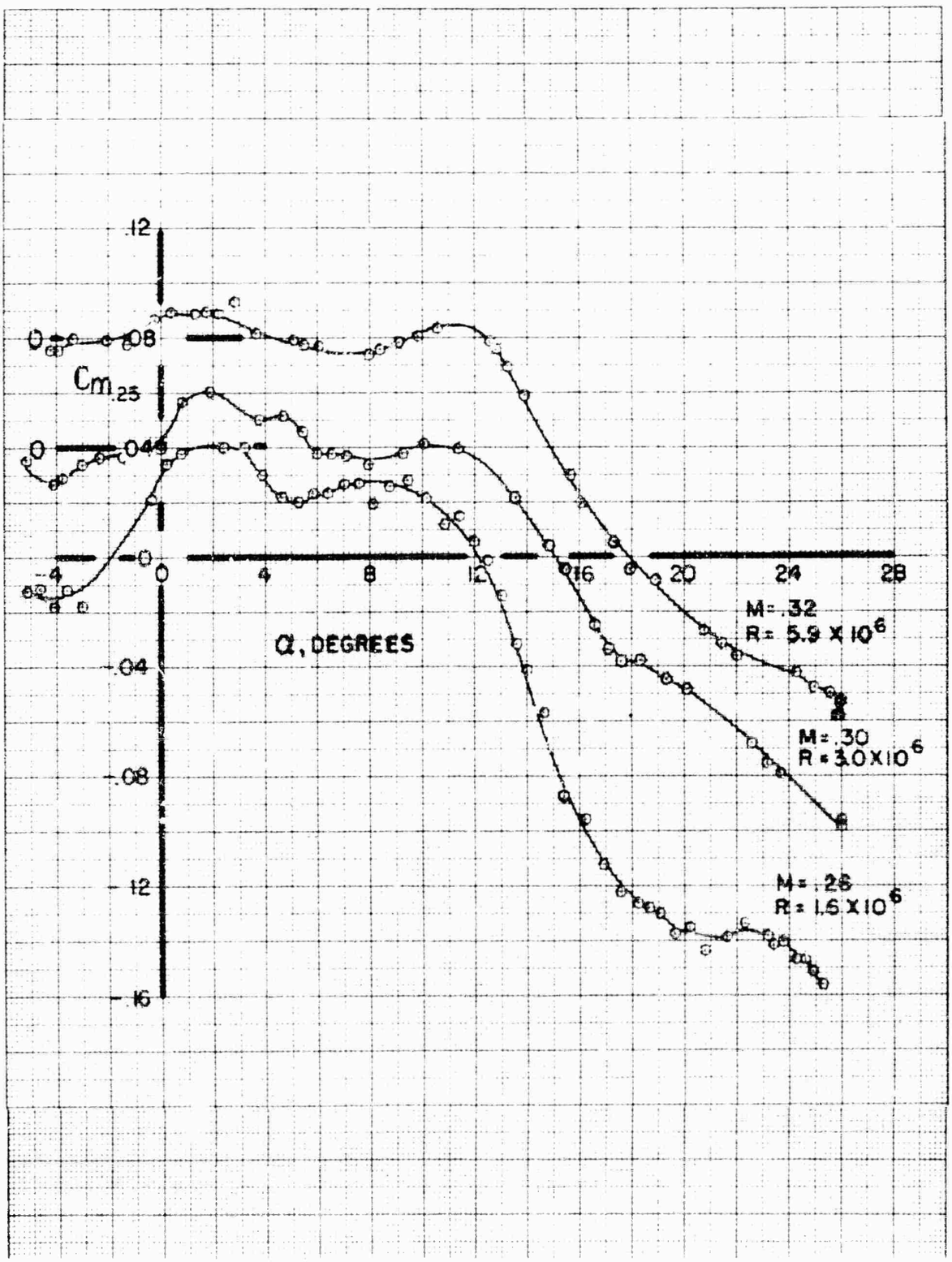


Figure 51A. Variation of Section Pitching Moment Coefficient With Angle of Attack, NACA Section 63A012

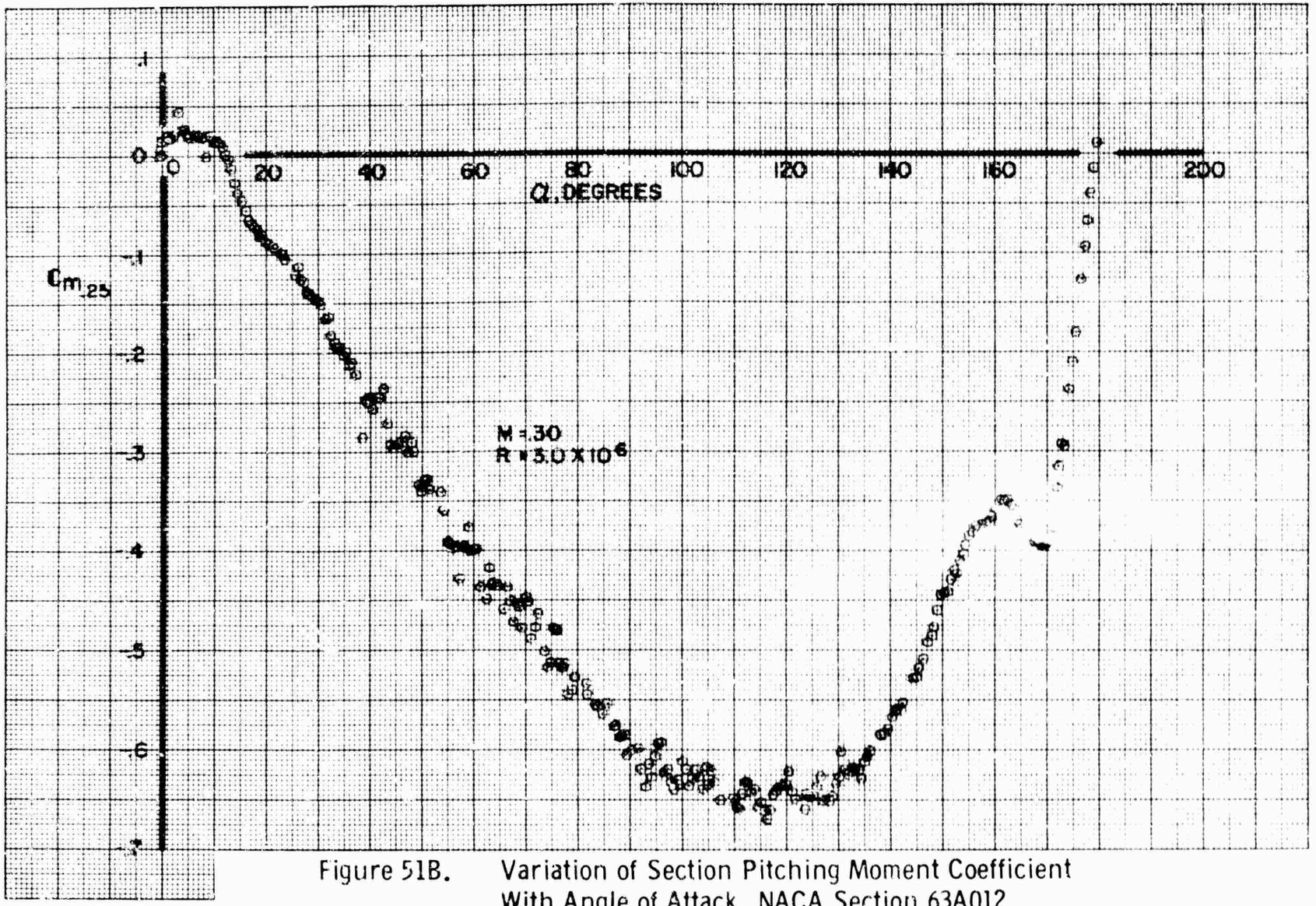


Figure 51B. Variation of Section Pitching Moment Coefficient With Angle of Attack, NACA Section 63A012

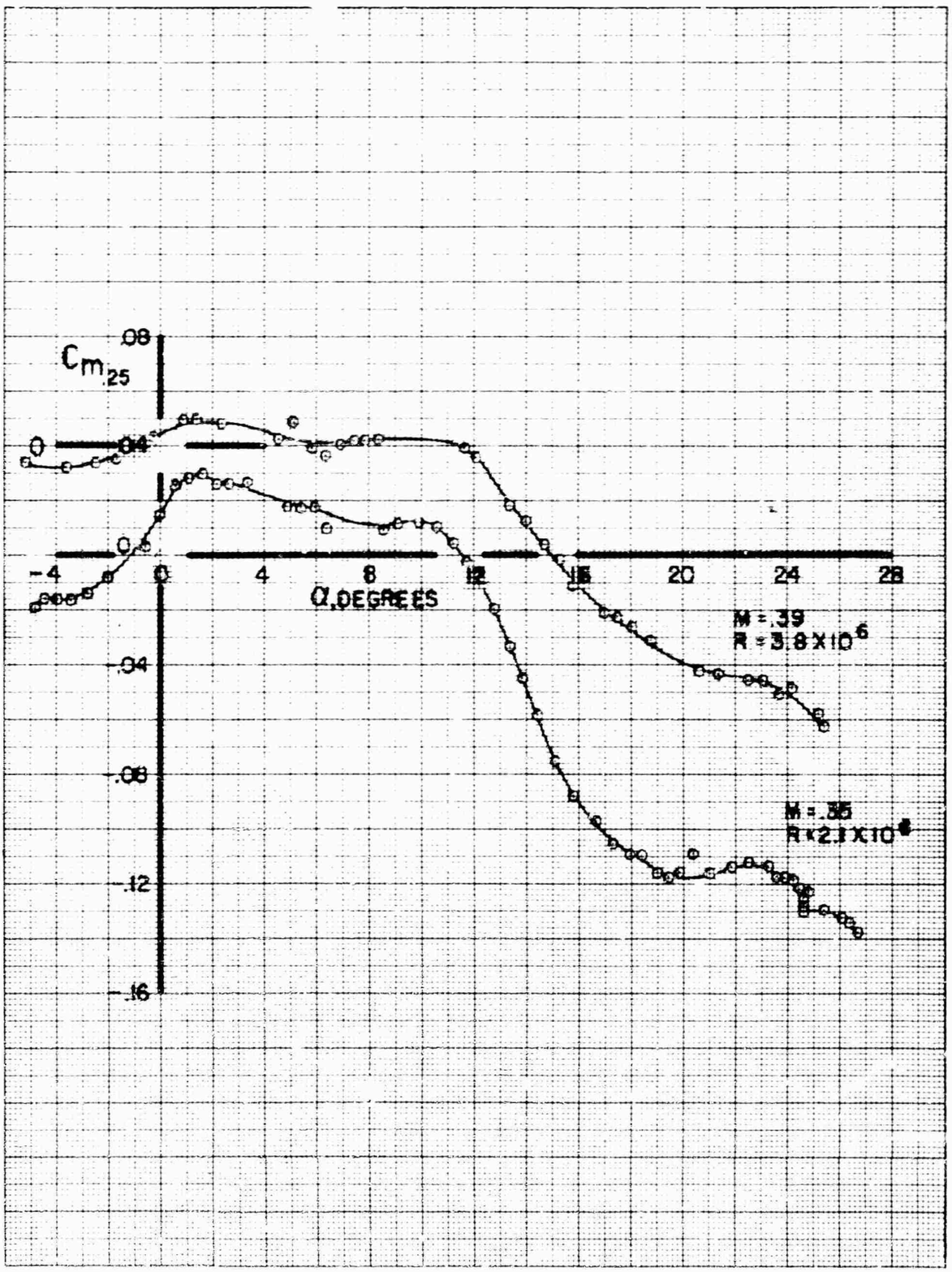


Figure 51C. Variation of Section Pitching Moment Coefficient With Angle of Attack, NACA Section 63A012

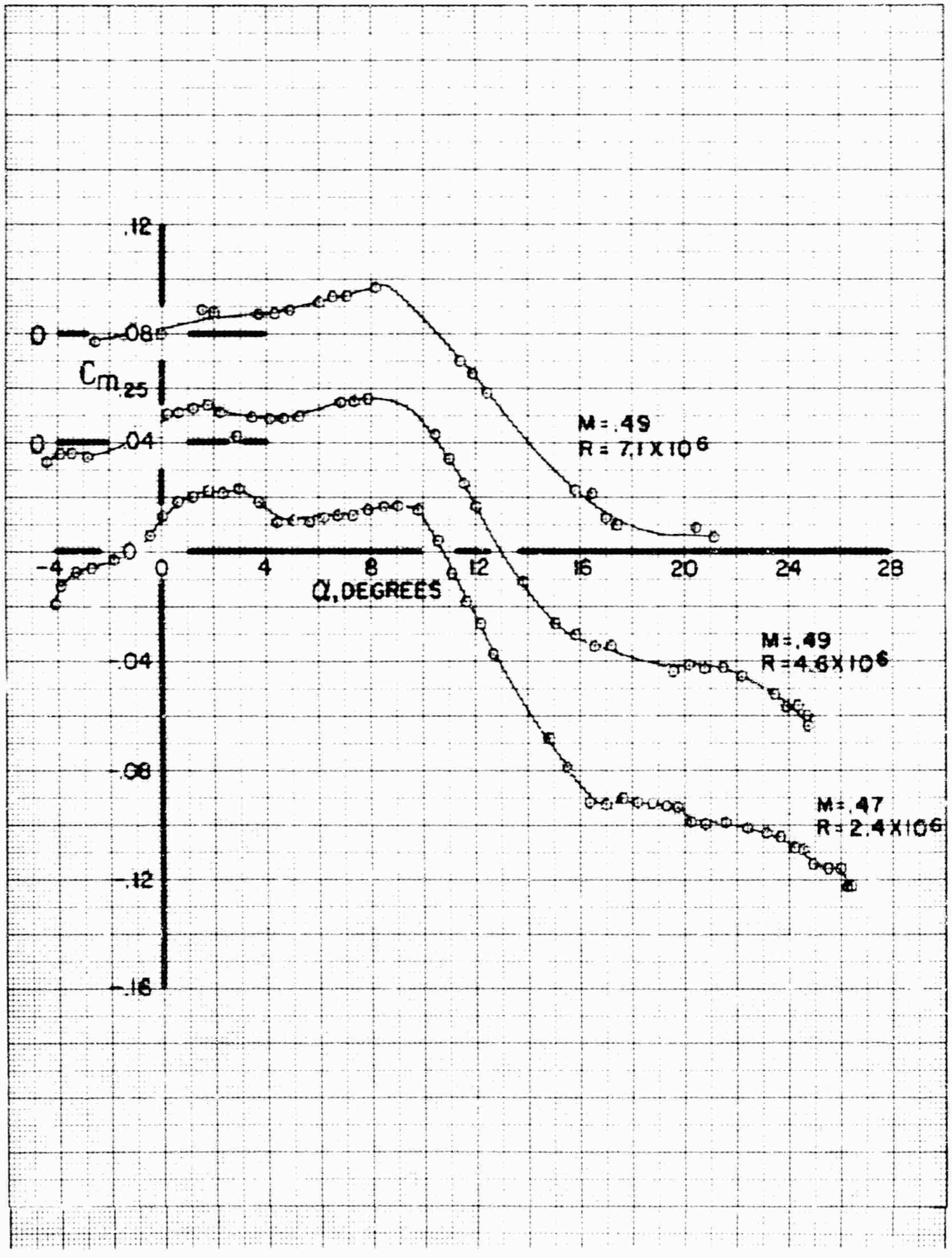


Figure 51D. Variation of Section Pitching Moment Coefficient With Angle of Attack, NACA Section 63A012

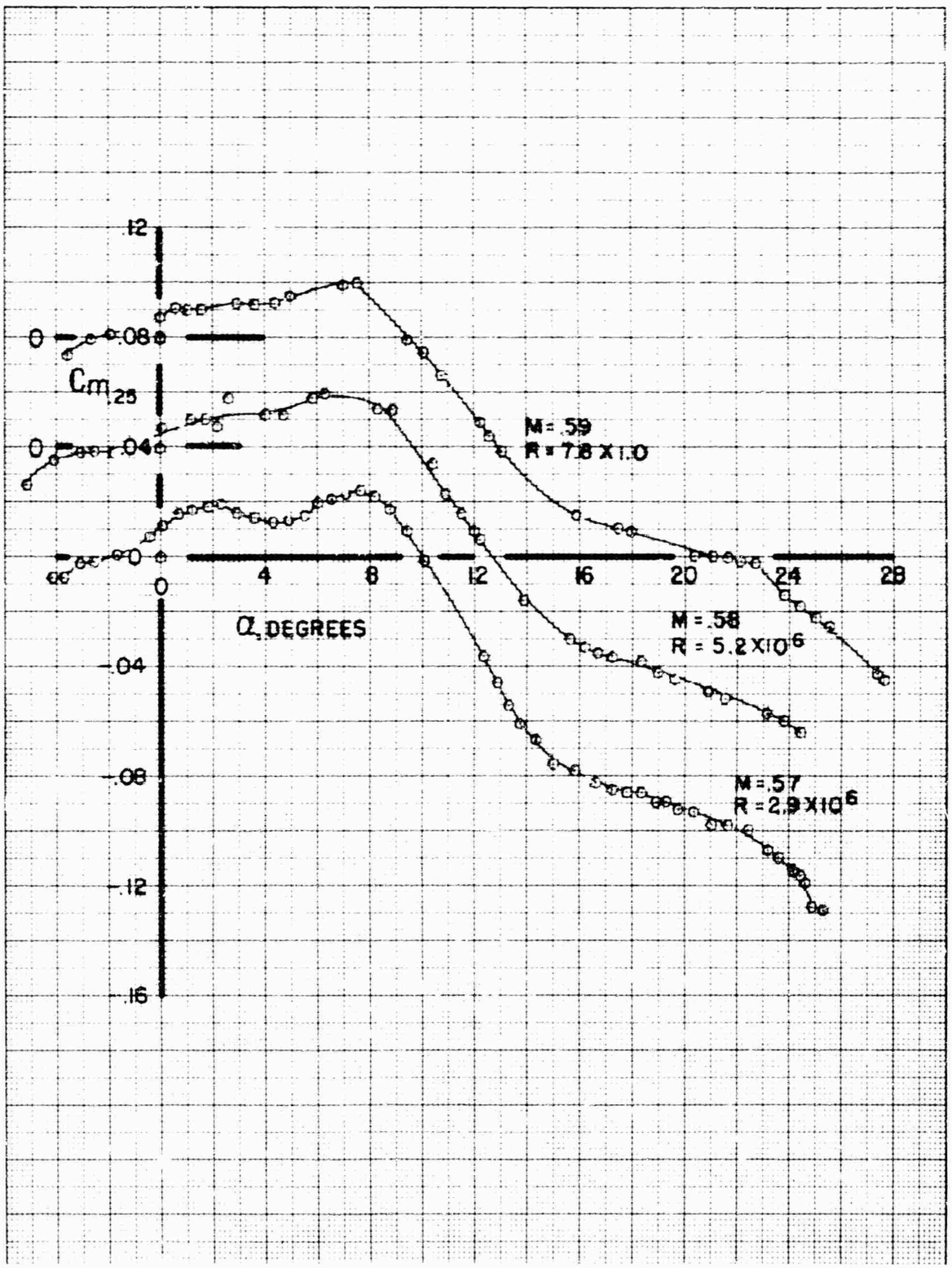


Figure 51E. Variation of Section Pitching Moment Coefficient With Angle of Attack, NACA Section 63A012

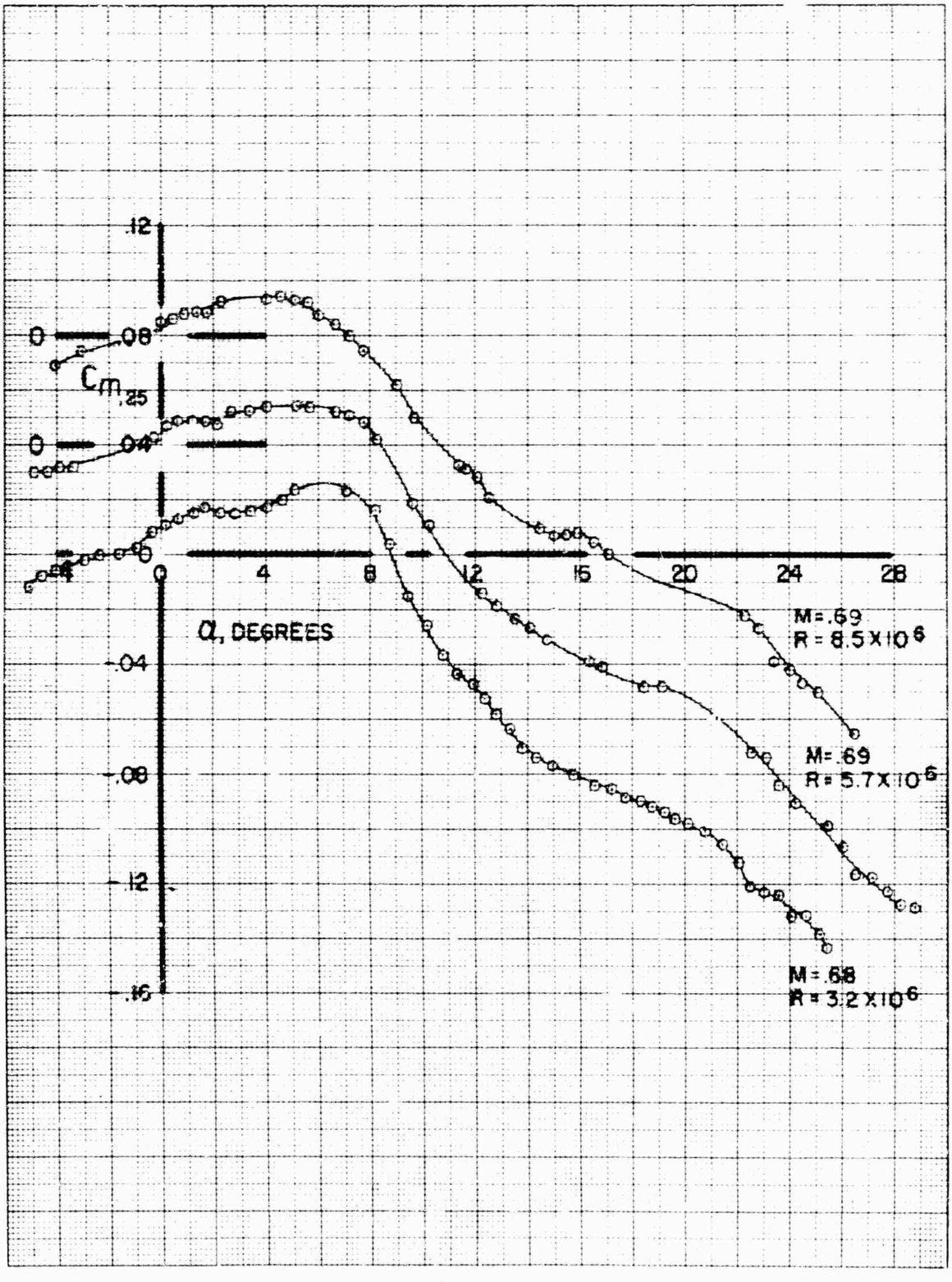


Figure 51F. Variation of Section Pitching Moment Coefficient With Angle of Attack, NACA Section 63A012

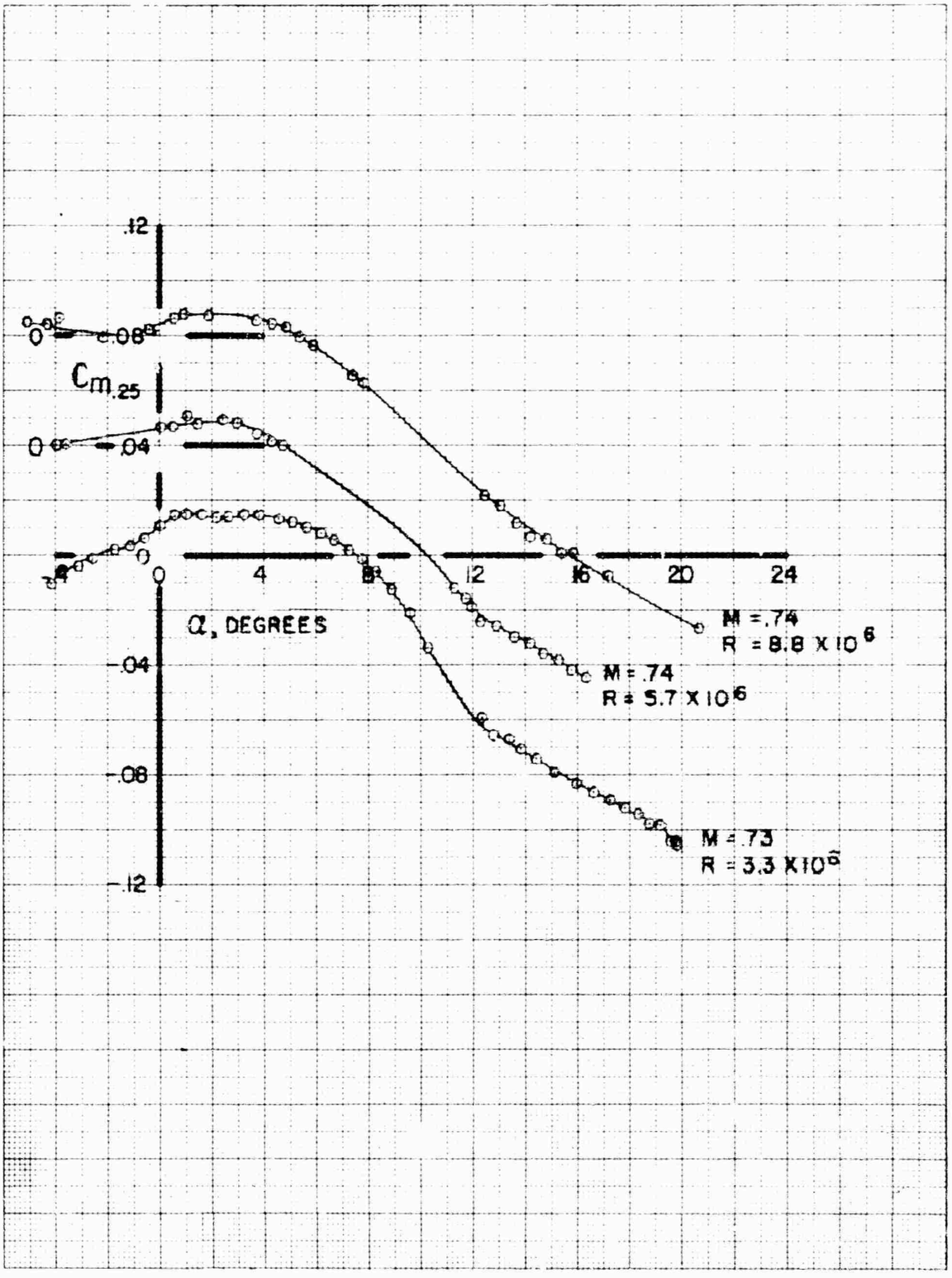


Figure 51G. Variation of Section Pitching Moment Coefficient With Angle of Attack, NACA Section 63A012

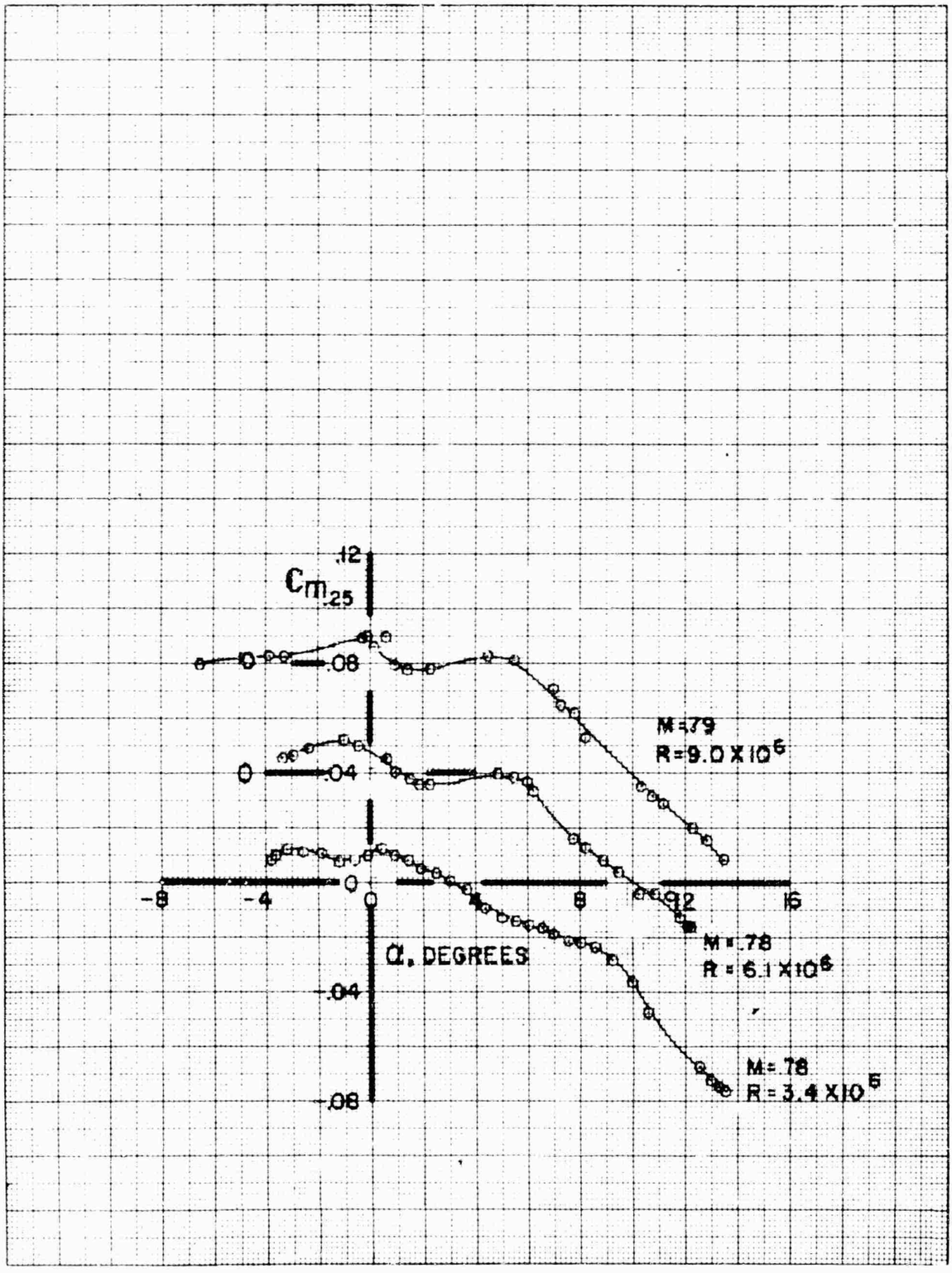


Figure 51H. Variation of Section Pitching Moment Coefficient With Angle of Attack, NACA Section 63A012

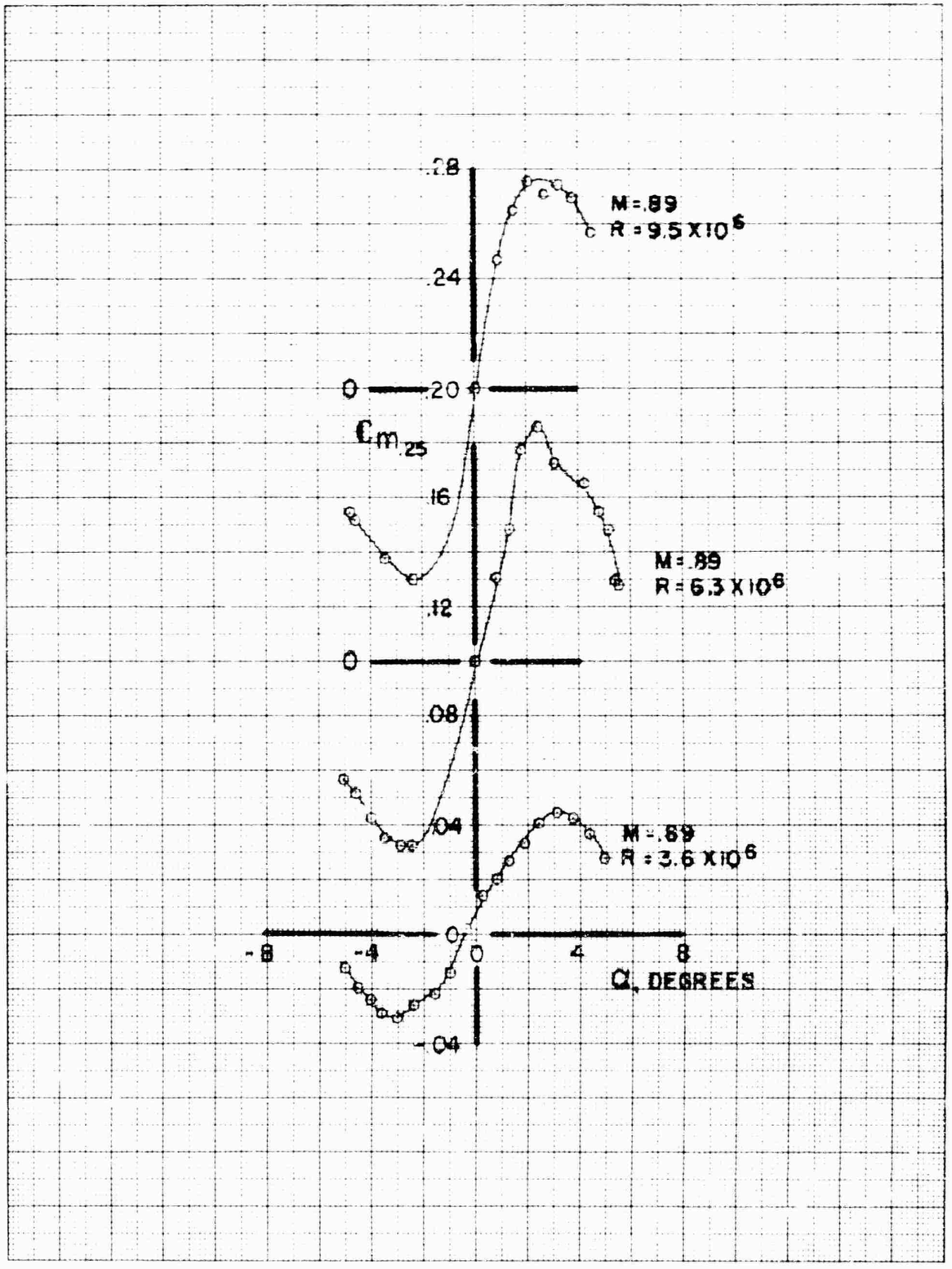


Figure 511. Variation of Section Pitching Moment Coefficient With Angle of Attack, NACA Section 63A012

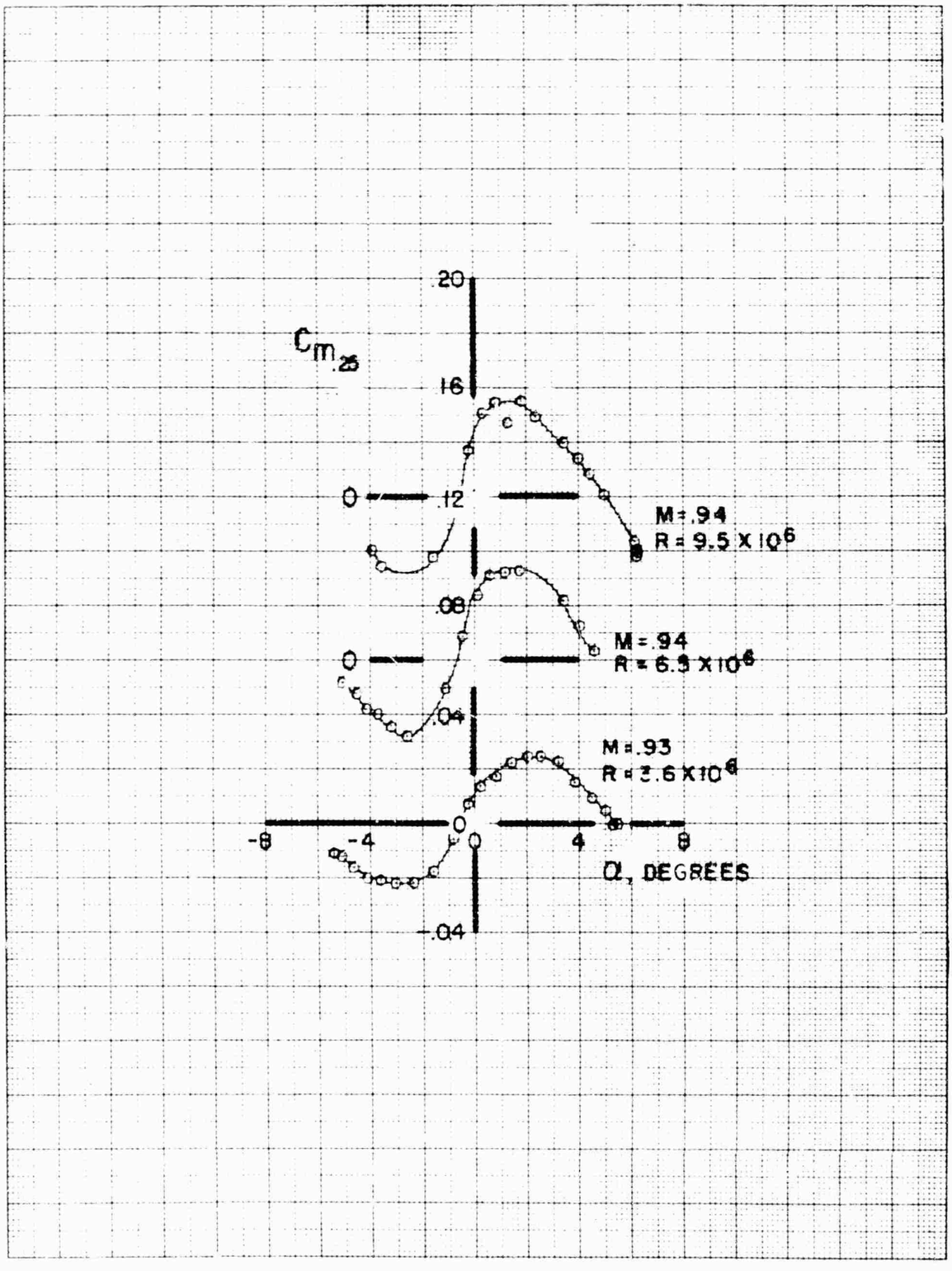


Figure 51J. Variation of Section Pitching Moment Coefficient With Angle of Attack, NACA Section 63A012

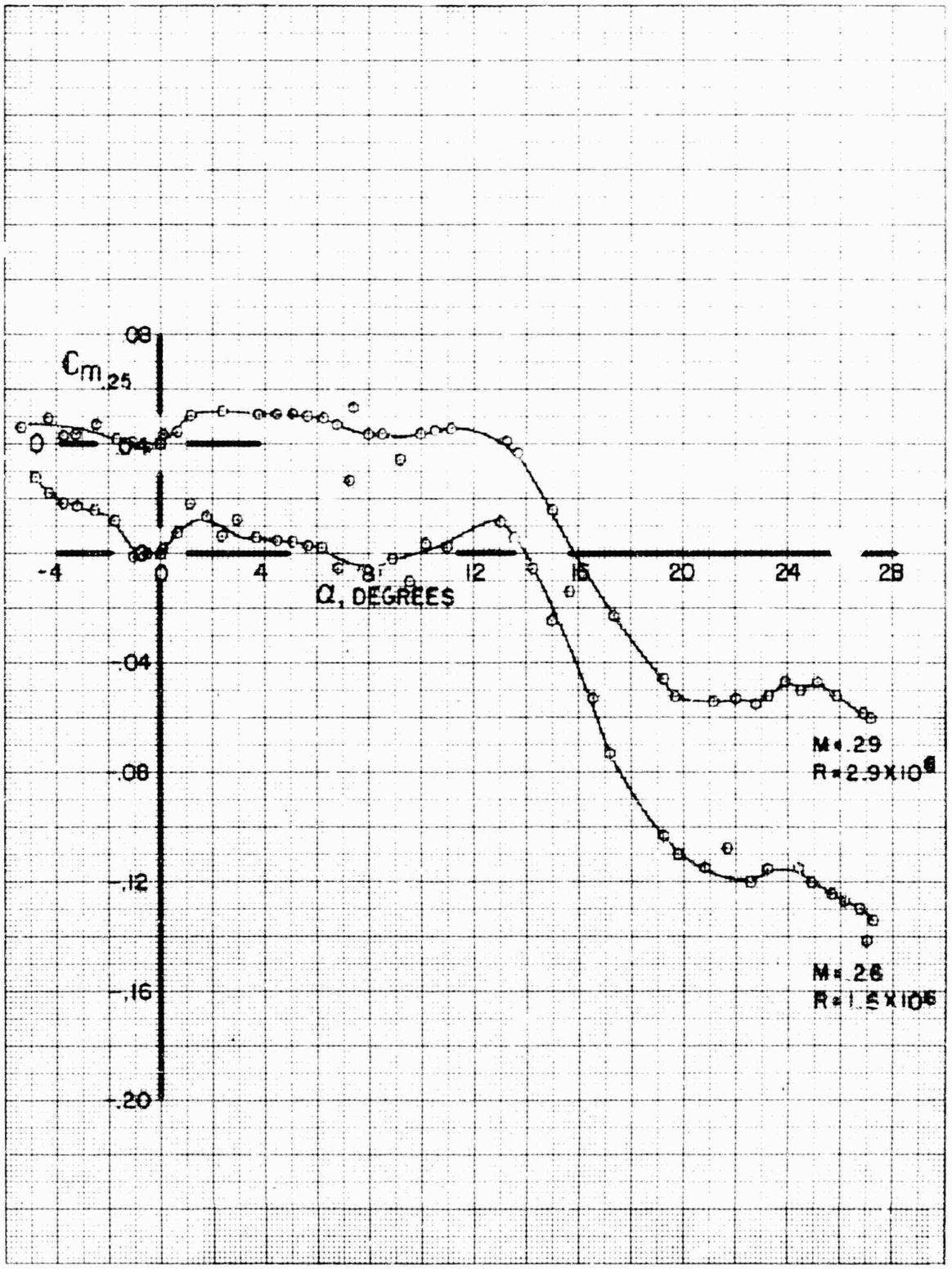


Figure 52A. Variation of Section Pitching Moment Coefficient With Angle of Attack, NACA Section 63A015

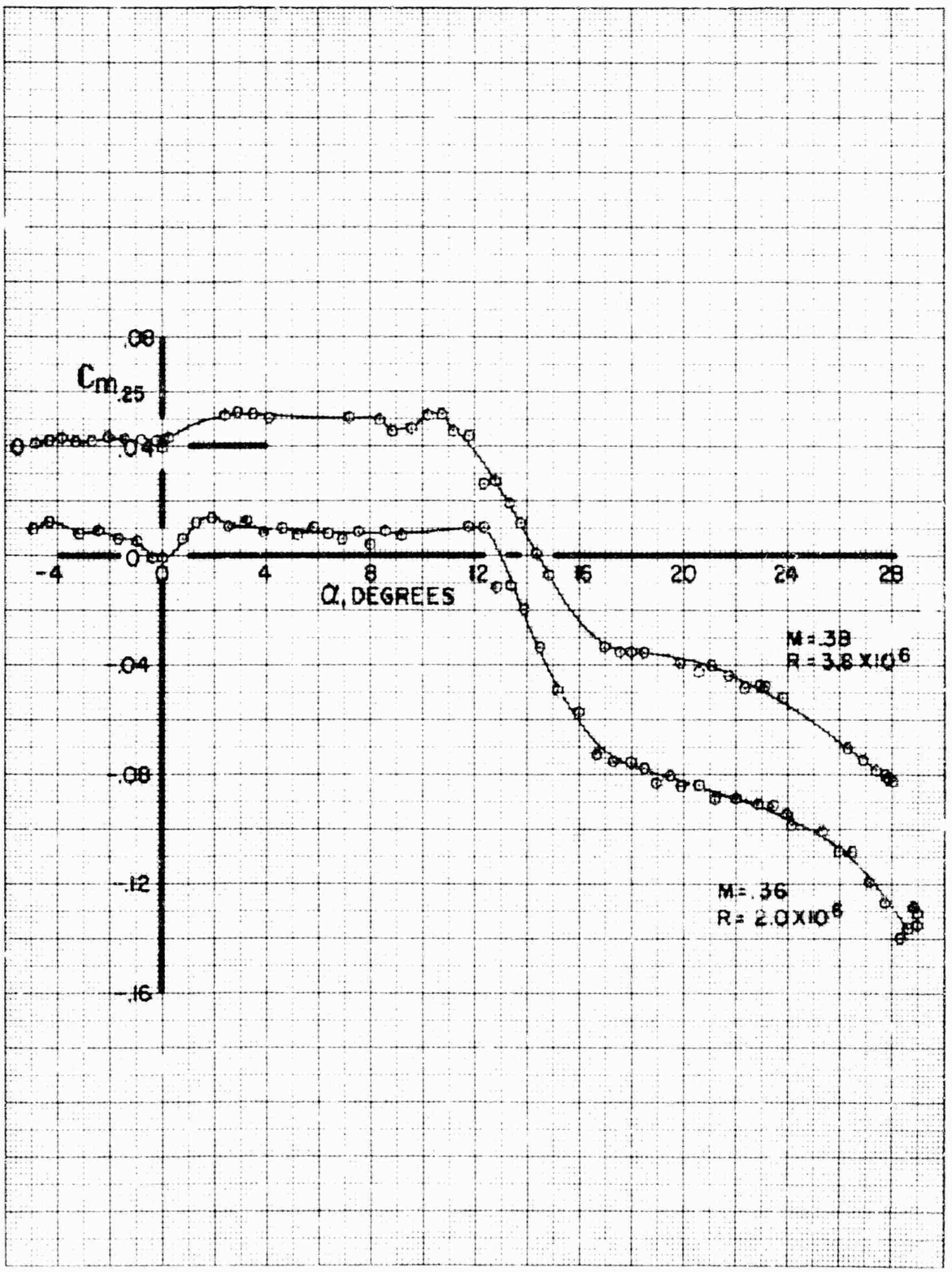


Figure 52B. Variation of Section Pitching Moment Coefficient With Angle of Attack, NACA Section 63A015

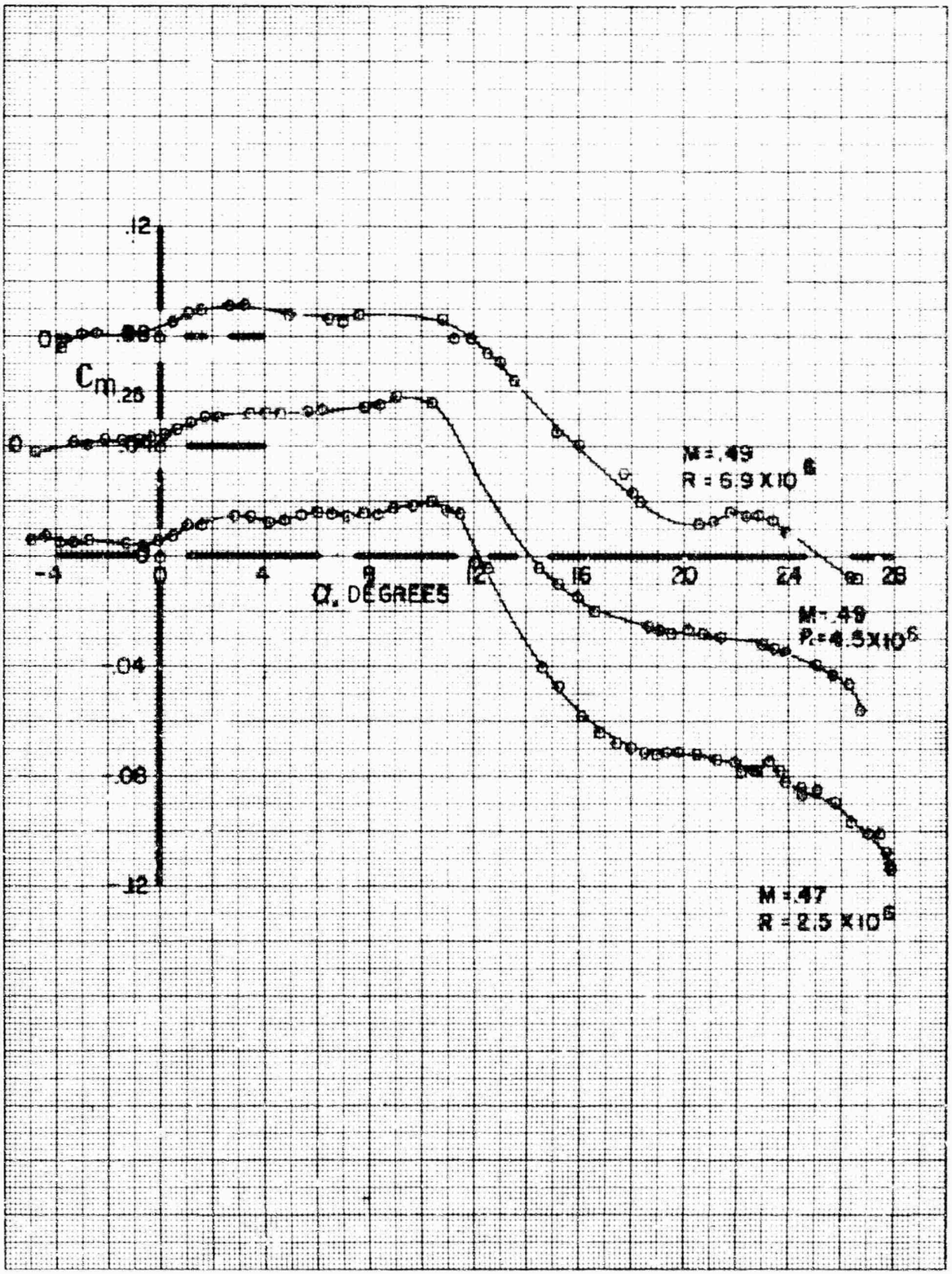


Figure 52C. Variation of Section Pitching Moment Coefficient With Angle of Attack, NACA Section 63A015

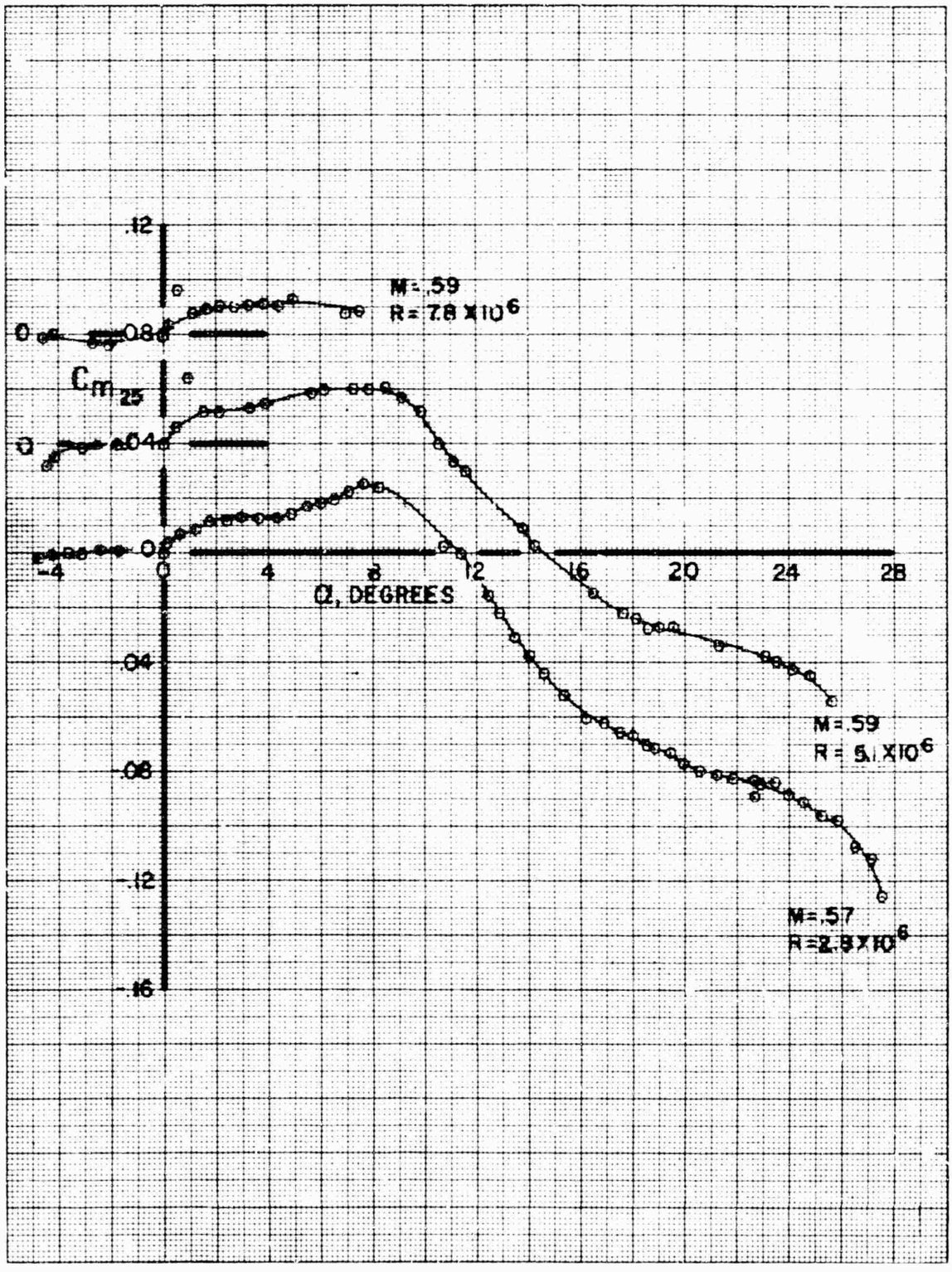


Figure 52D. Variation of Section Pitching Moment Coefficient With Angle of Attack, NACA Section 63A015

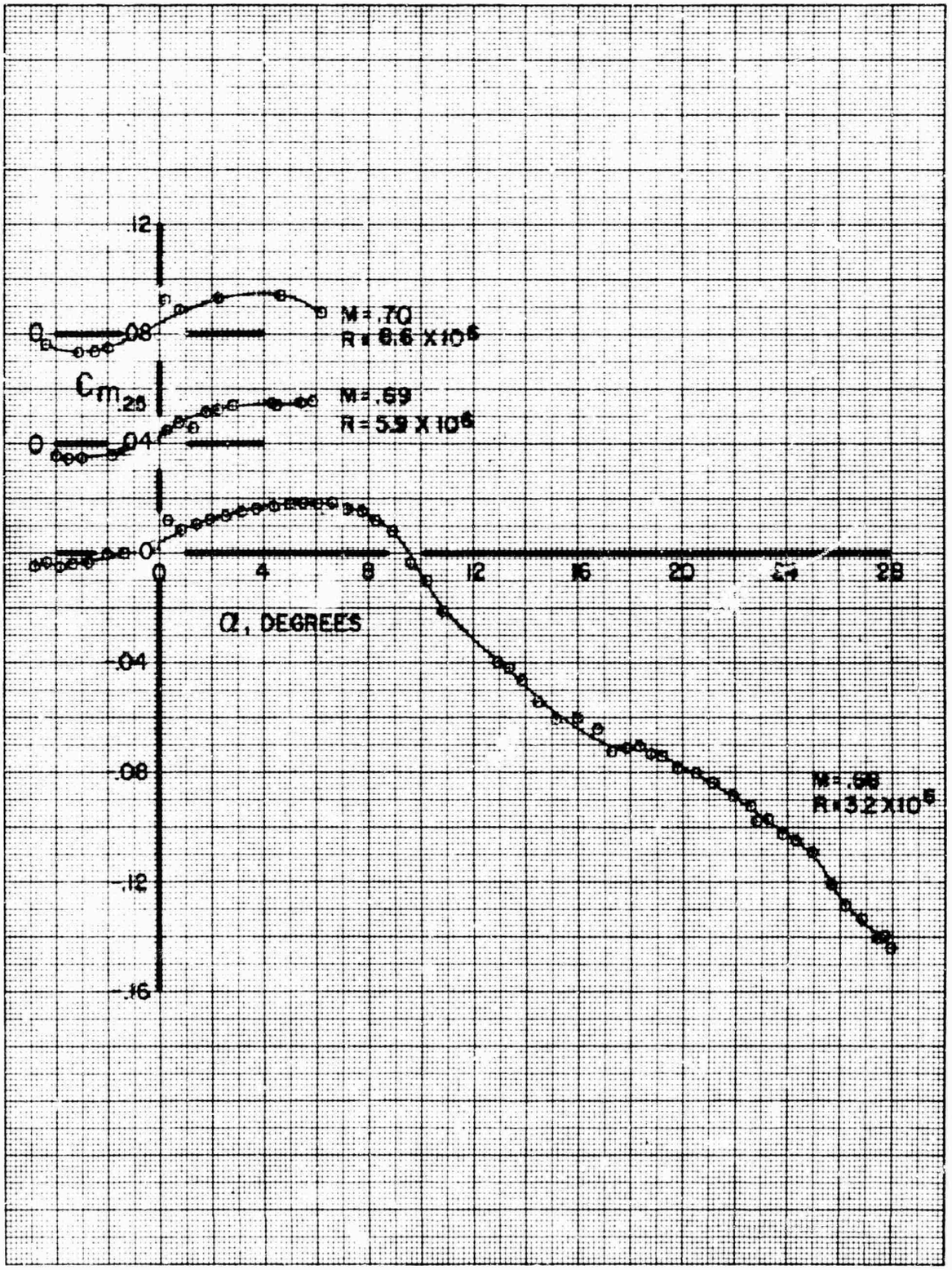


Figure 52E. Variation of Section Pitching Moment Coefficient With Angle of Attack, NACA Section 63A015

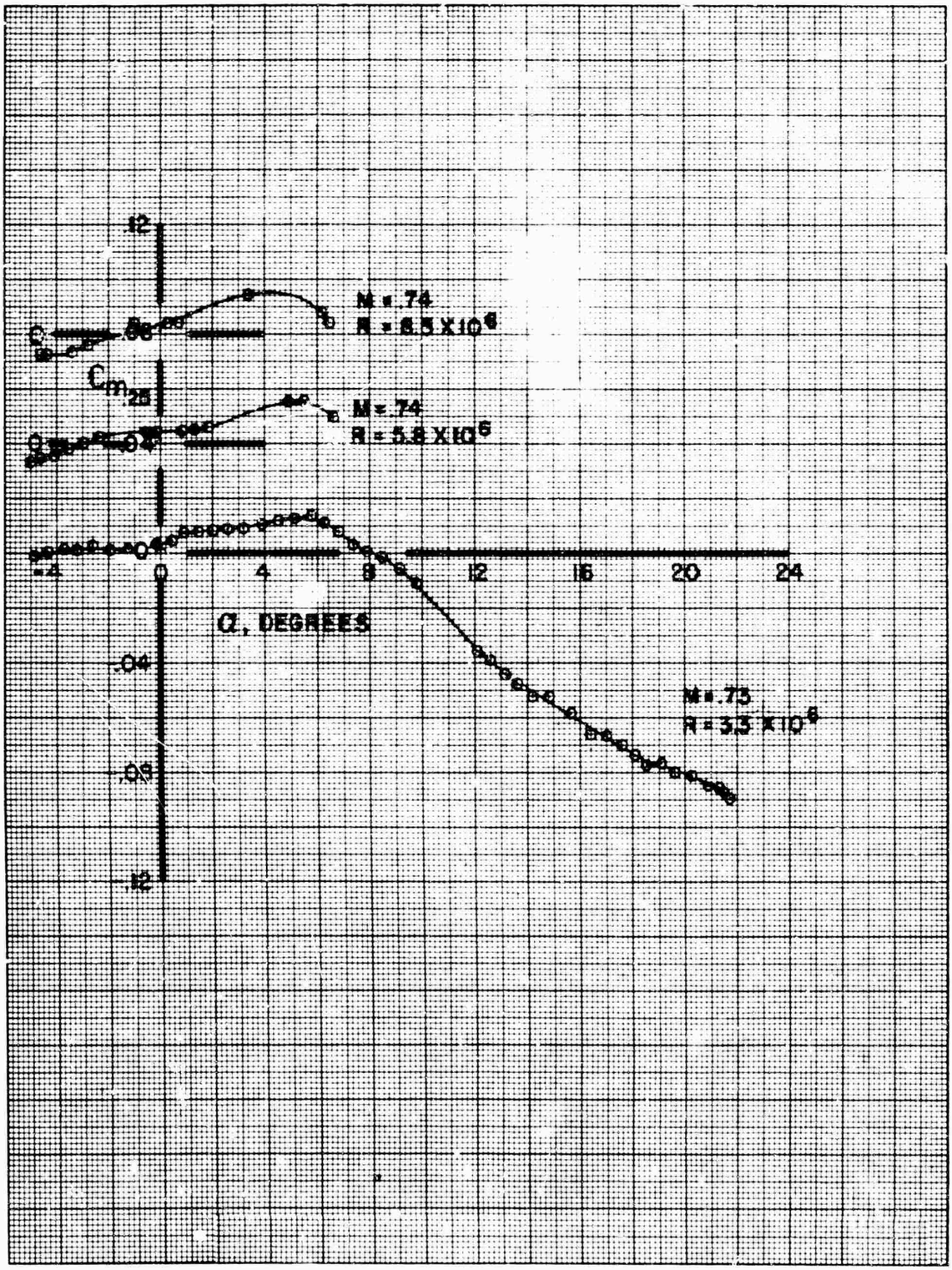


Figure 52F. Variation of Section Pitching Moment Coefficient With Angle of Attack, NACA Section 63A015

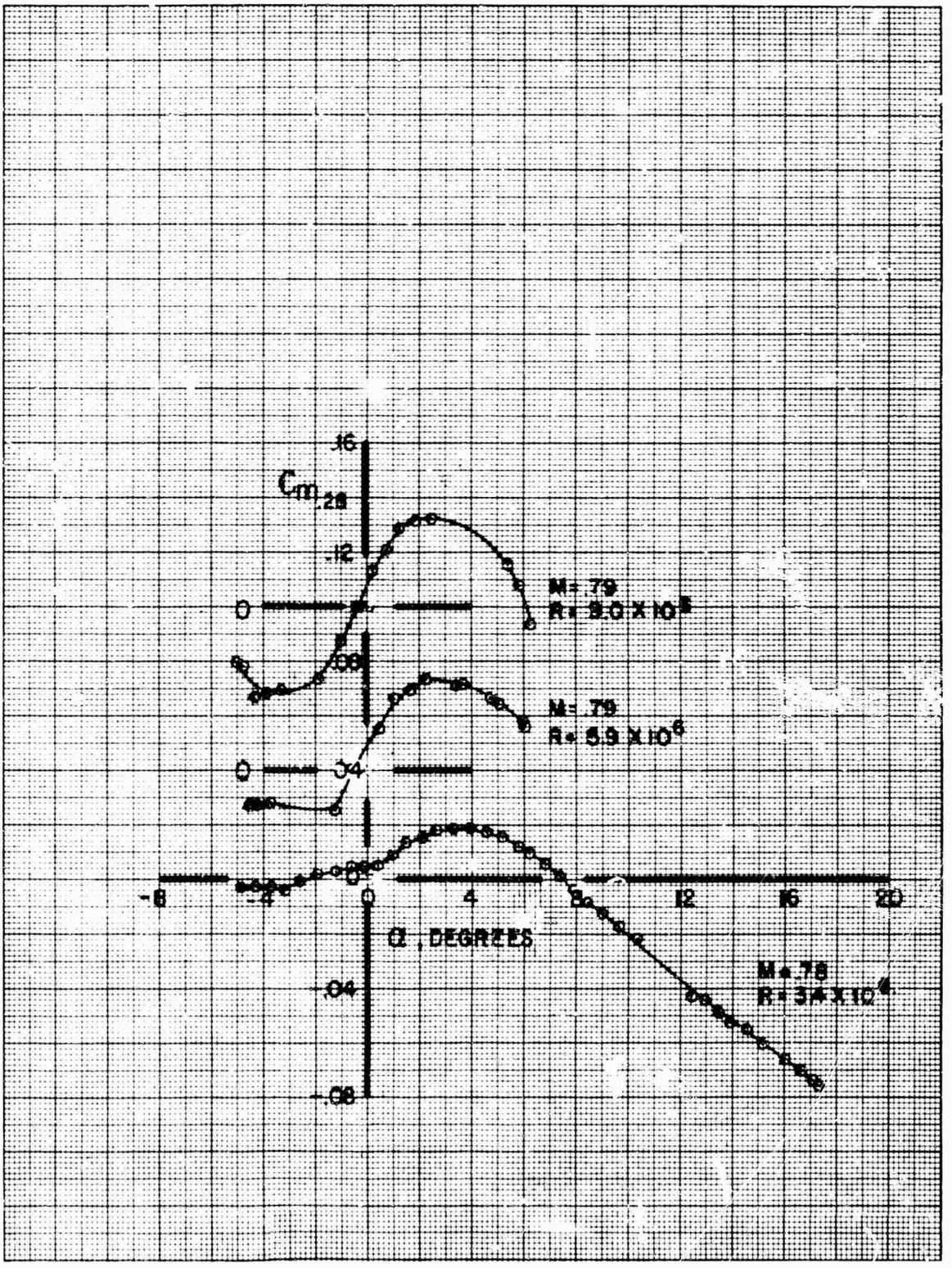


Figure 52G. Variation of Section Pitching Moment Coefficient With Angle of Attack, NACA Section 63A015

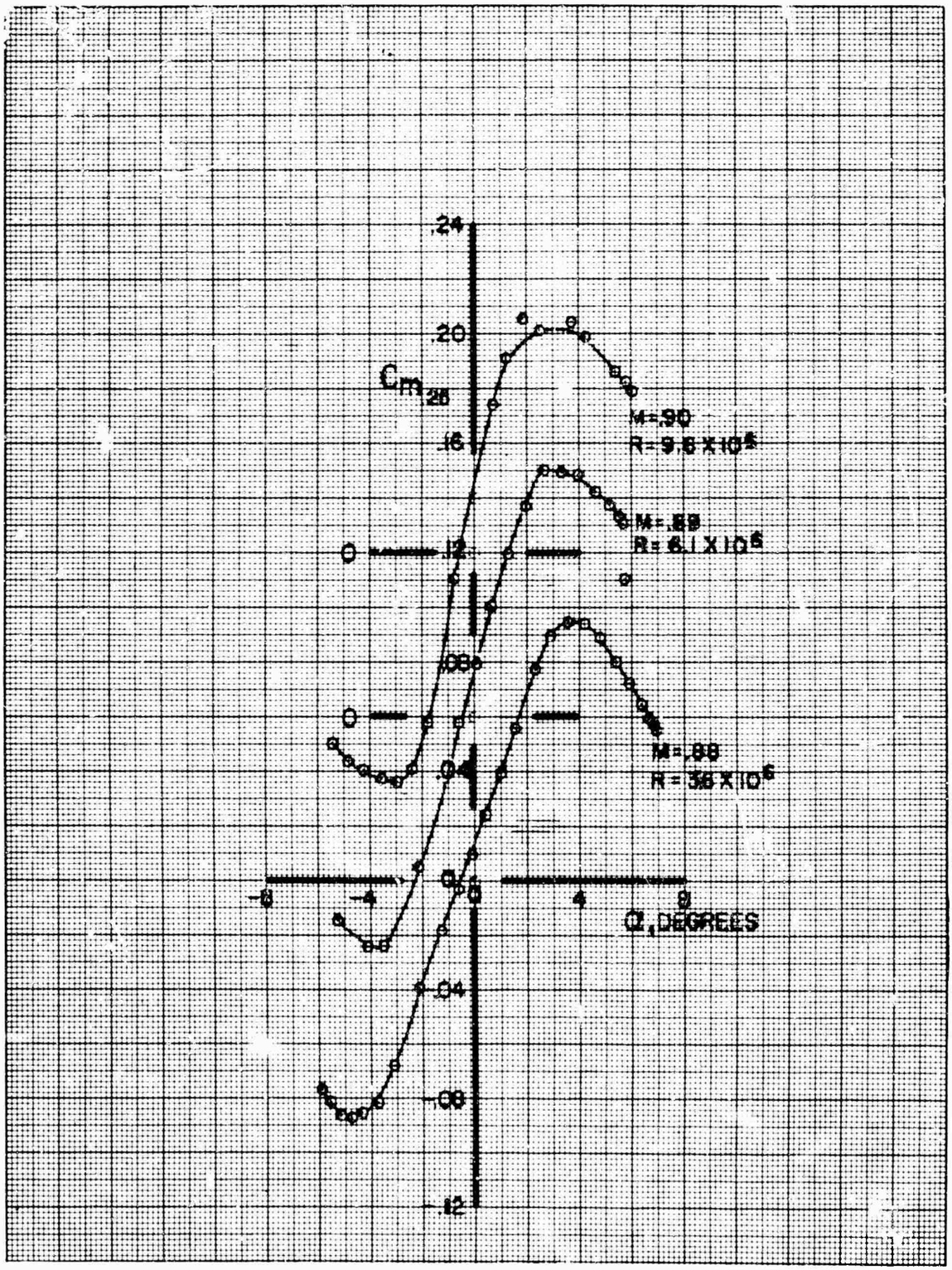


Figure 52H. Variation of Section Pitching Moment Coefficient With Angle of Attack, NACA Section 63A015

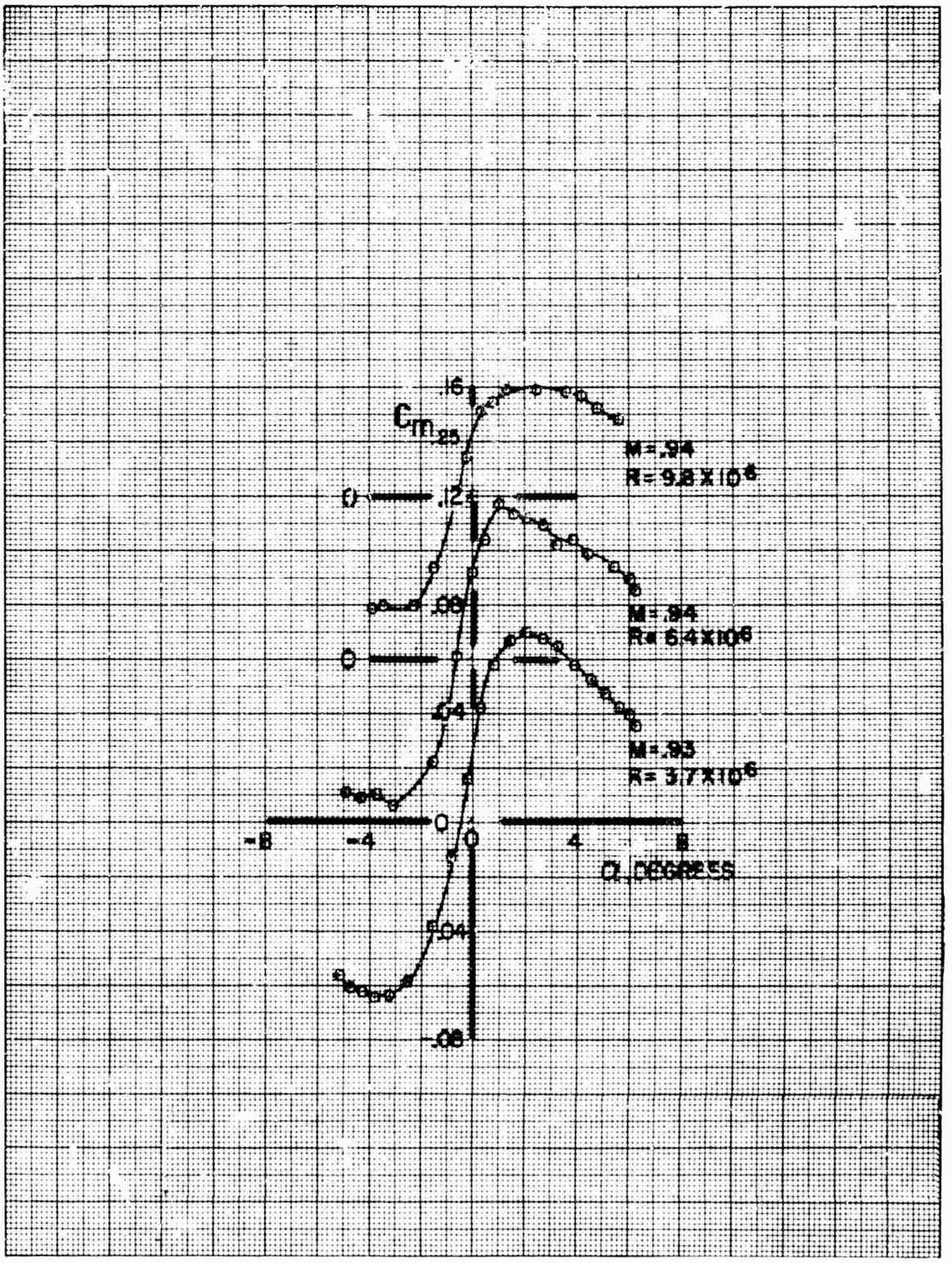


Figure 521. Variation of Section Pitching Moment Coefficient With Angle of Attack, NACA Section 63A015

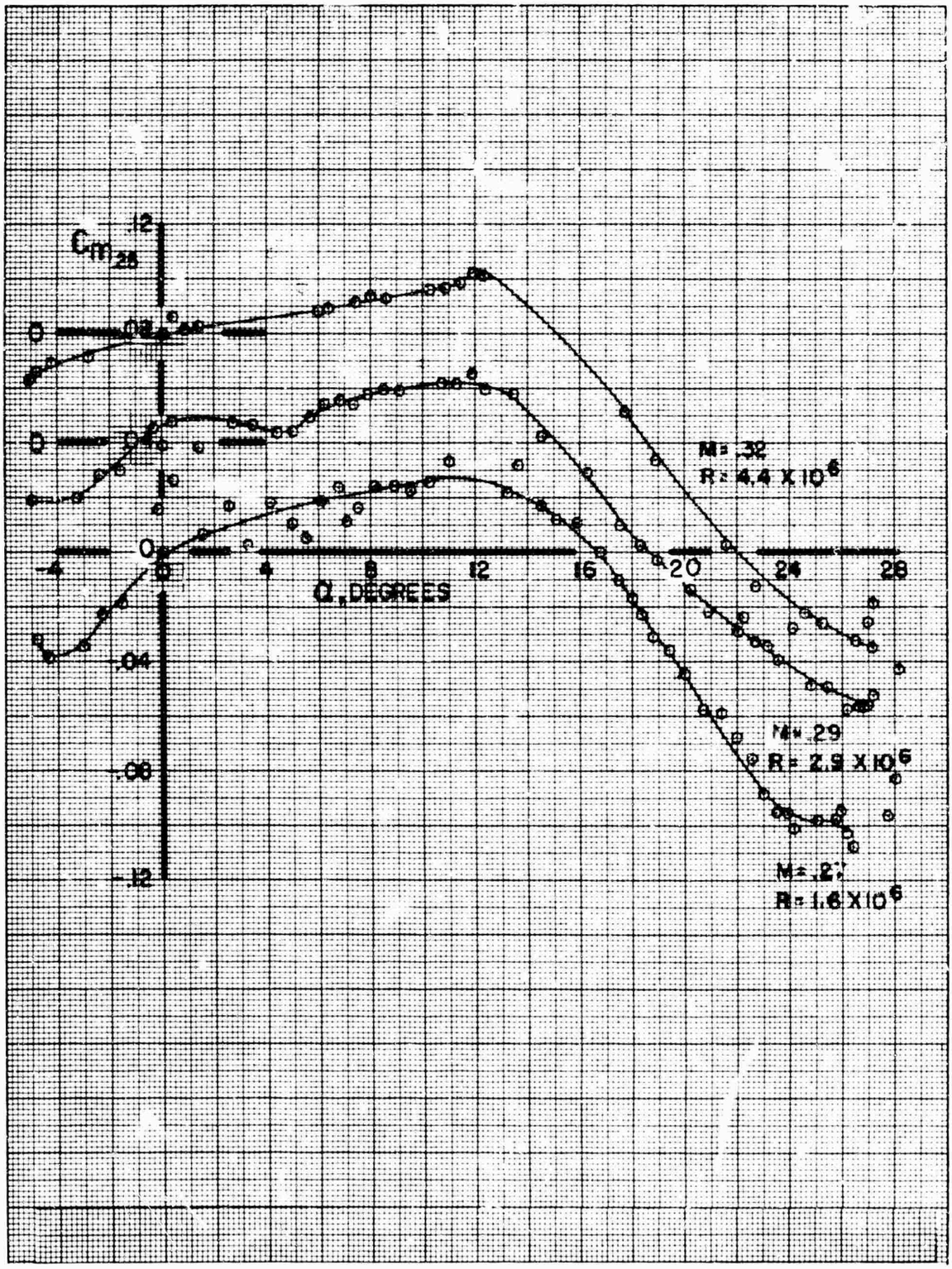


Figure 53A. Variation of Section Pitching Moment Coefficient With Angle of Attack, NACA Section 63A018

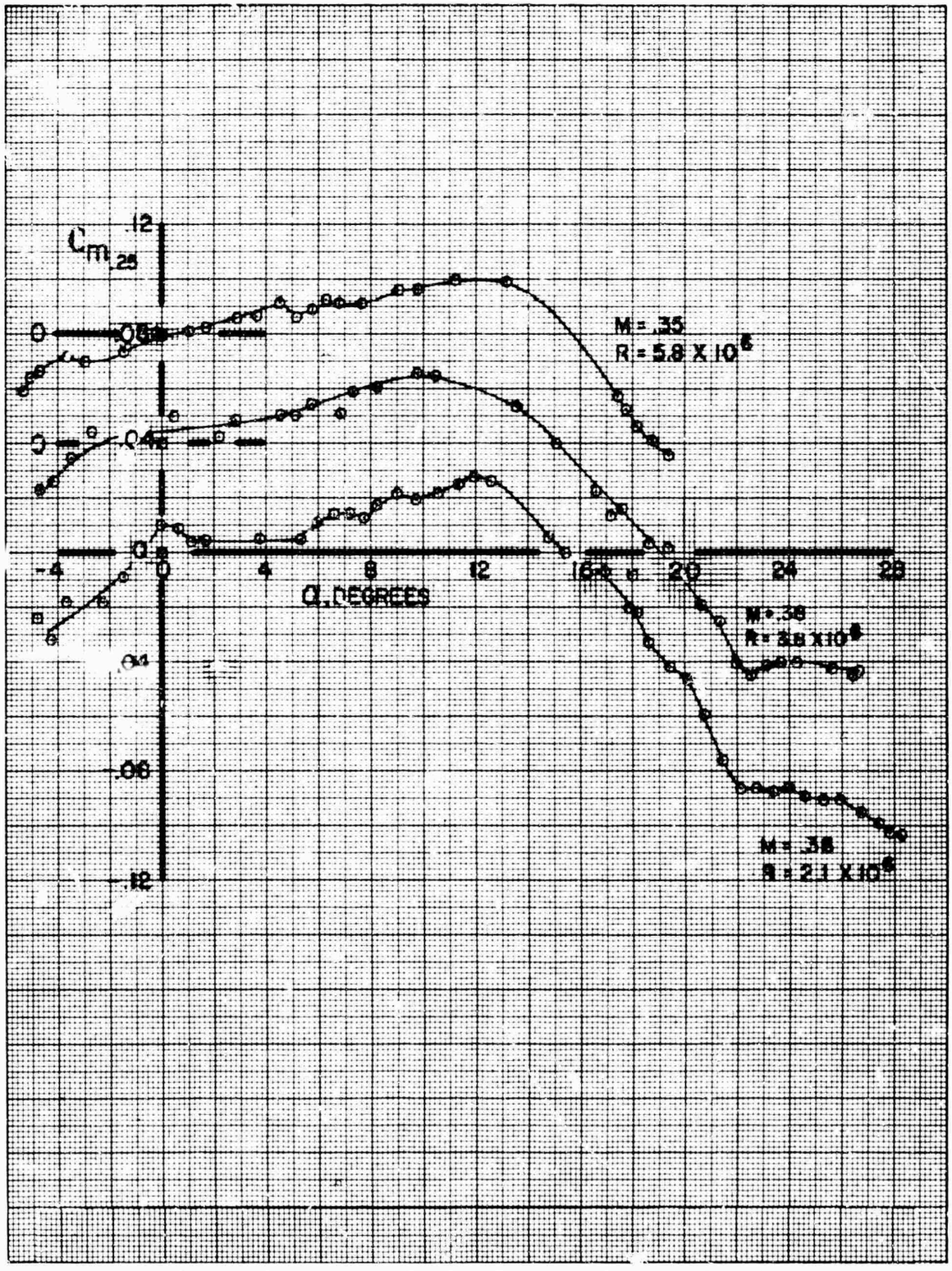


Figure 53B. Variation of Section Pitching Moment Coefficient With Angle of Attack, NACA Section 63A018

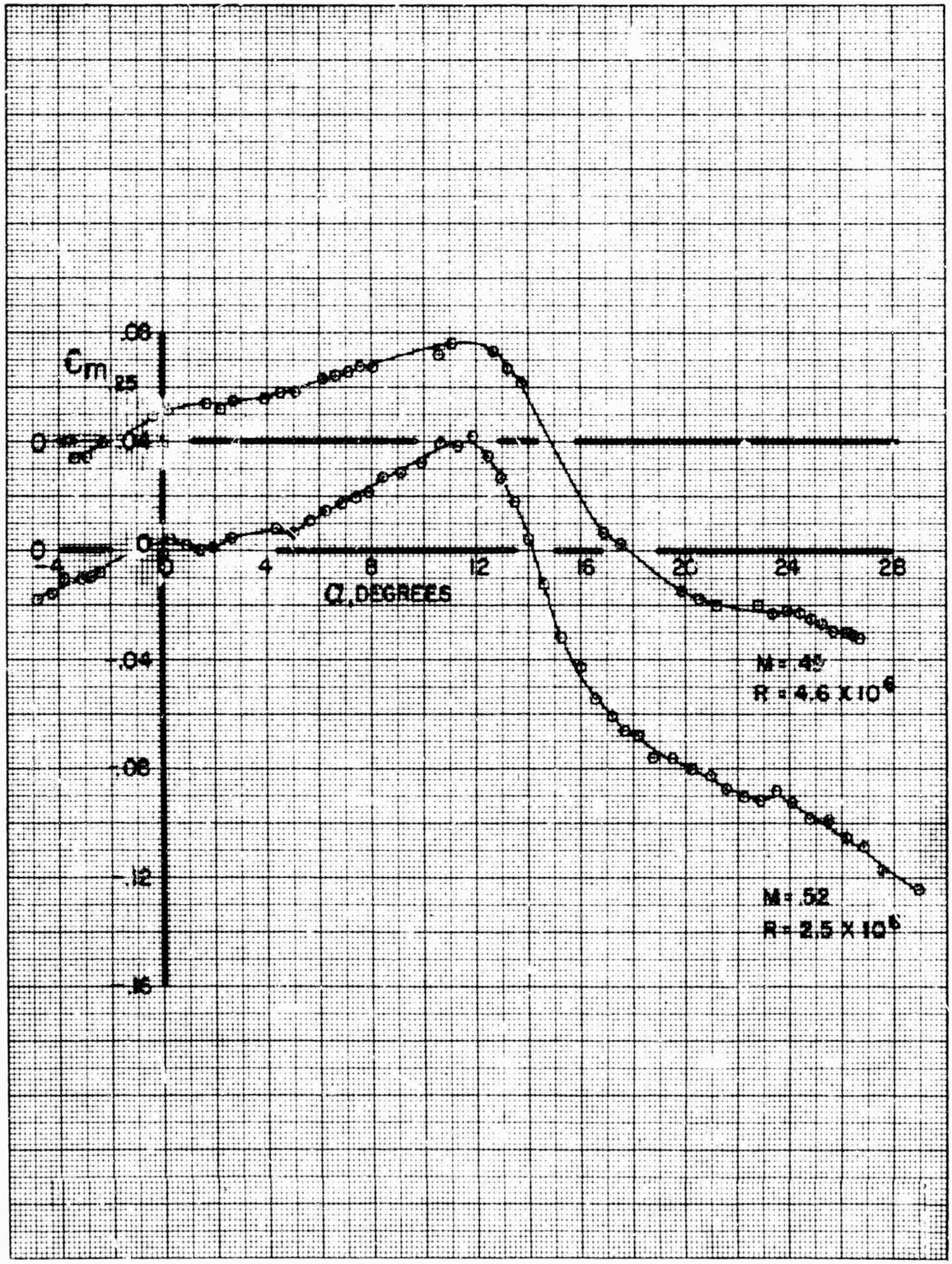


Figure 53C. Variation of Section Pitching Moment Coefficient With Angle of Attack, NACA Section 63A018

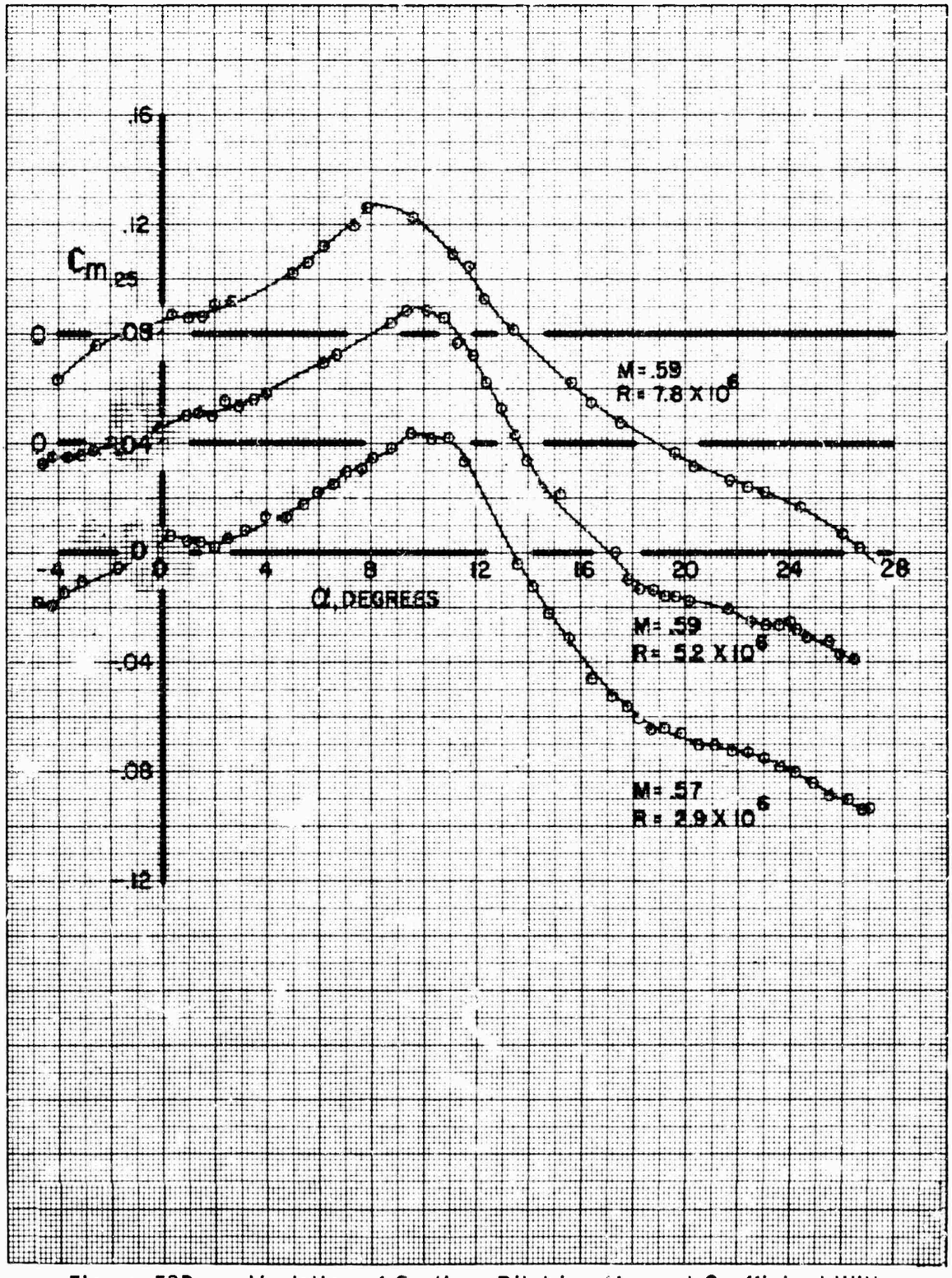


Figure 53D. Variation of Section Pitching Moment Coefficient With Angle of Attack, NACA Section 63A018

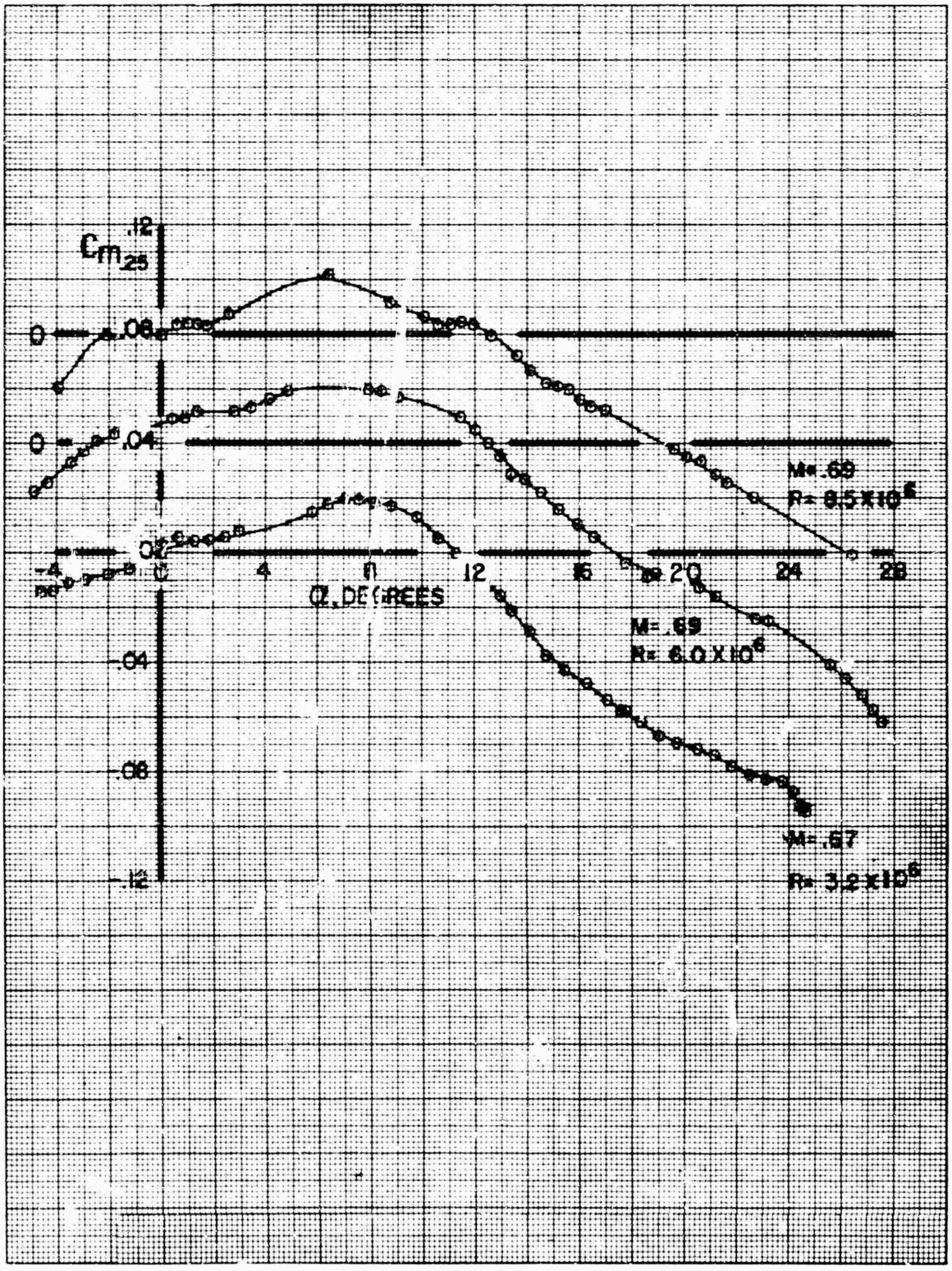


Figure 53E. Variation of Section Pitching Moment Coefficient With Angle of Attack, NACA Section 63A018

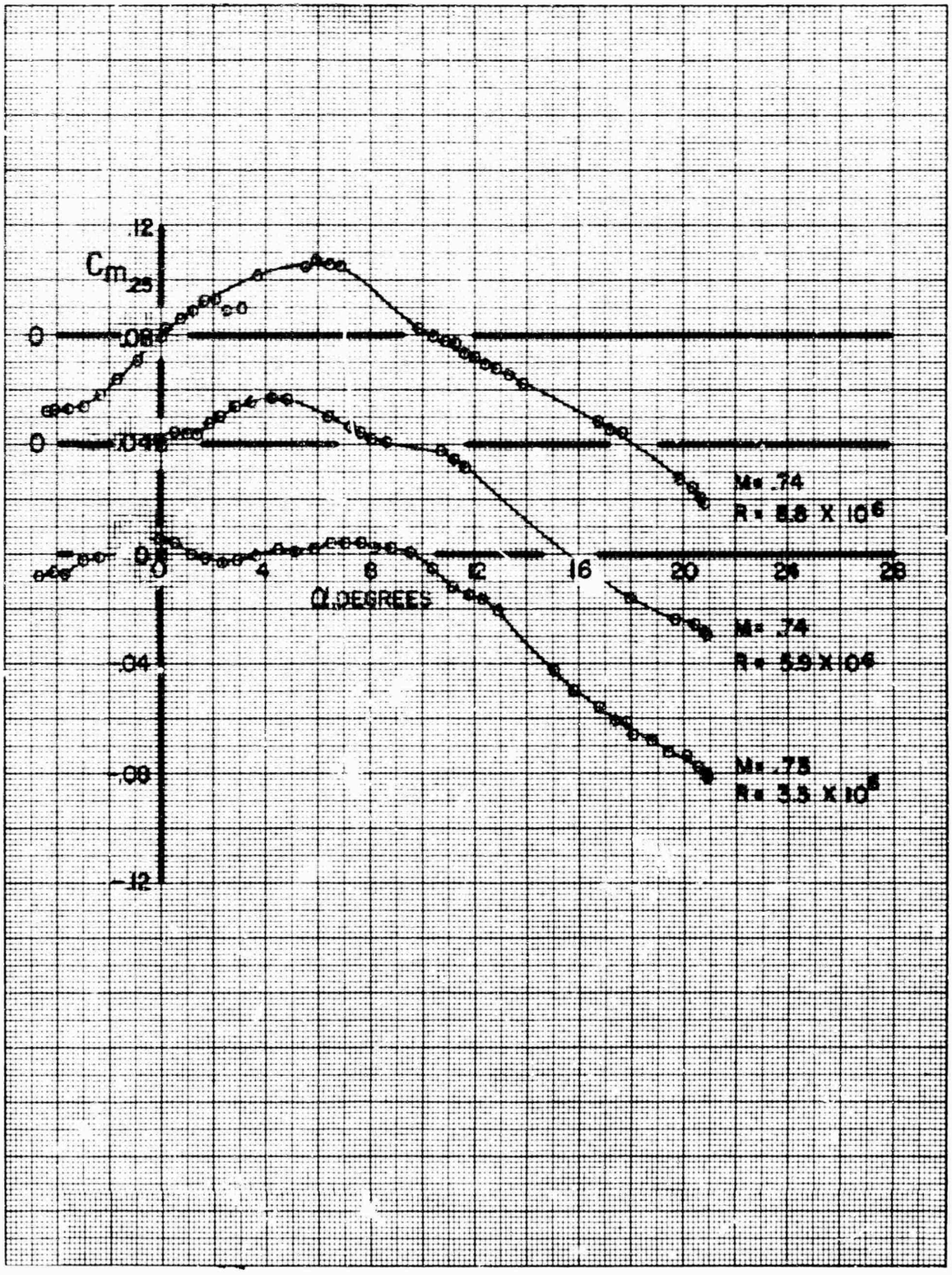


Figure 53F. Variation of Section Pitching Moment Coefficient With Angle of Attack, NACA Section 63A018

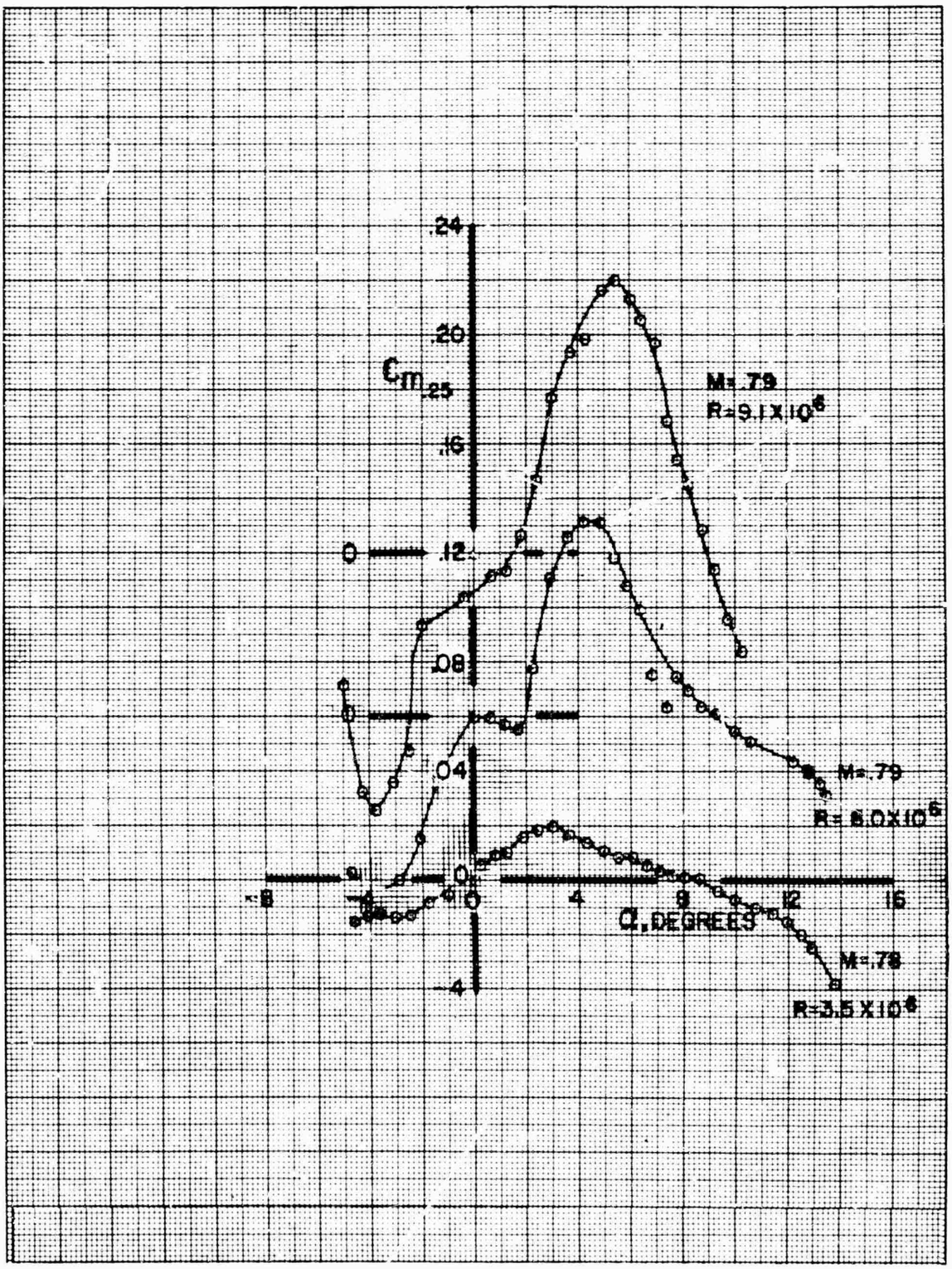


Figure 53G. Variation of Section Pitching Moment Coefficient With Angle of Attack, NACA Section 63A018

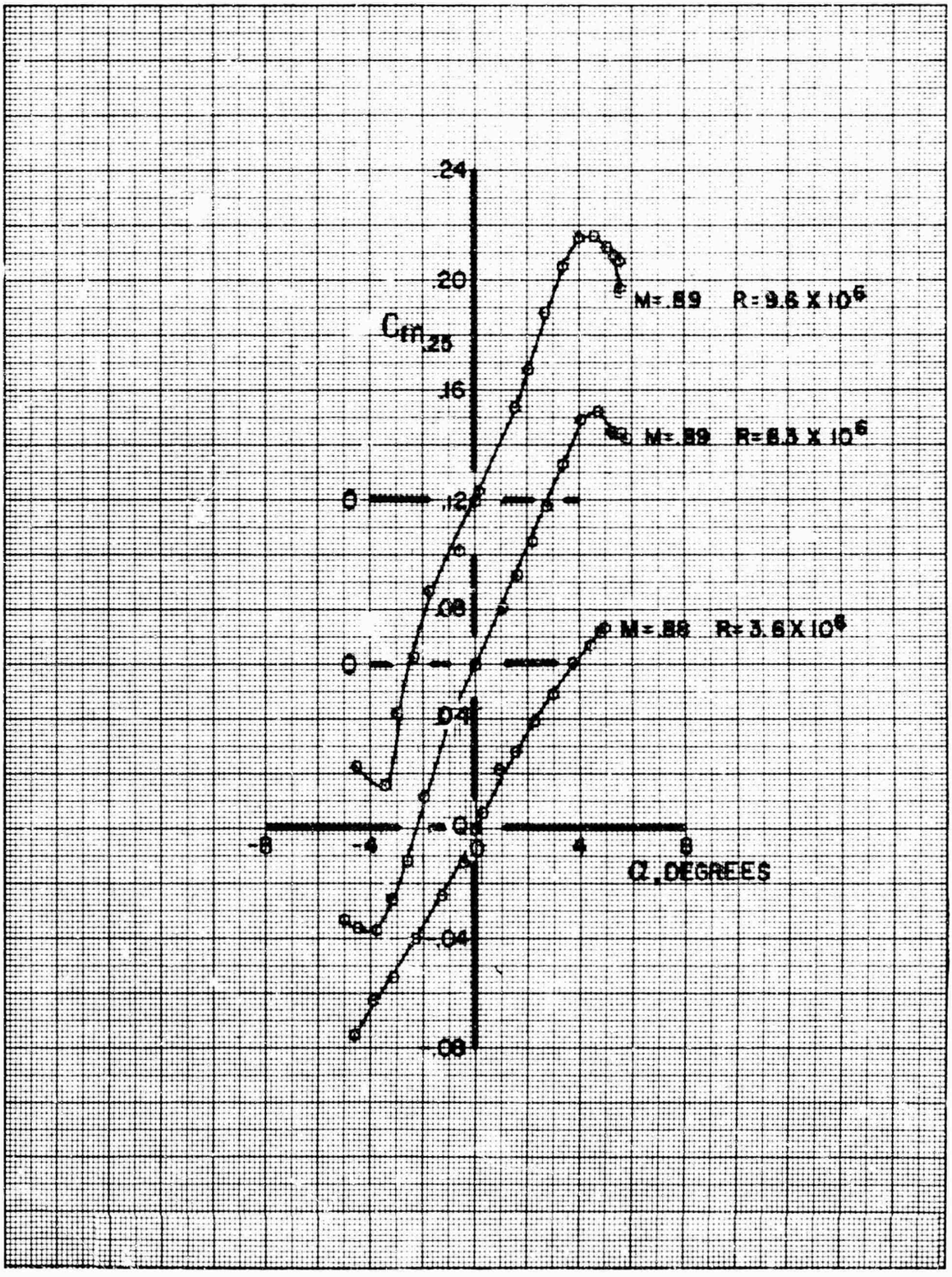


Figure 53H. Variation of Section Pitching Moment Coefficient With Angle of Attack, NACA Section 63A018

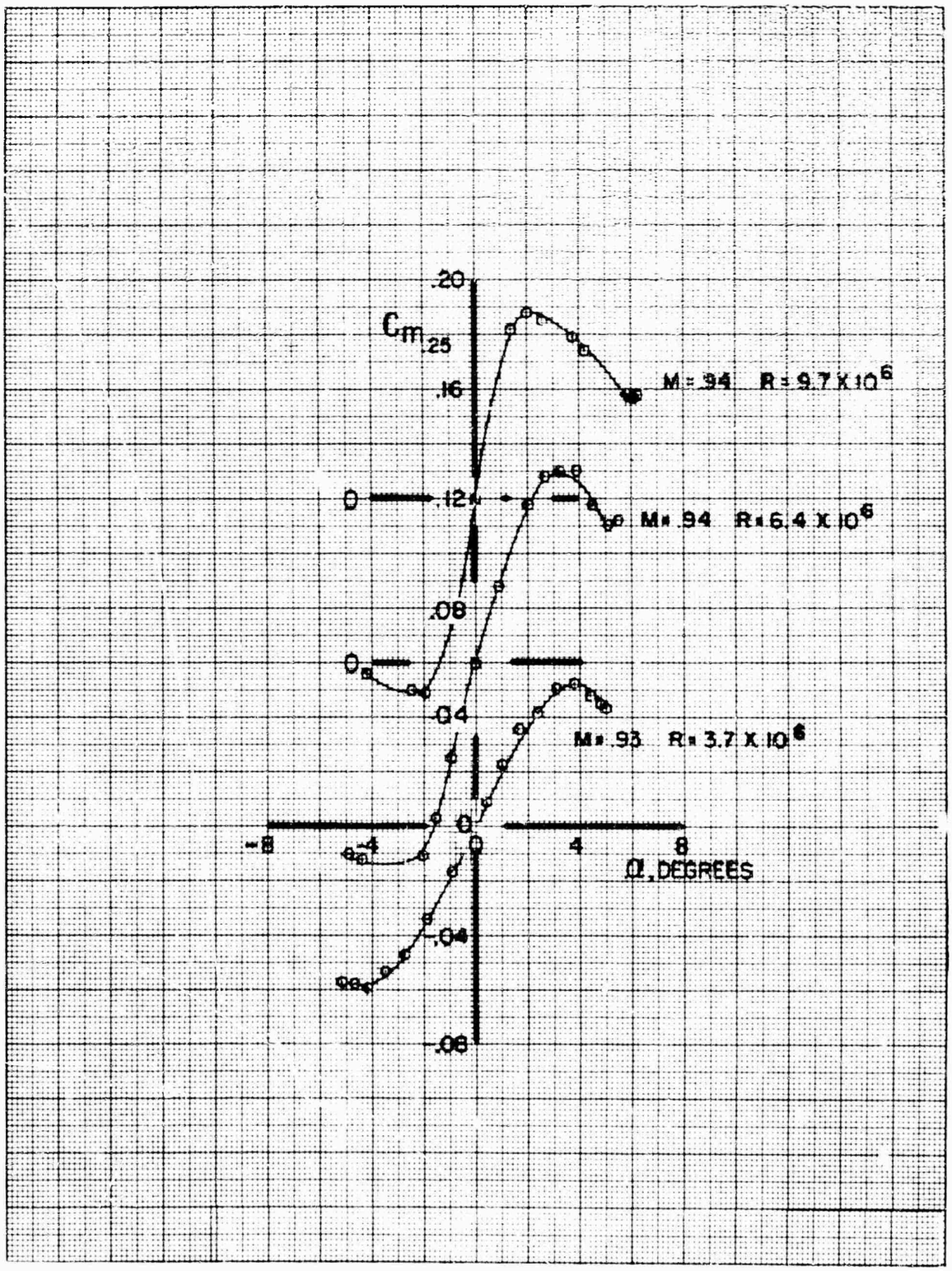


Figure 531. Variation of Section Pitching Moment Coefficient With Angle of Attack, NACA Section 63A018

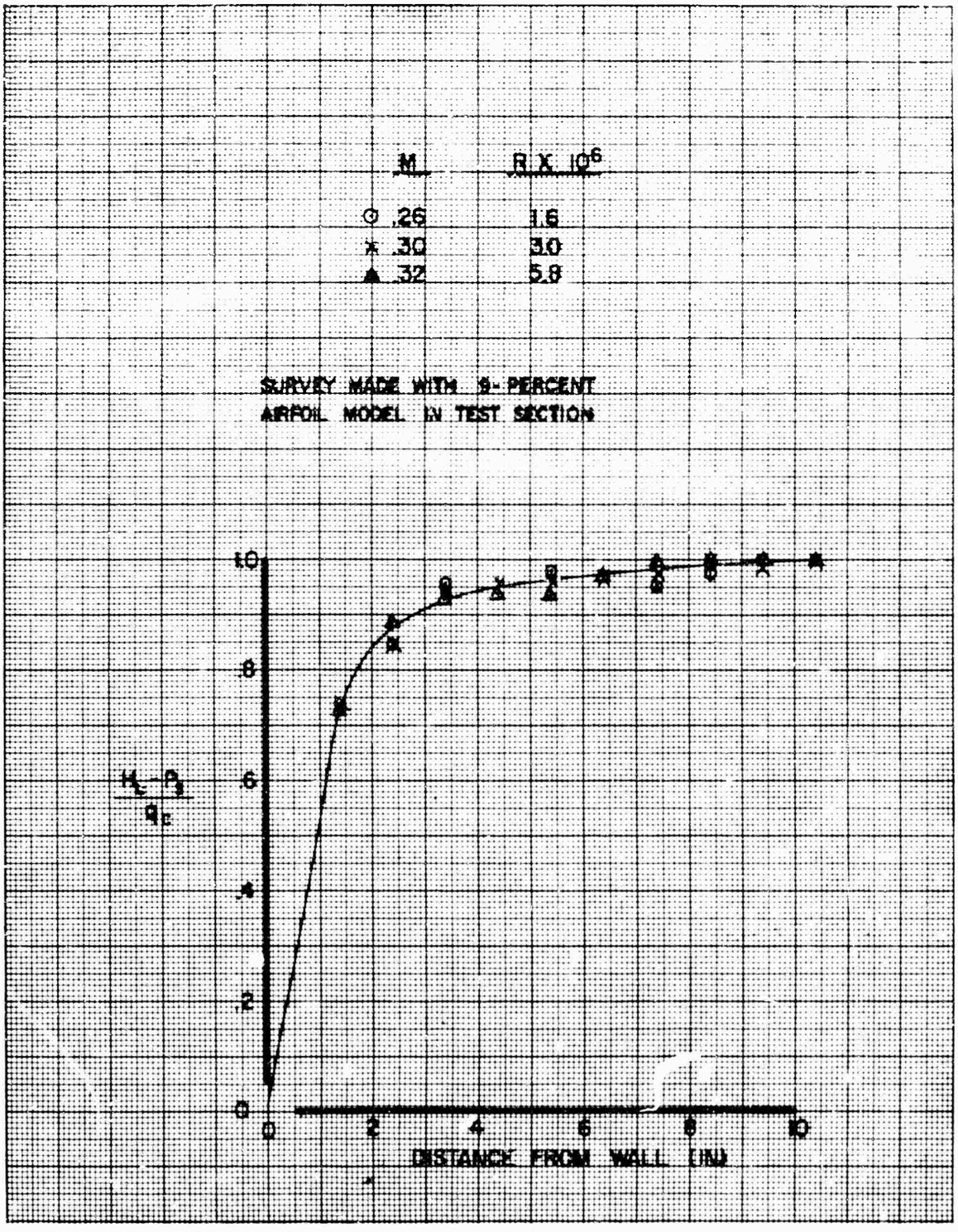


Figure 54A. Wind Tunnel Wall Boundary Layer

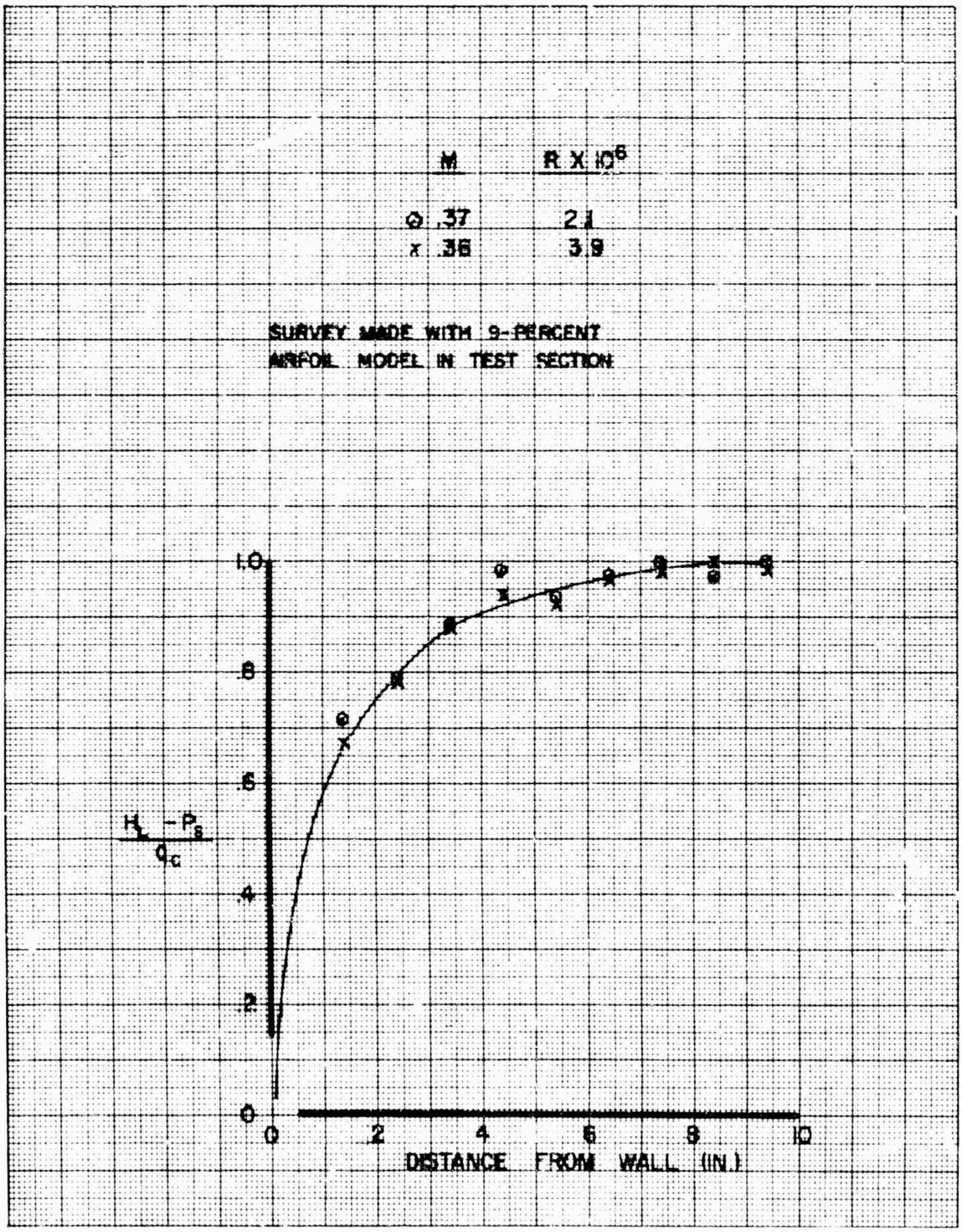


Figure 54B. Wind Tunnel Wall Boundary Layer

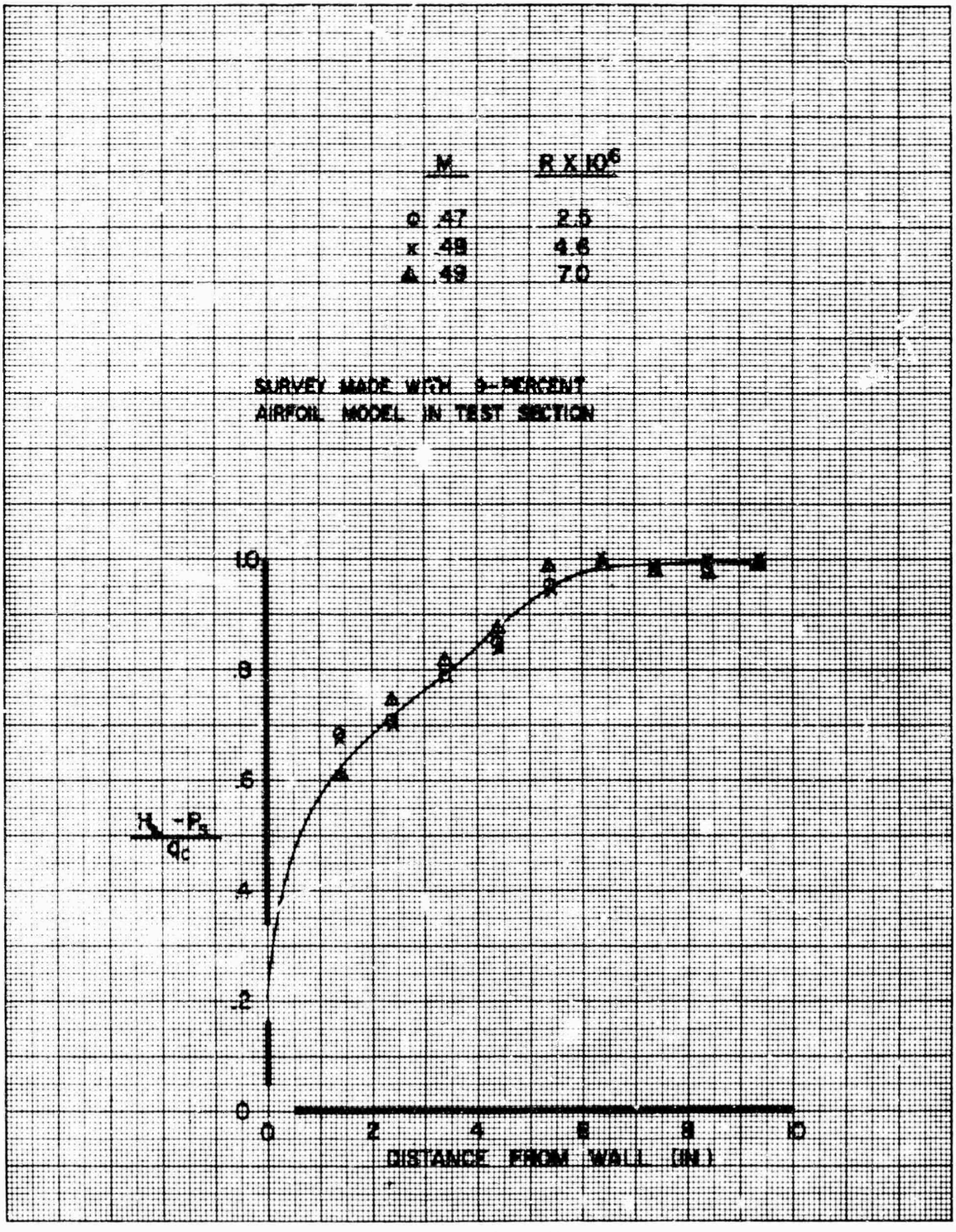


Figure 54C. Wind Tunnel Wall Boundary Layer

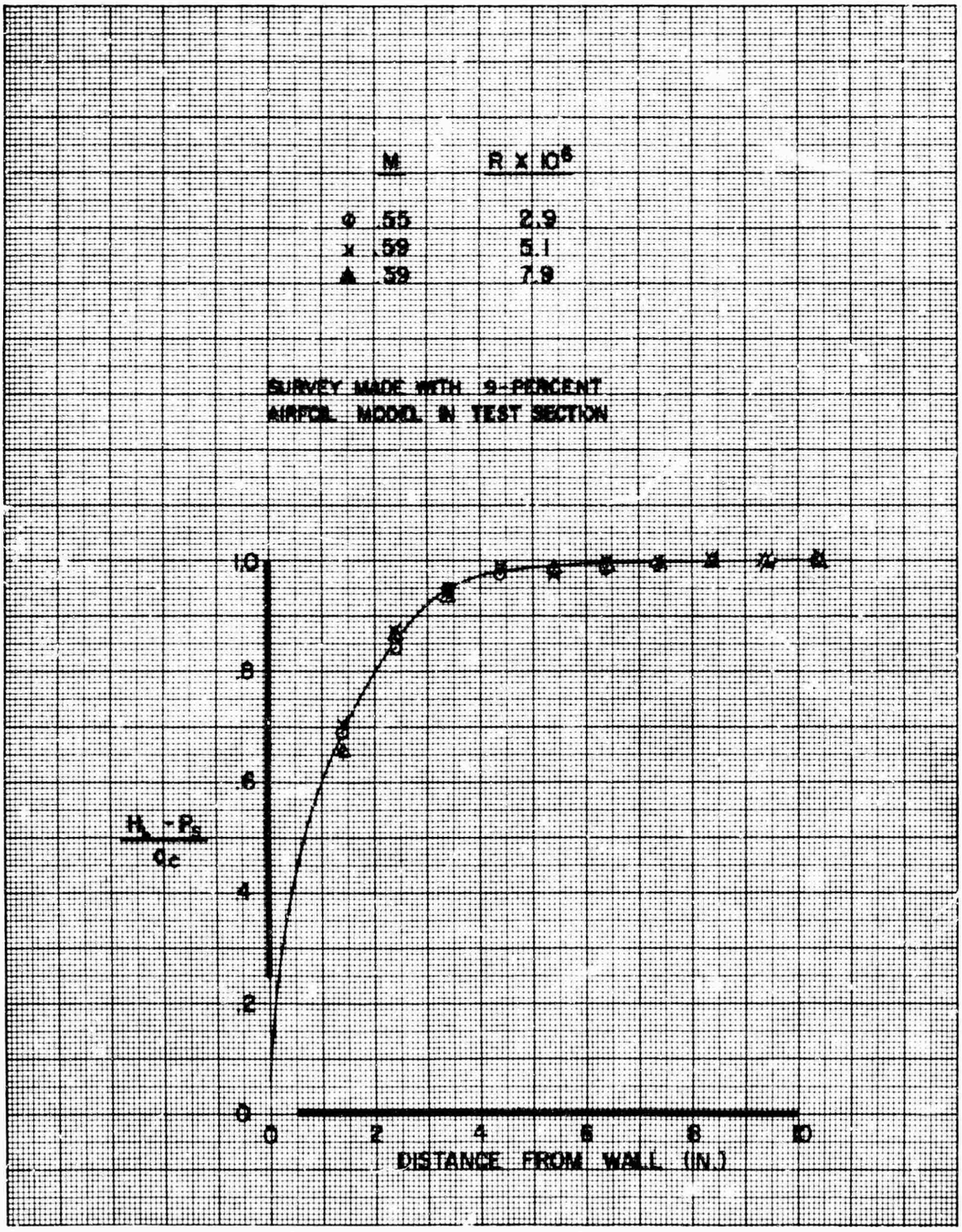


Figure 54D. Wind Tunnel Wall Boundary Layer

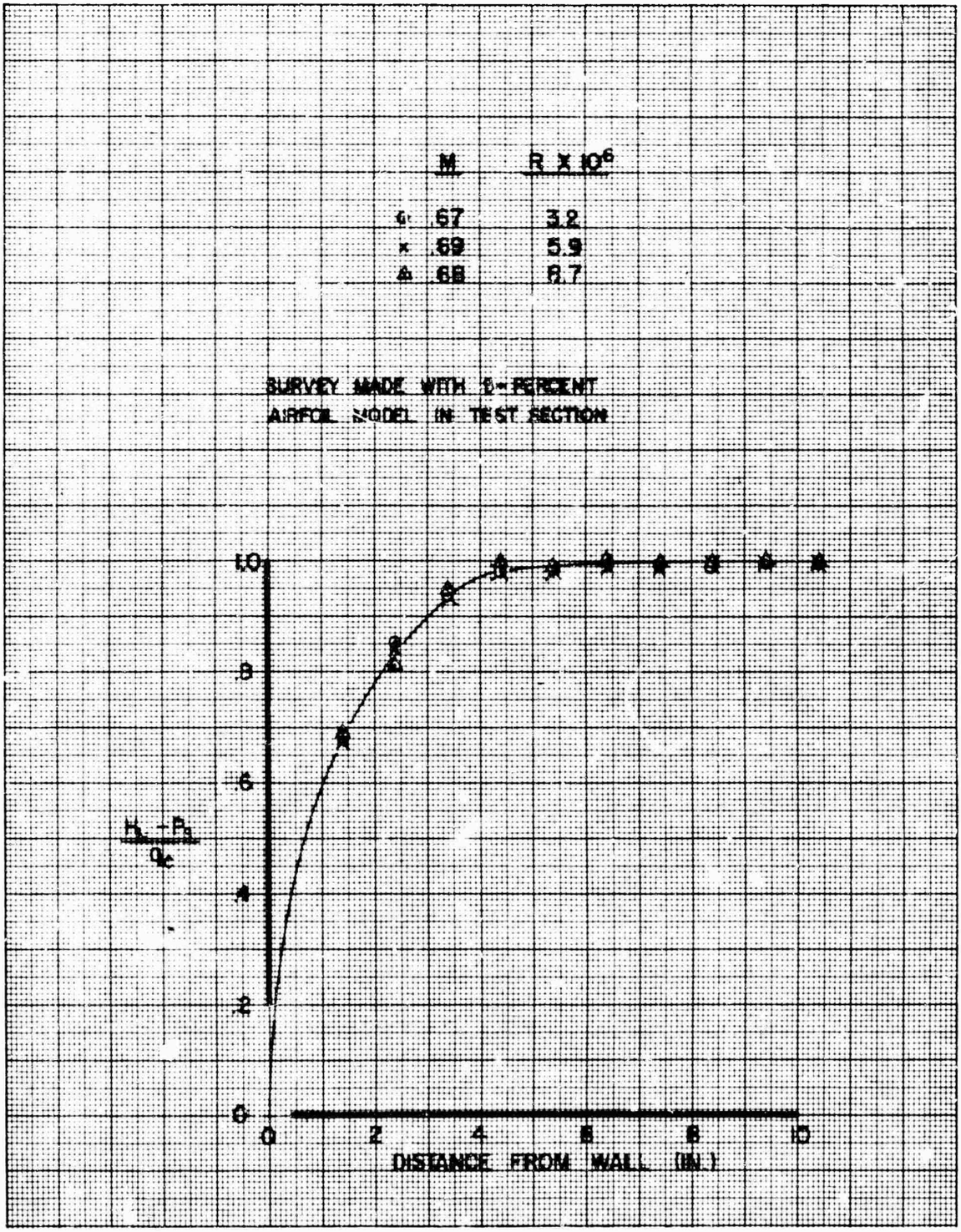


Figure 54E. Wind Tunnel Wall Boundary Layer

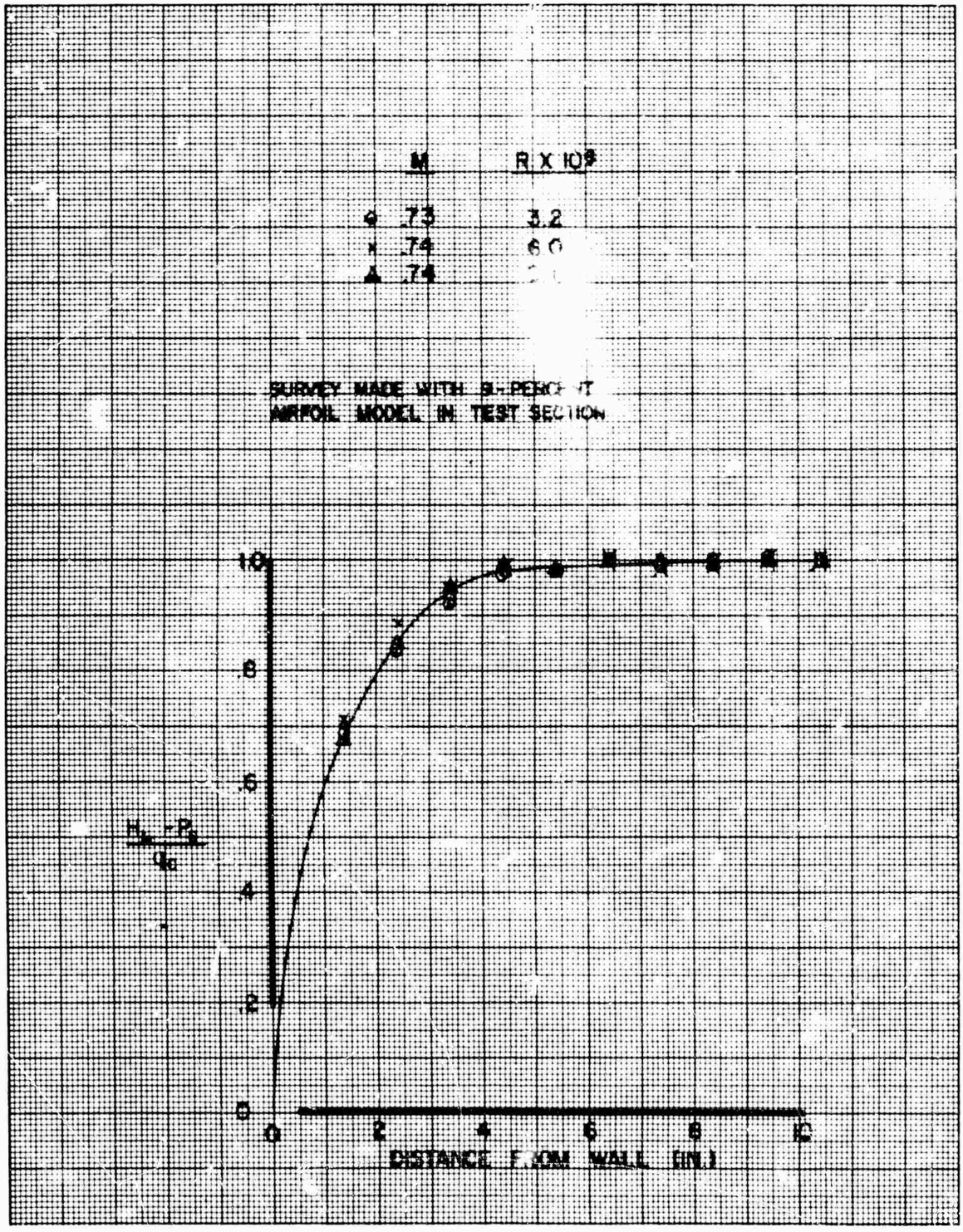


Figure 54F. Wind Tunnel Wall Boundary Layer

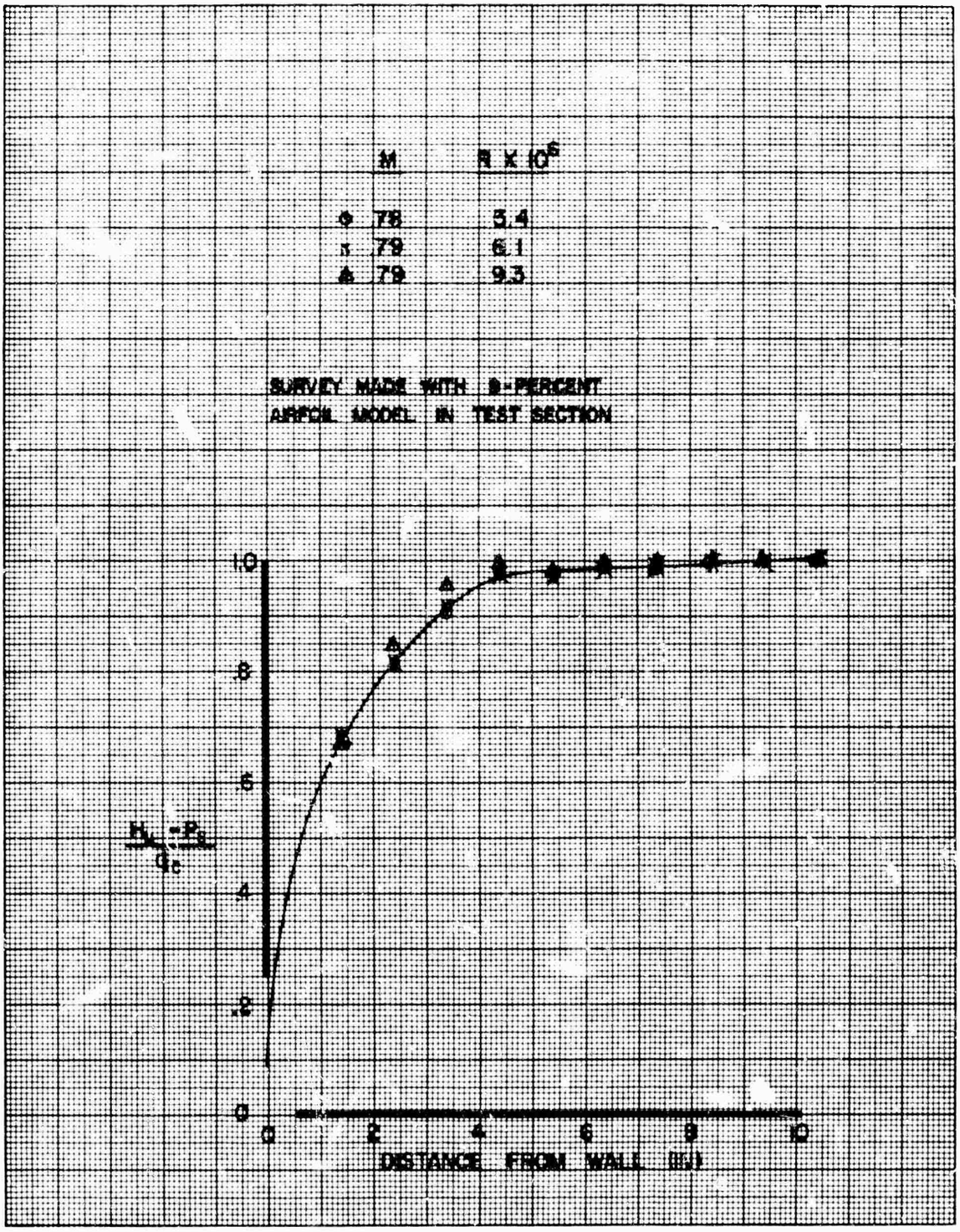


Figure 54G. Wind Tunnel Wall Boundary Layer

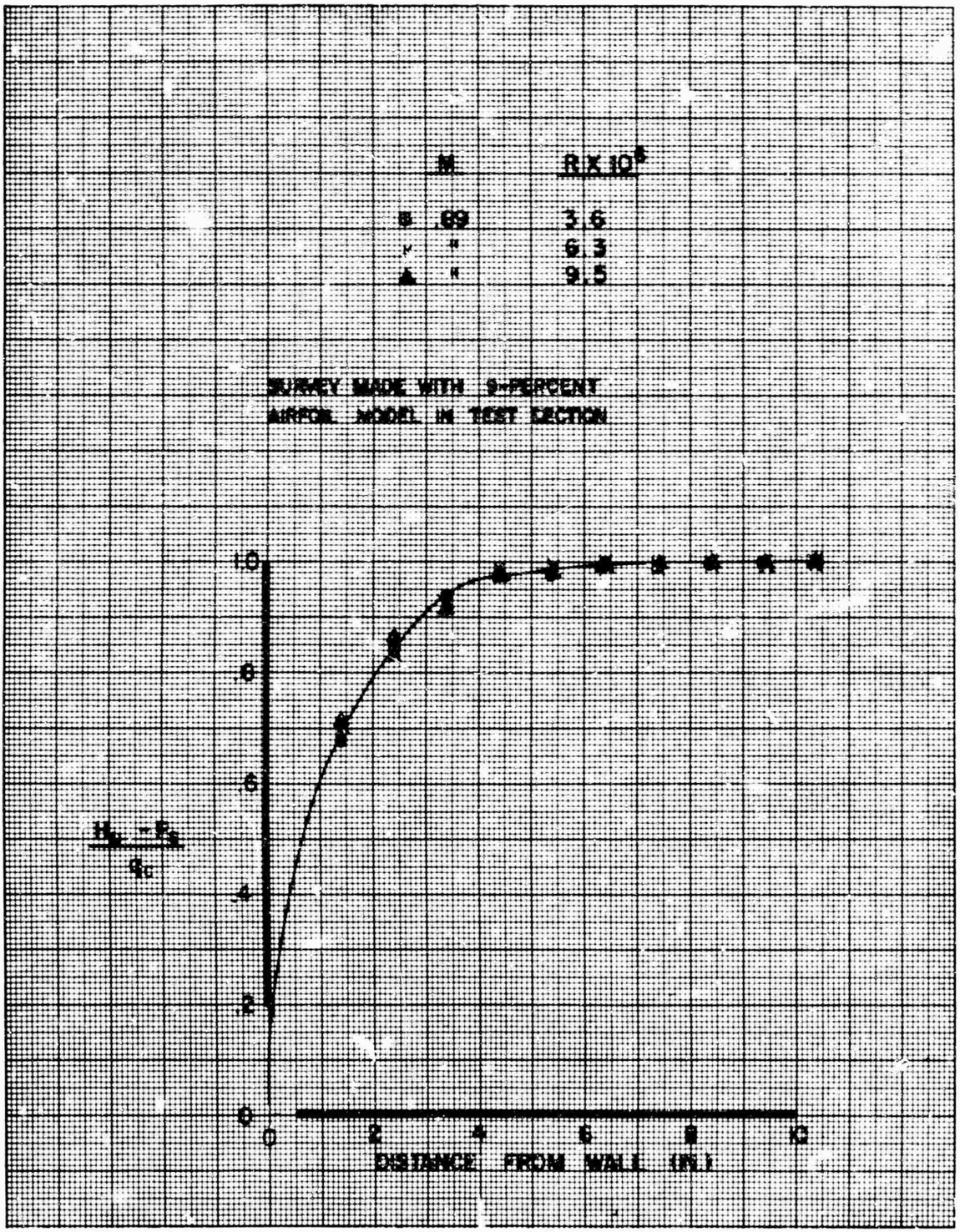


Figure 54H. Wind Tunnel Wall Boundary Layer

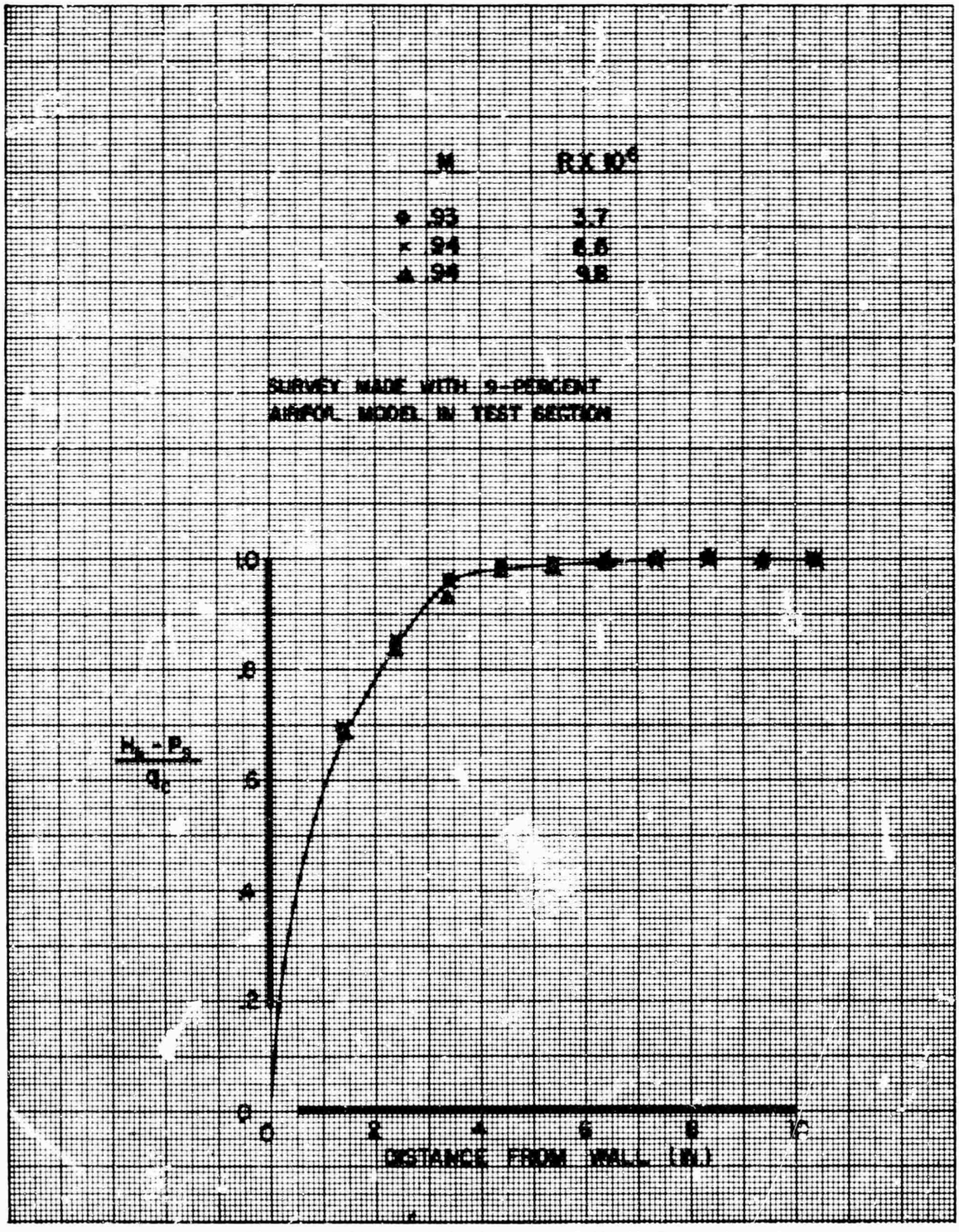


Figure 541. Wind Tunnel Wall Boundary Layer

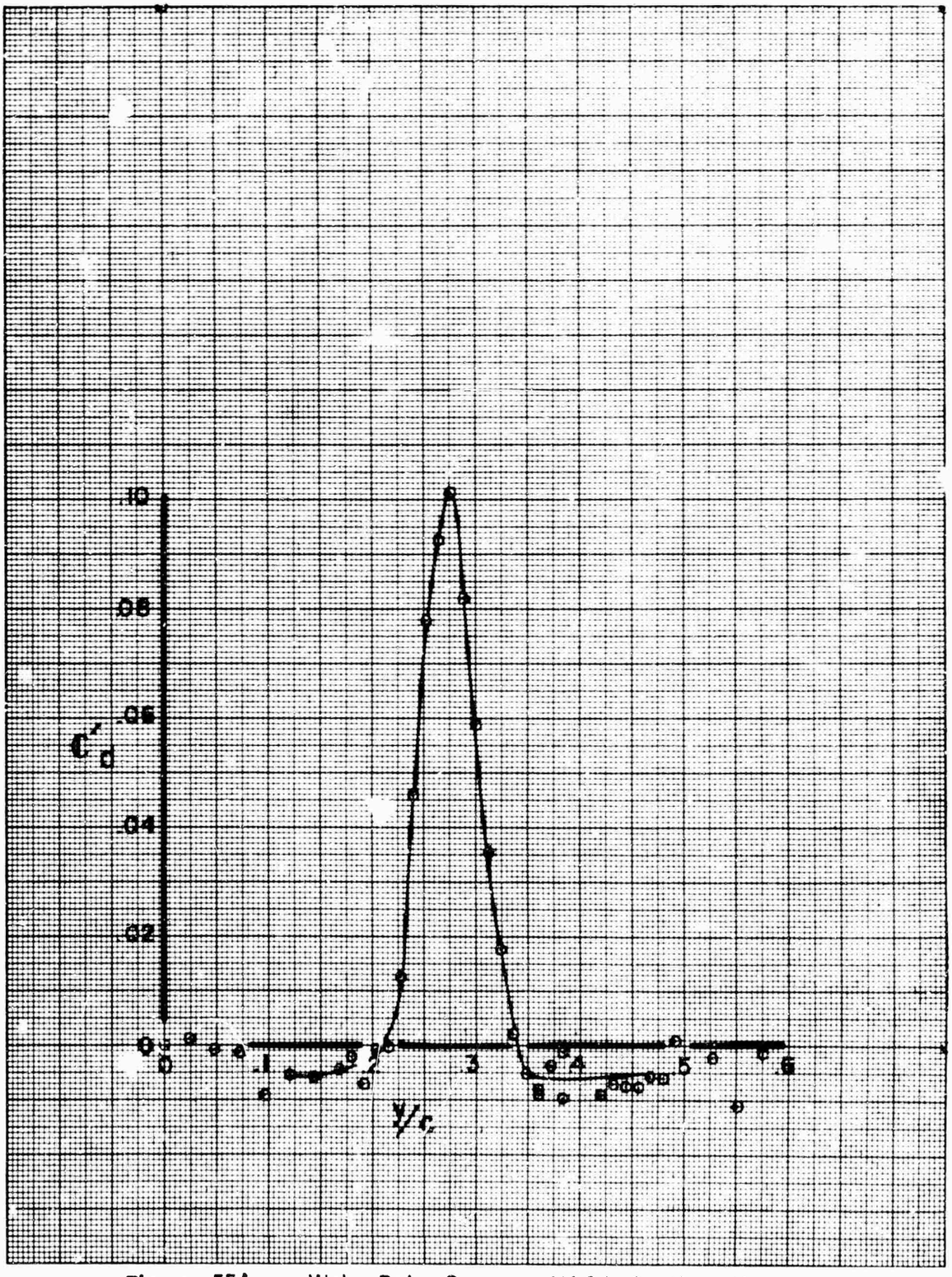


Figure 55A. Wake Rake Survey, NACA Section 63A009 - M = .59, R = 5.2 x 10^6

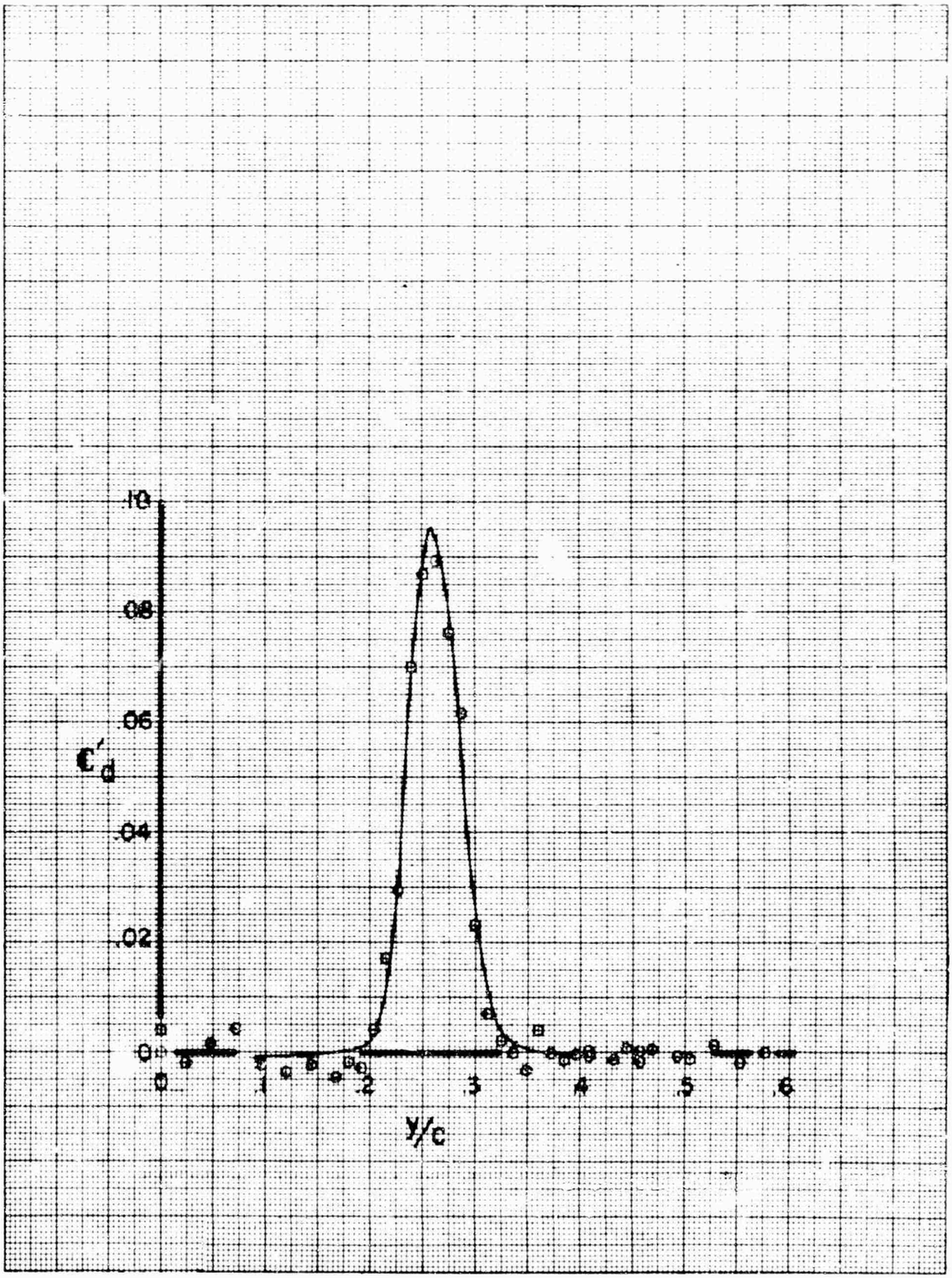


Figure 55B. Wake Rake Survey, NACA Section 63A009 - $M = .74$, $R = 6.0 \times 10^6$

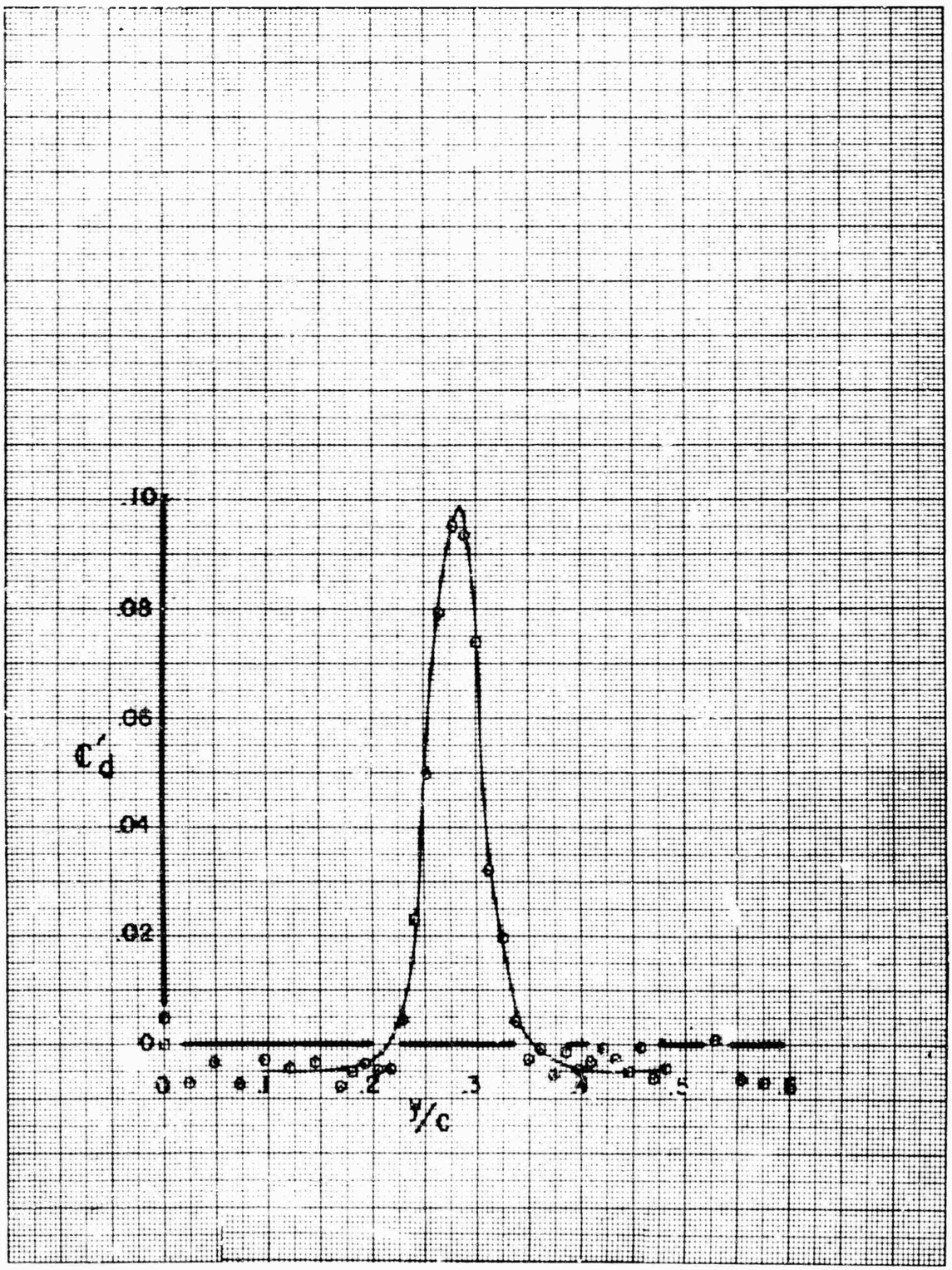


Figure 55C. Wake Rake Survey, NACA Section 63A009 - $M = .79$, $R = 6.0 \times 10^6$

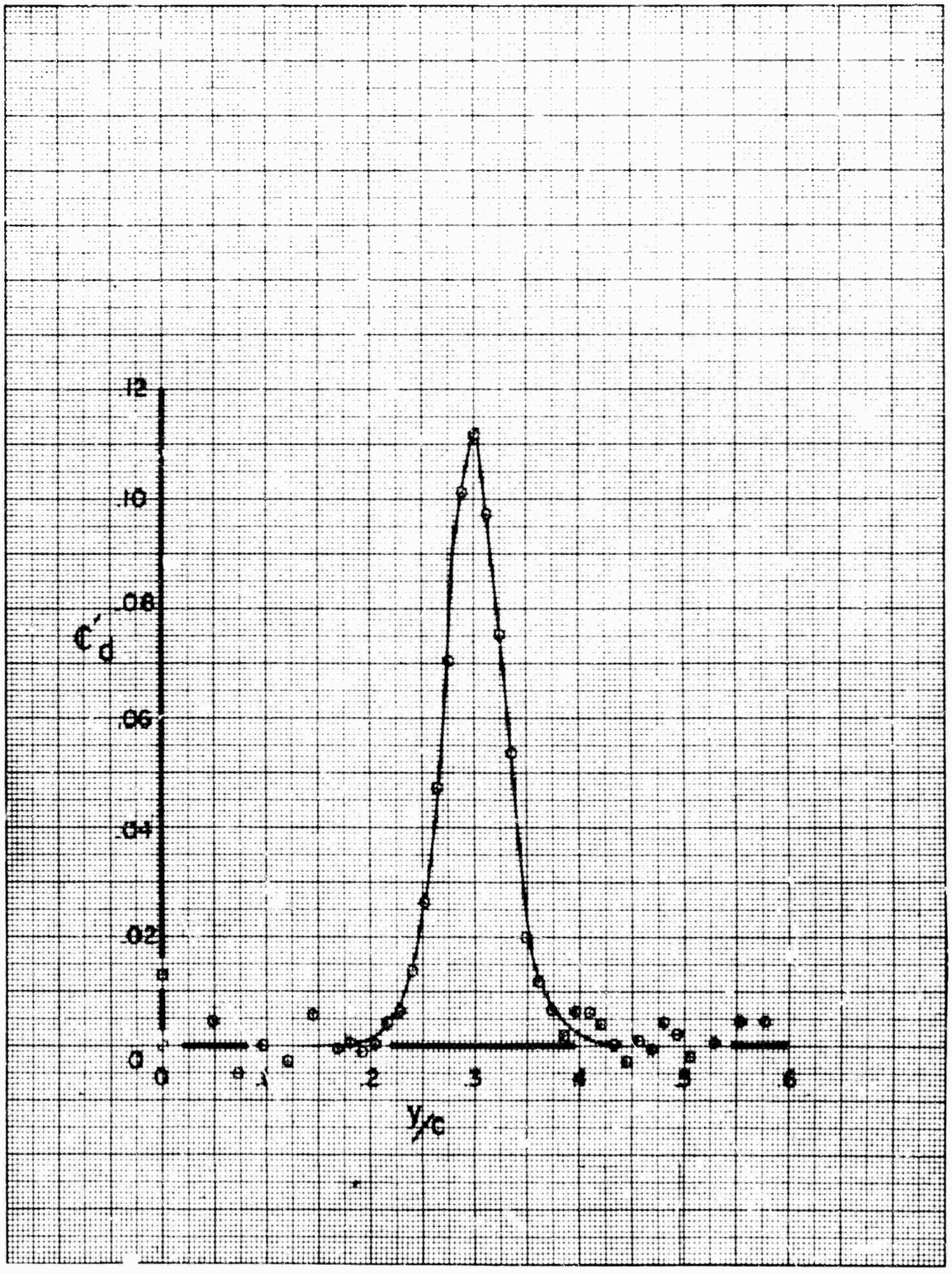


Figure 56A. Wake Rake Survey, NACA Section 63A012 - M = .59, R = 7.8 x 10^6

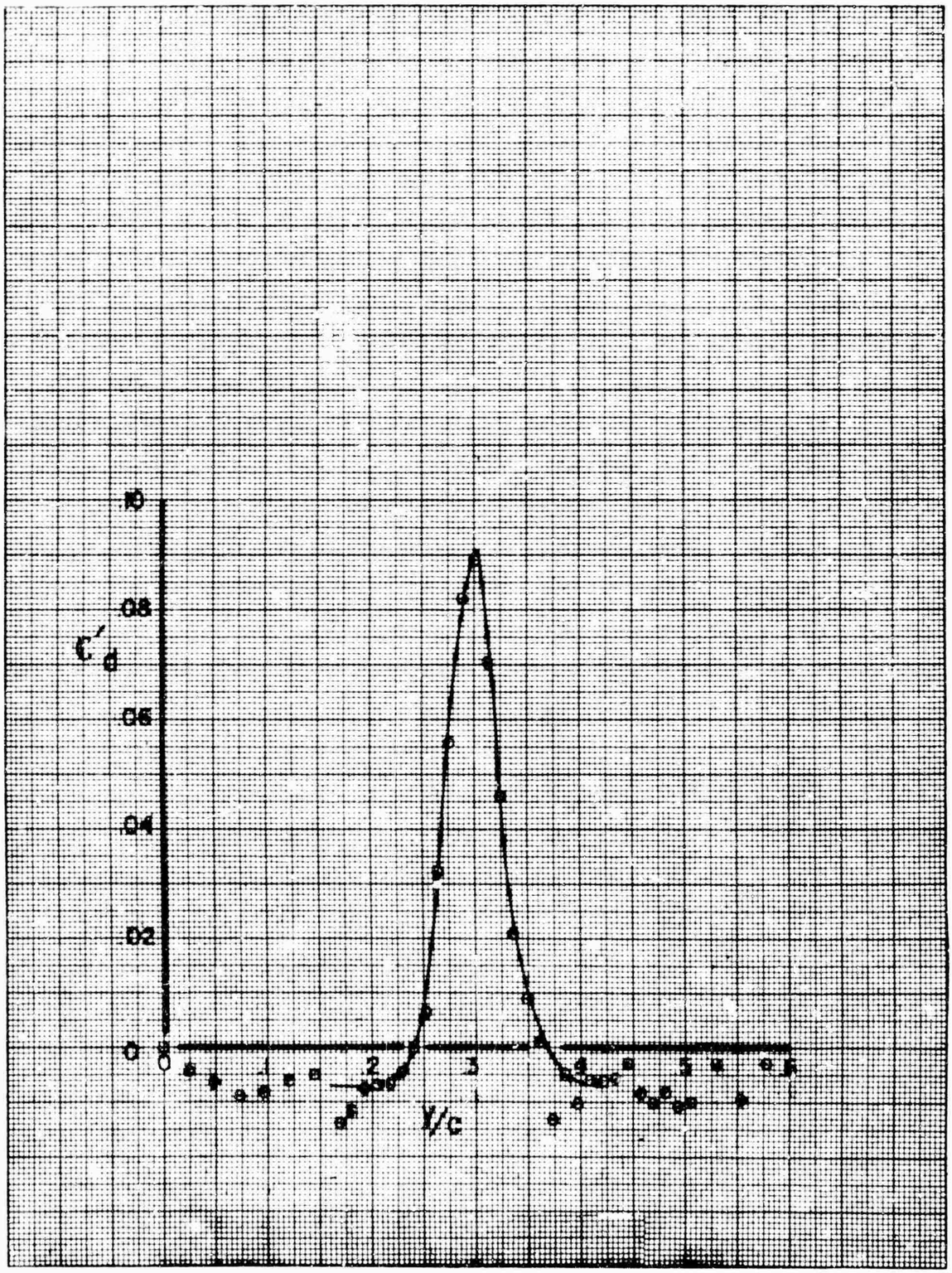


Figure 56B. Wake Rake Survey, NACA Section 63A012 - M = .69, R = 5.7 x 10^6

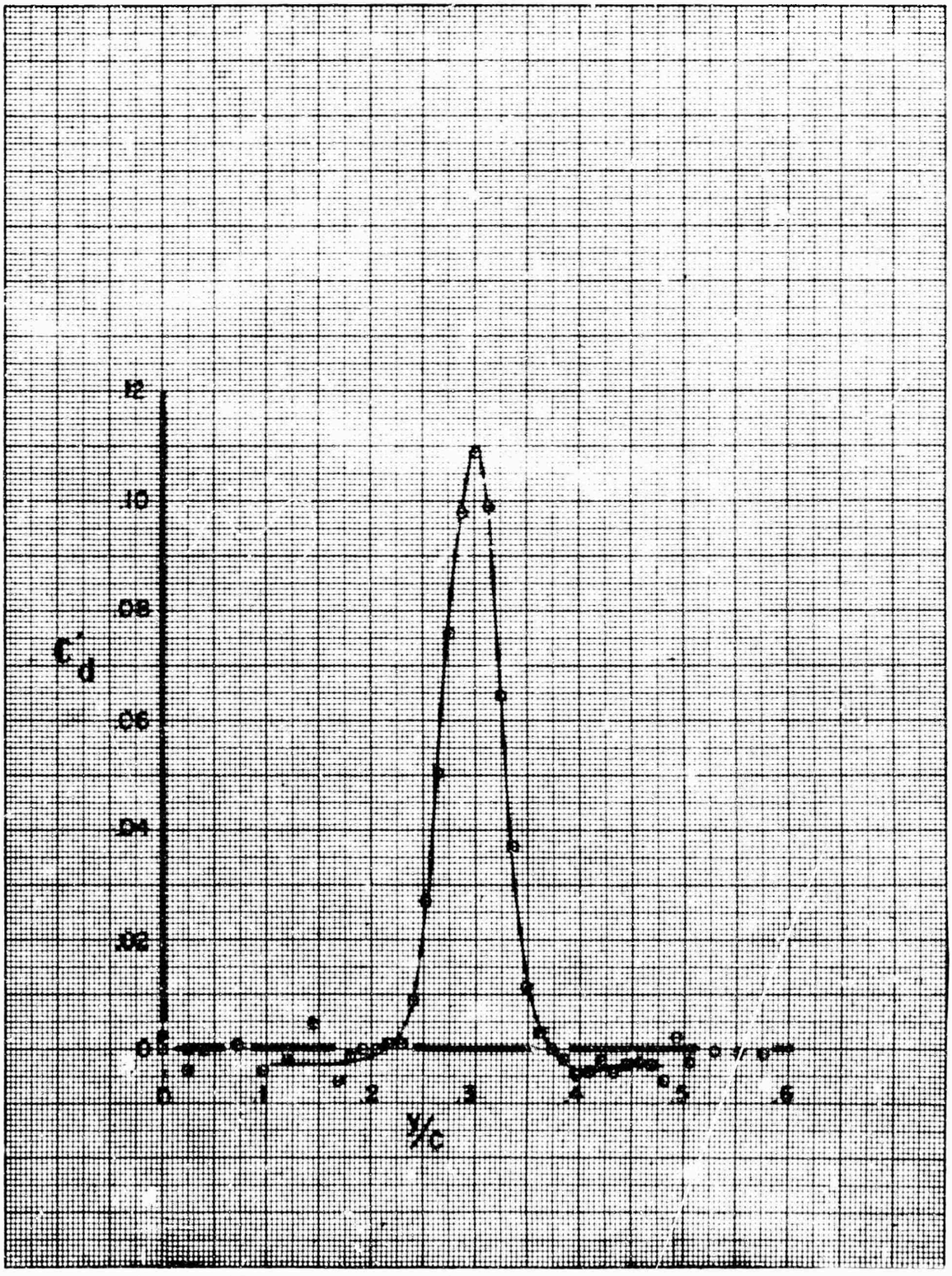


Figure 56C. Wake Rake Survey, NACA Section 63A012 - M = .74, R = 5.7 x 10^6

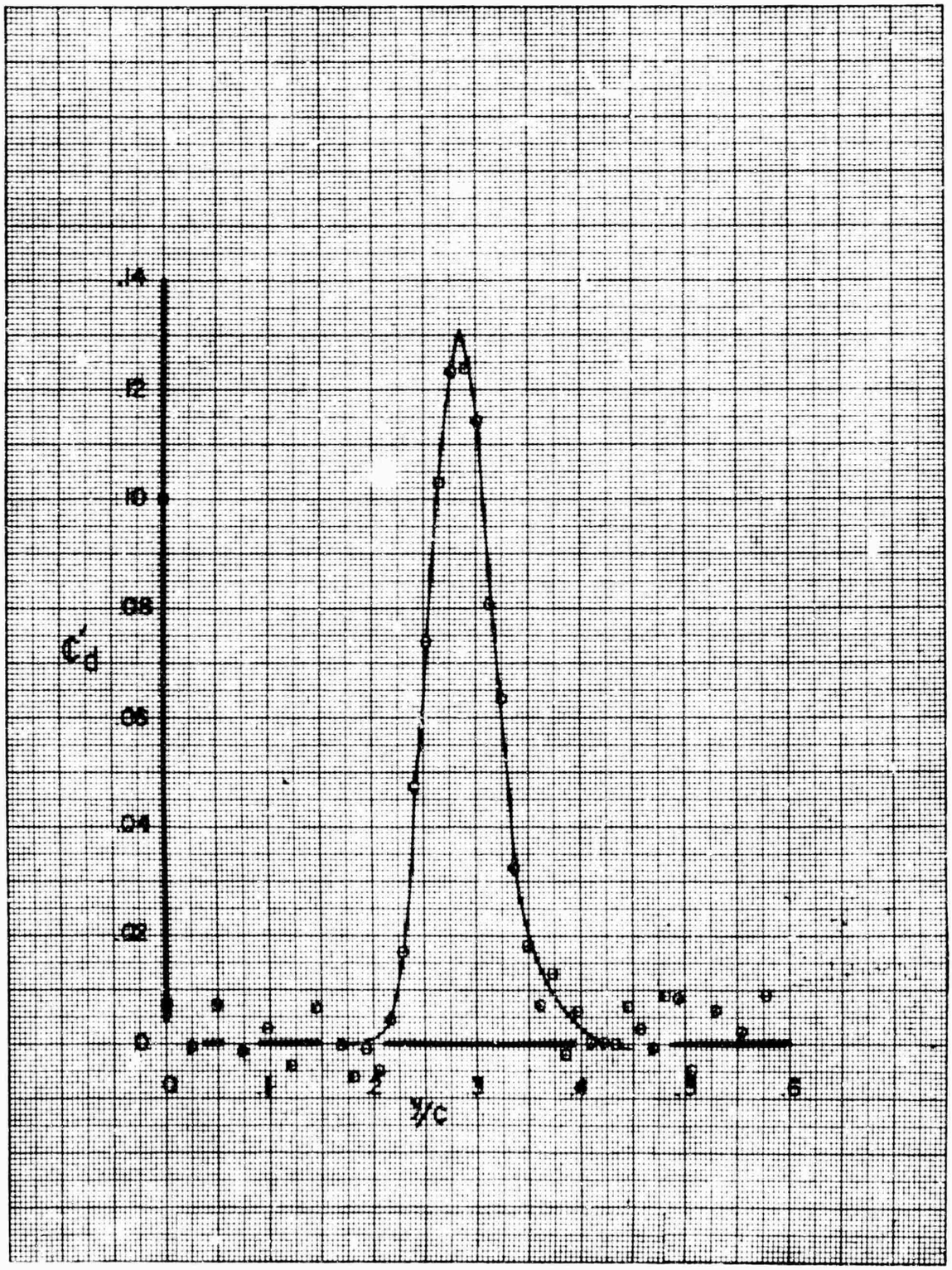


Figure 57A. Wake Rake Survey, NACA Section 63$_1$015 - M = .59, R = 5.1 x 10^6

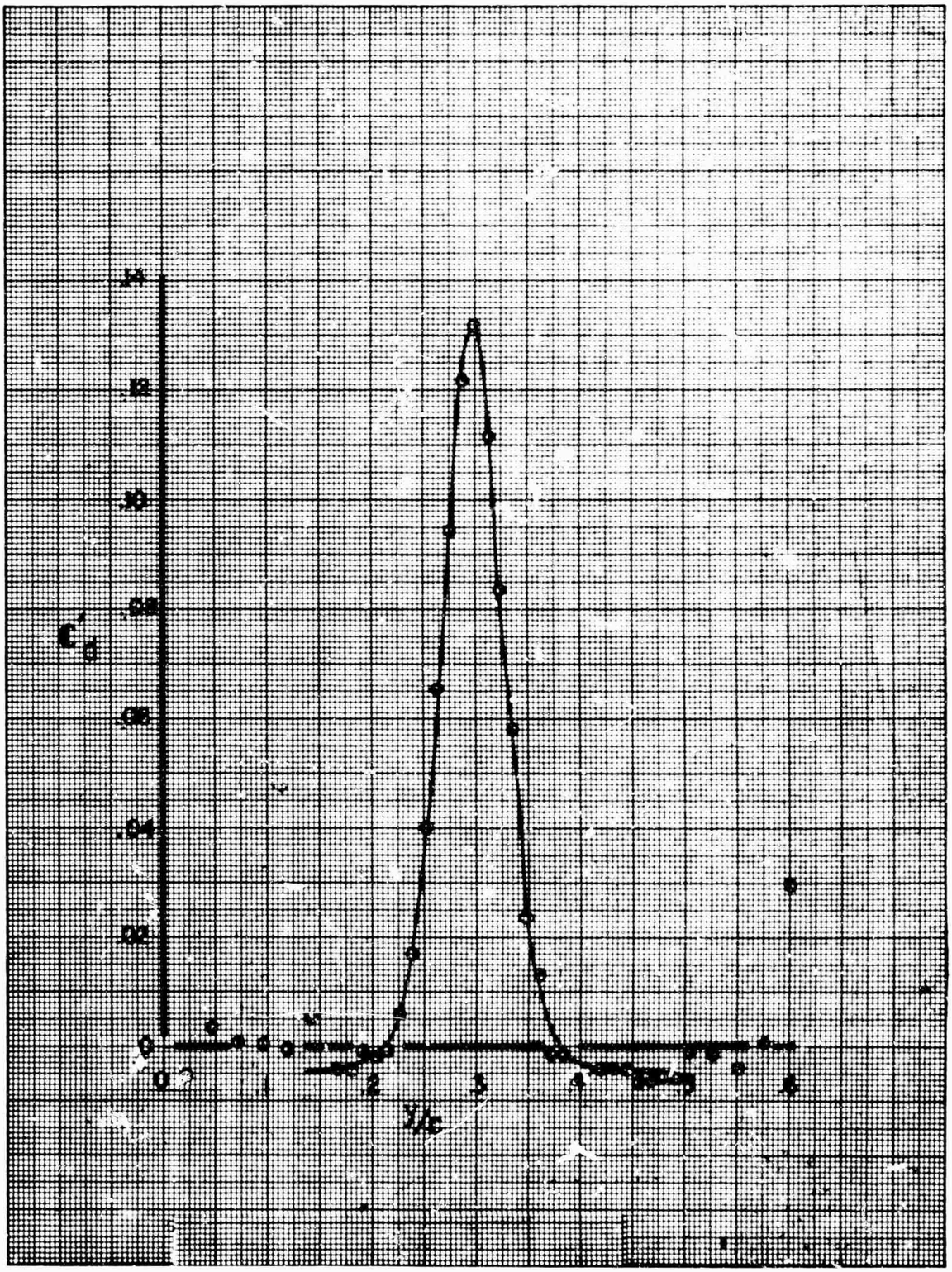


Figure 57B. Wake Rake Survey, NACA Section 63A015 - $M = .69$, $R = 5.9 \times 10^6$

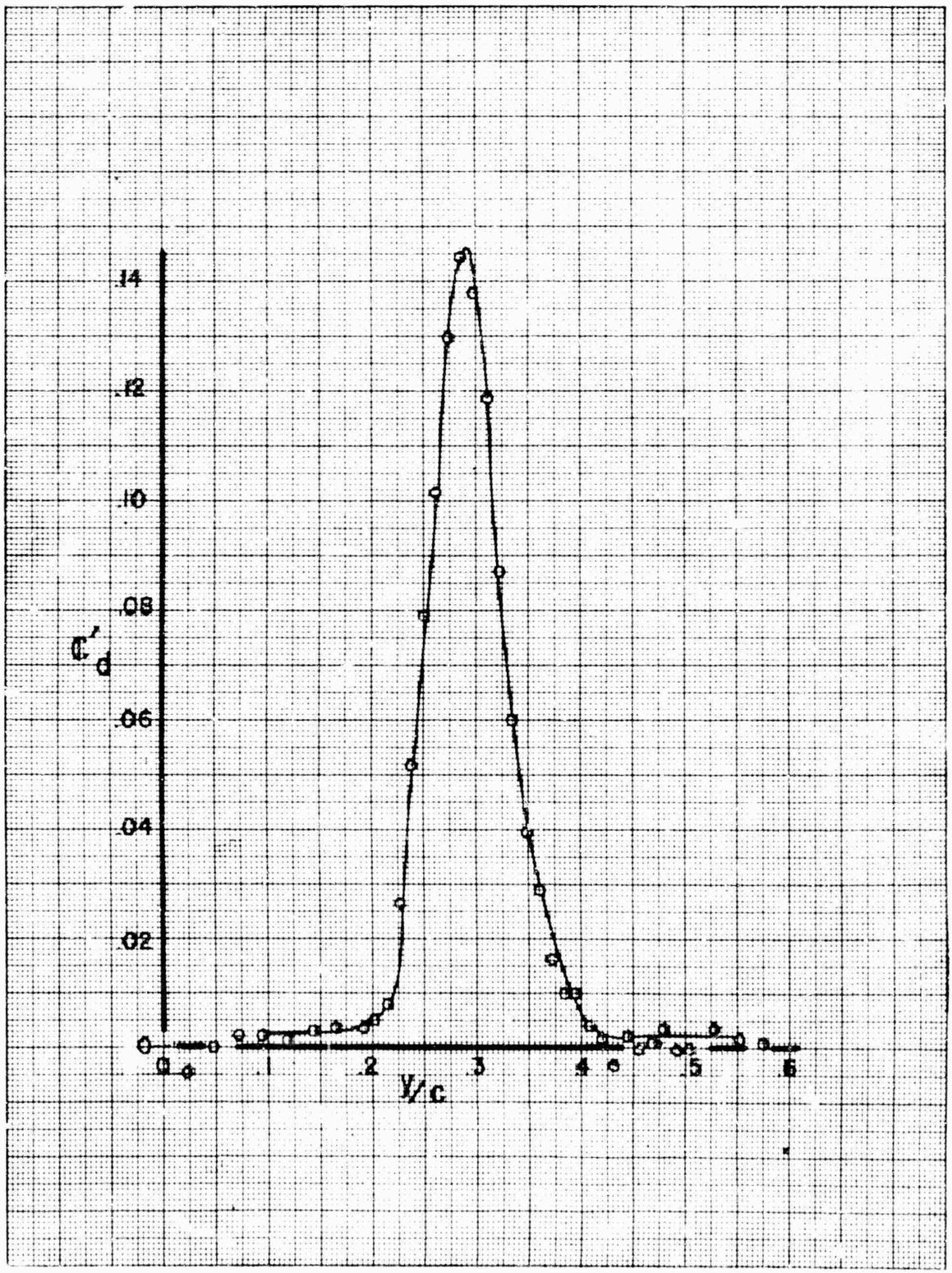


Figure 57C. Wake Rake Survey, NACA Section 63A015 - $M = .74$, $R = 5.8 \times 10^6$

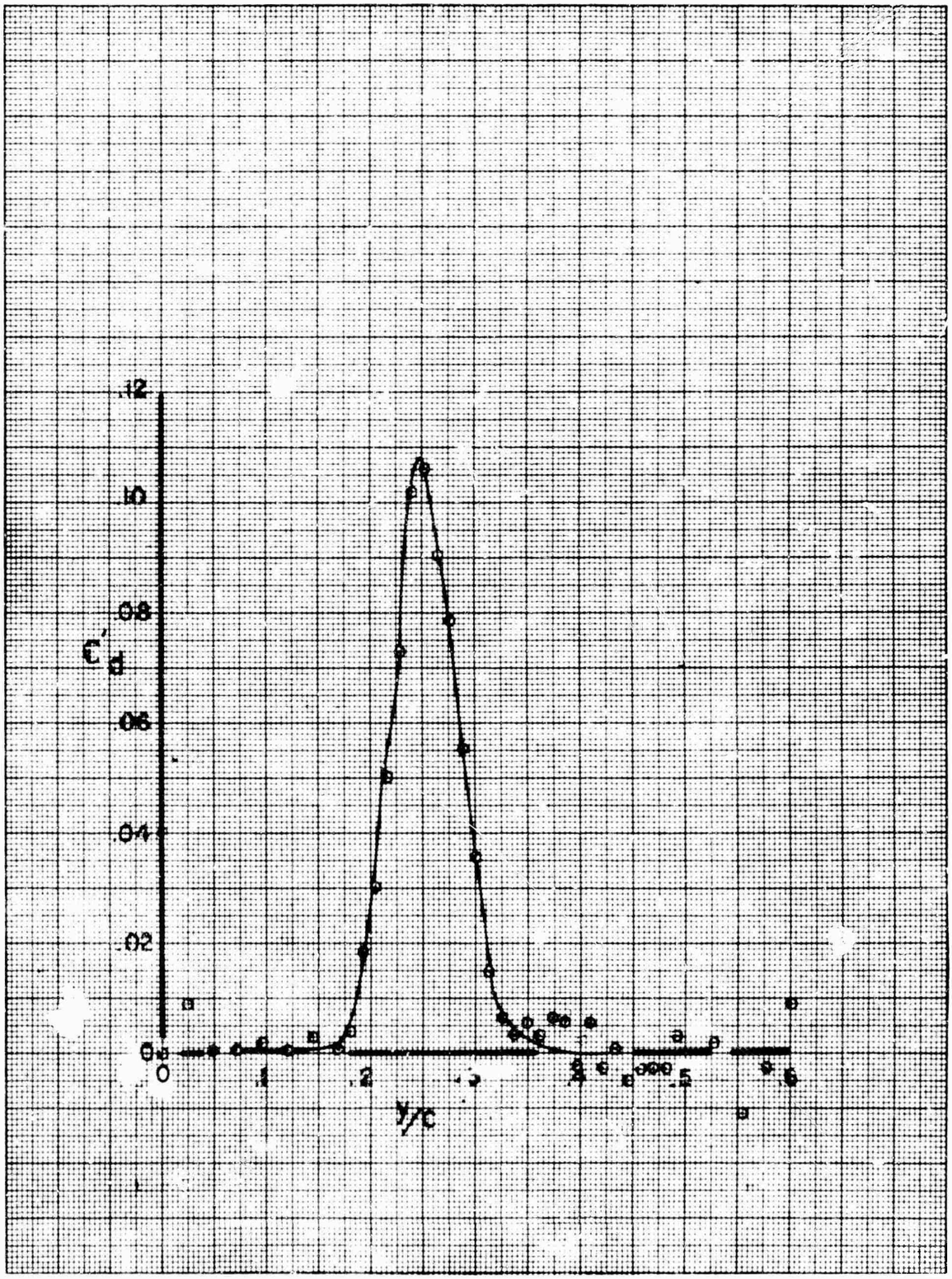


Figure 58A. Wake Rake Survey, NACA Section 63A018 - $M = .57$, $R = 2.9 \times 10^6$

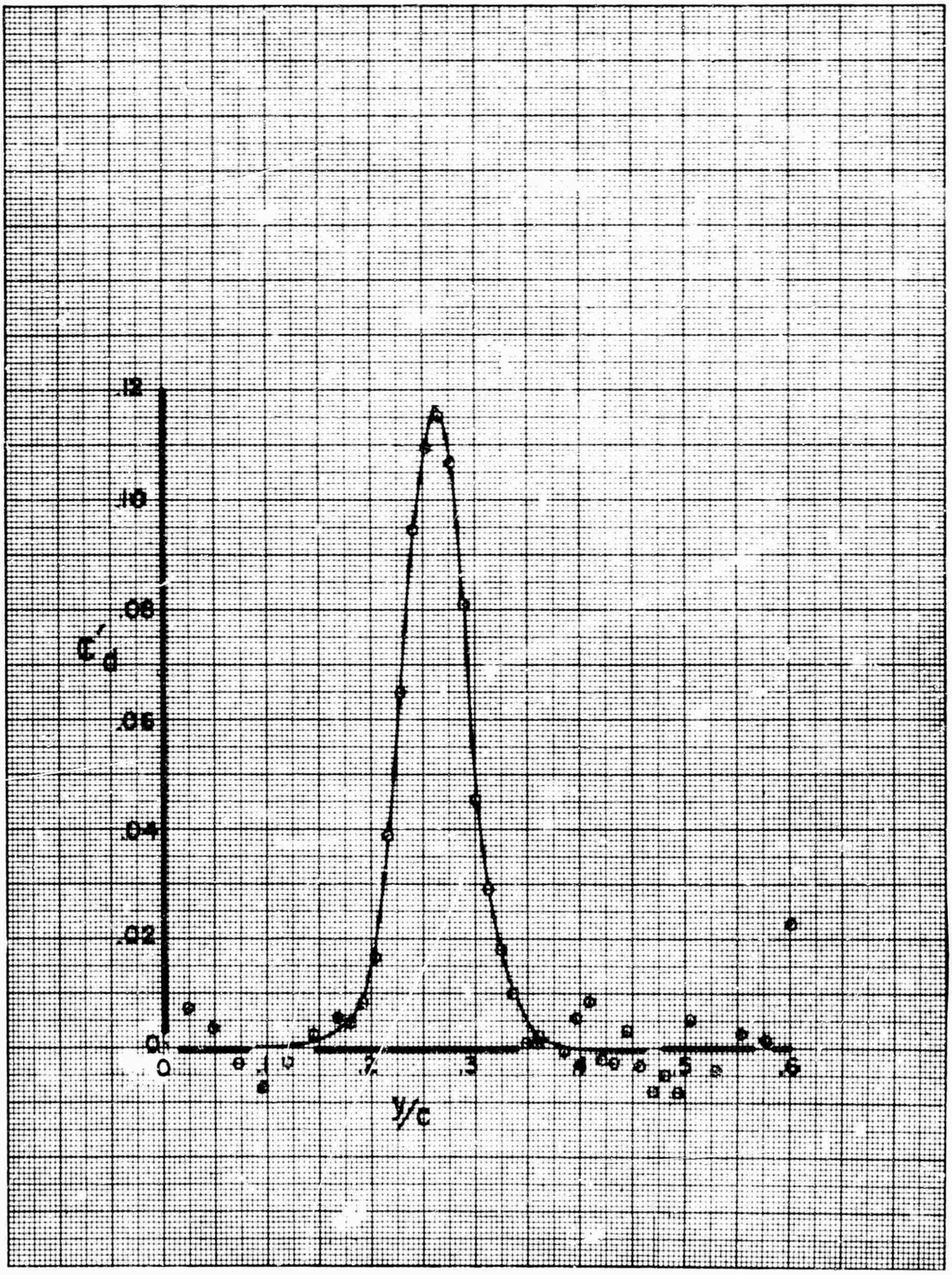


Figure 58B. Wake Rake Survey, NACA Section 63A018 - M = .59, R = 7.8 x 10^6

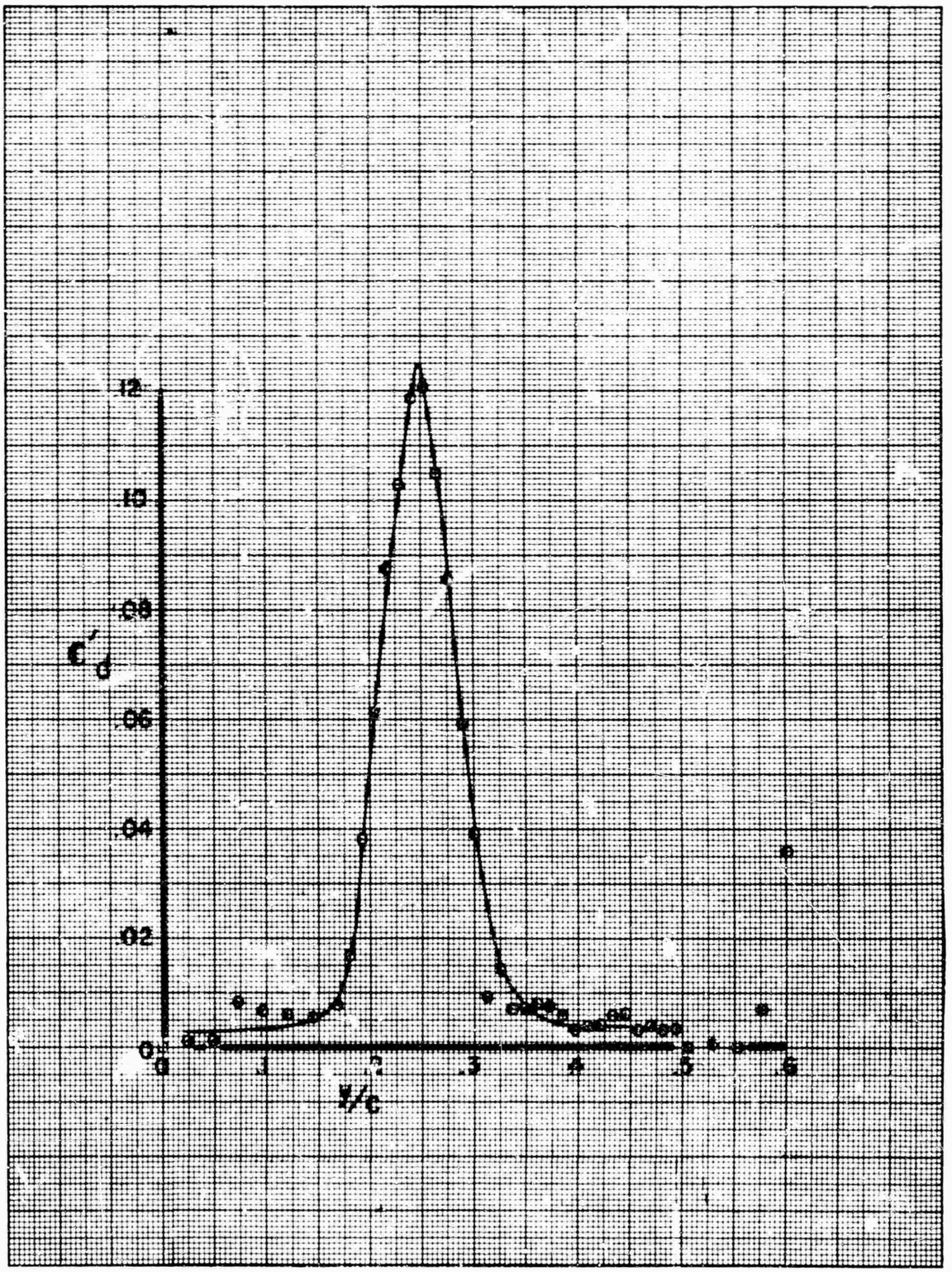


Figure 58C. Wake Rake Survey, NACA Section 63A018 - M = .64, R = 6.0 x 10^6

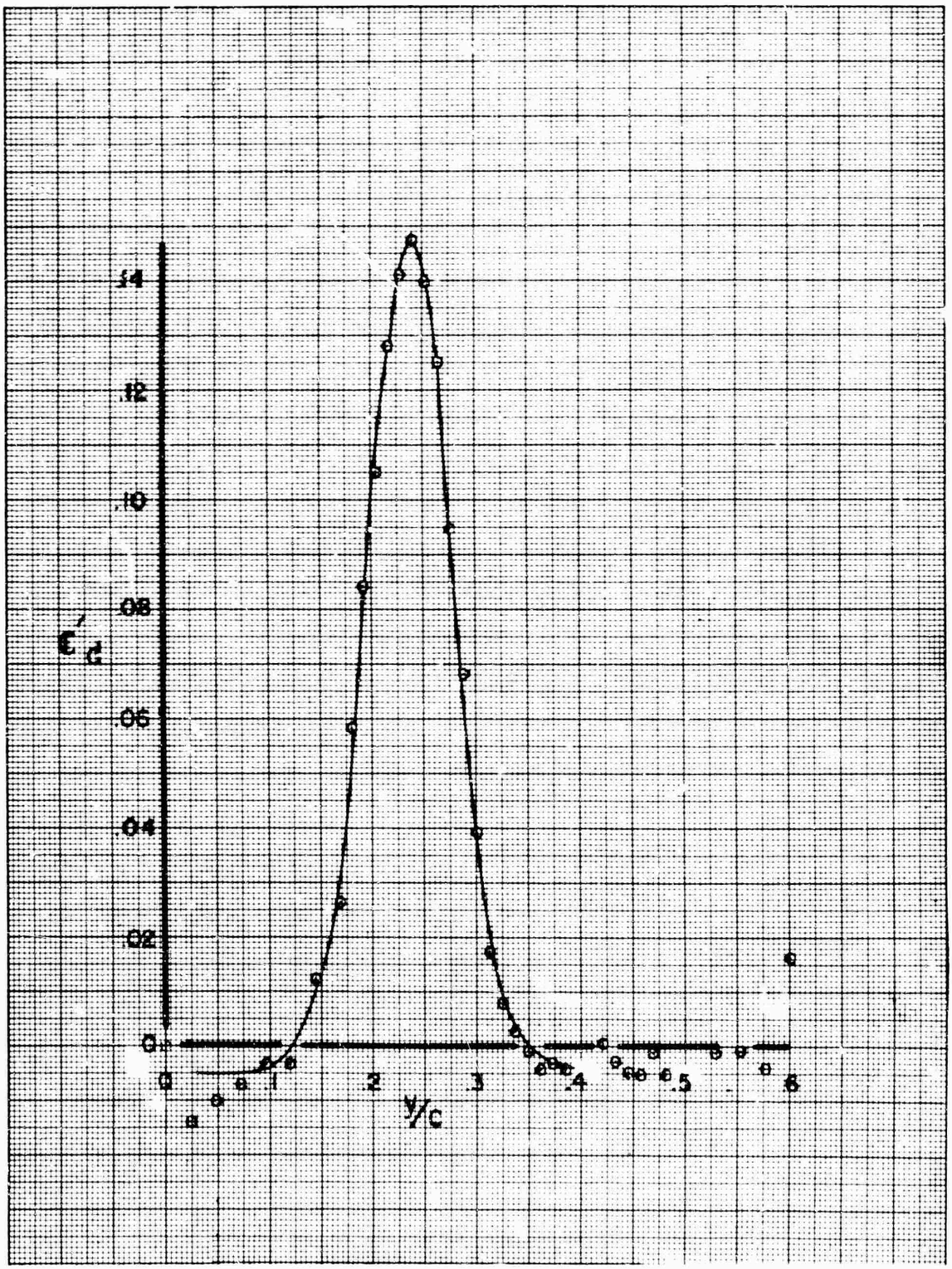


Figure 58D. Wake Rake Survey, NACA Section 63A018 - $M = .73$, $R = 3.3 \times 10^6$

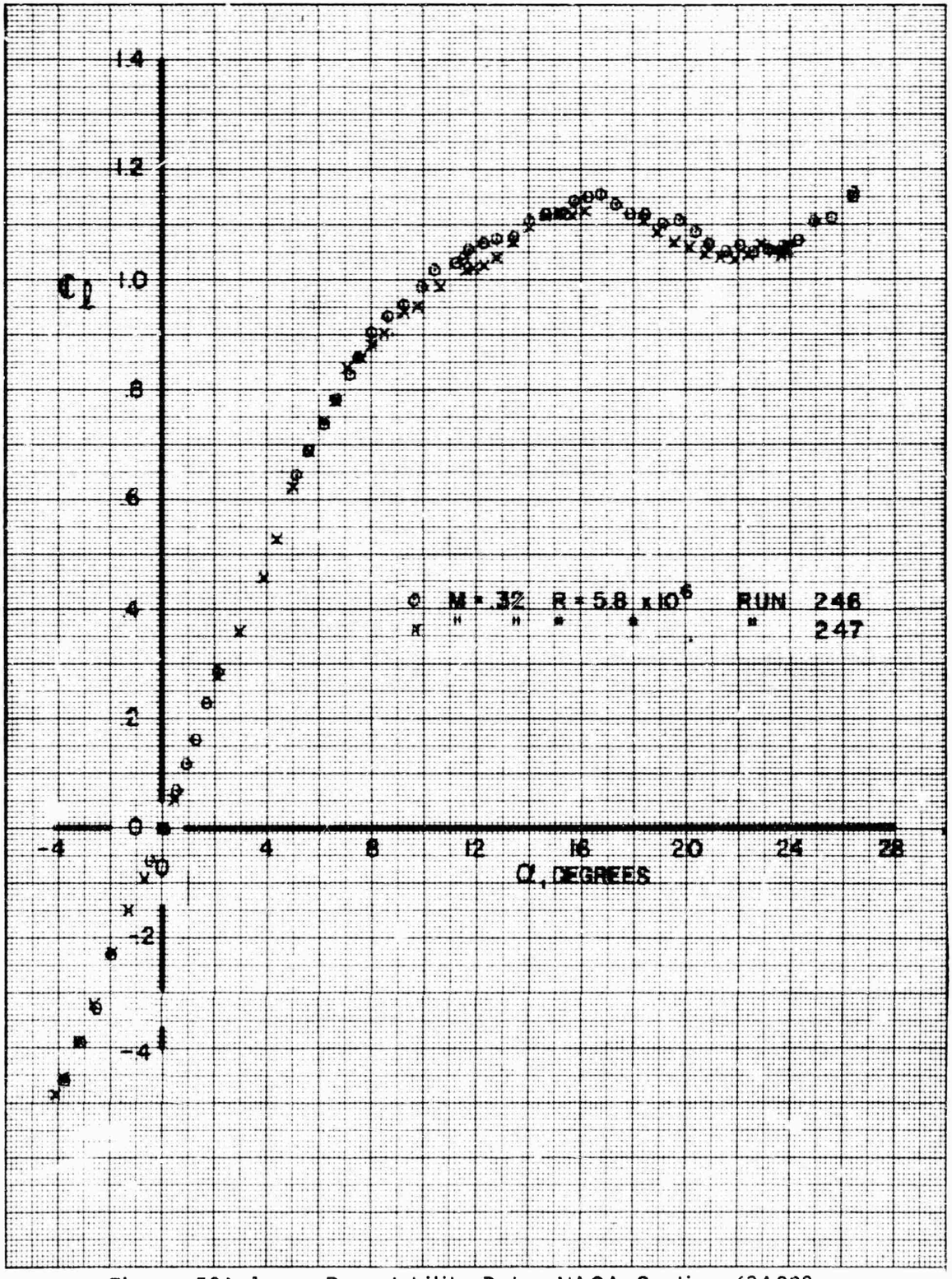


Figure 59A-1. Repeatability Data, NACA Section 63A009

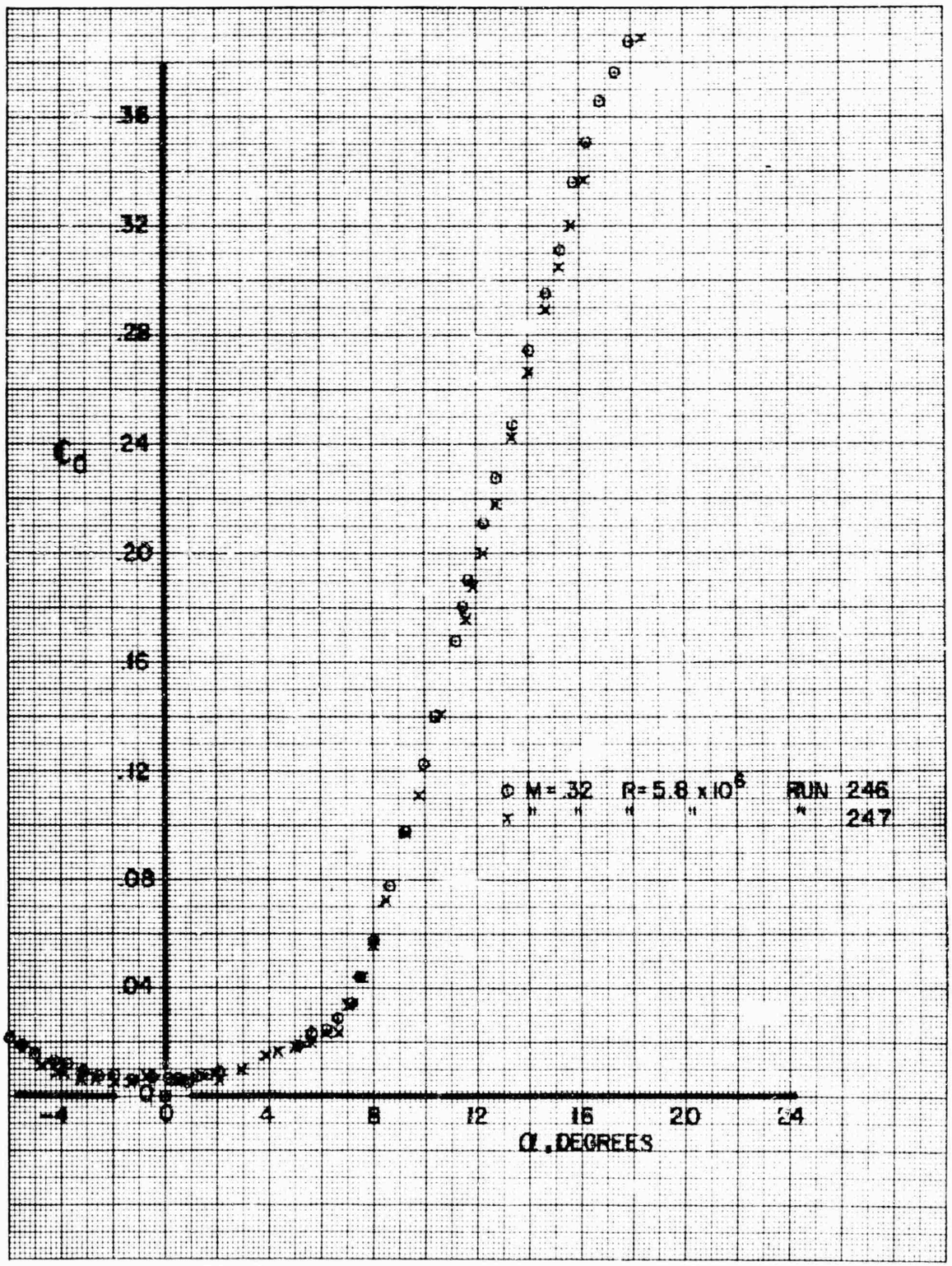


Figure 59A-2. Repeatability Data, NACA Section 63A009

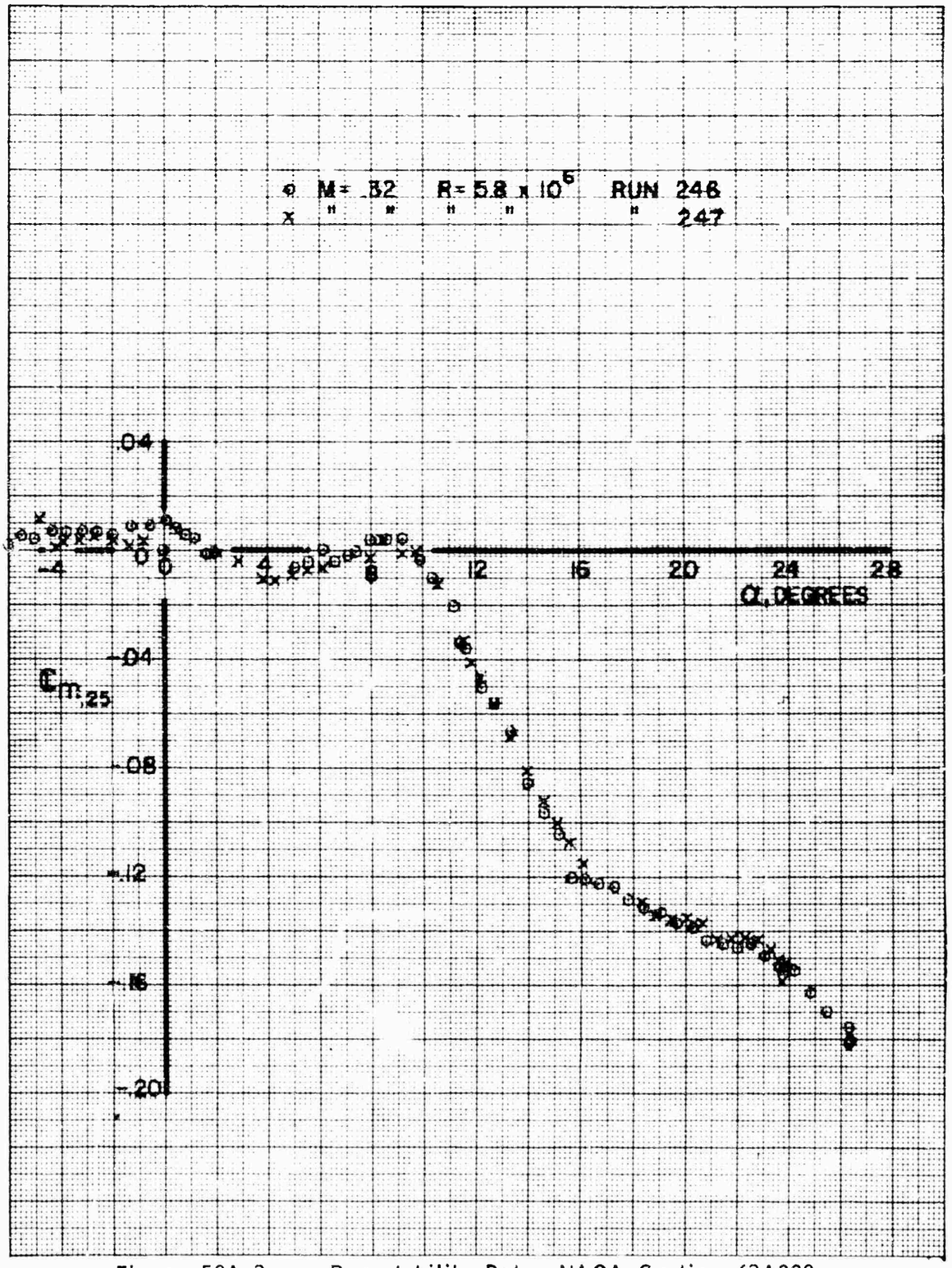


Figure 59A-3. Repeatability Data, NACA Section 63A009

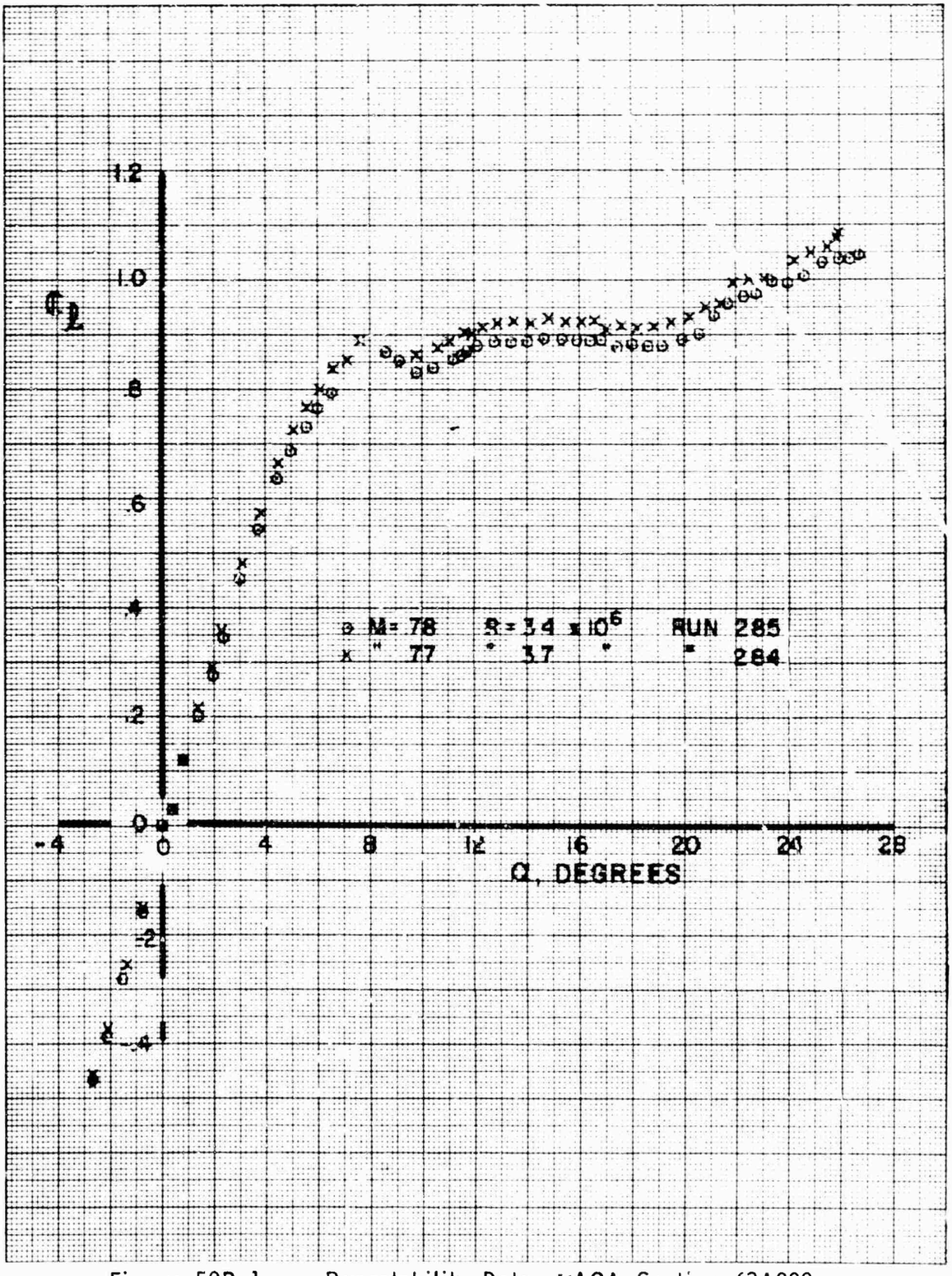


Figure 59B-1. Repeatability Data, NACA Section 63A009

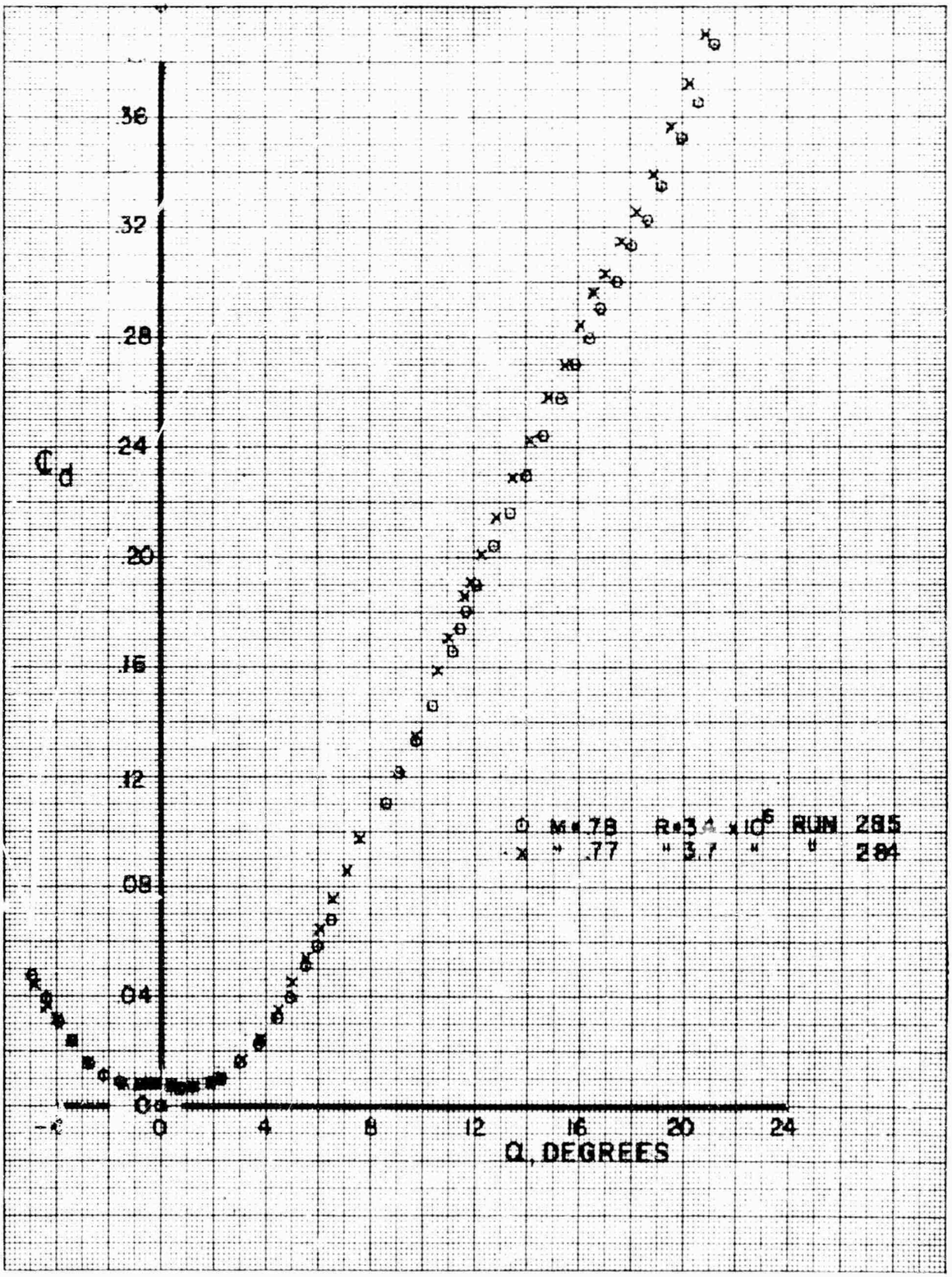


Figure 59B-2. Repeatability Data, NACA Section 63A009

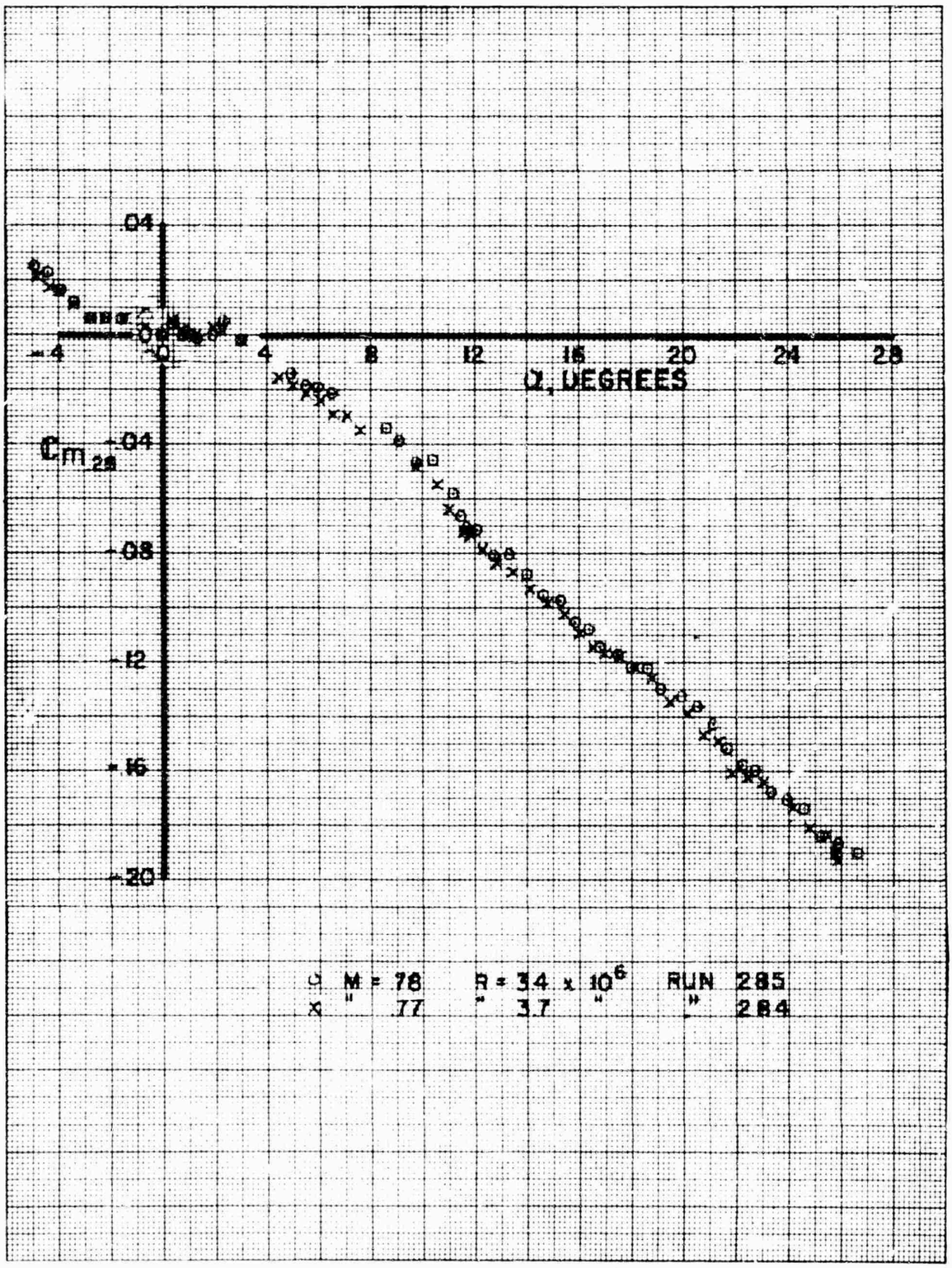


Figure 59B-3. Repeatability Data, NACA Section 63A009

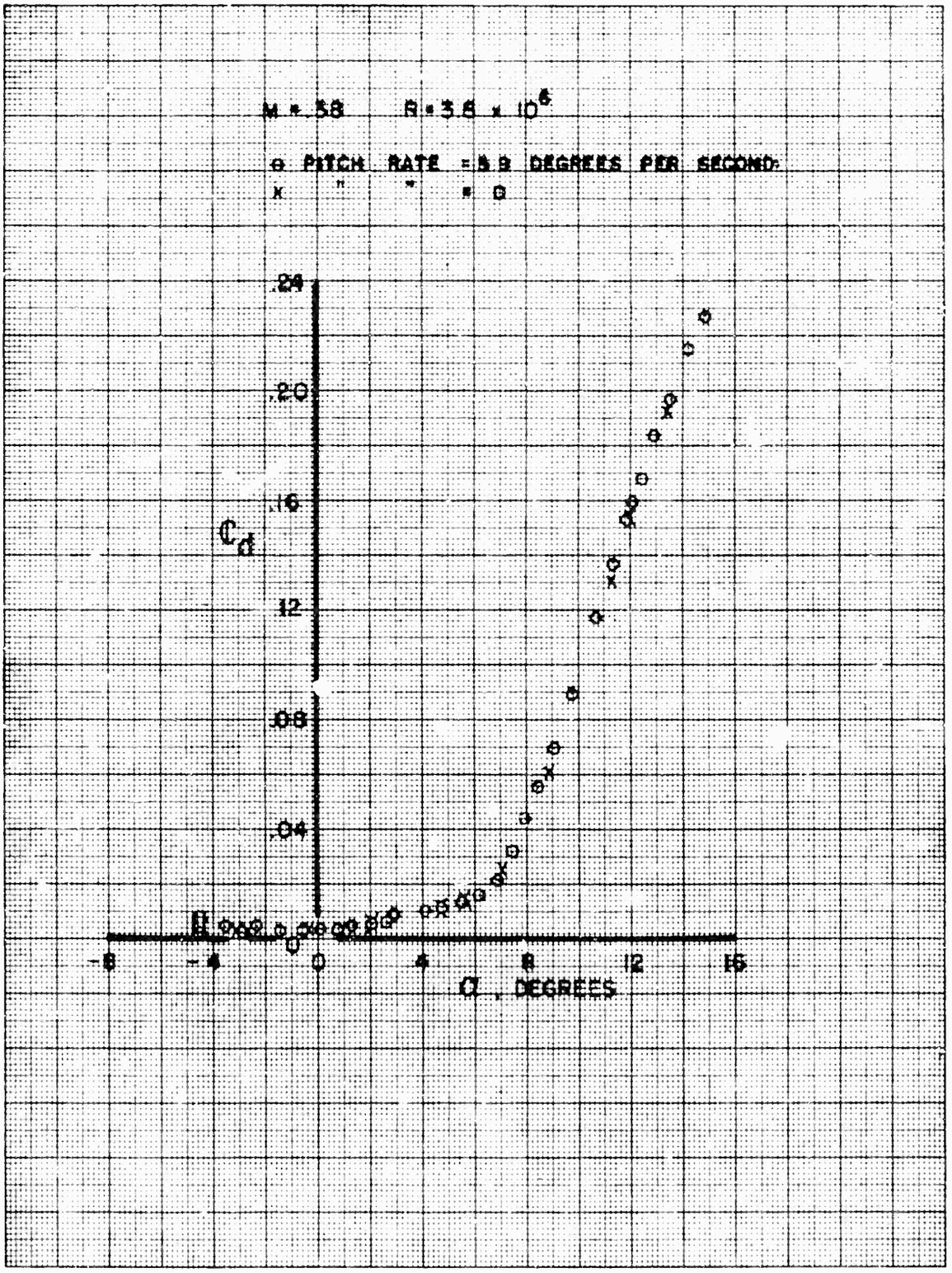


Figure 60A-1. Pitch Rate Comparison Data, NACA Section 63A009

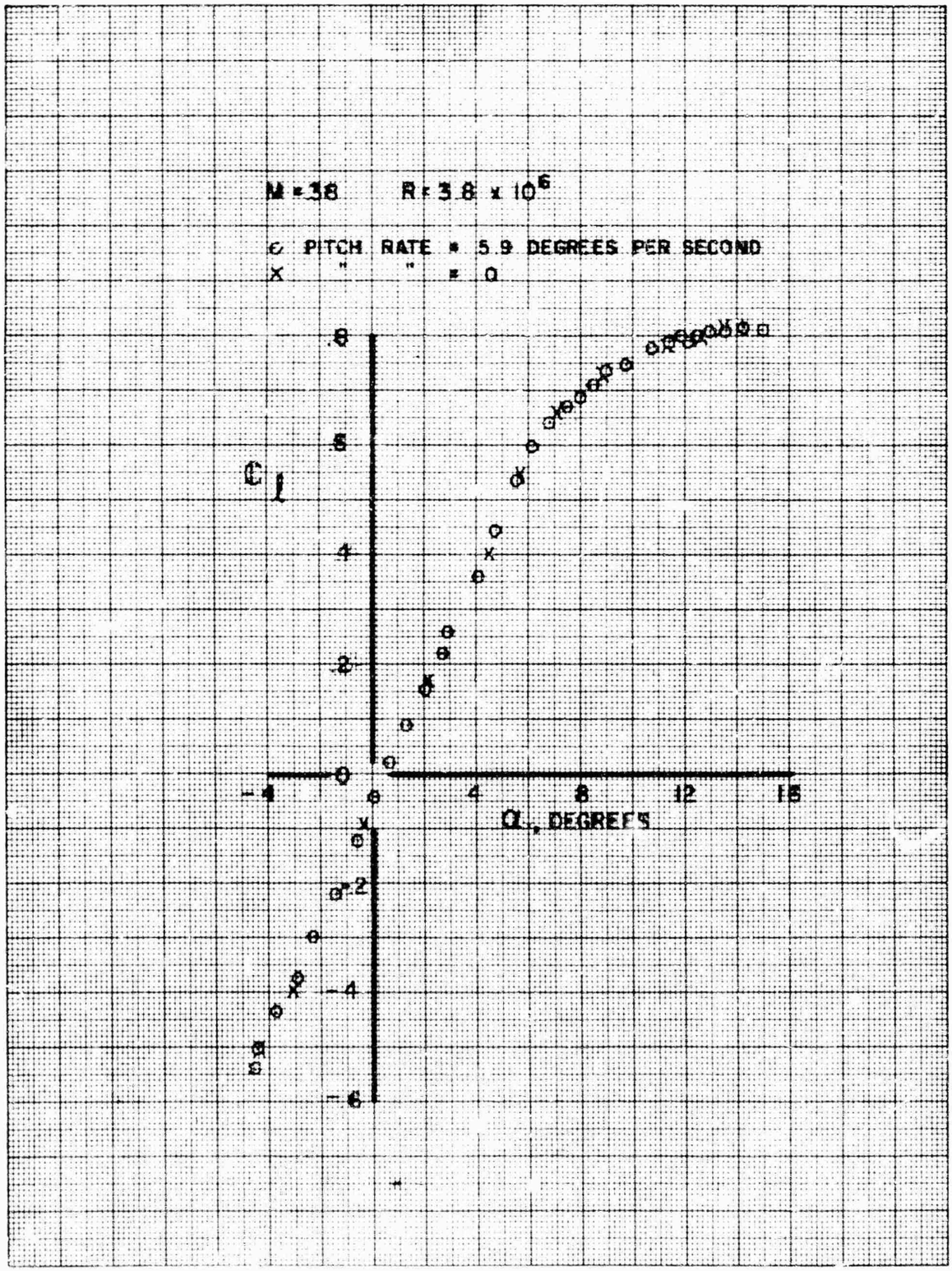


Figure 60A-2. Pitch Rate Comparison Data, NACA Section 63A009

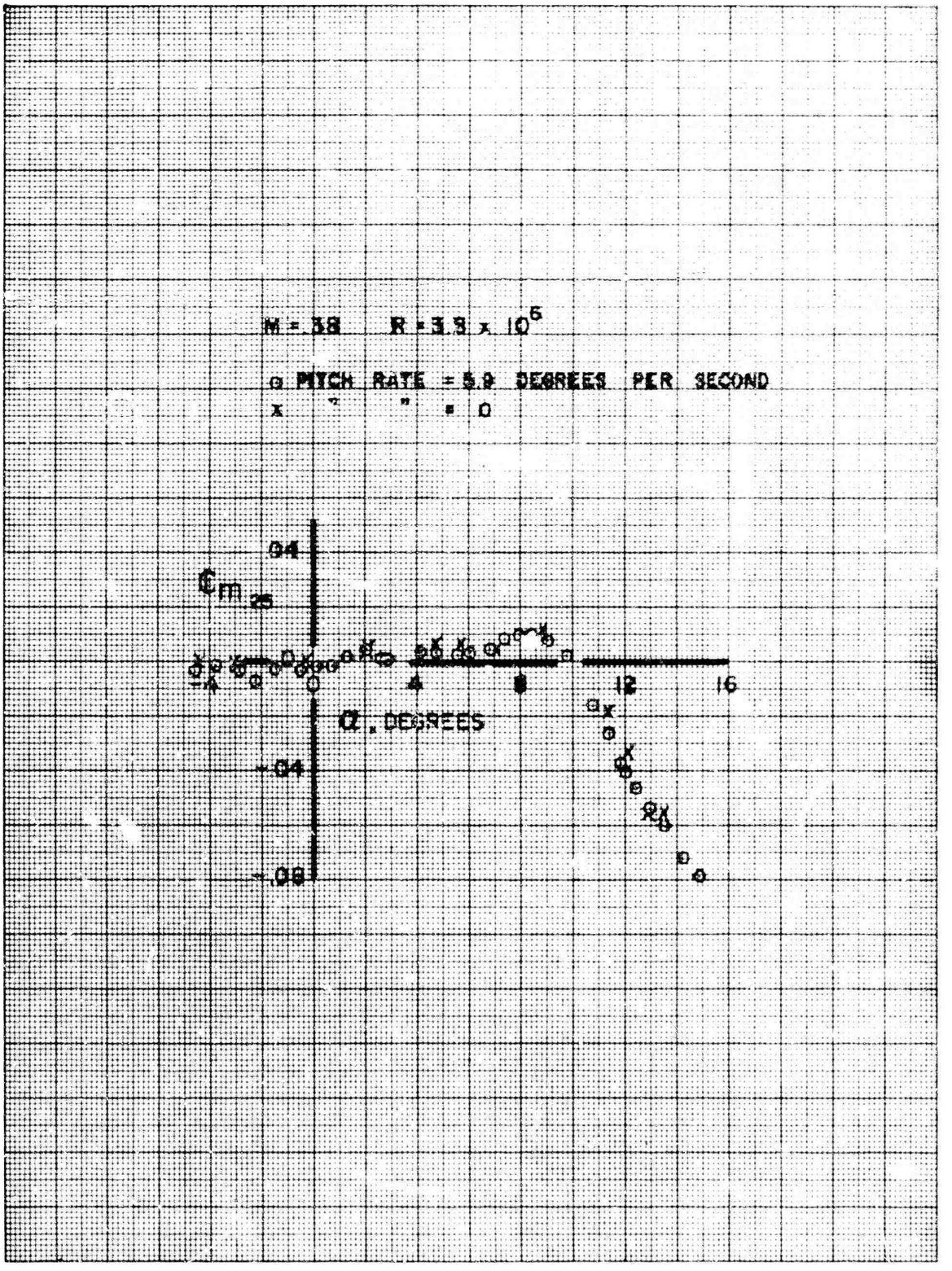


Figure 60A-3. Pitch Rate Comparison Data, NACA Section 63A009

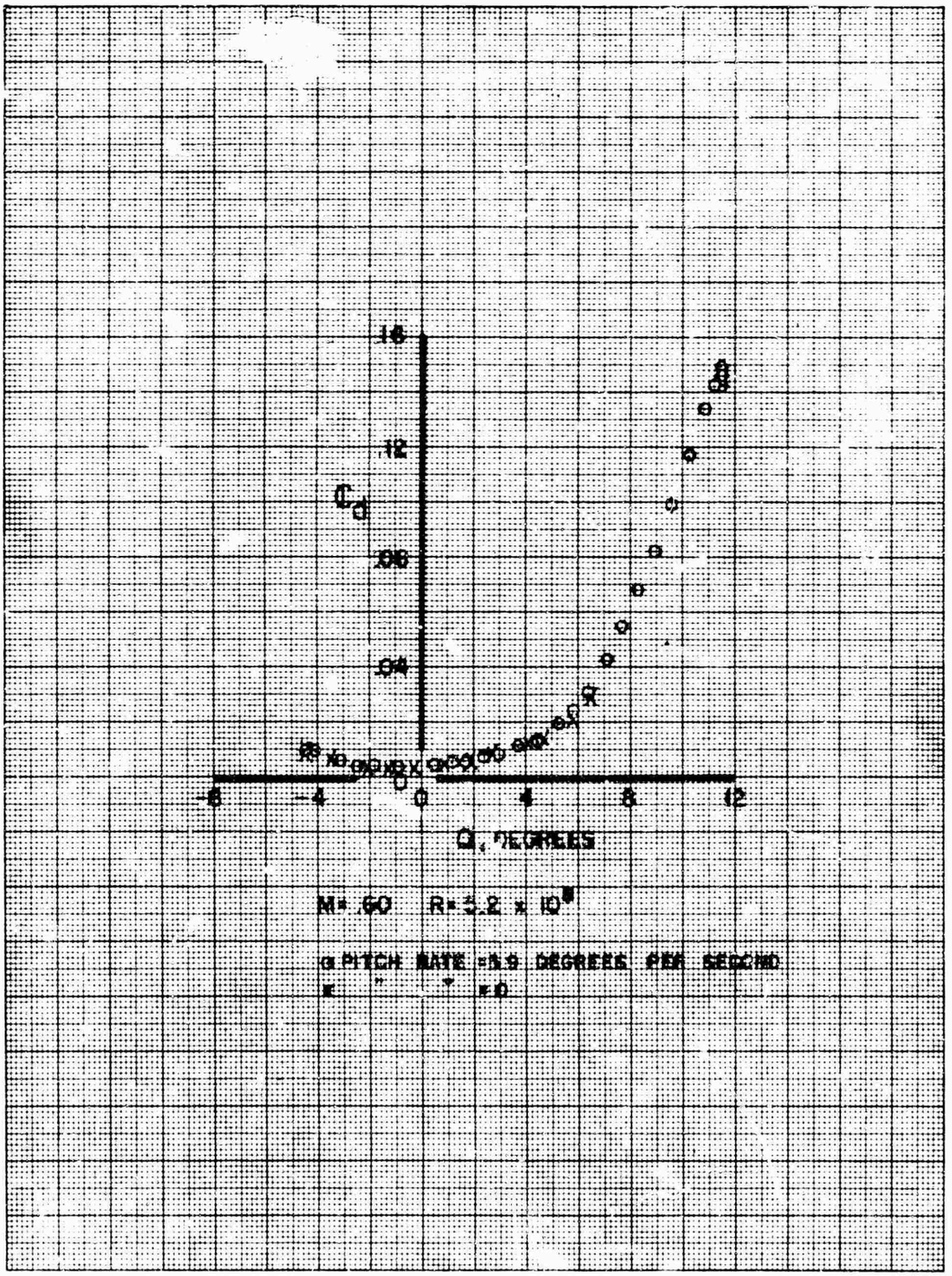


Figure 60B-1. Pitch Rate Comparison Data, NACA Section 63A009

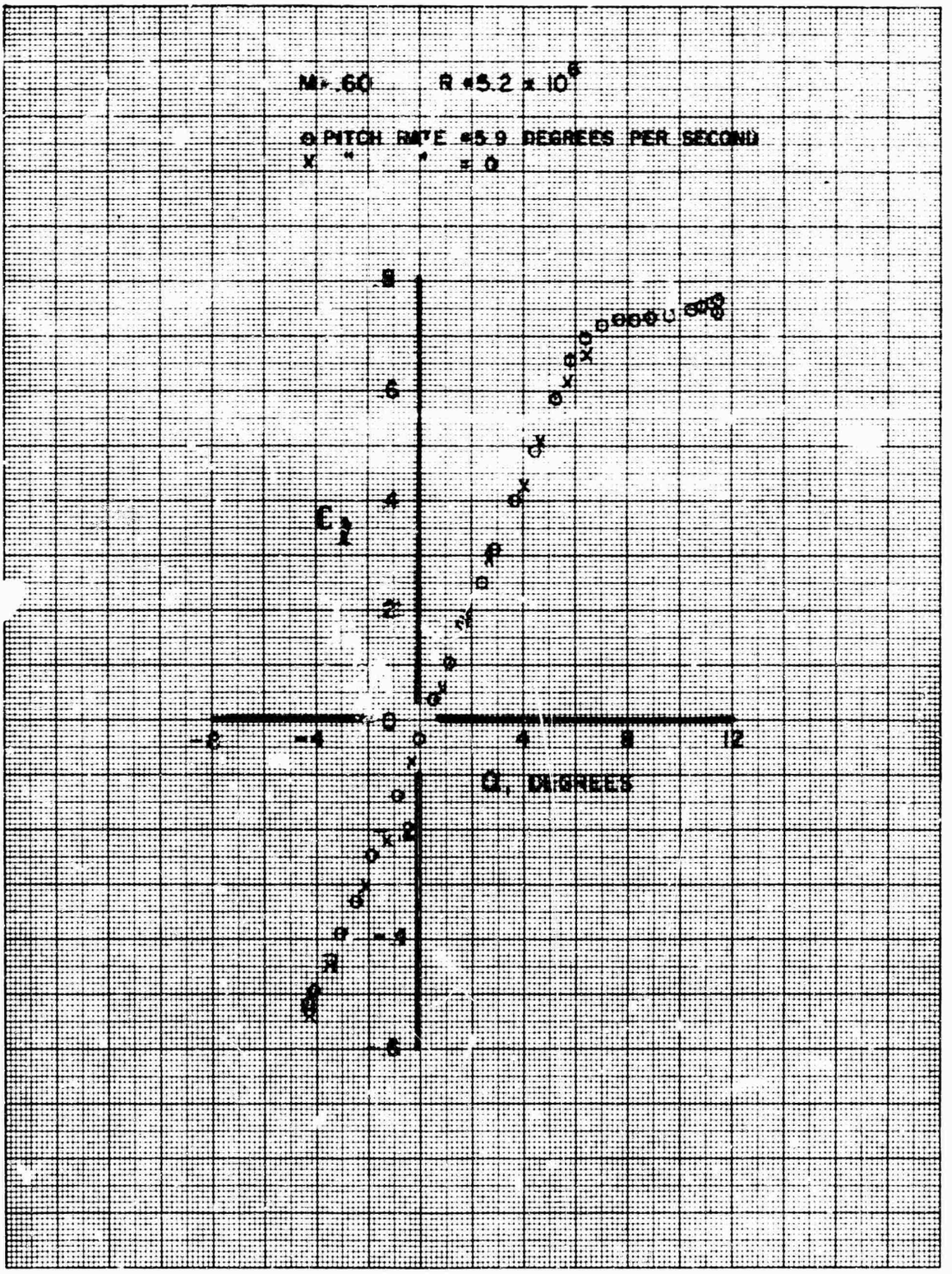


Figure 60B-2. Pitch Rate Comparison Data, NACA Section 63A009

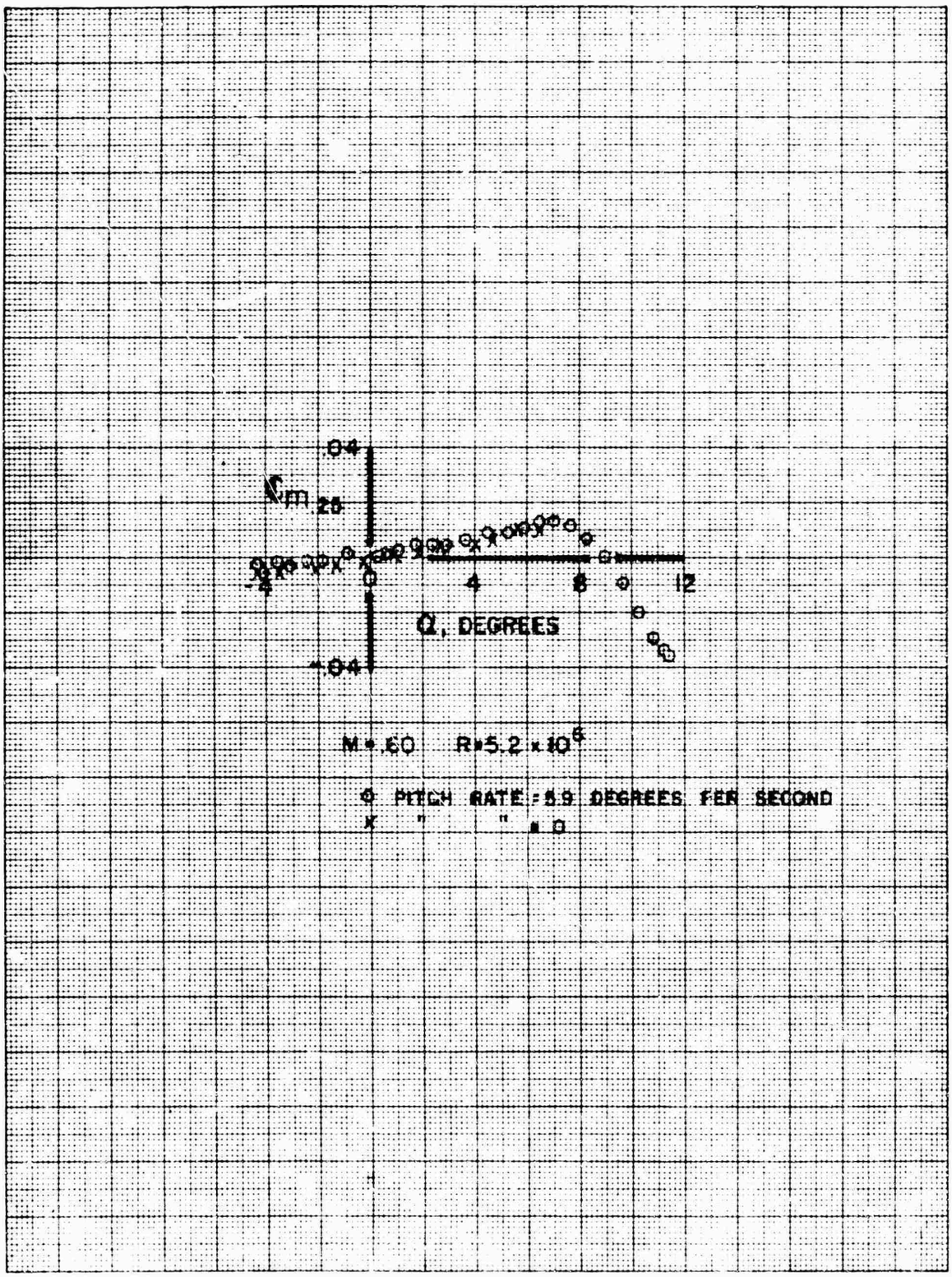


Figure 60B-3. Pitch Rate Comparison Data, NACA Section 63A009

BIBLIOGRAPHY

SECTION A - AIRFOIL TEST DATA AND DATA CORRELATION METHODS*

1. Abbott, I. H., von Doenhoff, A. E., and Stivers, Jr., L. S., Summary Of Airfoil Data, NACA Report 824, 1945.

2. Abbott, I. H. and von Doenhoff, A. E., Theory Of Wing Sections Including A Summary Of Airfoil Data, Dover Publications, Inc., New York, 1959.

3. Beavan, J. A., Sargent, R., North, R. J., and Burrows, P. M., Measurements Of Maximum Lift On 26 Airfoil Sections At High Mach Numbers, R and M No. 2678, Aeronautical Research Council, 1953.

4. Bullivant, W. K., Tests Of The NACA 0025 and 0035 Airfoils In The Full-Scale Wind Tunnel, NACA Report 708, 1941.

5. Busemann, A., Application Of Transonic Similarity, NACA TN 2687, April 1952.

6. Cleary, H. E., The Effects Of Reynolds Number On The Application Of NACA 16-Series Airfoil Characteristics To Propeller Design, NACA TN 2591, January 1952.

7. Critzos, C. C., Heyson, H. H., and Boswinkle, Jr., R. W., Aerodynamic Characteristics Of NACA 0012 Airfoil Section At Angles Of Attack From 0° to 180°, NACA TN 3361, January 1955.

7.1 Critzos, C. C., Aerodynamic Characteristics At High And Low Subsonic Mach Numbers Of The NACA 0012, 64_2-015 and 64_3-018 Airfoil Sections At Angles Of Attack From -2° to 30°, RM L54H06a, 1954. (Special release copy; limited circulation.)

8. Daley, B. N. and Humphreys, M. D., Effects Of Compressibility On The Flow Past Thick Airfoil Sections, NACA TN 1657, July 1948.

*References in Section A of the Bibliography are identified throughout the report as "A-" followed by the applicable reference number.

9. Daley, B. N., and Lord, D. R., Aerodynamic Characteristics of Several 6-Percent Thick Airfoils At Angles of Attack From 0^{o} to 20^{o} at High Subsonic Speeds, NACA TN 3424, May 1955.

10. Daley, B. N., and Dick, R. S., Effect of Thickness, Camber and Thickness Distribution on Airfoil Characteristics at Mach Numbers Up To 1.0, NACA TN 3607, March 1956.

11. Eggers, Jr., A. J., Aerodynamic Characteristics at Subcritical Mach Numbers of Two Airfoil Sections Having Sharp Leading Edges and Extreme Rearward Positions of Maximum Thickness, NACA RM A7C10, 6 November, 1947.

12. Gault, D. E., Boundary-Layer and Stalling Characteristics of the NACA 63-009 Airfoil Section, NACA TN 1894, June 1949.

13. Gault, D. E., A Correlation of Low-Speed, Airfoil-Section Stalling Characteristics With Reynolds Number and Airfoil Geometry, NACA TN 3963, March 1957.

14. Graham, D. J., Nitzberg, G. E., and Olson, R. N., A Systematic Investigation of Pressure Distributions at High Speeds Over Five Representative NACA Low-Drag and Conventional Airfoil Sections, NACA Report 832, 1945.

15. Harder, K. C., Transonic Similarity Rules for Lifting Wings, NACA TN 2724, June 1952.

16. Humphreys, M. D., and Robinson, R. A., The Effect of Changes in the Leading-Edge Radius on the Aerodynamic Characteristics of a Symmetrical, 9-Percent-Thick Airfoil at High-Subsonic Mach Numbers, NACA RM L9L09, 7 August , 1950.

17. Jacobs, E. N., Ward, K. E., and Pinkerton, R. M., The Characteristics of 78 Related Airfoil Sections From Tests in the Variable Density Wind Tunnel, NACA Report 460, 1932.

18. Jacobs, E. N., and Pinkerton, R. M., Tests in the Variable-Density Wind Tunnel of Related Airfoils Having the Maximum Camber Unusually Far Forward, NACA Report 537, 1935.

19. Jacobs, E. N., and Sherman, A., Airfoil Section Characteristics as Affected by Variations of the Reynolds Number, NACA Report 586, 1937.

20. Jacobs, E. N., Pinkerton, R. M., and Greenberg, H., Tests of Related Forward-Camber Airfoils in the Variable Density Wind Tunnel, NACA Report 610, 1937.

21. Jacobs, E. N., and Abbott, I. H., Airfoil Section Data Obtained in the NACA Variable-Density Tunnel As Affected By Support Interference and Other Corrections, NACA Report 669, 1939.

22. Koenig, D. G., Low-Speed Tests of Semispan-Wing Models at Angles of Attack From 0° to 180°, NASA Memo 2-27-59A, April 1959.

23. Kelley, J. A., Effects of Modifications to the Leading Edge Region On The Stalling Characteristics of the NACA 63_1 -012, NACA TN 2228, November 1950.

24. Ladson, C. L., Two-Dimensional Airfoil Characteristics of Four NACA 6A-Series Airfoils at Transonic Mach Numbers Up To 1.25, NACA RM L57F05, 6 August, 1957.

25. Ladson, C. L., Chordwise Pressure Distributions Over Several NACA 16-Series Airfoils at Transonic Mach Numbers Up To 1.25, NASA Memo 6-1-59L, June 1959.

26. Liepmann, H. W., and Roshko, A., Elements of Gas Dynamics, John Wiley and Sons, Inc., New York, 1957.

27. Lindsay, W. F., Daley, B. N., Humphreys, M. D., The Flow and Force Characteristics of Supersonic Airfoils at High Subsonic Speeds, NACA TN 1211, 1947.

28. Lindsay, W. F., Stevenson, D. B., and Daley, B. N., Aerodynamic Characteristics of 24 NACA 16-Series Airfoils at Mach Numbers Between 0.3 and 0.8, NACA TN 1546, September 1948.

29. Lindsay, W. F., and Humphreys, M. D., Tests of the NACA 64_1 -012 and 64_1 A-102 Airfoils at High Subsonic Mach Numbers, NACA RM L8D23, 9 July, 1948.

30. Loftin, Jr., L. K., and Poteat, M., Aerodynamic Characteristics of Several NACA Airfoil Sections at Seven Reynolds Numbers From 0.7×10^6 to 9.0×10^6, NACA RM L8B02, May 1948.

31. Loftin, Jr., L. K. and Bursnall, W. J., The Effects of Variations in Reynolds Number Between 3.0×10^6 and 25.0×10^6 Upon The Aerodynamic Characteristics of a Number of NACA 6-Series Airfoil Sections, NACA Report 964, 1950.

32. Loftin, Jr., L. K., Theoretical and Experimental Data For A Number of NACA 6A-Series Airfoil Sections, NACA Report 903, 1948.

33. Loftin, Jr., L. K., and Smith, H. A., Aerodynamic Characteristics of 15 NACA Airfoil Sections At 7 Reynolds Numbers from 0.7 x 10^6 to 9.0 x 10^6, NACA TN 1945, October 1949.

34. Loftin, Jr., L. K., and von Doenhoff, A. E., Exploratory Investigation at High and Low Subsonic Mach Numbers of Two Experimental 6-Percent-Thick Airfoil Sections Designed to Have High Maximum Lift Coefficients, NACA RM L51F06, 14 December, 1951.

35. Loftin, Jr., L. K., Airfoil Section Characteristics at High Angles of Attack, NACA TN 3241, August 1954.

36. Maki, R. L., and Hunton, L. W., An Investigation at Subsonic Speeds of Several Modifications to the Leading-Edge Region of the NACA 64A010 Airfoil Section Designed to Increase Maximum Lift, NACA TN 3871, December 1956.

37. McDevitt, J. B., A Correlation By Means of Transonic Similarity Rules of Experimentally Determined Characteristics of a Series of Symmetrical and Cambered Wings of Rectangular Planform, NACA Report 1253, 1955.

38. Mellenthin, J. A., The Flow About a Section of a Finite-Aspect-Ratio NACA 0015 Airfoil on a Transonic Bump, NACA TN 3036, October 1953.

39. Muse, T. C., Some Effects of Reynolds and Mach Numbers on the Lift of a NACA 0012 Rectangular Wing in the NACA 19-Foot Pressure Tunnel, NACA Wartime Report L-406, 1943.

40. Nelson, W. H., and McDevitt, J. B., The Transonic Characteristics of 22 Rectangular, Symmetrical Wing Models of Varying Aspect Ratio and Thickness, NACA TN 3501, June 1955.

41. Nelson, W. H., and Krumm, W. J., The Transonic Characteristics of 38 Cambered Rectangular Wings of Varying Aspect Ratio and Thickness Determined by the Transonic-Bump Technique, NACA TN 3502, June 1955.

42. Nitzberg, G. E., and Crandall, S. M., A Comparative Examination of Some Measurements of Airfoil Section Lift and Drag at Supercritical speeds, NACA TN 2825, November 1952.

43. Paradiso, N. J., Investigation at High and Low Subsonic Mach Numbers of Two Symmetrical 6-Percent-Thick Airfoil Sections Designed to Have High Maximum Lift Coefficients at Low Speeds, NACA RM L52102, 17 October, 1952.

44. Polentz, P. P., Comparison of the Aerodynamic Characteristics of the NACA 0010 and 0010-64 Airfoil Sections at High Subsonic Mach Numbers, RM A9G19, 7 October, 1949.

45. Pope, A., The Forces and Pressures Over An NACA 0015 Airfoil Through 180 Degrees Angle of Attack, David Guggenheim School of Aeronautics, Georgia Tech. Report E-102, February 1947.

46. Racisz, S. F., Effects of Independent Variations of Mach Number and Reynolds Number on the Maximum Lift Coefficients of Four NACA 6-Series Airfoil Sections, NACA TN 2824, November 1952.

47. Reigels, Dr. F. W., Aerofoil Sections, Butterworth Co., Ltd., London, 1961.

48. Schaefer, R. F., Loftin, Jr., L. K., and Horton, E. A., Two Dimensional Investigation of Five Related NACA Airfoil Sections Designed for Rotating Wing Aircraft, NACA TN 1922, July 1949.

49. Schaefer, R. F., and Smith, H. A., Aerodynamic Characteristics of the NACA 8-H-12 Airfoil Section at Six Reynolds Numbers From 1.8×10^6 to 11.0×10^6, NACA TN 1998, December 1949.

50. Schairer, G. S., "Systematic Wing Section Development", Journal of the Aeronautical Sciences, Volume 14, No. 1, January 1947.

51. Spreiter, J. R., and Steffen, P. J., Effect of Mach and Reynolds Numbers on Maximum Lift Coefficient, NACA TN 1044, 1946.

52. Spreiter, J. R., Similarity Laws for Transonic Flow About Wings of Finite Span, NACA TN 2273, January 1951.

53. Spreiter, J. R., On the Application of Transonic Similarity Rules to Wings of Finite Span, NACA Report 1153, 1953.

54. Stack, J., and von Doenhoff, A. E., Tests of 16 Related Airfoils at High Speeds, NACA Report 492, 1934.

55. Stack, J., Lindsay, W. F. and Littell, R. E., The Compressibility Burble and the Effects of Compressibility on Pressures and Forces Acting on an Airfoil, NACA Report 646, 1938.

56. Stack, J., Tests of Airfoils Designed to Delay the Compressibility Burble, NACA Report 763, 1943.

57. Stack, J. and Lindsay, W. F., Characteristics of Low-Aspect-Ratio Wings at Supercritical Mach Numbers, NACA Report 922, 1949.

58. Stivers, Jr., L. S. and Rice, Jr., F. J., Aerodynamic Characteristics of Four NACA Airfoil Sections Designed for Helicopter Rotor Blades, NACA Wartime Report L-29, February 1946.

59. Stivers, Jr., L. S., Effects of Subsonic Mach Number on the Forces and Pressure Distributions on Four NACA 64A-Series Airfoil Sections at Angles of Attack As High As 28°, NACA TN 3162, March 1954.

60. Summers, J. L. and Graham, D. J., Effects of Systematic Changes of Trailing-Edge Angle and Leading Edge Radius on the Variation With Mach Number of the Aerodynamic Characteristics of a 10-Per-Cent-Chord-Thick NACA Airfoil Section, NACA RM A9G18, September 1949.

61. Tetervin, N., Airfoil Section Data From Tests of Ten Practical Construction Sections of Helicopter Rotor Blades Submitted by the Sikorsky Aircraft Division, United Aircraft Corporation, NACA Wartime Report L-643, September 1944.

62. Van Dyke, M. D., High-Speed Subsonic Characteristics of 16 NACA 6-Series Airfoil Sections, NACA TN 2670, March 1952.

63. Wilson, Jr., H. B. and Horton, E. A., Aerodynamic Characteristics at High and Low Subsonic Mach Numbers of Four NACA 6-Series Airfoil Sections at Angles of Attack from -2° to 31°, NACA RM L53C20, 5 June, 1953.

SECTION B - ROTOR TEST DATA*

1. Carpenter, P. J., Effects of Compressibility on the Performance of Two Full Scale Helicopter Rotors, NACA Report 1078, 1952.

2. Carpenter, P. J., Lift and Profile-Drag Characteristics of an NACA 0012 Airfoil Section as Derived From Measured Helicopter-Rotor Hovering Performance, NACA TN 4357, September 1958.

*References in Section B of the Bibliography are identified throughout the report as "B-" followed by the applicable reference number.

3. Harris, Lt. E. R., and Velkoff, H. R., "An Aerodynamic Comparison of Two Airfoils Based Upon Full Scale Rotor Whirl Tests", Paper presented at the American Helicopter Society Fifth Annual Western Forum, September 1958.

4. Jewel, Jr., J. W. and Harrington, R. D., Effect of Compressibility On The Hovering Performance of Two 10-Foot Diameter Helicopter Rotors Tested in the Langley Full-Scale Tunnel, NACA RM L58B19, 21 April 1958.

5. Jewel, Jr., J. W., Compressibility Effects on the Hovering Performance of a Two-Blade 10-Foot Diameter Helicopter Rotor Operating at Tip Mach Numbers Up To 0.98, NASA TN D-245.

6. McCloud, III, J. L. and McCullough, G. B., Wind-Tunnel Tests of a Full-Scale Helicopter Rotor With Symmetrical and With Cambered Blade Sections at Advance Ratios From 0.3 to 0.4, NACA TN 4367, September 1958.

7. McCloud, III, J. L. and McCullough, G. B., Comparison of Calculated and Measured Stall Boundaries of a Helicopter Rotor at Advance Ratios From 0.3 to 0.4, NASA TN D-73, September 1959.

8. McCloud, III, J. L., Hall, L. P. and Brady, J. A., Full-Scale Wind Tunnel Tests of Blowing Boundary-Layer Control Applied to a Helicopter Rotor, NASA TN D-335, September 1960.

9. McCloud, III, J. L., Biggers, J. C. and Maki, R. L., Full Scale Wind Tunnel Tests of a Medium-Weight Utility Helicopter at Forward Speeds, NASA TN D-1887, May 1963.

10. Powell, Jr., R. D., Hovering Performance of a Helicopter Rotor Using NACA 8-H-12 Airfoil Sections, NACA TN 3237, August 1954.

11. Powell, Jr., R. D., Compressibility Effects on a Hovering Helicopter Rotor Having an NACA 0018 Root Airfoil Tapering to an NACA 0012 Tip Airfoil, NACA RM L57F26, September 1957.

12. Powell, Jr., R. D. and Carpenter, P. J., Low Tip Mach Number Stall Characteristics and High Tip Mach Number Compressibility Effects on a Helicopter Rotor Having an NACA 0009 Tip Airfoil Section, NACA TN 4355, July 1958.

13. Powell, Jr., R. D., Maximum Mean Lift Coefficient Characteristics at Low Tip Mach Numbers of a Hovering Helicopter Rotor Having an NACA 64_1 A012 Airfoil Section, NASA Memo 1-23-59L, February 1959.

14. Shivers, J. P. and Carpenter, P. J., Experimental Investigation on the Langley Helicopter Test Tower of Compressibility Effects on a Rotor Having NACA 632-015 Airfoil Sections, NACA TN 3850, December 1956.

15. Rabbott, Jr., J. P., Comparison of Theoretical and Experimental Model Helicopter Rotor Performance in Forward Flight, TCREC Technical Report 61-103, U. S. Army Transportation Research Command, Fort Eustis, Virginia, July 1961.

16. Shivers, J. P. and Carpenter, P. J., Effects of Compressibility on Rotor Hovering Performance and Synthesized Blade-Section Characteristics Derived from Measured Rotor Performance of Blades Having NACA 0015 Airfoil Tip Sections, NACA TN 4356, September 1958.

17. Shivers, J. P., High Speed Static-Thrust Tests of a Rotor Having NACA 63(215)A018 Airfoil Sections With and Without Vortex Generators Installed, NASA TN D-376, May 1960.

18. Shivers, J. P., Hovering Characteristics of a Rotor Having an Airfoil Section Designed for Flying-Crane Type of Helicopter, NASA TN D-742, April 1961.

19. Shivers, J. P., and Monahan, W. J., Hovering Characteristics of an Airfoil Section Designed for a Utility Type Helicopter, NASA TN D-1517, December 1962.

20. Sweet, G. E., Jenkins, Jr., J. L., and Winston, M. M., Wind-Tunnel Measurements on a Lifting Rotor at High Thrust Coefficients and High-Tip-Speed Ratios, NASA TN D-2462, September 1964.

DISTRIBUTION

US Army Materiel Command	1
US Army Mobility Command	1
US Army Aviation Materiel Command	5
US Army Aviation Materiel Laboratories	22
US Army Engineer R&D Laboratories	2
Army Research Office-Durham	1
US Army War College	1
US Army Command and General Staff College	1
US Army Aviation School	1
Air Force Systems Command, Wright-Patterson AFB	1
Air Force Flight Test Center, Edwards AFB	1
Air Proving Ground Center, Eglin AFB	1
Bureau of Naval Weapons	3
Bureau of Naval Research	1
US Naval Air Station, Patuxent River	1
David Taylor Model Basin	1
Marine Corps Liaison Officer, US Army Transportation School	1
Ames Research Center, NASA	1
Lewis Research Center, NASA	1
Manned Spacecraft Center, NASA	1
NASA Representative, Scientific and Technical Information Facility	2
Research Analysis Corporation	1
National Aviation Facilities Experimental Center	1
Defense Documentation Center	20
US Government Printing Office	1

APPENDIX

EQUATIONS TO DETERMINE AERODYNAMIC COEFFICIENTS

The equations used to obtain the aerodynamic coefficients are presented in detail below:

$$N = C_1 N_1 \cos \phi_1 + C_2 N_2 \cos \phi_2 - C_1 Y_1 \sin \phi_1 - C_2 Y_2 \sin \phi_2 - \left[\frac{\partial N_{1w}}{\partial \alpha} \alpha_B + \frac{\partial N_{2w}}{\partial \alpha} \alpha_B \right]$$

$$X = C_1 X_1 + C_2 X_2 - \left[\frac{\partial X_{1w}}{\partial \alpha} \alpha_B + \frac{\partial X_{2w}}{\partial \alpha} \alpha_B \right]$$

$$m = C_1 m_1 \cos \phi_1 + C_2 m_2 \cos \phi_2 - C_1 n_1 \sin \phi_1 - C_2 n_2 \sin \phi_2 - \left[\frac{\partial m_{1w}}{\partial \alpha} \alpha_B + \frac{\partial m_{2w}}{\partial \alpha} \alpha_B \right]$$

$$q = \frac{0.7 H_A M^2}{\sqrt{(1 + 0.2M^2)^7}}$$

$$c_l = \frac{N \cos \alpha - X \sin \alpha}{q S}$$

$$c_d = \frac{X \cos \alpha + N \sin \alpha}{q S}$$

$$c_{m_{.25}} = \frac{m}{q\ Sc}$$

$$\Delta\alpha_B = 0.5 \left[\left(\frac{\Delta\alpha_{B_1}}{N_1} \right) C_1 N_1 + \left(\frac{\Delta\alpha_{B_2}}{N_2} \right) C_2 N_2 + \left(\frac{\Delta\alpha_{B_1}}{m_1} \right) C_1 m_1 + \left(\frac{\Delta\alpha_{B_2}}{m_2} \right) C_2 m_2 \right]$$

$$\alpha_B = \alpha_n + \Delta\alpha_B$$

$$\alpha = \alpha_u + \Delta\alpha_F$$

where

C_1 , C_2 = Constant dependent on numbers of balances used in data reduction

H_A = Free stream total pressure, p.s.i.a.

M = Free stream Mach number

N = Total normal force acting on model, positive upwards; pounds.

N_1 , N_2 = Normal force measured by balances 1 and 2, positive upwards; pounds

S = Airfoil area, square inches = 384

X = Total chord force measured on model, positive aft; pounds

X_1 , X_2 = Chord force measured by balances 1 and 2, positive aft; pounds

Y_1 , Y_2 = Side force measured by balances 1 and 2, positive right; pounds

c = Airfoil chord, inches = 8

c_l = Section lift coefficient

c_d = Section drag coefficient

$c_{m_{.25}}$ = Section pitching moment coefficient about .25 airfoil chord

m = Total pitching moment measured about .25 airfoil chord, positive nose up; inch-pounds

m_1 , m_2 = Pitching moment about .25 airfoil chord measured by balances 1 and 2, positive nose up; inch-pounds

n_1 , n_2 = Yawing moment measured by balances 1 and 2, positive right; inch-pounds

q = Incompressible free stream dynamic pressure, p.s.i.a.

$\frac{\partial N_{1w}}{\partial \alpha}$, $\frac{\partial N_{2w}}{\partial \alpha}$ = Normal force weight tares for balances 1 and 2

$\frac{\partial X_{1w}}{\partial \alpha}$, $\frac{\partial X_{2w}}{\partial \alpha}$ = Chord force weight tares for balances 1 and 2

$\frac{\partial m_{1w}}{\partial \alpha}$, $\frac{\partial m_{2w}}{\partial \alpha}$ = Pitching moment weight tares for balances 1 and 2

α = Angle of attack with reference to airfoil chord line, positive nose up, degrees

α_n = Nominal angle of attack, degrees

α_B = Nominal angle of attack + balance deflection angle, degrees

$\Delta\alpha_B$ = Balance deflection angle, degrees

$\frac{\Delta\alpha_{B_1}}{N_1}$, $\frac{\Delta\alpha_{B_2}}{N_2}$ = Deflection of balances 1 and 2 per pound of normal force; degrees/pound

$\frac{\Delta\alpha_{B_1}}{m_1}$, $\frac{\Delta\alpha_{B_2}}{m_2}$ = Deflection of balances 1 and 2 per inch-pound of pitching moment; degrees/inch-pound

$\Delta\alpha_F$ = Flow inclination, degrees

ϕ_1 , ϕ_2 = Roll angles of balances 1 and 2, degrees